2013

Silica Polypeptide-Based Colloids: Physical Properties and Novel Materials

Cornelia Rosu
Louisiana State University and Agricultural and Mechanical College, crosu1@tigers.lsu.edu

SILICA POLYPEPTIDE-BASED COLLOIDS: PHYSICAL PROPERTIES AND NOVEL MATERIALS

A Dissertation

Submitted to the Graduate Faculty of
Louisiana State University and
Agricultural and Mechanical College
in partial fulfillment of the
requirements for the degree of
Doctor of Philosophy

in

The Department of Chemistry

by
Cornelia Rosu
B.S. "Al. I. Cuza", Iasi, 1996
M.S. Louisiana State University, 2010
August 2013

To my parents, Leontina and Pavel

"Appreciation is a wonderful thing.
It makes what is excellent in others
belong to us as well."
Voltaire

ACKNOWLEDGEMENTS

There are many people to whom I would like to thank and express my gratitude for assistance and support during the years of my doctoral program at Louisiana State University. First I would like to start with Professor Paul S. Russo, my major advisor. His scientific guidance, his constructive critique and the challenges which he decorated my research time helped me to become the scientist I am today. Most of all I want to thank him for the understanding and the moral support when I have passed through difficult times.

Equal gratitude is directed to Professor Ioan I. Negulescu and Professor William H. Daly for their support, guidance and expertise provided to me especially in the first years of my PhD. I am indebted to Dr. Rafael Cueto who kindly offered his knowledge and assistance all the time I needed. Professor John Pojman and Professor Donghui Zhang are also acknowledged for their time serving in my committee and also for helpful suggestions over the time.

Research around the LSU campus could not be possible without devoted people who assisted with training and conducting measurements. I hope I will be forgiven if somehow, by mistake, I forgot name: Dr. Dale Treleaven and Dr. Thomas Weldeghiorghis (NMR), Connie Davis (mass spectrometry), Dr. Dongmei Cao (Material Center, Patrick Taylor Hall), Ying Xiao and Dr. Matthew Brown (Socolofski Microscopy Lab, Life Sciences), Dr. Amitava Roy and Andrew Weber (CAMD).

I appreciate the collaboration with other research departments and universities: Professor Ernst Von Meerwall (Akron State University, Akron, OH), Professor Chanjoong Kim and his postdoc (Institute of Liquid Crystals, Kent State, OH), Professor Charles Han (Academy of

Science, Beijing, China) and Professor John DiTusa and his graduate student Yin Yan (Department of Physics, LSU).

I value the help of my colleagues from Dr. Russo's and Dr. Daly/Dr. Negulescu's groups: Dr. Erick Soto-Cantu, Dr. Derek Dorman, Dr. Javoris Hollingsworth, Melissa Collins, Wayne Huberty, Sourav Chaterjee, Xiaowei Tong, Brandon Curtis, Brad Blalock, Kyle Deville, Mohammad Abu-Laban, Daniel Hulgan, Dr. Lee Madsen, Dr. Cristina Stefanescu, Dr. Eduard Stefanescu and Brent Sellers. I particularly want to thank Dr. Sreelatha Balamurugan and Dr. Ionela Glover for their help and support.

National Science Foundation and Louisiana State University are deeply acknowledged for funding this work. I also want to thank Coates Travel Award Travel for sponsoring my participation to national symposiums. I thank American Chemical Society, Polymer Division for recognition of my research in polymers.

Not the last I want to thank from the bottom of my heart to my parents, Leontina and Pavel. I know these years were long for you, especially for you now, mother. I am also in-depth to my dear friends and my relatives. Thank you for your moral support when I was in need.

TABLE OF CONTENTS

LIST OF TABLES

LIST OF FIGURES

LIST OF SCHEMES

ABBREVIATIONS AND SYMBOLS

AEAPTMS	aminoethyl-aminopropyltrimethyl silane
APS	3-Aminopropyl triethoxysilane
B	Magnetic induction
CBL	Nε-Carbobenzyloxy-L-Lysine
d	Crystallite size or rod diameter
D_0	Diffusion coefficient extrapolated at zero concentration and magnitude of scattering angle vector
D_{app}	Apparent diffusion coefficient
DLS	Dynamic light scattering
DMAc	Dimethyl acetamide
DMF	Dimethyl formamide
DSC	differential scanning calorimetry
ESI	Electrospray Ionization
f	Fraction of polypeptide ashes
FITC	Fluorescein isothiocyanate
FTIR	Fourier transform infrared spectroscopy
FWHM	Full Width Half Maximum
$g^{(1)}(\tau)$	Normalized electric field autocorrelation function
GPC	Gel permeation chromatography
G′	Storage modulus
G″	Loss modulus
H	Henry

H_c	Coercive field
HRTEM	High Resolution Transmission Electron Microscopy
K	Shape factor
K	Kelvin
k_B	Boltzmann constant
LC	Liquid crystal
LECH	Light emitting colloidal hybrids
M	Molarity
MALDI-TOF	Matrix Assisted Laser Desorbtion-Ionization Time of Flight
MALS	Multi-angle Light Scattering
Mmol	milimolar
M_n	Number-average molecular weight
M_r	Remanent magnetization
M_s	Saturation magnetization
MTMS	Methyltrimethoxy silane
M_w	Weight-average molecular weight
N	Normality
NCA	N-carboxyanhydride
nm	Nanometer
NMR	Nuclear Magnetic Resonance
BTYR	o-Benzyloxy-L-Tyrosine
Oe	Oersted
PBLG	Poly(γ-benzyl-α-*L*-glutamate)

PBTY	Poly(o-benzyl-L-tyrosine)
PCBL	Poly(ε-carbobenzyloxy-*L*-lysine)
PCP	Polypeptide composite particle
PDI	Polydispersity index
PEP	Polypeptide
PICUP	Photo-induced Cross-linking of Unmodified Proteins
PLLeu	Poly(L-leucine)
PLYS, PLL	Poly(L-lysine)
PMDETA	Pentamethyldiethylene triamine
PSLG	Poly(γ-stearyl-α-*L*-glutamate)
PTYR	Poly(*L*-tyrosine)
q	Scattering vector magnitude
R_{app}	Apparent radius
R_h	Hydrodynamic radius
ROP	Ring-open polymerization
RPM	Rotation per minute
SAXS/WAXS	Small/Wide angle X-ray scattering
SEM	Scanning electron microscopy
SLG	γ-Stearyl-L-Glutamate
SQUID	Superconducting quantum interference device
Sspec.	Surface specific area
T	Absolute temperature
T	Tesla

T1	Spin-lattice relaxation time
TEM	Transmission electron microscopy
TEOS	Tetraethylortho silicate
TGA	Thermogravimetric analysis
TYR	Tyrosine
w	Mass weight
XPS	X-ray Photoelectron Spectroscopy
XRD	X-ray Powder Diffraction
β	Line broadening
Γ	Decay rate
η_0	Solvent viscosity
θ	Scattering angle
λ	Wavelength
λ_0	Wavelength in vacuo
μ_2	Second cumulant
σ	Grafting density
τ	Lag time

ABSTRACT

The investigation of polypeptide composite particles, PCPs, is described. The production of mesoporous and polycolloid architectures is also addressed. PCPs were prepared by both growing form and grafting to method. They consist of a core made of silica, silica-coated magnetite or silica-coated cobalt. Some of the particles were covalently labeled with fluorescein isothiocyanate. Several polypeptides were chosen for attachment on the core: poly(γ-stearyl-L-glutamate), PSLG, poly(N^{ε}-carbobenzyloxy-L-lysine), PCBL and poly(o-benzyl-L-tyrosine), PBTY.

Attachment of a well-characterized alkyne-end terminated PSLG and PCBL to an azide-functionalized particle yielded PCPs with a desired sparse coverage. A blend of techniques such as FTIR, XPS, TEM, HTEM, XRD, GPC, MALDI-TOF, DLS, and SQUID was used to confirm their production and to investigate their properties. The near superparamagnetic PCBL-CPs showed thinning behavior when subjected to stress. PSLG-CPs dispersed in different surfactant aqueous solutions and also enabled the immobilization by adsorption of a lipase from *Candida rugosa*. Dispersed in a liquid crystal PSLG matrix they rendered interesting morphologies.

Mesoporous silica structures, some called geodesics, were obtained by prolonged storage in a slightly basic solution of ammonium hydroxide. Treatment with 3mM NaOH of fluorescent silica and PCPS yielded interesting mesoporous structures. Silica fluorescent particles were easily up-taken in the living cells of the *Arabidopsis thaliana* leaf. A concentrated NaOH solution (~10%) was used to cleave the polypeptide shell and measure the molecular weight. The helix conformation of the shell and the molecular weight, were confirmed by GPC assays.

PCBL-CPs underwent to an inverse helix-to-coil transition in m-cresol as a function of temperature. The transition was followed by DLS, DSC, NMR T1 and SAXS. The results

obtained with the blend of these techniques suggested a complicated landscape for the transition. The conformational change is not a pure coil-to-helix transition, rather transient states were identified.

Polycolloid architectures were obtained by using enzymatic (*Horseradish peroxidase*) and photolytic catalysis (PICUP-Photo-induced Cross-linking of Unmodified Proteins). Comparison between the two approaches emphasized the facile preparation of the polycolloid structures by PICUP. The technique was suitable for preparation of different architectures obtained by patterning the reaction vessels. PICUP also enabled the formation of permanent magnetic PCP chains.

CHAPTER 1
PROGRESS IN SILICA POLYPEPTIDECOMPOSITE COLLOIDAL HYBRIDS: FROM SILICA CORES TO FUZZY SHELLS

1.1 Introduction

Colloids have been used for various purposes since the earliest records of civilization. People have used them in technological processes such as making paper, cosmetics and soaps involved in colloidal systems. Over time, the technical improvements allowed the design of well defined materials. One of these materials is colloidal silica, or silica sol, which consists of stable dispersions or sols of discrete particles made of amorphous silica particles. Nature is abundant in silicon sources such as quartz. One key difference between colloidal silica and quartz sand, having the same chemical formula (SiO_2), is in the size. The typical range of the silica grains is between 1 and 5 nm and usually is expanded in the growth process to a size range covering the nano and the micrometer scale. The other key difference is in crystallinity. Colloidal silica is usually amorphous while quartz is crystalline. Silica has advantages over other inorganic materials such as nontoxic to the living bodies, inexpensive cost of the production and its refractive index matches with a broad variety of solvents. The first part of this review will summarize the preparation methods and the myriad of application of silica colloids as good models to perform fundamental studies.

The range of the silica applications is considerably expanded when they are dye-labeled or/and they carry magnetic inclusions. For example, tagged colloidal particles can be used as tracers, in order to understand diffusion in colloidal dispersions or in very viscous liquids.[1-5] The magnetic inclusion inside the colloidal silica add a degree of complexity which makes the system very appealing especially for biological applications.[6] Martel et al. reported the manipulation of the colloidal magnetic beads at speeds in the order of 8 μm/s, along preplanned paths by

magnetostatic bacteria.[7] A section will provide a glimpse of the work involving only magnetite (Fe_3O_4) and cobalt (Co) superparamagnetic particles.

Core-shell particles having a well-defined solid core made of silica or a polymer have enhanced colloidal stability and robustness. In the past, few composite core-shell colloidal particles that have been made featured a homopolypeptide shell.[8-13] The exquisite advantage of these composite particles is that, in the same material, the chemical versatility of the polypeptide shell is combined with magnificent optical and physical properties of the core.[14-21] The combination between these properties and the features of the colloidal particles would be beneficial. The last section of this review will give a survey over the work done on the core-shell hybrid particles with special emphasis on silica polypeptide-based colloids.

1.2 Colloidal Silica

1.2.1 Historical Perspective on Colloidal Silica Sols

Among other colloidal systems, silica nanoparticles occupy a top position in the scientific research because of their facile preparation that makes them an extraordinary candidate for various applications. In this respect, researchers have to be able to tune the quality of these products which is dependent strongly on the size and the size distribution. Reports of stable concentrated silica sols that do not gel or precipitate for a long time became available in early 1940's. These reports on concentrated silica solution production were summarized by Iler in the first edition of his book.[22] Vail in 1925, Treadwell and Wieland in 1930 had prepared sols that contained more than 10% silica particles but were not stable to the gelling effect. Ammonia-stabilized sols were reported by Griessbach in 1933. Later in 1941 Bird et al. prepared 5- 10 nm sized particles by removing alkali from the dilute sodium silicate using hydrogen ion-exchange resin, followed by stabilization with dilute alkali and concentration of the solution. Later, White

et al. used the process of peptizing the gel to a sol by dispersion in a basic solution and heating. Better control on the size and the uniformity was achieved by Bechtold et al. in 1951. Bechtold's method was improved by Rule et al. by optimizing the concentrations of alkali used for stabilization.

1.2.2 One-Time Addition of Silicon Alkoxide

The first report on monodisperse silica particles formation through the hydrolysis and condensation of a silicon alkoxide, tetraethylorthosilicate (TEOS) in a mixture of alcohol, water and ammonia was made in 1956 by Kolbe et al.[23] The first systematic study and probably the most cited work on monodisperse colloidal silica prepared in the solution, was performed by Stöber et al. in 1968.[24] Particle sizes ranged from several hundred nanometers to 2 microns in diameter. The synthetic procedure utilized ammonia-catalyzed hydrolysis of silicon alkoxides of different chain lengths and subsequent condensation of the silicic acid in the alcoholic solutions. The key to the Stöber procedure is the use of highly pure tetraalkyl silicates obtained by redistillation. Since the Stöber report, the most popular silanization agent has been tetraethylorthosilicate, TEOS. The silicon atom in TEOS carries a partial positive charge which makes it susceptible by the nucleophilic attack. In the presence of water the silicate, Si—OEt, bonds are hydrolyzed yielding ethanol, EtOH, and a new silanol Si—OH bond. The silanol group reacts further with other TEOS molecules producing new Si—O—Si bonds. The result of this process is the formation of the dimers, trimers, etc. Further, the polymerization reaction gives cyclic molecules. These cyclic polymers form grains that will grow further in highly condensed particles by the addition of the new monomers.[25] The Stöber procedure is illustrated in the Scheme1.1.

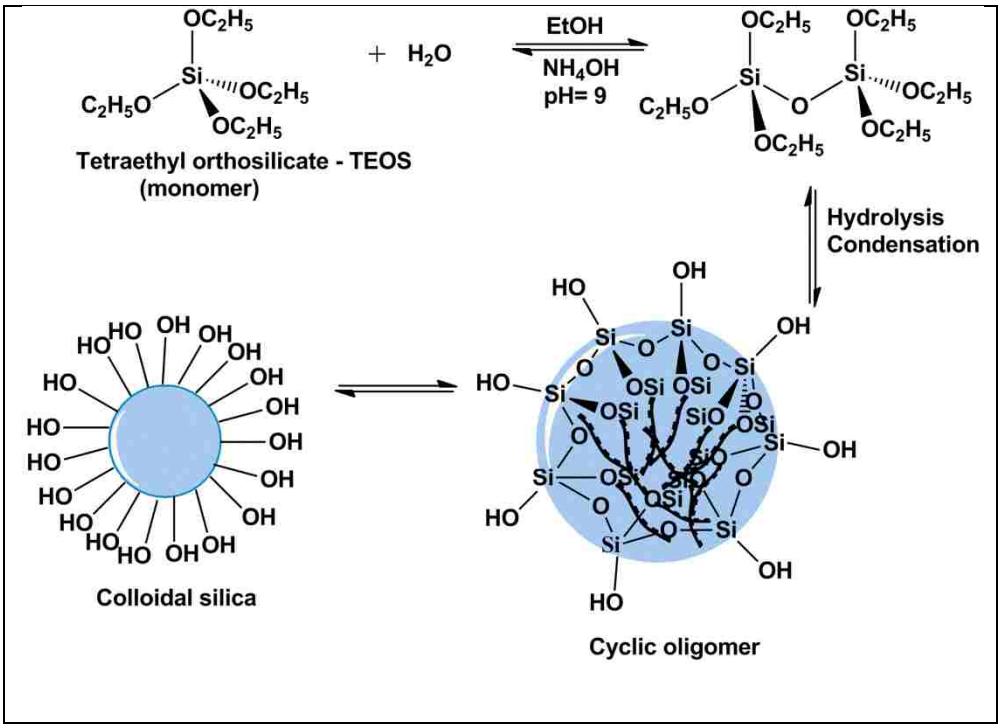

Scheme 1.1 Schematic illustration of Stöber method.

Silane-based polymers condense in a compact state, leaving —OH groups on the outside. The degree of this compact state depends on the reaction conditions, as shown by Van Helden et al.[26] Even though the hydrolysis-condensation reactions can occur on a wide range of the pH, only between 7-10 and in the absence of the salts, are all the condensed species ionized and therefore mutually repulsive.

Because TEOS is not water miscible, a small alcohol molecule is introduced to enable the miscibility between the two. Bogush et al. expanded the range of the reagent concentration and the reaction temperature and obtained 17% yield of suspension with narrow distribution and good control over sizes.[27] They proposed an expression to predict the diameter of the particle as a function of reagent concentrations:

$$d = A[H_2O]^2 \exp(-B[H_2O]^{1/2}) \qquad \text{Eq. 1.1}$$

where $A = [TEOS]^{1/2} \times (82 + 151[NH_3] + 1200[NH_3]^2 - 366[NH_3]^3)$ and

$B = 1.05 + 0.523[NH_3] - 0.128[NH_3]^2$

In this equation *d* is the average diameter in nanometers and the concentration of the reagents are expressed in mol L^{-1}.

Even though the earlier researchers on Stöber particles were focused mainly on the empirical prediction of the final size, they were also proposing models to understand the physical/chemical growth mechanisms of silica. Silica formation was divided into two events: nucleation and growth. The controlled aggregation model proposed by Bogush and co-workers considered that the nucleation and the growth of silica occurs as an aggregation process of the small silica grains of several nanometers in size.[27-29] Matsoukas et al. explained the nucleation through the monomer addition model: the nucleation arises as a result of the hydrolysis between two monomers followed by the growth through molecular addition.[30-32] These two models are akin condensation *versus* addition polymerization. Many studies concerning the growth of the silica particles were developed in the last years.[33-39] They improved and explained in more depth these two models.

One step growth process yielded, indeed, a broad range of sizes with narrow particle distribution but the drawback was the low solid weight fraction of the particles. The increase in the concentration of the TEOS resulted in heterodisperse sols because of the second nucleation. In order to attain narrow distributions, larger particles and good solid yield, Bogush et al. pioneered the regrowth method or the more popular seed method.[27]

1.2.3 Seed Method-A Route to Monodispersity

In a typical seed method experiment depicted in Scheme 1.2, a suspension of the silica particles is prepared and further amounts of the TEOS are added as a function of the desired size numbers.

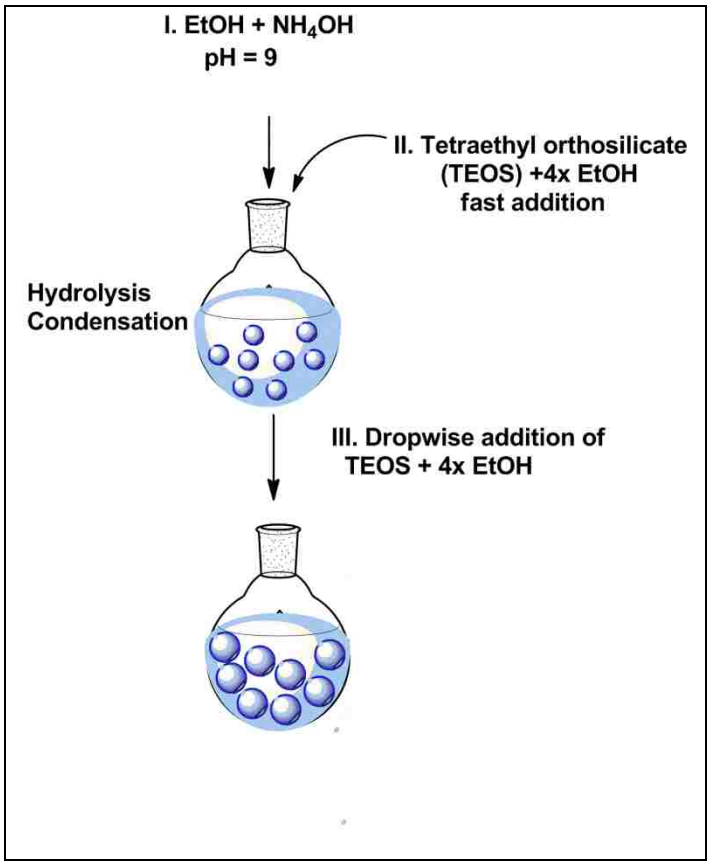

Scheme 1.2 Schematic illustration of seed method.

Bogush et al. used seeds of 170 nm, fabricated using distilled TEOS, and added various portions of TEOS equal to the TEOS volume used for seeds. After ten additions at 8 h intervals, the stable suspensions of silica colloids were analyzed and found to keep their spherical shape and narrow distributions, while size increased significantly. The mass fraction of solids increased to a theoretical limit of 24%. They correlated the size of the final particle with the volume of the TEOS used:

$$d = d_0 \left(\frac{V}{V_0}\right)^{1/3} \qquad Eq.\ 1.2$$

where d is the final average diameter, d_0 is the average seed diameter, V_0 is the volume (or moles) of TEOS used for the seed production and V is the total volume (moles) of TEOS added. It was also found that the use of TEOS as received in subsequent growth step did not impact the particle shape and distribution.

Extra purification of silicon precursors increases the cost of the production. Consequently, the combination of the original Stöber and the Bogush's seed methods were streamlined to use readily available tetraethylorthosilicate, TEOS. Zhang et al. obtained silica colloidal particles with uniform size, shape and composition following Bogush formulation.[40] The unique Zhang's contribution was to dilute TEOS 4 times with ethanol rather than to distill it. In the subsequent regrowth steps, the diluted TEOS was drop added continuously. This approach was inspired by previous reports on silica synthesis which showed that undesired sizes and shapes such as peanut-like cannot be avoided. The use of TEOS with no dilution over 8 h addition intervals led to a long period of the growth. In order to shorten the nucleation and the growth times and to suppress the undesired shapes and sizes, dilution of TEOS with ethanol was found to be an effective approach. The dilution increases the diffusion rate of the reagents and the nascent nuclei have a greater probability to grow, in the same time, by the condensation and the hydrolysis of the TEOS, without secondary nucleation occurrence. It also depresses the adhesion or aggregation of the particles.

The influence of the different dilution ratios, the temperature and the ammonia-ethanol ratios were also studied in depth. The method developed by Zhang et al. proved efficient in the

silica preparation, their sizes ranging from 150 nm to 1.2 μm with a percentage standard deviation from ±5% to ±1%.

Recently Watanabe et al. prepared monodisperse particles by the seed method using L-arginine for nucleation.[41] Monodisperse seeds were prepared by emulsion in a mixture containing L-arginine and TEOS. Various sizes of the particles were obtained by addition of TEOS to the original sol and additional small amounts of L-arginine. This method underlines the importance of the seed quality. Spherical and monodisperse seeds lead to even better colloid materials in terms of size dispersity after sequential growth by the TEOS addition. Other researchers reported silica prepared by seed method.[42-45]

Alternate sources of the silica captured the attention of the researchers in the recent years. For example, Balamurugan et al. prepared silica beads from *Sorghum vulgare* seed heads, an agricultural waste which apparently has no other potential use.[46] Despite such novel approaches, the high yield of the colloidal particles coupled with the narrow size distribution, the broad size range and the spherical shape make the seeded method the most effective approach to the silica particles with controllable size and shape.

1.3 Magnetic Cores

1.3.1 Magnetite

Ferrites are ceramic-like ferromagnetic materials, mainly composed of α-Fe_2O_3.[47] One of the first recognized magnetic materials from the ferrites family is magnetite, Fe_3O_4. Its discovery dates back in time to the old legend of the shepherd Magnés. His metal-tipped stick and the nails from his boots were attracted to the ground while he was herding his sheep on Mount Ida. When he dug in the ground to find what was pinning his boots on the ground, he found stones that today are referred to as lodestones and contain magnetite. The actual discovery of lodestones can

be attributed to either Greeks or Chinese. Magnetite is also used by magnetotactic bacteria, *Aquaspirilum magnetotacticum*, microorganisms found in fresh water. They contain fine Fe_3O_4 particles and are capable of orienting along the Earth's magnetic field which enables them to swim. In the laboratory, Smiltens et al. prepared large crystals of magnetite using a modified Bridgeman-Stackbarger procedure.[48] Over the years, several methods were developed to synthesize functional magnetic nanoparticles with controllable size and shape driven from their broad technological applications.

1.3.2 Coprecipitation Method

The preparation of the ferrofluids containing magnetite is usually performed in both acidic and basic solution by mixing the appropriate amounts of an iron (II) salt and iron (III) salt. Magnetite, Fe_3O_4, is the black precipitate obtained, a mixture of two oxides (Fe (II) and Fe (III)), $FeO{\bullet}Fe_2O_3$. The earliest coprecipitation preparation of Fe_3O_4 was accomplished by the Bureau of Mines.[49] Later, this technique was modified by Massart et al.; theirs is one of the most cited reports on the ferrofluid production.[50] In order to prevent the oxidation of the magnetite particles, Massart et al. stabilized the dispersion with different peptizing agents in both acidic and basic media. Philipse prepared magnetite-coated with silica[51] and stabilized the magnetic nuggets with oleic acid prior silica coating.[52] Coating magnetic particles with an inorganic matrix proved to be an efficient route to produce magnetic colloids. The iron surface has a high affinity toward silica. A silica shell not only prevents the magnetic particles from aggregation in different pH ranges but also provides a surface which can be further modified with various functionalities (Scheme 1.3).

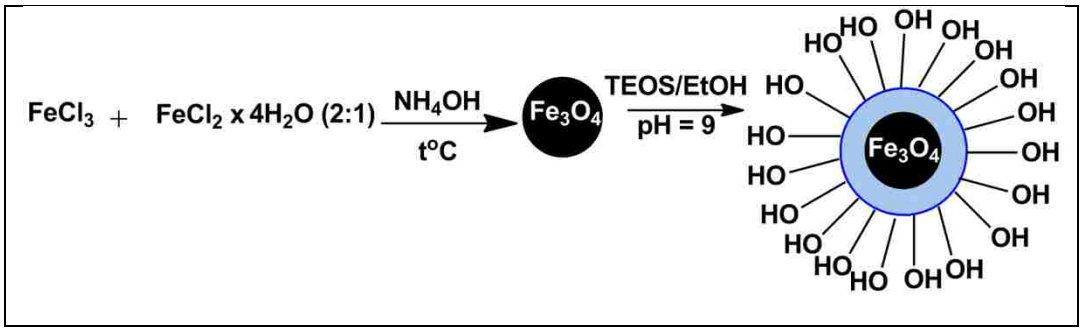

Scheme 1.3 Schematic route for preparation of the magnetite particles by coprecipitation method.

The coprecipitation, also called the sol-gel method, has been adopted more widely because the yield of the silica-coated magnetite or maghemite particles is high, even when the production of a uniform particle with a single magnetic inclusion is not very well controlled and this can be viewed as a drawback. Other advantages over other methods are: low cost, relatively mild reaction conditions and surfactant free. Still, this method is the main source of the magnetic fluids because, over the time, researchers added improvements to the original work of Massart and Philipse.

Wang et al. prepared silica-magnetite particles directly by reacting the magnetite sol with TEOS in a basic alcohol/water mixture.[53] The reaction conditions favored the coagulation of the particles. Aliev et al. devised a slow sol-gel process and used sodium silicate as a silica source.[54] The morphology of the final composite could not be well controlled because the silica coating was performed without pretreatment of the magnetic nugget. Several other reports dealt with ill-defined structure and morphology of the composite particles by ignoring the treatment of the magnetic cores before coating.[55-58] Stabilization with oleic acid was achieved by Lu et al.[59] Tsai et al. prepared water stable dispersions of the magnetite stabilized with tartaric acid.[60] Yang et al. reported a sol-gel approach optimized to control the preparation of the magnetite-silica particles by using electrostatically stabilized magnetite particles as seeds.[61] Deng et al. aimed to offer a

suitable method for the preparation of the uniform silica-coated magnetite by systematically studying the formation of such composite.[62] Their investigations revealed that low polar alcohols yielded irregular particle morphology while increasing the amount of TEOS gave more regular and monodisperse shapes. The catalyst, ammonia, and the ratio alcohol/water seemed to impact tremendously the shape and the dispersity of the final product.

Systematic studies should regard all parameters involved in the synthesis of the magnetic particles especially when the final particle is desired to have superparamagnetic properties which are directly related to the size of the magnetic grain, the smaller-the better. In this respect, Iida et al. found that varying the hydrolysis conditions, especially the ratio of the ferrous to ferric ions, led to larger Fe_3O_4 particles.[63] The magnetic properties could be controlled to some extent. When only ferrous sulfates or chloride salts were used in the preparation, the saturation magnetizations were 86.6 and 81.0 emu·g^{-1}. A significant drop in the saturation magnetization when compared with the bulk magnetite, ~91 emu·g^{-1}, was noted for samples prepared from both ferric and ferrous sulfates of chlorides, 46.7 and 55.4 emu·g^{-1}, respectively. The trend was attributed to the oxidation of the ferric ion during the preparation, leading to a ferrimagnetic material. Other reports obtained the same values.[64,65] Precipitation with a basic solution at temperatures below 60°C led to the preferential formation of the maghemite, while temperature over 80°C yielded magnetite.[58,66,67] Higher saturation magnetization, better crystallinity and smaller particle size were achieved by using ammonia solution instead of sodium hydroxide.[68,69] Also pouring the alkali solution as quickly as possible into magnetite forming mixture under vigorous stirring resulted in a black coloration but the size dispersity of the magnetic particles was broad. A slow pouring rate favors less nucleation and the crystalline grains grow all at the same time.[70] The nuclei number remains constant and the added monomer molecules condensate on the existing

grains. The coprecipitation method may remind the reader about living addition polymerization. The absence of chain termination and chain transfer reactions, and a higher rate of initiation than propagation ensure the growth of the polymer chains at a constant rate. Their lengths are similar and the polydispersity index low.

Oxygen removal is essential to obtain pure magnetite particles. Unwanted oxidation is prevented by the presence of an inert atmosphere (e.g. argon or nitrogen bubbling). This approach not only prevents against oxidation but enables a decrease in the particle size.[68,71] Liu et al. demonstrated that when the deionized water was not degassed and the synthesis proceed under ambient conditions without N_2 protection, a reddish-brown colloid was obtained, indicating the presence of other iron oxide phases as a consequence of Fe_3O_4 oxidation.[70] These phases impacted the magnetic properties of the desired magnetite by lowering the saturation magnetization or even arresting the superparamagnetic behavior. Small, superparamagnetic magnetite particles were prepared using coprecipitation by other research groups in various sizes: 6- 7 nm diameter with 2 nm silica shell,[72] 9.2 nm,[73] ~10 nm,[74,75] 10.4 and 12.3 nm. 6 and 12 nm,[76] and 10 and 40 nm.[77]

1.3.3 Emulsions

Preparation of colloids in the emulsion has been regarded as an effective method to either produce monodisperse silica particles or encapsulate magnetic inclusions into a silica or a polymer shell. This paragraph will describe the fabrication of both silica and magnetic silica coated particles. Emulsion is a general term to introduce micro/macro emulsions, reverse micelle or inverse microemulsion. The difference is made by the interplay between the water-in-oil emulsion's components. An amphiphilic surfactant is added in an attempt to lower the interfacial tension between water and oil. Each hydrophilic and hydrophobic part within the surfactant

molecule has its preferred solvent. Water-in-oil designates usually a mixture between the water and an alcohol, hydrocarbon or more sophisticated choices (such as supercritical carbon dioxide assisted emulsions).[78-91] Water and oil domains are separated by surfactant monolayers; hence, the unfavorable contact between water-oil is prevented. Macroemulsions are thermodynamically unstable in contrast with microemulsions. Nanosized emulsion droplets are formed spontaneously. Reverse micelles are equilibrium phases on a molecular scale and thus are thermodynamically stable. The control of the water/oil/surfactant content allows tuning over the size of the droplets, the nanoreactors, which contains the reagents. Consequently, the droplet uniformity is the crucial factor that will trigger the quality of the final product. Inside the droplets, the particle formation is a combination of the nucleation, growth, coagulation and flocculation, in some instance. The major advantage of the emulsion is the uniformity of the resulting particles. Reverse micelle is the most successful procedure used in the synthesis of the colloidal particles with narrow distribution because the nucleation occurs simultaneously at a large scale within the micelle and it is separated by the growth due to the intermicellar interactions. The reverse micelle phase consists of surfactant-encapsulated water droplets, the aqueous pool physically separated by the oily phase. The challenge is in controlling the size of the pool droplets to obtain fine and uniform particles.[92-97] Reverse micelle method yielded, over the years, a broad spectrum of silica- based materials and it is reflected in Scheme 1.4 by an example of the silica coating of metal particles (e.g. magnetite).

The optimum condition found for the preparation of such products seems to point to a gradual increase of pH up to 11-12 after immersing the silica precursor, usually tetraethyl orthosilicate, TEOS, in the water-ethanol phase. The condensation of TEOS must be catalyzed by a base or an acid. Ammonia is the most commonly used catalyst because it was noticed to

yield good spherical morphologies of the particulates. The optimal temperature should be kept below 25°C, because of the possible thermally induced phase inversions. The reaction time has been reported from few hours up to 48 h for a complete reaction. The control over the size of the silica-based particle is obtained by tuning the ratio between TEOS/water/surfactant.

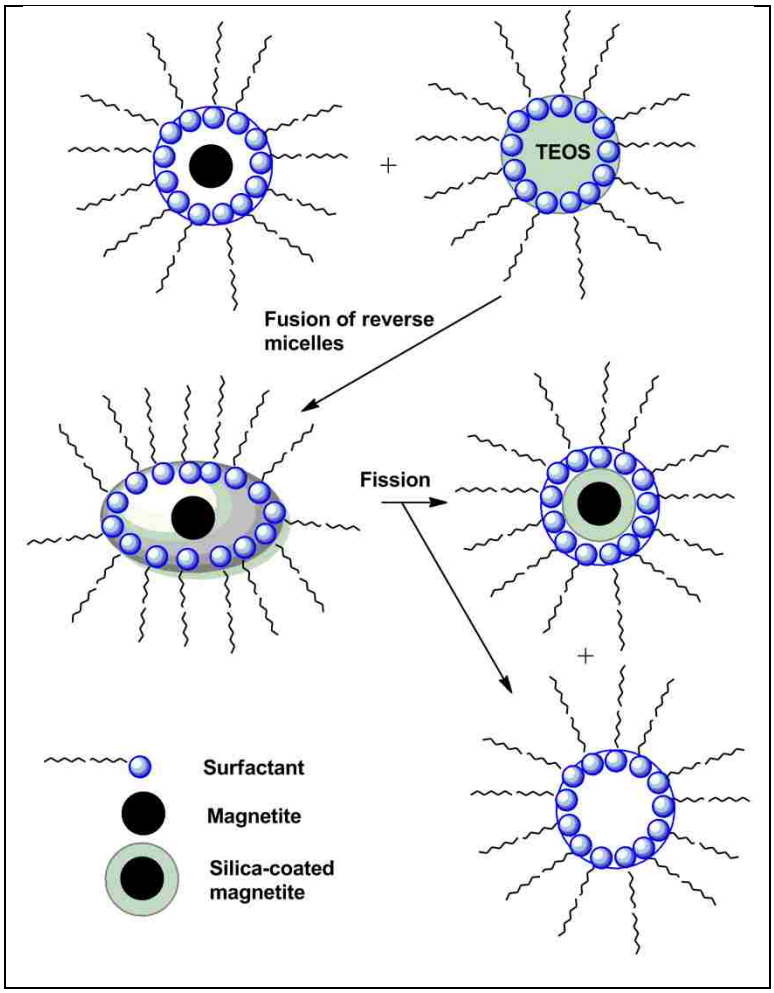

Scheme 1.4 Schematic illustration of the silica coating of metal particles using the reverse micelle.

The formation of the silica particle or the silica coatings by the reverse micellar system can be explained by a series of steps. Even a series of contradictory opinions was formulated upon the emulsion mechanism; the most agreed-upon path for a mono-emulsion involves the association of TEOS molecules within the micelles, as the first step, after its addition into the

emulsion phase. The catalyst then enables the hydrolysis of TEOS with the formation of the monomers. Nucleation occurs by condensation of monomers via inter- and intra-micellar exchange. Further nuclei growth is favored by addition of TEOS or by aggregation. Materials such as ferrofluids,[98-101] silica[102] and silica-coated particles either metal (Fe,[103] Co,[104-106]), oxide (Fe_2O_3,[51,107,108] Fe_3O_4,[109]), alloy type (NiFe,[110] Co-ferrite[111]) or mixed oxides ($MnFe_2O_4$,[112] $CoFe_2O_4$,[113] $ZnFe_2O_4$[114]) have been prepared.

Now let us take a look back over the microemulsion method and underline what might be considered as the future trends. Even the micelle itself is considered a nanoreactor. The main drawback is the still-poor control over the reactions and the reaction conditions that govern the formation of a high-quality product. Good spherical monodisperse particles were obtained but the method is still shadowed by the low yields of the final material. Yet, combination with other synthesis techniques (e.g. sol-gel,[115-121] hydrothermal/solvothermal[122]) can take various advantages: the fine and the tunable nucleus size obtained in the reverse micelle and the growth controlled by the stoichiometry through the sol- gel method. Combined techniques opened the door to more complex products. The layer-by-layer deposition of the opposite charged electrolytes onto the particle surface,[123] metal-doped carbon nanotubes[124,125] or polymer encapsulated nanoparticles[126] have been produced in the reverse micellar systems. One intensively explored trend is the assembly in 3D supermolecular lattices.[127-130] Driven by external fields (e.g. magnetic or electric), self-assembled crystalline structures are considered a future challenge. The new combination of different surfactants may give the rise of a better control over the morphology and the useful properties of the desired materials. Before ending this section it must be mentioned the several reviews dedicated to this subject.[131-136]

1.3.4 Solvothermal/Thermal Decomposition Routes

High level of the monodispersity and the size control over nanoparticles can be obtained using high-temperature methods. The thermal decomposition of organometallic precursors such as $Fe(acac)_3$, (acac=acetylacetonate), and $Fe(CO)_5$, (carbonyls), assisted by organic solvents and surfactants is a reliable way to monodisperse nanocrystallites ranging in diameter from 3 to 15 nm. Surfactants (ligand) are, in general, long-chain amines, fatty acids or both. They have a dual role: to mediate the growth during reaction and to prevent particle aggregation. A satisfactory stabilization requires at least six-carbon-long ligand.[137,138] A zerovalent metal precursor leads to the formation of a metal grain or cluster that can be subjected further to oxidation and give high-quality iron oxide particles. Cationic metal sources yield directly iron oxides. Control over the size distribution and the morphology is achieved by optimizing the ratios of the starting materials (iron precursor, solvents, and surfactants). In addition, temperature and time complete the map of decisive factors in controlling the size and the monodispersity.

Kwon et al. prepared iron oxide particles by thermal decomposition of the iron oleate complex in their effort to elucidate the kinetics.[139] The mechanism of the decomposition had been shown to evolve through intermediate species, which can act as monomers for iron oxide monocrystals, as shown in the Scheme 1.5. The sudden increase in the concentration of the nanocrystals (burst crystallization) as evidenced by TEM was followed by a rapid decrease in size distribution (size focusing) variance. Once the reaction time increased the iron cluster grew unevenly.

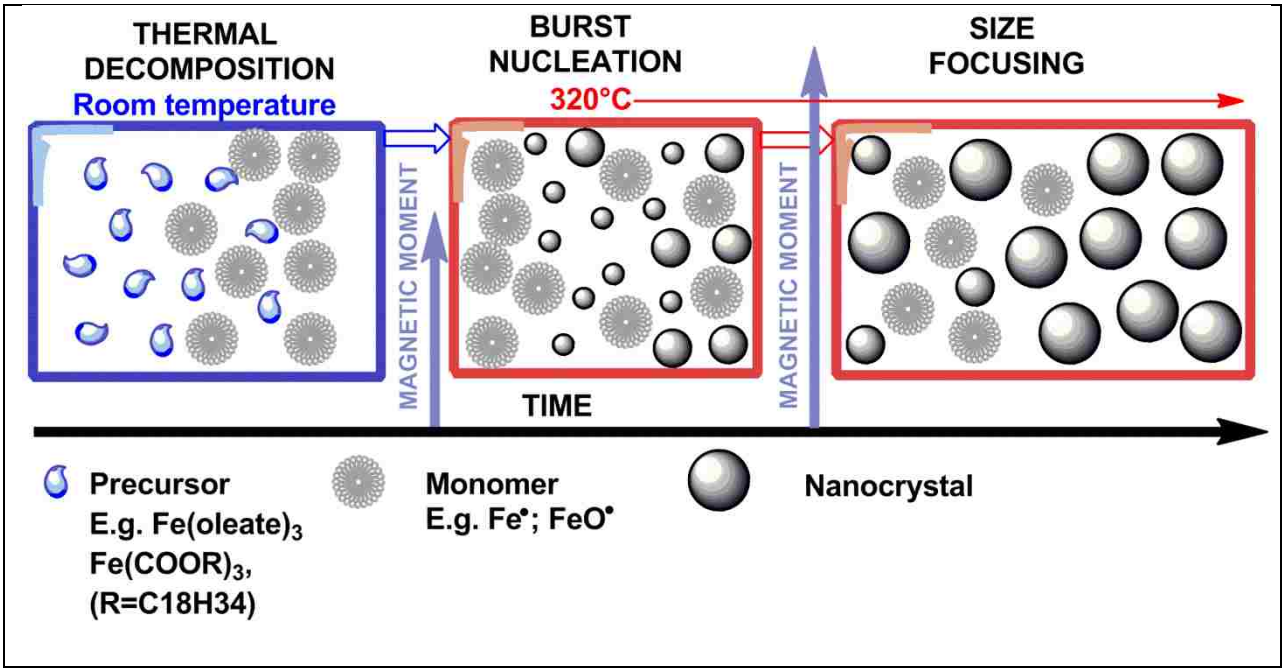

Scheme 1.5 Schematic representation of the size, morphology and magnetic properties as a function of the reaction temperature and reaction time for magnetite synthesized by thermal decomposition methods. Adapted from Reference 139.

The control over the ratio of surfactant to FeO(OH) led to a broad distribution of the sizes ranging from 8 to 55 nm, some with a high magnetization moment.[140-144] Even though the thermal decomposition process yields monodisperse particles with narrow distribution, it is not environmentally friendly and economic. For example, the $Fe(CO)_5$ precursor is highly toxic and ligands such as 1-octadecene and oleylamine are expensive.[145,146] Zhang et al. developed a green thermal chemistry using ethanol as solvent and 1,2-dodecanediol as ligand. The reaction mixture was held at 150°C in an autoclave for 24h. The iron clusters were comprised of 5 nm magnetite crystals.[147] Ultrafine magnetite powders are prepared by the hydrothermal, also called the solvothermal method. The aqueous media is the major advantage of this reaction but high pressure (greater than 2,000 psi), high temperature (higher than 200°C) and a good sealing is required once the mixture is placed into autoclave. The concentration of the iron source used in

preparation can tune the size of the magnetic crystal and the nanocluster.[148-152] The continuous hydrothermal process is a simple route to metal oxide particles of the specific size and morphology. Although this route is environmentally friendly and can be scaled up easily, the mechanism of particle formation has not been yet determined. Investigations on factors that contribute to evolution of continuous process were performed by Xu et al.[153] Particle size distribution variance and aggregation seemed to increase with increased concentration of polyvinyl alcohol, temperature and time.

The drawback of the conventional hydrothermal method is the slow kinetics at any specific temperature. In an effort to speed the crystallization kinetics, Komarneni et al. introduced a new approach termed microwave-solvothermal method.[154] The shorter time and thermal conditions allowed the production of particles in a 2 to 60 nm size range with good control over the variance dispersity. Balasubramanian et al. used DC thermal arc-plasma to prepare Fe_3O_4 powders having a high magnetization saturation, 88 emu·g^{-1}.[155]

1.4 Cobalt

Most common magnetic materials contain metal oxides. These are often mixtures of oxides, which imply that their magnetic properties are not always reproducible and well defined. Pure metals such as Fe, Co, Ni and their alloys are also good candidates in various fields of magnetism. The use of pure metals has difficulties arising from their instability toward oxidation in air. Once the particle size decreases, especially close to superparamagnetic limit (~10-15 nm), oxidation becomes easier. Thus the preparatory approaches require ways to improve the chemical stability of the particles. One of the metal particles with increased sensitivity to air exposure is the cobalt. Two crystal structures, face-centered cubic (fcc) and close-packed hexagonal (hcp) are specific to cobalt. These structures coexist at room temperature but at

elevated temperature (450°C) fcc is thermodynamically favored.[156] Consequently, the magnetic properties of cobalt greatly depend on the crystal nature and the temperature.[156-160]

The era of cobalt particles starts most probably with a report by Hess *et al*. in 1966. They thermally decomposed dicobalt octacarbonyl in solutions of different polymers.[161] A cobalt organometallic precursor has been used by Chaudret et al. to prepare cobalt particles and coated them with polyvinylpyrrolidone.[162] Coating procedures also included noble metals, used as insulating shells through the microemulsion method or other chemical approaches such as redox transmetallation.[163,164] Thus, Sobal et al. reported stable Ag-Co nanoparticles with cobalt as shell.[165] Gedanken et al. used a sonochemical procedure to obtain air-stable Co colloids.[166] The explanation behind the stability of the nanoparticles was the formation of a carbon shell on the particle surface. The pyrolysis of metal carbonyls was applied to produce Co, Fe, Ni and other magnetic materials. The solution phase metal salt reduction was involved in the preparation of the Co, CoO and FePt particles. Riffle et al. obtained magnetic cobalt dispersions in the presence of poly(dimethylsiloxane). The challenge in the above-mentioned reports was the control over stability and size. Particles were rather polydisperse and not very uniform.

The deposition of the silica shells on the magnetic particles as a stabilizer was used in several reports. The facile modification of the surface, the excellent stability of the aqueous solutions and the good control on the interparticle interaction, either in solution or within structures are few advantages that makes silica one of the best candidates for coating metal nanoparticles. Hematite (Fe_2O_3) spindles,[167] reduced to metallic iron in a dry state[168] and magnetite (Fe_3O_4) clusters[51,169-172] were successfully coated with silica. The complications in silica attachment arise due to the lack of functional groups, especially OH, on the metal surface. Therefore, it is necessary to use a primer to enable silica deposition. For example, in 1996, Liz-

Marzan et al. coated gold colloids with silica in a three-step deposition process.[173] First citric acid was used as stabilizer and afterwards was replaced with amino silane groups. Finally silica was attached to the surface of the particles through the Stöber method. This approach was used for noble metals which are chemically very stable. Matijevic et al. showed that a modified Stöber method could yield differently sized silica-coated silver particles without surface "conditioning" with amino silanes.[174] A very good control over the size and the colloid stability, following the Liz-Marzan et al. procedure, was reported by Kobayashi et al. in 2003.[175] They used a one-pot reaction, as shown in the Scheme 1.6, to prepare silica-coated cobalt particles with different Co core size and silica shell thickness.

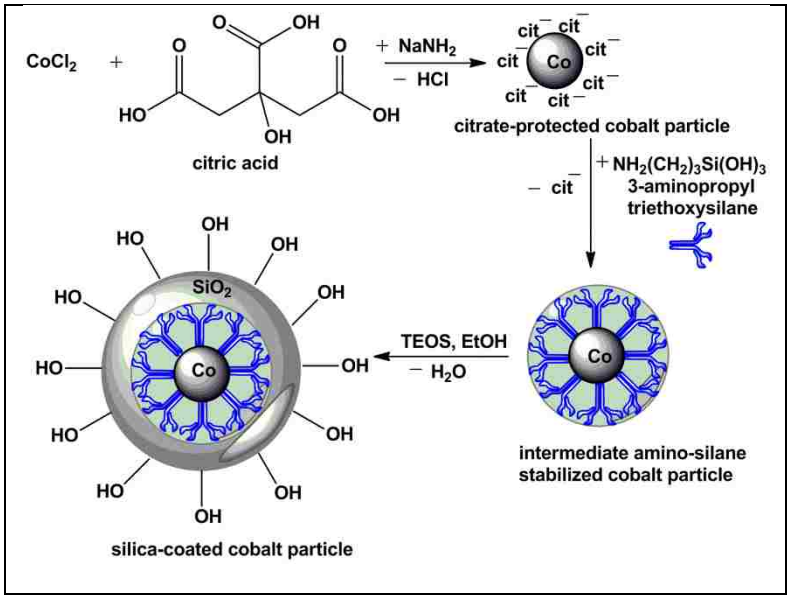

Scheme 1.6 Schematic of the surface reactions involved in the formation of silica- protected cobalt particles.

Further, the authors demonstrated that addition of the silica precursor, TEOS, improved the particle uniformity and the shape without altering the magnetic properties. Two crystal structures, face-centered cubic (fcc) and close-packed hexagonal (hcp) of silica-coated cobalt particles were identified after annealing at different temperature (200°-700°C). After annealing

at high temperature, these particles showed high magnetization saturation in the range of 120-180 emu·g^{-1} per cobalt.

1.5 Dye-labeling

Labeling of the colloidal silica with fluorophore molecules leads to composite materials with a broad spectrum of the applications. Various labeling agents can be incorporated into nanoparticles to yield fluorescent probes. Dye-doped nanoparticles, semi-conductor quantum dots (Q-dots) or fluorescent beads are considered good candidates for biolabels. Each class of these probes has drawbacks. Q-dots are small in size and photostable with tunable optical properties. Yet, their quantum efficiency lags when compared with the organic dyes. The real-time monitoring might be limited by their blinking emission. Furthermore, the UV range required for Q-dot excitation might be harmful for biological species. Upon UV excitation highly toxic Cd^{2+} ions are released as a consequence of the surface degradation. This process practically kills cells. A multitude of methods were designed for the production of such fluorescent colloids but the focus of this review is on the fluorescein isothiocyanate (FITC) encapsulated silica-based nanoparticles. Silica has been widely chosen for both, industry and laboratory research, because of the close refractive index match (dn/dc=0.143 mL·g^{-1}) with organic solvents such as chloroform, cyclohexane and hexadecane. In the early '90s Van Blaaderen et al. developed a facile method for the FITC-silica through two major steps.[176] First FITC was covalently bound to a silane coupling agent, 3-aminoproyltriethoxysilane, APS, and formed the FITC-APS molecule, as shown in Scheme 1.7.

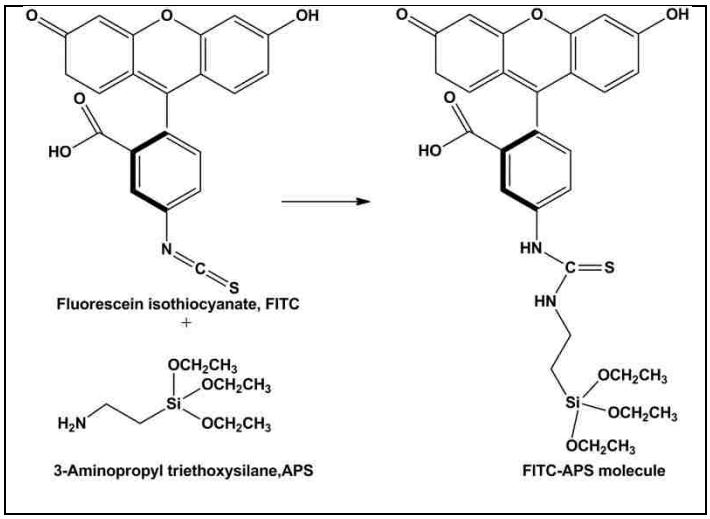

Scheme 1.7 Sketch of the FITC-APS molecule formation.

Second, the FITC-APS reaction product was incorporated in the Stöber mixture consisting of water, ammonia and TEOS used in the silica grains preparation. The procedure allowed the production of the silica either with a thin fluorescent shell or an inner layer. The later approach had as purpose the dye prevention from leaking or bleaching. A series of reports using a similar procedure to obtain fluorescent labeled particle was recorded.[177-181]

Fluorescent labeling of silica-based colloids having magnetic inclusions has received a growing interest because the range of their applications spans both fundamental and applied research. The labeling procedure is performed in the same manner as described above. The most widely used magnetic particles are either magnetite (Fe_3O_4) or maghemite (γ-Fe_2O_3).

1.6 Surface Functionalization and Characterization

The requirement for specific applications in nanotechnology poses great challenges to researchers to develop efficient preparatory methods and, most of all, to understand the impact of the composite particle on the environment for which they were targeted. Various techniques used can now offer a wide palette of hybrids with unique properties. But one of the key steps to such

materials is the surface functionalization. Therefore the section will outline some general aspects on surface tailoring and, afterwards, will focus mainly on amino-decorated silica surfaces.

The attachment of functional groups on particle surface governs their solubility and chemical functionality. The groups or the molecules attached on the particles, either by physical or covalent bonds, should provide a stable colloid suitable for further chemistries. One of the most employed ways to functional materials is silica coating which has advantages over the organic coating.[182,183] Naked metal nanoparticles are in some cases very air/moisture sensitive and a thin layer of silica protects against oxidation. Furthermore, the silica surface has terminal OH groups which can be easily reacted with other molecules by a simple chemistry. From this perspective, particles consisting of an especially magnetic core and a silica shell[59,62] have received particular interest in terms of their magnetic responsivity, controllable interparticle interactions by tuning the shell thickness and biocompatibility.[184] Posing a negative charge stable in the 6-7 pH range, the silica surface is an ideal model to mimic the behavior of the negatively charged biomolecules in physiological conditions.[185] Coatings with double layers of silicon led to materials suitable for the magnetic bioseparations and drug delivery. The first layer protects the core against degradation or etching in rough conditions and the external can be etched in basic or acidic conditions to a porous structure. Consequently, enhanced properties can be obtained such as high surface area. In this order of idea, Sen et al.[186] discovered a jump from 25 to 250 m^2g^{-1} while Deng et. al.[187] reported 365 m^2g^{-1}. On the other side, the silica shell can screen the magnetic response of the composite causing an increase in coercivity.[188-190] Thus, control over silica coatings is essential. Various functional groups can be attached to the surface such as —SH,[191-193] —COOH,[194-199] —N_3,[200-206] —CHO, vinyl, —Br[205,206] and biomolecules (e.g. oligonucleotides)[207,208] but in the next lines the focus will be placed on amine-functionalized

particles used as initiators in the *growing from* method which will be discussed in a following section. The wide used amine precursor is 3-aminopropyltriethoxy silane, APS. The activation of the silica surfaces with APS is carried out usually in organic solvents. The silane coupling agents react with the silanol groups to yield amino functions on the surface. In order to lower the cost of production, the surface modification in aqueous media was also devised. The later approach involves the hydrolysis of the amino precursor at pH 3 and, afterwards, the condensation with silanol groups resulting in siloxanes bridges.[209] Even though the chemistry behind aminoactivation is well established, it still suffers from controlling the loading and the reproducibility. The water content when organic solvents are used is an issue. Assink et al.[210] have shown by ^{1}H and ^{29}Si NMR that the rate of the hydrolysis is much faster than condensation. Thus, a safe approach to water free amino-particles involves the azeotropic distillation and the use of anhydrous solvents. A recent review of Yu et al. discusses the pros and shortcomings of the generally accepted amino-silanization mechanism for the surface activation.[211]

Polypeptide-based silica hybrids obtained by the *growing from* method involves the use of amine activated particles as the primary amine initiators in the ring opening polymerization, ROP, of N-carboxyanhydrides. In this respect, the development of techniques enabling the control over the amino moieties on the silica particle surface greatly influences the polypeptide load. Applications of hybrid particles may require either a dense[212,213] or sparse[214] activated surfaces. A crowded assortment of amine groups can be obtained either by the reaction of silica particles with aminosilanes[215] or the co-condensation between the silicate and amino precursors.[216] The preparation of the dense amino grafted surfaces needs to take in account the interaction between amine-amine and amine-silanol groups through H-bonding. Better control on

amino sites is provided by separating the amines and capping the free silanol groups, as shown in the Scheme 1.8.

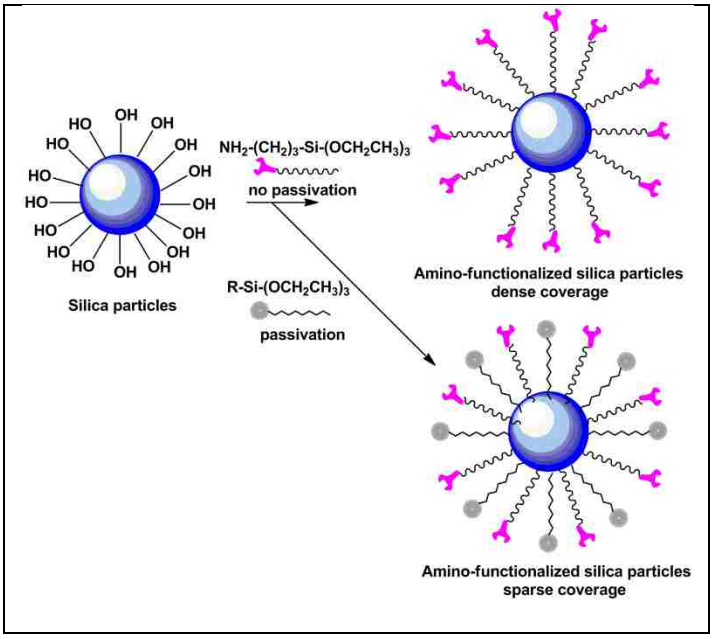

Scheme 1.8 Schematic illustration of the surface reactions involved in the formation of a dense and a sparse coverage with functional groups.

In order to manipulate the loading of functionalities on the surface, researchers have used various approaches. Mixtures of aminosilanes and alkylsilanes such as APS and methyl trimethoxysilane, MTMS were considered the easiest way to asses control over the grafting density.[217,218] Hydrolyzable templates placed on silica favored low loading (less than 0.2 mmol NH_2/g product).[219,220] Yet, after hydrolysis, the silanol-free groups are available for interaction with amine. The molecular imprinting and the thermolytic deprotection of carbamate silica to the corresponding amino silica have yielded particles with less than 0.23 or 0.27 NH_2/g of the matched set material.[221,222] The Jones group devised an unique method involving the immobilization of the bulky tritylimine and upon deprotection in acidic conditions revealed amines spaces between each other.[223] They also used benzyl spacers. Still the amine-amine and

amine-silanol interactions were assumed to be reduced or eliminated but no quantitative assay of OH groups was performed to verify the assumption.[223,224] Several groups have used only APS without any passivator and they have calculated the amount of the amino precursor per surface unit based on the concentration of the particle solution and total surface area of the colloid.[209,225-233] The key factor in the activation-passivation tandem seems to be the length of the two species. A long aminosilane and a short alkyl silane can reduce or eliminate the amine-silanol interactions but the H-bonding of amine-amine is still present. The amino end-capped chains can bend and either can hinder other functional groups or they become inaccessible for further molecule attachment. Consequently, a better approach to arrest such interactions will be the use of activator-passivator with comparable length. Such a method was devised by Heise group in late '90s. They have prepared 1-bromo-11-(trichlorosilyl)undecane and 1-trichlorosilylundecane and then grafted on the silica flat surface. The conversion of terminal bromine groups to azide by reaction with sodium azide, NaN_3, followed by the reduction in the presence of $LiAlH_4$ yielded a surface covalently grafted with amino groups.[234] Even though the reduction to amino groups is not performed azide-functionalized particles can be further used in click chemistry coupling.

Amine functions can modify the macroscopic surface properties. Nevertheless, these properties and the subsequent polypeptide grafting greatly depend on the density of amino groups per unit area, thus their quantification is necessary in order to maintain a control over the functionalization. Several methods such as fluorometry,[235-237] spectroscopy[238-240] and colorimetry[241,242] have been reported. Most of them involved only flat inorganic or organic surfaces. Some are more time consuming and expensive due to the cost of fluorophores. The success of these techniques in the quantification of amine moieties relies on their reactivity, their stability and their capability to attach labels and probes. Microscopy (electron and light) and

spectroscopy (e.g. X-ray Photoelectron Spectroscopy, XPS) give useful information about surface composition and binding energies, but their efficiency is limited mostly to flat surfaces. Moreover, a covalent attachment between the primary amino group and the label, in some cases, is required. That means the surface cannot be used for further application which is a major drawback. A standardized, fast, inexpensive and accurate determination of the amino moieties grafted on silica beads or other spherical surfaces is still under perfection. Recently Coussot et al.[243] and Noel et al.[244] quantified the protonated groups NH_3^+ with Coomasie Brilliant Blue, CBB and Orange II respectively, as the colorimetric reagents, but applicable to polymeric surfaces. Chen et al. devised a so-called fluorescent Fmoc-Cl method which was found to be 50 times more sensitive than the UV assay.[245] They have shown that the pendant amino groups from the silica particle surface produced stronger fluorescence than a smaller amine free in solutions. A facile and inexpensive method to determine the amino grafting density was innovated in this group using zeta potential.[246] Thermogravimetric analysis, TGA, is another convenient resource researchers exploit in amino assay. Devised by Bartholomé et al., the method uses the weight loss percentages which ultimately are converted to the grafting density.[8,247] Other groups have proposed improvements but overall Bartholome's approach remains the milestone.[248]

1.7 Shell

1.7.1 Synthetic Polypeptides and Their N-carboxyanhydride Precursors

The most economical and practical method for synthesis of polypeptides, especially homopolypeptides with long chains, is the polymerization of α-amino acid N-carboxyanhydrides, NCAs.[249,250] These amino acid precursors were discovered by coincidence when Hermann Leuchs attempted to purify N-ethoxycarbonyl or N-methoxycarbonyl amino acid chlorides by distillation and, at first, they were called Leuchs's anhydrides.[251-253] Even Leuchs

abandoned his work on this field because of misbelief in the existence of covalent polymers with molecular weights higher than 10,000 Da. Curtius et al.[254-257] and Wessley et al.[258-264] used primary amines, water and alcohol as initiators and reported for the first time high-molecular weight polypeptides. These reports helped the international community of researchers to acknowledge Staudinger's concept of covalent macromolecules.

The ring closure of NCA with phosgene was pioneered by Fuchs et al.[265] The method, widely used, was modified over the years to produce higher yields of NCAs.[266-268] The control over the gas amount was achieved by bubbling it into the solution[269] or by using derivatives such as diphosgene.[270,271] The phosgene approach has several disadvantages. Besides its high toxicity, phosgene generates HCl as a byproduct, which can lead to further side reactions during the NCA polymerization. Consequently, the complete removal of HCl from NCA mixture is essential. Since the anhydride's ring is very sensitive to moisture, the most common route to pure NCA is the recrystallization performed in an inert atmosphere and with anhydrous solvents. Another method, such as rephosgenation, was proposed by Dorman et al.[272] An important contribution to the field of NCA synthesis was pioneered by Daly et al. Substitution of phosgene with triphosgene, (bis(trichloromethyl chloroformate)), had been proven a viable route. The probability of the side reactions was greatly decreased because only 1/3 equivalent of triphosgene delivered in situ was enough to close the NCA's ring in high yield.[273,274] The mechanistic route involved in the preparation of the polypeptides using triphosgene is depicted in Scheme 1.9.

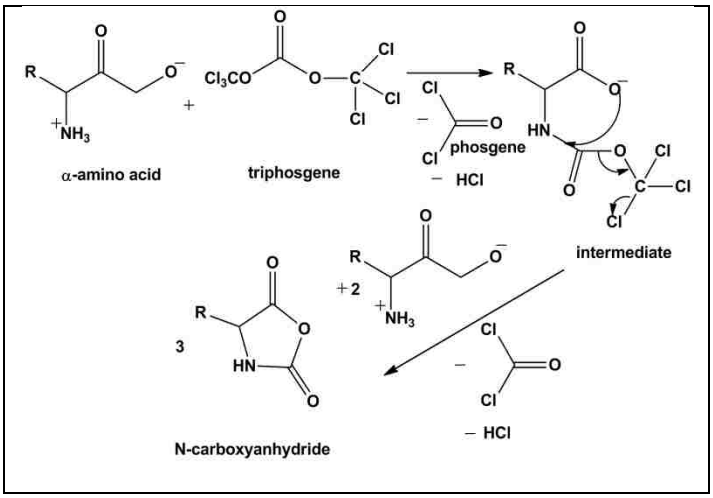

Scheme 1.9 Schematic of the synthesis of α-amino acid N-carboxyanhydrides, NCAs, with triphosgene. Adapted from References 273 and 274.

Wilder et al. also used triphosgene at room temperature.[275] A novel approach in the NCA purification was introduced by Poché et al.[276] Cold, oily NCA mixture prepared in ethylacetate was rinsed with icy water, neutralized with an icy solution of the sodium bicarbonate and finally dried with anhydrous $MgSO_4$. The behavior of NCA toward cold water runs against the common belief of the NCA moisturizing at room temperature. This method allows the decrease in the number of recrystallizations which also decreases the yield. Many researchers have been using this method or variations. Because the field of polypeptide precursors grew rapidly only representative work had been cited.

The work on the kinetics and the mechanism of the NCA polymerization was written by Szwarc in a comprehensive review.[277] N-carboxyanhydrides have several reactive sites that make the polymerization complicated. The carbamoyl (C-2) and carbonyl (C-5) are electrophile centers while NH (3) and α-C (C-4) are nucleophile sites, as shown in Figure 1.1

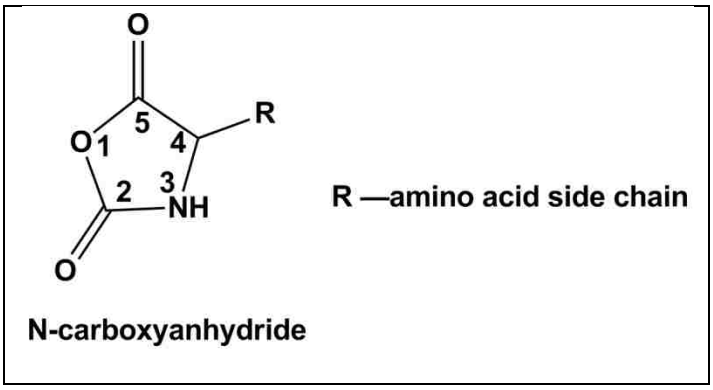

Figure 1.1 Representation of the amino acid N-carboxyanhydride structure.

No doubt, the polymerization path will depend mostly on the initiator's nature. One major advantage of NCAs widely exploited in the polypeptide synthesis relies on its ring capability to combine the activation of the C-5 carbonyl with the protection of the amino group. The activation of CO (C5) by the acylation of amino groups occurring at the room temperature or even lower, can render oligomerization products very difficult to separate from the desired polypeptide. Although reports of using N-unsubstituted NCAs were accounted, the route didn't attracted large interest.[278-284] NCAs are not stable upon storage for long periods of time and water traces attached to the crystal surface through H-bonds can initiate the polymerization in the solid state.

In order to overcome some of such complications, NCAs can be either subjected to N-protection chemistry or protected amino acids can be used in their synthesis. The attachment of an electron-withdrawing group to the nitrogen lowers its nucleophilic site in such a way that the reaction with phosgene or its derivatives is not favored in mild conditions. In an insightful anniversary review on NCAs, Kricheldorf compiled the routes to N- protection: cyclization of N-protected amino acids and attachment of a protecting group to a preformed NCA.[285]

Since the beginning of the 1940s, polypeptides synthesized by the ring opening polymerization of the corresponding NCAs served as models of natural polypeptides and proteins to investigate the relationship between their primary and secondary structures. Hence systematic studies regarded the elucidation of the synthetic homo- and copolypeptides structure. Polypeptides can adopt a multitude of conformational stable secondary structures depending on the nature of side chain substituent. The best-known are random coil, β-sheet and α- helix.[286-288]

Many studies were devoted to the elucidation of the NCA polymerization mechanism. NMR and IR spectroscopy were the most used analytical methods to detect the polymerization intermediate adducts and final products. Kricheldorf has published an important volume of work dedicated to the polypeptide formation mechanism.[285,289-297] The most common mechanism is through amines, whether primary, secondary or tertiary. The first NCA reaction, amine initiated, was reported by Fuchs[265] and Wessely.[260] Kinetic studies were conducted by Waley et al. on the polymerization of sarcosine NCA. The rate of the propagation was followed by the increase in the CO_2 pressure at constant volume. The titration of terminal amino groups at the onset of polymerization indicated the absence of the termination and, hence, the living character of the process. These findings were supported at that time by other researchers on other systems.[298-304] Scheme 1.10 displays a schematic of the primary amine mechanism. The amine initiator attacks the C-5 of the NCA monomer, which induces the ring opening and, further, the decarboxylation of the intermediate unstable carbamic acid or its zwitter-ion.[305] The new formed molecule will initiate the attack on another nearby NCA molecule.

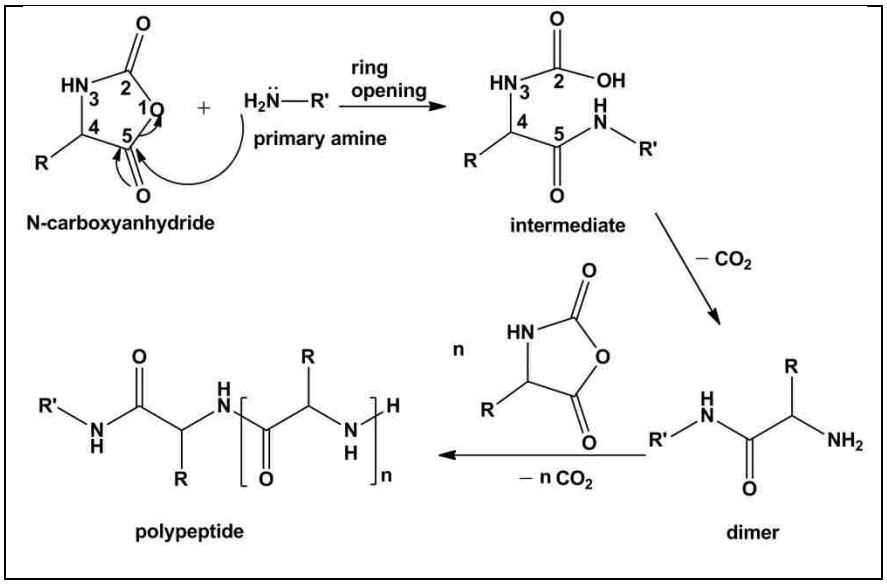

Scheme 1.10 Schematic of the initiation and growth steps involved in ring opening polymerization of NCAs initiated by a primary amine.

The new formed molecule will initiate the attack on another nearby NCA molecule. The overall step sequence in the reaction of the primary and secondary amines with NCA's studied with labeled isotopes[306] showed that decarboxylation occurs at C-2 of the intermediate. This step was not demonstrated as the rate-determining process. The reaction should depend either on the intermediate formation or on the ring opening between C-1 and C-5.[307,308] The NCA monomer feeds the growth of the living polymer. At a specific ratio monomer to initiator, M/I, the chains should grow in the same time, assuming rapid initiation compared with propagation. The fast initiation is achieved with strong nucleophiles. The formation of the polypeptide can adopt another pathway if the primary amine initiator is strong enough to deprotonate the intermediate carbamic acid, yielding a new adduct which further reacts with the NCA monomer and forms an intermediate anhydride (Scheme 1.11). Decarboxylation of the intermediate anhydride enables the formation of the corresponding polypeptide.

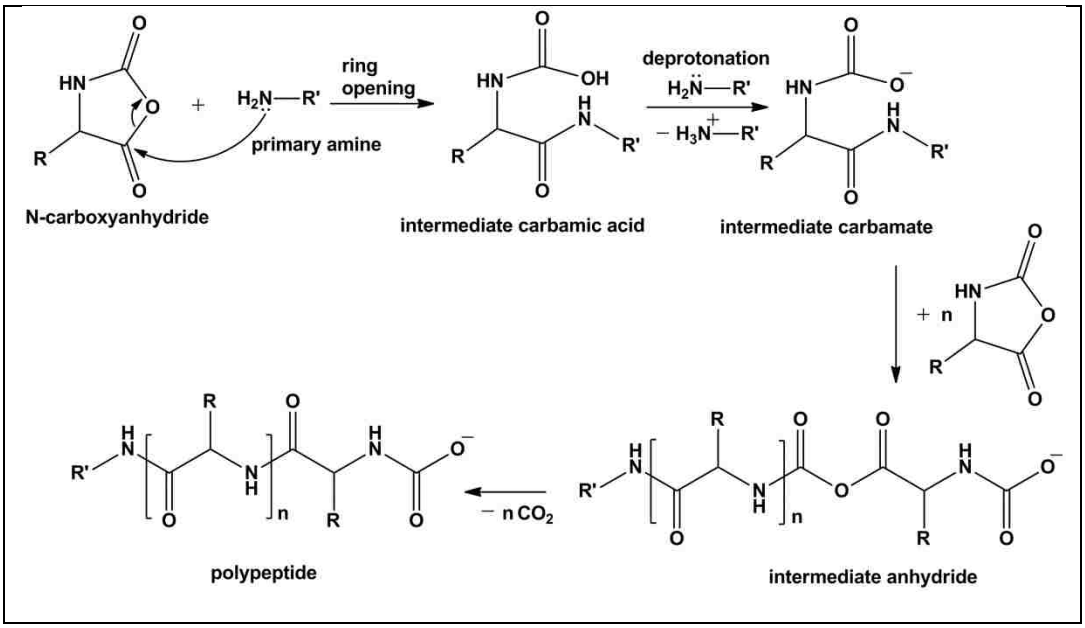

Scheme 1.11 Schematic of the initiation and growth steps involved in ring opening polymerization of NCAs initiated by a primary amine through carbamate mechanism.

Kricheldorf gave a critical overview on the previous work and used MALDI-TOF mass spectrometry among other techniques to better identify the end-group combinations.[297] Mass spectroscopy doesn't necessarily determine accurately the molecular weights and molecular weight distributions, MWD, of the polymer, but qualitatively it does offer a picture of the frequency distribution.[285] The polydispersity index, PDI, values depend strongly on the polymerization medium and, as well, on the solubility and the secondary structure of the forming polypeptide chain. Secondary reactions occurring during polymerization retard the propagation mechanism enabling the termination. Broad[296,309,310] and low[311] PDI's were reported accounting for the aforementioned reaction conditions. Mostly poly(alkyl glutamates) and poly(N-protected-L-lysine) were investigated but, also, other amino acid NCAs.[312,313] Optimum preparation of long chains with low PDI's can be achieved from soluble α-helix forming polypeptides and lowering the temperature to freezing point of water.[314,315] Therefore in the primary amine initiated NCA polymerizations it is challenging to control the chain-end functionality. The absence of the side

reaction results in a true living polymerization and the amino end-group is stable over a long time, as proven by Kricheldorf.[311]

The inherent problem in conventional NCA polymerization is the poor control over the reactivity of the growing chain due to side reactions. An important contribution in this field was brought by Deming's group. He studied many metal complexes such as zerovalent nickel[316,317] and cobalt[318] known to increase both the reaction selectivity and efficiency.[319] The manner in which these metal complexes react with NCAs is similar. Scheme 1.12 illustrates the n-carboxyanhydride polymerization initiated by the Ni(0) complex.

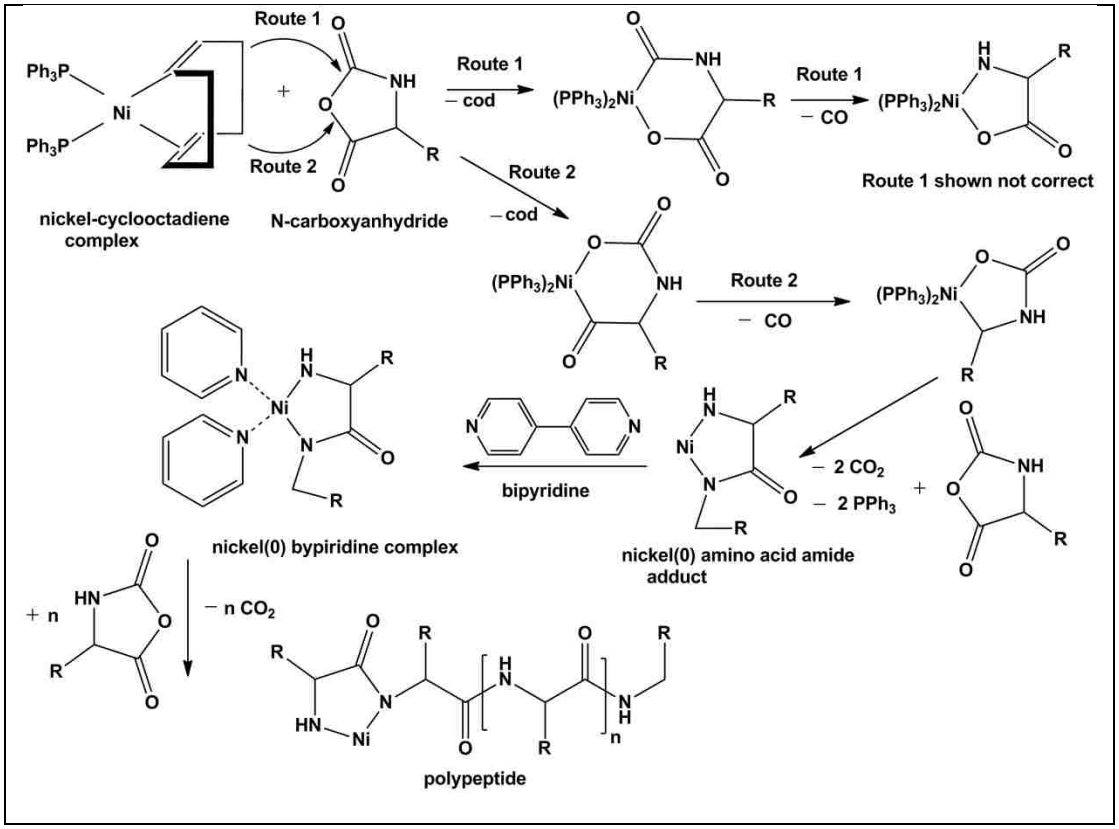

Scheme 1.12 Schematic of polymerizations of N-carboxyanhydrides initiated by Ni(0) complexes. Adapted from Reference 285.

The oxidative addition reactions are followed by the attachment of a second NCA molecule and yield six-membered amido-alkyl metallacyles. Further, these cyclic intermediates contract to a

five-membered ring upon addition of the NCA monomers. This process was explained to occur via proton migration from an amide group to the metal bound carbon, thus liberating the chain end from the metal. The cyclic intermediate was proposed as the active specie capable of initiating the nucleophilic attack of the amido group on the electrophilic C-5 of the NCA.[316-318,320] The large cycle formed as the result of the propagation could contract through CO_2 release. The amido amidate propagating species formed as a result of the proton transfer from the free amide to amidate group enables ring contraction. In fact, the end chain of the polymer becomes free and the metal chelate can migrate along the growing polymer.[321] Despite some ambiguity regarding the correct mechanistic route, Deming's work spans a variety of preparative applications. Variation of the metal allowed good control over the molecular weight and PDI of poly(glutamate)s, and the use of the different NCA precursors resulted in a broad range of homopolypeptides. No less important is the multitude of the architectural copolypeptides designed by using metal chelate initiation.[322-345]

The common theme of improving the classical amine-initiated polymerization initiators was also shared by other groups. Hadjichristidis conducted primary amine initiated polymerizations of NCAs under high vacuum conditions. [346-353] Even though doubts were placed on the purification efficiency of NCA monomer under high vacuum when compared with the recrystallization under an inert atmosphere, the polymerization of the γ-benzyl-L-glutamate NCA (BLG-NCA) and N-carbobenzyloxy-L-lysine NCA, (CBL-NCA) in DMF under high vacuum was found to have a living character. The main conclusion drawn by the authors outlines that the side reactions in the amine-initiated mechanism are a result of the impurities contained in the monomer. Furthermore, the continuous removal of CO_2 generated during the reaction can mediate the polymerization.[346-353] Low-polydispersity products were obtained with predictable

molecular weight but the method needs more insight on the chain-end characterization. In a recent report of Pickel et al., the preparation of the poly(o-benzyl-L-tyrosine), PoTYR, in DMF was performed both using high vacuum techniques and glovebox environment.[354] Polymers prepared by initiation with 1,6-diaminohexane in the high vacuum followed the normal amine pathway, the termination occurring with DMF. Products prepared in the glovebox showed initiation by both amine and activated monomer mechanisms and the termination yielded several species. The nano-assisted desorption/ionization time-of-flight mass spectrometry, NALDI-TOF MS, was used for the chain-end analysis and the conclusion pointed to the end-group fidelity obtained via high vacuum.[354]

N-trimethylsilylamines were used for controlled ring opening polymerization of NCAs by Cheng and coworkers.[355] The unique feature of this technique is that the amine end-groups are obtained after cleaving the protecting trimethylsilyl end-group. A narrow distribution was achieved and the ^{13}C NMR, the fast atom bombardment mass spectrometry, FAB-MS,[356] the matrix assisted laser adsorption ionization time of flight, MALDI-TOF,[355] and the electrospray ionization mass spectrometry, ESI-MS,[357] determined the nature of terminal groups. In order to avoid the formation of NCA anions during the polymerization, Schlaad et al. have utilized primary amine hydrochloride salts as initiating species. Their goal was to inhibit the polymerization through the activated monomer mechanism, obtaining in this way low dispersity. A drawback of this work points to the lack in the end-group determination. Higher values of molecular weight were obtained for products when compared with those theoretically computed.[358-360]

The identification of the terminal groups is also important from another point of view. For a long time in the NCA ring opening polymerization era it was believed that resulting

adducts were linear, unless branching was intentionally desired. One exception stated otherwise[361] until Kricheldorf confirmed the in situ formation of the cyclic polypeptides along with the linear ones.[297,362] Solvents with high nucleophilicity and donor ability such as pyridine, DMF, N-methylpyrrolidone, NMP, and dimethylsulfoxide, DMSO, were found to catalyze zwitterionic polymerizations.[363] The Scheme 1.13 displays the interactions between the polymerization species when the solvent involved is pyridine.

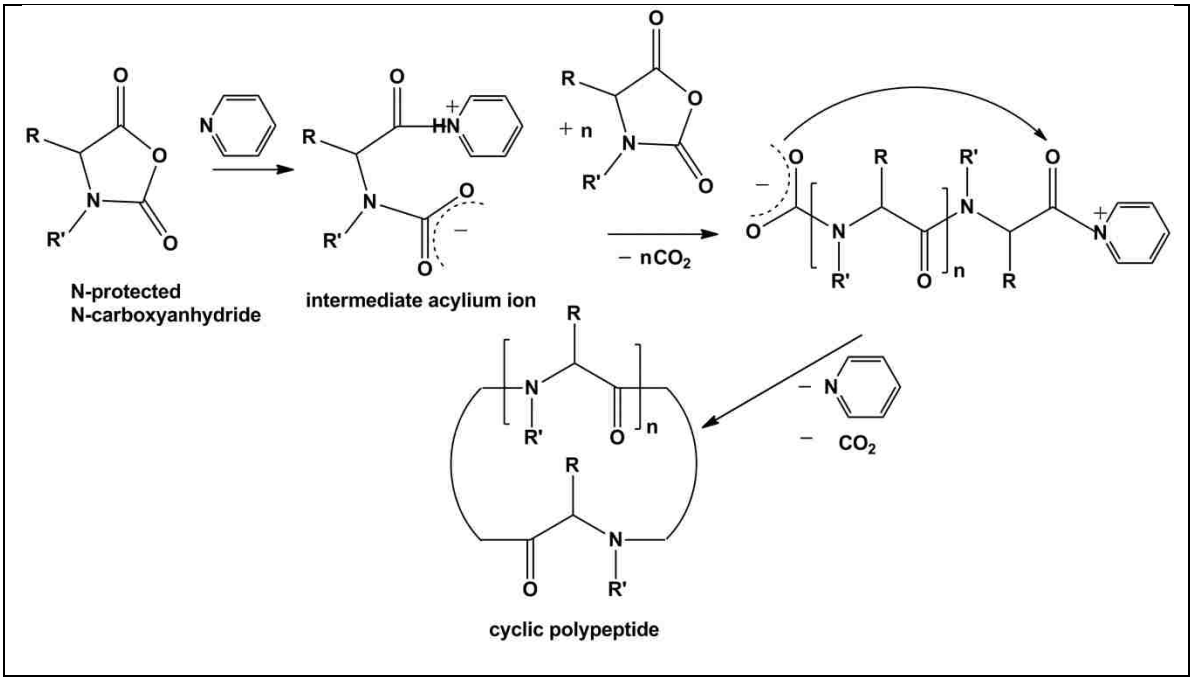

Scheme 1.13 General route of the pyridine-mediated ring opening polymerization of N-protected N-carboxyanhydrides via zwitterionic ionic intermediates. Adapted from Reference 285.

Consequently, the synthesis of homo- and copolypeptides in these solvents should take into account that the polymerization mixture might be a blend of most linear chains with cyclic "contaminations". Soluble polypeptides that adopt a random coil conformation showed a high tendency toward cyclization.[364] It has been known that traditional NCA ring opening polymerization leads to low-molecular weight polymers. Once removed (and usually discarded)

the remaining high-molecular weight polymer is very good (M_w/M_n ~ 1.2). Thus, it will be more efficient to fractionate and keep both high-molecular weight and low-molecular weight polymers.

From the perspective of the next section dedicated to core shell systems where the core consists of an inorganic hard sphere and a shell built from a fuzzy homopolypeptide, several words will be spent first on the enormous potential of polypeptides as shell materials. Depending on their side chain substituent, polypeptides can deliver a variety of versatile properties such as chirality, ability to form liquid crystals (LC), secondary structure structural changes as a response to external stimuli, etc. No less important than self assembly in spherical and cylindrical micelles or vesicles, the ability of polypeptides to form liquid crystalline phases has attracted a lot of interest. One of the most studied polypeptides is poly(γ-benzyl-L-glutamate), PBLG.[365] Most of the early publications concentrated on PBLG lyotropic LCs are mentioned in the book by Block.[366] The first reports of PBLG LC phases date in the 1950s[365,367,368] and since then an immense volume of the work was dedicated to its LC behavior.[366,369-388] Studies on glutamates with different side chain moieties were reviewed by Daly et al. [389] The Russo group focused on PBLG's and other glutamate-based liquid crystals, aggregation and gelation behavior.[274,390-407] The driving force behind such phenomenon is the change in the secondary structure and its effect on the phase behavior. Substituents attached to the side chains were found to induce thermotropic transition.

A very commonly used technique in the phase behavior for concentrated solutions of poly(glutamate ester)s was optical rotation dispersion, ORD. It has an advantage over circular dichroism, CD, because the interference from the solvent can be better discriminated. ORD can also deal very well with solutions prepared in solvents not suitable for CD. Most studies focused

on the characterization of the cholesteric phase.[407-409] It was found that the pitch of the cholesteric helix varies inversely proportional to the optical rotation. More or less recent investigations dealt with the specific features of helix formation and tried to simulate different models. Yet, below a critical point (temperature, molecular weight), the ORD signal suddenly became intense.[410] This jump in the intensity was attributed to the short range order of the long axes of the α helices. The orientational effect, as well the distorsions (disclinations) in the cholesteric phase were studied by varying temperature,[373,411] solvent,[412] polydispersity of the polymer[413,414] , surfactants,[415,416] and concentration.[417,418] Small-angle X-ray scattering, SAXS, and dynamic/static[373] light scattering, DLS/SLS, techniques added more information to the mechanism of helix formation and LC stabilization. A helices possess a high dipole moment which can be influenced by electric[381,419] and magnetic fields.[420,421] The helix order vector aligns parallel to an external field. Strong fields can hamper the formation of the cholesteric phase. Chiral and special solvents,[422-424] surfactants and fluorescent tags were additional tools used to influence the molecular orientation in the LC phases. The diffusion coefficients of the rod-like mesogens (PBLG) were measured by the means of the pulse field gradient nuclear magnetic resonance, PFG-NMR.[425-428] The diffusion coefficient for a solution of PBLG in chloroform at 30°C decreased from the isotropic to the cholesteric phase. The diffusion parallel, D^{II}, to the helix axis was higher than perpendicular, $D^{\perp}$. The diffusion behavior of the PBLG in concentrated solutions was found to follow Kirkwood theory. Very recently investigations with fluorescence photobleaching recovery, FPR, on the magnetically aligned fluorescein (FITC) labeled PBLG have found that the rate of the parallel diffusion in the direction of α-helix declined with the concentration while the rate perpendicular remained approximately constant. At low concentrations of the LC domain, the ratio between D^{II} and $D^{\perp}$ was 5 but at higher

concentrations it was 2. The molecular mobility and the flexure effects on the LC phase in m-cresol were studied by rheology.[372,429-435] Mesophases occurring as a result of the transition from various LC states were investigated in terms of stability.[436,437] The nature of the side chain substituents and their influence on the molecular orientation was studied by varying the temperature.[424] The work of Watanabe et al. on random copolymers made of different glutamates and on polyglutamates with mesogenic groups was dedicated to thermotropic phase behavior.[438-455] The pitch of the molecular helix was found to increase with the length of the n-alkyl chains and with the temperature.[456] A columnar hexagonal mesophase formed at temperatures below the cholesteric phase. Phase behavior of PBLG in m-cresol was also studied in depth.[457,458] Research performed by other groups used differential scanning calorimetry, DSC,[459] NMR,[425,460-462] electron spin resonance, ESR[463], X-ray photoelectron spectroscopy, XPS,[20] and CD to understand better the LC behavior. Polarized light microscopy, POM, was another technique used to visualize the morphologies of the LC phases and to calculate the order parameter.[384,464-466] Many other investigations were extended to poly(L-lysine),[467-470] poly(L-alanine),[471] poly(γ-benzyl-L-aspartate),[472,473] and other unusual polypeptides.[474]

The end of this section briefly summarizes the ability of polypeptides to undergo conformational transitions induced by the temperature, solvent, pH and surfactants. Doty[475], Blout[476] and Applequist[477] conducted pioneering studies on PBLG helix-coil transition. A well-defined transition temperature for PBLG in dichloroacetic acid, DCA, (37% vol.)-chloroform (63% vol.) mixture was identified.[478,479] The heat capacity associated to the transition was determined by calorimetry. Watanabe et al. measured the dielectric constant and electric birefringence of the PBLG in DCA–EDC, 1,2-dichloroethane, mixture. Addition of DCA in small amount (~0.1%) caused a sharp change of these properties and was assigned to the helix-

coil transition.[480] Ackermann et al. investigated the thermodynamics of PBLG in the same solvent mixture by polarimetric measurements.[481] The critical transition temperature increased with the PBLG concentration at constant solvent composition. This trend was also noted when the PBLG solutions had equal concentration but the amount of DCA increased. Both studies seem to agree that parameters such as transition enthalpy or cooperativity depend greatly on the concentration, the temperature and the solvent composition. The present trend in the literature concerns PBLG copolymers and the aggregation behavior based on the secondary structure changes.[482,483] Polytyrosine, PTYR, undergoes a helix-coil transition in mixtures of dimethylsulfoxide, DMSO, and DCA.[484,485] Upon addition of a strong base, NaOH, PTYR changed the helix conformation into the β- sheet.[486]Poly(N^{ϵ}-carbobenzyloxy-L-lysine), PCBL, has a reverse transition from helix to coil in m-cresol as a function of the temperature.[487-489] Poly(β-benzyl-L-aspartate) is another polypeptide known to change its conformation in m-cresol.[490] Deprotection of side chains of the PBLG, PCBL, etc., enables the pH-dependent conformational transitions.[491-493] Helix-to-helix[494] or helix-to-sheet[495,496] changes were also reported. A picture of the processes involved in the structural changes will be given in other chapters of this document.

1.8 Silica Polypeptide-based Hybrids

The past decades encountered a rapid development of micro- and nano-scale materials which found applications in wide areas such as medicine, industry and technology. Core-shell particles having a well-defined solid core made from silica and a shell comprised of a polymer can display a range of projected behaviors besides colloidal stability and robustness. From all core-shell particles, silica particles featuring a polypeptide shell have become lately an expanding field of research because of their potential applications, still in the incipient phase of

the exploration. In this section early reports on silica polypeptide hybrids will be summarized and, as well, trends in present research. Methods used in hybrid material synthesis such as *grafting to (onto)* and *growing from* will be compared and the shortcomings in designing the desired properties of the final product will be also addressed. The main steps involved in these two techniques are presented in Scheme 1.14.

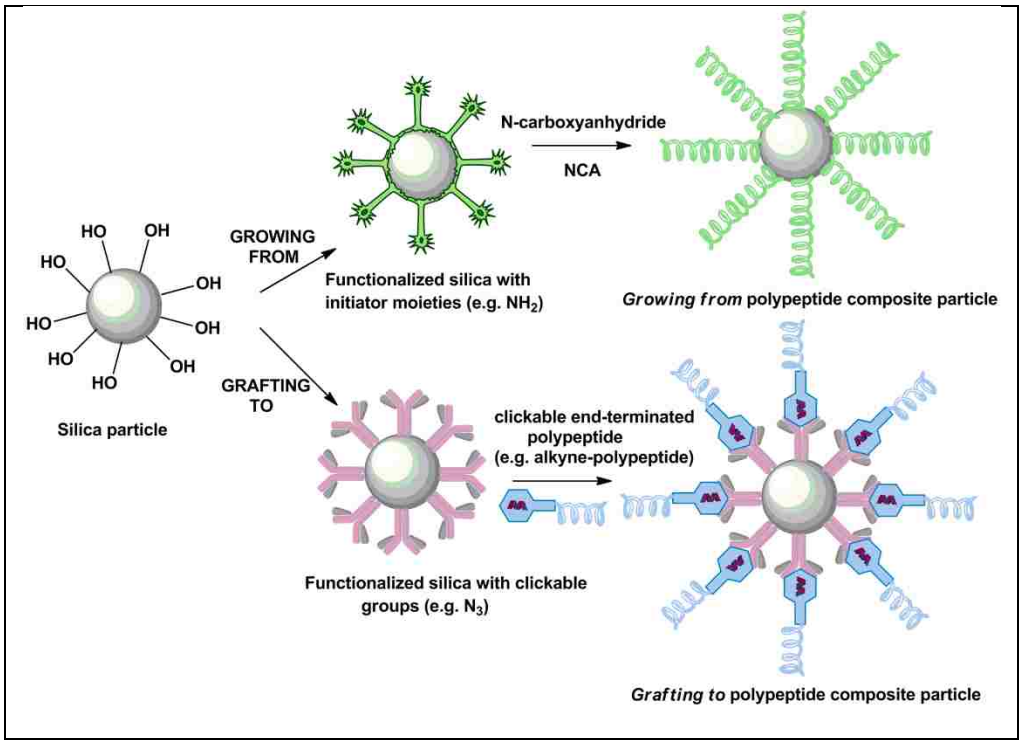

Scheme 1.14 Schematic illustration of the *growing from* and the *grafting to* methods.

The key feature of the polypeptide-grafted silica particles is the possibility to combine in one material the distinct secondary structures (α- helix, β- sheet, random coil) with the low cost, easy preparation and facile surface modification of the silica particles. As a consequence, these hybrids possess a broad range of functional and structural properties. In addition, a silica core with magnetic inclusions and the functional groups decorating the polypeptide chain give a colloid responsive to external stimuli such as magnetic and electric field, pH, solvent,

temperature and electrolytes. Besides using a silica spherical core, polypeptides were deposited on flat surfaces by the classical ROP of the corresponding NCA or by the vapor deposition.[15,18,19,234,489,497-507] Researchers were devoted to controlling the surface grafting density, to assessment of the orientation of the polypeptide chains, to growing multi-polypeptide layers, and, most importantly to explore the conformational changes in response to the external stimuli.

In the past years, a few composite core-shell colloidal particles have been made that featured a homopolypeptide shell.[8-13] In the Russo group the era of the polypeptide-silica hybrids started one decade and a half ago from the simple desire to design a better core for engineering star shaped polymers such as PSLG-a hairy rod-like polymer.[274,389,403,508] The step to discovering new and interesting properties these materials can display, was almost natural. Beautiful colloidal crystals were obtained from PCBL-grafted silica upon improving the uniformity of the silica cores.[232,233] The effect of polydispersity on the formation of colloidal crystal has been reported.[509,510] Soon it became obvious that methods to control the grafting density are necessary, as well as knowing the length of the polymer grown on the particle, usually by dissolving the silica core using etching procedures.

The emergence of the click chemistry or Huisgen 1,3-dipolar cycloadition[511] had made possible the control over the length of polymer attached to the core. This is the major advantage of the *grafting to* method: well-characterized polypeptide chains, further attached to the functionalized surface of the core, produce a uniform shell. Another feature of click chemistry is the possibility to match the end group of the preformed polymer with the reactive functional moiety grafted on the silica surface. The compatibility between the matching groups prevents interference with any other functional moieties on the silica surface or on the polymer. It also

favors the fast covalent grafting step over the other complementary processes (e.g. polymer chains can fold and give a nonreactive surface). The chemoselective and fast *grafting to* method is also known for its tolerance to a broad range of the functional groups.[512-517] The most popular among all is the cycloadition of an alkyne and azide groups *via* stable 1,2,3-triazole linkages, as shown in the Scheme 1.15.

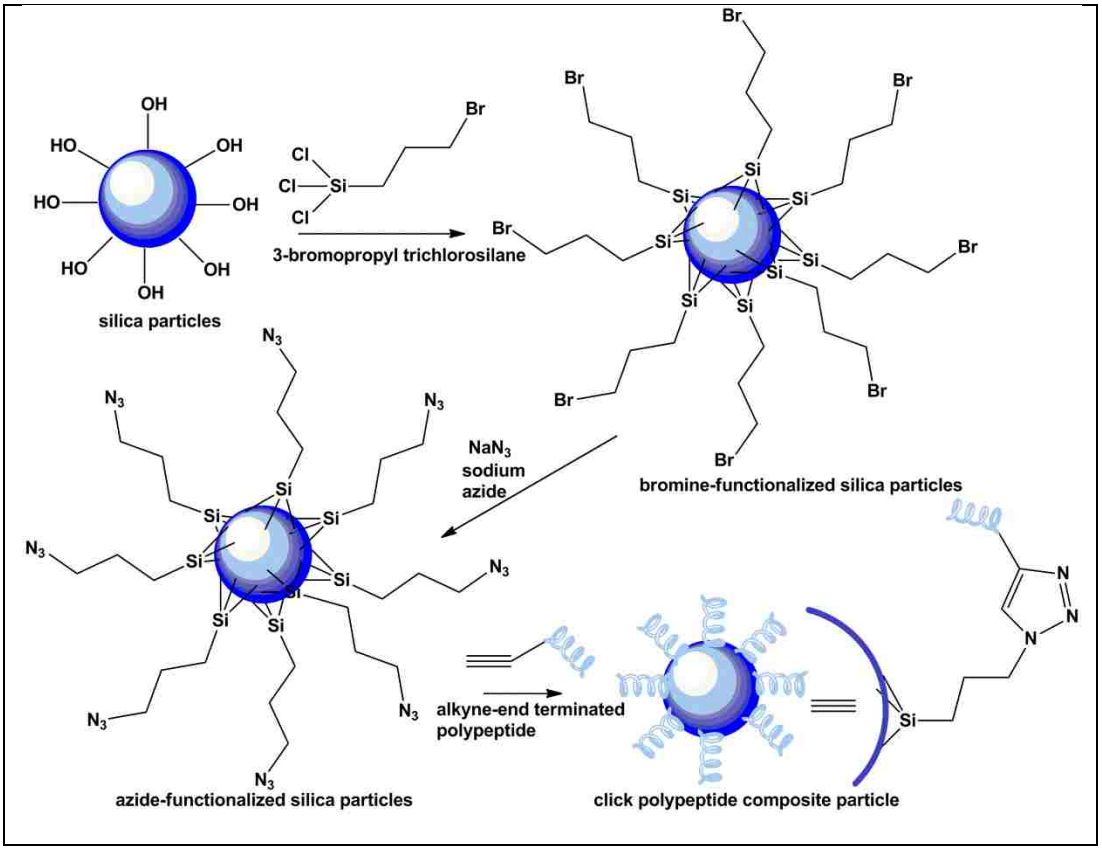

Scheme 1.15 Schematic of the surface reactions involved in the preparation of polypeptide composite particles using click chemistry.

Click chemistry was involved from the very beginning in coupling premade polymers or biomolecules to peptides, proteins, nucleic acids, viruses, cells, sugars and synthetic polymers.[518-523] Several groups reported block copolymers made of homopolypeptides.[238,524-533] Yet, few reports were recorded about click hybrid particles featuring a homopolypeptide shell or

other synthetic polymer.[205,206,534-536] The Russo group grafted an α-helical hydrophobic PSLG to silica particles.[204] These particles formed stable dispersions in a broad range of organic solvents such as THF, chloroform, dodecane and toluene. The molecular weight of the coupled polymer was calculated to be approximately 4600 Da based on the monomer-to-initiator ratio and a repeat unit weight of 381 $g \cdot mol^{-1}$. The GPC/MALS measurement returned a much higher value as listed in Table 1.1, an indication that some initiator molecules were probably inactive or yielded dead chains. At the same time, Gupta group used the tandem of the click chemistry and the ROP of NCAs to fabricate PBLG-, PLL- and PLGA-grafted silica particles with a high grafting density. The methodology was extended to obtain copolypeptide-grafted hybrids such as poly(L-lysine-b-poly-L-leucine), (PLL-b-PLLeu) silica particles. The molecular weights of the grafted polymers appear in Table 1.1.

Table 1.1 Polymer Name, Ratio of the Monomer to Initiator, Weight-average Molecular Weight, Polydispersity and the Corresponding Reference for Several Polymers Prepared for Click Chemistry

Polymer	[M]/[I]	M_w		PDI	Reference
		Theoretical	Actual		
Alkyne-PSLG	30	4,600	8,480	1.15	Balamurugan et al.
Alkyne-cbz-PLL	30	n/a	8,000	1.05	Kar et al.
Alkyne -PBLG	25	n/a	7,000	1.1	Kar et al.
Alkyne-p-methoxy-PBLG	30	n/a	9,500	1.08	Kar et al.
Alkyne-p-methoxy-PBLG	40	n/a	12,000	1.04	Kar et al.
Alkyne- PLGA	30	n/a	4,300	1.08	Kar et al.

Table 1.1 continued

Polymer	[M]/[I]	M_w		PDI	Reference
		Theoretical	Actual		
Alkyne- PLGA	30	n/a	5,000	1.04	Kar et al.
Alkyne-cbz-PLL-b-PLLeu	25:15	n/a	8,000	1.06	Kar et al.

Comparison of the results contained in Table1.1 also helps to underline some drawbacks in *grafting to* approach. Regardless of the available range of alkyne- amine initiators, good control over the desired molecular weight of the polypeptide is still not evident. For example, propargylamine, one of the most common primary initiators used in click chemistry, is not reactive enough. The initiation step needs to be fast in order to enable the propagation and the growth of the nascent chains in the same time. The preparation of the short polypeptides as well as very long ones still remains a challenge. Lately, new initiators that are more reactive were developed and offered a better control over polymerization. One of them, N-trimethylsilyl propargyl amine,[357] also used by the Gupta group seems to give low-polydispersity polymers and molecular weights that lie closer to those predicted from the monomer-to-initiator ratio.

Even if the polymer has a well-characterized molecular weight, once grafted onto the surface the loading on the particle still remains low leading to low yields. The attachment of the active functions on the particle surface needs to be adjusted in such a way that will avoid a crowded surface. Moreover a dense coverage will result in many sites with unreacted functional groups because of steric hindrance. In this situation, homopolypeptides carying a side chain and covering the core surface are forced to interpenetrate. Therefore, some properties of the final product might be affected. For example, a crowded shell may fail to undergo secondary

transitions in response to the external stimuli if that was the application targeted for the hybrid particle. In order to illustrate the aforementioned, Table 1.2 summarizes grafting densities obtained by the two groups for several click particles.

Table 1.2 Hybrid Particle Name, Core and Overall Size, Weight Loss, Grafting Density and Associated Reference for Polypeptide Composite Particles Prepared by Click Chemistry

Hybrid Particle	Diameter/nm, DLS)		Weight loss %	Grafting density/μmol·m^{-2}	Reference
	Core	Core+shell			
Silica-PSLG	140 ± 3	160 ± 10	30	1.48	Balamurugan et al.
Silica-PLGA-30	22 ± 3	37 ± 3	25	0.427	Kar et al.
Silica-PLGA-40	22 ± 3	38 ± 6	28.4	0.45	Kar et al.

Another disadvantage in the *grafting to* approach arises from the difficulty and the costly protocol to remove the copper traces from the final product. Used in tandem with a ligand, the common *N*, *N*, *N'*, *N'*, *N''*-pentamethyldiethylenetriamine, PMDETA, or recently used sulfonated bathophenanthroline,[200] the copper in the salt form (e.g. CuBr, CuI) catalyzes the coupling reaction between the azide and the alkyne functionalities through stable 1,2,3-triazole bonds. The presence of the metal in the click colloid can exert cytotoxic effects on metabolism in the living body, and thus hampers its use in biological applications. A step toward improving the utilization of this method was made by the innovation of the so-called copper-free click chemistry. Biorthogonal reactions use components inert to the biological environment and employ several classes of reagents. One class of molecules, cyclooctynes, coined by Wittig and Krebs[537] reacts selectively with the azide groups at ambient temperature. The activation energy of the classical Huisgens [3 + 2] cycloadition is high, 26 kcal/mol,[515] thus, elevated temperature and pressure are required to accelerate the rate of coupling. The copper-free chemistry has a lower activation

barrier, 18 kcal/mol of ring strain,[538] because of the unique feature of cyclooctynes, a highly strained ring, which confer them a higher reactivity at the ambient temperature and pressure. Recent developments were directed to increase even more the reactivity and selectivity of the cyclooctynes.[539-543] In depth view about the biorthogonal chemistry was also comprised in a review by Jewett and Bertozzi.[544] The drawback of the copper-free click-to approach concerns of the cost and the complicated chemistry behind the synthesis of these compounds. The future of this subclass of click chemistry is very promising in terms of the visualization of substructures in cells and conducting reactions *in vivo* (e.g. covalent labeling of biomolecules). The method will also allow the in depth study of the cellular machinery. Overall, click chemistry remains an expanding field of the research in nanotechnology. Recent reports used click chemistry to prepare macromolecular self-assembling building blocks, polypeptide-*g*-polyhedral silsesquioxane (POSS) copolymers from a mono-azido-functionalized POSS and poly(γ-propargyl-L-glutamates), PPLG.[545] The PPLG-POSS nanoparticles had superior thermal properties and better conformational stability compared to pure PPLG.

Disadvantages of the *grafting to* method can be circumvented by the *grafting from* technique. Historically *grafting from* method was used as an exclusive tool to grow polypeptide brushes on planar surfaces such as silicon wafers. The ring opening polymerization of NCAs was conducted in solution,[19,234,502,505,506,546-550] melt[504] and by vapor deposition.[18,501,551,552] One of the most-used polypeptides for grafting was PBLG.[553,554] The work by Fong and Russo demonstrated the successful growth of the PBLG on the spherical surface made of silica particles.[232,233] Lately, the same group demonstrated the grafting of PCBL in a controlled fashion and opened the door to copolypeptide shells, as shown in the Scheme 1.16.[218]

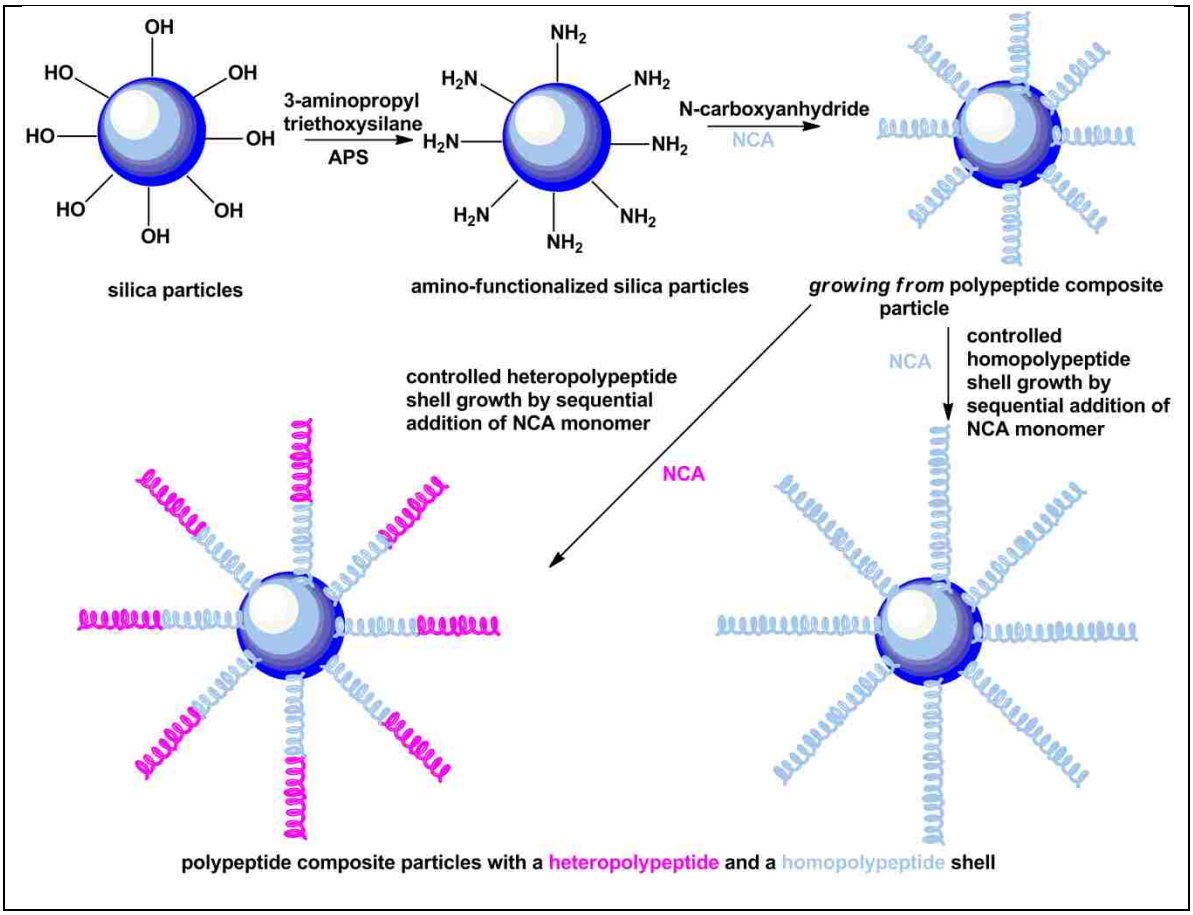

Scheme 1.16 Schematic of the surface reactions involved in the preparation of the polypeptide composite particles having a homopolypeptide and a heteropolypeptide shell.

Control over the shell thickness could be assured by the sequential addition of the NCA monomer. The Heise group expanded the work on stimuli-responsive polypeptide-based silica hybrids and investigated the optimal conditions of the polymerization to produce uniform shells.[248] Reactions carried out at 0°C seemed to give a core-shell structure whose hydrodynamic radius increased proportionally with the BLG-NCA monomer addition. The same polypeptide was grown on silica enclosing a magnetic (magnetite) nugget. Magnetic inclusions broaden the responsiveness spectrum of the hybrid particle.

Even though the polypeptide loading on the particles is much higher than click particles, the *grafting from* method suffers from several constrains which will be further addressed. First,

the control over the grafting density still needs to be improved. For this reason, the Russo group used the tandem passivator/activator (e.g. methyltrimethoxy silane, MTMS/aminoethyl-3-aminopropyltrimethoxy silane, AEAPTMS, MTMS/ 3-aminopropyltrimethoxy silane, APTMS) in the effort to avoid a densely polypeptide packed surface. Two sets of particles were prepared: one carrying a shell consisting of PCBL and the other had PBLG.[218] Methods to demonstrate the packing nature of the shell are limited because the molecular weight of the polymer is not easily accessible unless the hybrid particle is subjected to a "haircut". This aspect will be developed in a future paragraph. Information about the "densification" of the shell was gathered by a combination of light scattering and computation methods based on the core-shell form factor.[555-558]

$$I(qR) \propto R^6 \left[\frac{(m_1-1)}{2\pi}\left(\frac{3j_1(x)}{x} + f^3\frac{(m_2-m_1)}{(m_1-1)}\frac{3j_1(fx)}{fx}\right)\right] \qquad Eq.\,1.3$$

In this equation, R is the outer radius of the polypeptide silica core shell particle, $x = qR$, q is the scattering vector magnitude defined as $q = 4\pi n \cdot \sin(\theta/2)/\lambda_o$ (n is the solvent refractive index, θ the scattering angle and λ_o the wavelength in vacuum), j_1 is the first-order spherical Bessel function given by $\sin(x)/x^2 - \cos(x)/x$. The relative refractive indices were expressed as $m_1 = n_1/n_0$ and $m_2 = n_2/n_0$ with n_0, n_1 and n_2 the refractive indices for the solvent, the shell and the core, respectively. The term f designates the fraction belonging to the core from the total dimension of the particle: $f = (R\text{-t})/R$ (t-is the thickness of the shell). Well-solvated particles can be modeled using the refractive index contrast between the solvent, the shell and the core.[556,559] Suspensions of PCBL silica particles in pyridine showed a near agreement between their radius measured by DLS and SLS suggesting good solvation of a shell which was not densely packed. Setting the values of the refractive indices to 1.507 for the pyridine solvent,[560,561] 1.544 for the PCBL[562] and 1.445 for the

silica[563] adequate contrast was ensured to detect both entities: the core and the shell. In the Rayleigh-Gans-Debye limit[556,564] at zero scattering angle the scattering intensity is given by:

$$I_s(q=0) \propto \nu M^2 \left(\frac{dn}{dc}\right)^2 \qquad Eq.\,1.4$$

In this expression ν is the number density of particles, *dn*/*dc* is the differential refractive index increment and *M* is the mass. Under these conditions and assuming a hypothetical suspension containing only PCBL shell without core, light scattering at finite angles should return different values for both R_{SLS} (core-shell) and R_{core} (silica). The results didn't reflect this trend pointing once again to a good solvation of the shell, in contradiction with the situation of a highly packed one. Yet, this qualitative assessment couldn't associate the apparent thickness of the shell with its length even under the assumption that polypeptide is oriented perpendicular to the core surface.

The continuous reactivity of the chain ends was proven by sequential addition of the NCA (BLG-NCA) monomer.[218] The direct assay of the shell was facilitated by the thermogravimetric analysis. The weight loss at each step increased, indeed not linearly, with the monomer concentration and the results were confirmed by DLS measurements. The lower grafting efficiency could be explained by the formation of the untethered polymer in the polymerization mixture. This aspect was also noted by the Heise group.[248] The growth of the copolymers made of homopolypeptides on silica spheres was assessed. The importance of washings to remove the free, untethered polypeptide was reflected in the thermogravimetric curves. Approximately 25% weight loss difference was recorded between the unwashed and the washed sample. The reactions conducted at various temperatures (0°C and 20°C) showed good control over the shell thickness, especially at 0°C. This is in agreement with the findings that at 0°C the NCA doesn't react with moisture.

A sensitive and debatable issue is the determination of the molecular weight of the homopolypeptide grown on the surface. The most popular technique is etching the silica cores by hydrofluoric acid, HF. Soto Cantu et al. reported the ability to control the size of the silica when HF etchant was employed.[246] The etching method was adapted to the polypeptide composites from the extensively used treatment of the silica wafers.[565,566] Yet, no detailed study was conducted so far to determine the effect of etching conditions on the polypeptide shell. Questions if the degradation of the polypeptide can occur were asked and answers still wait. The Heise group was the first to combine molecular weights from GPC and mass of shell polymer from TGA to determine the number of polypeptide chains on a particle (0.4 chains/nm^2 or 2.5 nm^2 "parking area" *per* chain).[248] The obtained molecular weights of the PBLG ranged from 7,700 to 20,100 Da for polymerizations conducted at 0°C while the values for polymerizations performed at 20°C varied from 8,700 to 20,100 Da. The polydispersity indexes were 1.4 (0°C) and mostly 1.3 (20°C). The authors claimed that lower temperatures are better but a net difference in the molecular weights values cannot be distinguished. Moreover, the polymerization conducted at 20°C seemed to favor slightly lower PDI's. Some research groups have shown that polymerization in solvents such as DMF as Heise used can initiate the polymerization of the NCA, consequently competing with the initiation by the amino groups. The DMF initiation, as shown in the Scheme 1.17 was also studied by Kricheldorf.[285,363]

This competition arrests the formation of the high molecular weight polymer and yields polydisperse polymers, because the growth of the nascent chains occurs before, during and after the addition of initiator. Yet, the Heise group brought an important contribution to this field by engineering hybrids decorated with a copolypeptide shell. These results demonstrated the potential adaptability of the polymerization to a broader range of amino acids. The continuous

reactivity of the polypeptidic chains was consequently proven, which agreed with the Russo group reports.

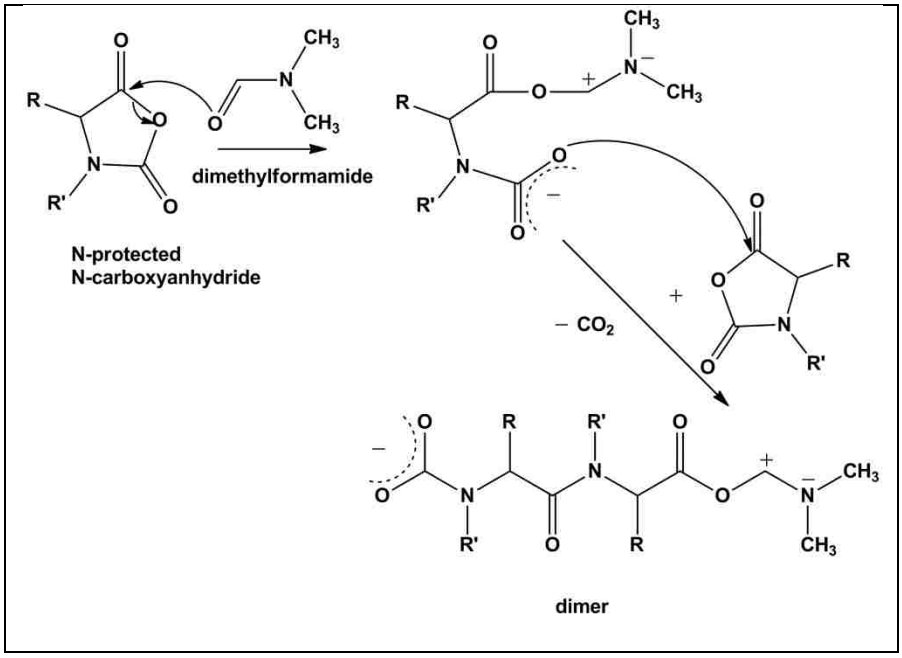

Scheme 1.17 Schematic of the initiation steps of solvent (DMF)-induced zwitterionic polymerization of N-protected N-carboxyanhydrides. Adapted from References 285, 296 and 363.

The stability of the polypeptide-based silica hybrids is of special interest from the perspective of their potential applications. The Russo group presented a study conducted on the aging PCBL-silica hybrids over one year since they were fabricated. It was found that, in time, particles tend to aggregate, a prerequisite of the shell interdigitation. Dynamic and static light scattering techniques recorded correlation functions characteristic to aggregate entities. Sonication over 30 min. reversed the aggregation: particles' size was similar with the one recorded right after the preparation. The downward tendency of μ_2/Γ^2, the DLS polydispersity index, similar with M_w/M_n in GPC, could be explained by the presence of the aggregate particles that could not be separated by the sonication. The polypeptide seemed to survive the treatment for the aggregate breakage. Liu et al. sonicated their PBLG-SiO_2-Fe_3O_4 composite particle in

DMF for 36 hours to test the presence of the polypeptide on the magnetic silica surface.[567] Still, the authors fail to display the thermograms of all steps involved in the preparation and also the size before and after sonication. Ostlund et al. have shown that prolonged sonication of PBLG alters greatly the chains.[568] The scission was noted to occur preferentially on the backbone between the weaker C–N bonds than the C–C or the side chain C–O bonds. The molecular weights dropped to less than half from the initial value, while the polymer retained its helical conformation. Consequently it is not clear how the sonication affected the grafted polypeptide on the Liu et al. magnetic silica surface or on those "de-aggregated" by the Russo group using sonication.

Another route employed in the production polypeptide-silica core shell particles is layer-by-layer, LbL, assembly, method exploited by Caruso group.[569,570] The method is mainly used as an efficient way to design capsules. This technique utilizes the electrostatic interactions between layers of oppositely charged polyelectrolytes which are sequentially deposited on a silica sacrificial template. In this manner, the charge is compensated at each layer.[571-573] The LbL method has the advantage of providing better control on the capsule dimensions.[574] Engineered as drug carriers, these capsules must be small and flexible to travel through the circulatory system's tiny vessels[575] without obstructing the blood stream. The LbL polymer assembly is not limited only to the electrostatic or the zwitterionic interaction. Lately, the LbL assembly was expanded on the H-bonding[576,577] and also on the DNA- DNA hybridization.[578] The continuous development of click chemistry enabled the LbL deposition of the click functional group "matched" polymers.[579-582] Once the desired number of layers is loaded on the sacrificial silica, the core template is removed by etching with HF. Afterwards, the capsule can be loaded with drugs for release purposes. Initially designed with one single void, the morphology of the

capsules was adjusted to create sub-compartmentalized micro-reactors by using liposomes.[583-589] The Caruso group took one step further in the field and produced crosslinked poly(L-glutamic acid), PLGA particles. The procedure employed positively charged amino-functionalized mesoporous silica particles which were further decorated by LbL deposition with PLGA carying cysteine residues.[590] Further, the final composite particle was obtained by disulfide crosslinking and the silica template removal. The polypeptide particles were found to degrade under cytoplasmic conditions and were stable under physiological conditions making them promising candidates as therapeutic carriers.

1.9 Future Trends and Applications of Polypeptide-based Silica Hybrids

Colloids with a soft shell, especially made of homopolypeptides, are extraordinary candidates for a broad range of applications. This section will outline several areas of the impact and also future trends in the polypeptide-based hybrid particles.

One important feature of the polypeptides, still not fully exploited, is their ability to self-assemble in spherical shapes, micelles. Hybrids carrying such shell can be envisioned as excellent models to mimic the self assembly and the action of viruses during the infection stage. Many other proteins have this ability to form the so-called virus-like particles but the polypeptide composite particles, PCPs, have the advantage of the sequence simplicity. Reports emphasized the great potential of the capsid structures resembling virions in designing vaccines that could replace the therapeutic monoclonal antibodies used in some disease treatments.[591] Having a well-defined core and a shell that can be adjusted to the intended shape and thickness, PCPs can be compelling models to understand the interplay forces between the viruses and the living cells within the body. Moreover, such capsids can be easily obtained from PCPs by etching the core with HF or NaOH. In addition, the control over the etching conditions can lead to various

mesoporous morphologies useful in the drug delivery. They can also serve as platforms to investigate the laborious work of the nature in virus construction and to unravel fundamental properties of the infecting bodies.[592]

Another area less explored is jamming. Before designing complex applications as previously mentioned one needs to understand the interactions between the colloid particles in different states, medium and external stimuli. The most studied soft matter, the colloidal hard spheres, was shown to render a slow relaxation dynamics under crowding conditions as a result of either repulsive or attractive forces. Jamming soft matter helps to better understand the relationship between the viscoelastic properties and the spatial correlations of the dynamics.[593] Jammed matter evolves from a flowing to a rigid state. Even though the dynamics change dramatically, the internal structure remains disordered in both solid and fluid phase, quite different than crystallization.[594-600] Rheology is one of the traditional tools used to investigate the dynamic behavior of colloidal suspensions: See Reference 601-602 for reviews.[601,602] The change in the polarization of dipolar composites under the influence of the external electromagnetic fields was another subject of interest for researchers.[602] Other techniques employed in jamming matter investigations such as sedimentation,[603,604] hydrostatic pressure[605] or elipsometry[606] gave insight into the short- and long-time dynamic properties of the colloidal core-shell particles. For example, Ross et al. used the generalized Mie theory applied to multiple spheres to study the relationship between the scattering matrix and the elipsometric scattering variables as a function of the nonconcentricity and the shell thickness.[606] Fluctuations in scattering modes enabled the design of a contrast model that could be used as a guide in the future light scattering experimentation. The mutual interactions between particles suspended in a liquid more or less viscous are greatly influenced by the particulate size. For simple fluids, the molecular size, and

nanometer scale, the behavior is well characterized by the hydrodynamic equations. Once the frontier of the micron scale is crossed one has to deal with the non-equilibrium dynamics, dictated by depletion.[607-628] This phenomenon does influence the stability of the suspension, as a result of the manner in particle interaction either in a confined volume or flowing along a surface.[629,630]

Largely studied systems comprised of core-shell particles confined in a polymer matrix were used as models to investigate the self-assembly phenomenon. A special interest was placed on mixtures of hard spheres and rod-like polymers. A milestone can be considered the work of Tracy and Pecora on ternary systems silica/PBLG/DMF at different concentrations.[631,632] The diffusion coefficients of 60.4 nm hard spheres suspended in PBLG of 70 nm in length could be measured simultaneously and were found to deviate from the theoretical predictions. Such deviation found in the rod and coil solutions suggested that the hydrodynamic interactions between the polymer chains play an important role. At first look one may question why such complex interaction should matter. It matters because the present and future technology is devoted to expand the frontier of the liquid dispersion by preparing complex composite liquids. Used as lubricants, paints, adhesives and ceramic precursors it is important to understand the interactions between each component within the liquid. The cytoplasm in the biological cells is another example of the complex fluids. The increased complexity of drug carriers, the targeted reactions at the cell level or the infiltration of infecting bodies under cell size, altogether, reflect the picture of the complicated interactions within the cell medium. From the biological point of view and the applications that may arise, the study of ternary systems using particles coated with a homopolypeptide shell suspended in the same or different helical polypeptide matrix as the shell, is not even in its infancy. Useful techniques recently emerging are devoted to offer high

resolution information on such advanced materials and their dynamics. Micro-rheology using optical tweezers is one of these methods.[633-637] Forces acting on single colloids without any mechanical contact that can be carried out in nano- and microfluidics can be measured. Trapped in the focal point of the strongly focused lasers, a particle is held and manipulated in the desirable medium enabling excellent insight especially on the pair interaction, the electrophoretic mobility and drag forces, respectively.[638] For example, DNA's uniform and non-uniform stretching was studied since the 1990's by Brochard and Pecora.[639] Attached to a magnetic bead with one end they could investigate the behavior of the DNA strand under different conditions. The progress in the field over the past decades enables today high resolution experiments on single cell adhesion[640] or parasite entity manipulation,[641] to name only a very few applications in the biological sciences.

One of the most extraordinary and unique features that polypeptides provide is their capability to undergo conformational changes as a function of the pH, temperature or solvent. Stimuli-responsive assembly such as polymeric micelles, capsules or polymersomes found a myriad of applications from cosmetics, pharmaceutics, and biotechnology to biomedicine. Steps toward introducing polypeptide-coated silica as biodegradable and easy-to-manipulate candidates to the field of such applications were made and this area continues to grow. Borase et al. entrapped Rhodamine B within the poly (L-glutamic) acid-based, PLGA, composites that was released when the pH of the aqueous solution was changed from acidic (pH=2) to basic (pH=10).[248] The Rhodamine B release mechanism can be considered a good model for future pH-responsive payload delivery. Furthermore, the feasibility of the bioconjugation was demonstrated by the attachment of a green fluorescent protein using NHS coupling chemistry. Aggregate particles were visualized by the means of fluorescence microscopy. Kar et al.[200]

explored the potential of the PLGA as a biodegradable platform in the preparation of the scaffolds for drug delivery,[642-652] MRI contrast agents[653,654] and tissue engineering applications.[655] Well-defined, aligned three-dimensional macroporous structures were produced from PLGA-grafted silica particles crosslinked with polyethyleneimine, PEI, upon ice templating approach with directional freezing. The PEI treatment had as role the stabilization of the scaffold against water disassembly. The presence of the PLGA makes possible the post-functionalization with other organic moieties for the purpose of tissue engineering applications. A devoted work to the field of biocompatible and biodegradable responsive materials has being elaborated by other research groups. Lecommandoux group has developed their polymersomes comprised of diblock copolymers, one being PLGA.[656] These self-assembled structures resemble in their structure primitive biological cells. Agut et al. demonstrated that poly[2-(dimethylamino)ethyl methacrylate]-*b*-poly(glutamic acid), the double hydrophilic block copolymers, DHBCs, self-assemble in micelles and polymersomes.[656] Their sizes and morphology could be varied as a function of the pH, the temperature, the composition of the DHBC and its isoelectric point and the PLGA block length. The separate response upon pH and temperature changes achieved with these models was considered a new route to stimuli-responsive carriers. Sanson et al. synthesized biocompatible block copolymers from poly(trimethylene carbonate)-b-poly(L-glutamic acid), PTMC-b-PLGA that formed vesicles and their sizes and dispersities were controlled under different conditions (e.g. polymer concentration, nature of organic phase, etc.).[657,658] The polyelectrolytic PLGA corona responded to the pH changes. The encapsulation of superparamagnetic maghemite, γ-Fe_2O_3, within the membrane of the vesicles by a nanoprecipitation process enhanced their responsiveness: they could be guided under external magnetic fields.[659] Furthermore, by loading with an antitumor drug such as doxorubicin

hydrochloride, DOX, their use as complex drug carriers and as potential candidates for controlled drug release by radio frequency magnetic hyperthermia was proven. Not the last, polymersomes fully based on the PLGA and the carbohydrate (galactose) building blocks prepared by the click glycosilation have shown various morphologies triggered by the reaction conditions and they also aligned to the raw of the nanosized drug carriers targeted for drug delivery.[660]

No matter the procedure involved in the preparation of such void-polypeptide shell, the so-called either polymersomes, micelles, vesicles, capsids or caposomes, the future of these self-assembled morphologies is directed toward manufacturing more complex structures with enhanced responsiveness, biocompatibility and multiple compartments. The future availability of such advanced materials was already demonstrated, for example, by Caruso's caposomes used as platforms to future therapeutic cells and organocells.[583,588] In the same order of ideas, polypeptide-based silica hybrids remain a field in continuous exploration and development with compelling future applications ranging from biomedicine to simple cosmetics.

1.10 References and Notes

(1) Koenderink, G. H.; Philipse, A. P. Rotational and translational self-diffusion in colloidal sphere suspensions and the applicability of generalized Stokes-Einstein relations. *Langmuir* **2000**, *16*, 5631-5638.

(2) Koenderink, G. H.; Philipse, A. P.; Kluijtmans, S. Sphere dynamics in isotropic colloidal rod fluids. *Journal of Physics-Condensed Matter* **2000**, *12*, A339-A343.

(3) Lettinga, M. P.; van Kats, C. M.; Philipse, A. P. Rotational diffusion of tracer spheres in packings and dispersions of colloidal spheres studied with time-resolved phosphorescence anisotropy. *Langmuir* **2000**, *16*, 6166-6172.

(4) Lettinga, M. P.; van Zandvoort, M.; van Kats, C. M.; Philipse, A. P. Phosphorescent colloidal silica spheres as tracers for rotational diffusion studies. *Langmuir* **2000**, *16*, 6156-6165.

(5) Schartl, W. Crosslinked spherical nanoparticles with core-shell topology. *Adv. Mater.* **2000**, *12*, 1899.

(6) Salgueirino-Maceira, V.; Correa-Duarte, M. A. Increasing the complexity of magnetic core/shell structured nanocomposites for biological applications. *Adv. Mater.* **2007**, *19*, 4131-4144.

(7) Martel, S.; Tremblay, C. C.; Ngakeng, S.; Langlois, G. Controlled manipulation and actuation of micro-objects with magnetotactic bacteria. *Applied Physics Letters* **2006**, *89*.

(8) Bartholome, C.; Beyou, E.; Bourgeat-Lami, E.; Chaumont, P.; Zydowicz, N. Nitroxide-mediated polymerizations from silica nanoparticle surfaces: "Graft from" polymerization of styrene using a triethoxysilyl-terminated alkoxyamine initiator. *Macromolecules* **2003**, *36*, 7946-7952.

(9) Jordi, M. A.; Seery, T. A. P. Quantitative determination of the chemical composition of silica-poly(norbornene) nanocomposites. *J. Am. Chem. Soc.* **2005**, *127*, 4416-4422.

(10) Liu, J.; Pelton, R.; Hrymak, A. N. Properties of poly(N-isopropylacrylamide)-grafted colloidal silica. *Journal of Colloid and Interface Science* **2000**, *227*, 408-411.

(11) Maitra, P.; Ding, J.; Huang, H.; Wunder, S. L. Poly(ethylene oxide) silanated nanosize fumed silica: DSC and TGA characterization of the surface. *Langmuir* **2003**, *19*, 8994-9004.

(12) Seebergh, J. E.; Berg, J. C. Depletion Flocculation of Aqueous, Electrosterically-Stabilized Latex Dispersions. *Langmuir* **1994**, *10*, 454-463.

(13) Shirai, Y.; Shirai, K.; Tsubokawa, N. Effective grafting of polymers onto ultrafine silica surface: Photopolymerization of vinyl monomers initiated by the system consisting of trichloroacetyl groups on the surface and Mn-2(CO)(10). *Journal of Polymer Science Part A-Polymer Chemistry* **2001**, *39*, 2157-2163.

(14) Achatz, D. E.; Heiligtag, F. J.; Li, X.; Link, M.; Wolfbeis, O. S. Colloidal silica nanoparticles for use in click chemistry-based conjugations and fluorescent affinity assays. *Sensors and Actuators B: Chemical* **2010**, *150*, 211-219.

(15) Chang, Y. C.; Frank, C. W. Grafting of poly(γ-benzyl-L-glutamate) on chemically modified silicon oxide surfaces. *Langmuir* **1996**, *12*, 5824-5829.

(16) Enriquez, E. P.; Gray, K. H.; Guarisco, V. F.; Linton, R. W.; Mar, K. D.; Samulski, E. T. Behavior of Rigid Macromolecules In Self-Assembly at An Interface. *Journal of Vacuum Science & Technology a-Vacuum Surfaces and Films* **1992**, *10*, 2775-2782.

(17) Machida, S.; Sano, K.; Sasaki, H.; Yoshiki, M.; Mori, Y. Preparation of Monolayer of Poly(γ-Benzyl-L-Glutamate) by Chemical-Reaction On A Silicon Crystal-Surface. *Journal of the Chemical Society-Chemical Communications* **1992**, 1626-1628.

(18) Wang, Y. L.; Chang, Y. C. Synthesis and conformational transition of surface-tethered polypeptide: Poly(L-glutamic acid). *Macromolecules* **2003**, *36*, 6503-6510.

(19) Wieringa, R. H.; Siesling, E. A.; Werkman, P. J.; Angerman, H. J.; Vorenkamp, E. J.; Schouten, A. J. Surface grafting of poly(L-glutamates). 2. Helix orientation. *Langmuir* **2001**, *17*, 6485-6490.

(20) Worley, C. G.; Linton, R. W.; Samulski, E. T. Electric-Field-Enhanced Self-Assembly of A-Helical Polypeptides. *Langmuir* **1995**, *11*, 3805-3810.

(21) Yu, M. E.; Deming, T. J. Synthetic polypeptide mimics of marine adhesives. *Macromolecules* **1998**, *31*, 4739-4745.

(22) Iler, R. K. *Colloid Chemistry of Silica and Silicates*; Cornell University Press, 1955.

(23) Kolbe, G., Jena, Germany, 1956.

(24) Stober, W.; Fink, A.; Bohn, E. *Journal of Colloid and Interface Science* **1968**, *26*, 62-69.

(25) Brinker, C. J. S., G.W. *Sol-Gel Science: the Physics and Chemistry of Sol-Gel Processing*; Academis Press: Boston, 2004.

(26) Van Helden, A. K.; Jansen, J. W.; Vrij, A. Preparation and Characterization of Spherical Monodisperse Silica Dispersions in Nonaqueous Solvents. *Journal of Colloid and Interface Science* **1981**, *81*, 354-368.

(27) Bogush, G. H.; Tracy, M. A.; Zukoski, C. F. Preparation of Monodisperse Silica Particles - Control of Size and Mass Fraction. *Journal of Non-Crystalline Solids* **1988**, *104*, 95-106.

(28) Bogush, G. H.; Zukoski, C. F. Studies of the Kinetics of the Precipitation of Uniform Silica Particles Through the Hydrolysis and Condensation of Silicon Alkoxides. *Journal of Colloid and Interface Science* **1991**, *142*, 1-18.

(29) Bogush, G. H.; Zukoski, C. F. Uniform Silica Particle-Precipitation - An Aggregative Growth-Model. *Journal of Colloid and Interface Science* **1991**, *142*, 19-34.

(30) Matsoukas, T.; Gulari, E. Dynamics of Growth of Silica Particles From Ammonia-Catalyzed Hydrolysis of Tetra-Ethyl-Orthosilicate. *Journal of Colloid and Interface Science* **1988**, *124*, 252-261.

(31) Matsoukas, T.; Gulari, E. Monomer-Addition Growth With A Slow Initiation Step - A Growth-Model For Silica Particles From Alkoxides. *Journal of Colloid and Interface Science* **1989**, *132*, 13-21.

(32) Matsoukas, T.; Gulari, E. Self-Sharpening Distributions Revisited Polydispersity In Growth By Monomer Addition. *Journal of Colloid and Interface Science* **1991**, *145*, 557-562.

(33) Vanblaaderen, A.; Kentgens, A. P. M. Particle Morphology and Chemical Microstructure of Colloidal Silica Spheres Made From Alkoxysilanes. *Journal of Non-Crystalline Solids* **1992**, *149*, 161-178.

(34) Brinker, C. J. S., G.W. *Sol-Gel Science*; Academic Press: San Diego, 1990.

(35) Walcarius, A.; Despas, C.; Bessiere, J. Molecular sieving with amorphous monodisperse silica beads. *Microporous and Mesoporous Materials* **1998**, *23*, 309-313.

(36) Boukari, H.; Long, G. G.; Harris, M. T. Polydispersity during the formation and growth of the Stober silica particles from small-angle X-ray scattering measurements. *Journal of Colloid and Interface Science* **2000**, *229*, 129-139.

(37) Green, D. L.; Lin, J. S.; Lam, Y. F.; Hu, M. Z. C.; Schaefer, D. W.; Harris, M. T. Size, volume fraction, and nucleation of Stöber silica nanoparticles. *Journal of Colloid and Interface Science* **2003**, *266*, 346-358.

(38) Vogelsberger, W.; Seidel, A.; Breyer, T. Kinetics of sol particle formation as a function of pH studied by viscosity measurements in silica solutions. *Langmuir* **2002**, *18*, 3027-3033.

(39) Smith, D. D.; Sibille, Z.; Cronise, R. J.; Hunt, A. J.; Oldenburg, S. J.; Wolfe, D.; Halas, N. J. Effect of microgravity on the growth of silica nanostructures. *Langmuir* **2000**, *16*, 10055-10060.

(40) Zhang, J. H.; Zhan, P.; Wang, Z. L.; Zhang, W. Y.; Ming, N. B. Preparation of monodisperse silica particles with controllable size and shape. *J. Mater. Res.* **2003**, *18*, 649-653.

(41) Watanabe, R.; Yokoi, T.; Kobayashi, E.; Otsuka, Y.; Shimojima, A.; Okubo, T.; Tatsumi, T. Extension of size of monodisperse silica nanospheres and their well-ordered assembly. *Journal of Colloid and Interface Science* **2011**, *360*, 1-7.

(42) Chang, S. M.; Lee, M.; Kim, W.-S. Preparation of large monodispersed spherical silica particles using seed particle growth. *Journal of Colloid and Interface Science* **2005**, *286*, 536-542.

(43) Chen, H. M.; Hu, T.; Zhang, X. M.; Huo, K. F.; Chu, P. K.; He, J. H. One-Step Synthesis of Monodisperse and Hierarchically Mesostructured Silica Particles with a Thin Shell. *Langmuir* **2011**, *26*, 13556-13563.

(44) Rao, K. S.; El-Hami, K.; Kodaki, T.; Matsushige, K.; Makino, K. A novel method for synthesis of silica nanoparticles. *Journal of Colloid and Interface Science* **2005**, *289*, 125-131.

(45) Wang, J. Z.; Sugawara, A.; Shimojima, A.; Okubo, T. Preparation of Anisotropic Silica Nanoparticles via Controlled Assembly of Presynthesized Spherical Seeds. *Langmuir* **2011**, *26*, 18491-18498.

(46) Balamurugan, M.; Saravanan, S. Producing nanosilica from Sorghum vulgare seed heads. *Powder Technology* **2012**, *224*, 345-350.

(47) Sugimoto, M. The past, present, and future of ferrites. *Journal of the American Ceramic Society* **1999**, *82*, 269-280.

(48) Rado, G. T. S., H. *Magnetism VIII: Spin Arrangements and Crystal Structure, Domains, and Micromagnetics*; Academic Press Inc.: London, 1963.

(49) Khalafalla, S. E.; Reimers, G. W. Preparation of Dilution-Stable Aqueous Magnetic Fluids. *Ieee Transactions on Magnetics* **1980**, *16*, 178-183.

(50) Massart, R. Preparation of Aqueous Magnetic Liquids In Alkaline and Acidic Media. *Ieee Transactions on Magnetics* **1981**, *17*, 1247-1248.

(51) Philipse, A. P.; Vanbruggen, M. P. B.; Pathmamanoharan, C. Magnetic Silica Dispersions - Preparation and Stability of Surface-Modified Silica Particles With A Magnetic Core. *Langmuir* **1994**, *10*, 92-99.

(52) van Ewijk, G. A.; Vroege, G. J.; Philipse, A. P. Convenient preparation methods for magnetic colloids. *Journal of Magnetism and Magnetic Materials* **1999**, *201*, 31-33.

(53) Wang, H.; Nakamura, H.; Yao, K.; Maeda, H.; Abe, E. Effect of solvents on the preparation of silica-coated magnetic particles. *Chemistry Letters* **2001**, 1168-1169.

(54) Aliev, F. G.; Correa-Duarte, M. A.; Mamedov, A.; Ostrander, J. W.; Giersig, M.; Liz-Marzan, L. M.; Kotov, N. A. Layer-by-layer assembly of core-shell magnetite nanoparticles: Effect of silica coating on interparticle interactions and magnetic properties. *Adv. Mater.* **1999**, *11*, 1006-1010.

(55) Bruce, I. J.; Taylor, J.; Todd, M.; Davies, M. J.; Borioni, E.; Sangregorio, C.; Sen, T. Synthesis, characterisation and application of silica-magnetite nanocomposites. *Journal of Magnetism and Magnetic Materials* **2004**, *284*, 145-160.

(56) Klotz, M.; Ayral, A.; Guizard, C.; Menager, C.; Cabuil, V. Silica coating on colloidal maghemite particles. *Journal of Colloid and Interface Science* **1999**, *220*, 357-361.

(57) Solinas, S.; Piccaluga, G.; Morales, M. P.; Serna, C. J. Sol-gel formation of γ-Fe2O3/SiO2 nanocomposites. *Acta Materialia* **2001**, *49*, 2805-2811.

(58) Zhang, L.; Papaefthymiou, G. C.; Ziolo, R. F.; Ying, J. Y. Novel γ-Fe_2O_3/SiO_2 magnetic nanocomposites via sol-gel matrix-mediated synthesis. *Nanostructured Materials* **1997**, *9*, 185-188.

(59) Lu, Y.; Yin, Y. D.; Mayers, B. T.; Xia, Y. N. Modifying the surface properties of superparamagnetic iron oxide nanoparticles through a sol-gel approach. *Nano Letters* **2002**, *2*, 183-186.

(60) Tsai, Y. L.; Chun, C. H.; Ou, J. L.; Huang, C. K.; Chen, C. C. Magnetic Fe_3O_4 nanoparticles synthesized for preparations of silica-coated composites. *Desalination* **2006**, *200*, 97-99.

(61) Yang, D.; Hu, J. H.; Fu, S. K. Controlled Synthesis of Magnetite-Silica Nanocomposites via a Seeded Sol-Gel Approach. *J. Phys. Chem. C* **2009**, *113*, 7646-7651.

(62) Deng, Y. H.; Wang, C. C.; Hu, J. H.; Yang, W. L.; Fu, S. K. Investigation of formation of silica-coated magnetite nanoparticles via sol-gel approach. *Colloids and Surfaces a-Physicochemical and Engineering Aspects* **2005**, *262*, 87-93.

(63) Iida, H.; Takayanagi, K.; Nakanishi, T.; Osaka, T. Synthesis of Fe_3O_4 nanoparticles with various sizes and magnetic properties 14 by controlled hydrolysis. *Journal of Colloid and Interface Science* **2007**, *314*, 274-280.

(64) Babes, L.; Denizot, B.; Tanguy, G.; Le Jeune, J. J.; Jallet, P. Synthesis of iron oxide nanoparticles used as MRI contrast agents: A parametric study. *Journal of Colloid and Interface Science* **1999**, *212*, 474-482.

(65) Tronc, E.; Belleville, P.; Jolivet, J. P.; Livage, J. Transformation of Ferric Hydroxide Into Spinel by Fe(II) Adsorption. *Langmuir* **1992**, *8*, 313-319.

(66) Shen, L. F.; Laibinis, P. E.; Hatton, T. A. Bilayer surfactant stabilized magnetic fluids: Synthesis and interactions at interfaces. *Langmuir* **1999**, *15*, 447-453.

(67) Ziolo, R. F.; Giannelis, E. P.; Weinstein, B. A.; Ohoro, M. P.; Ganguly, B. N.; Mehrotra, V.; Russell, M. W.; Huffman, D. R. Matrix-Mediated Synthesis of Nanocrystalline γ-Fe_2O_3 - A New Optically Transparent Magnetic Material. *Science* **1992**, *257*, 219-223.

(68) Hong, R. Y.; Li, J. H.; Li, H. Z.; Ding, J.; Zheng, Y.; Wei, D. G. Synthesis of Fe3O4 nanoparticles without inert gas protection used as precursors of magnetic fluids. *Journal of Magnetism and Magnetic Materials* **2008**, *320*, 1605-1614.

(69) Hu, C. Q.; Gao, Z. H.; Yang, X. R. Fabrication and magnetic properties of Fe_3O_4 octahedra. *Chemical Physics Letters* **2006**, *429*, 513-517.

(70) Liu, Z. L.; Wang, H. B.; Lu, Q. H.; Du, G. H.; Peng, L.; Du, Y. Q.; Zhang, S. M.; Yao, K. L. Synthesis and characterization of ultrafine well-dispersed magnetic nanoparticles. *Journal of Magnetism and Magnetic Materials* **2004**, *283*, 258-262.

(71) Kim, D. K.; Zhang, Y.; Voit, W.; Rao, K. V.; Muhammed, M. Synthesis and characterization of surfactant-coated superparamagnetic monodispersed iron oxide nanoparticles. *Journal of Magnetism and Magnetic Materials* **2001**, *225*, 30-36.

(72) He, Y. P.; Wang, S. Q.; Li, C. R.; Miao, Y. M.; Wu, Z. Y.; Zou, B. S. Synthesis and characterization of functionalized silica-coated Fe_3O_4 superparamagnetic nanocrystals for biological applications. *Journal of Physics D-Applied Physics* **2005**, *38*, 1342-1350.

(73) Bumb, A.; Brechbiel, M. W.; Choyke, P. L.; Fugger, L.; Eggeman, A.; Prabhakaran, D.; Hutchinson, J.; Dobson, P. J. Synthesis and characterization of ultra-small superparamagnetic iron oxide nanoparticles thinly coated with silica. *Nanotechnology* **2008**, *19*.

(74) Kang, Y. S.; Risbud, S.; Rabolt, J. F.; Stroeve, P. Synthesis and characterization of nanometer-size Fe_3O_4 and γ-Fe_2O_3 particles. *Chem. Mat.* **1996**, *8*, 2209.

(75) Kang, Y. S.; Risbud, S.; Rabolt, J. F.; Stroeve, P. Synthesis and characterization of nanometer-size Fe_3O_4 and γ-Fe_2O_3 particles (vol 8, pg 2210, 1996). *Chem. Mat.* **1998**, *10*, 1733-1733.

(76) Kim, D. K.; Mikhaylova, M.; Zhang, Y.; Muhammed, M. Protective Coating of Superparamagnetic Iron Oxide Nanoparticles. *Chem. Mat.* **2003**, *15*, 1617-1627.

(77) Petcharoen, K.; Sirivat, A. Synthesis and characterization of magnetite nanoparticles via the chemical co-precipitation method. *Materials Science and Engineering: B* **2012**, *177*, 421-427.

(78) Fremgen, D. E.; Smotkin, E. S.; Gerald, R. E.; Klingler, R. J.; Rathke, J. W. Microemulsions of water in supercritical carbon dioxide: an in-situ NMR investigation of micelle formation and structure. *Journal of Supercritical Fluids* **2001**, *19*, 287-298.

(79) Anim-Mensah, A. R.; Ilias, S. Solubilization of TX-100 (TM) and PEG-PPG-PEG in Liquid Carbon Dioxide. *Separation Science and Technology* **2010**, *45*, 1901-1907.

(80) Clarke, M. J.; Harrison, K. L.; Johnston, K. P.; Howdle, S. M. Water in supercritical carbon dioxide microemulsions: Spectroscopic investigation of a new environment for aqueous inorganic chemistry. *J. Am. Chem. Soc.* **1997**, *119*, 6399-6406.

(81) Cummings, S.; Enick, R.; Rogers, S.; Heenan, R.; Eastoe, J. Amphiphiles for supercritical CO_2. *Biochimie* **2012**, *94*, 94-100.

(82) Holmes, J. D.; Lyons, D. M.; Ziegler, K. J. Supercritical fluid synthesis of metal and semiconductor nanomaterials. *Chem.-Eur. J.* **2003**, *9*, 2144-2150.

(83) Ikushima, Y.; Saito, N.; Hatakeda, K.; Arai, M. Water/AOT/ethane microemulsion under supercritical conditions as a reaction medium. *Journal of Supercritical Fluids* **1998**, *13*, 217-224.

(84) Klostermann, M.; Strey, R.; Sottmann, T.; Schweins, R.; Lindner, P.; Holderer, O.; Monkenbusch, M.; Richter, D. Structure and dynamics of balanced supercritical CO_2-microemulsions. *Soft Matter* **2012**, *8*, 797-807.

(85) Roberts, C. B.; Thompson, J. B. Investigation of cosolvent effects on the solvation of AOT reverse micelles in supercritical ethane. *Journal of Physical Chemistry B* **1998**, *102*, 9074-9080.

(86) Sagisaka, M.; Oike, D. K.; Mashimo, Y.; Yoda, S.; Takebayashi, Y.; Furuya, T.; Yoshizawa, A.; Sakai, H.; Abe, M.; Otake, K. Water/supercritical CO_2 microemulsions with mixed surfactant systems. *Langmuir* **2008**, *24*, 10116-10122.

(87) Stone, M. T.; Smith, P. G.; da Rocha, S. R. P.; Rossky, P. J.; Johnston, K. P. Low interfacial free volume of stubby surfactants stabilizes water-in-carbon dioxide microemulsions. *Journal of Physical Chemistry B* **2004**, *108*, 1962-1966.

(88) Sui, R. H.; Charpentier, P. Synthesis of Metal Oxide Nanostructures by Direct Sol-Gel Chemistry in Supercritical Fluids. *Chemical Reviews* **2012**, *112*, 3057-3082.

(89) Wai, C. M.; Ohde, H. Synthesizing nanoparticles in supercritical carbon dioxide. *Journal of the Chinese Institute of Chemical Engineers* **2001**, *32*, 253-261.

(90) Wei, J. J.; Su, B. G.; Xing, H. B.; Zhang, H.; Yang, Q. W.; Ren, Q. L. Progress in Supercritical CO_2 Microemulsions with Hydrocarbon Surfactants. *Progress in Chemistry* **2009**, *21*, 1141-1148.

(91) Ye, X. G.; Wai, C. M. Making nanomaterials in supercritical fluids: A review. *J Chem. Educ.* **2003**, *80*, 198-204.

(92) O'Connor, C. J.; Kolesnichenko, V.; Carpenter, E.; Sangregorio, C.; Zhou, W. L.; Kumbhar, A.; Sims, J.; Agnoli, F. Fabrication and properties of magnetic particles with nanometer dimensions. *Synthetic Metals* **2001**, *122*, 547-557.

(93) O'Connor, C. J.; Seip, C. T.; Carpenter, E. E.; Li, S. C.; John, V. T. Synthesis and reactivity of nanophase ferrites in reverse micellar solutions. *Nanostructured Materials* **1999**, *12*, 65-70.

(94) Willard, M. A.; Kurihara, L. K.; Carpenter, E. E.; Calvin, S.; Harris, V. G. Chemically prepared magnetic nanoparticles. *International Materials Reviews* **2004**, *49*, 125-170.

(95) Pileni, M. P. Water-In-Oil Colloidal Droplets Used As Microreactors. *Advances in Colloid and Interface Science* **1993**, *46*, 139-163.

(96) Pileni, M. P. The role of soft colloidal templates in controlling the size and shape of inorganic nanocrystals. *Nature Materials* **2003**, *2*, 145-150.

(97) Pileni, M. P.; Zemb, T.; Petit, C. Solubilization by Reverse Micelles - Solute Localization and Structure Perturbation. *Chemical Physics Letters* **1985**, *118*, 414-420.

(98) Raj, K.; Moskowitz, B.; Casciari, R. Advances In Ferrofluid Technology. *Journal of Magnetism and Magnetic Materials* **1995**, *149*, 174-180.

(99) Perez, J. A. L.; Quintela, M. A. L.; Mira, J.; Rivas, J.; Charles, S. W. Advances in the preparation of magnetic nanoparticles by the microemulsion method. *Journal of Physical Chemistry B* **1997**, *101*, 8045-8047.

(100) Lopez-Perez, J. A.; Lopez-Quintela, M. A.; Mira, J.; Rivas, J. Preparation of magnetic fluids with particles obtained in microemulsions. *Ieee Transactions on Magnetics* **1997**, *33*, 4359-4362.

(101) Mira, J.; Lopez-Perez, J. A.; Lopez-Quintela, M. A.; Rivas, J. In *Synthesis and Properties of Mechanically Alloyed and Nanocrystalline Materials, Pts 1 and 2 - Ismanam-96*; Fiorani, D., Magini, M., Eds. 1997; Vol. 235-, p 297-302.

(102) Zhao, L.; Zhao, Y. F.; Han, Y. Pore Fabrication in Various Silica-Based Nanoparticles by Controlled Etching. *Langmuir* **2010**, *26*, 11784-11789.

(103) Tartaj, P.; Serna, C. J. Synthesis of monodisperse superparamagnetic Fe/silica nanospherical composites. *J. Am. Chem. Soc.* **2003**, *125*, 15754-15755.

(104) Cavalier, M.; Walls, M.; Lisiecki, I.; Pileni, M. P. How Can the Nanocrystallinity of 7 nm Spherical Co Nanoparticles Dispersed in Solution Be Improved? *Langmuir* **2011**, *27*, 5014-5020.

(105) Pileni, M. P. Reverse micelles used as templates: a new understanding in nanocrystal growth. *Journal of Experimental Nanoscience* **2006**, *1*, 13-27.

(106) Tago, T.; Hatsuta, T.; Nagase, R.; Kishida, M.; Wakabayashi, K. Preparation of silica-coated Co-Fe_3O_4 nanoparticles and their magnetic properties. *Kagaku Kogaku Ronbunshu* **2001**, *27*, 288-290.

(107) Pileni, M. P.; Ngo, A. T. Mesoscopic structures maghemite nanocrystals: Fabrication, magnetic properties, and uses. *Chemphyschem* **2005**, *6*, 1027-1034.

(108) Yi, D. K.; Lee, S. S.; Papaefthymiou, G. C.; Ying, J. Y. Nanoparticle architectures templated by SiO_2/Fe_2O_3 nanocomposites. *Chem. Mat.* **2006**, *18*, 614-619.

(109) Im, S. H.; Herricks, T.; Lee, Y. T.; Xia, Y. N. Synthesis and characterization of monodisperse silica colloids loaded with superparamagnetic iron oxide nanoparticles. *Chemical Physics Letters* **2005**, *401*, 19-23.

(110) Ban, I.; Drofenik, M.; Makovec, D. In *Current Research in Advanced Materials and Processes*; Uskokovic, D. P., Milonjic, S. K., Rakovic, D. I., Eds. 2005; Vol. 494, p 161-165.

(111) Gyergyek, S.; Makovec, D.; Kodre, A.; Arcon, I.; Jagodic, M.; Drofenik, M. Influence of synthesis method on structural and magnetic properties of cobalt ferrite nanoparticles. *Journal of Nanoparticle Research* **2010**, *12*, 1263-1273.

(112) Vestal, C. R.; Zhang, Z. J. Synthesis and magnetic characterization of Mn and Co spinel ferrite-silica nanoparticles with tunable magnetic core. *Nano Letters* **2003**, *3*, 1739-1743.

(113) Vestal, C. R.; Zhang, Z. J. Magnetic spinel ferrite nanoparticles from microemulsions. *International Journal of Nanotechnology* **2004**, *1*, 240-263.

(114) Grasset, F.; Labhsetwar, N.; Li, D.; Park, D. C.; Saito, N.; Haneda, H.; Cador, O.; Roisnel, T.; Mornet, S.; Duguet, E.; Portier, J.; Etourneau, J. Synthesis and magnetic characterization of zinc ferrite nanoparticles with different environments: Powder, colloidal solution, and zinc ferrite-silica core-shell nanoparticles. *Langmuir* **2002**, *18*, 8209-8216.

(115) Cellesi, F.; Tirelli, N. Sol-gel synthesis at neutral pH in W/O microemulsion: A method for enzyme nanoencapsulation in silica gel nanoparticles. *Colloids and Surfaces a-Physicochemical and Engineering Aspects* **2006**, *288*, 52-61.

(116) Chen, Q.; Larismaa, J.; Keski-Honkola, A.; Vilonen, K.; Soderberg, O.; Hannula, S. P. Effect of Synthesis Time on Morphology of Hollow Porous Silica Microspheres. *Materials Science-Medziagotyra* **2012**, *18*, 66-71.

(117) Inada, M.; Enomoto, N.; Hojo, J. Synthesis and photocatalytic activity of mesoporous SiO_2-TiO_2. *Research on Chemical Intermediates* **2010**, *36*, 115-120.

(118) Liu, Y. M.; Wu, Y. C. Synthesis of europium-doped silica microspheres using the sol-gel microencapsulation method. *J. Sol-Gel Sci. Technol.* **2012**, *63*, 36-44.

(119) Oh, C.; Lee, Y. G.; Choi, T. S.; Jon, C. U.; Oh, S. G. Facile synthesis of PEG-silica hybrid particles using one-step sol-gel reaction in aqueous solution. *Colloids and Surfaces a-Physicochemical and Engineering Aspects* **2009**, *349*, 145-150.

(120) Scholz, S.; Lercher, J. A. Hierarchically Structured Millimeter-Sized (Organo) Silica Spheres with a Macroporous Shell and a Meso/Microporous Core. *Chem. Mat.* **2011**, *23*, 2091-2099.

(121) Tapeinos, C.; Kartsonakis, I.; Liatsi, P.; Daniilidis, I.; Kordas, G. Synthesis and characterization of magnetic nanocontainers. *Journal of the American Ceramic Society* **2008**, *91*, 1052-1056.

(122) Lin, J. C.; Dipre, J. T.; Yates, M. Z. Microemulsion-directed synthesis of molecular sieve fibers. *Chem. Mat.* **2003**, *15*, 2764-2773.

(123) Shchukin, D. G.; Sukhorukov, G. B. Nanoparticle synthesis in engineered organic nanoscale reactors. *Adv. Mater.* **2004**, *16*, 671-682.

(124) Ago, H.; Ohshima, S.; Uchida, K.; Komatsu, T.; Yumura, M. Carbon nanotube synthesis using colloidal solution of metal nanoparticles. *Physica B-Condensed Matter* **2002**, *323*, 306-307.

(125) Saito, T.; Ohshima, S.; Xu, W. C.; Ago, H.; Yumura, M.; Iijima, S. Size control of metal nanoparticle catalysts for the gas-phase synthesis of single-walled carbon nanotubes. *Journal of Physical Chemistry B* **2005**, *109*, 10647-10652.

(126) Shangguan, T.; Cabral-Lilly, D.; Purandare, U.; Godin, N.; Ahl, P.; Janoff, A.; Meers, P. A novel N-acyl phosphatidylethanolamine-containing delivery vehicle for spermine-condensed plasmid DNA. *Gene Therapy* **2000**, *7*, 769-783.

(127) Legrand, J.; Petit, C.; Pileni, M. P. Domain shapes and superlattices made of 8 nm cobalt nanocrystals: Fabrication and magnetic properties. *Journal of Physical Chemistry B* **2001**, *105*, 5643-5646.

(128) Pileni, M. P. Magnetic fluids: Fabrication, magnetic properties, and organization of nanocrystals. *Advanced Functional Materials* **2001**, *11*, 323-336.

(129) Pileni, M. P. Nanocrystal self-assemblies: Fabrication and collective properties. *Journal of Physical Chemistry B* **2001**, *105*, 3358-3371.

(130) Courty, A.; Richardi, J.; Albouy, P. A.; Pileni, M. P. How To Control the Crystalline Structure of Supracrystals of 5-nm Silver Nanocrystals. *Chem. Mat.* **2011**, *23*, 4186-4192.

(131) Asua, J. M. Miniemulsion polymerization. *Progress in Polymer Science* **2002**, *27*, 1283-1346.

(132) Dickinson, E. Food emulsions and foams: Stabilization by particles. *Current Opinion in Colloid & Interface Science* **2010**, *15*, 40-49.

(133) Lopez-Quintela, M. A.; Tojo, C.; Blanco, M. C.; Rio, L. G.; Leis, J. R. Microemulsion dynamics and reactions in microemulsions. *Current Opinion in Colloid & Interface Science* **2004**, *9*, 264-278.

(134) Uskokovic, V.; Drofenik, M. Synthesis of materials within reverse micelles. *Surface Review and Letters* **2005**, *12*, 239-277.

(135) Fletcher, P. D. I.; Howe, A. M.; Robinson, B. H. The kinetics of solubilisate exchange between water droplets of a water-in-oil microemulsion. *Journal of the Chemical Society, Faraday Transactions 1: Physical Chemistry in Condensed Phases* **1987**, *83*, 985-1006.

(136) Faraji, M.; Yamini, Y.; Rezaee, M. Magnetic Nanoparticles: Synthesis, Stabilization, Functionalization, Characterization, and Applications. *Journal of the Iranian Chemical Society* **2010**, *7*, 1-37.

(137) Hyeon, T.; Lee, S. S.; Park, J.; Chung, Y.; Na, H. B. Synthesis of Highly Crystalline and Monodisperse Maghemite Nanocrystallites without a Size-Selection Process. *J. Am. Chem. Soc.* **2001**, *123*, 12798-12801.

(138) Sun, S. H.; Zeng, H.; Robinson, D. B.; Raoux, S.; Rice, P. M.; Wang, S. X.; Li, G. X. Monodisperse MFe_2O_4 (M = Fe, Co, Mn) nanoparticles. *J. Am. Chem. Soc.* **2004**, *126*, 273-279.

(139) Kwon, S. G.; Piao, Y.; Park, J.; Angappane, S.; Jo, Y.; Hwang, N. M.; Park, J. G.; Hyeon, T. Kinetics of monodisperse iron oxide nanocrystal formation by "heating-up" process. *J. Am. Chem. Soc.* **2007**, *129*, 12571-12584.

(140) Angermann, A.; Topfer, J. Synthesis of magnetite nanoparticles by thermal decomposition of ferrous oxalate dihydrate. *J. Mater. Sci.* **2008**, *43*, 5123-5130.

(141) Goya, G. F.; Berquo, T. S.; Fonseca, F. C.; Morales, M. P. Static and dynamic magnetic properties of spherical magnetite nanoparticles. *Journal of Applied Physics* **2003**, *94*, 3520-3528.

(142) Roca, A. G.; Morales, M. P.; O'Grady, K.; Serna, C. J. Structural and magnetic properties of uniform magnetite nanoparticles prepared by high temperature decomposition of organic precursors. *Nanotechnology* **2006**, *17*, 2783-2788.

(143) Roca, A. G.; Morales, M. P.; Serna, C. J. Synthesis of monodispersed magnetite particles from different organometallic precursors. *Ieee Transactions on Magnetics* **2006**, *42*, 3025-3029.

(144) Ravikumar, C.; Bandyopadhyaya, R. Mechanistic Study on Magnetite Nanoparticle Formation by Thermal Decomposition and Coprecipitation Routes. *J. Phys. Chem. C* **2011**, *115*, 1380-1387.

(145) Li, D.; Jiang, D. L.; Chen, M.; Xie, J. M.; Wu, Y. Y.; Dang, S. C.; Zhang, J. X. An easy fabrication of monodisperse oleic acid-coated Fe_3O_4 nanoparticles. *Materials Letters* **2010**, *64*, 2462-2464.

(146) Wu, S.; Sun, A. Z.; Zhai, F. Q.; Wang, J.; Xu, W. H.; Zhang, Q.; Volinsky, A. A. Fe_3O_4 magnetic nanoparticles synthesis from tailings by ultrasonic chemical co-precipitation. *Materials Letters* **2011**, *65*, 1882-1884.

(147) Zhang, S. J.; Liu, X. H.; Zhou, L. P.; Peng, W. J. Magnetite nanostructures: One-pot synthesis, superparamagnetic property and application in magnetic resonance imaging. *Materials Letters* **2012**, *68*, 243-246.

(148) Daou, T. J.; Pourroy, G.; Begin-Colin, S.; Greneche, J. M.; Ulhaq-Bouillet, C.; Legare, P.; Bernhardt, P.; Leuvrey, C.; Rogez, G. Hydrothermal synthesis of monodisperse magnetite nanoparticles. *Chem. Mat.* **2006**, *18*, 4399-4404.

(149) Ge, J. P.; Hu, Y. X.; Biasini, M.; Beyermann, W. P.; Yin, Y. D. Superparamagnetic magnetite colloidal nanocrystal clusters. *Angew. Chem.-Int. Edit.* **2007**, *46*, 4342-4345.

(150) Ge, J. P.; Hu, Y. X.; Biasini, M.; Dong, C. L.; Guo, J. H.; Beyermann, W. P.; Yin, Y. D. One-step synthesis of highly water-soluble magnetite colloidal nanocrystals. *Chem.-Eur. J.* **2007**, *13*, 7153-7161.

(151) Mizutani, N.; Iwasaki, T.; Watano, S.; Yanagida, T.; Kawai, T. Size control of magnetite nanoparticles in hydrothermal synthesis by coexistence of lactate and sulfate ions. *Current Applied Physics* **2010**, *10*, 801-806.

(152) Zhang, Z. J.; Chen, X. Y.; Wang, B. N.; Shi, C. W. Hydrothermal synthesis and self-assembly of magnetite (Fe_3O_4) nanoparticles with the magnetic and electrochemical properties. *Journal of Crystal Growth* **2008**, *310*, 5453-5457.

(153) Xu, C. B.; Teja, A. S. Continuous hydrothermal synthesis of iron oxide and PVA-protected iron oxide nanoparticles. *Journal of Supercritical Fluids* **2008**, *44*, 85-91.

(154) Komarneni, S.; Katsuki, H. Nanophase materials by a novel microwave-hydrothermal process. *Pure Appl. Chem.* **2002**, *74*, 1537-1543.

(155) Balasubramaniam, C.; Khollam, Y. B.; Bannerjee, I.; Bakare, P. P.; Date, S. K.; Das, A. K.; Bhoraskar, S. DC thermal arc-plasma preparation of nanometric and stoichiometric spherical magnetite (Fe_3O_4) powders. *Materials Letters* **2004**, *58*, 3958-3962.

(156) Dinega, D. P.; Bawendi, M. G. A solution-phase chemical approach to a new crystal structure of cobalt. *Angew. Chem.-Int. Edit.* **1999**, *38*, 1788-1791.

(157) Tracy, J. B.; Weiss, D. N.; Dinega, D. P.; Bawendi, M. G. Exchange biasing and magnetic properties of partially and fully oxidized colloidal cobalt nanoparticles. *Physical Review B* **2005**, *72*.

(158) Mazaleyrat, F.; Ammar, M.; LoBue, M.; Bonnet, J. P.; Audebert, P.; Wang, G. Y.; Champion, Y.; Hytch, M.; Snoeck, E. Silica coated nanoparticles: Synthesis, magnetic properties and spin structure. *Journal of Alloys and Compounds* **2009**, *483*, 473-478.

(159) Mourdikoudis, S.; Simeonidis, K.; Tsiaoussis, I.; Dendrinou-Samara, C.; Angelakeris, M.; Kalogirou, O. Impact of synthesis parameters on structural and magnetic characteristics of Co-based nanoparticles. *Journal of Nanoparticle Research* **2009**, *11*, 1477-1484.

(160) Yin, X. J.; Peng, K.; Hu, A. P.; Zhou, L. P.; Chen, J. H.; Du, Y. W. Preparation and characterization of core-shell structured Co/SiO_2 nanosphere. *Journal of Alloys and Compounds* **2009**, *479*, 372-375.

(161) Hess, P. H.; Parker, P. H. Polymers For Stabilization of Colloidal Cobalt Particles. *Journal of Applied Polymer Science* **1966**, *10*, 1915-&.

(162) Ould-Ely, T.; Amiens, C.; Chaudret, B.; Snoeck, E.; Verelst, M.; Respaud, M.; Broto, J. M. Synthesis of nickel nanoparticles. Influence of aggregation induced by modification of poly(vinylpyrrolidone) chain length on their magnetic properties. *Chem. Mat.* **1999**, *11*, 526-+.

(163) Rivas, J.; Sanchez, R. D.; Fondado, A.; Izco, C.; Garciabastida, A. J.; Garciaotero, J.; Mira, J.; Baldomir, D.; Gonzalez, A.; Lado, I.; Quintela, M. A. L.; Oseroff, S. B. Structural And Magnetic Characterization of Co Particles Coated With Ag. *Journal of Applied Physics* **1994**, *76*, 6564-6566.

(164) Carpenter, E. E.; Sangregorio, C.; O'Connor, C. J. Effects of shell thickness on blocking temperature of nanocomposites of metal particles with gold shells. *Ieee Transactions on Magnetics* **1999**, *35*, 3496-3498.

(165) Sobal, N. S.; Hilgendorff, M.; Mohwald, H.; Giersig, M.; Spasova, M.; Radetic, T.; Farle, M. Synthesis and structure of colloidal bimetallic nanocrystals: The non-alloying system Ag/Co. *Nano Letters* **2002**, *2*, 621-624.

(166) Nikitenko, S. I.; Koltypin, Y.; Palchik, O.; Felner, I.; Xu, X. N.; Gedanken, A. Synthesis of highly magnetic, air-stable iron iron carbide nanocrystalline particles by using power ultrasound. *Angew. Chem.-Int. Edit.* **2001**, *40*, 4447.

(167) Ohmori, M.; Matijevic, E. Preparation and Properties of Uniform Coated Colloidal Particles .7. Silica On Hematite. *Journal of Colloid and Interface Science* **1992**, *150*, 594-598.

(168) Ohmori, M.; Matijevic, E. Preparation and Properties of Uniform Coated Inorganic Colloidal Particles .8. Silica On Iron. *Journal of Colloid and Interface Science* **1993**, *160*, 288-292.

(169) Correa-Duarte, M. A.; Giersig, M.; Kotov, N. A.; Liz-Marzan, L. M. Control of packing order of self-assembled monolayers of magnetite nanoparticles with and without SiO_2 coating by microwave irradiation. *Langmuir* **1998**, *14*, 6430-6435.

(170) Lu, Y.; Yin, Y.; Mayers, B. T.; Xia, Y. Modifying the Surface Properties of Superparamagnetic Iron Oxide Nanoparticles through a Sol-Gel Approach. *Nano Letters* **2002**, *2*, 183-186.

(171) Liu, Q. X.; Xu, Z. H.; Finch, J. A.; Egerton, R. A novel two-step silica-coating process for engineering magnetic nanocomposites. *Chem. Mat.* **1998**, *10*, 3936-3940.

(172) Tago, T.; Hatsuta, T.; Miyajima, K.; Kishida, M.; Tashiro, S.; Wakabayashi, K. Novel synthesis of silica-coated ferrite nanoparticles prepared using water-in-oil microemulsion. *Journal of the American Ceramic Society* **2002**, *85*, 2188-2194.

(173) Liz-Marzan, L. M.; Giersig, M.; Mulvaney, P. Homogeneous silica coating of vitreophobic colloids. *Chem. Commun.* **1996**, 731-732.

(174) Hardikar, V. V.; Matijevic, E. Coating of nanosize silver particles with silica. *Journal of Colloid and Interface Science* **2000**, *221*, 133-136.

(175) Kobayashi, Y.; Horie, M.; Konno, M.; Rodriguez-Gonzalez, B.; Liz-Marzan, L. M. Preparation and Properties of Silica-Coated Cobalt Nanoparticlesâ€ *The Journal of Physical Chemistry B* **2003**, *107*, 7420-7425.

(176) Vanblaaderen, A.; Vrij, A. Synthesis and characterization of colloidal dispersions of fluorescent, monodisperse silica spheres. *Langmuir* **1992**, *8*, 2921-2931.

(177) Makarova, O. V.; Ostafin, A. E.; Miyoshi, H.; Norris, J. R.; Meisel, D. Adsorption and encapsulation of fluorescent probes in nanoparticles. *Journal of Physical Chemistry B* **1999**, *103*, 9080-9084.

(178) Nyffenegger, R.; Quellet, C.; Ricka, J. Synthesis of Fluorescent, Monodisperse, Colloidal Silica Particles. *Journal of Colloid and Interface Science* **1993**, *159*, 150-157.

(179) Verhaegh, N. A. M.; Vanblaaderen, A. Dispersions of Rhodamine-Labeled Silica Spheres - Synthesis, Characterization, and Fluorescence Confocal Scanning Laser Microscopy. *Langmuir* **1994**, *10*, 1427-1438.

(180) Wang, L.; Tan, W. H. Multicolor FRET silica nanoparticles by single wavelength excitation. *Nano Letters* **2006**, *6*, 84-88.

(181) Yang, W.; Zhang, C. G.; Qu, H. Y.; Yang, H. H.; Xu, J. G. Novel fluorescent silica nanoparticle probe for ultrasensitive immunoassays. *Anal. Chim. Acta* **2004**, *503*, 163-169.

(182) Bakalova, R.; Zhelev, Z.; Aoki, I.; Ohba, H.; Imai, Y.; Kanno, I. Silica-shelled single quantum dot micelles as imaging probes with dual or multimodality. *Anal. Chem.* **2006**, *78*, 5925-5932.

(183) Zhelev, Z.; Ohba, H.; Bakalova, R. Single quantum dot-micelles coated with silica shell as potentially non-cytotoxic fluorescent cell tracers. *J. Am. Chem. Soc.* **2006**, *128*, 6324-6325.

(184) Giaume, D.; Poggi, M.; Casanova, D.; Mialon, G.; Lahlil, K.; Alexandrou, A.; Gacoin, T.; Boilot, J. P. Organic functionalization of luminescent oxide nanoparticles toward their application as biological probes. *Langmuir* **2008**, *24*, 11018-11026.

(185) Vroman, L. Surface Charge, Protein Adsorption, and Thrombosis. *Science* **1974**, *184*, 585-586.

(186) Sen, T.; Sebastianelli, A.; Bruce, I. J. Mesoporous silica-magnetite nanocomposite: Fabrication and applications in magnetic bioseparations. *J. Am. Chem. Soc.* **2006**, *128*, 7130-7131.

(187) Deng, Y.; Qi, D.; Deng, C.; Zhang, X.; Zhao, D. Superparamagnetic high-magnetization microspheres with an Fe_3O_4@SiO_2 core and perpendicularly aligned mesoporous SiO2 shell for removal of microcystins. *J. Am. Chem. Soc.* **2008**, *130*, 28.

(188) Coskun, M.; Korkmaz, M.; Firat, T.; Jaffari, G. H.; Shah, S. I. Synthesis of SiO2 coated $NiFe_2O_4$ nanoparticles and the effect of SiO_2 shell thickness on the magnetic properties. *Journal of Applied Physics* **2010**, *107*.

(189) Zhou, B.; Liu, Z. G.; Wang, X. J.; Sui, Y.; Huang, X. Q.; Lu, Z.; Su, W. H. Effect of SiO_2 coating on the magnetic properties of Ni-Zn ferrite. *Physica B-Condensed Matter* **2010**, *405*, 374-378.

(190) Zhu, J. H.; Wei, S. Y.; Lee, I. Y.; Park, S.; Willis, J.; Haldolaarachchige, N.; Young, D. P.; Luo, Z. P.; Guo, Z. H. Silica stabilized iron particles toward anti-corrosion magnetic polyurethane nanocomposites. *Rsc Advances* **2012**, *2*, 1136-1143.

(191) Kao, H. M.; Shen, T. Y.; Wu, J. D.; Lee, L. P. Control of ordered structure and morphology of cubic mesoporous silica SBA-1 via direct synthesis of thiol-functionalization. *Microporous and Mesoporous Materials* **2008**, *110*, 461-471.

(192) Westcott, S. L.; Oldenburg, S. J.; Lee, T. R.; Halas, N. J. Formation and adsorption of clusters of gold nanoparticles onto functionalized silica nanoparticle surfaces. *Langmuir* **1998**, *14*, 5396-5401.

(193) Yu, Y.; Addai-Mensah, J.; Losic, D. Functionalized diatom silica microparticles for removal of mercury ions. *Science and Technology of Advanced Materials* **2012**, *13*.

(194) Chang, B. S.; Guo, J.; Liu, C. Y.; Qian, J.; Yang, W. L. Surface functionalization of magnetic mesoporous silica nanoparticles for controlled drug release. *J. Mater. Chem.* **2010**, *20*, 9941-9947.

(195) Chong, A. S. M.; Zhao, X. S. Design of large-pore mesoporous materials for immobilization of penicillin G acylase biocatalyst. *Catalysis Today* **2004**, *93-5*, 293-299.

(196) Kralj, S.; Drofenik, M.; Makovec, D. Controlled surface functionalization of silica-coated magnetic nanoparticles with terminal amino and carboxyl groups. *Journal of Nanoparticle Research* **2011**, *13*, 2829-2841.

(197) Kumar, R.; Roy, I.; Hulchanskyy, T. Y.; Goswami, L. N.; Bonoiu, A. C.; Bergey, E. J.; Tramposch, K. M.; Maitra, A.; Prasad, P. N. Covalently dye-linked, surface-controlled, and bioconjugated organically modified silica nanoparticles as targeted probes for optical imaging. *ACS Nano* **2008**, *2*, 449-456.

(198) Schiestel, T.; Brunner, H.; Tovar, G. E. M. Controlled surface functionalization of silica nanospheres by covalent conjugation reactions and preparation of high density streptavidin nanoparticles. *Journal of Nanoscience and Nanotechnology* **2004**, *4*, 504-511.

(199) Zeng, Z.; Yu, J.; Guo, Z. X. Preparation of polymer/silica composite nanoparticles bearing carboxyl groups on the surface via emulsifier-free emulsion copolymerization. *Journal of Polymer Science Part a-Polymer Chemistry* **2005**, *43*, 2826-2835.

(200) Kar, M.; Pauline, M.; Sharma, K.; Kumaraswamy, G.; Sen Gupta, S. Synthesis of Poly-L-glutamic Acid Grafted Silica Nanoparticles and Their Assembly into Macroporous Structures. *Langmuir* **2011**, *27*, 12124-12133.

(201) Tissandier, C.; Diop, N.; Martini, M.; Roux, S.; Tillernent, O.; Hamaide, T. One-Pot Synthesis of Hybrid Multifunctional Silica Nanoparticles with Tunable Coating by Click Chemistry in Reverse W/O Microemulsion. *Langmuir* **2012**, *28*, 209-218.

(202) Wu, T.; Zhang, Q. Q.; Hu, J. M.; Zhang, G. Y.; Liu, S. Y. Composite silica nanospheres covalently anchored with gold nanoparticles at the outer periphery of thermoresponsive polymer brushes. *J. Mater. Chem.* **2012**, *22*, 5155-5163.

(203) Coll, C.; Mondragon, L.; Martinez-Manez, R.; Sancenon, F.; Marcos, M. D.; Soto, J.; Amoros, P.; Perez-Paya, E. Enzyme-Mediated Controlled Release Systems by Anchoring Peptide Sequences on Mesoporous Silica Supports. *Angew. Chem.-Int. Edit.* **2011**, *50*, 2138-2140.

(204) Balamurugan, S. S.; Soto-Cantu, E.; Cueto, R.; Russo, P. S. Preparation of Organosoluble Silica-Polypeptide Particles by "Click" Chemistry. *Macromolecules* **2010**, *43*, 62-70.

(205) Ranjan, R.; Brittain, W. J. Tandem RAFT polymerization and click chemistry: An efficient approach to surface modification. *Macromol. Rapid Commun.* **2007**, *28*, 2084-2089.

(206) Ranjan, R.; Brittain, W. J. Combination of living radical polymerization and click chemistry for surface modification. *Macromolecules* **2007**, *40*, 6217-6223.

(207) Park, S. J.; Taton, T. A.; Mirkin, C. A. Array-based electrical detection of DNA with nanoparticle probes. *Science* **2002**, *295*, 1503-1506.

(208) Mout, R.; Moyano, D. F.; Rana, S.; Rotello, V. M. Surface functionalization of nanoparticles for nanomedicine. *Chemical Society Reviews* **2012**, *41*, 2539-2544.

(209) Quang, D. V.; Sarawade, P. B.; Hilonga, A.; Kim, J. K.; Chai, Y. G.; Kim, S. H.; Ryu, J. Y.; Kim, H. T. Preparation of amino functionalized silica micro beads by dry method for supporting silver nanoparticles with antibacterial properties. *Colloids and Surfaces a-Physicochemical and Engineering Aspects* **2011**, *389*, 118-126.

(210) Assink, R. A.; Kay, B. D. Sol-gel kinetics I. Functional group kinetics. *Journal of Non-Crystalline Solids* **1988**, *99*, 359-370.

(211) Rother, D.; Sen, T.; East, D.; Bruce, I. J. Silicon, silica and its surface patterning/activation with alkoxy- and amino-silanes for nanomedical applications. *Nanomedicine* **2012**, *6*, 281-300.

(212) Acosta, E. J.; Carr, C. S.; Simanek, E. E.; Shantz, D. F. Engineering nanospaces: Iterative synthesis of melamine-based dendrimers on amine-functionalized SBA-15 leading to complex hybrids with controllable chemistry and porosity. *Adv. Mater.* **2004**, *16*, 985.

(213) Ford, D. M.; Simanek, E. E.; Shantz, D. F. Engineering nanospaces: ordered mesoporous silicas as model substrates for building complex hybrid materials. *Nanotechnology* **2005**, *16*, S458-S475.

(214) Luechinger, M.; Prins, R.; Pirngruber, G. D. Functionalization of silica surfaces with mixtures of 3-aminopropyl and methyl groups. *Microporous and Mesoporous Materials* **2005**, *85*, 111-118.

(215) Beck, J. S.; Vartuli, J. C.; Roth, W. J.; Leonowicz, M. E.; Kresge, C. T.; Schmitt, K. D.; Chu, C. T. W.; Olson, D. H.; Sheppard, E. W.; McCullen, S. B.; Higgins, J. B.; Schlenker, J. L. A New Family of Mesoporous Molecular-Sieves Prepared With Liquid-Crystal Templates. *J. Am. Chem. Soc.* **1992**, *114*, 10834-10843.

(216) Burkett, S. L.; Sims, S. D.; Mann, S. Synthesis of hybrid inorganic-organic mesoporous silica by co-condensation of siloxane and organosiloxane precursors. *Chem. Commun.* **1996**, 1367-1368.

(217) Luechinger, M.; Prins, R.; Pirngruber, G. D. Functionalization of silica surfaces with mixtures of 3-aminopropyl and methyl groups. *Microporous and Mesoporous Materials* **2005**, *85*, 111-118.

(218) Soto-Cantu, E.; Turksen-Selcuk, S.; Qiu, J. H.; Zhou, Z.; Russo, P. S.; Henk, M. C. Silica-Polypeptide Composite Particles: Controlling Shell Growth. *Langmuir* **2011**, *26*, 15604-15613.

(219) Wulff, G.; Heide, B.; Helfmeier, G. Molecular Recognition Through The Exact Placement of Functional-Groups On Rigid Matrices Via a Template Approach. *J. Am. Chem. Soc.* **1986**, *108*, 1089-1091.

(220) Wulff, G.; Heide, B.; Helfmeier, G. Enzyme-Analog Built Polymers .24. On The Distance Accuracy of Functional-Groups In Polymers And Silicas Introduced by a Template Approach. *Reactive Polymers* **1987**, *6*, 299-310.

(221) Katz, A.; Davis, M. E. Molecular imprinting of bulk, microporous silica. *Nature* **2000**, *403*, 286-289.

(222) Bass, J. D.; Katz, A. Thermolytic Synthesis of Imprinted Amines in Bulk Silica. *Chem. Mat.* **2003**, *15*, 2757-2763.

(223) McKittrick, M. W.; Jones, C. W. Toward single-site functional materials-preparation of amine-functionalized surfaces exhibiting site-isolated behavior. *Chem. Mat.* **2003**, *15*, 1132-1139.

(224) McKittrick, M. W.; Jones, C. W. Modulating the reactivity of an organometallic catalyst via immobilization on a spatially patterned silica surface. *Chem. Mat.* **2005**, *17*, 4758-4761.

(225) Khosroshahi, M. E.; Ghazanfari, L. Synthesis and functionalization of SiO2 coated Fe3O4 nanoparticles with amine groups based on self-assembly. *Materials Science & Engineering C-Materials for Biological Applications* **2012**, *32*, 1043-1049.

(226) Lombardo, M. V.; Videla, M.; Calvo, A.; Requejo, F. G.; Soler-Illia, G. Aminopropyl-modified mesoporous silica SBA-15 as recovery agents of Cu(II)-sulfate solutions: Adsorption efficiency, functional stability and reusability aspects. *Journal of Hazardous Materials* **2012**, *223*, 53-62.

(227) Nikolic, M. P.; Giannakopoulos, K. P.; Bokorov, M.; Srdic, V. V. Effect of surface functionalization on synthesis of mesoporous silica core/shell particles. *Microporous and Mesoporous Materials* **2012**, *155*, 8-13.

(228) Martin-Palma, R. J.; Manso, M.; Perez-Rigueiro, J.; Garcia-Ruiz, J. P.; Martinez-Duart, J. M. Surface biofunctionalization of materials by amine groups. *J. Mater. Res.* **2004**, *19*, 2415-2420.

(229) Recio-Sanchez, G.; Dominguez-Canizares, G.; Manso, M.; Preda, I.; Torres-Costa, V.; Gutierrez, A.; Soriano, L.; Martin-Palma, R. J. Surface Functionalization of Nanostructured Porous Silicon by APTS: Toward the Fabrication of Electrical Biosensors of Bacterium Escherichia coli. *Current Nanoscience* **2011**, *7*, 178-182.

(230) Silvan, M. M.; Messina, G. M. L.; Montero, I.; Satriano, C.; Ruiz, J. P. G.; Marletta, G. Aminofunctionalization and sub-micrometer patterning on silicon through silane doped agarose hydrogels. *J. Mater. Chem.* **2009**, *19*, 5226-5233.

(231) Liu, D.; Li, Y.; Deng, J.; Yang, W. Synthesis and characterization of magnetic Fe_3O_4-silica-poly(Î³-benzyl-L-glutamate) composite microspheres. *Reactive and Functional Polymers* **2011**, *71*, 1040-1044.

(232) Fong, B.; Russo, P. S. Organophilic colloidal particles with a synthetic polypeptide coating. *Langmuir* **1999**, *15*, 4421-4426.

(233) Fong, B.; Turksen, S.; Russo, P. S.; Stryjewski, W. Colloidal crystals of silica-homopolypeptide composite particles. *Langmuir* **2004**, *20*, 266-269.

(234) Heise, A.; Menzel, H.; Yim, H.; Foster, M. D.; Wieringa, R. H.; Schouten, A. J.; Erb, V.; Stamm, M. Grafting of polypeptides on solid substrates by initiation of N-carboxyanhydride polymerization by amino-terminated self-assembled monolayers. *Langmuir* **1997**, *13*, 723-728.

(235) Ivanov, V. B.; Behnisch, J.; Hollander, A.; Mehdorn, F.; Zimmermann, H. Determination of functional groups on polymer surfaces using fluorescence labelling. *Surface and Interface Analysis* **1996**, *24*, 257-262.

(236) Xing, Y. J.; Borguet, E. Specificity and sensitivity of fluorescence labeling of surface species. *Langmuir* **2007**, *23*, 684-688.

(237) Janolino, V. G.; Swaisgood, H. E. A Spectrophotometric Assay For Solid-Phase Primary Amino-Groups. *Applied Biochemistry and Biotechnology* **1992**, *36*, 81-85.

(238) Aflori, M.; Drobota, M.; Timpu, D.; Barboiu, V. Studies of amine treatments influence on poly(ethyleneterepthalate) films. *Optoelectronics and Advanced Materials-Rapid Communications* **2008**, *2*, 291-295.

(239) Kay, C.; Lorthioir, O. E.; Parr, N. J.; Congreve, M.; McKeown, S. C.; Scicinski, J. J.; Ley, S. V. Solid-phase reaction monitoring - Chemical derivatization and off-bead analysis. *Biotechnology and Bioengineering* **2000**, *71*, 110-118.

(240) Gude, M.; Ryf, J.; White, P. D. An accurate method for the quantitation of Fmoc-derivatized solid phase supports. *Letters in Peptide Science* **2002**, *9*, 203-206.

(241) Kaiser, E.; Colescot.Rl; Bossinge.Cd; Cook, P. I. Color Test For Detection of Free Terminal Amino Groups In Solid-Phase Synthesis Of Peptides. *Analytical Biochemistry* **1970**, *34*, 595.

(242) McCaman, M. W.; Robins, E. Fluorimetric Method For Determination of Phenylalanine In Serum. *Journal of Laboratory and Clinical Medicine* **1962**, *59*, 885.

(243) Coussot, G.; Faye, C.; Ibrahim, A.; Ramonda, M.; Dobrijevic, M.; Le Postollec, A.; Granier, F.; Vandenabeele-Trambouze, O. Aminated dendritic surfaces characterization: a rapid and versatile colorimetric assay for estimating the amine density and coating stability. *Analytical and Bioanalytical Chemistry* **2011**, *399*, 2295-2302.

(244) Noel, S.; Liberelle, B.; Robitaille, L.; De Crescenzo, G. Quantification of Primary Amine Groups Available for Subsequent Biofunctionalization of Polymer Surfaces. *Bioconjugate Chem.* **2011**, *22*, 1690-1699.

(245) Chen, Y.; Zhang, Y. Q. Fluorescent quantification of amino groups on silica nanoparticle surfaces. *Analytical and Bioanalytical Chemistry* **2011**, *399*, 2503-2509.

(246) Soto-Cantu, E.; Cueto, R.; Koch, J.; Russo, P. S. Synthesis and Rapid Characterization of Amine-Functionalized Silica. *Langmuir* **2012**, *28*, 5562-5569.

(247) Bartholome, C.; Beyou, E.; Bourgeat-Lami, E.; Chaumont, P.; Lefebvre, F.; Zydowicz, N. Nitroxide-mediated polymerization of styrene initiated from the surface of silica nanoparticles. In situ generation and grafting of alkoxyamine initiators. *Macromolecules* **2005**, *38*, 1099-1106.

(248) Borase, T.; Iacono, M.; Ali, S. I.; Thornton, P. D.; Heise, A. Polypeptide core-shell silica nanoparticles with high grafting density by N-carboxyanhydride (NCA) ring opening polymerization as responsive materials and for bioconjugation. *Polymer Chemistry* **2012**, *3*, 1267-1275.

(249) Kricheldorf, H. R. *α-Aminoacid-N-Carboxyanhydrides and Related Materials* Springer: Berlin Heidelberg New York, 1987.

(250) Kricheldorf, H. R. *Models of Biopolymers by Ring-Opening Polymerization.*; CRC Press: Boca Raton, FL., 1990.

(251) Leuchs, H. Glycine-carbonic acid. *Berichte Der Deutschen Chemischen Gesellschaft* **1906**, *39*, 857-861.

(252) Leuchs, H.; Geiger, W. Concerning the anhydride on α-amino-N-carbonic acids and that of α-amino acids. *Berichte Der Deutschen Chemischen Gesellschaft* **1908**, *41*, 1721-1726.

(253) Leuchs, H.; Manasse, W. The isomerism of carboethoxy-glycylglycine ester. *Berichte Der Deutschen Chemischen Gesellschaft* **1907**, *40*, 3235-3249.

(254) Curtius, T. The formation of urea from azide from mono- and dialkyl acetic acid. *Journal Fur Praktische Chemie-Leipzig* **1930**, *125*, 152-156.

(255) Curtius, T. The migration of the alkalised malonic acids in α-amino acids. *Journal Fur Praktische Chemie-Leipzig* **1930**, *125*, 211-218.

(256) Curtius, T.; Sieber, W. Conversion of malonic acid in glycocoll and of methyl-malonic acid in α-alanine. *Berichte Der Deutschen Chemischen Gesellschaft* **1921**, *54*, 1430-1437.

(257) Curtius, T.; Sieber, W. Conversion of alkylated malonic acid in α-amino-acids. (II. Announcement - Synthesis of β-phenyl α-alanine and the α-amino-n-butyric acid). *Berichte Der Deutschen Chemischen Gesellschaft* **1922**, *55*, 1543-1558.

(258) Sigmund, F.; Wessely, F. Research on the α-amino-Nu-carbonic acid anhydrides. II. *Hoppe-Seylers Zeitschrift Fur Physiologische Chemie* **1926**, *157*, 91-105.

(259) Wessely, F.; Sigmund, F. Investigations on α-amino-N-carbonic acid anhydrides. III. (On knowledge of highly molecular compounds). *Hoppe-Seylers Zeitschrift Fur Physiologische Chemie* **1926**, *159*, 102-119.

(260) Wessely, F. Analysis of α-amino-N-carbonic acid anhydride. I. *Hoppe-Seylers Zeitschrift Fur Physiologische Chemie* **1925**, *146*, 72-90.

(261) Wessely, F.; John, M. Examinations on α-amino-N-carbonic acid anhydrides. V. Ancillary reactions of the decomposition of pyridin. *Hoppe-Seylers Zeitschrift Fur Physiologische Chemie* **1927**, *170*, 38-43.

(262) Wessely, F.; Riedl, K.; Tuppy, H. Untersuchungen Uber A-Amino-N-Carbonsaureanhydride .6. *Monatshefte Fur Chemie* **1950**, *81*, 861-872.

(263) Wessely, F.; Schlogl, K.; Wawersich, E. Konstitutionsermittlung Von Peptiden .3. Uber Eine Schonende Methode Zur Umwandlung Von Peptiden In Hydantoinpeptide .7. Uber Peptide. *Monatshefte Fur Chemie* **1952**, *83*, 1439-1447.

(264) Wessely, F.; Swoboda, W. Zur Darstellung Reiner Sekundarer Und Tertiarer Amine. *Monatshefte Fur Chemie* **1951**, *82*, 621-627.

(265) Fuchs, F. On N-carbonic acid-anhydride. *Berichte Der Deutschen Chemischen Gesellschaft* **1922**, *55*, 2943-2943.

(266) Coleman, D.; Farthing, A. C. Synthetic Polypeptides .2. Properties of Oxazolid-2-5-Diones and An Initial Study of The Preparation Of Polypeptides Therefrom. *Journal of the Chemical Society* **1950**, 3218-3222.

(267) Farthing, A. C. Synthetic Polypeptides .1. Synthesis of Oxazolid-2-5-Diones And A New Reaction of Glycine. *Journal of the Chemical Society* **1950**, 3213-3217.

(268) Farthing, A. C.; Reynolds, R. J. W. Anhydro-N-carboxy-DL-β-phenylalanine. *Nature* **1950**, *165*, 647-647.

(269) Fuller, W. D.; Verlander, M. S.; Goodman, M. Procedure for facile synthesis of amino-acid N-carboxyanhydrides. *Biopolymers* **1976**, *15*, 1869-1871.

(270) Cornille, F.; Copier, J.-L.; Senet, J.-P.; Robin, Y.; Isochem Paris Cedex US Patent 6479665, (Nov. 12, 2002).

(271) Oya, M.; Katakai, R.; Nakai, H.; Iwakura, Y. Novel synthesis of N-carboxy-α-amino acid anhydride. *Chemistry Letters* **1973**, 1143-1144.

(272) Dorman, L. C.; Shiang, W. R.; Meyers, P. A. Purification of γ-benzyl and γ-methyl L-glutamate N-carboxyanhydrides by rephosgenation. *Synthetic Communications* **1992**, *22*, 3257-3262.

(273) Daly, W. H.; Poché, D. The preparation of N-carboxyanhydrides of α-amino acids using bis(trichloromethyl)carbonate. *Tetrahedron Letters* **1988**, *29*, 5859-5862.

(274) Poche, D. S.; Daly, W. H.; Russo, P. S. Synthesis and some solution properties of poly(γ-stearyl α,L-glutamate). *Macromolecules* **1995**, *28*, 6745-6753.

(275) Wilder, R.; Mobashery, S. The use of triphosgene in preparation of n-carboxy-α-amino acid anhydrides. *Journal of Organic Chemistry* **1992**, *57*, 2755-2756.

(276) Poche, D. S.; Moore, M. J.; Bowles, J. L. An unconventional method for purifying the N-carboxyanhydride derivatives of γ-alkyl-L-glutamates. *Synthetic Communications* **1999**, *29*, 843-854.

(277) Szwarc, M. The kinetics and mechanism of N-carboxy-α-amino-acid anhydride (NCA) polymerisation to poly-amino acids. *Advance in Polymer Science* **1965**, *4*, 1-65.

(278) Dewey, R. S.; Schoenew.Ef; Joshua, H.; Paleveda, W. J.; Schwam, H.; Barkemey.H; Arison, B. H.; Veber, D. F.; Strachan, R. G.; Milkowsk.J; Denkewal.Rg; Hirschma.R Synthesis of peptides in aqueous medium .7. Preparation and use of 2,5-thiazolidinediones in peptide synthesis. *Journal of Organic Chemistry* **1971**, *36*, 49.

(279) Denkewal.Rg; Veber, D. F.; Holly, F. W.; Hirschma.R Studies on total synthesis of an enzyme .i. Objective and strategy. *J. Am. Chem. Soc.* **1969**, *91*, 502.

(280) Veber, D. F.; Hirschma.R; Denkewal.Rg Synthesis of peptides in aqueous medium .6. Synthesis of an unsymmetrical cystine peptide fragment of insulin. *Journal of Organic Chemistry* **1969**, *34*, 753.

(281) Dewey, R. S.; Schoenew.Ef; Joshua, H.; Paleveda, W. J.; Schwam, H.; Barkemey.H; Arison, B. H.; Veber, D. F.; Denkewal.Rg; Hirschma.R Synthesis of peptides in aqueous medium .v. Preparation and use of 2,5-thiazolidinediones (ntas) . Use of ^{13}C-H nuclear magnetic resonance signal as internal standard for quantitative studies. *J. Am. Chem. Soc.* **1968**, *90*, 3254.

(282) Hirschma.R; Strachan, R. G.; Schwam, H.; Schoenew.Ef; Joshua, H.; Barkemey.B; Veber, D. F.; Paleveda, W. J.; Jacob, T. A.; Beesley, T. E.; Denkewal.Rg Controlled synthesis of peptides in aqueous medium .3. Use of leuchs anhydrides in synthesis of

dipeptides . Mechanism and control of side reactions. *Journal of Organic Chemistry* **1967**, *32*, 3415.

(283) Veber, D. F.; Pfister, K.; Hirschma.R Synthesis of α-methyl-DLG-glutathione. *J. Med. Chem.* **1967**, *10*, 968.

(284) Denkewal.Rg; Schwam, H.; Strachan, R. G.; Beesley, T. E.; Veber, D. F.; Schoenew.Ef; Barkemey.H; Paleveda, W. J.; Jacob, T. A.; Hirschma.R Controlled synthesis of peptides in aqueous medium .I. Use of α-amino acid N-carboxyanhydrides. *J. Am. Chem. Soc.* **1966**, *88*, 3163.

(285) Kricheldorf, H. R. Polypeptides and 100 years of chemistry of α-amino acid N-carboxyanhydrides. *Angew. Chem.-Int. Edit.* **2006**, *45*, 5752-5784.

(286) Bloom, S. M.; Deloze, C.; Fasman, G. D.; Blout, E. R. Effect of amino acid composition on conformations of synthetic polypeptides, polymers and copolymers of l-methionine S-methyl-L-cysteine and L-valine. *J. Am. Chem. Soc.* **1962**, *84*, 458.

(287) Blout, E. R.; Deloze, C.; Bloom, S. M.; Fasman, G. D. The dependence of the conformations of synthetic polypeptides on amino acid composition. *J. Am. Chem. Soc.* **1960**, *82*, 3787-3789.

(288) Voet, D.; Voet, J. G.; 2nd ed.; Wiley: New York, 1995; Vol. Chapter 2.

(289) Kricheldorf, H. R. Mechanism of NCA-polymerization .4. Synthesis and reactions of N-acyl-NCA. *Makromolekulare Chemie-Macromolecular Chemistry and Physics* **1977**, *178*, 905-939.

(290) Kricheldorf, H. R. Mechanism of NCA-polymerization .5. Catalysis by secondary-amines. *Makromolekulare Chemie-Macromolecular Chemistry and Physics* **1977**, *178*, 1959-1970.

(291) Kricheldorf, H. R. Mechanism of the NCA polymerization .6. Investigations on cocatalysts of the base-initiated nca polymerization. *Journal of Polymer Science Part a-Polymer Chemistry* **1979**, *17*, 97-109.

(292) Kricheldorf, H. R.; Bosinger, K. Mechanism of nca-polymerization .3. Amine catalyzed polymerization of sarcosine-NCA and sarcosine-NTA. *Makromolekulare Chemie-Macromolecular Chemistry and Physics* **1976**, *177*, 1243-1258.

(293) Kricheldorf, H. R.; Mulhaupt, R. Mechanism of the NCA polymerization .7. Primary and secondary amine-initiated polymerization of β-amino acid NCAs. *Makromolekulare Chemie-Macromolecular Chemistry and Physics* **1979**, *180*, 1419-1433.

(294) Kricheldorf, H. R.; Mulhaupt, R. Mechanism of NCA polymerization .8. The base-initiated polymerization of β-amino acid NCAs. *Journal of Macromolecular Science-Chemistry* **1980**, *A14*, 349-377.

(295) Kricheldorf, H. R.; Mang, T. C-13-NMR sequence-analysis, .20. Stereospecificity of the polymerization of D,L-Leu-NCA and D,L-Val-NCA. *Makromolekulare Chemie-Macromolecular Chemistry and Physics* **1981**, *182*, 3077-3098.

(296) Kricheldorf, H. R.; Von Lossow, C.; Schwarz, G. Primary amine and solvent-induced polymerizations of L- or D,L-phenylalanine N-carboxyanhydride. *Macromol. Chem. Phys.* **2005**, *206*, 282-290.

(297) Kricheldorf, H. R.; Von Lossow, C.; Schwarz, G. Tertiary amine catalyzed polymerizations of α-amino acid N-carboxyanhydrides: The role of cyclization. *Journal of Polymer Science Part a-Polymer Chemistry* **2006**, *44*, 4680-4695.

(298) Hanby, W. E.; Waley, S. G.; Watson, J. Synthetic polypeptides. 1. *Journal of the Chemical Society* **1950**, 3009-3013.

(299) Hanby, W. E.; Waley, S. G.; Watson, J. Synthetic polypeptides. 2. Polyglutamic acid. *Journal of the Chemical Society* **1950**, 3239-3249.

(300) Waley, S. G.; Watson, J. The kinetics of the polymerization of carbonic anhydrides. *J. Am. Chem. Soc.* **1948**, *70*, 2299-2300.

(301) Waley, S. G.; Watson, J. The kinetics of the polymerization of sarcosine carbonic anhydride. *Proceedings of the Royal Society of London Series A-Mathematical and Physical Sciences* **1949**, *199*, 499-517.

(302) Fessler, J. H.; Ogston, A. G. Studies of the sedimentation, diffusion and viscosity of some sarcosine polymers in aqueous solution. *Transactions of the Faraday Society* **1951**, *47*, 667.

(303) Pope, M. T.; Weakley, T. J.; Williams, R. J. P. Distribution of molecular weights in some polyesters and polypeptides. *Journal of the Chemical Society* **1959**, 3442-3446.

(304) Lundberg, R. D.; Doty, P. POLYPEPTIDES. 17. A study of the kinetics of the primary amine-initiated polymerization of n-carboxy-anhydrides with special reference to configurational and stereochemical effects. *J. Am. Chem. Soc.* **1957**, *79*, 3961-3972.

(305) Frankel, M.; Katchalski, E. Derivatives of N-carboxy-α-amino acid esters. *J. Am. Chem. Soc.* **1943**, *65*, 1670-1674.

(306) Heyns, K.; Schultze, H.; Brockmann, R. Zum mechanismus der polymerisation von aminosaure-n-carbonsaureanhydriden - untersuchungen zum isotopie-effekt. 2. *Annalen Der Chemie-Justus Liebig* **1958**, *611*, 33-39.

(307) Ballard, D. G.; Bamford, C. H. Kinetics of the formation of polypeptides from N-carboxy-α-amino-acid anhydrides. *Nature* **1953**, *172*, 907-908.

(308) Ballard, D. G. H.; Bamford, C. H. Studies in polymerization .7. The polymerization of n-carboxy-α-amino acid anhydrides. *Proceedings of the Royal Society of London Series A-Mathematical and Physical Sciences* **1954**, *223*, 495-520.

(309) Flory, P. J. Fundamental principles of condensation polymerization. *Chemical Reviews* **1946**, *39*, 137-197.

(310) Kricheldorf, H. R.; Schwarz, G. Cyclic polymers by kinetically controlled step-growth polymerization. *Macromol. Rapid Commun.* **2003**, *24*, 359-381.

(311) Kricheldorf, H. R.; von Lossow, C.; Schwarz, G. Primary amine-initiated polymerizations of alanine-NCA and sarcosine-NCA. *Macromol. Chem. Phys.* **2004**, *205*, 918-924.

(312) Kanazawa, H.; Ohashi, Y. Polymerization of N-carboxy anhydrides of L- and DL-valine, and L- and DL-phenylalanine in the solid state. *Molecular Crystals and Liquid Crystals Science and Technology Section A-Molecular Crystals and Liquid Crystals* **1996**, *276*, A45-A54.

(313) Kanazawa, H.; Ohashi, Y.; Sasada, Y.; Kawai, T. Polymerization of N-carboxy amino-acid anhydrides in the solid-state .2. Relation between polymerizability and molecular arrangement in N-leucine NCA and L-alanine NCA crystals. *Journal of Polymer Science Part B-Polymer Physics* **1982**, *20*, 1847-1862.

(314) Vayaboury, W.; Giani, O.; Collet, H.; Commeyras, A.; Schue, F. Synthesis of N-ε-protected-L-lysine and γ-benzyl-L-glutamate N-carboxyanhydrides (NCA) by carbamoylation and nitrosation. *Amino Acids* **2004**, *27*, 161-167.

(315) Vayaboury, W.; Giani, O.; Cottet, H.; Deratani, A.; Schue, F. Living polymerization of α-amino acid N-carboxyanhydrides (NCA) upon decreasing the reaction temperature. *Macromol. Rapid Commun.* **2004**, *25*, 1221-1224.

(316) Deming, T. J. Facile synthesis of block copolypeptides of defined architecture. *Nature* **1997**, *390*, 386-389.

(317) Deming, T. J. Amino acid derived nickelacycles: Intermediates in nickel-mediated polypeptide synthesis. *J. Am. Chem. Soc.* **1998**, *120*, 4240-4241.

(318) Deming, T. J. Cobalt and iron initiators for the controlled polymerization of α-amino acid-N-carboxyanhydrides. *Macromolecules* **1999**, *32*, 4500-4502.

(319) Collman, J. P.; Hegedus, L. S.; Norton, J. R.; Fink, R. G. *Principles and Applications of Organotransition Metal Chemistry 2nd edn.* ; Uinversity Science Books: Mill Valley, CA, 1987.

(320) Deming, T. J.; Curtin, S. A. Chain initiation efficiency in cobalt- and nickel-mediated polypeptide synthesis. *J. Am. Chem. Soc.* **2000**, *122*, 5710-5717.

(321) Deming, T. J. Methodologies for preparation of synthetic block copolypeptides: materials with future promise in drug delivery. *Advanced Drug Delivery Reviews* **2002**, *54*, 1145-1155.

(322) Bellomo, E. G.; Wyrsta, M. D.; Pakstis, L.; Pochan, D. J.; Deming, T. J. Stimuli-responsive polypeptide vesicles by conformation-specific assembly. *Nature Materials* **2004**, *3*, 244-248.

(323) Breedveld, V.; Nowak, A. P.; Sato, J.; Deming, T. J.; Pine, D. J. Rheology of block copolypeptide solutions: Hydrogels with tunable properties. *Macromolecules* **2004**, *37*, 3943-3953.

(324) Brzezinska, K. R.; Curtin, S. A.; Deming, T. J. Polypeptide end-capping using functionalized isocyanates: Preparation of pentablock copolymers. *Macromolecules* **2002**, *35*, 2970-2976.

(325) Brzezinska, K. R.; Deming, T. J. Synthesis of ABA triblock copolymers via acyclic diene metathesis polymerization and living polymerization of α-amino acid-N-carboxyanhydrides. *Macromolecules* **2001**, *34*, 4348-4354.

(326) Brzezinska, K. R.; Deming, T. J. Synthesis of AB diblock copolymers by atom-transfer radical polymerization (ATRP) and living polymerization of α-amino acid-N-carboxyanhydrides. *Macromolecular Bioscience* **2004**, *4*, 566-569.

(327) Cha, J. N.; Birkedal, H.; Euliss, L. E.; Bartl, M. H.; Wong, M. S.; Deming, T. J.; Stucky, G. D. Spontaneous formation of nanoparticle vesicles from homopolymer polyelectrolytes. *J. Am. Chem. Soc.* **2003**, *125*, 8285-8289.

(328) Cha, J. N.; Stucky, G. D.; Morse, D. E.; Deming, T. J. Biomimetic synthesis of ordered silica structures mediated by block copolypeptides. *Nature* **2000**, *403*, 289-292.

(329) Cheng, J. J.; Deming, T. J. Controlled polymerization of β-lactams using metal-amido complexes: Synthesis of block copoly(β-peptides). *J. Am. Chem. Soc.* **2001**, *123*, 9457-9458.

(330) Cui, H. G.; Krikorian, V.; Thompson, J.; Nowak, A. P.; Deming, T. J.; Pochan, D. J. Preparation and characterization of synthetic polypeptide single crystals with controlled thickness. *Macromolecules* **2005**, *38*, 7371-7377.

(331) Curtin, S. A.; Deming, T. J. Initiators for end-group functionalized polypeptides via tandem addition reactions. *J. Am. Chem. Soc.* **1999**, *121*, 7427-7428.

(332) Deming, T. J. Polypeptide hydrogels via a unique assembly mechanism. *Soft Matter* **2005**, *1*, 28-35.

(333) Deming, T. J. In *Peptide Hybrid Polymers*; Klok, H. A., Schlaad, H., Eds. 2006; Vol. 202, p 1-18.

(334) Deming, T. J. Synthetic polypeptides for biomedical applications. *Progress in Polymer Science* **2007**, *32*, 858-875.

(335) Deming, T. J. Regenerative medicine: Noodle gels for cells. *Nat Mater* **2010**, *9*, 535-536.

(336) Goodwin, A. A.; Bu, X. H.; Deming, T. J. Reactions of α-amino acid-N-carboxyanhydrides (NCAs) with organometallic palladium(0) and platinum(0) compounds: structure of a metallated NCA product and its role in polypeptide synthesis. *Journal of Organometallic Chemistry* **1999**, *589*, 111-114.

(337) Holowka, E. P.; Deming, T. J. Synthesis and Crosslinking of L-DOPA Containing Polypeptide Vesicles. *Macromolecular Bioscience* **2010**, *10*, 496-502.

(338) Holowka, E. P.; Pochan, D. J.; Deming, T. J. Charged polypeptide vesicles with controllable diameter. *J. Am. Chem. Soc.* **2005**, *127*, 12423-12428.

(339) Li, Z. B.; Deming, T. J. Tunable hydrogel morphology via self-assembly of amphiphilic pentablock copolypeptides. *Soft Matter* **2010**, *6*, 2546-2551.

(340) McKenna, B. J.; Birkedal, H.; Bartl, M. H.; Deming, T. J.; Stucky, G. D. Micrometer-sized spherical assemblies of polypeptides and small molecules by acid-base chemistry. *Angew. Chem.-Int. Edit.* **2004**, *43*, 5652-5655.

(341) Nowak, A. P.; Sato, J.; Breedveld, V.; Deming, T. J. Hydrogel formation in amphiphilic triblock copolypeptides. *Supramolecular Chemistry* **2006**, *18*, 423-427.

(342) Pakstis, L. M.; Ozbas, B.; Hales, K. D.; Nowak, A. P.; Deming, T. J.; Pochan, D. Effect of chemistry and morphology on the biofunctionality of self-assembling diblock copolypeptide hydrogels. *Biomacromolecules* **2004**, *5*, 312-318.

(343) Pochan, D. J.; Pakstis, L.; Ozbas, B.; Nowak, A. P.; Deming, T. J. SANS and Cryo-TEM study of self-assembled diblock copolypeptide hydrogels with rich nano- through microscale morphology. *Macromolecules* **2002**, *35*, 5358-5360.

(344) Schaefer, K. E.; Keller, P.; Deming, T. J. Thermotropic polypeptides bearing side-on mesogens. *Macromolecules* **2006**, *39*, 19-22.

(345) Wong, M. S.; Cha, J. N.; Choi, K. S.; Deming, T. J.; Stucky, G. D. Assembly of nanoparticles into hollow spheres using block copolypeptides. *Nano Letters* **2002**, *2*, 583-587.

(346) Aliferis, T.; Iatrou, H.; Hadjichristidis, N. Living polypeptides. *Biomacromolecules* **2004**, *5*, 1653-1656.

(347) Gitsas, A.; Floudas, G.; Mondeshki, M.; Spiess, H. W.; Aliferis, T.; Iatrou, H.; Hadjichristidis, N. Control of Peptide Secondary Structure and Dynamics in Poly(γ-benzyl-L-glutamate)-b-polyalanine Peptides. *Macromolecules* **2008**, *41*, 8072-8080.

(348) Hadjichristidis, N.; Iatrou, H.; Pitsikalis, M.; Mays, J. Macromolecular architectures by living and controlled/living polymerizations. *Progress in Polymer Science* **2006**, *31*, 1068-1132.

(349) Hadjichristidis, N.; Iatrou, H.; Pitsikalis, M.; Sakellariou, G. Synthesis of Well-Defined Polypeptide-Based Materials via the Ring-Opening Polymerization of α-Amino Acid N-Carboxyanhydrides. *Chemical Reviews* **2009**, *109*, 5528-5578.

(350) Iatrou, H.; Hadjichristidis, N. Multiresponsive vesicles from well-defined polypeptides: Formation of gene vesicles. *Abstracts of Papers of the American Chemical Society* **2007**, *234*.

(351) Karatzas, A.; Bilalis, P.; Iatrou, H.; Pitsikalis, M.; Hadjichristidis, N. Synthesis of well-defined functional macromolecular chimeras based on poly(ethylene oxide) or poly(N-vinyl pyrrolidone). *Reactive & Functional Polymers* **2009**, *69*, 435-440.

(352) Kirkwood, K. M.; Leal, L. G.; Vlassopoulos, D.; Driva, P.; Hadjichristidis, N. Stress Relaxation of Comb Polymers with Short Branches. *Macromolecules* **2009**, *42*, 9592-9608.

(353) Papadopoulos, P.; Floudas, G.; Schnell, I.; Klok, H. A.; Aliferis, T.; Iatrou, H.; Hadjichristidis, N. "Glass transition" in peptides: Temperature and pressure effects. *J. Chem. Phys.* **2005**, *122*.

(354) Pickel, D. L.; Politakos, N.; Avgeropoulos, A.; Messman, J. M. A Mechanistic Study of α-(Amino acid)-N-carboxyanhydride Polymerization: Comparing Initiation and Termination Events in High-Vacuum and Traditional Polymerization Techniques. *Macromolecules* **2009**, *42*, 7781-7788.

(355) Zhang, Y. F.; Lu, H.; Lin, Y.; Cheng, J. J. Water-Soluble Polypeptides with Elongated, Charged Side Chains Adopt Ultrastable Helical Conformations. *Macromolecules* **2011**, *44*, 6641-6644.

(356) Lu, H.; Cheng, J. J. Hexamethyldisilazane-mediated controlled polymerization of α-Amino acid N-carboxyanhydrides. *J. Am. Chem. Soc.* **2007**, *129*, 14114.

(357) Lu, H.; Cheng, J. J. N-trimethylsilyl amines for controlled ring-opening polymerization of amino acid N-carboxyanhydrides and facile end group functionalization of polypeptides. *J. Am. Chem. Soc.* **2008**, *130*, 12562.

(358) Dimitrov, I.; Kukula, H.; Colfen, H.; Schlaad, H. Advances in the synthesis and characterization of polypeptide-based hybrid block copolymers. *Macromolecular Symposia* **2004**, *215*, 383-393.

(359) Dimitrov, I.; Schlaad, H. Synthesis of nearly monodisperse polystyrene-polypeptide block copolymers via polymerisation of N-carboxyanhydrides. *Chem. Commun.* **2003**, 2944-2945.

(360) Schlaad, H.; Klok, H.-A.; Springer Berlin / Heidelberg: 2006; Vol. 202, p 53-73.

(361) Bilek, L.; Derkosch, J.; Michl, H.; Wessely, F. Uber die zersetzung von α-amino-n-carbonsaureanhydriden mit pyridin und pyridinderivaten - zur frage der bildung von hohermolekularen cyklopeptiden. *Monatshefte Fur Chemie* **1953**, *84*, 717-740.

(362) Kricheldorf, H. R.; Von Lossow, C.; Schwarz, G. Imidazole-initiated polymerizations of α-amino acid N-carboxyanhydrides - Simultaneous chain-growth and step-growth polymerization. *Journal of Polymer Science Part a-Polymer Chemistry* **2005**, *43*, 5690-5698.

(363) Kricheldorf, H. R.; von Lossow, C.; Schwarz, G. Cyclic polypeptides by solvent-induced polymerizations of α-amino acid N-carboxyanhydrides. *Macromolecules* **2005**, *38*, 5513-5518.

(364) Kricheldorf, H. R.; Von Lossow, C.; Schwarz, G.; Fritsch, D. Chain extension and cyclization of telechelic polysarcosines. *Macromol. Chem. Phys.* **2005**, *206*, 1165-1170.

(365) Elliott, A.; Ambrose, E. J. Evidence of chain folding in polypeptides and proteins. *Discussions of the Faraday Society* **1950**, 246.

(366) Block, H. *Poly(γ-benzyl-L-glutamate) and other Glutamic Acid Containing Polymers*; Gordon and Breach: New York, 1983.

(367) Robinson, C. Liquid-crystalline structures in solutions of a polypeptide. *Transactions of the Faraday Society* **1956**, *52*, 571.

(368) Robinson, C.; Ward, J. C.; Beevers, R. B. Liquid crystalline structure in polypeptide solutions .2. *Discussions of the Faraday Society* **1958**, 29.

(369) Hentschke, R.; Herzfeld, J. Isotropic, nematic, and columnar ordering in systems of persistent flexible hard-rods. *Physical Review A* **1991**, *44*, 1148-1155.

(370) Horton, J. C.; Donald, A. M. Phase-separation in the poly(γ-benzyl-α, L-glutamate) benzyl alcohol system and its role in gelation. *Polymer* **1991**, *32*, 2418-2427.

(371) Kamio, Y.; Watanabe, J.; Kajikawa, K.; Takezoe, H.; Fukuda, A.; Toyooka, T.; Ishii, T. 2nd-harmonic generation in noncentrosymmetric p-nitroaniline spontaneously crystallized by quenching from lyotropic liquid-crystalline poly(γ-benzyl-L-glutamate). *Japanese Journal of Applied Physics Part 1-Regular Papers Short Notes & Review Papers* **1991**, *30*, 1710-1714.

(372) Shukla, P. Thermodynamics and kinetics of gelation in the poly(γ-benzyl α,L-glutamate) benzyl alcohol system. *Polymer* **1992**, *33*, 365-372.

(373) Shukla, P.; Muthukumar, M. Supramolecular structure investigation of poly(γ-benzyl, α-L-glutamate)-benzyl alcohol system by static light-scattering. *Journal of Polymer Science Part B-Polymer Physics* **1991**, *29*, 1373-1387.

(374) Korenaga, T.; Oikawa, H.; Nakanishi, H. Spinodal decomposition and gel structure of quenched poly(γ-benzyl L-glutamate)-toluene solutions. *Journal of Macromolecular Science-Physics* **1997**, *36*, 487-501.

(375) Lin, J. P.; Abe, A.; Furuya, H.; Okamoto, S. Liquid crystal formation coupled with the coil helix transition in the ternary system poly(γ-benzyl L-glutamate) dichloroacetic acid dichloroethane. *Macromolecules* **1996**, *29*, 2584-2589.

(376) Machida, S.; Urano, T. I.; Sano, K.; Kato, T. Response of a hydrogen-bonded liquid crystal to an applied electric field accelerated by a poly(γ-benzyl L-glutamate) chemical reaction alignment film. *Langmuir* **1997**, *13*, 576-580.

(377) Meddour, A.; Canet, I.; Loewenstein, A.; Pechine, J. M.; Courtieu, J. Observation of enantiomers, chiral by virtue of isotopic-substitution, through deuterium NMR in a polypeptide liquid-crystal. *J. Am. Chem. Soc.* **1994**, *116*, 9652-9656.

(378) Ugaz, V. M.; Cinader, D. K.; Burghardt, W. R. X-ray scattering investigation of highly concentrated poly(benzyl glutamate) solutions under shear flow. *Journal of Rheology* **1998**, *42*, 379-394.

(379) Veron, A.; Gomes, A. E.; Leal, C. R.; Van der Klink, J.; Martins, A. F. NMR study of flow and viscoelastic properties of PBLG/m-cresol lyotropic liquid crystal. *Molecular Crystals and Liquid Crystals Science and Technology Section a-Molecular Crystals and Liquid Crystals* **1999**, *331*, 2359-2367.

(380) Walker, L. M.; Wagner, N. J. SANS analysis of the molecular order in poly(γ-benzyl L-glutamate) deuterated dimethylformamide (PBLG/d-DMF) under shear and during relaxation. *Macromolecules* **1996**, *29*, 2298-2301.

(381) Chen, T.; Lin, J. P.; Tian, X. H.; Liu, P. H.; Lin, S. L.; Lu, X. W.; Zhou, D. F. Effect of electric field on phase behavior of polypeptide liquid crystals. *Acta Polymerica Sinica* **2004**, 145-148.

(382) Hamley, I. W. Liquid crystal phase formation by biopolymers. *Soft Matter* **2010**, *6*, 1863-1871.

(383) Ibarboure, E.; Papon, E.; Rodriguez-Hernandez, J. Nanostructured thermotropic PBLG-PDMS-PBLG block copolymers. *Polymer* **2007**, *48*, 3717-3725.

(384) Ibarboure, E.; Rodriguez-Hernandez, J.; Papon, E. Thermotropic liquid crystal behavior on PBLG-PDMS-PBLG triblock copolymers. *Journal of Polymer Science Part a-Polymer Chemistry* **2006**, *44*, 4668-4679.

(385) Marx, A.; Bottcher, B.; Thiele, C. M. Enhancing the Orienting Properties of Poly(γ-benzyl-L-glutamate) by means of Additives. *Chem.-Eur. J.* **2010**, *16*, 1656-1663.

(386) Solgadi, A.; Jean, L.; Marie-Claire, L.; Rouden, J.; Courtieu, J.; Meddour, A. NMR in chiral polypeptide liquid crystals: the problem of amines. *Tetrahedron-Asymmetry* **2007**, *18*, 1511-1516.

(387) Tsuboi, K.; Marcelletti, E.; Matsumoto, H.; Ashizawa, M.; Minagawa, M.; Furuya, H.; Tanioka, A.; Abe, A. Preparation of poly(γ-benzyl-L-glutamate) nanofibers by electrospinning from isotropic and biphasic liquid crystal solutions. *Polymer Journal* **2012**, *44*, 360-365.

(388) Yen, C. C.; Taguchi, Y.; Tokita, M.; Watanabe, J. Spontaneous Formation of Polar Liquid Crystal in Lyotropic Solution of Helical Poly(γ-Benzyl Glutamate). *Molecular Crystals and Liquid Crystals* **2010**, *516*, 91-98.

(389) Daly, W. H.; Poché, D.; Negulescu, I. I. Poly (γ-Alkyl-α,L-glutamate)s, derived from long chain paraffinic alcohols. *Progress in Polymer Science* **1994**, *19*, 79-135.

(390) Doucet, G. J.; Qiu, J.; Russo, P. S. Effect of Length on the Diffusion of a Rodlike Polymer at Concentrations Spanning the Isotropic-Lyotropic Transition. *Journal of Physical Chemistry B* **2010**, *114*, 4777-4782.

(391) Ricks, H. L.; Nakamatsu, J.; Daly, W. H.; Russo, P. S. Poly(γ-stearyl-α,L-glutamate) lyotropic liquid crystals. *Abstracts of Papers of the American Chemical Society* **1996**, *211*, 175-POLY.

(392) Russo, P. S.; Baylis, M.; Bu, Z. M.; Stryjewski, W.; Doucet, G.; Temyanko, E.; Tipton, D. Self-diffusion of a semiflexible polymer measured across the lyotropic liquid-crystalline-phase boundary. *J. Chem. Phys.* **1999**, *111*, 1746-1752.

(393) Schmidtke, S.; Russo, P.; Nakamatsu, J.; Buyuktanir, E.; Turfan, B.; Temyanko, E.; Negulescu, L. Thermoreversible gelation of isotropic and liquid crystalline solutions of a "sticky" rodlike polymer. *Macromolecules* **2000**, *33*, 4427-4432.

(394) Schmidtke, S.; Russo, P. S.; Nakamatsu, J.; Negulescu, I. I. Gelation of a "sticky" rodlike polymer. *Abstracts of Papers of the American Chemical Society* **2000**, *219*, U494-U494.

(395) Sohn, D.; Yu, H.; Nakamatsu, J.; Russo, P. S.; Daly, W. H. Monolayer properties of a fuzzy rod polymer: Poly(γ-stearyl α, L-glutamate). *Journal of Polymer Science Part B-Polymer Physics* **1996**, *34*, 3025-3034.

(396) Tipton, D. L.; Russo, P. S. Thermoreversible gelation of a rodlike polymer. *Macromolecules* **1996**, *29*, 7402-7411.

(397) Wang, X. L.; Daly, W. H.; Russo, P.; Ngu-Schwemlein, M. Synthesis of paucidisperse poly(γ-benzyl-α,L-glutamate) oligomers and star polymers with rigid arms. *Biomacromolecules* **2001**, *2*, 1214-1219.

(398) Bu, Z.; Tipton, D. L.; Poche, D. S.; Negulescu, I.; Daly, W. H.; Russo, P. S. Self-diffusion of semiflexible rods in dilute and concentrated isotropic solutions. *Abstracts of Papers of the American Chemical Society* **1993**, *205*, 43-POLY.

(399) Bu, Z. M.; Russo, P. S.; Tipton, D. L.; Negulescu, I. I. self-diffusion of rodlike polymers in isotropic solutions. *Macromolecules* **1994**, *27*, 6871-6882.

(400) Camins, B.; Russo, P. S. Following polymer gelation by depolarized dynamic light-scattering from optically and geometrically anisotropic latex-particles. *Langmuir* **1994**, *10*, 4053-4059.

(401) Chowdhury, A. H.; Russo, P. S. Late stages of phase-separation gelation of isotropic solutions of rod-like polymers by video microscopy. *J. Chem. Phys.* **1990**, *92*, 5744-5750.

(402) Delong, L. M.; Russo, P. S. Thermodynamic and dynamic behavior of semiflexible polymers in the isotropic-phase. *Macromolecules* **1991**, *24*, 6139-6155.

(403) Jamil, T.; Russo, P. S.; Daly, W. H.; Negulescu, I. Static and dynamic light-scattering of a random coil polymer in rodlike polymer-solution. *Macromolecular Symposia* **1994**, *79*, 81-85.

(404) Russo, P. S.; Cao, T. Phase-behavior in a ternary rod coil solvent system - poly(γ-benzyl-α,L-glutamate) nylon-6/m-cresol. *Molecular Crystals and Liquid Crystals* **1988**, *157*, 501-514.

(405) Russo, P. S.; Magestro, P.; Miller, W. G. Gelation of poly(γ-benzyl-α,L-glutamate). *Acs Symposium Series* **1987**, *350*, 152-180.

(406) Tipton, D. L.; Russo, P. S. Dynamic light-scattering in gels. *Abstracts of Papers of the American Chemical Society* **1993**, *205*, 42-POLY.

(407) Russo, P. S.; Miller, W. G. Coexistence of liquid-crystalline phases in poly(γ-benzyl-α,L-glutamate)-dimethylformamide. *Macromolecules* **1983**, *16*, 1690-1693.

(408) Patel, D. L.; Dupre, D. B. Spherulite morphology in liquid-crystals of polybenzylglutamates - optical-rotatory power and effect of magnetic-field. *Journal of Polymer Science Part B-Polymer Physics* **1980**, *18*, 1599-1607.

(409) Dupre, D. B.; Parthasarathy, R. Mesophase formation in solutions of semirigid polymers - poly(γ-benzyl-L-glutamate) liquid-crystals. *Acs Symposium Series* **1989**, *384*, 130-141.

(410) Patel, D. L.; Dupre, D. B. Optical-rotatory behavior of polypeptide solutions in the liquid-crystal and pretransitional regions. *J. Chem. Phys.* **1980**, *72*, 2515-2524.

(411) Kosho, H.; Tanaka, Y.; Ichizuka, T.; Kawauchi, S.; Watanabe, J. Distinct temperature dependence of cholesteric pitch in lyotropic cholesteric solutions of polypeptide. *Polymer Journal* **1999**, *31*, 199-202.

(412) Minich, E. A.; Nowak, A. P.; Deming, T. J.; Pochan, D. J. Rod-rod and rod-coil self-assembly and phase behavior of polypeptide diblock copolymers. *Polymer* **2004**, *45*, 1951-1957.

(413) Hashimoto, T.; Ebisu, S.; Inaba, N.; Kawai, H. Supramolecular structure of polypeptides in concentrated-solutions and films .2. Small-angle light-scattering from cholesteric mesophase. *Polymer Journal* **1981**, *13*, 701-713.

(414) Itou, S. Lyotropic liquid-crystalline structures of synthetic polypeptides .1. Molecular-weight dependence of the cholesteric pitch on poly(γ-benzyl L-glutamate) solutions. *Molecular Crystals and Liquid Crystals* **1989**, *172*, 201-210.

(415) Rao, M. V. R.; Atreyi, M.; Pantar, A. V. Surfactant bound polypeptides .2. Liquid-crystalline behavior of triton x-100 bound poly-γ-benzyl-L-glutamate. *Liquid Crystals* **1987**, *2*, 889-893.

(416) Rao, M. V. R.; Pantar, A. V.; Atreyi, M. Surfactant bound polypeptides .1. Conformation in solution and solid-state of poly (γ-benzyl-L-glutamate)-Triton X-100. *International Journal of Biological Macromolecules* **1987**, *9*, 337-342.

(417) Hashimoto, T.; Inaba, N.; Ebisu, S.; Kawai, H. Supramolecular structure of polypeptides in concentrated-solutions and films .3. Inhomogeneous twisting of cholesteric mesophase as clarified from multiple-order light-scattering maxima. *Polymer Journal* **1981**, *13*, 897-910.

(418) Shiau, C. C.; Labes, M. M. Correlation of pitch with concentration and molecular-weight in poly(γ-benzyl glutamate) lyophases. *Macromolecules* **1989**, *22*, 328-332.

(419) Block, H.; Shaw, C. P. 2nd-harmonic generation in poly(α-amino acid) and poly(isocyanate) films. *Polymer* **1992**, *33*, 2459-2462.

(420) Iizuka, E. Electric and magnetic orientation of macromolecules. *Applied Polymer Symposia* **1985**, 131-147.

(421) Iizuka, E.; Kiriki, T.; Abe, K. Electric and magnetic orientation of a thermotropic-liquid crystalline polypeptide. *Polymer Journal* **1991**, *23*, 1507-1510.

(422) Shiau, C. C.; Labes, M. M. Control of the pitch of synthetic polypeptide lyotropic phases utilizing a chiral solvent. *Molecular Crystals and Liquid Crystals* **1985**, *124*, 125-130.

(423) Okosh, K.; San, N.; Suzaki, G.; Tokita, M.; Magos, J.; Watanabe, J. Smectic liquid crystal observed in thermotropic system of rigid-rod poly(γ-octadecyl L-glutamate). *Japanese Journal of Applied Physics Part 2-Letters* **2002**, *41*, L720-L722.

(424) Watanabe, J.; Sakajiri, K.; Okoshi, K.; Kawauchi, S.; Magoshi, J. Columnar liquid crystals in polypeptides, 1 Columnar hexagonal phase observed in lyotropic solutions of poly(γ-octadecyl-1-glutamate) dissolved in amphiphilic solvents, such as octadecylamine, octadecyl alcohol, and octadecanoic acid. *Macromol. Chem. Phys.* **2001**, *202*, 1004-1009.

(425) Yin, Y. G.; Zhao, C. H.; Sasaki, A.; Kimura, H.; Kuroki, S.; Ando, I. Diffusional behavior of polypeptides in the isotropic, biphasic, and liquid crystalline phases as studied by the pulse field-gradient spin-echo H-1 NMR method. *Macromolecules* **2002**, *35*, 5910-5915.

(426) Ando, I.; Yin, Y. G.; Zhao, C. H.; Kanesaka, S.; Kuroki, S. Diffusion of rod-like polypeptides in the liquid crystalline and isotropic phases as studied by high field-gradient NMR spectroscopy. *Macromolecular Symposia* **2005**, *220*, 61-73.

(427) Kanesaka, S.; Kimura, H.; Kuroki, S.; Ando, I.; Fujishige, S. Diffusional behavior of poly(diethylsiloxane) in the liquid crystalline and isotropic phases as studied by high field-gradient NMR. *Macromolecules* **2004**, *37*, 453-458.

(428) Kuroki, S.; Kamiguchi, K. Diffusional behavior of poly(γ-benzyl l-glutamate) in concentrated solution as studied by the field-gradient H-1 NMR methods. *Polymer Journal* **2008**, *40*, 223-227.

(429) Larson, R. G.; Mead, D. W. Toward a quantitative theory of the rheology of concentrated-solutions of stiff polymers. *Journal of Polymer Science Part B-Polymer Physics* **1991**, *29*, 1271-1285.

(430) Kiss, G. Rheology of concentrated solutions of poly(γ-benzyl-glutamate) - Reflections. *Journal of Polymer Science Part B-Polymer Physics* **1996**, *34*, 2263-2266.

(431) Kiss, G.; Porter, R. S. Rheology of concentrated-solutions of poly(γ-benzyl-glutamate). *Journal of Polymer Science Part C-Polymer Symposium* **1978**, 193-211.

(432) Kiss, G.; Porter, R. S. Rheology of concentrated-solutions of helical polypeptides. *Journal of Polymer Science Part B-Polymer Physics* **1980**, *18*, 361-388.

(433) Kiss, G.; Porter, R. S. Rheo-optical studies of liquid-crystalline solutions of helical polypeptides. *Molecular Crystals and Liquid Crystals* **1980**, *60*, 267.

(434) Kiss, G.; Porter, R. S. Rheology of concentrated solutions of poly(γ-benzyl-glutamate). *Journal of Polymer Science Part B-Polymer Physics* **1996**, *34*, 2271-2289.

(435) Chaffey, C. E.; Porter, R. S. On the origin of negative normal stresses in sheared or lyotropic liquid-crystals. *Journal of Rheology* **1985**, *29*, 281-305.

(436) Emelyanenko, A. V. Analytical description for the chiral nematic state in terms of molecular parameters. *Physical Review E* **2003**, *67*.

(437) Emelyanenko, A. V.; Osipov, M. A.; Dunmur, D. A. Molecular theory of helical sense inversions in chiral nematic liquid crystals. *Physical Review E* **2000**, *62*, 2340-2352.

(438) Park, B.; Kinoshita, Y.; Takezoe, H.; Watanabe, J. Ferroelectricity in the lyotropic cholesteric phase of poly L-glutamate. *Japanese Journal of Applied Physics Part 2-Letters* **1998**, *37*, L136-L138.

(439) Mohanty, B.; Komoto, T.; Watanabe, J.; Ando, I.; Shiibashi, T. Conformation aspect of poly(γ-oleyl l-glutamate) with long flexible side-chains as studied by variable-temperature c-13 cp/mas nmr-spectroscopy. *Macromolecules* **1989**, *22*, 4451-4455.

(440) Mohanty, B.; Watanabe, J.; Ando, I.; Sato, K. Proton nmr relaxation study of molecular-motion in poly(γ-normal-octadecyl L-glutamate) and poly(γ-oleyl L-glutamate). *Macromolecules* **1990**, *23*, 4908-4911.

(441) Watanabe, J.; Nagase, T.; Ichizuka, T. Thermotropic polypeptides .7. Temperature-dependence of cholesteric pitches in poly[γ-benzyl L-glutamate)-co-(γ-dodecyl L-glutamate)s]. *Polymer Journal* **1990**, *22*, 1029-1033.

(442) Kasuya, S.; Sasaki, S.; Watanabe, J.; Fukuda, Y.; Uematsu, I. Thermotropic cholesteric mesophases in copoly(γ-n-alkyl L-glutamate)s. *Polymer Bulletin* **1982**, *7*, 241-248.

(443) Ono, H.; Watanabe, J.; Abe, A. Studies on sidechain crystallization of poly(γ-n-alkyl L-glutamate). *Kobunshi Ronbunshu* **1988**, *45*, 69-77.

(444) Tsukahara, M.; Yamanobe, T.; Komoto, T.; Watanabe, J.; Ando, I.; Uematsu, I. Conformation and molecular packing of normal-alkyl side-chains protruding from α-helical poly(L-glutamates) as studied by C-13 CP/MAS NMR-spectroscopy. *Journal of Molecular Structure* **1987**, *159*, 345-353.

(445) Watanabe, J.; Fukuda, Y.; Gehani, R.; Uematsu, I. Thermotropic polypeptides .1. Investigation of cholesteric mesophase properties of poly(γ-methyl D-glutamate-co-γ-hexyl D-glutamate)s. *Macromolecules* **1984**, *17*, 1004-1009.

(446) Watanabe, J.; Goto, M.; Nagase, T. Thermotropic polypeptides .3. Investigation of cholesteric mesophase properties of poly(γ-benzyl L-glutamate-co-γ-dodecyl L-glutamates) by circular dichroic measurements. *Macromolecules* **1987**, *20*, 298-304.

(447) Watanabe, J.; Imai, K.; Gehani, R.; Uematsu, I. Structural differences between 2 crystal modifications of poly (γ-benzyl L-glutamate). *Journal of Polymer Science Part B-Polymer Physics* **1981**, *19*, 653-665.

(448) Watanabe, J.; Nagase, T. Thermotropic polypeptides .4. Thermotropic cholesteric mesophase of copolyglutamates based on γ-benzyl L-glutamate and γ-alkyl L-glutamate. *Polymer Journal* **1987**, *19*, 781-784.

(449) Watanabe, J.; Nagase, T. Thermotropic polypeptides .5. Temperature-dependence of cholesteric pitches exhibiting a cholesteric sense inversion. *Macromolecules* **1988**, *21*, 171-175.

(450) Watanabe, J.; Naka, M.; Watanabe, K.; Uematsu, I. Structure and mechanical-properties of poly(γ-methyl glutamate) films .2. *Polymer Journal* **1978**, *10*, 569-582.

(451) Watanabe, J.; Ono, H. X-ray evidence of an α-helical coiled coil in poly(γ-dodecyl l-glutamate). *Macromolecules* **1986**, *19*, 1079-1083.

(452) Watanabe, J.; Ono, H.; Uematsu, I.; Abe, A. Thermotropic polypeptides .2. Molecular packing and thermotropic behavior of poly(L-glutamates) with long normal-alkyl side-chains. *Macromolecules* **1985**, *18*, 2141-2148.

(453) Watanabe, J.; Sasanuma, Y.; Endo, A.; Uematsu, I. Crystalline complex between poly(γ-methyl L-glutamate) and dimethyl phthalate. *Polymer* **1984**, *25*, 698-705.

(454) Watanabe, J.; Uematsu, I. Anomalous properties of poly(γ-benzyl l-glutamate) film composed of unusual 7/2 helices. *Polymer* **1984**, *25*, 1711-1717.

(455) Yamanobe, T.; Tsukahara, M.; Komoto, T.; Watanabe, J.; Ando, I.; Uematsu, I.; Deguchi, K.; Fujito, T.; Imanari, M. Conformation and dynamic aspects of poly(γ-normal-octadecyl L-glutamate) in the solid-state and liquid-crystalline state as studied by variable-temperature C-13 CP/MAS NMR-spectroscopy. *Macromolecules* **1988**, *21*, 48-50.

(456) Watanabe, J.; Tominaga, T. Thermotropic liquid-crystals in polypeptides with mesogenic side-chains .1. *Macromolecules* **1993**, *26*, 4032-4036.

(457) Yen, C. C.; Edo, S.; Oka, H.; Tokita, M.; Watanabe, J. Phase diagram for solutions of α-helical poly(L-glutamate)s in m-cresol including isotropic, cholesteric, and columnar phases. *Macromolecules* **2008**, *41*, 3727-3733.

(458) Yen, C. C.; Taguchi, Y.; Tokita, M.; Watanabe, J. Polar nematic phase in lyotropic solutions of poly(γ-benzyl glutamate) and its temperature instability as detected by SHG measurement. *Macromolecules* **2008**, *41*, 2755-2758.

(459) Neagu, E.; Neagu, R.; Daly, W. H.; Negulescu, I. I. dielectric relaxations in thermotropic liquid-crystalline polypeptides. *IEEE Transactions on Electrical Insulation* **1993**, *28*, 122-127.

(460) Murata, K.; Katoh, E.; Kuroki, S.; Ando, I. A study of the conformational stability of poly(β-benzyl L-aspartate), poly(γ-benzyl L-glutamate) and poly(β-benzyl L-aspartate)/poly(γ-benzyl L-glutamate) blend in the solid state by variable-temperature C-13 CP/MAS NMR. *Journal of Molecular Structure* **2004**, *689*, 223-235.

(461) Yamane, Y.; Kobayashi, M.; Kimura, H.; Kuroki, S.; Ando, I. Diffusional behavior of amino acids in solid-phase reaction field as studied by H-1 pulsed-field-gradient spin-echo NMR method. *Polymer* **2002**, *43*, 1767-1772.

(462) Yin, Y. G.; Zhao, C. H.; Kuroki, S.; Ando, I. Diffusion of rodlike polypeptides with different main-chain lengths in the thermotropic liquid crystalline state as studied by the field-gradient H-1 NMR method. *Macromolecules* **2002**, *35*, 2335-2338.

(463) Hanabusa, K.; Yanagisawa, K.; Higashi, J. I.; Shirai, H.; Hayakawa, T.; Hojo, N. Thermotropic liquid-crystalline poly(L-glutamate) esters with long alkyl chain containing

aromatic segment at terminal position. *Journal of Polymer Science Part a-Polymer Chemistry* **1990**, *28*, 825-835.

(464) Hanski, S.; Houbenov, N.; Ruokolainen, J.; Chondronicola, D.; Iatrou, H.; Hadjichristidis, N.; Ikkala, O. Hierarchical ionic self-assembly of rod-comb block copolypeptide-surfactant complexes. *Biomacromolecules* **2006**, *7*, 3379-3384.

(465) Kitaev, V.; Schillen, K.; Kumacheva, E. Supramolecular structures of poly(γ-benzyl-L-glutamate) self-assembled on mica surface. *Journal of Polymer Science Part B-Polymer Physics* **1998**, *36*, 1567-1577.

(466) Monzen, K.; Hiraoka, K.; Uematsu, Y.; Date, M. Banded texture induced by an electric field in polymeric liquid crystalline solution. *Polymer Journal* **1998**, *30*, 499-507.

(467) Gallot, B.; Fafiotte, M.; Fissi, A.; Pieroni, O. Liquid-crystalline structure of poly(L-lysine) containing azobenzene units in the side chain. *Macromol. Rapid Commun.* **1996**, *17*, 493-501.

(468) Gallot, B.; Fafiotte, M.; Fissi, A.; Pieroni, O. Poly(L-lysine) containing azobenzene units in the side chains: Influence of the degree of substitution on liquid crystalline structure and thermotropic behaviour. *Liquid Crystals* **1997**, *23*, 137-146.

(469) Gallot, B.; Guillermain, C.; Fissi, A.; Pieroni, O. Thermotropic photochromic polypeptides: Polyornithine and polylysine bearing azobenzene units in the side chains. *Molecular Crystals and Liquid Crystals Science and Technology Section a-Molecular Crystals and Liquid Crystals* **1999**, *330*, 1309-1317.

(470) Guillermain, C.; Gallot, B. Synthesis and liquid crystalline structures of poly (L-lysine) containing undecanamidobiphenyl units in the side chains. *Liquid Crystals* **2002**, *29*, 141-153.

(471) Murata, K.; Kuroki, S.; Ando, I. A study of the conformational stability of poly(L-alanine), poly(D-alanine), poly(L-isoleucine), polyglycine and poly(L-valine) and their polypeptide blends in the solid-state by C-13 CP/MAS NMR. *Polymer* **2002**, *43*, 6871-6878.

(472) Kanesaka, S.; Kamiguchi, K.; Kanekiyo, M.; Kuroki, S.; Ando, I. Diffusional Behavior of poly(β-benzyl L-aspartate) in the rodlike, random-coil, and intermediate forms as studied by high field-gradient H-1 NMR spectroscopy. *Biomacromolecules* **2006**, *7*, 1323-1328.

(473) Sakajiri, K.; Kawasaki, E.; Watanabe, J. Distinct complex precipitating from racemic solution of poly(β-benzyl L-aspartate) and poly(β-benzyl D-aspartate). *Macromolecules* **2001**, *34*, 7238-7240.

(474) Hanabusa, K.; Kobayashi, C.; Koyama, T.; Masuda, E.; Shirai, H.; Kondo, Y.; Takemoto, K.; Iizuka, E.; Hojo, N. Functional metal-porphyrazine derivatives and their

polymers. 15. Synthesis and properties of poly(γ-benzyl-L-glutamate)s containing covalently bound metalphthalocyanine moieties in the side-chains. *Makromolekulare Chemie-Macromolecular Chemistry and Physics* **1986**, *187*, 753-761.

(475) Doty, P.; Yang, J. T. Polypeptides .7. Poly-γ-benzyl-L-glutamate - the helix-coil transition in solution. *J. Am. Chem. Soc.* **1956**, *78*, 498-500.

(476) Blout, E. R.; Lenormant, H. Reversible configurational changes in poly-L-lysine hydrochloride induced by water. *Nature* **1957**, *179*, 960-963.

(477) Applequist, J. On helix-coil equilibrium in polypeptides. *J. Chem. Phys.* **1963**, *38*, 934.

(478) Karasz, F. E.; Oreilly, J. M.; Bair, H. E. Thermal helix-coil transition in poly-γ-benxyl-L-glutamate. *Nature* **1964**, *202*, 693.

(479) Karasz, F. E.; Oreilly, J. M.; Bair, H. E. Helix-coil transition in poly-ε-carbobenzoxy-L-lysine. *Biopolymers* **1965**, *3*, 241.

(480) Watanabe, H.; Yoshioka, K.; Wada, A. Electrooptical and dielectric investigations on the conformation and the electrical properties of poly-γ-benzyl-L-glutamate in mixed solvents. *Biopolymers* **1964**, *2*, 91-101.

(481) Ackerman.T; Neumann, E. Experimental thermodynamics of helix-random coil transition .1. Influence of polymer concentration and solvent composition in PBG-DCA-EDC system. *Biopolymers* **1967**, *5*, 649.

(482) Itoh, T.; Hatanaka, T.; Ihara, E.; Inoue, K. Helix-coil transformation of poly(γ-benzyl-L-glutamate) with polystyrene attached to the N or C terminus in trifluoroacetic acid-chloroform mixtures. *Polymer Journal* **2012**, *44*, 189-194.

(483) Lin, J. P.; Zhu, G. Q.; Zhu, X. M.; Lin, S. L.; Nose, T.; Ding, W. W. Aggregate structure change induced by intramolecular helix-coil transition. *Polymer* **2008**, *49*, 1132-1136.

(484) Wen, K. J.; Woody, R. W. Conformational studies of poly(l-tyrosine) - helix-coil transition in dimethyl sulfoxide dichloroacetic acid mixtures. *Biopolymers* **1975**, *14*, 1827-1840.

(485) Yasui, S. C.; Keiderling, T. A. Vibrational circular-dichroism of polypeptides .6. Polytyrosine α-helical and random-coil results. *Biopolymers* **1986**, *25*, 5-15.

(486) Watanabe, K.; Muto, K.; Ishii, T. Conformational analysis of poly(L-tyrosine) and tyrosyl oligomers based on backbone circular dichroism spectra obtained by fluorescence-detected circular dichroism. *Biospectroscopy* **1997**, *3*, 103-111.

(487) Fasman, G. D.; Idelson, M.; Blout, E. R. Synthesis and conformation of high molecular weight poly-ε-carbobenzyloxy-L-lysine and poly-L-lysine.HCL. *J. Am. Chem. Soc.* **1961**, *83*, 709.

(488) Hayashi, T.; Emi, S.; Nakajima, A. Helix-coil transition of poly(ε-carbobenzyloxy-L-lysine) in m-cresol. *Polymer* **1975**, *16*, 396-400.

(489) Wang, Y. L.; Chang, Y. C. Synthesis and conformational transition of surface-tethered polypeptide: Poly(L-lysine). *Macromolecules* **2003**, *36*, 6511-6518.

(490) Wada, A. Dielectric evidence of chemical relaxation in the helix-coil transition of polypeptides. *Chemical Physics Letters* **1971**, *8*, 211-213.

(491) Ho, G. H.; Ho, T. I.; Hsieh, K. H.; Su, Y. C.; Lin, P. Y.; Yang, J.; Yang, K. H.; Yang, S. C. γ-polyglutamic acid produced by Bacillus subtilis (natto): Structural characteristics, chemical properties and biological functionalities. *Journal of the Chinese Chemical Society* **2006**, *53*, 1363-1384.

(492) Dzwolak, W.; Smirnovas, V. A conformational α-helix to β-sheet transition accompanies racemic self-assembly of polylysine: an FT-IR spectroscopic study. *Biophysical Chemistry* **2005**, *115*, 49-54.

(493) Mezo, G.; Kajtar, J.; Nagy, I.; Szekerke, M.; Hudecz, F. Carrier design: Synthesis and conformational studies of poly(L-lysine) based branched polypeptides with hydroxyl groups in the side chains. *Biopolymers* **1997**, *42*, 719-730.

(494) Sakajiri, K.; Satoh, K.; Yen, C. C.; Tokita, M.; Watanabe, J. Helix-helix transition of poly(β-phenylpropyl L-aspartate) embedded in stable helical poly(γ-phenylethyl glutamate) matrix. *Polymer* **2011**, *52*, 5053-5057.

(495) Floudas, G.; Spiess, H. W. Self-Assembly and Dynamics of Polypeptides. *Macromol. Rapid Commun.* **2009**, *30*, 278-298.

(496) Sallach, R. E.; Wei, M.; Biswas, N.; Conticello, V. P.; Lecommandoux, S.; Dluhy, R. A.; Chaikof, E. L. Micelle density regulated by a reversible switch of protein secondary structure. *J. Am. Chem. Soc.* **2006**, *128*, 12014-12019.

(497) Zheng, W. W.; Frank, C. W. Surface-Initiated Vapor Deposition Polymerization of Poly (γ-benzyl-L-glutamate): Optimization and Mechanistic Studies. *Langmuir* **2010**, *26*, 3929-3941.

(498) Lee, N. H.; Christensen, L. M.; Frank, C. W. Morphology of vapor-deposited poly(α-amino acid) films. *Langmuir* **2003**, *19*, 3525-3530.

(499) Lee, N. H.; Frank, C. W. Surface-initiated vapor polymerization of various α-amino acids. *Langmuir* **2003**, *19*, 1295-1303.

(500) Chang, Y. C.; Frank, C. W. Vapor deposition-polymerization of α-amino acid N-carboxy anhydride on the silicon(100) native oxide surface. *Langmuir* **1998**, *14*, 326-334.

(501) Chang, Y. C.; Frank, C. W. In *Organic Thin Films: Structure and Applications*; Frank, C. W., Ed. 1998; Vol. 695, p 142-157.

(502) Jaworek, T.; Neher, D.; Wegner, G.; Wieringa, R. H.; Schouten, A. J. Electromechanical properties of an ultrathin layer of directionally aligned helical polypeptides. *Science* **1998**, *279*, 57-60.

(503) Menzel, H.; Heise, A.; Yim, H.; Foster, M. D.; Wieringa, R. H.; Schouten, A. J. In *Organic Thin Films: Structure and Applications*; Frank, C. W., Ed. 1998; Vol. 695, p 131-141.

(504) Wieringa, R. H.; Schouten, A. J. Oriented thin film formation by surface graft polymerization of γ-methyl L-glutamate N-carboxyanhydride in the melt. *Macromolecules* **1996**, *29*, 3032-3034.

(505) Wieringa, R. H.; Siesling, E. A.; Geurts, P. F. M.; Werkman, P. J.; Vorenkamp, E. J.; Erb, V.; Stamm, M.; Schouten, A. J. Surface grafting of poly (L-glutamates). 1. Synthesis and characterization. *Langmuir* **2001**, *17*, 6477-6484.

(506) Wieringa, R. H.; Siesling, E. A.; Werkman, P. J.; Vorenkamp, E. J.; Schouten, A. J. Surface grafting of poly(L-glutamates). 3. Block copolymerization. *Langmuir* **2001**, *17*, 6491-6495.

(507) Wang, Y. L.; Chang, Y. C. Grafting of homo- and block co-polypeptides on solid substrates by an improved surface-initiated vapor deposition polymerization. *Langmuir* **2002**, *18*, 9859-9866.

(508) Poche, D. S.; Russo, P. S.; Daly, W. H. Solution characterization of linear and star-branched semiflexible polymers of γ-stearyl-α,l-glutamate. *Abstracts of Papers of the American Chemical Society* **1990**, *200*, 211-POLY.

(509) Phan, S. E.; Russel, W. B.; Cheng, Z. D.; Zhu, J. X.; Chaikin, P. M.; Dunsmuir, J. H.; Ottewill, R. H. Phase transition, equation of state, and limiting shear viscosities of hard sphere dispersions. *Physical Review E* **1996**, *54*, 6633-6645
.

(510) Phan, S. E.; Russel, W. B.; Zhu, J. X.; Chaikin, P. M. Effects of polydispersity on hard sphere crystals. *J. Chem. Phys.* **1998**, *108*, 9789-9795.

(511) Huisgen, R. *1,3-Dipolar Cycloaddition Chemistry*; Wiley: New York, 1984.

(512) Kolb, H. C.; Finn, M. G.; Sharpless, K. B. Click chemistry: Diverse chemical function from a few good reactions. *Angew. Chem.-Int. Edit.* **2001**, *40*, 2004.

(513) Kolb, H. C.; Sharpless, K. B. The growing impact of click chemistry on drug discovery. *Drug Discovery Today* **2003**, *8*, 1128-1137.

(514) Tornoe, C. W.; Christensen, C.; Meldal, M. Peptidotriazoles on solid phase: [1,2,3]-triazoles by regiospecific copper(I)-catalyzed 1,3-dipolar cycloadditions of terminal alkynes to azides. *Journal of Organic Chemistry* **2002**, *67*, 3057-3064.

(515) Himo, F.; Lovell, T.; Hilgraf, R.; Rostovtsev, V. V.; Noodleman, L.; Sharpless, K. B.; Fokin, V. V. Copper(I)-catalyzed synthesis of azoles. DFT study predicts unprecedented reactivity and intermediates. *J. Am. Chem. Soc.* **2005**, *127*, 210-216
.

(516) Rostovtsev, V. V.; Green, L. G.; Fokin, V. V.; Sharpless, K. B. A stepwise Huisgen cycloaddition process: Copper(I)-catalyzed regioselective "ligation" of azides and terminal alkynes. *Angew. Chem.-Int. Edit.* **2002**, *41*, 2596.

(517) Golas, P. L.; Matyjaszewski, K. Click chemistry and ATRP: A beneficial union for the preparation of functional materials. *Qsar & Combinatorial Science* **2007**, *26*, 1116-1134.

(518) Le Droumaguet, B.; Velonia, K. Click chemistry: A powerful tool to create polymer-based macromolecular chimeras. *Macromol. Rapid Commun.* **2008**, *29*, 1073-1089.

(519) McCormick, C. L.; Sumerlin, B. S.; Lokitz, B. S.; Stempka, J. E. RAFT-synthesized diblock and triblock copolymers: thermally-induced supramolecular assembly in aqueous media. *Soft Matter* **2008**, *4*, 1760-1773.

(520) Gragert, M.; Schunack, M.; Binder, W. H. Azide/Alkyne-"Click"-Reactions of Encapsulated Reagents: Toward Self-Healing Materials. *Macromol. Rapid Commun.* **2010**, *32*, 419-425.

(521) Li, N. W.; Binder, W. H. Click-chemistry for nanoparticle-modification. *J. Mater. Chem.* **2010**, *21*, 16717-16734.

(522) Schulz, M.; Tanner, S.; Barqawi, H.; Binder, W. H. Macrocyclization of Polymers via Ring-Closing Metathesis and Azide/Alkyne-"Click"-Reactions: An Approach to Cyclic Polyisobutylenes. *Journal of Polymer Science Part a-Polymer Chemistry* **2010**, *48*, 671-680.

(523) Binder, W. H.; Sachsenhofer, R. 'Click' chemistry in polymer and material science: An update. *Macromol. Rapid Commun.* **2008**, *29*, 952-981.

(524) Agut, W.; Taton, D.; Lecommandoux, S. A versatile synthetic approach to polypeptide based rod-coil block copolymers by click chemistry. *Macromolecules* **2007**, *40*, 5653-5661.

(525) Sanda, F.; Gao, G. Z.; Masuda, T. Helical polymer carrying helical grafts from peptide-based acetylene macromonomers: Synthesis. *Macromolecular Bioscience* **2004**, *4*, 570-574.

(526) Rao, J. Y.; Zhang, Y. F.; Zhang, J. Y.; Liu, S. Y. Facile Preparation of Well-Defined AB(2) Y-Shaped Miktoarm Star Polypeptide Copolymer via the Combination of Ring-Opening Polymerization and Click Chemistry. *Biomacromolecules* **2008**, *9*, 2586-2593.

(527) Schatz, C.; Louguet, S.; Le Meins, J. F.; Lecommandoux, S. Polysaccharide-block-polypeptide Copolymer Vesicles: Towards Synthetic Viral Capsids. *Angew. Chem.-Int. Edit.* **2009**, *48*, 2572-2575.

(528) Schatz, C.; Lecommandoux, S. Polysaccharide-Containing Block Copolymers: Synthesis, Properties and Applications of an Emerging Family of Glycoconjugates. *Macromol. Rapid Commun.* **2010**, *31*, 1664-1684.

(529) Habraken, G. J. M.; Peeters, M.; Thornton, P. D.; Koning, C. E.; Heise, A. Selective Enzymatic Degradation of Self-Assembled Particles from Amphiphilic Block Copolymers Obtained by the Combination of N-Carboxyanhydride and Nitroxide-Mediated Polymerization. *Biomacromolecules* **2011**, *12*, 3761-3769.

(530) Kramer, J. R.; Deming, T. J. Glycopolypeptides with a Redox-Triggered Helix-to-Coil Transition. *J. Am. Chem. Soc.* **2012**, *134*, 4112-4115.

(531) Tang, H. Y.; Zhang, D. H. Multi-functionalization of helical block copoly(α-peptide)s by orthogonal chemistry. *Polymer Chemistry* **2011**, *2*, 1542-1551
.

(532) Upadhyay, K. K.; Le Meins, J. F.; Misra, A.; Voisin, P.; Bouchaud, V.; Ibarboure, E.; Schatz, C.; Lecommandoux, S. Biomimetic Doxorubicin Loaded Polymersomes from Hyaluronan-block-Poly(γ-benzyl glutamate) Copolymers. *Biomacromolecules* **2009**, *10*, 2802-2808.

(533) Wang, R.; Chen, G. T.; Du, F. S.; Li, Z. C. Preparation and aggregation behavior of mannose-terminated poly(ethylene glycol)-b-poly(L-leucine) in water. *Colloids and Surfaces B-Biointerfaces* **2011**, *85*, 56-62.

(534) Chang, L. M.; Li, Y.; Chu, J.; Qi, J. Y.; Li, X. Preparation of core-shell molecularly imprinted polymer via the combination of reversible addition-fragmentation chain transfer polymerization and click reaction. *Anal. Chim. Acta* **2012**, *680*, 65-71.

(535) Chang, L. M.; Li, Y.; Chu, J.; Qi, J. Y.; Li, X. Preparation of core-shell molecularly imprinted polymer via the combination of reversible addition-fragmentation chain transfer polymerization and click reaction. *Anal. Chim. Acta* **2010**, *680*, 65-71.

(536) Li, G. L.; Xu, L. Q.; Tang, X. Z.; Neoh, K. G.; Kang, E. T. Hairy Hollow Microspheres of Fluorescent Shell and Temperature-Responsive Brushes via Combined Distillation-Precipitation Polymerization and Thiol-ene Click Chemistry. *Macromolecules* **2010**, *43*, 5797-5803.

(537) Wittig, G.; Krebs, A. Zur existenz niedergliedriger cycloalkine .1. *Chemische Berichte-Recueil* **1961**, *94*, 3260-3275.

(538) Turner, R. B.; Goebel, P.; Mallon, B. J.; Jarrett, A. D. Heats o hydrogenation .9. Cyclic acetylenes and some miscellaneous olefins. *J. Am. Chem. Soc.* **1973**, *95*, 790-792.

(539) Baskin, J. M.; Prescher, J. A.; Laughlin, S. T.; Agard, N. J.; Chang, P. V.; Miller, I. A.; Lo, A.; Codelli, J. A.; Bertozzi, C. R. Copper-free click chemistry for dynamic in vivo imaging. *Proceedings of the National Academy of Sciences of the United States of America* **2007**, *104*, 16793-16797.

(540) Codelli, J. A.; Baskin, J. M.; Agard, N. J.; Berozzi, C. R. Second-generation difluorinated cyclooctynes for copper-free click chemistry. *J. Am. Chem. Soc.* **2008**, *130*, 11486-11493.

(541) Rodionov, V. O.; Fokin, V. V.; Finn, M. G. Mechanism of the ligand-free Cu-I-catalyzed azide-alkyne cycloaddition reaction. *Angew. Chem.-Int. Edit.* **2005**, *44*, 2210-2215.

(542) Devaraj, N. K.; Upadhyay, R.; Hatin, J. B.; Hilderbrand, S. A.; Weissleder, R. Fast and Sensitive Pretargeted Labeling of Cancer Cells through a Tetrazine/trans-Cyclooctene Cycloaddition. *Angew. Chem.-Int. Edit.* **2009**, *48*, 7013-7016.

(543) Han, H. S.; Devaraj, N. K.; Lee, J.; Hilderbrand, S. A.; Weissleder, R.; Bawendi, M. G. Development of a Bioorthogonal and Highly Efficient Conjugation Method for Quantum Dots Using Tetrazine-Norbornene Cycloaddition. *J. Am. Chem. Soc.* **2010**, *132*, 7838.

(544) Jewett, J. C.; Bertozzi, C. R. Cu-free click cycloaddition reactions in chemical biology. *Chemical Society Reviews* **2010**, *39*, 1272-1279.

(545) Lin, Y.-C.; Kuo, S.-W. Hierarchical self-assembly and secondary structures of linear polypeptides graft onto POSS in the side chain through click chemistry. *Polymer Chemistry* **2012**, *3*, 162-171.

(546) Oosterling, M.; Willems, E.; Schouten, A. J. End-grafting of (co)polyglutamates and (co)polyaspartates onto si-oh containing surfaces. *Polymer* **1995**, *36*, 4463-4470.

(547) Oosterling, M.; Willems, E.; Schouten, A. J. Conformation and orientation of end-grafted (co)polyglutamates and (co)polyaspartates. *Polymer* **1995**, *36*, 4485-4490.

(548) Wang, J.; Gibson, M. I.; Barbey, R.; Xiao, S. J.; Klok, H. A. Nonfouling Polypeptide Brushes via Surface-initiated Polymerization of N-ε-oligo(ethylene glycol)succinate-L-lysine N-carboxyanhydride. *Macromol. Rapid Commun.* **2009**, *30*, 845-850.

(549) Luijten, J.; Vorenkamp, E. J.; Schouten, A. J. Reversible helix sense inversion in surface-grafted poly(β-phenethyl-L-aspartate) films. *Langmuir* **2007**, *23*, 10772-10778.

(550) Luijten, J.; Groeneveld, D. Y.; Nijboer, G. W.; Vorenkamp, E. J.; Schouten, A. J. Cross-linking-induced permanently perpendicular helix orientation in surface-grafted polyglutamate films. *Langmuir* **2007**, *23*, 8163-8169.

(551) Wu, J. C.; Wang, Y. L.; Chen, C. C.; Chang, Y. C. Biomimetic synthesis of silica films directed by polypeptide brushes. *Chem. Mat.* **2008**, *20*, 6148-6156.

(552) Duran, H.; Ogura, K.; Nakao, K.; Vianna, S. D. B.; Usui, H.; Advincula, R. C.; Knoll, W. High-Vacuum Vapor Deposition and in Situ Monitoring of N-Carboxy Anhydride Benzyl Glutamate Polymerization. *Langmuir* **2009**, *25*, 10711-10718.

(553) Barbosa, M. E. M.; Montembault, V.; Cammas-Marion, S.; Ponchel, G.; Fontaine, L. Synthesis and characterization of novel poly(γ-benzyl-L-glutamate) derivatives tailored for the preparation of nanoparticles of pharmaceutical interest. *Polymer International* **2007**, *56*, 317-324.

(554) Guo, J. S.; Huang, Y. B.; Jing, X. B.; Chen, X. S. Synthesis and characterization of functional poly(γ-benzyl-L-glutamate) (PBLG) as a hydrophobic precursor. *Polymer* **2009**, *50*, 2847-2855.

(555) Aden, A. L.; Kerker, M. Scattering of electromagnetic waves from 2 concentric spheres. *Journal of Applied Physics* **1951**, *22*, 1242-1246.

(556) Kerker, M. *The scattering of Light and Other Electromagnetic Radiation* Academic Press: New York, 1969.

(557) Korgel, B. A.; van Zanten, J. H.; Monbouquette, H. G. Vesicle size distributions measured by flow field-flow fractionation coupled with multiangle light scattering. *Biophysical Journal* **1998**, *74*, 3264-3272.

(558) Wyatt, P. J. Differential light scattering - a physical method for identifying living bacterial cells. *Applied Optics* **1968**, *7*, 1879.

(559) Wyatt, P. J. Cell wall thickness, size distribution, refractive index ratio and dry weight content of living bacteria (*Staphylococcus-aureus*). *Nature* **1970**, *226*, 277.

(560) Cappelli, C.; Mennucci, B.; Cammi, R.; Rizzo, A. Quantum mechanical polarizable continuum model approach to the Kerr effect of pure liquids. *Journal of Physical Chemistry B* **2005**, *109*, 18706-18714.

(561) Zeffert, B. M.; Coulter, P. B.; Macy, R. The absence of quaternary salt formation between phosphoryl chloride and pyridine. *J. Am. Chem. Soc.* **1953**, *75*, 751-753.

(562) Qiu, J. Ph. D. DissertationLouisiana State University, 2007.

(563) Szekeres, M.; Kamalin, O.; Schoonheydt, R. A.; Wostyn, K.; Clays, K.; Persoons, A.; Dekany, I. Ordering and optical properties of monolayers and multilayers of silica spheres deposited by the Langmuir-Blodgett method. *J. Mater. Chem.* **2002**, *12*, 3268-3274.

(564) Huglin, M. B. *Specific Refractive Index Increments.* ; Academic Press: New York, 1972.

(565) Bu, M. Q.; Melvin, T.; Ensell, G. J.; Wilkinson, J. S.; Evans, A. G. R. A new masking technology for deep glass etching and its microfluidic application. *Sensors and Actuators a-Physical* **2004**, *115*, 476-482.

(566) van Kats, C. M.; Johnson, P. M.; van den Meerakker, J.; van Blaaderen, A. Synthesis of monodisperse high-aspect-ratio colloidal silicon and silica rods. *Langmuir* **2004**, *20*, 11201-11207.

(567) Liu, D.; Li, Y.; Deng, J. P.; Yang, W. T. Synthesis and characterization of magnetic Fe_3O_4-silica-poly(γ-benzyl-L-glutamate) composite microspheres. *Reactive & Functional Polymers* **2011**, *71*, 1040-1044.

(568) Ostlund, S. G.; Striegel, A. M. Ultrasonic degradation of poly(γ-benzyl-L-glutamate), an archetypal highly extended polymer. *Polymer Degradation and Stability* **2008**, *93*, 1510-1514.

(569) Caruso, F.; Caruso, R. A.; Mohwald, H. Nanoengineering of inorganic and hybrid hollow spheres by colloidal templating. *Science* **1998**, *282*, 1111-1114.

(570) Donath, E.; Sukhorukov, G. B.; Caruso, F.; Davis, S. A.; Mohwald, H. Novel hollow polymer shells by colloid-templated assembly of polyelectrolytes. *Angew. Chem.-Int. Edit.* **1998**, *37*, 2202-2205.

(571) Becker, A. L.; Johnston, A. P. R.; Caruso, F. Layer-By-Layer-Assembled Capsules and Films for Therapeutic Delivery. *Small* **2010**, *6*, 1836-1852.

(572) Becker, A. L.; Johnston, A. P. R.; Caruso, F. Peptide Nucleic Acid Films and Capsules: Assembly and Enzymatic Degradation. *Macromolecular Bioscience* **2010**, *10*, 488-495.

(573) Becker, A. L.; Zelikin, A. N.; Johnston, A. P. R.; Caruso, F. Tuning the Formation and Degradation of Layer-by-Layer Assembled Polymer Hydrogel Microcapsules. *Langmuir* **2009**, *25*, 14079-14085.

(574) Johnston, A. P. R.; Cortez, C.; Angelatos, A. S.; Caruso, F. Layer-by-layer engineered capsules and their applications. *Current Opinion in Colloid & Interface Science* **2006**, *11*, 203-209.

(575) Wiedeman, M. P. Dimensions of blood vessels from distributing artery to collecting vein. *Circulation Research* **1963**, *12*, 375.

(576) Zelikin, A. N.; Li, Q.; Caruso, F. Disulfide-stabilized poly(methacrylic acid) capsules: Formation, cross-linking, and degradation behavior. *Chem. Mat.* **2008**, *20*, 2655-2661.

(577) Zelikin, A. N.; Li, Q.; Caruso, F. Degradable polyelectrolyte capsules filled with oligonucleotide sequences. *Angew. Chem.-Int. Edit.* **2006**, *45*, 7743-7745.

(578) Johnston, A. P. R.; Zelikin, A. N.; Caruso, F. Assembling DNA into advanced materials: From nanostructured films to Biosensing and delivery systems. *Adv. Mater.* **2007**, *19*, 3727-3730.

(579) Such, G. K.; Quinn, J. F.; Quinn, A.; Tjipto, E.; Caruso, F. Assembly of ultrathin polymer multilayer films by click chemistry. *J. Am. Chem. Soc.* **2006**, *128*, 9318-9319.

(580) Such, G. K.; Tjipto, E.; Postma, A.; Johnston, A. P. R.; Caruso, F. Ultrathin, responsive polymer click capsules. *Nano Letters* **2007**, *7*, 1706-1710.

(581) Chong, S. F.; Chandrawati, R.; Stadler, B.; Park, J.; Cho, J. H.; Wang, Y. J.; Jia, Z. F.; Bulmus, V.; Davis, T. P.; Zelikin, A. N.; Caruso, F. Stabilization of Polymer-Hydrogel Capsules via Thiol-Disulfide Exchange. *Small* **2009**, *5*, 2601-2610.

(582) Yan, Y.; Ochs, C. J.; Such, G. K.; Heath, J. K.; Nice, E. C.; Caruso, F. Bypassing Multidrug Resistance in Cancer Cells with Biodegradable Polymer Capsules. *Adv. Mater.* **2010**, *22*, 5398.

(583) Chandrawati, R.; Hosta-Rigau, L.; Vanderstraaten, D.; Lokuliyana, S. A.; Stadler, B.; Albericio, F.; Caruso, F. Engineering Advanced Capsosomes: Maximizing the Number of Subcompartments, Cargo Retention, and Temperature-Triggered Reaction. *ACS Nano* **2010**, *4*, 1351-1361.

(584) Chandrawati, R.; Stadler, B.; Postma, A.; Connal, L. A.; Chong, S. F.; Zelikin, A. N.; Caruso, F. Cholesterol-mediated anchoring of enzyme-loaded liposomes within disulfide-stabilized polymer carrier capsules. *Biomaterials* **2009**, *30*, 5988-5998.

(585) Hosta-Rigau, L.; Stadler, B.; Yan, Y.; Nice, E. C.; Heath, J. K.; Albericio, F.; Caruso, F. Capsosomes with Multilayered Subcompartments: Assembly and Loading with Hydrophobic Cargo. *Advanced Functional Materials* **2010**, *20*, 59-66.

(586) Stadler, B.; Chandrawati, R.; Goldie, K.; Caruso, F. Capsosomes: Subcompartmentalizing Polyelectrolyte Capsules Using Liposomes. *Langmuir* **2009**, *25*, 6725-6732.

(587) Stadler, B.; Chandrawati, R.; Price, A. D.; Chong, S. F.; Breheney, K.; Postma, A.; Connal, L. A.; Zelikin, A. N.; Caruso, F. A Microreactor with Thousands of Subcompartments: Enzyme-Loaded Liposomes within Polymer Capsules. *Angew. Chem.-Int. Edit.* **2009**, *48*, 4359-4362.

(588) Chandrawati, R.; van Koeverden, M. P.; Lomas, H.; Caruso, F. Multicompartment Particle Assemblies for Bioinspired Encapsulated Reactions. *J. Phys. Chem. Lett.* **2011**, *2*, 2639-2649.

(589) Driever, C. D.; Mulet, X.; Johnston, A. P. R.; Waddington, L. J.; Thissen, H.; Caruso, F.; Drummond, C. J. Converging layer-by-layer polyelectrolyte microcapsule and cubic lyotropic liquid crystalline nanoparticle approaches for molecular encapsulation. *Soft Matter* **2011**, *7*, 4257-4266.

(590) Chang, D. H. C.; Johnston, A. P. R.; Wark, K. L.; Breheney, K.; Caruso, F. Engineered Bacterially Expressed Polypeptides: Assembly into Polymer Particles with Tailored Degradation Profiles. *Angew. Chem.-Int. Edit.* **2012**, *51*, 460-464.

(591) Peabody, D. S.; Manifold-Wheeler, B.; Medford, A.; Jordan, S. K.; do Carmo Caldeira, J.; Chackerian, B. Immunogenic Display of Diverse Peptides on Virus-like Particles of RNA Phage MS2. *Journal of Molecular Biology* **2008**, *380*, 252-263.

(592) McPherson, A. Micelle formation and crystallization as paradigms for virus assembly. *Bioessays* **2005**, *27*, 447-458.

(593) Maccarrone, S.; Brambilla, G.; Pravaz, O.; Duri, A.; Ciccotti, M.; Fromental, J. M.; Pashkovski, E.; Lips, A.; Sessoms, D.; Trappe, V.; Cipelletti, L. Ultra-long range correlations of the dynamics of jammed soft matter. *Soft Matter* **2010**, *6*, 5514-5522.

(594) Cerbino, R.; Vailati, A. Near-field scattering techniques: Novel instrumentation and results from time and spatially resolved investigations of soft matter systems. *Current Opinion in Colloid & Interface Science* **2009**, *14*, 416-425.

(595) Cipelletti, L.; Ramos, L.; Manley, S.; Pitard, E.; Weitz, D. A.; Pashkovski, E. E.; Johansson, M. Universal non-diffusive slow dynamics in aging soft matter. *Faraday Discussions* **2003**, *123*, 237-251.

(596) Coniglio, A.; Abete, T.; de Candia, A.; Del Gado, E.; Fierro, A. Dynamical heterogeneities: from glasses to gels. *Journal of Physics-Condensed Matter* **2008**, *20*.

(597) Duri, A.; Sessoms, D. A.; Trappe, V.; Cipelletti, L. Resolving Long-Range Spatial Correlations in Jammed Colloidal Systems Using Photon Correlation Imaging. *Physical Review Letters* **2009**, *102*.

(598) Head, D. A. Critical Scaling and Aging in Cooling Systems Near the Jamming Transition. *Physical Review Letters* **2009**, *102*.

(599) Loppinet, B.; Stiakakis, E.; Vlassopoulos, D.; Fytas, G.; Roovers, J. Reversible thermal gelation in star polymers: An alternative route to jamming of soft matter. *Macromolecules* **2001**, *34*, 8216-8223.

(600) Rahmani, Y.; van der Vaart, K.; van Dam, B.; Hu, Z.; Chikkadi, V.; Schall, P. Dynamic heterogeneity in hard and soft sphere colloidal glasses. *Soft Matter* **2012**, *8*, 4264-4270.

(601) Siebenburger, M.; Fuchs, M.; Ballauff, M. Core-shell microgels as model colloids for rheological studies. *Soft Matter* **2012**, *8*, 4014-4024.

(602) Lhuillier, D.; Nadim, A. Rheology of suspensions of mass-polarized particles in a gravitational field. *Chemical Engineering Communications* **2010**, *197*, 76-91.

(603) Abade, G. C.; Cichocki, B.; Ekiel-Jezewska, M. L.; Nagele, G.; Wajnryb, E. Diffusion, sedimentation, and rheology of concentrated suspensions of core-shell particles. *J. Chem. Phys.* **2012**, *136*.

(604) Piazza, R.; Buzzaccaro, S.; Secchi, E. The unbearable heaviness of colloids: facts, surprises, and puzzles in sedimentation. *Journal of Physics-Condensed Matter* **2012**, *24*.

(605) Colin, J. Shape evolution of a core-shell spherical particle under hydrostatic pressure. *Physical Review E* **2012**, *85*.

(606) Ross, D. J.; Sigel, R. Mie scattering by soft core-shell particles and its applications to ellipsometric light scattering. *Physical Review E* **2012**, *85*.

(607) Aarts, D.; Tuinier, R.; Lekkerkerker, H. N. W. Phase behaviour of mixtures of colloidal spheres and excluded-volume polymer chains. *Journal of Physics-Condensed Matter* **2002**, *14*, 7551-7561.

(608) Boek, E. S.; Coveney, P. V.; Lekkerkerker, H. N. W. Computer simulation of rheological phenomena in dense colloidal suspensions with dissipative particle dynamics. *Journal of Physics-Condensed Matter* **1996**, *8*, 9509-9512.

(609) Bolhuis, P. G.; Lekkerkerker, H. N. W. Light-scattering and sedimentation equilibrium of a concentrated multicomponent hard rod dispersion. *Physica A* **1993**, *196*, 375-388.

(610) de Folter, J. W. J.; de Villeneuve, V. W. A.; Aarts, D.; Lekkerkerker, H. N. W. Rigid sphere transport through a colloidal gas-liquid interface. *New Journal of Physics* **2010**, *12*.

(611) Deschepper, I. M.; Cohen, E. G. D.; Pusey, P. N.; Lekkerkerker, H. N. W. Long-time diffusion in suspensions of interacting charged colloids. *Journal of Physics-Condensed Matter* **1989**, *1*, 6503-6506.

(612) Finsy, R.; Devriese, A.; Lekkerkerker, H. Light-scattering study of the diffusion of interacting particles. *Journal of the Chemical Society-Faraday Transactions Ii* **1980**, *76*, 767-775.

(613) Finsy, R.; Moreels, E.; Bottger, A.; Lekkerkerker, H. Study of the relation between diffusion and sedimentation of charged silica sols by dynamic light-scattering, ultracentrifugation, and turbidimetry. *J. Chem. Phys.* **1985**, *82*, 3812-3816.

(614) Kopswerkhoven, M. M.; Vrij, A.; Lekkerkerker, H. N. W. On the relation between diffusion, sedimentation, and friction. *J. Chem. Phys.* **1983**, *78*, 2760-2763.

(615) Lekkerke.Hn; Laidlaw, W. G. Onsager symmetry relations and spectral distribution of scattered light. *Physical Review A* **1972**, *5*, 1604.

(616) Lekkerke.Hn; Laidlaw, W. G. Onsager symmetry relations and maximum number of propagating hydrodynamic modes. *Physical Review A* **1974**, *9*, 431-434.

(617) Lekkerkerker, C. G. Linear transport-equation - degenerate case c=1. 1. Full-range theory. *Proceedings of the Royal Society of Edinburgh Section a-Mathematics* **1976**, *75*, 259-282.

(618) Lekkerkerker, H. N. W. Brownian-motion and hydrodynamic fluctuations near convective instability point. *Physica A* **1975**, *80*, 415-420.

(619) Lekkerkerker, H. N. W. Osmotic equilibrium treatment of the phase-separation in colloidal dispersions containing nonadsorbing polymer-molecules. *Colloids and Surfaces* **1990**, *51*, 419-426.

(620) Lekkerkerker, H. N. W.; Coulon, P.; Luyckx, R. Dispersion forces between closed shell atoms. *Physica A* **1977**, *88*, 375-384.

(621) Lekkerkerker, H. N. W.; Stroobants, A. On the spinodal instability of highly asymmetric hard-sphere suspensions. *Physica A* **1993**, *195*, 387-397.

(622) Mao, Y.; Cates, M. E.; Lekkerkerker, H. N. W. Depletion force in colloidal systems. *Physica A* **1995**, *222*, 10-24.

(623) Overbeek, J. T. G.; Verhoeckx, G. J.; Debruyn, P. L.; Lekkerkerker, H. N. W. On understanding microemulsions .2. Thermodynamics of droplet-type microemulsions. *Journal of Colloid and Interface Science* **1987**, *119*, 422-441.

(624) Oversteegen, S. M.; Lekkerkerker, H. N. W. The importance of correlations in free-volume models for depletion phenomena. *Physica a-Statistical Mechanics and Its Applications* **2002**, *310*, 181-196.

(625) Oversteegen, S. M.; Lekkerkerker, H. N. W. On the accuracy of the Derjaguin approximation for depletion potentials. *Physica a-Statistical Mechanics and Its Applications* **2004**, *341*, 23-39.

(626) ten Brinke, A. J. W.; Bailey, L.; Lekkerkerker, H. N. W.; Maitland, G. C. Rheology modification in mixed shape colloidal dispersions. Part I: pure components. *Soft Matter* **2007**, *3*, 1145-1162.

(627) Vrij, A.; Penders, M.; Rouw, P. W.; Dekruif, C. G.; Dhont, J. K. G.; Smits, C.; Lekkerkerker, H. N. W. Phase-transition phenomena in colloidal systems with attractive and repulsive particle interactions. *Faraday Discussions* **1990**, *90*, 31-40.

(628) Xian, X.; Petukhov, A. V.; Snel, M. M. E.; Dolbnya, I. P.; Aarts, D.; Vroege, G. J.; Lekkerkerker, H. N. W. Depletion-induced colloidal crystals at a wall characterised by small-angle X-ray diffraction. *Journal of Applied Crystallography* **2003**, *36*, 597-601.

(629) Allia, P.; Tiberto, P. Dynamic effects of dipolar interactions on the magnetic behavior of magnetite nanoparticles. *Journal of Nanoparticle Research* **2011**, *13*, 7277-7293.

(630) Almenar, L.; Rauscher, M. Dynamics of colloids in confined geometries. *Journal of Physics-Condensed Matter* **2011**, *23*.

(631) Tracy, M. A.; Garcia, J. L.; Pecora, R. An investigation of the microstructure of a rod sphere composite liquid. *Macromolecules* **1993**, *26*, 1862-1868.

(632) Tracy, M. A.; Pecora, R. Synthesis, characterization, and dynamics of a rod sphere composite liquid. *Macromolecules* **1992**, *25*, 337-349.

(633) Ashkin, A. Forces of a single-beam gradient laser trap on a dielectric sphere in the ray optics regime. *Biophysical Journal* **1992**, *61*, 569-582.

(634) Block, S. M.; Blair, D. F.; Berg, H. C. Compliance of bacterial flagella measured with optical tweezers. *Nature* **1989**, *338*, 514-518.

(635) Block, S. M.; Goldstein, L. S. B.; Schnapp, B. J. Bead movement by single kinesin molecules studied with optical tweezers. *Nature* **1990**, *348*, 348-352.

(636) Svoboda, K.; Block, S. M. Biological applications of optical forces. *Annual Review of Biophysics and Biomolecular Structure* **1994**, *23*, 247-285.

(637) Wright, W. H.; Sonek, G. J.; Berns, M. W. Parametric study of the forces on microspheres held by optical tweezers. *Applied Optics* **1994**, *33*, 1735-1748.

(638) Gutsche, C.; Elmahdy, M. M.; Kegler, K.; Semenov, I.; Stangner, T.; Otto, O.; Ueberschar, O.; Keyser, U. F.; Krueger, M.; Rauscher, M.; Weeber, R.; Harting, J.; Kim, Y. W.; Lobaskin, V.; Netz, R. R.; Kremer, F. Micro-rheology on (polymer-grafted) colloids using optical tweezers. *Journal of Physics-Condensed Matter* **2011**, *23*.

(639) Brochardwyart, F.; Hervet, H.; Pincus, P. Unwinding of polymer-chains under forces or flows. *Europhysics Letters* **1994**, *26*, 511-516.

(640) Castelain, M.; Rouxhet, P. G.; Pignon, F.; Magnin, A.; Piau, J. M. Single-cell adhesion probed in-situ using optical tweezers: A case study with *Saccharomyces cerevisiae*. *Journal of Applied Physics* **2012**, *111*.

(641) Hegge, S.; Uhrig, K.; Streichfuss, M.; Kynast-Wolf, G.; Matuschewski, K.; Spatz, J. P.; Frischknecht, F. Direct Manipulation of Malaria Parasites with Optical Tweezers Reveals Distinct Functions of Plasmodium Surface Proteins. *ACS Nano* **2012**, *6*, 4648-4662.

(642) Meng, F. H.; Zhong, Z. Y.; Feijen, J. Stimuli-Responsive Polymersomes for Programmed Drug Delivery. *Biomacromolecules* **2009**, *10*, 197-209.

(643) Auzenne, E.; Donato, N. J.; Li, C.; Leroux, E.; Price, R. E.; Farquhar, D.; Klostergaard, J. Superior therapeutic profile of poly-L-glutamic acid-paclitaxel copolymer compared with Taxol in xenogeneic compartmental models of human ovarian carcinoma. *Clinical Cancer Research* **2002**, *8*, 573-581.

(644) Buescher, J. M.; Margaritis, A. Microbial biosynthesis of polyglutamic acid biopolymer and applications in the biopharmaceutical, biomedical and food industries. *Critical Reviews in Biotechnology* **2007**, *27*, 1-19.

(645) Li, C. Poly(L-glutamic acid) - anticancer drug conjugates. *Advanced Drug Delivery Reviews* **2002**, *54*, 695-713.

(646) Li, C.; Newman, R. A.; Wu, Q. P.; Ke, S.; Chen, W.; Hutto, T.; Kan, Z. X.; Brannan, M. D.; Charnsangavej, C.; Wallace, S. Biodistribution of paclitaxel and poly(L-glutamic acid)-paclitaxel conjugate in mice with ovarian OCa-1 tumor. *Cancer Chemotherapy and Pharmacology* **2000**, *46*, 416-422.

(647) Li, C.; Wallace, S. Polymer-drug conjugates: Recent development in clinical oncology. *Advanced Drug Delivery Reviews* **2008**, *60*, 886-898.

(648) Li, C.; Yu, D. F.; Newman, R. A.; Cabral, F.; Stephens, L. C.; Hunter, N.; Milas, L.; Wallace, S. Complete regression of well-established tumors using a novel water-soluble poly(L-glutamic acid) paclitaxel conjugate. *Cancer Research* **1998**, *58*, 2404-2409.

(649) Melancon, M. P.; Li, C. Multifunctional Synthetic Poly(L-Glutamic Acid)-Based Cancer Therapeutic and Imaging Agents. *Molecular Imaging* **2011**, *10*, 28-42.

(650) Milas, L.; Mason, K. A.; Hunter, N.; Li, C.; Wallace, S. Poly(L-glutamic acid)-paclitaxel conjugate is a potent enhancer of tumor radiocurability. *International Journal of Radiation Oncology Biology Physics* **2003**, *55*, 707-712.

(651) Oldham, E. A.; Li, C.; Ke, S.; Wallace, S.; Huang, P. Comparison of action of paclitaxel and poly(L-glutamic acid)paclitaxel conjugate in human breast cancer cells. *International Journal of Oncology* **2000**, *16*, 125-132.

(652) Singer, J. W.; Baker, B.; De Vries, P.; Kumar, A.; Shaffer, S.; Vawter, E.; Bolton, M.; Garzone, P. In *Polymer Drugs in the Clinical Stage: Advantages and Prospects*; Maeda, H., Kabanov, A., Kataoka, K., Okano, T., Eds. 2003; Vol. 519, p 81-99.

(653) Lu, Z. R.; Ye, F. R.; Vaidya, A. Polymer platforms for drug delivery and biomedical imaging. *Journal of Controlled Release* **2007**, *122*, 269-277.

(654) Ye, F. R.; Ke, T. Y.; Jeong, E. K.; Wang, X. L.; Sung, Y. G.; Johnson, M.; Lu, Z. R. Noninvasive visualization of in vivo drug delivery of poly(L-glutamic acid) using contrast-enhanced MRI. *Molecular Pharmaceutics* **2006**, *3*, 507-515.

(655) Hsieh, C. Y.; Tsai, S. P.; Wang, D. M.; Chang, Y. N.; Hsieh, H. J. Preparation of γ-PGA/chitosan composite tissue engineering matrices. *Biomaterials* **2005**, *26*, 5617-5623.

(656) Agut, W.; BruÌ‚let, A.; Schatz, C.; Taton, D.; Lecommandoux, S. b. pH and Temperature Responsive Polymeric Micelles and Polymersomes by Self-Assembly of Poly[2-(dimethylamino)ethyl methacrylate]-b-Poly(glutamic acid) Double Hydrophilic Block Copolymers. *Langmuir* **2010**, *26*, 10546-10554.

(657) Sanson, C.; Le Meins, J. F.; Schatz, C.; Soum, A.; Lecommandoux, S. Temperature responsive poly(trimethylene carbonate)-block-poly(L-glutamic acid) copolymer: polymersomes fusion and fission. *Soft Matter* **2010**, *6*, 1722-1730.

(658) Sanson, C.; Schatz, C.; Le Meins, J. F.; Brulet, A.; Soum, A.; Lecommandoux, S. Biocompatible and Biodegradable Poly(trimethylene carbonate)-b-Poly (L-glutamic acid) Polymersomes: Size Control and Stability. *Langmuir* **2010**, *26*, 2751-2760.

(659) Sanson, C.; Diou, O.; Thevenot, J.; Ibarboure, E.; Soum, A.; Brulet, A.; Miraux, S.; Thiaudiere, E.; Tan, S.; Brisson, A.; Dupuis, V.; Sandre, O.; Lecommandoux, S. Doxorubicin Loaded Magnetic Polymersomes: Theranostic Nanocarriers for MR Imaging and Magneto-Chemotherapy. *ACS Nano* **2011**, *5*, 1122-1140.

(660) Huang, J.; Bonduelle, C.; Thevenot, J.; Lecommandoux, S.; Heise, A. Biologically Active Polymersomes from Amphiphilic Glycopeptides. *J. Am. Chem. Soc.* **2012**, *134*, 119-122.

CHAPTER 2
PREPARATION AND CHARACTERIZATION OF STRATIFIED COLLOIDAL SILICA

2.1 Introduction

The fast expansion of nanotechnology to a broad range of vital fields of science and technology provides opportunity to develop new advanced materials with excellent properties and facile control over such features. These fields relate to pigments,[1] catalysts,[2] chromatography,[3] dynamic behavior,[4] drug delivery,[5] bioimaging,[6] photonics,[7,8] etc. The road to such materials usually starts with the preparation of simple particulates. For the most advanced materials, the quality of the core, in terms of control over size and shape, is of great importance. This requirement demands improved ways to prepare and to characterize the colloidal suspensions.

Silica, SiO_2, is probably the most widely used filler in the development of the composite materials. Abundant natural silica is not amenable for scientific and technological applications because it is blended with metal traces. The purification of silica from natural sources will raise, consequently, the price of the production. Research-grade silica is mostly prepared by synthetic methods as pure and amorphous powders. One of the bottom-up routes to silica particles is the sol-gel method. This approach involves the hydrolysis and condensation of the silica precursors, tetraethylorthosilicate, TEOS, metal alkoxides, or inorganic salts such as sodium silicate in acidic or basic conditions. The basic environment provided by aqueous ammonia is milder during the preparation of particulate suspensions than the acidic medium used to generate gel-like products. A two-step process—hydrolysis of silicon alkoxide precursor to silicic acid followed by base-catalyzed alcohol condensation is used to make certain materials. Today silica colloid is synonymous with Stöber silica because the work published by Stöber et al. in 1968

became the most popular way to quasi-uniform particles.[9] Yet, several years before, Kolbe observed the formation of silica particles through the hydrolysis and condensation of TEOS in mixtures of water, alcohol and ammonia.[10] Some other reports were also known before the dawn of the Stöber era.[11] The drawbacks of the Stöber's approach, such as slow and costly TEOS distillation and the fast addition of TEOS to the basic alcoholic solution, have received much attention by other researchers attempting to obtain inexpensive monodisperse silica particulates.[12] Bogush et al.[12] and then Zhang et al.[13] developed a seeded growth technique to improve the spherical shape and uniformity, and to also increase the size of the particles. The contribution of latter authors was substantial in the field of colloids because it allowed the production of high-quality materials in terms of size and shape. Over the years research in the silica production was directed in improving the original Stöber method with focus on controlling the size distribution and shape.[14,15]

Silica formation was studied extensively from a kinetics point of view in an attempt to describe the growth mechanism. Two models have been proposed: monomer addition[16,17] and controlled aggregation.[12,18,19] The size of the primary particles is a commonly studied aspect, and researchers reported values from 2-4 nm to over 20 nm.[18,20-23] A review has appeared.[24]

Amorphous silica was found to be appealing for biomedical applications. Even though studies performed on the cytotoxicity were sometimes contradictory, in general silica is considered nontoxic for living bodies.[25] Monodisperse particles with a spherical shape are excellent candidates for photonic crystals applications.[26] Upon treatment with hydrofluoric acid, HF, or with base, NaOH, plain silica can be modeled into mesoporous structures which find applications in drug encapsulation and drug delivery.[27-29] The nature of the silica surface makes possible the decoration with functional groups which enables the attachment of polymers,

polypeptides, enzymes, etc. It is easy, then, to consider amorphous silica particles as an excellent platform to vital applications stemming from their properties.

Particle characterization typically uses tools such as electron microscopy (TEM and SEM) and light scattering. Flow field flow fractionation, F4, has emerged lately not only as a size evaluation method but also as a reliable utensil to separate colloid suspensions over a broad range (1 - 1000 nm) of sizes.[30] A member of the F4 family of techniques is asymmetric flow field-flow fractionation, AF4, introduced by Giddings.[31] The combination of AF4 with on-line detectors such as multi-angle light scattering, MALS, emerged as a powerful tool with enhanced sensitivity and high resolution information on particle morphology, composition and stability in a liquid media.[32-34] The AF4-MALS method is considered today an effective and viable alternate route to characterization of macromolecules[34-36] and especially non-spherical[37] and spherical particles.[33,38-44] More details about this technique are presented in a recent review article[45] and the theoretical background is described largely by Podzimek in his book.[46]

The present chapter describes a method to prepare a silica suspension in which particles of different size are separated into vertical layers. The layer separation occurred over a period of time in basic conditions. After their stratification each layer was collected separately and characterized by TEM, light scattering and AF4-MALS. Comparison of the size information gained by these techniques showed a tremendous improvement in particle dispersity. The mild basic conditions allowed a slow etching process of silica beads into mesoporous structures. The stability of the colloidal particles in time was also studied. Fractionation performed by AF4-MALS enabled the evaluation of the sizes within a given layer, along with information about the size distribution within that band. AF4/MALS was effective not only in the determination of the

intriguing mesoporous morphologies discovered in the silica layers but also in detecting the presence of degraded particles. These findings were also confirmed by TEM and DLS assays.

2.2. Materials

Tetraethyl orthosilicate, TEOS, (>90% purity) was purchased from Sigma-Aldrich. Absolute anhydrous ethyl alcohol 200 proof ACS/USP grade was obtained from Pharmco-AAPER. Ammonium hydroxide 28-30% ACS grade was purchased from BDH Aristar. All reagents were used without further purification. Deionized water (18 $M\Omega \bullet cm^{-1}$) was drawn from a Barnstead Nanopure water purification system.

2.3 Results and Discussion

2.3.1 Preparation and Characterization of Stratified Silica Colloid

The production of silica particles separated naturally by layers is illustrated in Scheme 2.1. A modification of the Stöber, Bogush and Zhang procedures was employed, albeit water was not used as in Stöber and Bogush approaches. The amount of water used was only from the ammonium hydroxide solution (28-30%). Briefly, a basic alcoholic solution (pH = 9) was obtained by mixing absolute ethanol with aqueous ammonium hydroxide for 15-20 min to achieve homogenization. Separately reagent grade TEOS was diluted 4x with absolute ethanol and rapidly added to the basic alcohol solution under vigorous stirring. After 2 h of reaction the white-bluish colloidal suspension was left undisturbed at least 12 h and, afterwards, was stored in tall bottles (8-8.5" in height, 3-4" in diameter). More preparatory details are described in Chapter 8, Sections 8.1, 8.1.1 and 8.1.2. At least six batches were prepared in both medium- (~500 mL) and large-scale (~1250 mL). The purpose of multiple batches was to test the method reproducibility in terms of yield, particle size and shape.

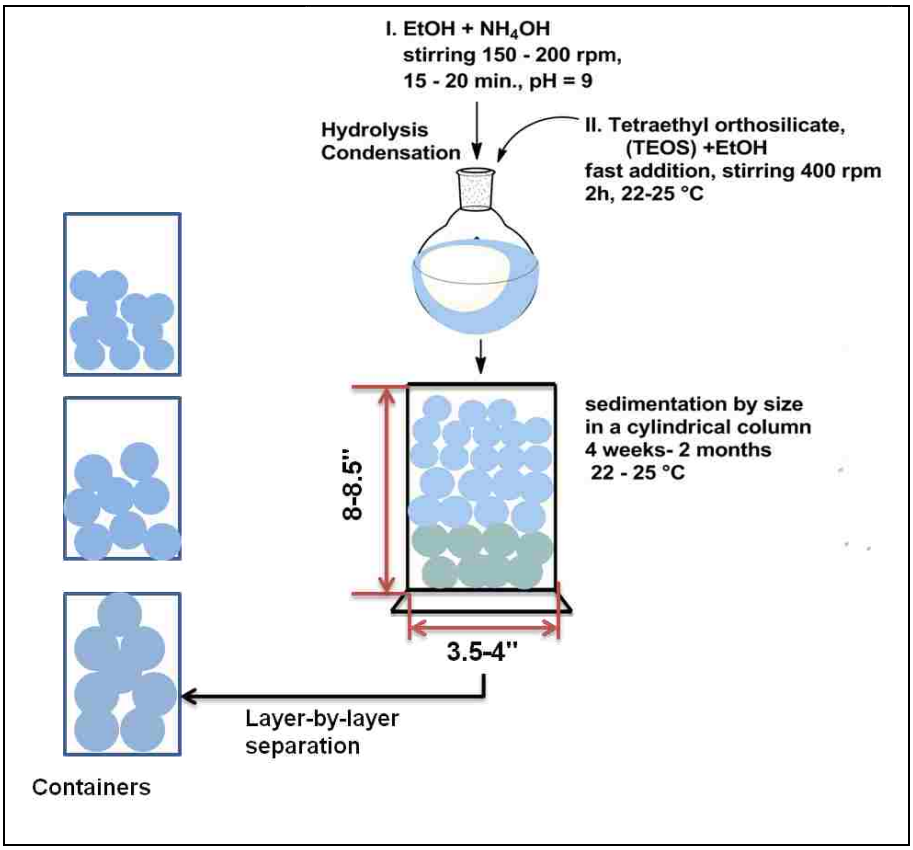

Scheme 2.1 Production of the stratified silica colloid (Not drawn to scale).

After preparation, the resting silica colloid began to separate into layers. The process took place from 4 weeks to almost 2 months. Each layer was collected separately. The particles were not washed. They were kept in the original basic conditions. The morphology of the particles was visualized by TEM. Figure 2.1 depicts particles from a batch which separated into two layers. Particles were uniform in size and spherical in shape. A tendency to pack into flower-like structures is evident in the TEM images. Undesired shapes such as peanut, were not observed. The peanut morphology occurs as a consequence of particle aggregation during the growth process.[13] The absence of such shapes demonstrates the importance of TEOS dilution with ethanol. The dilution slows the diffusion of the silane precursor to the silica nascent nuclei and

the growth evolves on a constant scale within the batch. These results are in good agreement with the report by Zhang et al.[13]

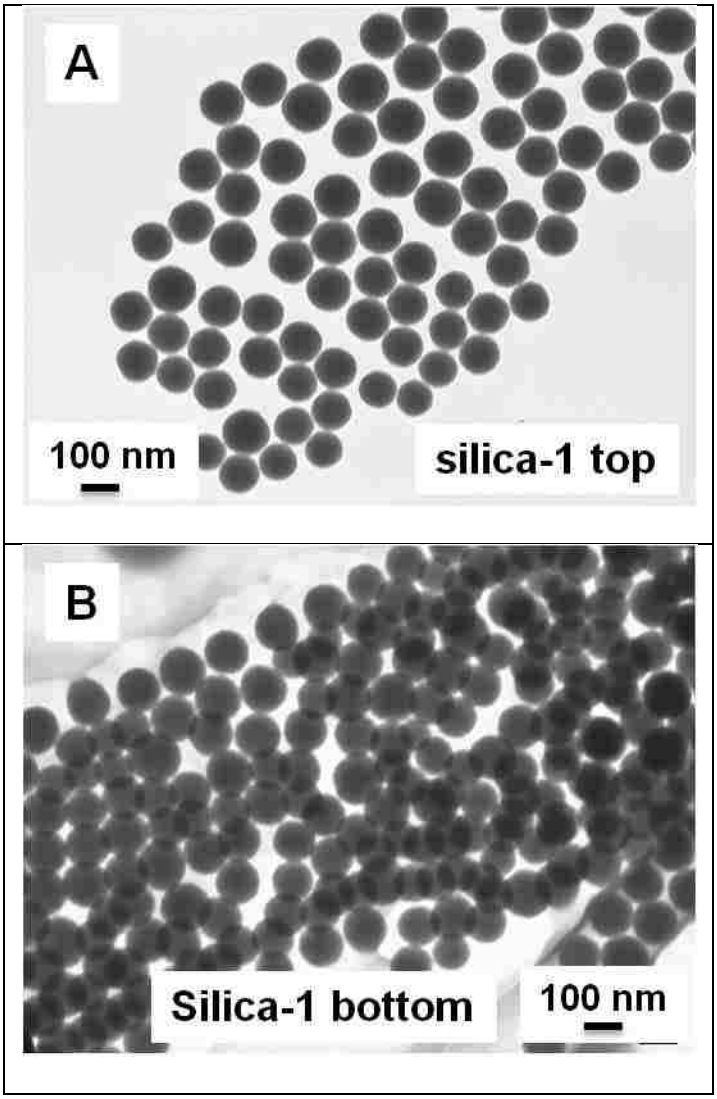

Figure 2.1 TEM images of silica-1 (CR5119) from different layers: top (A) and bottom (B).

Particles in the top layer, Figure 2.1A, were slightly bigger than those in the bottom layer, Figure 2.1B. The silica particles displayed in Figure 2.1A and Figure 2.1B have the consistency of hard solids. A softer appearance was observed for other batches and it is shown in Figure 2.2.

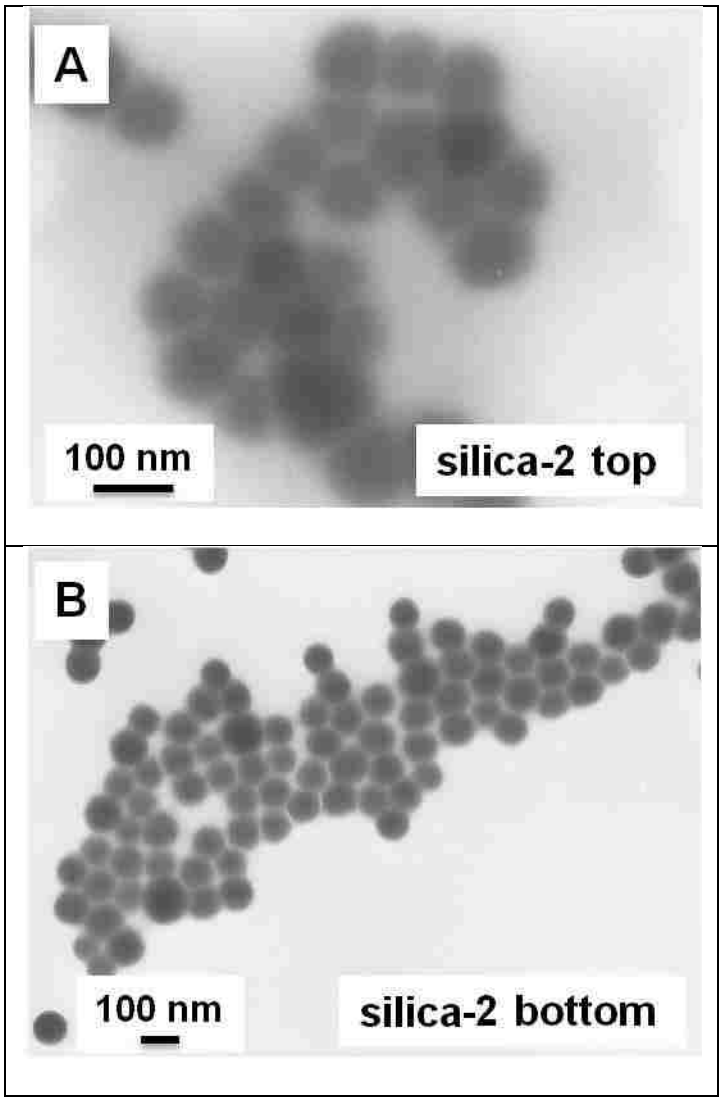

Figure 2.2 TEM images showing the soft appearance of the silica-2 (CR5134) cores.

In silica preparation the hydrolysis and the condensation of the TEOS have as result the formation of crosslinked siloxanes networks on top of each other. The soft morphology suggests either the silicon layers are not arranged in a very compacted structure or the basic conditions "soften" the spheres. They had a lower contrast in the electron beam as seen in Figures 2.2A and Figure 2.2B.

Measurements by DLS and AF4/MALS were also involved in the characterization of the silica particles. Figure 2.3 displays the DLS and AF4 profiles of the silica-1 (CR5119) and silica-3 (CR6133A) particles.

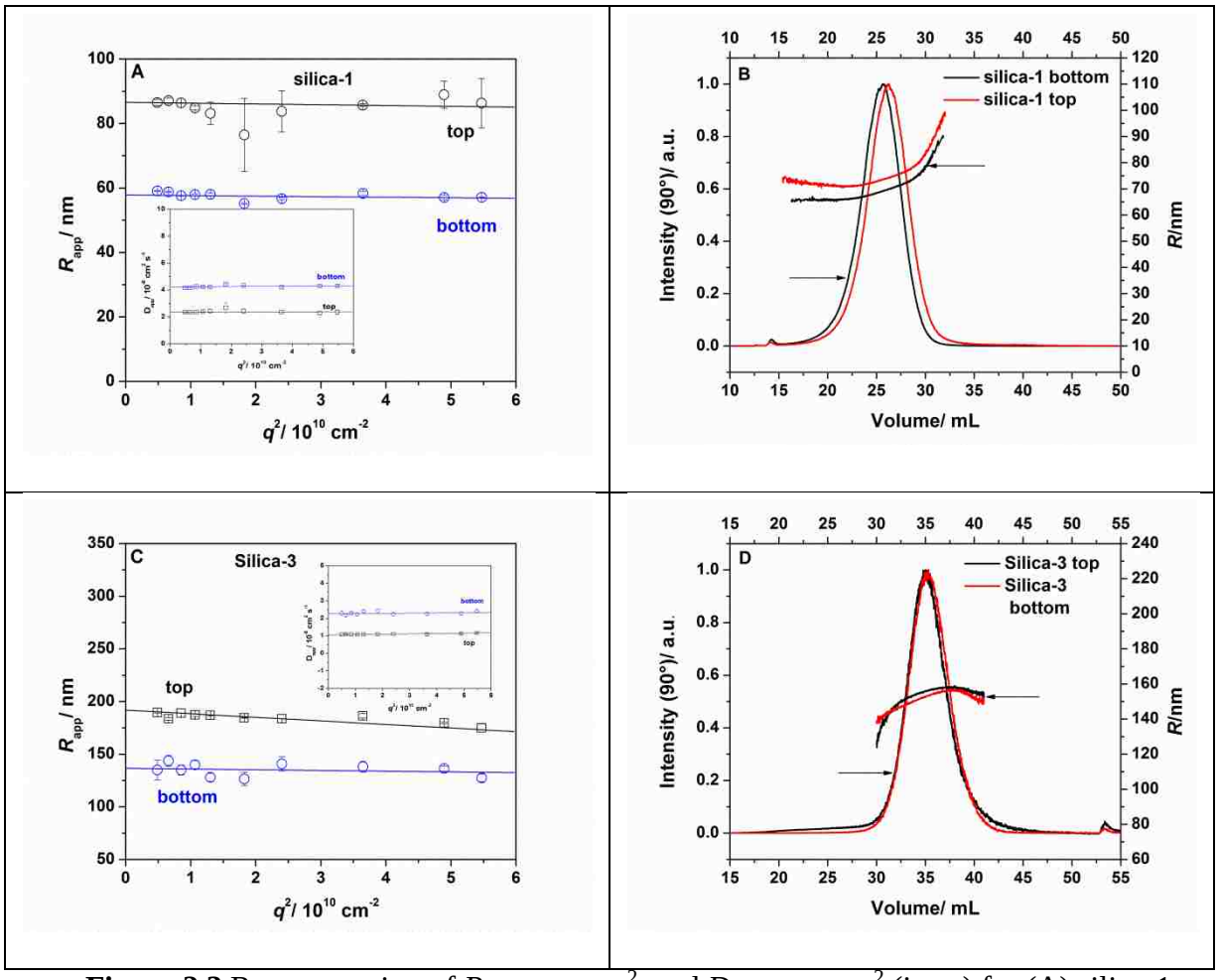

Figure 2.3 Representation of R_{app} versus q^2, and D_{app} versus q^2 (inset) for (A) silica-1 (CR5119) and (C) silica-3 (CR6133A) and AF4-MALS elugrams for (B) silica-1 (CR5119) and (D) silica-3 (CR6133A).

The sizes, summarized in Table 2.1, were larger for the top layer than for the bottom layer, in agreement with TEM.

DLS and AF4 along with TEM data suggest that the sedimentation of the particles was a density-driven process. The lighter yet larger silica collected at the top layer while the denser but

smaller particles sank to the bottom. The difference between DLS and AF4 size values is made by the way the radius is calculated.

Table 2.1 Silica Top and Bottom Layers and Their Radius from DLS and AF4

Silica	*R*(DLS)/nm	*R*(AF4)/nm
Silica-1(CR5119) top	84 ± 4.9%	75.5 ± 0.7%
Silica-1(CR5119) bottom	57.5 ± 5.2%	69.2 ± 0.5%
Silica-3(CR6133A) top	270 ± 3.3%	154.5 ± 2%
Silica-3(CR6133A) bottom	107 ± 1.2%	153 ± 1%

In AF4, the radius is obtained by fitting a spherical form factor applicable to a sphere with no internal structure. The obtained size is equal to the size of a uniform, simple sphere that matches the measured form factor. Sometimes this radius is erroneously referred to as the geometric radius. DLS fits the radius of a sphere with the radius calculated from the measured translational diffusion coefficients based on Stokes-Einstein relationship:

$$D = \frac{k_B T}{6\,\pi \eta_0 R} \qquad Eq.\,2.1$$

where D is the measured translational diffusion coefficient at the absolute temperature T, k_B is the Boltzmann constant, η_0 is the solvent viscosity and R is the radius. Both techniques assume a hard sphere model; consequently the reliability of the calculation depends on how well the actual particles adhere to the simple, uniform spherical model in terms of the shape and consistency. In Figure 2.3B the slight angle dependency noted for the top layer suggests either a distribution of the particles within the layer or a deviation from the sphere shape. Figure 2.3D reflects an average radius calculated by AF4.

The silica particles shown in Figure 2.1 were obtained in good yields. The method used allows for scale-up of the production. The cost of these particles is very low (assuming student salary $62/day, cost of reagents/3 medium batches ~$40, utilities/day ~$35 and a total of three medium batches produced which gives 15 g of particles, the total cost is $137/15g or ~$10/1g of silica) when compared with particles produced by the emulsion method. It is known that silica obtained in a reverse micelle have good uniformity but the major drawback is the very low yield. Figure 2.4 displays silica particles prepared in a sol-gel and a reverse micelle approach.

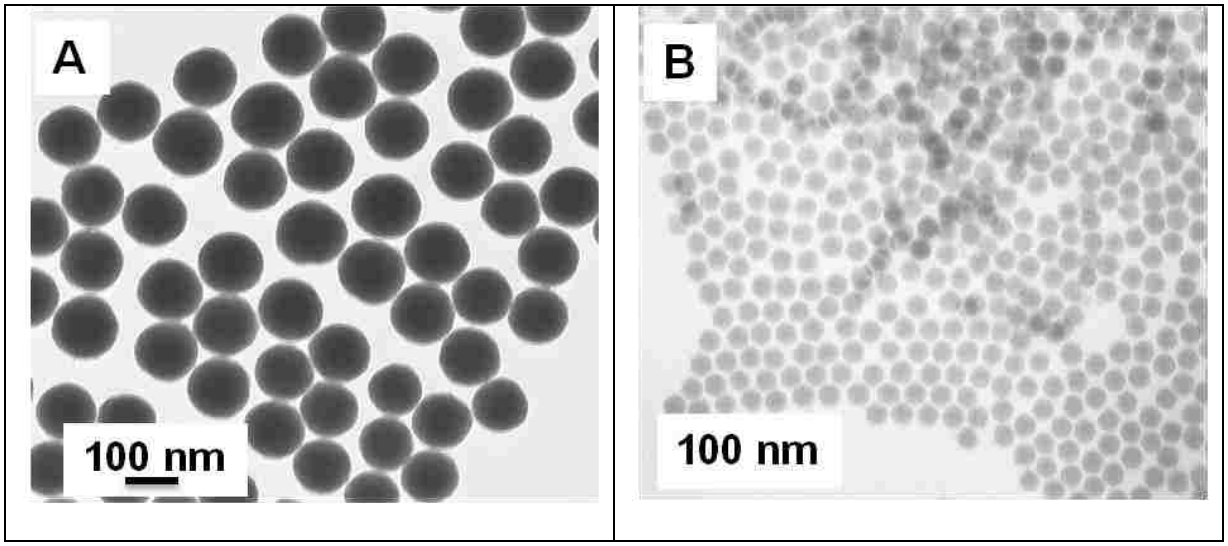

Figure 2.4 Silica particles obtained by (A) the sol-gel method (D = 122 ± 11 nm) and (B) the reverse micelle method (D = 33.5 ± 1.1 nm).

Even though the uniformity is worse for sol-gel silica, Figure 2.4A, than for particles obtained by the reverse micelle method; Figure 2.4B, the sol-gel method is an excellent way to produce monodisperse particles by the regrowth process in which new layers of TEOS are built on the particles used as seeds. The reproducibility of the silica colloids depends was satisfactory and depends on the reagent purity. Table 2.2 reflects the sizes of silica batches prepared at different times. In time, reagents can absorb traces of moisture while they had been used resulting in an alteration of their quality. This influences the growth of the silica colloid.

Table 2.2 Silica Sample and the Radius by TEM, AF4 and DLS Measured After Synthesis and From the Top Layer of Four Separate Batches.

Silica*	R(AF4)/nm	*R*(TEM)/nm	*R*(AF4)/nm	*R*(DLS)/nm
Silica-1(CR5119)	80 ± 0.7%	61 ± 4.5%	75.5 ± 0.7%	84 ± 3.5%
Silica-2(CR5134)	80 ± 2%	53 ± 4%	54± 2%	58 ± 0.6%
Silica-4(CR6184)	115 ± 0.5%	118 ± 4.5	104 ± 0.7%	118 ± 1.8%
Silica-5(CR6155)	63 ± 6%	84 ± 6.2%	80 ± 0.5%	114.5 ± 1.1%

*The size of the batch was medium, 500mL.

The slight deviations depicted in the Table 2.2 will be addressed later.

2.3.2 Colloidal Stability of the Stratified Silica

The development in advanced materials field, featuring core-shell architecture, qualified silica particles as a best candidate for such products. Among a variety of cores that can be prepared, silica has the main advantage of easy surface modification with functional groups. Figure 2.5 shows, for comparison reasons, standard polystyrene beads and standard colloidal silica spheres. The shape of the polystyrene, Figure 2.5A, prepared by emulsion method is better than the silica obtained in the sol-gel process, Figure 2.5B. Despite the undesired shapes, Figure 2.5B inset, silica remains the most widely used material as a core for a large palette of composite particles.

Many studies involved silica sols over the years but less studied is the colloidal stability over a long period of time. One might expect that the spherical shape is preserved for quite a long time. Still, silica can undergo changes in its structure and the result is reflected in Figure 2.6. The mesoporous structures called geodesics, were found in the top layer of the silica-1 batch, Figure 2.6A. Intriguing is the size of these structures when compared with the original top layer sol. The total diameter was calculated from the TEM images as 320 nm (± 3.4%) and the pore diameter as 70 nm (± 6.7%). The initial particles had a diameter of 122 nm (± 9%). The size

increased almost three times. The geodesics from silica-3 top sample, Figure 2.6B, had a size comparable with the original particles (~300 nm in diameter).

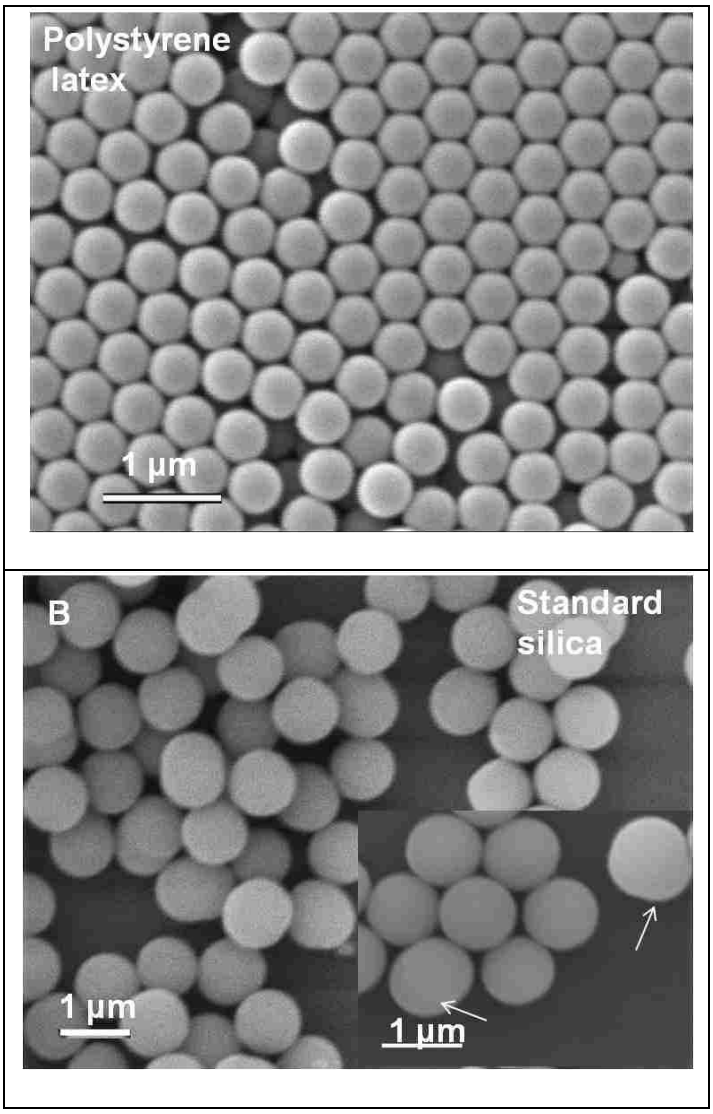

Figure 2.5 SEM pictures of (A) standard polystyrene latex and (B) standard silica, (inset) undesired silica shapes.

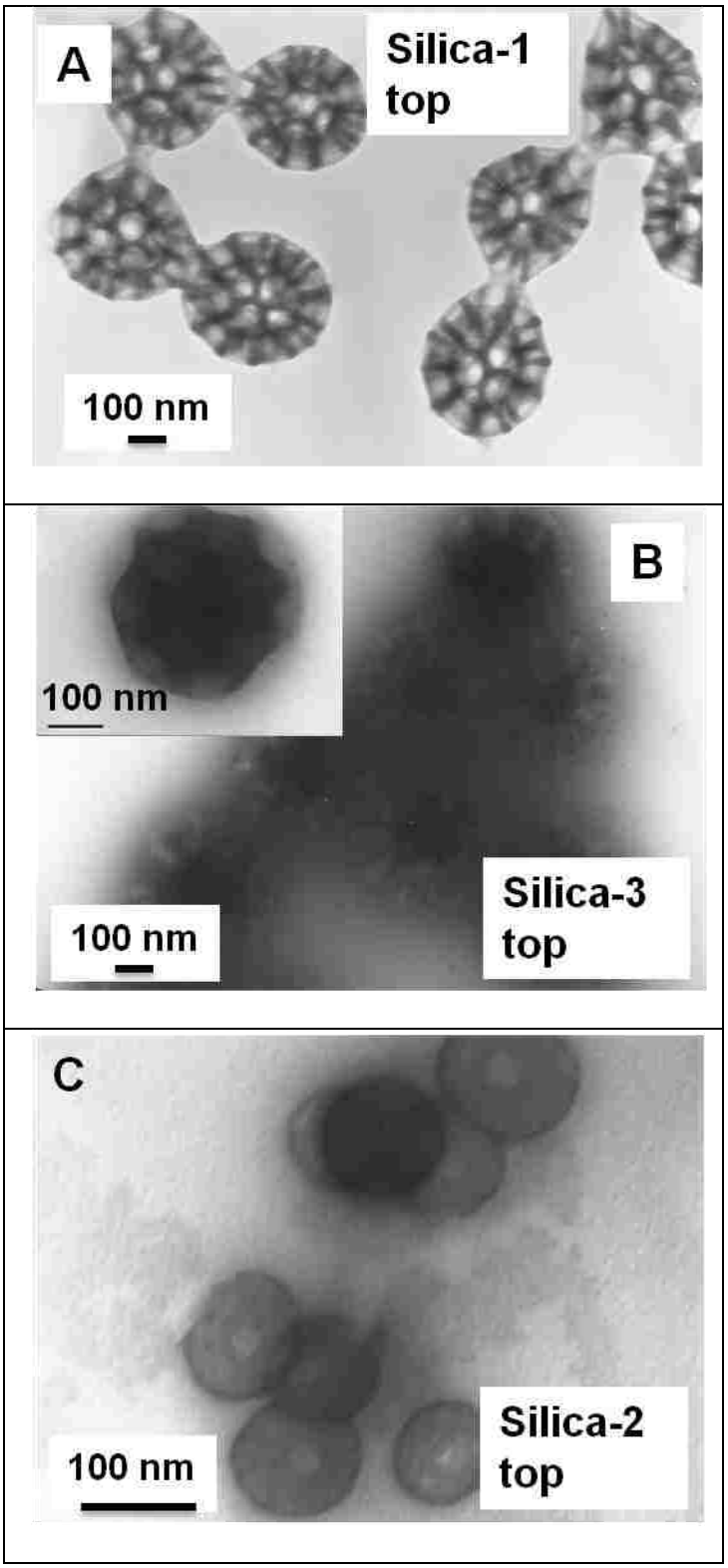

Figure 2.6 TEM micrographs of the cavitated structures: geodesics discovered in (A) silica-1 top and (B) silica-3 top and hollow discovered in (C) silica-2 top.

Figure 2.6C displays a hollow morphology found in the silica-2 top. Unlike the above particles, these ones shrank a little (~90 nm average diameter) when compared with the original ones (~100 nm average diameter). A common feature can be noted for all these three samples: all the non-solid morphologies were found in the top layer which is in a good agreement with the finding that the top layer consists of lighter particulates. The evolution of these particles from plain spheres to the mesoporous spheres is still not fully understood. Because the reaction and the storage conditions were the same for all the samples presented in this work, the parameters that could impact the formation of such structures are the size and the polymerization degree of the TEOS into crosslinked networks. Indeed, in early studies on silica sols, Van Helden et al. demonstrated that the core of a silica bead had a lower density than the outer surface.[47] Water trapped inside the silica hydrolyzes the siloxanes Si—O—Si bonds to Si—OH. The appearance of the mesoporous silica in TEM images can be correlated to different rate etching of more or less crosslinked siloxane networks. The formation of the silica was performed at pH 9, as well as their storage. The TEM pictures displayed in Figure 3.6 suggests that the etching took place from the interior to the exterior. It can be implied that the core of the silica beads had a less compacted siloxane network. This idea is in agreement with Van Helden et al.[47] and more recently with Gross et al.[48] Studying the effect of the pH on the silica chemistry, Gross et al. showed that pH 7 resulted in the most highly polymerized networks while at pH 11 the structure was the least inter-bonded. The condensation of the silica occurred faster at pH 7 while the hydrolysis was faster at pH 11. Higher pH (~12) was found to dissolve silica almost instantaneously. This aspect will be presented in Chapter 4. Gross et al. correlated the observed expansion and contraction of the silica spheres to the degree of the silica polymerization into a compact network. These observations were also confirmed by Liu et al.[49] and Park et al.[50] In the incipient stages of the

silica formation, the nascent silica beads have a less dense structure govern by the medium's pH. During reaction it might be possible a slight "pH dilution" due to byproducts which favors the formation of more compact siloxane networks. Moreover, the size of the surface pores should be smaller, hence preventing the penetration of the etchant molecules to the particle interior. The geodesics depicted in Figure 2.6A show an empty core with tunnels pointing to the exterior. Most probably the etching started as an interior process causing, in time, the expansion of the particles. This process can be compared to an ant hill; as the insects excavate their homes, the dirt is piled up on the outside. The Figure 2.6B depicts geodesics with a still filled core but the tunnels are just empty voids. The particles were etched from the outside which might explain the nearly constant size when compared with the original sol. This is intriguing because based on the size of the plain particles, this mesoporous spheres should behave more like the first geodesics shown in Figure 2.6A. The hollow structure, Figure 2.6C, probably result from etching at both the surface and the interior. The surface could undergo a slight modification due to the siloxanes hydrolysis which, at some extent, can close the pores of the remaining particle. This might be suggested by the presence of the outer silica membrane seen at higher electron density contrast. The core of the beads was etched by the etchant/water molecules trapped inside. In order to verify the series of assumptions made, the same layer of the silica-2 and silica-3 was monitored by AF4 at different times of the storage. The data are presented in Table 2.3.

Table 2.3 Silica Top Layers and Their Radius at Different Storage Times Measured by AF4

Silica	R^{a*}/nm	R^{b*}/nm
Silica-2 top	54 ± 2%	44 ± 0.8%
Silica-3 top	130 ± 1%	154.5 ± 2%

*a and b are different storage times; Δ(a,b) was 2-4 weeks.

Indeed the silica-3 underwent to a size increase over the time suggesting a dense siloxanes network which, upon etching, could swell. On the other side, silica-2 shrank but this observation is not a surprise since the TEM analysis showed a low electron density contrast particles, an attribute of a light siloxanes interbonded networks.

The mesoporous particles presented by this work can be obtained in high yields. Once formed, they can be washed with ethanol and water and stored in an acidic solution which stops the hydrolysis of the siloxane bonds. The geodesics, especially the ones seen in Figure 2.6A can be used as good fillers in the membrane manufacture. Furthermore, the mesoporous particles can be functionalized with the reactive groups. The functional moieties can be further used as platforms to attach biomolecules or other macromolecules.

The colloidal stability and the size preservation should take into account the duration, temperature and other conditions of storage. Particles kept even in a mild basic pH undergo to a slow etching process enabled in this case by the aqueous ammonia. Therefore, the size of the particles can change dramatically over the time. As proof-of-concept, Figure 2.7 reflects silica particles immediately after separation into layers and after more than one year of storage. The original sol separation into layers contained particles of spherical shape. They had the appearance of a hard core, as shown in Figure 2.7A. The sizes obtained by AF4/MALS measurements suggest a uniform silica density. Figure 2.7B reflects the stratification driven by weight: the bottom stratum contained the largest particles while the top had the smallest. After one year, the top layer, Figure 2.7C, had spherical particles. They retained the tendency of the hexagonal packing. Figure 2.7D depicts the middle layer with particles having a different architecture. The spheres underwent to a surface modification, a process which caused their morphology to change into one similar with a core-shell rather than a hard core (Figure 2.7D,

inset). The edges of the particles are not clear and the fuzziness around the area of the darker contrast is obvious. The bottom layer, Figure 2.7E, had a more pronounced fuzziness, as clearly seen in the zoom in area presented in the inset.

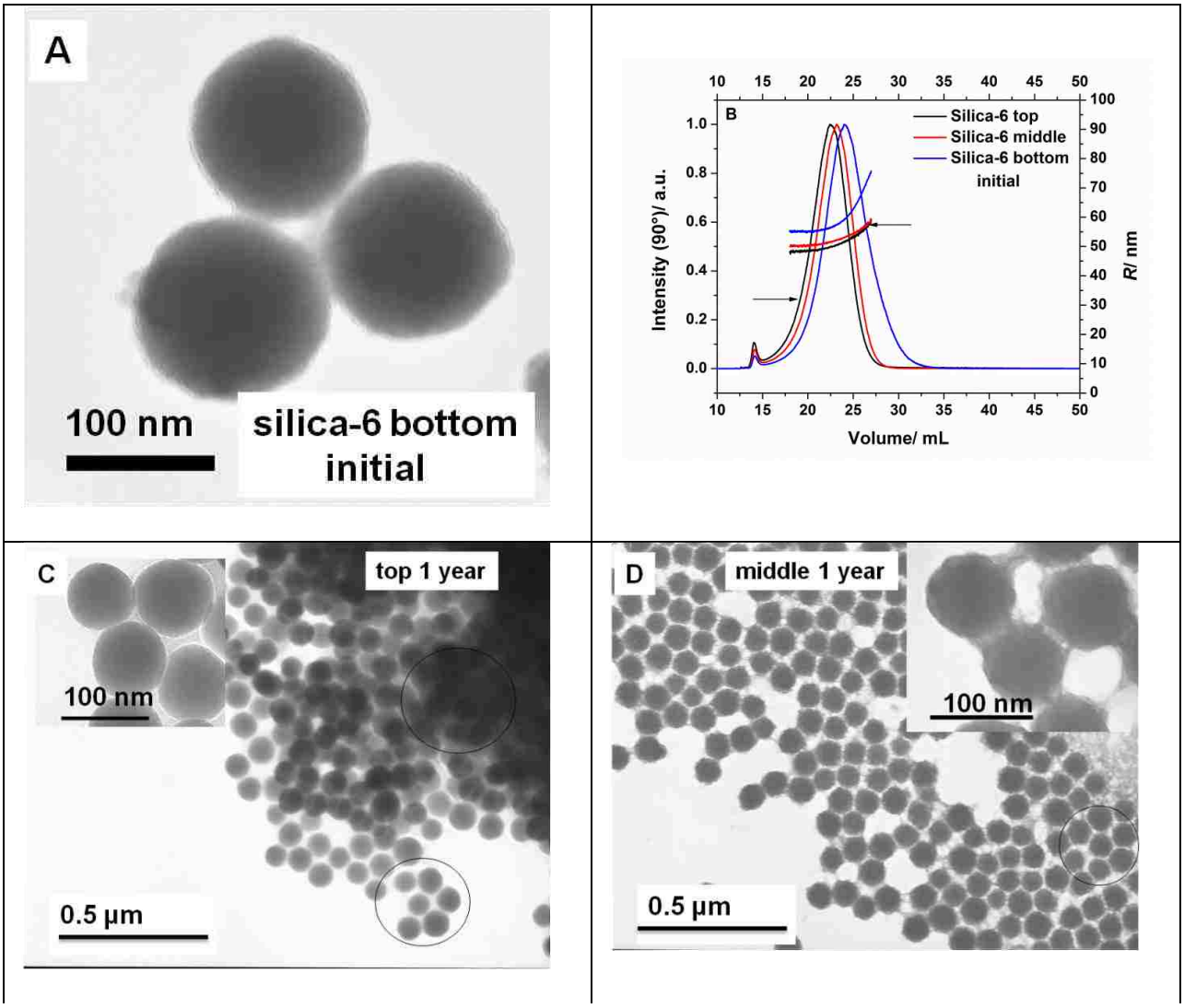

Figure 2.7 Silica-6 (CR51): (A) TEM image of the initial bottom layer particles showing their spherical structure, (B) AF4-MALS chromatogram of the initial separated sol reflecting an expected trend of the layer sizes: top the smallest, (C) TEM image of the top layer (higher magnification, inset) after one year, (D) TEM image of the middle layer (higher magnification, inset) after one year, (E) TEM image of the bottom layer (zoom in, inset) after one year and (F) Radius, R_{app}, versus scattering vector magnitude, q, and (inset) diffusion coefficients, D_{app} versus scattering vector magnitude after one year showing the new trend of the layer sizes: bottom the smallest. One year samples were stored in the initial basic conditions.

Figure 2.7 continued

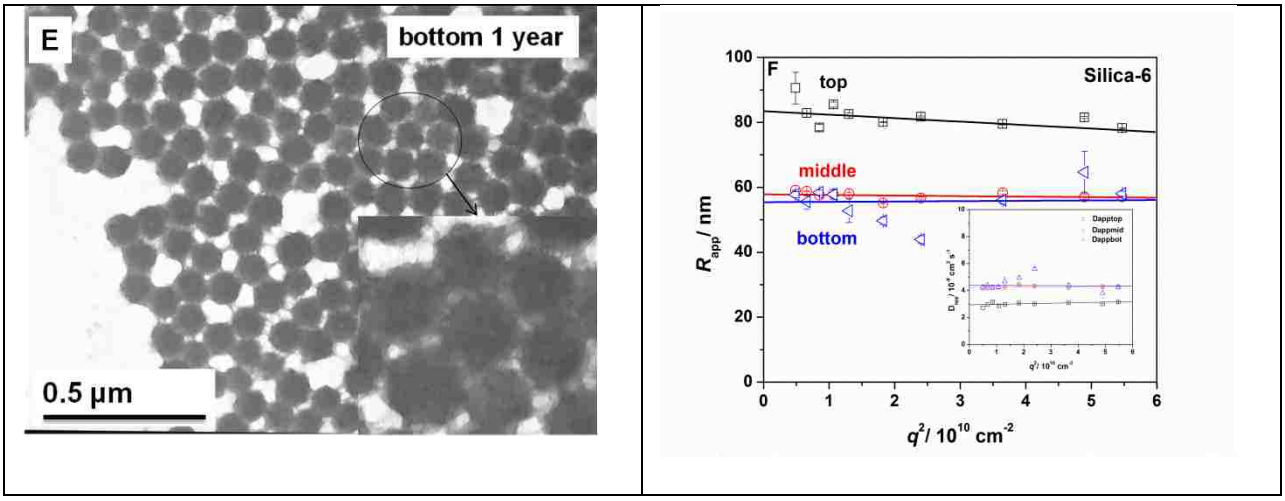

All three layered particles were able to self-assemble into a hexagonally close-packed structure, as a consequence of their uniform sizes and regular shapes. Hence, the silica beads obtained by this strategy are expected to possess photonic crystal properties. Nanoscale silica coated particles, similar in size with the particles presented in this work (200-300 nm), were found to exhibit optical properties applicable in the visible part of the spectrum.[51] The sizes returned by DLS showing a reverse trend when compared with the initial values obtained by AF4/MALS assay. Reasons for this finding will be addressed in a next paragraph.

In the experiment described in the preceding paragraph it was demonstrated that silica particles do change their sizes over time. Since silica are used as standard in many applications, concerns rise on their stability. In a simple experiment, standard silica (200 nm) more than one year old, were analyzed by TEM, DLS and AF4/MALS. The results are presented in Figure 2.8. The size modification is clearly visible in Figure 2.8A. Most of particles not only lost their spherical shape but began to develop a core-shell structure even their storage was not in a mild basic solution as silica-6. They should appear as the standard silica presented in Figure 2.5B.

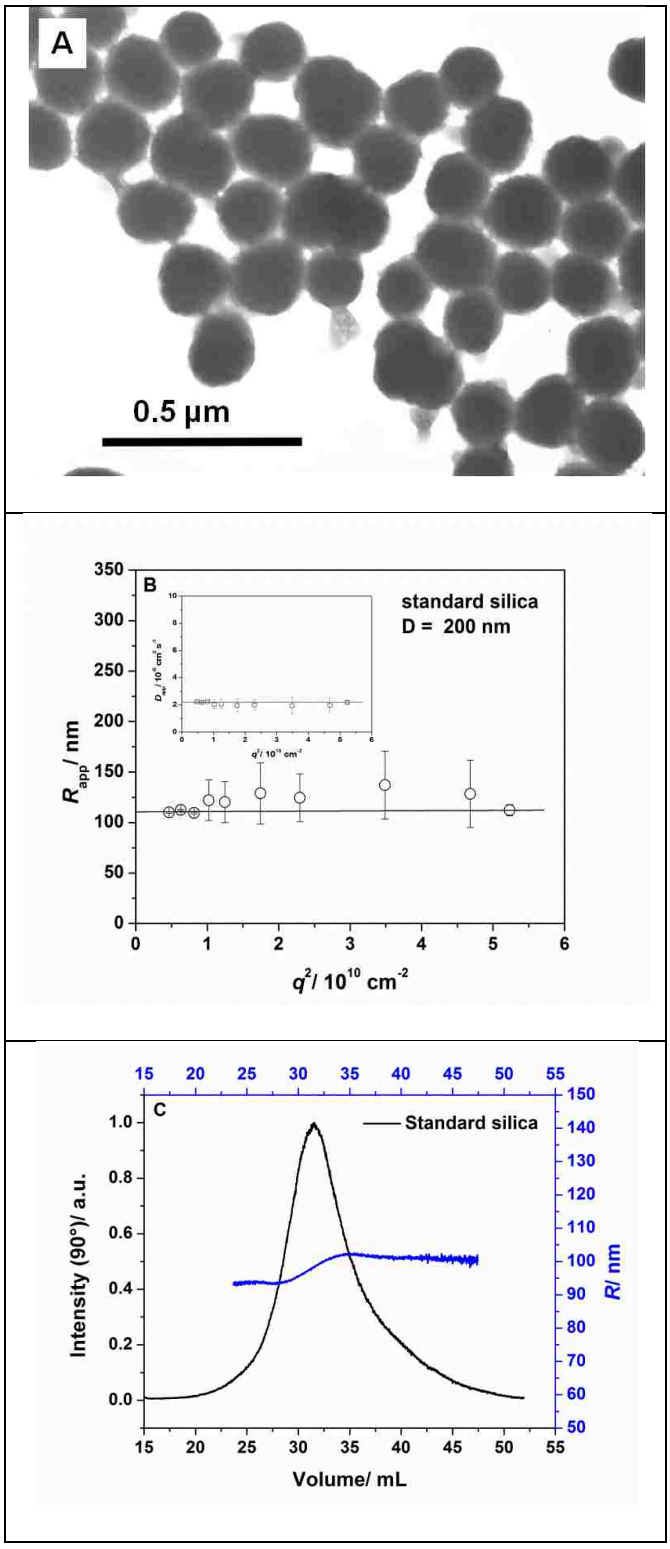

Figure 2.8 Standard silica (>one year): (A) TEM image, (B) apparent radius, R_{app}, and apparent diffusion coefficients, D_{app}, (inset) as a function of the scattering vector magnitude from DLS and (C) AF4-MALS chromatogram.

The DLS results, Figure 2.8B, showed no angle dependency of the radius but the points do not align nicely on the fitted line. In the AF4/MALS chromatogram, the ascendant slope rather than flat of the radius points to a slight distribution of the standard particles. Regardless of silica's application from raw to standard material, it is clear that the stability of the size and shape is not a long time feature.

As stated before, these silica particles separated into layers were not washed to remove the base. Therefore a question might rise concerning the effect of the washings on the stratification. Figure 2.9 depicts a batch of silica particles kept in different conditions after extensive washings were performed with ethanol and water.

Figure 2.9 Silica seed particles stored in different conditions; from left to right: the original sol, in water, in water and ammonium hydroxide (pH=9) and in ethanol.

The leftmost bottle is shown in its initial basic conditions as a comparison. No matter the pH, either neutral (silica in only ethanol and only water) or basic (9) (silica in water and ammonia) all showed the tendency to separate into layers in the same manner as the initial sol.

2.4 Applications

2.4.1 Fractionation of Colloids by AF4/MALS Using Inexpensive Silica as a Study Model

The continuous expanding of the advanced materials comprising colloidal particles demands the production of a large variety of particles in terms of size and shape. Not all involve an inexpensive process of production as silica does. In some applications, a narrow distribution is necessary, in others specific shapes are targeted. The fabrication of multiple batches to attain the desired particle uniformity and shape can make the final product really expensive. AF4/MALS is a technique that allows a good separation of particles by size and fractions of these particles eluting at different times can be collected. Silica can serve as a good model to demonstrate the capability of the AF4/MALS to resolve accurately even degraded batches of the particles. To prove the concept, silica-1 was chosen. Figure 2.10 shows the evolution of silica-1 over one year, monitored by AF4/MALS. As discussed before, silica-1 separated into two layers, Figure 2.10A, with the top layer eluting in AF4 instrument last, meaning larger particles. After one year the top stratum had a broader distribution with a shoulder eluting near the end, Figure 2.10B. The plot of the radius versus the elution volume showed an improved slope near flat. The trace of the bottom layer, Figure 2.10C, showed bigger particles and a shoulder similar with the top layer. Comparing the initial AF4/MALS traces with those recorded after one year, it can be seen that particles changed their size and/or shape. The top layer had initially larger particles but, in time, the middle became the smaller particle layer. Only the shoulder for both, top and bottom layers, overlapped in the same region of the elution time.

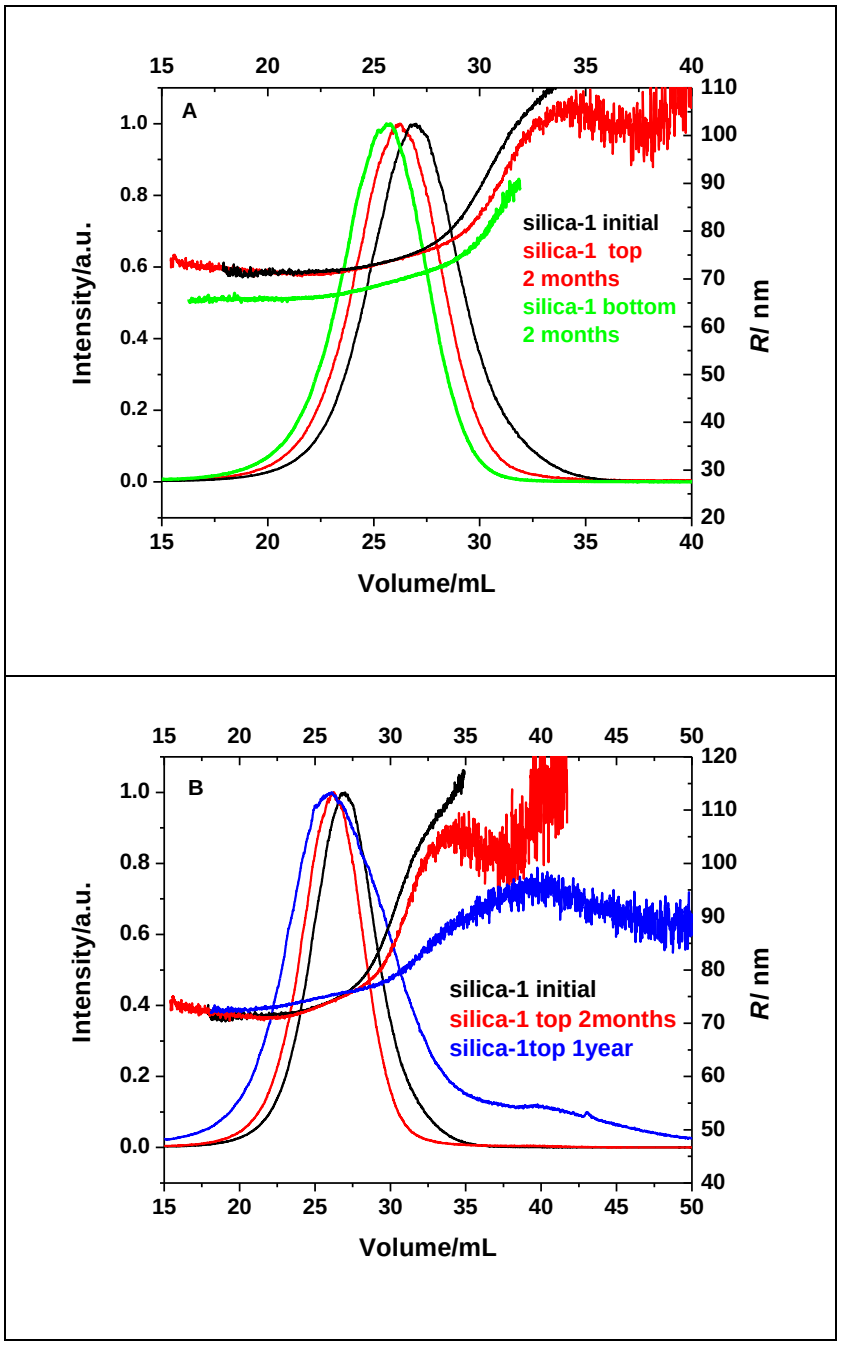

Figure 2.10 Comparison of the size distribution: silica all layers after 2 months(A), top layer after one year (B), bottom layer after one year (C) and silica all layers after one year (D).

Figure 2.10 continued

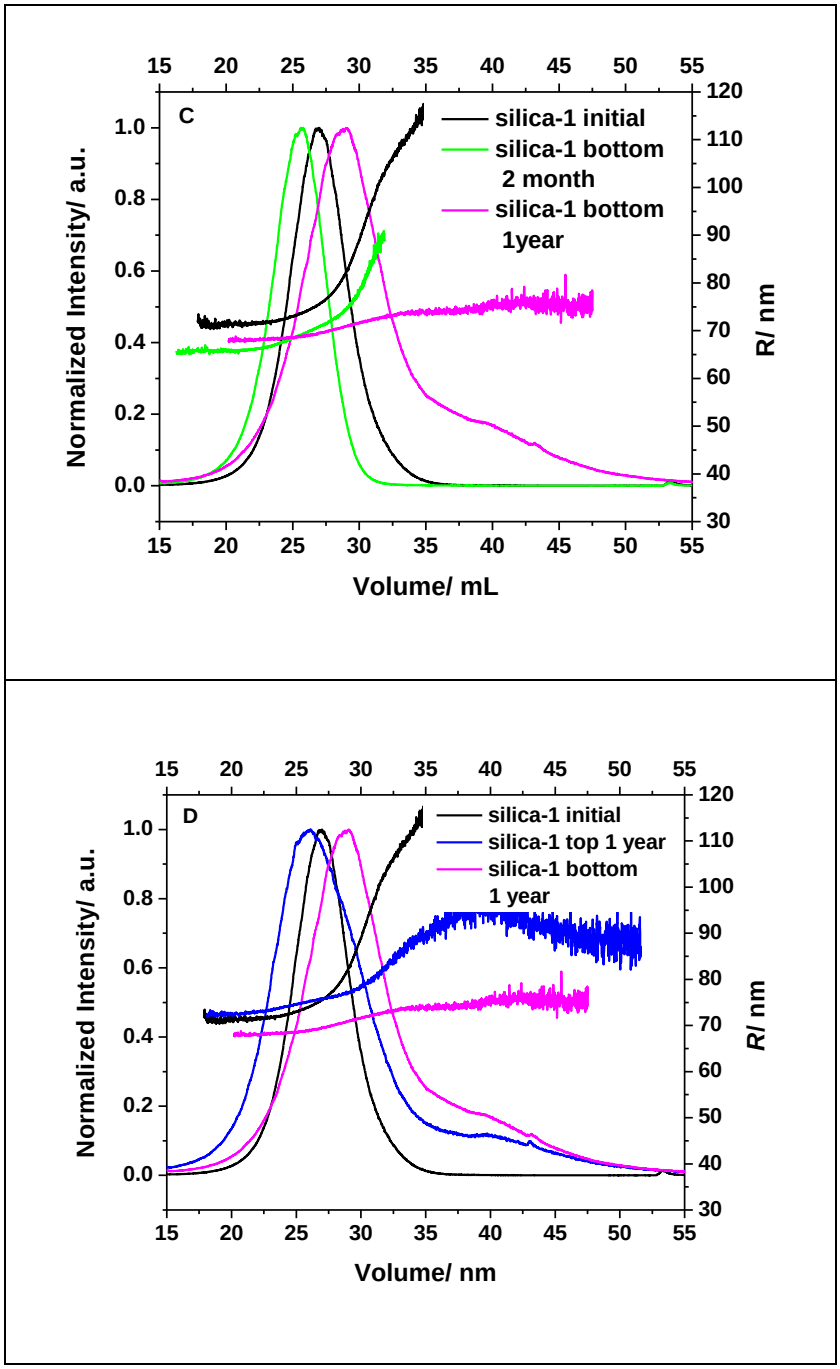

The radius slope for the region where the most particles eluted is almost flat when compared with the old standard silica, as shown in Figure 2.11A.

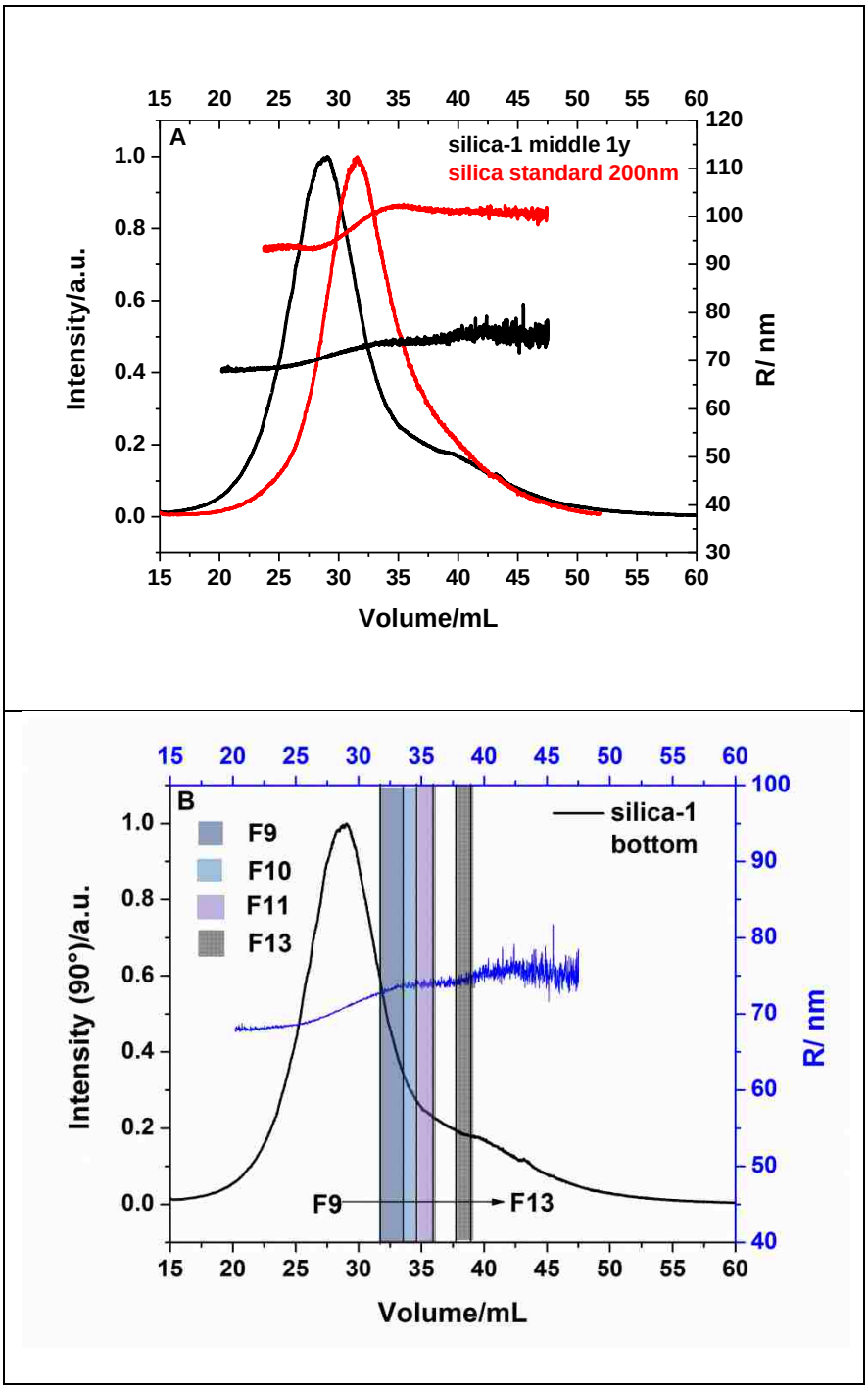

Figure 2.11 AF4-MALS traces of: (A) standard silica and silica-1 bottom 1 year and (B) silica-1 bottom 1 year showing the fractions collected.

Silica-1 bottom was elected for fractionation. Figure 2.11B reflects the slices collected at different elution volumes. The content of the fractions was analyzed by TEM and DLS and the results are presented for comparison in Figure 2.12.

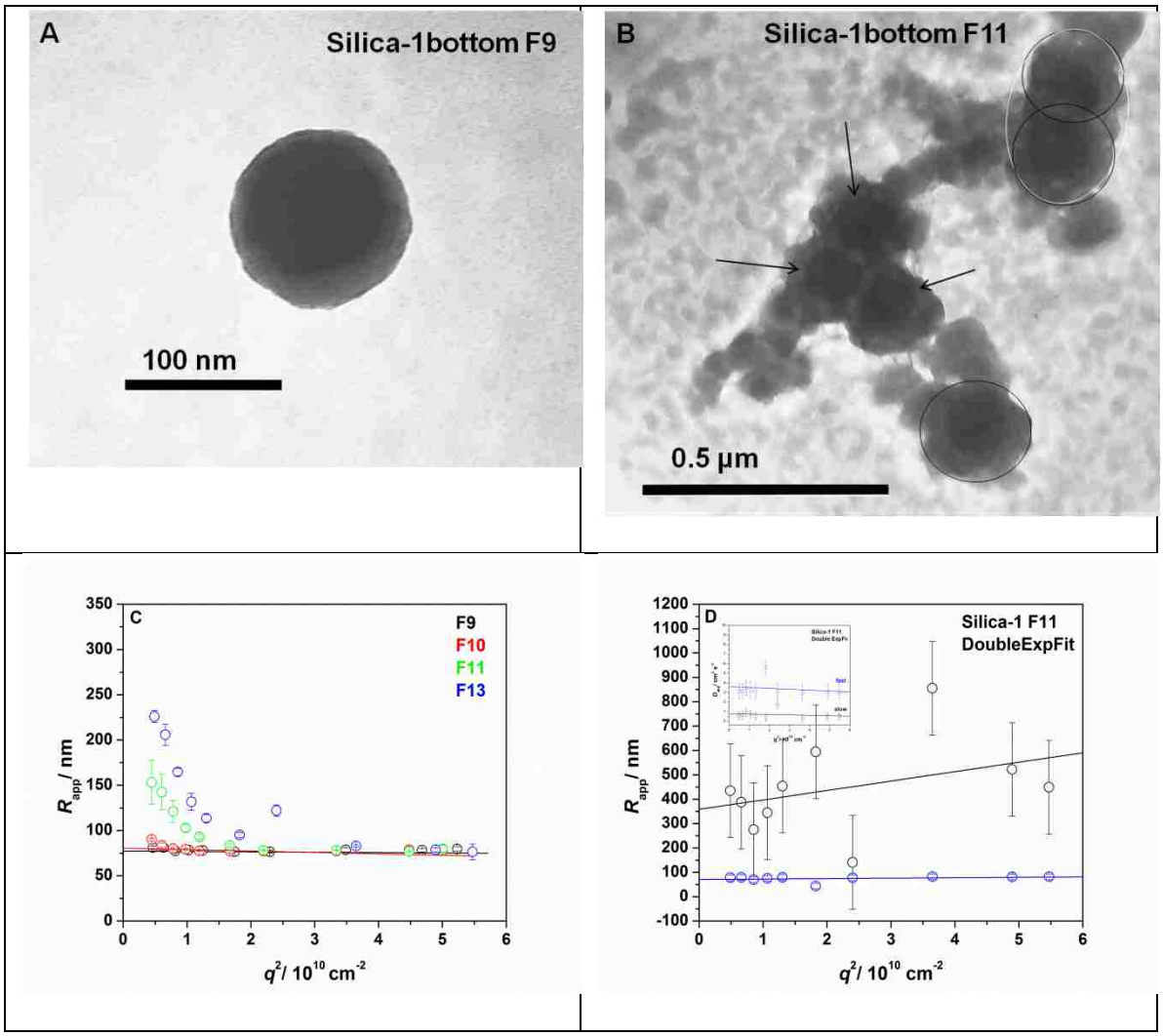

Figure 2.12 TEM images of the silica-1 bottom from (A) fraction 9, F9, (B) fraction 11, F11, and DLS radius, *R*, versus scattering vector magnitude, *q*, of silica-1 bottom for (C) F9, F10, F11, F13 following third cumulant and one exponential analysis and (D) F11 following double exponential fitting algorithm (diffusion coefficients as a function of *q*, inset).

Fractions up to F10 contained spherical particles with good uniformity as shown in Figure 2.12A. The particle fraction corresponding to the shoulder eluting near end had lost their hard

core spherical appearance. Remnants of the original beads can still be seen, sparsely, but most of the new shapes suggest the agglomeration of several denaturized beads. The new shape could be assigned to a core-shell as well as to an ellipsoid shape, as marked with a white frame. The DLS results presented in Figure 2.12C shows the radius of the particles as a function of the scattering vector. No angle dependency can be seen up to F9 but higher fractions showed a curvature at lower angles whilst at higher q values they aligned on the flat region of the fit line. It was evident that the fitting analysis taken as an average over the third cumulant and one exponential algorithm did not suffice an accurate reflection of the shape. To determine more precisely the trend of the size, two exponentials formalism was employed in analyzing the F11 particles. Indeed, as shown in Figure 2.12D two distributions can be seen: one diffusing fast and one slower (inset). The fast mode corresponded to the smaller particles and the slow was attributed to the larger aggregates seen in TEM image, Figure 2.12B. The trend of the radius for the slow diffusers, ascendant with the increased angle, is a fingerprint of the aggregation which is in agreement with the TEM images.

Several remarks should be addressed on the formalism used to analyze the particles size by both light scattering techniques, DLS and AF4/MALS. The AF4 instrument with online light scattering detection uses Wyatt Astra software, version 5.3.4.1.3 which by routine uses a spherical model for spheres. For a solid sphere the form factor, $P(qR)$, is expressed by:

$$P(qR) = \frac{9}{(qR)^6}(sin(qR) - qRcos(qR))^2 \qquad Eq.\,2.2$$

As demonstrated by Soto-Cantu et al. the fitting to a sphere form factor and data quality were better at lower angles than higher, a drawback of the Wyatt's machine nonlinear least squared fit formalism.[52] They also underlined the importance of using the best shape corresponding form

factor. The fit using a core-shell form factor improved the high angle data analysis. For the silica particles described in this work, it is clear that such formalism can tremendously improve the quality of the data. A core-shell form factor is expressed as follow:[52]

$$I(qR) \propto R^6 \left[\frac{m_1 - 1}{2\pi}\left(\frac{3j_1(x)}{x} + f\frac{3(m_2 - m_1)}{m_1 - 1}\frac{3j_1(fx)}{fx}\right)\right]^2 \quad Eq.\,2.3$$

where $x = qR$, j_1 is the spherical Bessel function expressed as:

$$j_1(x) = \frac{sinx}{x^2} - \frac{cosx}{x} \quad Eq.\,3.4$$

In the same formula, f is the fraction of the linear particle calculated as R-t/R with R the overall core-shell radius and t is the thickness of the shell, m_1 is the ratio between the relative indices of the shell to solvent refractive index, n_1/n_0 and m_2 is the same ratio of the core to solvent relative indices of refractive index, n_2/n_0.

Particle artifacts as seen in the F11 might require more sophisticated form factors. For an accurate analysis, a core-shell model also encounters its own challenges. In a case of a composite core-shell particle made of a hard core and a confined organic shell it is relatively simple to determine the refractive index of the core and the shell. For silica in the core-shell structure it is crucial to determine the refractive index of the lighter silica shell and the denser silica core. Without these parameters any form factor formalism might fail on improving the spherical approach. Despite the difficulties in shape representation when data analysis is performed to qualitatively evaluate the size distribution and uniformity, AF4/MALS technique can be reliably used to resolve difficult and more expensive samples.

2.4.2 Silica Seeds-Support for Preparation of Uniform Fluorescent Probes

Silica particles prepared by the approach described above can be used as seeds in the regrowth process by sequential addition of the diluted TEOS. More details on this regrowth

process are presented in Chapter 8. Bogush et al. demonstrated the close correlation between the quality of the silica seeds in terms of the uniformity and the quality of the final silica particle. Spherical shape visibly improved and also the uniformity.[12] In addition, the regrowth process can be used to prepare fluorescent particles by the incorporation of fluorescent molecules. The fluorophore, in this case the fluorescein isothiocyanate, FITC, was covalently incorporated as a molecule with the 3-aminopropyltriethoxy silane, APS. The addition of the fluorescent tag does not impact negatively the shape of the grown silica particles. Moreover, sequential additions of TEOS protect the dye against leaking and bleaching and also add more to the quality of the final particle. Such fluorescent particles are shown in Figure 2.13. The fluorescent particles shown in Figure 2.13A were uniform in size and had a polydispersity comparable with standard particles. TEM images taken on several hundreds of particles did not revealed undesired shapes. That means particles grew in the same time during regrowth process without adhesion or secondary nucleation. Fluorescent silica prepared from the seeds can be used in applications such as labeling, *in vivo* imaging and fluorescent probes. Figure 2.13B reflects a fluorescence image of the particles purposely bleached in a chosen area. The bleached area (inset) appears darker but snapshots taken at different times of bleaching showed the particles retained ~ 50% from the initial fluorescence intensity (Figure 2.13C). Several other samples were subjected to the same treatment and for a longer time. The decrease noticed was as less as 70%. Another exquisite application that can be designed is in drug delivery and drug encapsulation. Silica covalently tagged with FITC can be transformed into mesoporous spheres, still fluorescent. This aspect is largely described in Chapter 4.

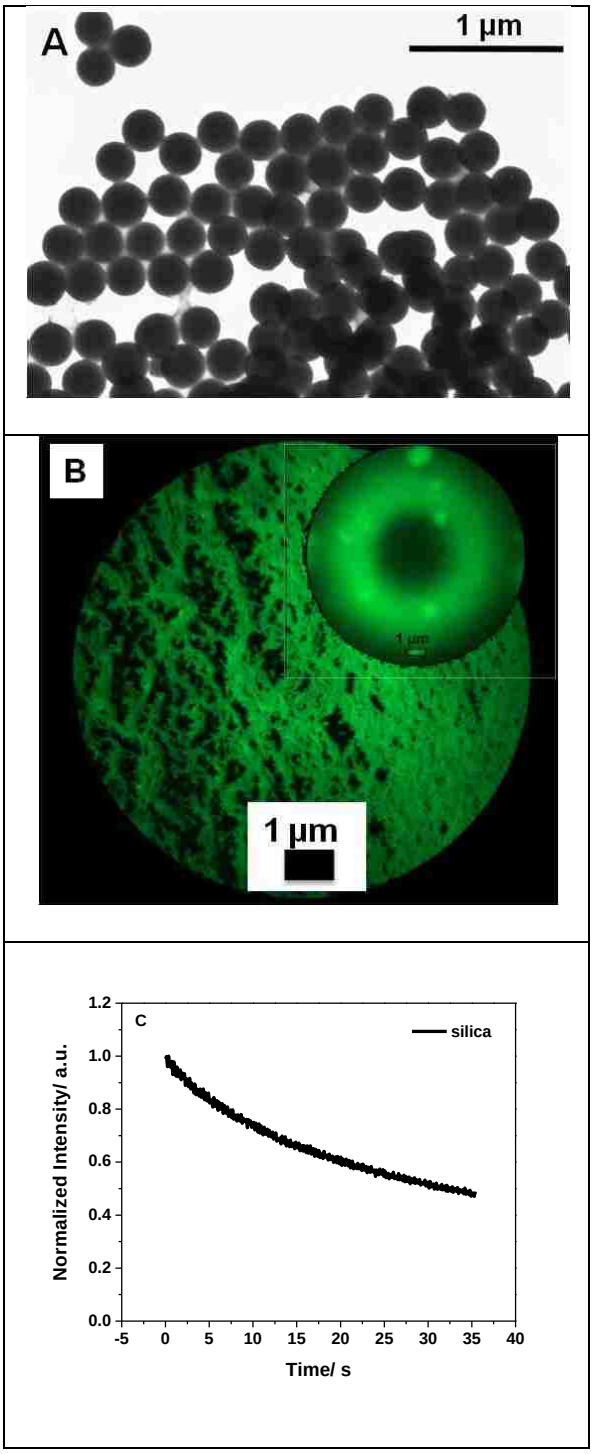

Figure 2.13 TEM image of the fluorescent silica particles obtained by the seeded method (D = 280 nm ± 4%), (B) fluorescence image of non-bleached particles (powder) (inset, bleached in aqueous solution) and (C) fluorescence intensity of the bleached particles (in solution, ethanol solvent) using illumination through a fluorescence microscope.

2.5 Conclusion

In summary, this work demonstrated that stratified silica colloid can be obtained by sedimentation in the initial conditions of the preparation. The process is slow and takes place between four weeks and two months, depending on the batch and the seed size. The separation of the particles is mostly a density-driven process, due to the degree of the polymerization of the TEOS into interbonded networks. In addition, the use of less water than in the original Stöber and Bogush methods can also had a contribution to the manner the TEOS hydrolyzes and condenses into more or less compact crosslinked networks. In the central part of the silica bead, the TEOS is less crosslinked than in the outer part of the particle. TEM, DLS and AF4/MALS were three reliable techniques used in the characterization of the stratified colloid. They revealed the morphology and the uniformity of the spheres from each layer. The storage for a longer time in the basic ammonia solution yielded mesoporous structures, some called geodesics, others displaying hollow architecture. The morphology of the mesoporous particles gave a qualitative image of the TEOS networks within the particles. The softness of the bead core was suggested by the low-contrast appearance of the porous spheres in the electron beam. Using the approach described, again slow in time, monodisperse seeds can be obtained in high yields. Once noted to form, the mesoporous structures can be separated from the original sol by washings and neutralization to an acidic pH that stops the etching of siloxanes network. The stability of the silica particles was also studied. It was found that the size and the shape preservation is not a long time feature. Particles, even standard silica, changed the shapes and broaden their distribution. In some cases, layer sizes reversed after more than one year of storage. It should be pointed out that standard particles should be monitored in time for shape degradation and replaced as often as needed. Asymmetric flow field flow fractionation, AF4, was used as a

reliable technique to resolve a challenging sample of the degraded silica particles. Fractions were collected and visualized by TEM. The size measurements by DLS agreed with the AF4-MALS data. Data were analyzed using the spherical model. The new morphologies noted require adequate form factors in data fitting analysis. Despite all challenges encounter in analysis formalism, AF4/MALS remains a reliable tool to characterize and separate particles by size and shape. Hence, silica particles presented in this work are a good model to study more expensive particles. Moreover, the recovery of the still uniform and spherical silica beads from the degraded old sample was demonstrated by AF4 fractionation. The silica seeds prepared by this approach can be covalently tagged with fluorescent moieties. The regrowth process with sequential additions of TEOS yields particles resistant a longer time to bleaching. All particles from initial batches to those slowly etched into mesoporous structure retained their tendency to self-organize in 2D hexagonal arrays.

2.6 References and Notes

(1) Yuan, J. J.; Zhou, S. X.; Gu, G. X.; Wu, L. M. Encapsulation of organic pigment particles with silica via sol-gel process. *J. Sol-Gel Sci. Technol.* **2005**, *36*, 265-274.

(2) Beakley, L. W.; Yost, S. E.; Cheng, R.; Chandler, B. D. Nanocomposite catalysts: Dendrimer encapsulated nanoparticles immobilized in sol-gel silica. *Applied Catalysis a-General* **2005**, *292*, 124-129.

(3) Leinweber, F. C.; Tallarek, U. Chromatographic performance of monolithic and particulate stationary phases - Hydrodynamics and adsorption capacity. *J. Chromatogr. A* **2003**, *1006*, 207-228.

(4) Vrij, A.; Penders, M.; Rouw, P. W.; Dekruif, C. G.; Dhont, J. K. G.; Smits, C.; Lekkerkerker, H. N. W. Phase-transition phenomena in colloidal systems with attractive and repulsive particle interactions. *Faraday Discussions* **1990**, *90*, 31-40.

(5) Avnir, D.; Coradin, T.; Lev, O.; Livage, J. Recent bio-applications of sol-gel materials. *J. Mater. Chem.* **2006**, *16*, 1013-1030.

(6) Sharma, P.; Brown, S.; Walter, G.; Santra, S.; Moudgil, B. Nanoparticles for bioimaging. *Advances in Colloid and Interface Science* **2006**, *123â€“126*, 471-485.

(7) Dotera, T. In *Israel Journal of Chemistry* 2011; Vol. 51, p 1197-1205.

(8) Dziomkina, N. V.; Vancso, G. J. Colloidal crystal assembly on topologically patterned templates. *Soft Matter* **2005**, *1*, 265-279.

(9) Stober, W.; Fink, A.; Bohn, E. Controlled Growth of Monodisperse Silica Spheres in the Micron Size Range. *Journal of Colloid and Interface Science* **1968**, *26*, 62-69.

(10) Kolbe, G., The Complex Chemical Behavior of Silica. Jena, Germany, 1956.

(11) Iler, R. K. *Colloid Chemistry of Silica and Silicates*; Cornell University Press, 1955.

(12) Bogush, G. H.; Tracy, M. A.; Zukoski, C. F. Preparation of monodisperse silica particles - control of size and mass fraction. *Journal of Non-Crystalline Solids* **1988**, *104*, 95-106.

(13) Zhang, J. H.; Zhan, P.; Wang, Z. L.; Zhang, W. Y.; Ming, N. B. Preparation of monodisperse silica particles with controllable size and shape. *J. Mater. Res.* **2003**, *18*, 649-653.

(14) Rao, K. S.; El-Hami, K.; Kodaki, T.; Matsushige, K.; Makino, K. A novel method for synthesis of silica nanoparticles. *Journal of Colloid and Interface Science* **2005**, *289*, 125-131.

(15) Park, S. K.; Do Kim, K.; Kim, H. T. Preparation of silica nanoparticles: determination of the optimal synthesis conditions for small and uniform particles. *Colloids and Surfaces A-Physicochemical and Engineering Aspects* **2002**, *197*, 7-17.

(16) Matsoukas, T.; Gulari, E. Dynamics of growth of silica particles from ammonia-catalyzed hydrolysis of tetra-ethyl-orthosilicate. *Journal of Colloid and Interface Science* **1988**, *124*, 252-261.

(17) Matsoukas, T.; Gulari, E. Monomer-addition growth with a slow initiation step - a growth-model for silica particles from alkoxides. *Journal of Colloid and Interface Science* **1989**, *132*, 13-21.

(18) Bogush, G. H.; Zukoski, C. F. Studies of the kinetics of the precipitation of uniform silica particles through the hydrolysis and condensation of silicon alkoxides. *Journal of Colloid and Interface Science* **1991**, *142*, 1-18.

(19) Bogush, G. H.; Zukoski, C. F. Uniform silica particle-precipitation-an aggregative growth-model. *Journal of Colloid and Interface Science* **1991**, *142*, 19-34.

(20) Bailey, J. K.; Mecartney, M. L. Formation of colloidal silica particles from alkoxides. *Colloids and Surfaces* **1992**, *63*, 151-161.

(21) Lee, K. T.; Sathyagal, A. N.; McCormick, A. V. A closer look at an aggregation model of the Stober process. *Colloids and Surfaces A-Physicochemical and Engineering Aspects* **1998**, *144*, 115-125.

(22) Green, D. L.; Lin, J. S.; Lam, Y. F.; Hu, M. Z. C.; Schaefer, D. W.; Harris, M. T. Size, volume fraction, and nucleation of Stober silica nanoparticles. *Journal of Colloid and Interface Science* **2003**, *266*, 346-358.

(23) Rahman, I. A.; Vejayakumaran, P.; Sipaut, C. S.; Ismail, J.; Abu Bakar, M.; Adnan, R.; Chee, C. K. An optimized sol-gel synthesis of stable primary equivalent silica particles. *Colloids and Surfaces a-Physicochemical and Engineering Aspects* **2007**, *294*, 102-110.

(24) Ab Rahman, I.; Padavettan, V. Synthesis of Silica Nanoparticles by Sol-Gel: Size-Dependent Properties, Surface Modification, and Applications in Silica-Polymer Nanocomposites-A Review. *Journal of Nanomaterials* **2012**.

(25) Petushkov, A.; Ndiege, N.; Salem, A. K.; Larsen, S. C.; James, C. F. In *Advances in Molecular Toxicology*; Elsevier: 2010; Vol. Volume 4, p 223-266.

(26) Xia, Y. N.; Gates, B.; Yin, Y. D.; Lu, Y. Monodispersed colloidal spheres: Old materials with new applications. *Adv. Mater.* **2000**, *12*, 693-713.

(27) El-Toni, A. M.; Khan, A.; Ibrahim, M. A.; Labis, J. P.; Badr, G.; Al-Hoshan, M.; Yin, S.; Sato, T. Synthesis of double mesoporous core-shell silica spheres with tunable core porosity and their drug release and cancer cell apoptosis properties. *Journal of Colloid and Interface Science* **2012**, *378*, 83-92.

(28) Park, S. J.; Kim, Y. J. Size-Dependent Shape Evolution of Silica Nanoparticles into Hollow Structures. *Langmuir* **2008**, *24*, 12134-12137.

(29) Zhang, Q.; Ge, J. P.; Goebl, J.; Hu, Y. X.; Lu, Z. D.; Yin, Y. D. Rattle-Type Silica Colloidal Particles Prepared by a Surface-Protected Etching Process. *Nano Research* **2009**, *2*, 583-591.

(30) Beckett, R.; Hart, B. T. *Environmental Particles*; Lewis Publisher: Boca Raton, FL, 1993.

(31) Giddings, J. C. Field-flow fractionation-analysis of macromolecular, colloidal, and particulate materials. *Science* **1993**, *260*, 1456-1465.

(32) Isaacson, C. W.; Bouchard, D. Asymmetric flow field flow fractionation of aqueous C-60 nanoparticles with size determination by dynamic light scattering and quantification by liquid chromatography atmospheric pressure photo-ionization mass spectrometry. *J. Chromatogr. A* **2010**, *1217*, 1506-1512.

(33) Schmidt, B.; Loeschner, K.; Hadrup, N.; Mortensen, A.; Sloth, J. J.; Koch, C. B.; Larsen, E. H. Quantitative Characterization of Gold Nanoparticles by Field-Flow Fractionation Coupled Online with Light Scattering Detection and Inductively Coupled Plasma Mass Spectrometry. *Anal. Chem.* **2011**, *83*, 2461-2468.

(34) Viebke, C.; Williams, P. A. The influence of temperature on the characterization of water-soluble polymers using asymmetric flow field-flow-fractionation coupled to multiangle laser light scattering. *Anal. Chem.* **2000**, *72*, 3896-3901.

(35) Li, S. L.; Nickels, J.; Palmer, A. F. Liposome-encapsulated actin-hemoglobin (LEAcHb) artificial blood substitutes. *Biomaterials* **2005**, *26*, 3759-3769.

(36) Qureshi, R. N.; Kok, W. T.; Schoenmakers, P. J. Fractionation of human serum lipoproteins and simultaneous enzymatic determination of cholesterol and triglycerides. *Anal. Chim. Acta* **2009**, *654*, 85-91.

(37) Guan, X.; Cueto, R.; Russo, P.; Qi, Y. D.; Wu, Q. L. Asymmetric Flow Field-Flow Fractionation with Multiangle Light Scattering Detection for Characterization of Cellulose Nanocrystals. *Biomacromolecules* **2012**, *13*, 2671-2679.

(38) Chuan, Y. P.; Fan, Y. Y.; Lua, L.; Middelberg, A. P. J. Quantitative analysis of virus-like particle size and distribution by field-flow Fractionation. *Biotechnology and Bioengineering* **2008**, *99*, 1425-1433.

(39) Hagendorfer, H.; Kaegi, R.; Parlinska, M.; Sinnet, B.; Ludwig, C.; Ulrich, A. Characterization of Silver Nanoparticle Products Using Asymmetric Flow Field Flow Fractionation with a Multidetector Approach - a Comparison to Transmission Electron Microscopy and Batch Dynamic Light Scattering. *Anal. Chem.* **2012**, *84*, 2678-2685.

(40) Lattuada, M.; Olivo, C.; Gauer, C.; Storti, G.; Morbidelli, M. Application of Asymmetric Flow-Field Flow Fractionation to the Characterization of Colloidal Dispersions Undergoing Aggregation. *Langmuir* **2012**, *26*, 7062-7071.

(41) McEvoy, M.; Razinkov, V.; Wei, Z. P.; Casas-Finet, J. R.; Tous, G. I.; Schenerman, M. A. Improved Particle Counting and Size Distribution Determination of Aggregated Virus Populations by Asymmetric Flow Field-Flow Fractionation and Multiangle Light Scattering Techniques. *Biotechnology Progress* **2011**, *27*, 547-554.

(42) Pease, L. F.; Lipin, D. I.; Tsai, D. H.; Zachariah, M. R.; Lua, L. H. L.; Tarlov, M. J.; Middelberg, A. P. J. Quantitative Characterization of Virus-like Particles by Asymmetrical

Flow Field Flow Fractionation, Electrospray Differential Mobility Analysis, and Transmission Electron Microscopy. *Biotechnology and Bioengineering* **2009**, *102*, 845-855.

(43) Von der Kammer, F.; Baborowski, M.; Tadjiki, S.; Von Tumpling, W. Colloidal particles in sediment pore waters: Particle size distributions and associated element size distribution in anoxic and re-oxidized samples, obtained by FFF-ICP-MS coupling. *Acta Hydrochimica Et Hydrobiologica* **2004**, *31*, 400-410.

(44) Xu, H.; Yan, F.; Monson, E. E.; Kopelman, R. Room-temperature preparation and characterization of poly (ethylene glycol)-coated silica nanoparticles for biomedical applications. *Journal of Biomedical Materials Research Part A* **2003**, *66A*, 870-879.

(45) Baalousha, M.; Stolpe, B.; Lead, J. R. Flow field-flow fractionation for the analysis and characterization of natural colloids and manufactured nanoparticles in environmental systems: A critical review. *J. Chromatogr. A* **2011**, *1218*, 4078-4103.

(46) Podzimek, S. In *Light Scattering, Size Exclusion Chromatography and Asymmetric Flow Field Flow Fractionation*; John Wiley & Sons, Inc., p 259-305.

(47) Van Helden, A. K.; Jansen, J. W.; Vrij, A. Preparation and Characterization of Spherical Monodisperse Silica Dispersions in Nonaqueous Solvents. *Journal of Colloid and Interface Science* **1981**, *81*, 354-368.

(48) Gross, A. F.; Le, V. H.; Kirsch, B. L.; Riley, A. E.; Tolbert, S. H. Correlations between silica chemistry and structural changes in hydrothermally treated hexagonal silica/surfactant composites examined by in situ X-ray diffraction. *Chem. Mat.* **2001**, *13*, 3571-3579.

(49) Liu, S.; Wong, Y.; Wang, Y.; Wang, D.; Han, M. Y. Controlled Release and Absorption Resonance of Fluorescent Silica-Coated Platinum Nanoparticles. *Advanced Functional Materials* **2007**, *17*, 3147-3152.

(50) Park, S.-J.; Kim, Y.-J.; Park, S.-J. Size-Dependent Shape Evolution of Silica Nanoparticles into Hollow Structures. *Langmuir* **2008**, *24*, 12134-12137.

(51) Lu, Y.; Yin, Y.; Li, Z.-Y.; Xia, Y. Synthesis and Self-Assembly of Au@SiO_2 Coreâ˚Shell Colloids. *Nano Letters* **2002**, *2*, 785-788.

(52) Soto-Cantu, E.; Cueto, R.; Koch, J.; Russo, P. S. Synthesis and Rapid Characterization of Amine-Functionalized Silica. *Langmuir* **2012**, *28*, 5562-5569.

CHAPTER 3
POLYPEPTIDE COMPOSITE PARTICLES BY CLICK CHEMISTRY: PREPARATION, CHARACTERIZATION AND APPLICATIONS OF MAGNETIC POLYPEPTIDE-BASED SILICA COLLOIDS SYNTHESIZED BY CLICK CHEMISTRY

3.1 Introduction

Hybrid materials made of inorganic cores and polymeric and biological shells have received an extensive research focus in the recent years. Their popularity arises from the unique properties they display and are not achieved by either shell or core alone.[1-10] Colloidal silica, either carying or lacking a magnetic nugget, are probably the most popular candidates for preparation of hybrid materials due to their low cost of fabrication, easy route of synthesis, resistance against oxidation and surface availability for post-functionalization with different moieties. Many applications were already found for such colloids especially in biosensing, separations, photonics and drug delivery. Recently a series of reviews summarized the progress in the field with special emphasis on the applications.[7,11-15] Among these kinds of composite materials, silica particles furnished with a homopolypeptide shell are of special interest.

Polypeptides exist in a well-defined ordered secondary structure (α-helix, β-sheet, random coil) and retain such conformation even in solution.[16-18] Different moieties anchored to the side chains allow them to respond when subjected to external stimuli such as pH, magnetic field, temperature or solvent.[19-25] Poly(Nε-carbobenzyloxy-L-lysine), PCBL is known for its reversible transition from random coil to α-helix in m-cresol as a function of temperature.[26-29] Cleavage of the benzyl side chain yields a water soluble composite material responsive to pH changes. One polypeptide that is less studied than its homolog poly(γ-benzyl-L-glutamate), PBLG, is poly(γ-stearyl-L-glutamate), PSLG. Besides being soluble in a wide range of organic solvents, PSLG exhibits a semiflexible rodlike structure: an α-helical backbone surrounded by

long flexible side chains positioned perpendicular to the helix axis giving the polypeptide a hairy constitution.[30-33] PSLG has both lyotropic and thermotropic properties due to the good solubility of pendant stearyl chains in desirable solvents and due to libration of these same side chains at high temperatures.[34-36]

Polypeptide and other biomolecular grafts on silica particles were obtained mainly by *growing from* and *grafting to* approaches. In the *grafting from* method the free amine decorated silica particles initiate the polymerization of particular amino acid N-carboxyanhydride, NCA, via ring opening polymerization. Early reports from this group dealt with the fabrication of both PBLG- and PCBL-coated silica particles. The former formed beautiful colored colloidal crystals.[37,38] Control over the thickness of the shell can be achieved by rationally choosing the ratio of the initiator to the monomer. Soto-Cantu et al. demonstrated the facile preparation of the composite particles in this manner opening the door to the copolymeric shells.[39] This method enables the formation of a uniformly dense shell on the core surface in a few steps, but the main disadvantage arises from the difficulty to evaluate the molecular weight of the grafted polypeptide accurately. The cleavage of the shell is available through treatment with hydrofluoric acid, HF, but besides etching the silica, HF may alter the polypeptide chain. The decrease in the size core with etching time was also studied by this group.[40] Recently the Heise group prepared polypeptide core-shell silica particles by *grafting from* with a high load of polypeptide.[41] Treatment with HF enabled access to the molecular weight of the shell by GPC means. The controlled polymerizations at 0°C and 25°C afforded polymers with molecular weights ranging from 7 to 20 kDa. Liu et al. prepared magnetic composites with silica coated magnetite core and PBLG shell with relatively high saturation magnetization.[42] On the other side, the *grafting to* method solves this challenging issue. The premade polymer is well-

characterized prior to the covalent attachment on the surface. Click chemistry has the main advantage of "matching" binding groups with an affinity for each other,[43,44] hence proving the selectivity of this approach. The drawback of the click methodology still remains the lower polymer loading and the efficient attachment of higher molecular weight polymer due to the steric hindrance. Few reports have been devoted to the attachment of polymers on silica particles[45-51] and even fewer on composite materials obtained by clicking a polypeptide on the same inorganic core. In this group, Balamurugan et al. attached 8 kDa PSLG on silica particles with 57,000 PSLG molecules per particle particles (±16%).[52] The higher-than-expected value of the molecular weight suggested that not all initiator molecules lead to growing polymer chains. Kar et al. have used N-trimethylsilyl propargyl amine in an effort to lower the polydispersity of the polypeptide and to have better control over the polymerization. The highest molecular weight of alkyne-poly(L-glutamic acid) obtained after deprotection of alkyne-poly(p-methoxy-benzyl-L-glutamate) was 12 kDa (M_w/M_n= 1.04).[53] The same methodology was employed to synthesize poly(L-lysine), PLL (~8 kDa by NMR, M_w/M_n= 1.05 by GPC) by deprotection of the PCBL homolog.[54] A block copolymer consisting of poly(L-lysine) and poly(L-leucine), PLL-b-PLLeu, (8 KDa, M_w/M_n= 1.1), was also used to prepare complex conjugate particles. Several reports have described the use of Huisgen 1,3-dipolar cycloadition to make block polymers consisting of homopolypeptides.[55-64]

The basis of click chemistry pioneered by Sharpless is coupling azide- and alkyne-terminated reactants through a very stable 1,2,3-triazole cycle, in the presence of a Cu(I) salt catalyst. The technique has been used to obtain a wide range of materials with a broad range of applications. Recently several reviews appeared which described the quintessence of this progressing field.[65-71] PSLG grafted on membranes allowed an increase in activity retention and

thermal stability of lipases immobilized on them. This behavior was attributed to the hydrophobic interaction between the long stearyl chains and lipase.[72,73] Further self-assembly of PSLG deposited on flat surfaces produced a flowerlike morphology[74] which was used to support biomimetic membranes.[75]

This work is devoted to expanding the field of multifunctional homopolypeptide-grafted silica composite particles using the *grafting to* approach. Designing responsive materials is a continuous challenge from the perspective of targeting very specific applications. Thus, a step forward was made to increase the responsiveness of click materials. Hybrid fluorescent PSLG and PCBL composite colloids furnished with a silica coated magnetite core were prepared. The lipase from *Candida rugosa*, was attached to the stearyl chains of PSLG particles demonstrating that the geometry of the surface doesn't hinder the capability of the lipase to adhere to the pendant chains. Magnetic and fluorescent particles were dispersed in a rodlike, liquid crystal forming solution of the same polymer, PSLG, to investigate the effect of external fields on mixture behavior. Water-soluble materials can be produced by cleaving protective side groups. In this way a PCBL shell can be converted to poly(L-lysine), PLL, yielding an aqueous dispersion of particles. The similarity between stearyl chains and some surfactant molecules enabled the dispersion of the PSLG click particles in diluted aqueous solutions. The rheological behavior of magnetic composite particles was also investigated.

3.2 Materials

L-glutamic acid (99%), stearyl alcohol (octadecanol) (99%), *tert*-butanol, (99.5%), anhydrous dichloromethane, anhydrous tetrahydrofuran, THF, *N,N,N',N',N''*-pentamethyldiethylenetriamine (PMDETA) (99%), CuBr (99.99%), propargylamine (98%), tetraethoxysilane (98%), triethylamine (99.5%) were purchased from Aldrich and used as

received. Nε-carbobenzyloxy-L-lysine (99%) was obtained from Acros Organic. Lipase from Candida Rugosa was purchased from Sigma Aldrich. Triphosgene was obtained from TCI America. (3-Bromopropyl)trichlorosilane was purchased from Gelest. All other chemicals were reagent grade and used without further purification.

3.3 Results and Discussion

3.3.1 Characterization of Polypeptide-based Hybrid Colloids.

Magneto- fluorescent azide-functionalized particles were obtained through several steps, as shown in Scheme 3.1. The magnetite core was produced by a sol-gel process involving coprecipitation of iron salts (Fe^{+2} and Fe^{+3}) in a mole ratio of 1:2. The citric acid protection was removed by dialysis and was replaced with a silica layer. The inorganic silicon protective coverage was realized by a modification of the Stöber procedure. In order to make the particles fluorescent, a layer of silica and an adduct made of 3-aminopropyltriethoxysilane, APS, and fluorescein isothiocyanate, FITC, was covalently attached onto the silica coated magnetite. Prevention against dye bleaching was possible by coating with another layer of silica. The condensation of (3-bromopropyl)trichlorosilane onto silica yielded the bromo-functionalized particles, as the precursors for the final product azide-functionalized colloid. The later was obtained by conversion of bromine functions to azide by nucleophilic substitution with NaN_3 in DMF in the presence of tetrabutylammonium iodide as catalyst. The final click product was obtained by coupling the premade alkyne-end terminated polypeptide and azide-end terminated particles through 1,3-Huisgen cycloadition using CuBr as catalyst and PMDETA as ligand. PMDETA enhances the rate of copper-catalyzed type azide-alkyne cycloadition in an organic environment. The alkyne polymer was prepared by ring opening polymerization of the

corresponding N-carboxyanhydrides initiated by the propargyl amine used as an initiator. This procedure is illustrated in Scheme 3.2.

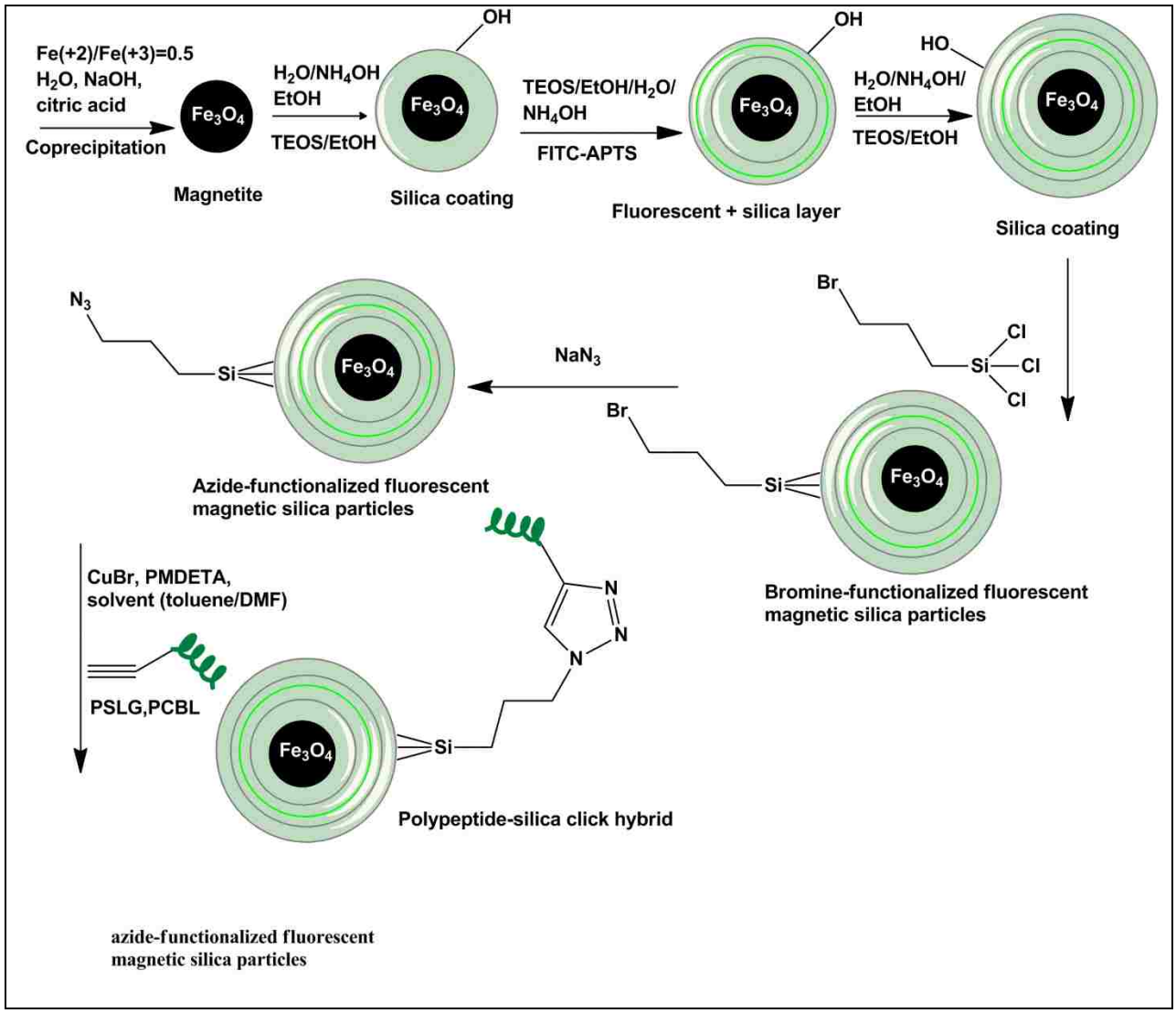

Scheme 3.1 . Synthetic route for preparation of magnetic fluorescent azide-functionalized particles.

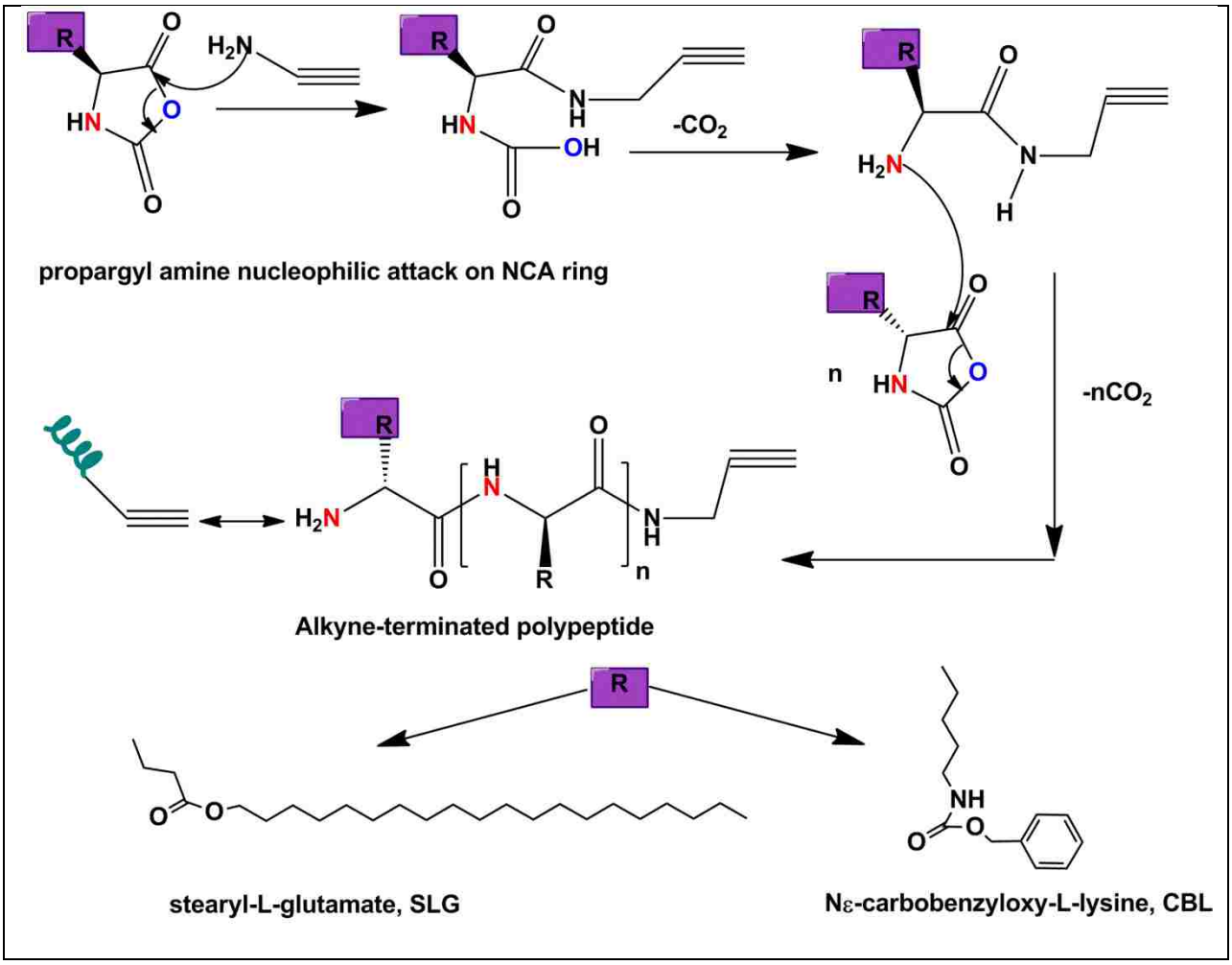

Scheme 3.2 Schematic representation of alkyne-terminated polypeptide preparation.

Preparation of the magnetite cores by the coprecipitation method and their protective coating with silica was confirmed using HRTEM, XRD and FTIR. Figure 3.1A shows the image of the relatively uniform magnetite particles with the average size of 11 nm in diameter. The diffraction lattice can also be easily observed. After preparation magnetite colloid had a layer of citrate ions on the surface to prevent against oxidation and to ensure a good dissolution in aqueous solutions. The presence of citrate ions was evidenced by FTIR (Figure 3.1 C inset). The specific band corresponding to C=O can be seen at 1628 cm^{-1} and the broad OH signal is clearly visible at ~3500 cm^{-1}. A magnetite's specific Fe—O—Fe stretch is reflected in the IR spectra by

the peak centered at 571 cm^{-1}. In biomedical applications, some organic coatings are not desirable because they might be toxic to the living body.

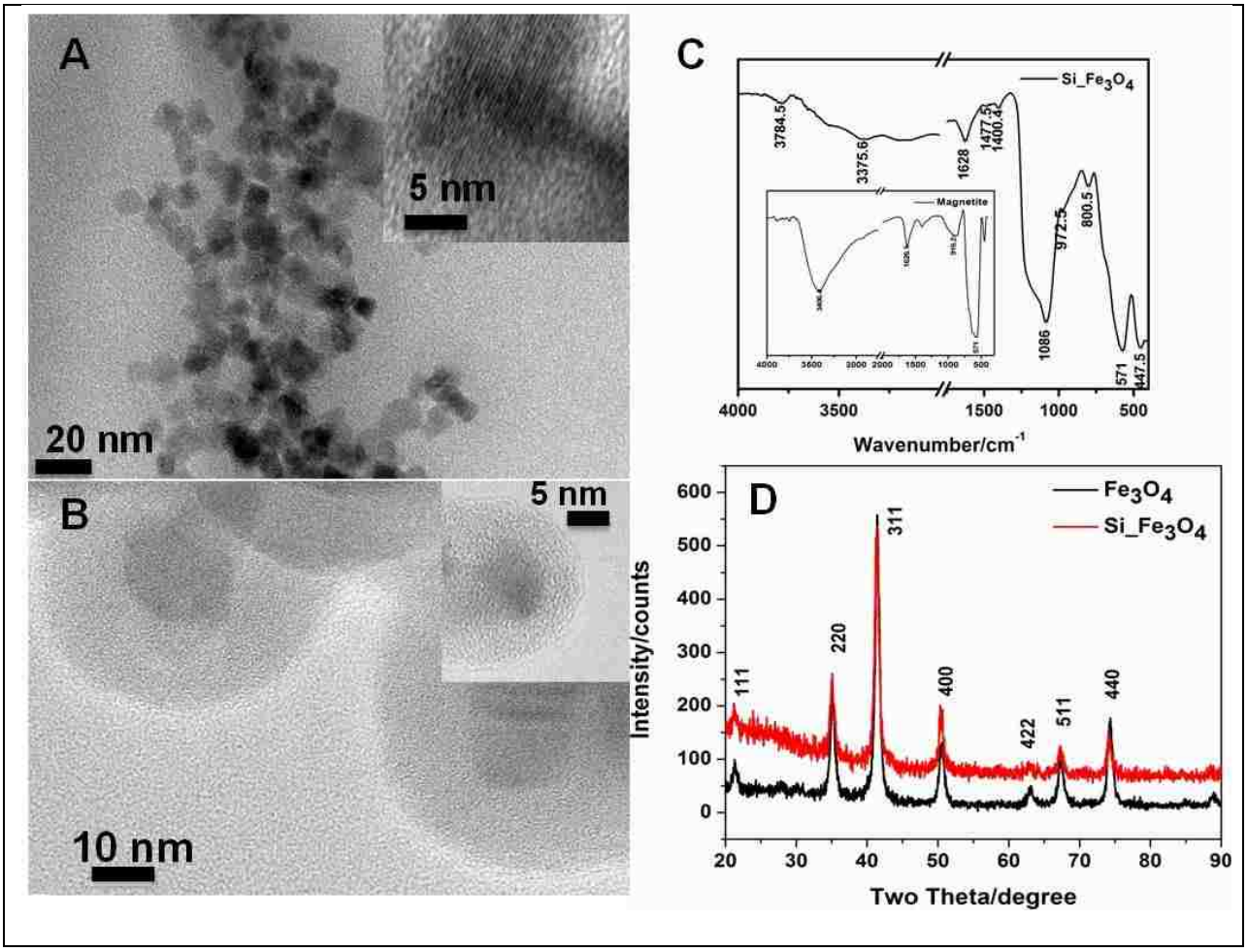

Figure 3.1 HRTEM images (A and B), FTIR (C) and XRD (D) spectra of naked magnetite and silica-coated magnetite (CR472 and CR615).

Removal of the citrate coating by dialysis is evidenced by the disappearance of the OH broad peak at 3500 cm^{-1} in the silica-coated magnetite particles. Only insignificant traces of the citrate are suggested by the small shoulder at 1628 cm^{-1}. The ratio between the specific band of silica (Si—O—Si) centered at 1086 cm^{-1} and iron (Fe—O—Fe, 571 cm^{-1}) suggested the presence of a thin silica layer on the surface. This thin coverage was also confirmed by XRD as shown in Figure 3.1D. Indeed the images recorded with the high-resolution electron microscope (Figure

1B inset) show an approximately 4.5 nm thick coating. Additional information on crystal nature was gathered by XRD. Magnetite has an inverse spinel structure described by a cubic close packing with tetrahedral sites occupied by Fe^{+3} and octahedral sites randomly shared by either Fe^{+3} or Fe^{+2} with the same proportions. Based on this arrangement, the structural formula can be written as $[Fe^{+3}](Fe^{+2}Fe^{+3})O_4$.[76] Under air exposure, Fe^{+2} can easily be oxidized and the magnetite crystallite will have an iron deficit, but this was not observed in the present synthesized magnetite. The characteristic peak 311 was located at 2θ = 41.4° and perfectly matched the standard values of pure magnetite taken from the NIST file no. 19-0629. Calculations based on the Scherer equation made the evaluation of the crystallite (coherent diffraction domain) size for both pure magnetite and silica coated particles possible. The measured values were 11 nm for the first and 19 nm for the latter.

$$d = \frac{K \times \lambda}{\beta \times cos\ \theta}, \quad \text{Eq. 3.1}$$

where d is the crystallite diameter, K is the shape factor, λ is the X-ray wavelength, β is the line broadening at half the maximum intensity (FWHM) for 311 peak and θ is the Bragg angle.

The increase in silica shell thickness after the protection against dye leaking and bleaching is clearly shown in the Figure 3.1B. The inorganic silica coating thickness increased from 4.5 nm to about 15 – 17 nm.

Another technique frequently used in particle characterization is X-ray photoelectron spectroscopy. The confirmation of products obtained at each step presented in Scheme 3.1 and Scheme 3.2 was also possible using XPS as shown in Figure 3.2. The nature of the Fe ions valence can be determined from 2p core-level spectra.[77] The spectrum displayed in Figure 3.2A shows the bonding energy of Fe $2p_{3/2}$ centered at 710 eV and Fe $2p_{1/2}$ at 723.8 eV.

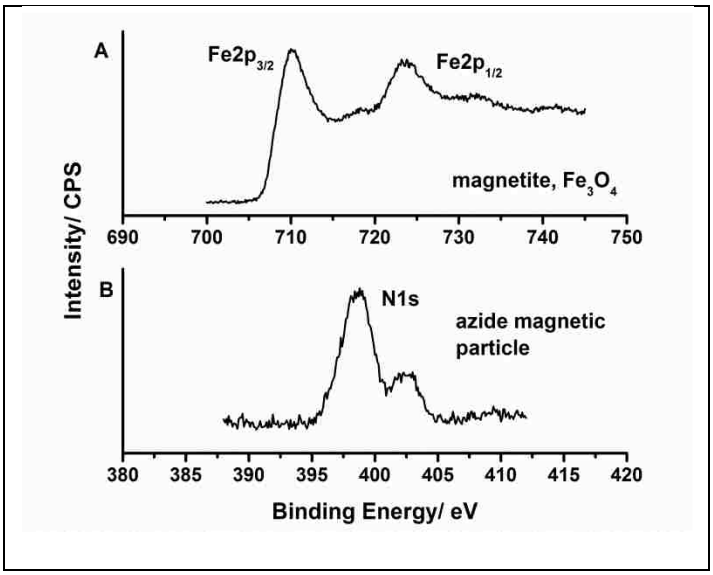

Figure 3.2 High-resolution XPS survey scans of (A) Fe 2p for magnetite and (B) N1s for azide-functionalized magnetite.

It is known that Fe ions bond with carboxylate groups belonging to protective acids.[78] This linkage is reflected in an XPS spectrum by the presence of the C1s peak at 286.7 eV. The C−C bonds from the acid's alkyl chain also contribute to the occurrence of this signal. The peak for free acid was not found. XPS confirmed the successful coating with silica and was reflected by the specific peaks Si2s (152.4 eV), Si2p (104.5 eV) (Figure 3.3)[79]. The covalent fluorescent doping with FITC-APS complex was confirmed by the N1s (396.5 eV) signal and the increased C1s (286.7 eV) (Figure 3.3). Further indication of a protective silica layer coating was evident from XPS spectrum by the disappearance of the N1s peak at 396.5 eV and a visible decrease in C 1s intensity (Figure 3.3). The coating of the surface with bromine groups was evident from the survey spectrum of bromine-functionalized particles.

Figure 3.4A shows the specific peaks corresponding to Br3d at 68 eV and Br3p at 181.5 eV as well as other elements present on the particle surface. Conversion of bromine groups to azide groups was evidenced by the disappearance of bromine peaks and the occurrence of azide N1s centered at 400 eV. A noticeable decrease in the C1s signal was also observed.

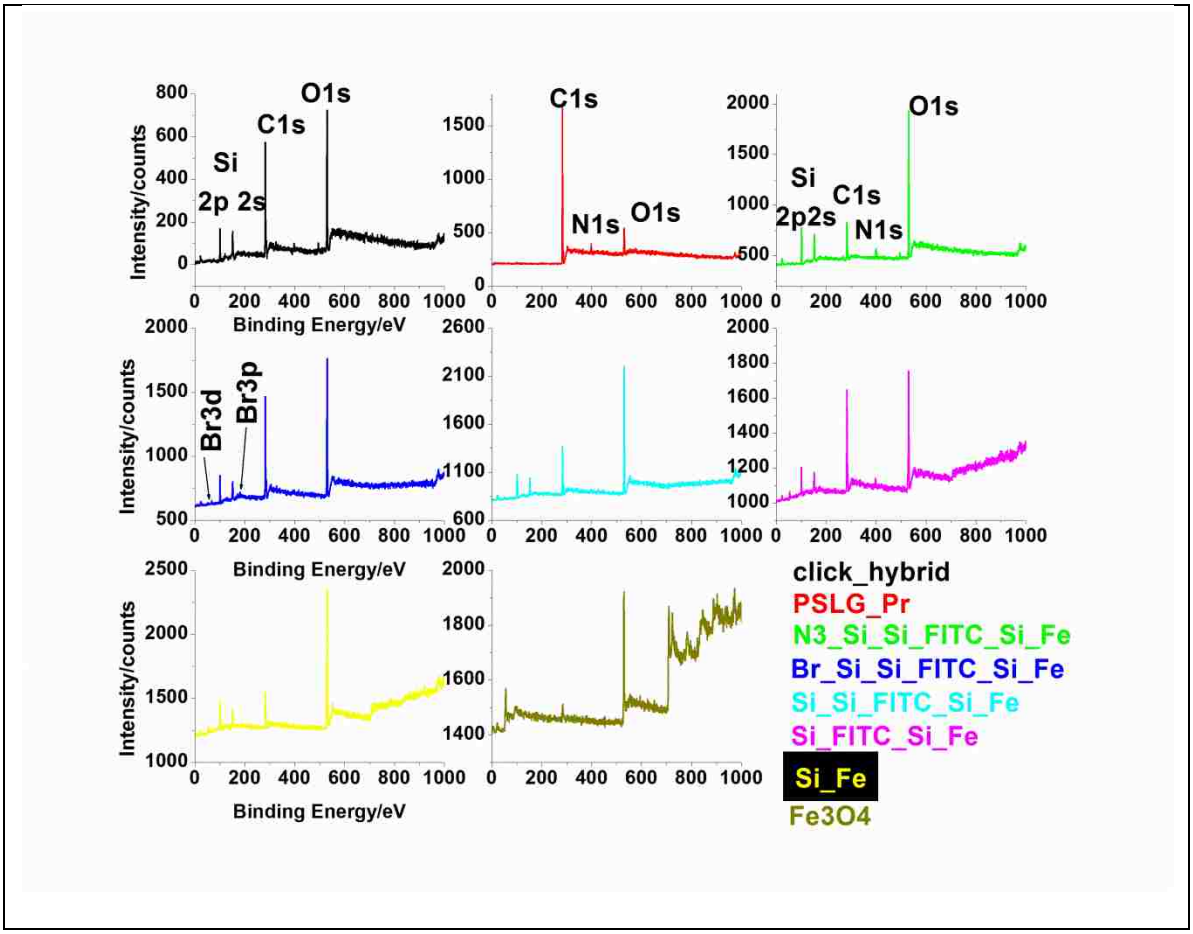

Figure 3.3 XPS survey scans of all steps involved in the preparation of the PSLG-click hybrid.

The replacement of the bromine moieties with bulky azide can hinder the carbon situated on the particle surface. A high-resolution spectrum (Figure 3.2B) gave more information on the structure of the azide-functionalized particles. The bonds from the azide were reflected in the N1s double peaks at 400 and 402.8 eV.[80,81] The electron deficiency of the azide's middle nitrogen can be seen by the less intense peak at 402.8 eV.[81]

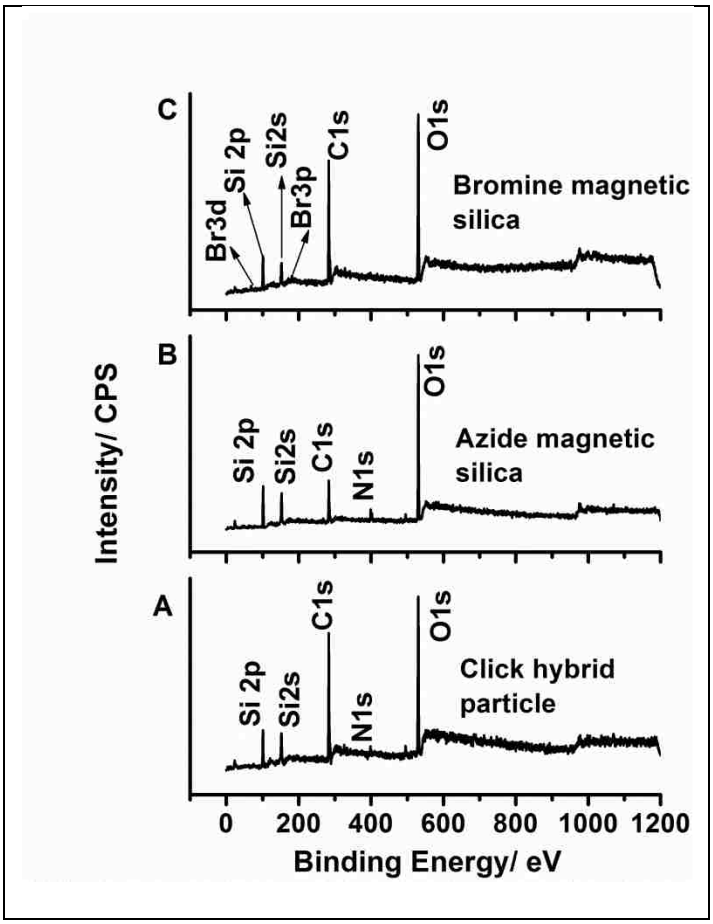

Figure 3.4 XPS-survey scans for (A) click-hybrid particle, (B) azide magnetic silica and (C) bromine magnetic silica.

The immobilization of polypeptide on the particle surface through click chemistry was evident in the XPS survey of the click-hybrid (Figure 3.3 and Figure 3.4). A consistent decrease in the N1s signal was recorded for the click-hybrid. The contribution to the N1s signal in the click hybrid is made by the nitrogen from the polypeptide backbone and possible unreacted azide groups. The polypeptide packs into stiff rod-like structure. This conformation might hinder the nitrogen from the backbone. Also some free azide groups can be hidden due to polypeptide chains which can bend or collapse on the surface. Another reason can be a light grafting density of the chains on the particle surface. The increase of the C1s signal for the click particle, Figure 3.4A, when

compared with the signal for the same element recorded for azide magnetic silica, Figure 3.4B, clearly proved the attachment of the polypeptide onto the particle surface.

One of the advantages of the *grafting to* when compared to the *growing from* method is that the former allows the characterization of the polymer which will constitute the shell. The molecular weights of the polypeptides (Table 3.1) were determined by GPC/MALS (Figure 3.5), using dn/dc=0.08 ± 0.002 $mL \cdot g^{-1}$ (PSLG) in THF and dn/dc=0.123 ± 0.002 $mL \cdot g^{-1}$ (PCBL) in DMF.

Table 3.1 Molecular Weights and Polydispersity Index for Alkyne-Polypeptides.

Polymer	[M]/[I]	Theoretical M	M_n/Da	M_w/Da	M_w/M_n
Pr-PSLG	100:1	38,300	25,700 ± 3%	30,000 ± 4%	1.17 ± 1%
Pr-PCBL	100:1	26,400	5,300 ± 3%	6,000 ± 5%	1.11 ± 2%

The average molecular weight values returned by GPC/MALS based on monomer to initiator ratio showed that some initiator molecules could lead to dormant chains or were simply inactive. The amine-initiated mechanism was confirmed by the MALDI-TOF analysis which allows the identification of end groups. A range of single peaks was observed for both polypeptides: from *m/z* = 1731 to 5056 Da (Figure 3.5B) with the mass difference of 381 units matching the SLG repeat units and from *m/z* = 1404 to 6379 Da (Figure 3.5C) with a mass difference of 262 units identical with the molecular weight of CBL repeat units. The average molecular weight values returned by GPC/MALS based on monomer to initiator ratio showed that some initiator molecules could lead to dormant chains or were simply inactive.

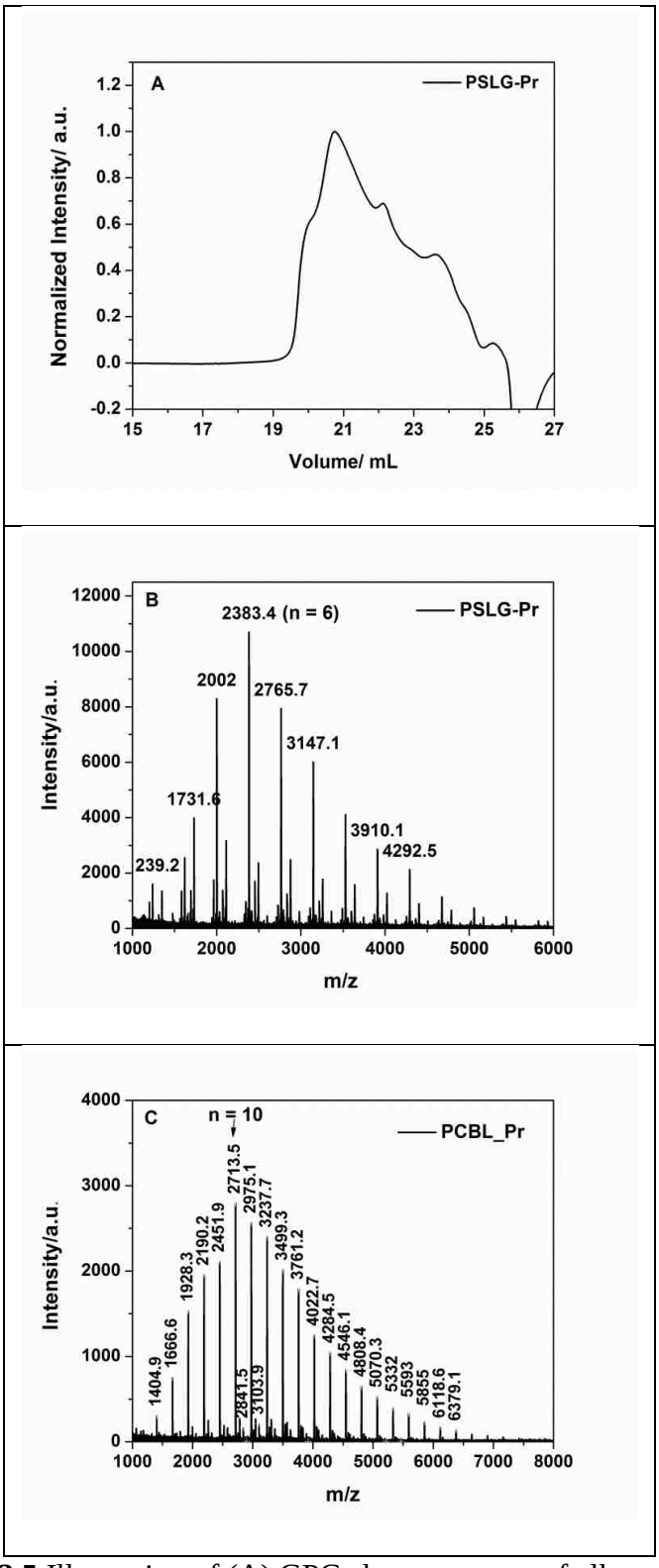

Figure 3.5 Illustration of (A) GPC chromatogram of alkyne-PSLG recorded in THF (the *dn*/*dc* was taken as 0.080 ± 0.002 mL·g^{-1}); MALDI-TOF MS of (B) poly(γ-stearyl-L-glutamate) and (C) poly(*N*ε-carbobenzyloxy-L-lysine) prepared with propargyl amine.

The amine-initiated mechanism was confirmed by the MALDI-TOF analysis which allows the identification of end groups. A range of single peaks was observed for both polypeptides: from *m/z* = 1731 to 5056 Da (Figure 3.5B) with the mass difference of 381 units matching the SLG repeat units and from *m/z* = 1404 to 6379 Da (Figure 3.5C) with a mass difference of 262 units identical with the molecular weight of CBL repeat units. The peak centered at *m/z* = 2713 in Figure 3.5C corresponds to decameric protonated fragment, CBL, with an incorporated initiator propargylamine as end-group. All adducts recorded in the chromatograms have a supplemental 35-39 units which might be explained by the adherence of potassium (K^+) to the fragments.

Polypeptides are known to adopt different secondary structures dependent on the solvent, temperature and pH changes.[16] PSLG is helical in solvents such as THF, toluene and chloroform. A single turn of the helix requires 3.6 monomer units with a projected diameter of 5.4 Å. If a degree of polymerization of about 78 computed from GPC/MALS data is taken into consideration, the number of turns is 20. The helical structure is stabilized by H-bonding between the N—H and C=O backbone groups. This twisting gives the polypeptide a rodlike behavior. PSLG does not undergo any conformational transitions when compared with PCBL. The lower molecular weight measured by GPC for the latter polypeptide has raised concerns on its helical conformation. The degree of the polymerization indicates 23 monomer units and points to a very short helix of about 6 turns. The formation of the helical secondary structure requires between 10 and 18 monomers per turn, on average, depending on the polypeptide. The unique feature of PCBL is its capability to undergo an inverse-type reversible helix-coil transition in a single organic solvent, m-cresol, as a function of temperature.[82] Upon deprotection of the side chains, poly(L-lysine) becomes sensitive to pH changes from acidic to basic. FTIR technique was exclusively used to investigate the structure of the polypeptides untethered and

tethered to the particle surface. Figure 3.6 illustrates the IR spectra of alkyne-PSLG and PSLG-click hybrid particle.

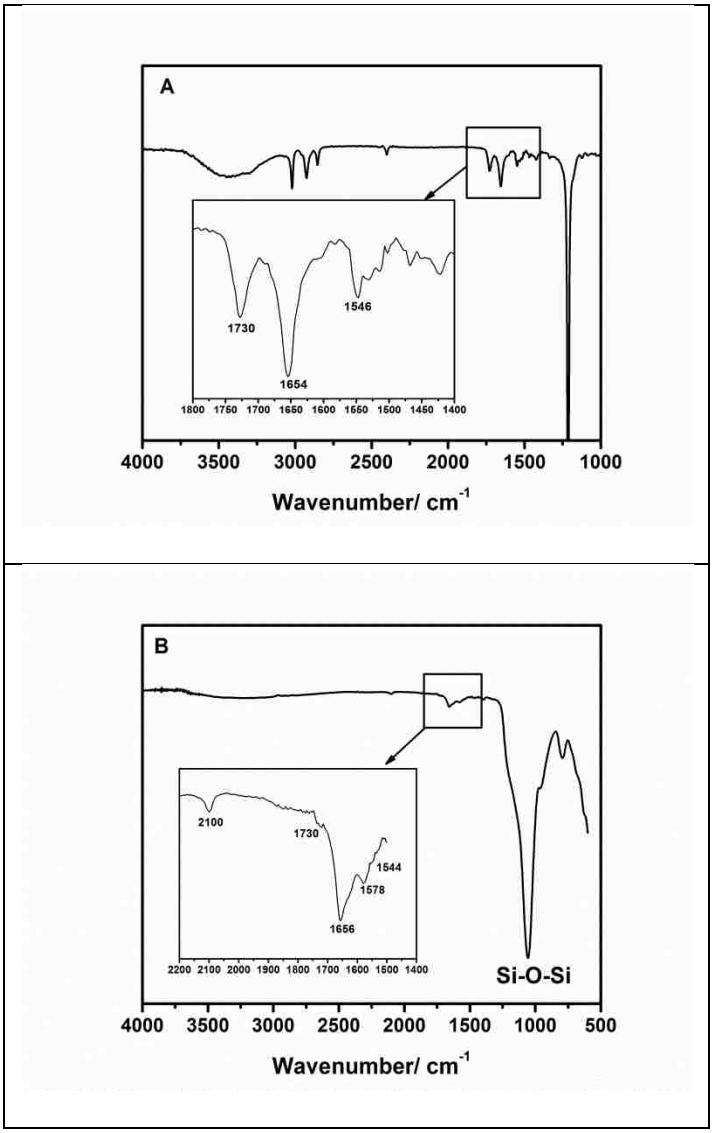

Figure 3.6 FTIR spectra of (A) alkyne-PSLG and the expanded region from 1800 to 1400 cm^{-1} and (B) PSLG-click hybrid particle and the expanded region from 2200 to 1400 cm^{-1}.

Both IR spectra were recorded in chloroform solution. Figure 3.6A shows the specific bands of amide I at 1654 cm^{-1} and amide II at 1546 cm^{-1} which are characteristic of amide α-helical structure. The N—H stretching of the amide A along with the N—H endgroups stretch, overlapped in the region from 3500 to 3200 cm^{-1}. The peaks visible between 3000 and 2800 cm^{-1}

correspond to asymmetric and symmetric vibrations of the hydrocarbon side chain $(CH_2)_{18}$. The C=O ester stretching of the polypeptide can be seen at 1730 cm^{-1}. Figure 3.6B shows that PSLG retained the helical conformation after grafting on the spherical surface. The characteristic peaks of the polypeptide described above are visible at the same wavenumbers within experimental error. The supplemental peak centered at 2100 cm^{-1} is assigned to azide groups, which is in agreement with XPS data showing free azide moieties on the surface. The specific signal of the Si—O—Si band is also visible at 1095 cm^{-1}. The same trend was followed by the PCBL click hybrid and is shown in Figure 3.7.

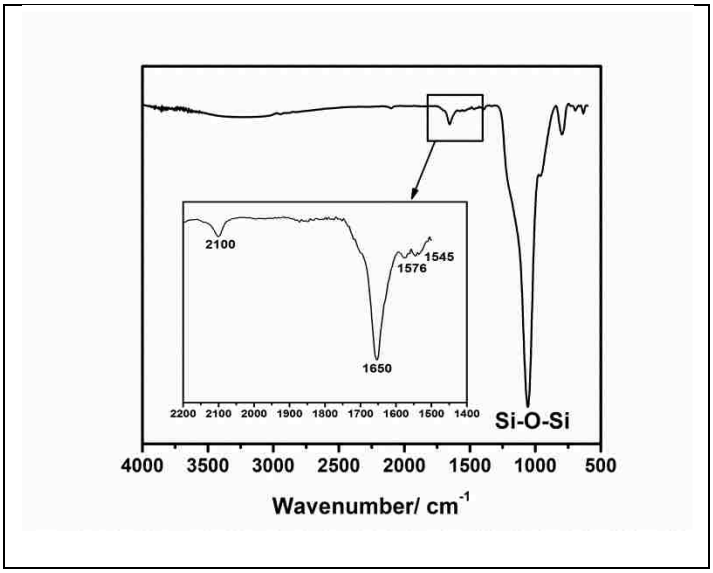

Figure 3.7 FTIR spectrum of the PCBL-click hybrid (CR6176) and the expanded region from 2200 to 1400 cm^{-1}.

Dynamic light scattering was used to estimate the size of the magnetic particles. Figure 3.8 doesn't reflect the true size of the individual PSLG click hybrid particle. Moreover the particles tended to cluster due to the magnetic anisotropy and most probably to the stickiness of the side chains toward each other and to dodecane, the solvent used in measurements.

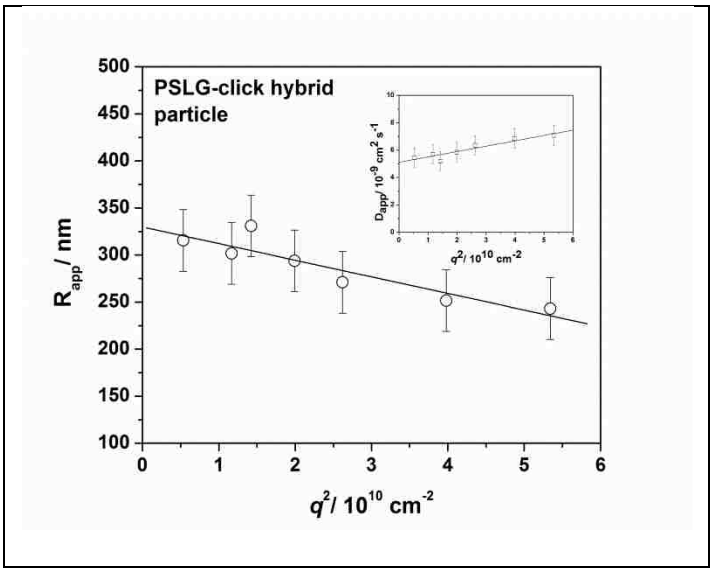

Figure 3.8 Apparent radius and the associated diffusion coefficients (inset) measured at seven different angles using DLS (CR715).

The elevated temperature at which the measurements were performed (50°C) couldn't overcome the cluster formation. A cluster noticed at lower angles seemed to be an agglomeration of 10 individual particles with a diameter of 60 nm for PSLG click particles. The same cluster size behavior of about 10 particles each was also noted for PCBL particles in DMF (Figure 3.9) pointing to the anisotropic nature of the composite particle encasing magnetite cores. The anisotropy can be explained on the basis of a small remanent magnetization. The TEM measurements indicated a size of 60 nm in diameter for PSLG click composite particle and 55 nm for PCBL click hybrid particle.

Thermogravimetric analysis, TGA, provided information about the loading on the particle at each step. Figure 3.10 shows the TGA traces recorded in both nitrogen and air atmosphere. The TGA profile, Figure 3.10B, shows the weight loss difference when the decomposition took place under nitrogen and air atmosphere. The supplemental 0.7% weight loss recorded under air conditions can be attributed to oxidation of Fe(+2) to Fe(+3).

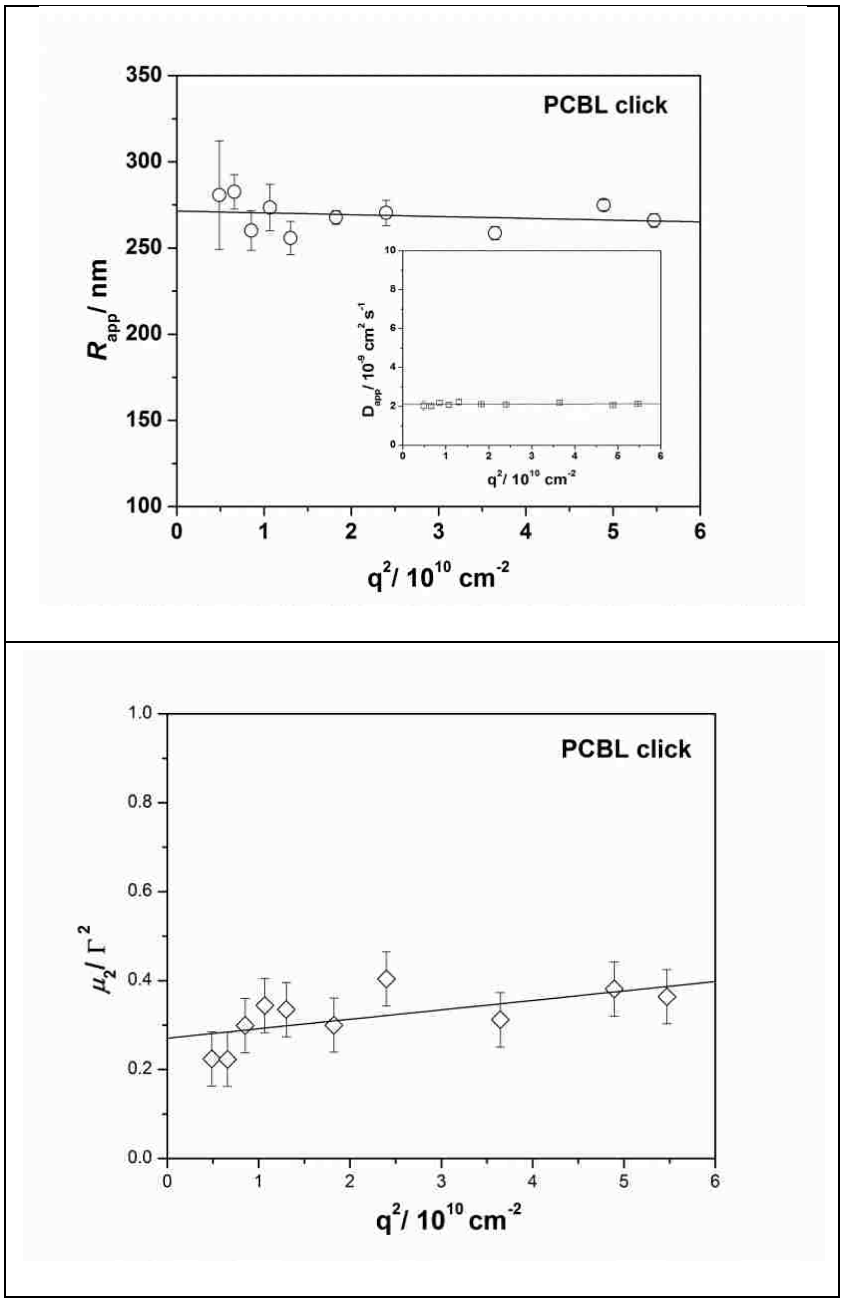

Figure 3.9 Typical DLS data collected for PCBL-click hybrid particle in DMF; (A, inset) apparent diffusion coefficients, D_{app}, as a function of the scattering vector magnitude, q, extrapolated to $q = 0$, (A) apparent radius, R_{app}, as a function of the scattering vector magnitude, q, and (B) polydispersity index, μ_2/Γ^2.

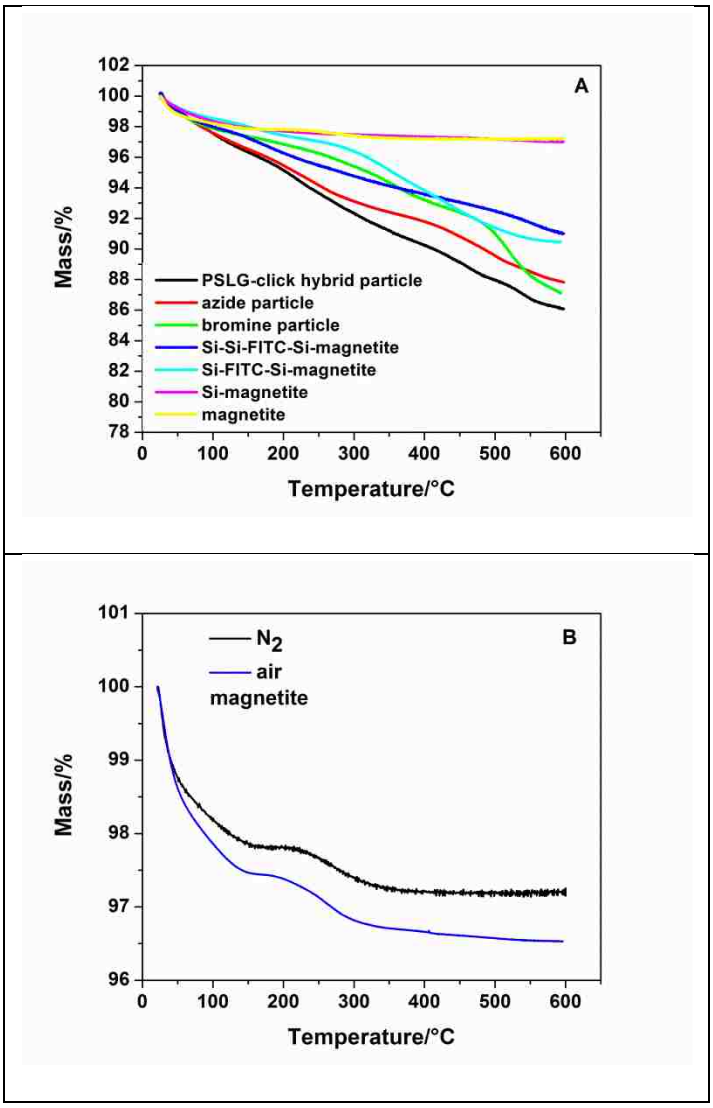

Figure 3.10 TGA thermograms for PSLG click-hybrid and the intermediate steps followed in the synthesis.

All thermograms discussed here on were obtained under nitrogen. TGA curves, Figure 3.10A, clearly shows the successful protective silica coating performed after the cores were doped with FITC: less decomposition can be seen in the double layered silica cores. This also shows the increased thermal stability of the fluorescent particle. The weight loss up to 200°C in the case of the click-hybrid can be attributed to the adsorbed water and probably to the unreacted azide functional groups. The decomposition range from 200 to 600°C corresponds to tethered polypeptide. The mass difference gave 6% coverage with polypeptide for both PSLG and PCBL

click hybrid particles. The thermograms associated with PCBL click product are presented in the Figure 3.11.

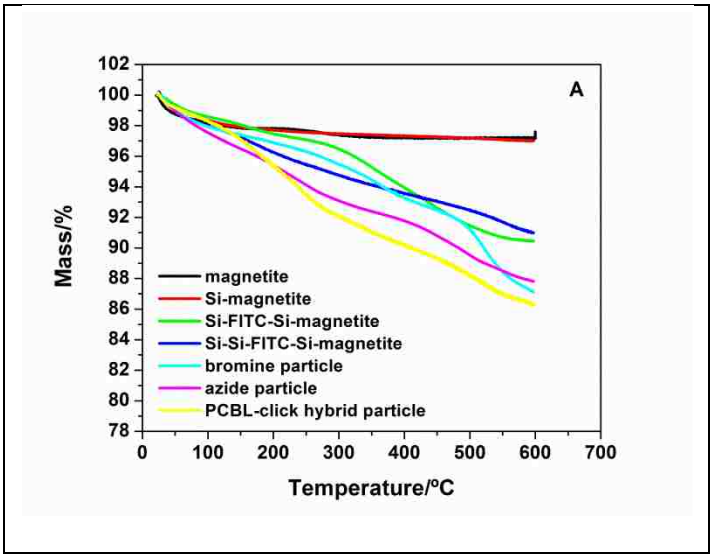

Figure 3.11 Decomposition profiles for products obtained at each step involving PCBL- click hybrid particle.

TGA data were further converted in grafting densities, σ, using the following equation:[52]

$$\sigma = \frac{f^{-1}w_{200-600} - w_{silica} \times (1 - f^{-1}w_{200-600})}{M \times S_{spec} \times (1 - f^{-1}w_{200-600})} \times 10^6 \, , \mu\text{mol} \cdot \text{m}^{-2} \quad \text{Eq. 2}$$

where f is the fraction of polypeptide ashes, $w_{200\text{-}600}$ is the weight loss of the polypeptide between 200 and 600°C, w_{silica} is the weight loss of the silica in the 200-600°C temperature interval, M is the molecular weight of the polypeptide ($g \cdot mol^{-1}$) and S_{spec} is the surface specific area ($m^2 \cdot g^{-1}$). S_{spec} was calculated considering the density of the silica 1.98 $g \cdot cm^{-3}$ and a core radius of 25 nm from TEM measurements. The values calculated are summarized in Table 3.2.

Table 3.2 Sample Name, Grafting Density and Chains per Particle

Sample	Grafting density/μmol· m^{-2}	Chains per particle
PSLG click	$0.03 \pm 1.5 \times 10^{-3}$	125 ± 6
PCBL click	$0.12 \pm 6 \times 10^{-3}$	800 ± 40

The magnetic properties of the particles were investigated with a SQUID device. Figure 3.12 displays the hysteresis loops for pure magnetite and click-hybrid.

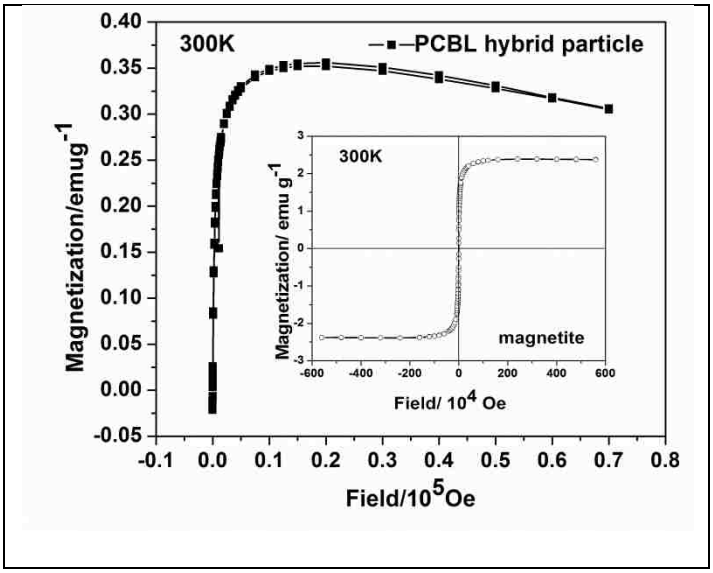

Figure 3.12 Hysteresis loops for pure magnetite and click-hybrid (CR6176).

The magnetic properties of the particles greatly depend on their size. A close inspection of magnetization curve for pure magnetite shows no hysteresis loop at 300K. This behavior is characteristic to superparamagnetic particles with a grain size up to a critical value of 20 nm.[83] The native magnetite showed a slow approach to saturation at a high field and no coercivity, H_c. Grafting layers of different natures onto the magnetite surface was reflected by the shape and the decrease in magnetization for the polypeptide click hybrid as shown in Figure 3.12. The coercive field necessary to obtain zero magnetization was 100 Oe. Overall the click composite particle exhibited insignificant remnant magnetization, M_r, and a low coercive field, H_c. Moreover the final product can be considered a nearly superparamagnetic material.

3.4 Applications of Polypeptide-based Click Hybrids.

3.4.1 Immobilization of *Candida Rugosa* Lipase

The PSLG click hybrid is an ideal support for immobilization of lipases known for their increased activity when in contact with a hydrophobic substrate.[84] The adsorption of the lipase to the click particles was performed in neutral pH phosphate buffer and is illustrated in Scheme 3.3. Details on the preparation are available in Chapter 8.

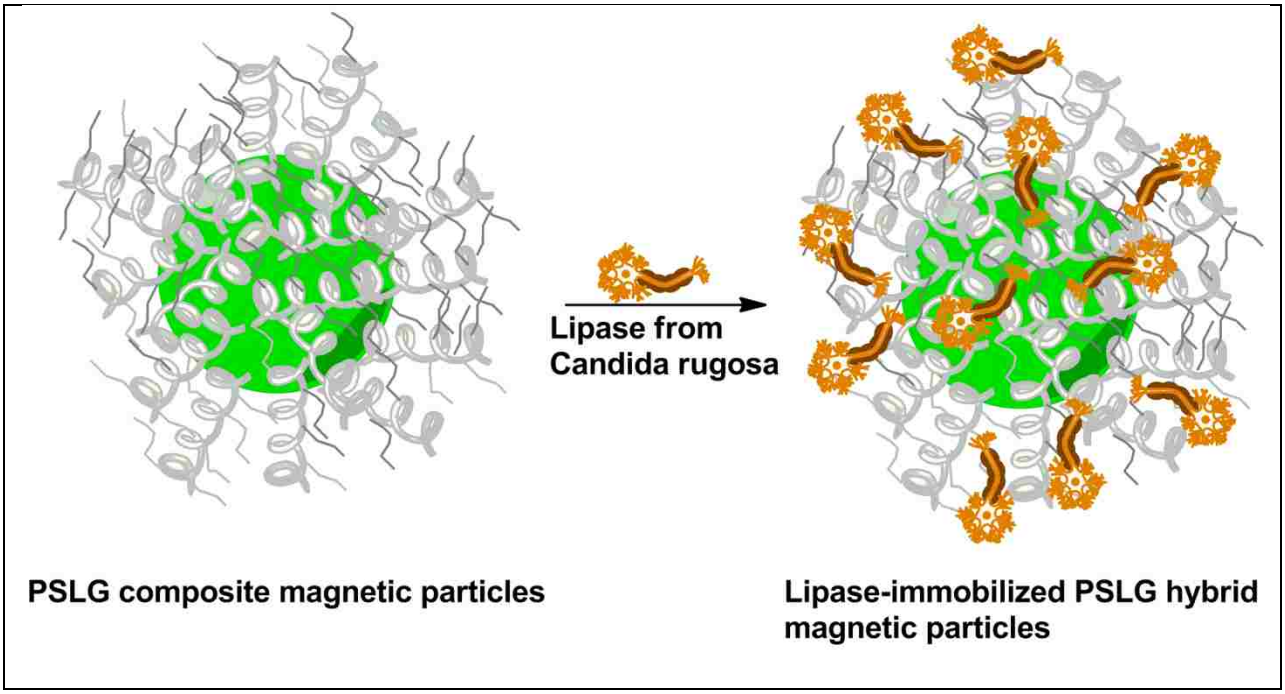

Scheme 3.3 Representation for the adsorption of lipase from *Candida rugosa* onto the PSLG-click composite particles

The disposition of the stearyl chains pointing out of the helical backbone allows a facile interaction with the hydrophobic part of the lipase. During adsorption, the lipase experiences important conformational rearrangements which uncovers the so-called "open state".[73] Further, the lipase is able to recognize the hydrophobic site of the carrier, in this case the stearyl chains, and adhere to them. The main issue with the immobilization of the enzymes on the substrates is their poor catalytic activity due to the steric hindrance between the carrier molecules (substrate)

and enzyme.[85] Spacer arms were incorporated to reduce undesirable interactions between the enzyme and the substrate.[86] Therefore, it is very important to have a lightly grafted substrate to enhance the enzyme's activity. Because PSLG-click hybrid had a low coverage with polypeptide chains, it was expected to easily immobilize the lipase. The TGA analysis gave the loading with lipase of the click particle as shown in Figure 3.13.

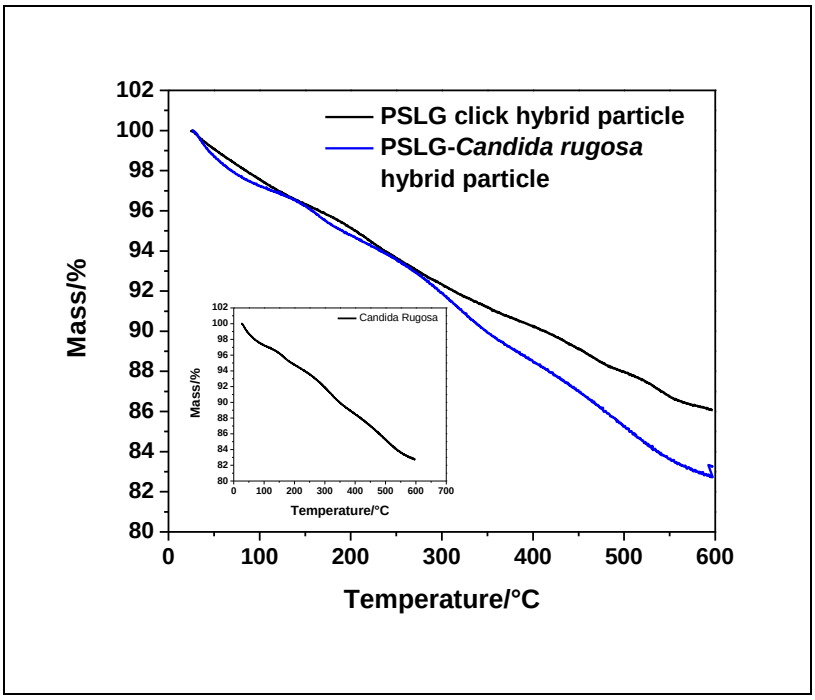

Figure 3.13 TGA traces of the lipase from *Candida rugosa* (inset), PSLG-click hybrid particle and PSLG-*Candida rugosa* hybrid particle.

A close inspection of the two traces for the PSLG-click hybrid particle and the immobilized enzyme particle revealed a 4% loading with lipase. The comparison between 6% coverage with polypeptide and the percent of enzyme loading, gives 66% immobilization efficiency. The immobilized-lipase-click hybrid material has several advantages when compared with hydrophobic flat surfaces. Due to its small size, the colloid particle carying the enzyme can access tiny areas. Furthermore, the magnetic inclusions enable the control in-out of the particles, consequently the material is easily recovered and reusable. In addition, the immobilization onto

the hydrophobic sites promotes the purification of the enzyme. The reversible incorporation of the lipase enables the recovery of the support particles after the enzyme inactivation. Finally the PSLG is a biofriendly substrate which can be used to mimic the tethering of the enzymes on natural macromolecules.[87-89]

3.4.2 Suspension of PSLG-click Colloids in the Rodlike Polypeptide Matrix.

PSLG click hybrid particles were suspended in a 40 wt% solution of PSLG in toluene at 1 wt% mass fraction. Figure 3.14A shows the texture of the particles 2 days after preparation. Columns made of particles seemed to arrange in a more or less organized network. It was also evident that the particles were well-dispersed in the mixture. An external magnetic field was applied to test whether the particles were able to respond and align. Particles aligned relatively fast (15- 20 min.) as shown in Figure 3.14C.

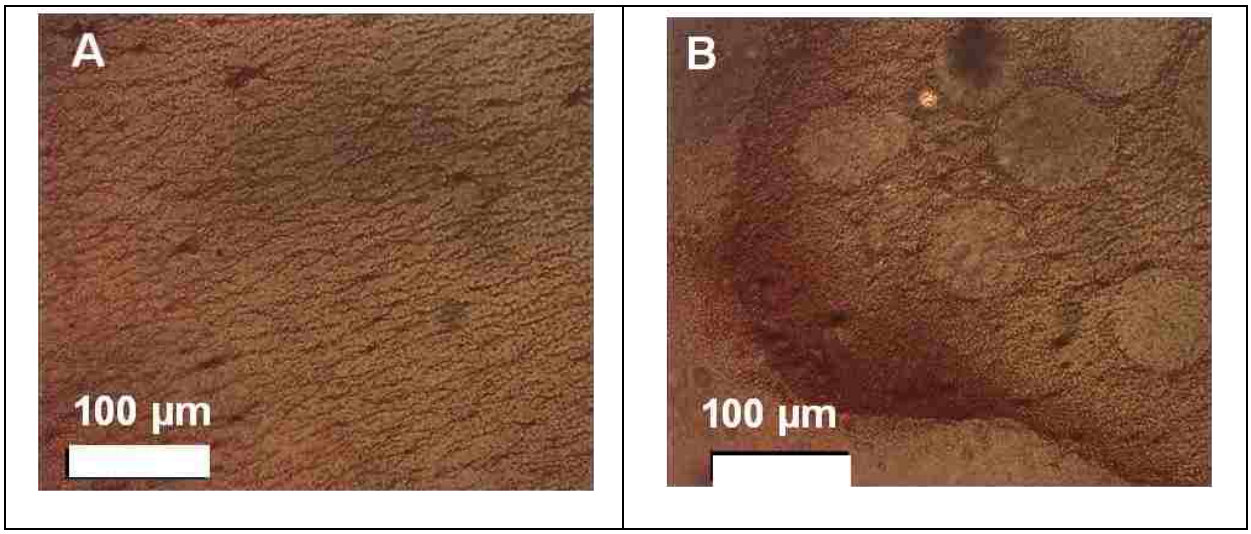

Figure 3.14 POM micrographs of 1 wt% PSLG-click hybrid particles (CR715) suspended in 40% PSLG/toluene taken at room temperature: (A) thin column arrangement after two days, (B) nascent ring-like texture after two days, (C, D) different orientations adopted by composite particles under applied magnetic field, (E, F cross polars) well-defined ring-like patterns after 6 days, and (G, H cross polars) thick columns of particles after 6 days in the absence of the applied magnetic field.

Figure 3.14 continued

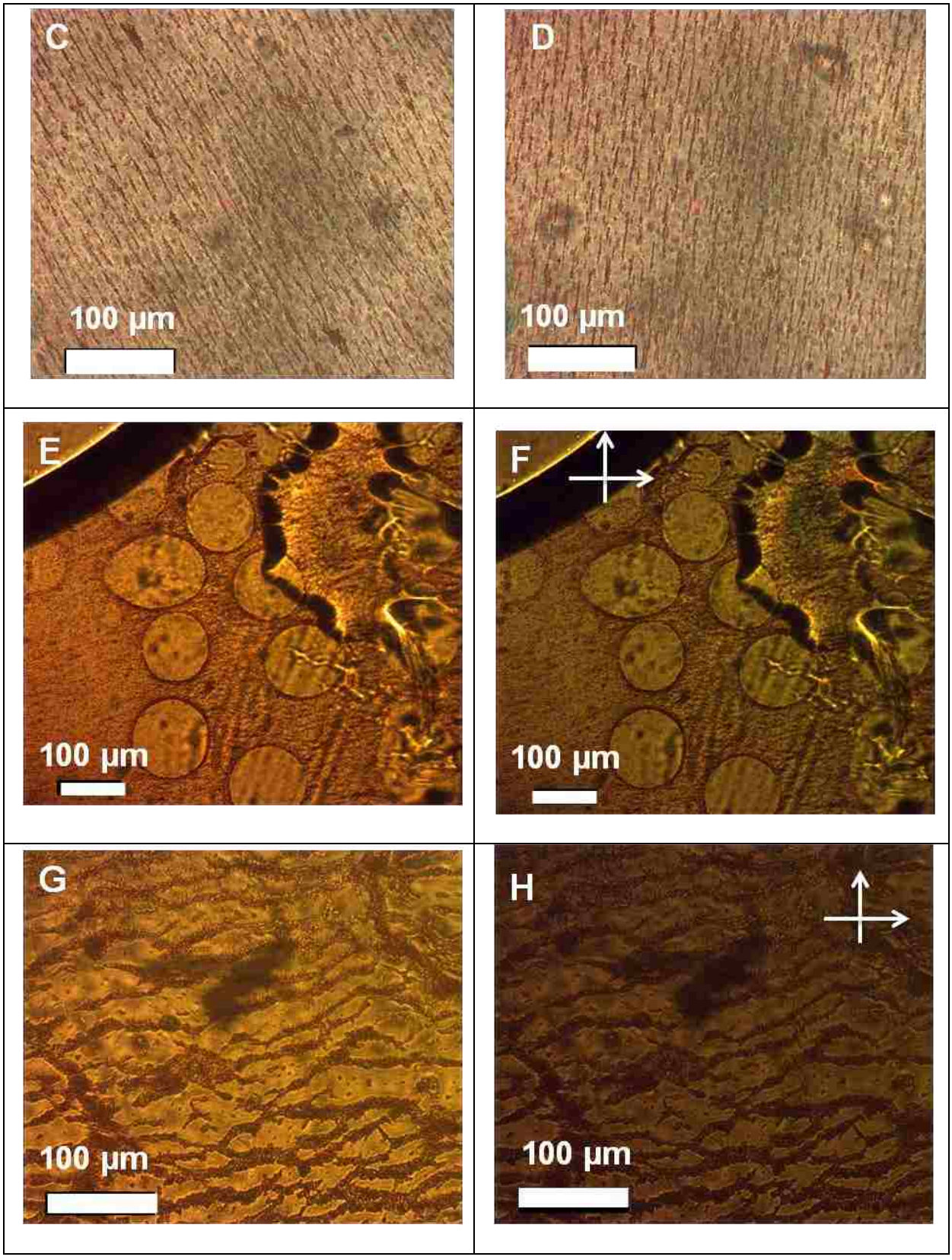

Furthermore the orientation of the magnetic field was changed to test if the particles were "locked" in the chain-like texture. Figure 3.14D clearly reflects the ability of the particles to reorient accordingly with the different direction of the applied magnetic field.[90] Interesting patterns resembling rings were observed nucleating as shown in Figure 3.14B. After more days these rings were well-defined and pretty uniform in size. In Figure 3.14E and F the coexistence of isotropic droplets and an anisotropic region can be seen.[91] These droplets were essentially free of particles. This might suggest that the particles had a higher affinity for the isotropic phase than the anisotropic area. Most likely, the particles were depleted from the droplet interface and were more compacted in the isotropic phase. In the absence of an applied magnetic field, the network observed initially (Figure 3.14A) changed the morphology. Particles were compacted in more thickly isotropic columns. They seemed to be expelled by the liquid regions which also appeared isotropic. Along with these patterns, spot-like textures, isotropic in nature were also visible (Figure 3.15). After 8 days the particles seemed to be depleted from the isotropic liquid phase. Thick random bands can be seen in Figure 3.15C and D right underneath the glass wall, "floating" above the LC phase. The formation of these morphologies in the mixture of particles coated with a shell similar to the suspension matrix can be explained by the interaction of the particles and the matrix molecules. PSLG in toluene assumes a rod-like conformation and at high concentrations can form cholesteric liquid crystals, LC. Large particles or clusters can induce topological defects in the LC orientation.[92,93] The sparse presence of the fingerprint morphology of the cholesteric PSLG supports the fact that particles deformed the nascent LC. The cholesteric domains, once formed, seemed not to be impacted by the particle presence. The magnetic clusters were probably bigger than the distance between the cholesteric bands.[94]

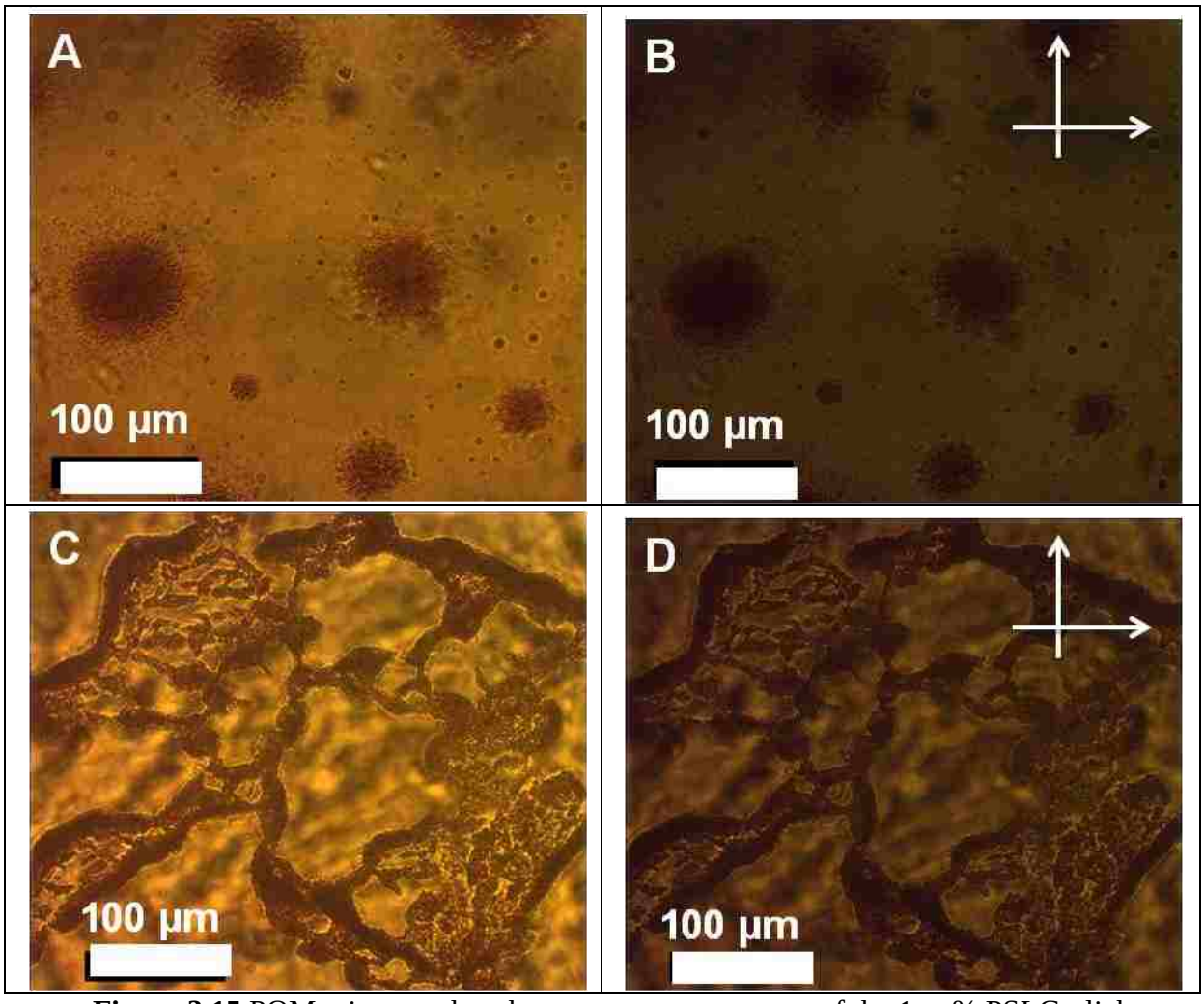

Figure 3.15 POM micrographs taken at room temperature of the 1 wt% PSLG-click hybrid particles (CR715) in 40 wt% PSLG/toluene: (A, B) cluster texture and (C, D) random stripe texture formed after 8 days.

Hence these clusters couldn't interpenetrate into these bands, rather the particles were expelled (Figure 3.16). The combination of polypeptide magnetic particles with liquid crystals made of rodlike polypeptides can be useful platforms to study the new and improved LC mixtures with tunable properties.

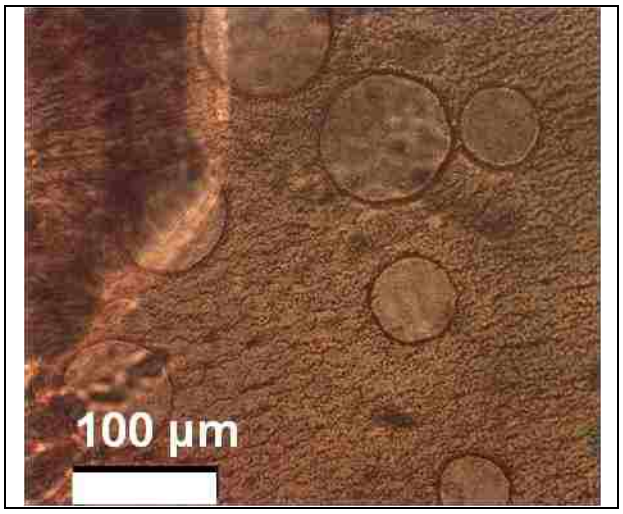

Figure 3.16 POM micrograph showing cholesteric patterns along with ring-like texture for 1 wt% PSLG-click hybrid particles (CR715) in 40 wt% PSLG/toluene.

The highly dispersed state of the particles in the polymer matrix attained by these preliminary experiments, can prove useful for the discovery of new morphologies and the development of new composite liquid crystal-colloid mixtures.

3.4.3 Soap-like Aqueous Suspensions of PSLG -click Particles in Surfactant Driven Media.

Magnetic particles carrying a hydrophobic shell consisting of poly(γ-stearyl-L-glutamate), PSLG, were found to disperse in aqueous surfactant solutions. Four surfactants were chosen: sodium dodecyl sulfate, SDS, cetyl trimethylammonium bromide, CTAB, Pluronic, and Genapol. The stearyl chains are very similar to the hydrophobic part of the surfactant. As shown in Figure 3.17 the click magnetic particles formed stable suspensions in SDS, CTAB, Genapol and partial in Pluronic. The suspended particles kept their magnetic properties. The mechanism of dissolution can be explained on the basis of hydrophobic-hydrophobic interactions. These interactions can cause the formation of localized micelles between the arms of the polypeptide helices anchored on the particle surface and the hydrophobic tail of the surfactant, with the surfactant's hydrophilic head pointing to the aqueous phase.

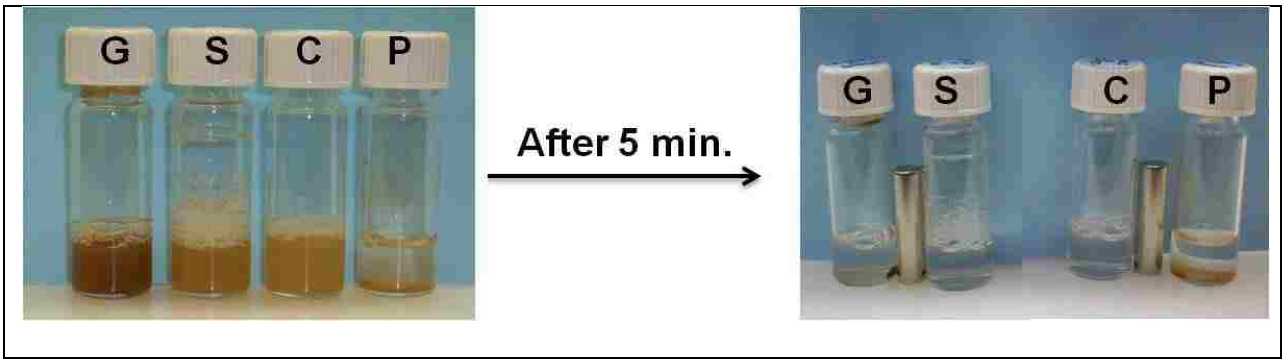

Figure 3.17 PSLG click hybrid particles suspended in Genapol (G), SDS (S), CTAB (C) and Pluronic (P).

The easy access of the surfactant molecules to the polypeptide side chains is also favored by the sparse populated particle surface.

3.4.4 Rheological Behavior of PCBL-click Particles

Magnetic particles were subjected to shear stress to measure their viscoelastic behavior. Figure 3.18A reflects the shear thinning behavior of the polypeptide-coated magnetic particles suspended in DMF (c = 1.5 wt%) in the absence of an applied magnetic field. This behavior was compared with standard magnetic latex suspended in water which showed thinning under stress, Figure 3.18B. The elastic modulus, G', was higher than viscous modulus, G'', suggesting that the material behaved like a viscoelastic solid. The agglomerated structures present in the magnetic suspension began to break with applied force but, at the same time, they probably recombined reversibly in other smaller aggregate morphologies. This is suggested by the profile of the storage and loss modulus, G′ and G″ respectively. They seemed to be frequency independent.[95] In the absence of magnetic field, a magnetorheological fluid was expected to behave similarly to a Newtonian fluid,[96] but Figure 3.18A shows that the PCBL click particles had a non-Newtonian flow behavior, a characteristic of stiff materials.

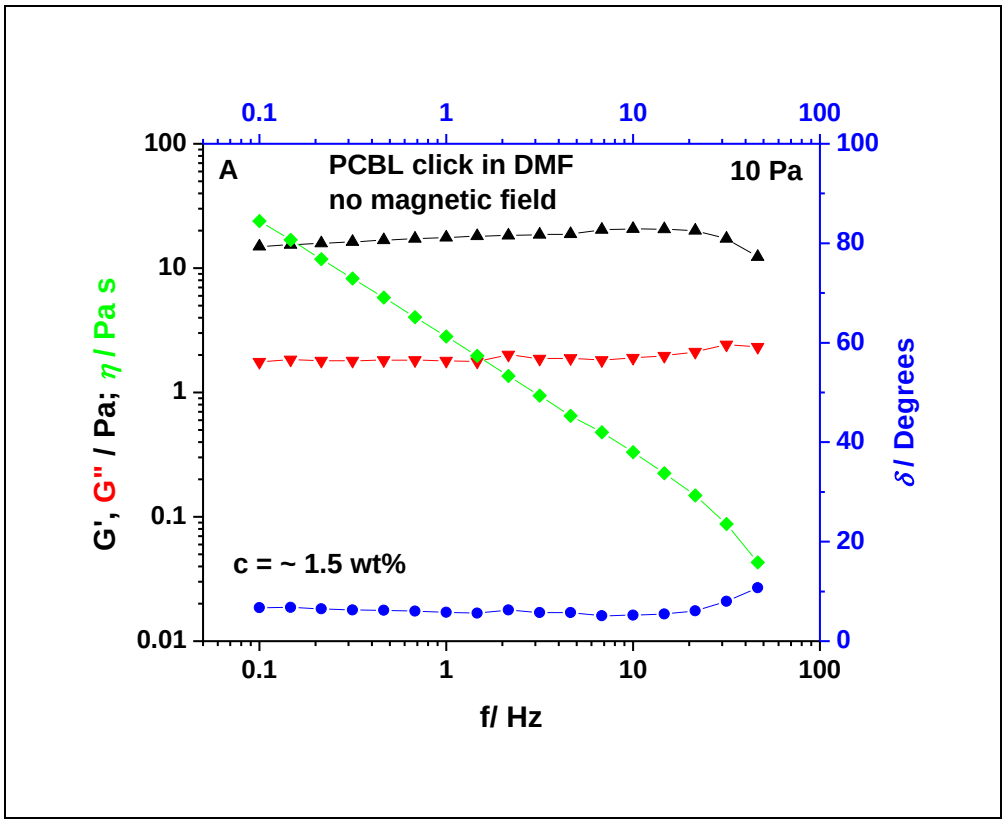

Figure 3.18 Illustration of the rheological behavior: (A) storage (G′) modulus, loss (G″) modulus, viscosity, η and phase angle, δ, as functions of frequency sweeps for PCBL click hybrid in DMF (no magnetic field applied), shear rate kept at 10Pa, (B) storage (G′) modulus, lost (G″) modulus, viscosity, η and phase angle, δ, as functions of shear stress for standard magnetic latex 0.5 μm in water (no magnetic field), frequency kept at 1 Hz, (C) storage (G′) modulus, loss (G″) modulus, viscosity, η and phase angle, δ, as functions of shear stress for PCBL-click hybrid in DMF (under applied magnetic field applied parallel to the rheometer plates), frequency kept at 1 Hz, (D) storage (G′) modulus, lost (G″) modulus as functions of shear stress for PCBL-click hybrid particle under and no applied magnetic field, frequency kept at 1 Hz and (E) storage (G′) modulus, lost (G″) modulus, viscosity, η and phase angle, δ, as functions of frequency sweeps for PCBL click hybrid in m-cresol (no magnetic field applied), shear rate kept at 100 Pa.

Figure 3.18 continued

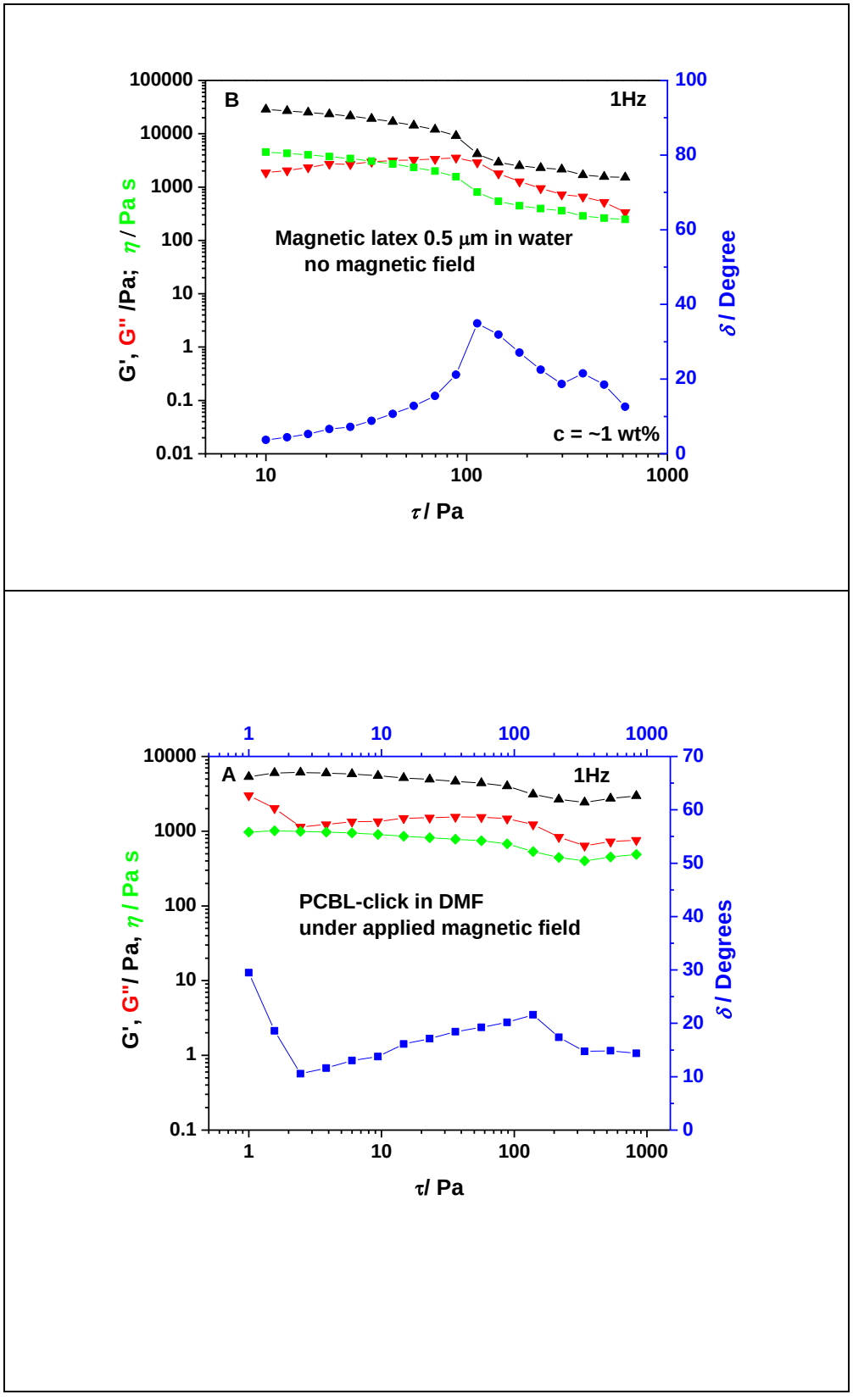

Figure 3.18 continued

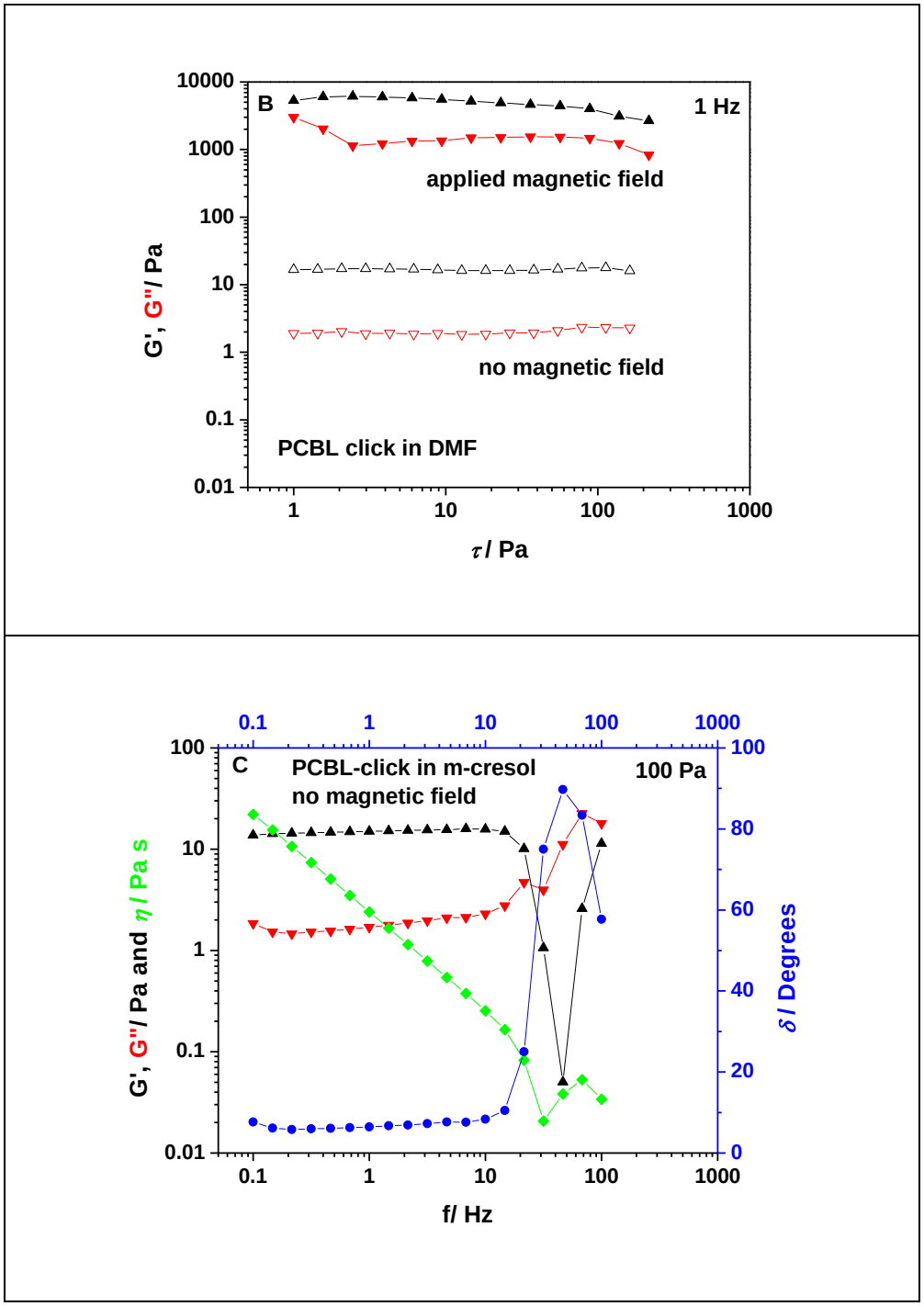

Under an applied magnetic field, Figure 3.18C, the rheological properties of the suspension changed dramatically. The G' and G'' moduli increased with at least two orders of magnitude, Figure 3.18D.[95,97] Under the magnetic field, the clustery suspension arranged in column-like microstructures due to the induced magnetic polarization and the resulting dipole-dipole interactions between the particles. At low frequencies the structure of the cluster remains fairly constant. Once the shear rate increases, the elastic modulus, G', decreases and the loss modulus, G'', increases. The fluid tended to approach the Newtonian behavior. Also the close proximity of up to an almost crossover point between G' and G'' attained at higher frequencies suggested that polypeptide coated particles might gel. Under an applied magnetic field, the viscosity decreased to a critical value and then suddenly increased, pointing to the magnetorheological effect. This effect is due to the flow hindrance by the aggregate and columns formed within the sheared suspension. It can also be speculated that the polypeptide can have an important role in such behavior. The polypeptide grafted onto the surface was very short and had the ability to pack into very rigid helices of 6 turns each. Once a shearing force is applied the particles are more or less reversibly jammed. Jammed together, the chains might interpenetrate. As a result, a local compacted structure can form, close in appearance with a liquid crystalline phase. The carrier (solvent) viscosity didn't seem to impact the magnitude of the G' and G'' as shown in Figure 3.18E. These preliminary results demonstrate that polypeptide composite particles can be used to study jamming effects under stress. Applied magnetic fields can be used to tune the rheological properties of the colloidal system.

3.5 Conclusion

Hybrid composite particles featuring a homopolypeptide shell were prepared by click chemistry. To increase the range of responsiveness, these FITC covalently labeled particles were furnished

with a magnetic core consisting of magnetite. The characterization of the products obtained at each step was performed with different range techniques. XRD confirmed the spinel structure of the magnetite and gave an average crystallite size of about 11 nm, in good agreement with the HRTEM analysis. Silica protection of the naked magnetite core was monitored by FTIR, HRTEM and XRD. The first protective layer of SiO_2 was 4 nm thick as determined by both HRTEM and XRD. After functionalization with azide groups, the well-characterized polypeptides, PSLG and PCBL respectively, were easy attached using the versatile Huisgen's 1,3 cycloadition yielding stable dispersions in THF and DMF. After grafting to the spherical surface, the two polypeptides retained their α-helical structure as proven by FTIR. The surface of the composite particle had a low population of polypeptide chains, 125 for PSLG and about 800 for PCBL-click particles. The composition of the surface was evaluated by XPS. The sparse coverage with polymer chains was also evidenced by the presence of the at N1s peak specific to azide moiety at very low intensity along with FTIR spectra showing the signal of azide functional group centered at 2100 cm^{-1}. SQUID investigation showed the superparamagnetic behavior of the colloid particle. The low grafting density enabled a good efficiency of enzyme immobilization. Lipase from *Candida rugosa* was incorporated by adsorption onto the PSLG-click particles yielding a product which can be further used as a versatile candidate to mimic the enzyme tethering to natural molecules. Upon suspension in the surfactant aqueous solutions, the PSLG-click particles formed stable dispersions. The surfactant molecules seemed to intermediate the dispersion of the PSLG into the hydrophilic media. Subjected to stress, the PCBL-click particles behaved as a stiff material showing shear thinning behavior.

3.6 References and Notes

(1) Gangopadhyay, R.; De, A. Conducting polymer nanocomposites: A brief overview. *Chem. Mat.* **2000**, *12*, 608-622.

(2) Janczak, C. M.; Aspinwall, C. A. Composite nanoparticles: the best of two worlds. *Analytical and Bioanalytical Chemistry* **2012**, *402*, 83-89.

(3) Kalele, S.; Gosavi, S. W.; Urban, J.; Kulkarni, S. K. Nanoshell particles: synthesis, properties and applications. *Current Science* **2006**, *91*, 1038-1052.

(4) Li, H. F.; Zhang, H. M.; Guo, X. L. Preparation of Micro-/Nano- Nonspherical Polymer Particles. *Progress in Chemistry* **2011**, *23*, 1196-1210.

(5) Maity, A.; Biswas, M. Recent progress in conducting polymer, mixed polymer-inorganic hybrid nanocomposites. *Journal of Industrial and Engineering Chemistry* **2006**, *12*, 311-351.

(6) Milonjic, S. K. In *Advanced Materials for High Technology Applications*; Uskokovic, D. P., Ed. 1996; Vol. 214, 197-204.

(7) Parveen, S.; Misra, R.; Sahoo, S. K. Nanoparticles: a boon to drug delivery, therapeutics, diagnostics and imaging. *Nanomedicine-Nanotechnology Biology and Medicine* **2012**, *8*, 147-166.

(8) Saunders, B. R. Hybrid polymer/nanoparticle solar cells: Preparation, principles and challenges. *Journal of Colloid and Interface Science* **2012**, *369*, 1-15.

(9) Zou, H.; Wu, S. S.; Shen, J. Polymer/silica nanocomposites: Preparation, characterization, properties, and applications. *Chemical Reviews* **2008**, *108*, 3893-3957.

(10) Chaudhuri, R. G.; Paria, S. Core/Shell Nanoparticles: Classes, Properties, Synthesis Mechanisms, Characterization, and Applications. *Chemical Reviews* **2012**, *112*, 2373-2433.

(11) Colombo, M.; Carregal-Romero, S.; Casula, M. F.; Gutierrez, L.; Morales, M. P.; Bohm, I. B.; Heverhagen, J. T.; Prosperi, D.; Parak, W. J. Biological applications of magnetic nanoparticles. *Chemical Society Reviews* **2012**, *41*, 4306-4334.

(12) Rumenapp, C.; Gleich, B.; Haase, A. Magnetic Nanoparticles in Magnetic Resonance Imaging and Diagnostics. *Pharmaceutical Research* **2012**, *29*, 1165-1179.

(13) Balazs, A. C.; Emrick, T.; Russell, T. P. Nanoparticle polymer composites: Where two small worlds meet. *Science* **2006**, *314*, 1107-1110.

(14) Lee, J. E.; Lee, N.; Kim, T.; Kim, J.; Hyeon, T. Multifunctional Mesoporous Silica Nanocomposite Nanoparticles for Theranostic Applications. *Accounts Chem. Res.* **2011**, *44*, 893-902.

(15) Piao, Y.; Burns, A.; Kim, J.; Wiesner, U.; Hyeon, T. Designed Fabrication of Silica-Based Nanostructured Particle Systems for Nanomedicine Applications. *Advanced Functional Materials* **2008**, *18*, 3745-3758.

(16) Block, H. *Poly(γ-benzyl-L-glutamate) and other Glutamic Acid Containing Polymers*; Gordon and Breach: New York, 1983.

(17) Kricheldorf, H. R. Polypeptides and 100 years of chemistry of alpha-amino acid N-carboxyanhydrides. *Angew. Chem.-Int. Edit.* **2006**, *45*, 5752-5784.

(18) Deming, T. J. In *Peptide Hybrid Polymers*; Klok, H. A., Schlaad, H., Eds. 2006; Vol. 202, p 1-18.

(19) Brinkhuis, R. P.; Rutjes, F.; van Hest, J. C. M. Polymeric vesicles in biomedical applications. *Polymer Chemistry* **2010**, *2*, 1449-1462.

(20) Guo, Y.; Xia, F.; Xu, L.; Li, J.; Yang, W. S.; Jiang, L. Switchable Wettability on Cooperative Dual-Responsive Poly-L-lysine Surface. *Langmuir* **2010**, *26*, 1024-1028.

(21) Huang, Y. C.; Arham, M.; Jan, J. S. Alkyl chain grafted poly(L-lysine): self-assembly and biomedical application as carriers. *Soft Matter* **2010**, *7*, 3975-3983.

(22) Huang, Y. C.; Yang, Y. S.; Lai, T. Y.; Jan, J. S. Lysine-block-tyrosine block copolypeptides: Self-assembly, cross-linking, and conjugation of targeted ligand for drug encapsulation. *Polymer* **2011**, *53*, 913-922.

(23) Knoop, R. J. I.; de Geus, M.; Habraken, G. J. M.; Koning, C. E.; Menzel, H.; Heise, A. Stimuli Responsive Peptide Conjugated Polymer Nanoparticles. *Macromolecules* **2010**, *43*, 4126-4132.

(24) Lowik, D.; Leunissen, E. H. P.; van den Heuvel, M.; Hansen, M. B.; van Hest, J. C. M. Stimulus responsive peptide based materials. *Chemical Society Reviews* **2010**, *39*, 3394-3412.

(25) Nakayama, M.; Okano, T. Multi-targeting cancer chemotherapy using temperature-responsive drug carrier systems. *Reactive & Functional Polymers* **2011**, *71*, 235-244.

(26) Fasman, G. D.; Idelson, M.; Blout, E. R. Synthesis and conformation of high molecular weight poly-ε-carbobenzyloxy-L-lysine and poly-L-lysine.HCl. *J. Am. Chem. Soc.* **1961**, *83*, 709-&.

(27) Hayashi, T.; Emi, S.; Nakajima, A. Helix-coil transition of poly(ε-carbobenzyloxy-L-lysine) in m-cresol. *Polymer* **1975**, *16*, 396-400.

(28) Matsuoka, M.; Norisuye, T.; Teramoto, A.; Fujita, H. Solution properties of synthetic polypeptides .15. Helix-coil transition in poly(ε-carbobenzyloxy L-lysine). *Biopolymers* **1973**, *12*, 1515-1532.

(29) Omura, I.; Teramoto, A.; Fujita, H. Dielectric-dispersion of polypeptide solutions .2. Helix-coil transition of "poly(ε-carbobenzoxy-L-lysine) in m-cresol. *Macromolecules* **1975**, *8*, 284-290.

(30) Daly, W. H.; Poché, D.; Negulescu, I. I. Poly (γ-Alkyl-α, L-glutamate)s, derived from long chain paraffinic alcohols. *Progress in Polymer Science* **1994**, *19*, 79-135.

(31) Jamil, T.; Russo, P. S.; Daly, W. H.; Negulescu, I. Static and dynamic light-scattering of a random coil polymer in rodlike polymer-solution. *Macromolecular Symposia* **1994**, *79*, 81-85.

(32) Poche, D. S.; Daly, W. H.; Russo, P. S. Synthesis and some solution properties of poly(γ-stearyl α, L-glutamate). *Macromolecules* **1995**, *28*, 6745-6753.

(33) Jamil, T.; Russo, P. S.; Negulescu, I.; Daly, W. H.; Schaefer, D. W.; Beaucage, G. Light-scattering from random coils dispersed in solutions of rodlike polymers. *Macromolecules* **1994**, *27*, 171-178.

(34) Schmidtke, S.; Russo, P.; Nakamatsu, J.; Buyuktanir, E.; Turfan, B.; Temyanko, E.; Negulescu, I. I. Thermoreversible gelation of isotropic and liquid crystalline solutions of a "sticky" rodlike polymer. *Macromolecules* **2000**, *33*, 4427-4432.

(35) Watanabe, J.; Sakajiri, K.; Okoshi, K.; Kawauchi, S.; Magoshi, J. Columnar liquid crystals in polypeptides, 1 Columnar hexagonal phase observed in lyotropic solutions of poly(γ-octadecyl-L-glutamate) dissolved in amphiphilic solvents, such as octadecylamine, octadecyl alcohol, and octadecanoic acid. *Macromol. Chem. Phys.* **2001**, *202*, 1004-1009.

(36) Watanabe, J.; Takashina, Y. Columnar liquid-crystals in polypeptides. 1. A columnar hexagonal liquid-crystal observed in poly(γ-octadecyl L-glutamate). *Macromolecules* **1991**, *24*, 3423-3426.

(37) Fong, B.; Russo, P. S. Organophilic colloidal particles with a synthetic polypeptide coating. *Langmuir* **1999**, *15*, 4421-4426.

(38) Fong, B.; Turksen, S.; Russo, P. S.; Stryjewski, W. Colloidal crystals of silica-homopolypeptide composite particles. *Langmuir* **2004**, *20*, 266-269.

(39) Soto-Cantu, E.; Turksen-Selcuk, S.; Qiu, J. H.; Zhou, Z.; Russo, P. S.; Henk, M. C. Silica-Polypeptide Composite Particles: Controlling Shell Growth. *Langmuir* **2011**, *26*, 15604-15613.

(40) Soto-Cantu, E.; Cueto, R.; Koch, J.; Russo, P. S. Synthesis and Rapid Characterization of Amine-Functionalized Silica. *Langmuir* **2012**, *28*, 5562-5569.

(41) Borase, T.; Iacono, M.; Ali, S. I.; Thornton, P. D.; Heise, A. Polypeptide core-shell silica nanoparticles with high grafting density by N-carboxyanhydride (NCA) ring opening polymerization as responsive materials and for bioconjugation. *Polymer Chemistry* **2012**, *3*, 1267-1275.

(42) Liu, D.; Li, Y.; Deng, J.; Yang, W. Synthesis and characterization of magnetic Fe_3O_4-silica-poly(Î³-benzyl-l-glutamate) composite microspheres. *Reactive and Functional Polymers* **2011**, *71*, 1040-1044.

(43) Kolb, H. C.; Finn, M. G.; Sharpless, K. B. Click chemistry: Diverse chemical function from a few good reactions. *Angew. Chem.-Int. Edit.* **2001**, *40*, 2004.

(44) Rostovtsev, V. V.; Green, L. G.; Fokin, V. V.; Sharpless, K. B. A stepwise Huisgen cycloaddition process: Copper(I)-catalyzed regioselective "ligation" of azides and terminal alkynes. *Angew. Chem.-Int. Edit.* **2002**, *41*, 2596.

(45) Ranjan, R.; Brittain, W. J. Tandem RAFT polymerization and click chemistry: An efficient approach to surface modification. *Macromol. Rapid Commun.* **2007**, *28*, 2084-2089.

(46) Ranjan, R.; Brittain, W. J. Combination of living radical polymerization and click chemistry for surface modification. *Macromolecules* **2007**, *40*, 6217-6223.

(47) Ranjan, R.; Brittain, W. J. Synthesis of high density polymer brushes on nanoparticles by combined RAFT polymerization and click chemistry. *Macromol. Rapid Commun.* **2008**, *29*, 1104-1110.

(48) Chen, J. C.; Xiang, J. M.; Cai, Z. W.; Yong, H.; Wang, H. D.; Zhang, L. H.; Luo, W. Q.; Min, H. Synthesis of Hydrophobic Polymer Brushes on Silica Nanoparticles Via the Combination of Surface-Initiated ATRP, ROP and Click Chemistry. *J. Macromol. Sci., Pure Appl. Chem.* **2010**, *47*, 655-662.

(49) Sun, D. X.; Miao, X.; Zhang, K. J.; Kim, H.; Yuan, Y. G. Triazole-forming waterborne polyurethane composites fabricated with silane coupling agent functionalized nano-silica. *Journal of Colloid and Interface Science* **2011**, *361*, 483-490.

(50) Yilmaz, G.; Kumbaraci, V.; Talinli, N.; Tatar, P.; Demirel, A. L.; Yagci, Y. Photoinduced Grafting of Polystyrene onto Silica Particles by Ketene Chemistry. *Journal of Polymer Science Part a-Polymer Chemistry* **2012**, *50*, 2517-2520.

(51) Li, Y.; Benicewicz, B. C. Functionalization of Silica Nanoparticles via the Combination of Surface-Initiated RAFT Polymerization and Click Reactions. *Macromolecules* **2008**, *41*, 7986-7992.

(52) Balamurugan, S. S.; Soto-Cantu, E.; Cueto, R.; Russo, P. S. Preparation of Organosoluble Silica-Polypeptide Particles by "Click" Chemistry. *Macromolecules* **2010**, *43*, 62-70.

(53) Kar, M.; Pauline, M.; Sharma, K.; Kumaraswamy, G.; Sen Gupta, S. Synthesis of Poly-L-glutamic Acid Grafted Silica Nanoparticles and Their Assembly into Macroporous Structures. *Langmuir* **2011**, *27*, 12124-12133.

(54) Kar, M.; Vijayakumar, P. S.; Prasad, B. L. V.; Sen Gupta, S. Synthesis and Characterization of Poly-L-lysine-Grafted Silica Nanoparticles Synthesized via NCA Polymerization and Click Chemistry. *Langmuir* **2010**, *26*, 5772-5781.

(55) Agut, W.; Agnaou, R.; Lecommandoux, S.; Taton, D. Synthesis of block copolypeptides by click chemistry. *Macromol. Rapid Commun.* **2008**, *29*, 1147-1155.

(56) Sanda, F.; Gao, G. Z.; Masuda, T. Helical polymer carrying helical grafts from peptide-based acetylene macromonomers: Synthesis. *Macromolecular Bioscience* **2004**, *4*, 570-574.

(57) Agut, W.; Brulet, A.; Taton, D.; Lecommandoux, S. Thermoresponsive micelles from jeffamine-b-poly(L-glutamic acid) double hydrophilic block copolymers. *Langmuir* **2007**, *23*, 11526-11533.

(58) Deng, L.; Shi, K.; Zhang, Y. Y.; Wang, H. M.; Zeng, J. G.; Guo, X. Z.; Du, Z. J.; Zhang, B. L. Synthesis of well-defined poly(N-isopropylacrylamide)-b-poly(L-glutamic acid) by a versatile approach and micellization. *Journal of Colloid and Interface Science* **2008**, *323*, 169-175.

(59) Schatz, C.; Louguet, S.; Le Meins, J. F.; Lecommandoux, S. Polysaccharide-block-polypeptide Copolymer Vesicles: Towards Synthetic Viral Capsids. *Angew. Chem.-Int. Edit.* **2009**, *48*, 2572-2575.

(60) Liu, G.; Dong, C. M. Photoresponsive Poly(S-(o-nitrobenzyl)-L-cysteine)-b-PEO from a L-Cysteine N-Carboxyanhydride Monomer: Synthesis, Self-Assembly, and Phototriggered Drug Release. *Biomacromolecules* **2012**, *13*, 1573-1583.

(61) Parrish, B.; Breitenkamp, R. B.; Emrick, T. PEG- and peptide-grafted aliphatic polyesters by click chemistry. *J. Am. Chem. Soc.* **2005**, *127*, 7404-7410.

(62) Tang, H. Y.; Zhang, D. H. Multi-functionalization of helical block copoly(α-peptide)s by orthogonal chemistry. *Polymer Chemistry* **2011**, *2*, 1542-1551.

(63) Upadhyay, K. K.; Le Meins, J. F.; Misra, A.; Voisin, P.; Bouchaud, V.; Ibarboure, E.; Schatz, C.; Lecommandoux, S. Biomimetic Doxorubicin Loaded Polymersomes from Hyaluronan-block-Poly(γ-benzyl glutamate) Copolymers. *Biomacromolecules* **2009**, *10*, 2802-2808.

(64) Wang, R.; Chen, G. T.; Du, F. S.; Li, Z. C. Preparation and aggregation behavior of mannose-terminated poly(ethylene glycol)-b-poly(L-leucine) in water. *Colloids and Surfaces B-Biointerfaces* **2011**, *85*, 56-62.

(65) Arosio, D.; Bertoli, M.; Manzoni, L.; Scolastico, C. Click chemistry to functionalise peptidomimetics. *Tetrahedron Letters* **2006**, *47*, 3697-3700.

(66) Binder, W. H.; Sachsenhofer, R. 'Click' chemistry in polymer and material science: An update. *Macromol. Rapid Commun.* **2008**, *29*, 952-981.

(67) Golas, P. L.; Matyjaszewski, K. Marrying click chemistry with polymerization: expanding the scope of polymeric materials. *Chemical Society Reviews* **2010**, *39*, 1338-1354.

(68) Gragert, M.; Schunack, M.; Binder, W. H. Azide/Alkyne-"Click"-Reactions of Encapsulated Reagents: Toward Self-Healing Materials. *Macromol. Rapid Commun.* **2010**, *32*, 419-425.

(69) Kolb, H. C.; Sharpless, K. B. The growing impact of click chemistry on drug discovery. *Drug Discovery Today* **2003**, *8*, 1128-1137.

(70) Le Droumaguet, B.; Velonia, K. Click chemistry: A powerful tool to create polymer-based macromolecular chimeras. *Macromol. Rapid Commun.* **2008**, *29*, 1073-1089.

(71) Li, N. W.; Binder, W. H. Click-chemistry for nanoparticle-modification. *J. Mater. Chem.* **2010**, *21*, 16717-16734.

(72) Deng, H. T.; Xu, Z. K.; Liu, Z. M.; Wu, J.; Ye, P. Adsorption immobilization of Candida rugosa lipases on polypropylene hollow fiber microfiltration membranes modified by hydrophobic polypeptides. *Enzyme and Microbial Technology* **2004**, *35*, 437-443.

(73) Deng, H. T.; Xu, Z. K.; Wu, J.; Ye, P.; Liu, Z. M.; Seta, P. A comparative study on lipase immobilized polypropylene microfiltration membranes modified by sugar-containing polymer and polypeptide. *Journal of Molecular Catalysis B-Enzymatic* **2004**, *28*, 95-100.

(74) Sohn, D.; Kitaev, V.; Kumacheva, E. Self-assembly of substituted polyglutamates on solid substrates: The side-chain effect. *Langmuir* **1999**, *15*, 1698-1702.

(75) Sackmann, E. Supported membranes: Scientific and practical applications. *Science* **1996**, *271*, 43-48.

(76) Jean, M.; Nachbaur, V.; Le Breton, J. M. Synthesis and characterization of magnetite powders obtained by the solvothermal method: Influence of the Fe3+ concentration. *Journal of Alloys and Compounds* **2012**, *513*, 425-429.

(77) Schrupp, D.; Sing, M.; Tsunekawa, M.; Fujiwara, H.; Kasai, S.; Sekiyama, A.; Suga, S.; Muro, T.; Brabers, V. A. M.; Claessen, R. Surface electronic structure and Verwey-transition of magnetite studied by photoemission spectroscopy. *Annalen Der Physik* **2004**, *13*, 78-80.

(78) Zhang, L.; He, R.; Gu, H. C. Oleic acid coating on the monodisperse magnetite nanoparticles. *Applied Surface Science* **2006**, *253*, 2611-2617.

(79) Morel, A. L.; Nikitenko, S. I.; Gionnet, K.; Wattiaux, A.; Lai-Kee-Him, J.; Labrugere, C.; Chevalier, B.; Deleris, G.; Petibois, C.; Brisson, A.; Simonoff, M. Sonochemical approach to the synthesis of Fe_3O_4@SiO_2 core-shell nanoparticles with tunable properties. *ACS Nano* **2008**, *2*, 847-856.

(80) Collman, J. P.; Devaraj, N. K.; Eberspacher, T. P. A.; Chidsey, C. E. D. Mixed azide-terminated monolayers: A platform for modifying electrode surfaces. *Langmuir* **2006**, *22*, 2457-2464.

(81) Wollman, E. W.; Kang, D.; Frisbie, C. D.; Lorkovic, I. M.; Wrighton, M. S. Photosensitive self-assembled monolayers on gold - photochemistry of surface-confined aryl azide and cyclopentadienylmanganese tricarbonyl. *J. Am. Chem. Soc.* **1994**, *116*, 4395-4404.

(82) Matsumot.T; Nishioka, N.; Teramoto, A.; Fujita, H. Dielectric-dispersion of polypeptide solutions .1. Once-broken rod polypeptide based on γ-benzyl L-glutamate. *Macromolecules* **1974**, *7*, 824-831.

(83) Marchegiani, G.; Imperatori, P.; Mari, A.; Pilloni, L.; Chiolerio, A.; Allia, P.; Tiberto, P.; Suber, L. Sonochemical synthesis of versatile hydrophilic magnetite nanoparticles. *Ultrasonics Sonochemistry* **2012**, *19*, 877-882.

(84) Sarda, L.; Desnuelle, P. Action de la lipase pancreatique sur les esters en emulsion. *Biochimica Et Biophysica Acta* **1958**, *30*, 513-521.

(85) Kulik, E. A.; Kato, K.; Ivanchenko, M. I.; Ikada, Y. Trypsin immobilization on to polymer surface through grafted layer and its reaction with inhibitors. *Biomaterials* **1993**, *14*, 763-769.

(86) Ozyilmaz, G. The effect of spacer arm on hydrolytic and synthetic activity of Candida rugosa lipase immobilized on silica gel. *Journal of Molecular Catalysis B-Enzymatic* **2009**, *56*, 231-236.

(87) Deng, H. T.; Lin, Y.; Wang, J. J.; Liu, Z. Y.; Ma, M.; Zheng, F. Comparative study on the immobilization of lipase on chitosan gels modified by different hydrophobic groups. *Surface Review and Letters* **2009**, *16*, 323-327.

(88) Deng, H. T.; Wang, J. J.; Ma, M.; Liu, Z. Y.; Zheng, F. Hydrophobic surface modification of chitosan gels by stearyl for improving the activity of immobilized lipase. *Chinese Chemical Letters* **2009**, *20*, 995-999.

(89) Ye, P.; Jiang, J.; Xu, Z. K. Adsorption and activity of lipase from Candida rugosa on the chitosan-modified poly(acrylonitrile-co-maleic acid) membrane surface. *Colloids and Surfaces B-Biointerfaces* **2007**, *60*, 62-67.

(90) Diestra-Cruz, H.; Rinaldi, C.; Acevedo, A. Rheological, optical, and thermal characterization of temperature-induced transitions in liquid crystal ferrosuspensions. *Journal of Applied Physics* **2012**, *111*.

(91) Vollmer, D.; Hinze, G.; Ullrich, B.; Poon, W. C. K.; Cates, M. E.; Schofield, A. B. Formation of self-supporting reversible cellular networks in suspensions of colloids and liquid crystals. *Langmuir* **2005**, *21*, 4921-4930.

(92) Stark, H. Director field configurations around a spherical particle in a nematic liquid crystal. *European Physical Journal B* **1999**, *10*, 311-321.

(93) Stark, H.; Stelzer, J.; Bernhard, R. Water droplets in a spherically confined nematic solvent: A numerical investigation. *European Physical Journal B* **1999**, *10*, 515-523.

(94) Qi, H.; Hegmann, T. Formation of periodic stripe patterns in nematic liquid crystals doped with functionalized gold nanoparticles. *J. Mater. Chem.* **2006**, *16*, 4197-4205.

(95) Claracq, J.; Sarrazin, J.; Montfort, J. P. Viscoelastic properties of magnetorheological fluids. *Rheologica Acta* **2004**, *43*, 38-49.

(96) Ginder, J. M. Behavior of magnetorheological fluids. *Mrs Bulletin* **1998**, *23*, 26-29.

(97) Hu, B.; Fuchs, A.; Huseyin, S.; Gordaninejad, F.; Evrensel, C. Supramolecular magnetorheological polymer gels. *Journal of Applied Polymer Science* **2006**, *100*, 2464-2479.

CHAPTER 4
POLYPEPTIDE-BASED SILICA HYBRID PARTICLES: A NOVEL APPROACH TO ENGINEER MESOPOROUS CORES AND MEASURE THE HAIRY SHELLS

4.1 Introduction

Silica colloids have been heavily researched for several decades, due to the range of applications they can display. Their unique properties such as low cytotoxicity, facile preparation, easy control over interparticle interaction, stability at the physiological pH range (6-7) and, most of all, the easy modification of their surfaces with functional groups, qualify silica particles as excellent candidates for biomedical applications such as drug delivery, cell separation and photonics.[1,2] Several review articles have appeared on these subjects.[3-6] Silica colloids are prepared usually from alkylorthosilanes in the sol-gel process pioneered by Stöber et al. in 1968, and, since then, they have been known by the colloid community as Stöber silica.[7] Many other reports were recorded over the years on modifying the Stöber procedure to improving the particle uniformity.[8,9] The emulsion method gives more monodisperse colloids but the shortcoming is the low yield.[10,11] Particles with a narrow size distribution typically have uniform physical properties desired in the application process.

The rapid development of biotechnology and biomedicine asks for advanced silica colloids. Physically or covalently loaded with dyes, fluorescent particles are used as probes and also for *in vivo* imaging purposes. They can encapsulate a magnetic nugget making them responsive to external stimuli such as electric and magnetic fields, but this aspect will not be developed in this chapter. From the multitude of the fluorescent agents, fluorescein isothiocyanate, FITC proves to be a good choice due to its high quantum efficiency when compared with self-quenching. Viger et al. studied the reduction of self-quenching in fluorescent silica coated silver particles.[12] Fluorescent particles were obtained using a silane coupling agent,

3-aminopropyltriethoxy silane, APS, in two steps. First the dye was chemically bound to the APS and then silver silica particles were prepared in a reverse micelle. These particles provided higher detection ability and lower self-quenching when compared with unbound dye molecules. The stability against photodegradation depends on the fluorophore recycling time or the life of excited state. A similar approach was employed by Santra et al. in the preparation of the FITC labeled silica nanoparticles for bioimaging applications.[13] Lu et al. prepared robust fluorescent silica particles in a two step process involving the sol gel technique.[14] They followed the Stöber procedure and added the APS-FITC complex to grow silica fluorescent particles. Further, after washings were performed, these particles were treated with supplemental amount of TEOS. Upon standing 12 h, a pure silica outer layer was deposited. In order to close the pores through which the dye might leak, the suspension was treated with sodium silicate, Na_2SiO_3, at pH 10.0, and acid exchange resin. This procedure suppressed the penetration of the protons inside the particle and, consequently, arrested their attack on the dye-containing networks.

Significant progress has been made in the past two decades on modification of the outer surface of silica with organic polymers. [15,16] A large variety of composite particles was designed but few featured a shell made of homopolypeptide.[17-23] Polypeptides were grown, first, on different flat surfaces.[15,16] Oosterling et al. reported, for the first time, aerosil silica grafted with poly(L-aspartates) and poly(L-glutamates).[24] Tsubokawa et al. used carbon black as a core and grafted poly (γ-methyl-L-glutamate) by ring opening polymerization of the corresponding N-carboxyanhydride initiated by the amino groups attached to the carbon black surface.[25] These early reports dealt with issues such as low grafting density, colloidal stability and uniformity. Also, the determination of the helix orientation was a real challenge. In 1999, the Russo group reported polypeptide-coated silica particles with improved uniformity and higher polypeptide

loading.[19] The uniformity of the poly(carbobenzyloxy-L-lysine), PCBL silica particles was confirmed by the formation of beautiful colloidal crystals.[20] Once the uniformity was improved, the real challenge was to measure the molecular weight of the polypeptide grafted on the surface and compute the grafting density. The problem could be circumvented by the younger and rapidly evolving technique, click chemistry, which can attach ready-made and fully characterized polymer s to the cores. Balamurugan et al.[17] and Kar et al.[21,22] prepared silica particles featuring a homopolypeptide and a copolypeptide shell by attaching a well-characterized polymer with an alkyne terminus to a silica surface decorated with azide groups. This technique allows a facile evaluation of the number of chains grafted on the particle. Yet, the main drawback of the click chemistry remains the lower polymer loading or lower grafting densities when compared with the more popular *growing from* approach. Control over the population of the functional groups used as initiators in the *growing from* method was demonstrated by Soto-Cantu et al. using the tandem activator-pasivator in the functionalization step.[23] The Russo group also established a correlation between zeta potential and the number of the amino groups attached to the silica surface[26] and opened the door to copolymeric shells.[23] Recently, the Heise group was able to combine the thermogravimetric assays and gel permeation chromatography to measure the molecular weight of the polypeptides attached to the silica surface by the *growing from* technique.[18] The cleavage of the polypeptide was facilitated by the treatment of the polypeptide composite particle with hydrofluoric acid as an etchant. Strong bases such as NaOH and KOH were also used but mainly for the purpose of obtaining silica mesoporous particles. Regardless of the nature of the etchant used, acid or base, a new question arises: is the polypeptide's helical conformation surviving such treatment? The conservation and the stability of the polypeptide

structure, especially the helix is of great importance in tailoring the applications of these composite materials.

A newly emerged subclass of colloid particles is the so-called mesoporous silica. The possibility to create particles with complex morphologies, composition and internal structures makes them attractive for applications such as catalysis, separations, diagnostic, coatings, optics and electronics.[27,28] Several techniques have been employed in developing porous structures such as swelling with supercritical carbon dioxide,[29,30] microfluidic devices,[31,32] spray drying[33-35] or etching with hydrofluoric acid.[36-40] More recently template synthesis[41-43] received increased attention. The removal of the polymer template caused the particles to shrink. Moreover, the control over the size and morphology of the final product was not optimal. Lately an important emphasis is placed on using NaOH as an etchant to tailor the internal morphology of the colloid.[44] Basic conditions can also be ensured by ammonium hydroxide. For example, Grzelczak et al. obtained carbon nanotubes encapsulated in the hollow silica shells resembling wormlike structures.[45]Chapter 2 of the dissertation is dedicated to ammonia etching.

Ranging from rattle-type or yolk-shell to sponge-like these configurations are very appealing, as demonstrated by Zhang et al.[46] Chen et al obtained mesoporous silica resembling pomegranate fruit-like morphology and also foam-like structures. These simple synthetic procedures enable the scale-up of the methodology. Even if the method involved was so-called "surface-protected etching" or just simple aging, the rational use of NaOH facilitated the creation of desirable silica morphologies.[47,48] The base route is much milder when compared with the acidic variant (safety issues, longer time required to complete reaction, etc.), etching with hydrofluoric acid, widely used for treatment of flat silicon substrates.[49,50]

In this chapter, a simple and efficient route to transform polypeptide composite particles, PCPs, or silica core-polypeptide shell particles into mesoporous colloids, while releasing all or some of the shell polypeptide is considered. The focus is on NaOH as etchant and poly(N^{ε}-carbobenzyloxy-L-lysine), PCBL and poly(L-tyrosine), PTYR as polypeptide. The etching method is applied to nonfluorescent and fluorescent PCPs and also to bare fluorescent silica particles as a control. The effect of polypeptide coverage on the porosity and morphology of etched silica is assessed. A real challenge in the characterization of growing-from core-shell colloids is the determination of the molecular weight of the shell polymers. This problem is addressed by subjecting the polymers cleaved from the surface during the etching process to analysis by GPC/MALS. The conformation of these polymers, as revealed by their fractal dimension, is compared to that of polymer prepared normally (not by from surface initiation). In order to address the question of the shell polypeptide degradation, normally produced polymer is also subjected to NaOH etching.

4.2 Experimental

The synthetic procedure describing the production of mesoporous particles and shell cleavage is illustrated in Scheme 4.1. Details on the particle preparation are available in Chapter 8. The black arrows represent the routes to nonfluorescent polypeptide composite particles, PCP, while the green denote the preparation steps for fluorescent particles.

4.3 Results and Discussion

4.3.1 Architectural Particles: Mesoporous Non-Fluorescent Silica

Silica cores were prepared following combined seeded and Stöber procedure with modifications.[7,9,51-53] Fluorescent particles were obtained by covalent incorporation of the adduct made of flourescein isothiocyanate and 3-aminopropyl triethoxysilane, FITC-APS.

Tetraorthoethylsilicate, TEOS, diluted four times with EtOH was also added to build a thin silica layer on top of the dye. Afterwards, another layer of silica was deposited to prevent dye leaking and bleaching. The surface of the silica spheres was furnished with amino functional groups facilitated by the use of APS as the silane agent.[26] On the left side, the nonfluorescent aminofunctionalized silica particles were obtained by the treatment with APS in the same fashion as described for the fluorescent particles. The *growing from* approach was used to grow the polypeptide shell around the core by ring opening polymerization of the corresponding N-carboxyanhydrides, the polypeptide precursors, initiated by the amino groups decorating the surface of silica beads.[18-20,23,54] Composite particles, either poly(N^{ε}-carbobenzyloxy-L-lysine), PCBL or poly(*o*-benzyl-L-tyrosine), PBTY were converted to water soluble colloidal materials, poly(L-lysine), PLYS and poly(L-tyrosine), PTYR respectively, by deprotection of the polypeptide side chains with a solution of HBr/CH_3COOH (33%). The preparatory steps of non- and fluorescent polypeptide composite particles are presented in Scheme 4.1.

Thermogravimetric analysis, TGA, confirmed the presence of the polypeptide on the silica surface. Figure 4.1 shows the percent polypeptide loading on the core for protected and deprotected hybrid materials, as well as the weight difference after debenzylation.

The percent mass loading with polypeptides before and after etching is summarized in the Table 4.1. After preparation, particles were visualized by transmission electron microscopy, TEM, (Figure 4.2).

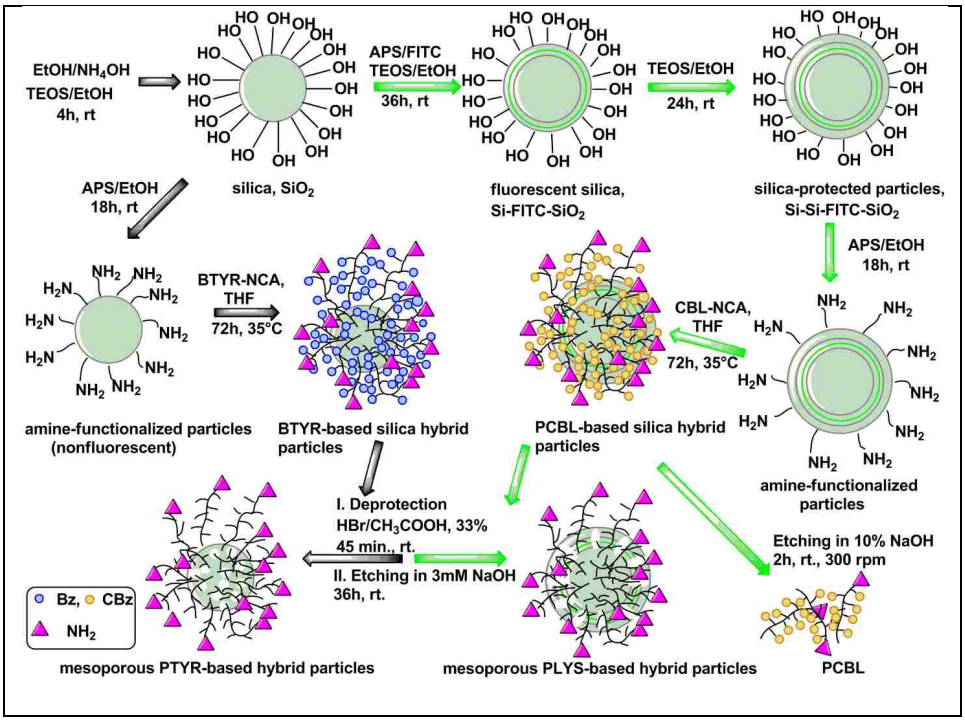

Scheme 4.1 Schematic illustration of the preparation of polypeptide-coated silica mesoporous hybrids using 3mM aqueous NaOH and shell cleavage using ~ 10% NaOH. The black arrows designate the non-fluorescent PCPs while the green are for fluorescent counterparts.

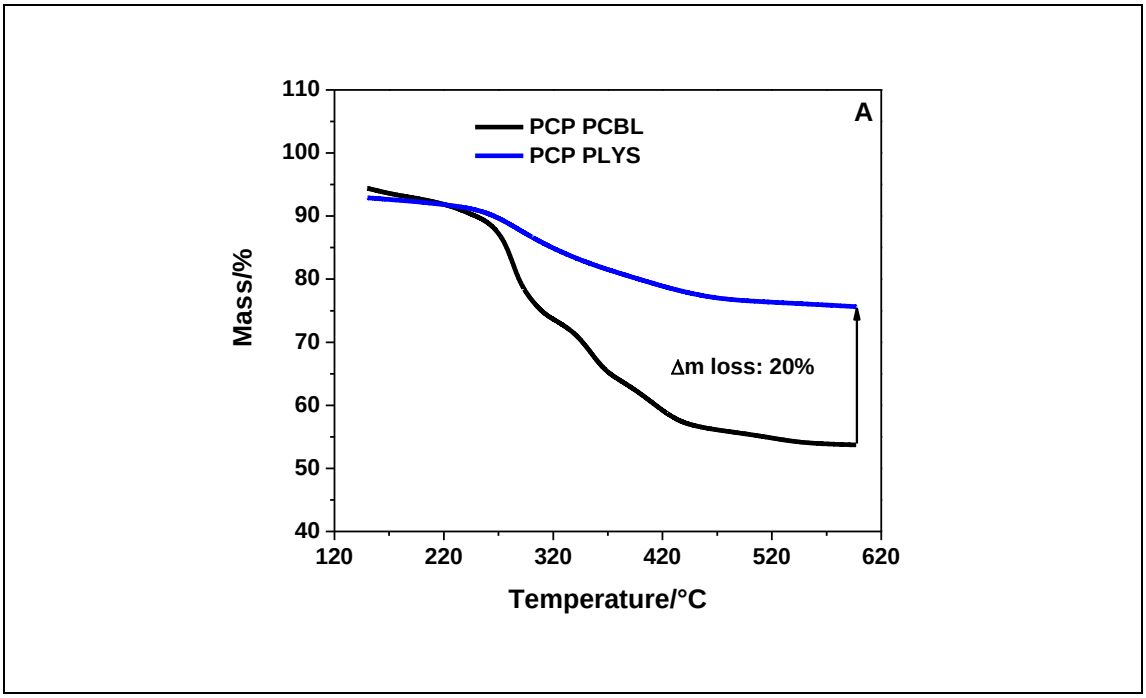

Figure 4.1 TGA traces before and after deprotection for PCP PCBL-coated silica hybrid (CR7160) (A) and PCP PBTY-coated silica hybrid (CR7161) (B).

Figure 4.1 continued

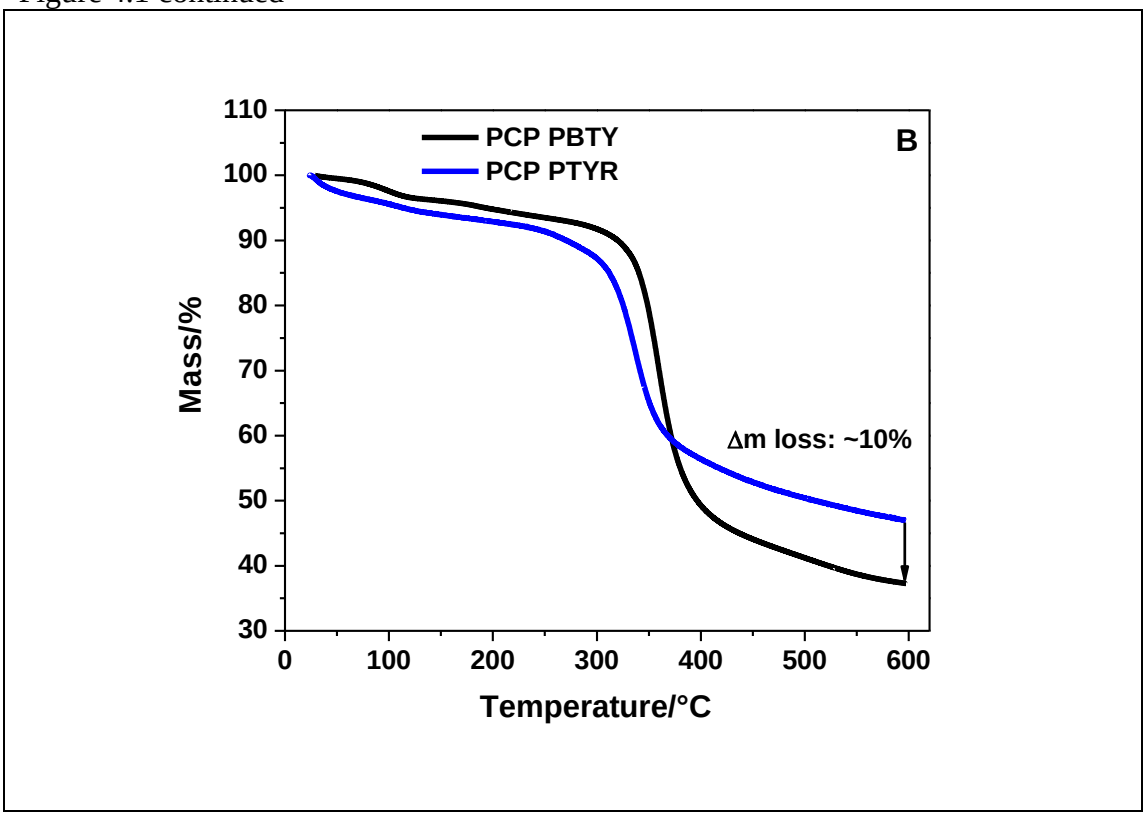

Table 4.1 Polypeptide Composite Particles, PCP, and the Percent Mass Loading with Polypeptide

PCP	Mass Loading/%
PCBL-silica	35
PLYS-silica	15
PBTY-silica	55
PTYR-silica	45

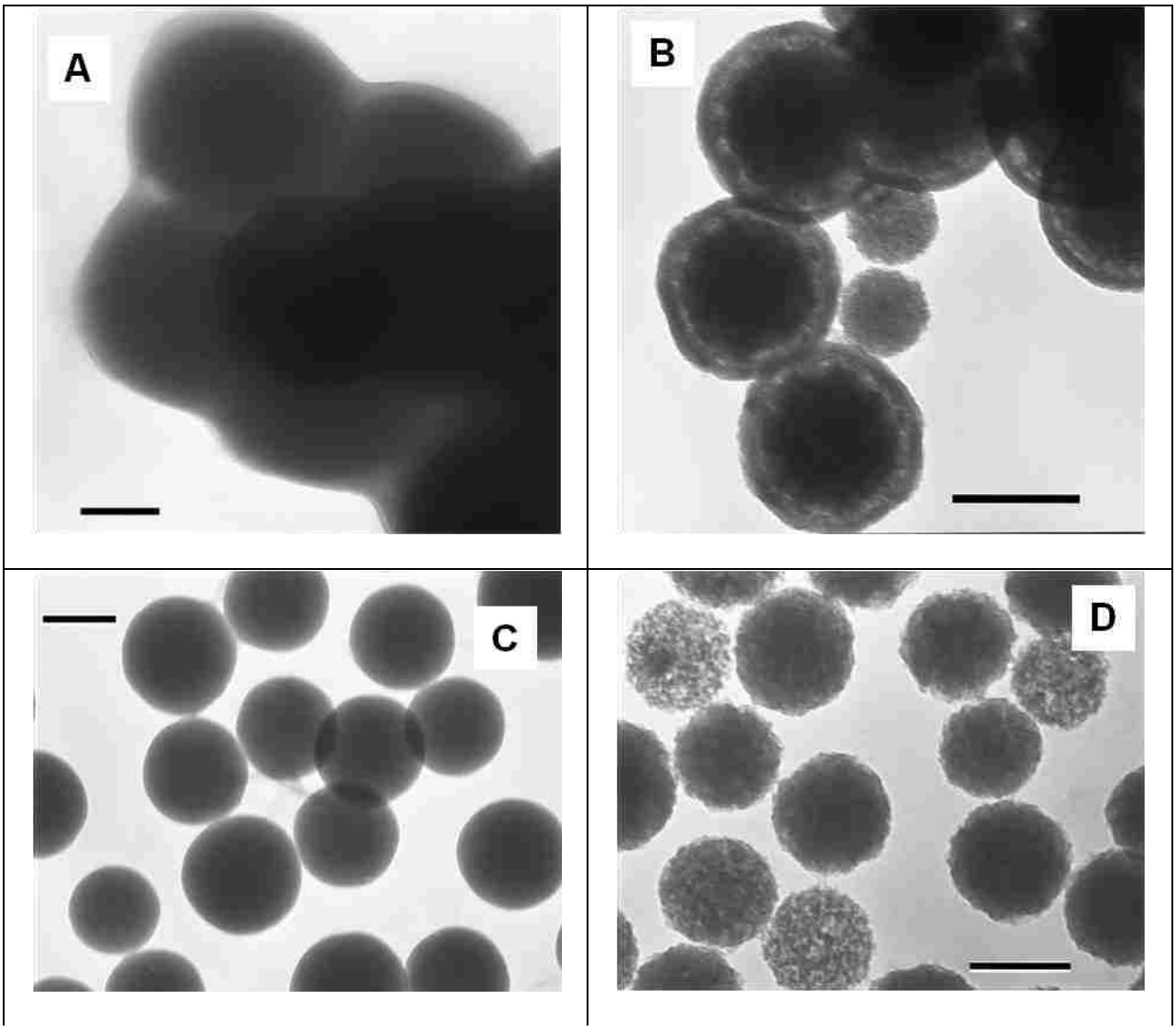

Figure 4.2 TEM images showing the morphology of the polypeptide composite particles before and after etching with a 3mM NaOH solution (pH= 12.6): (A) PCP PCBL (CR7160), (B) PCP PLYS (CR88A), (C) PCP PBTY (CR7161), (D) PCP PTYR-(CR88B), (E) bare fluorescent silica (CR760Atop) and (F) bare fluorescent silica after etching (CR828). Scale bars 100 nm.

Figure 4.2 continued

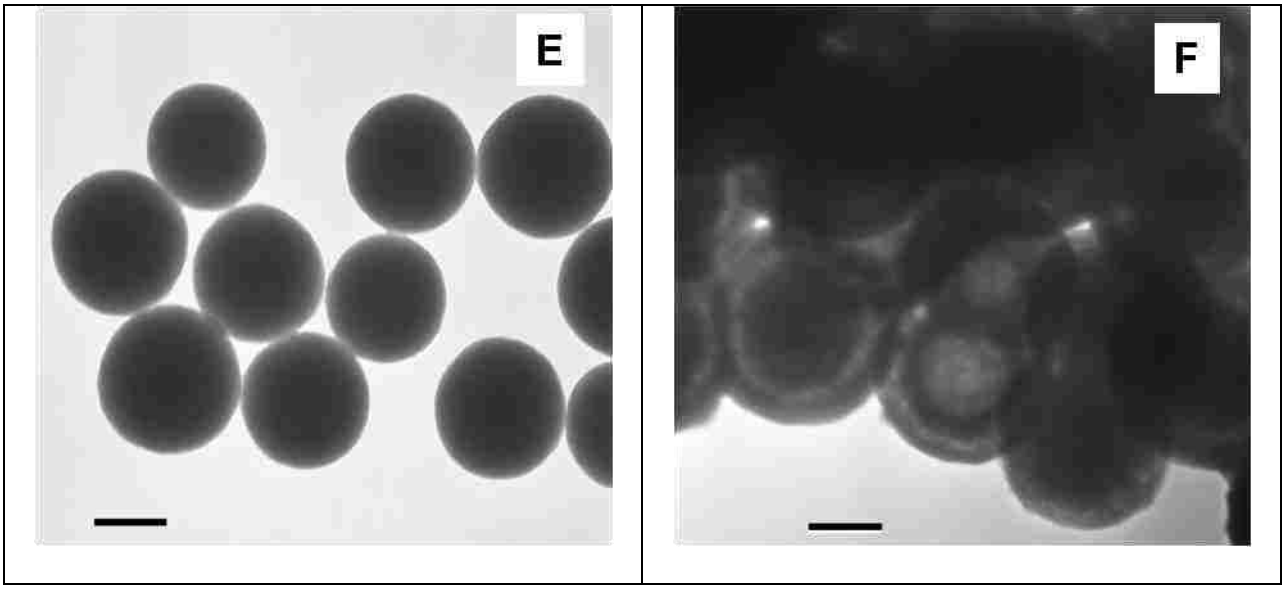

In order to make the polypeptide corona visible, the sample of PCP PCBL displayed in Figure 4.2A was stained by exposure to OsO_4 vapors. To guard against the possibility that polymer was deposited at the particle surface as the solvent was wicked off and dried down, Soto-Cantu and co-authors added a bare silica control particle that could be identified by a cobalt inclusion. Guided by this experiment, here it is assumed that no such dry-down artifacts occur. [23]. It is clearly shown that the core has a shadow around assigned to the polypeptide shell when compared, for example, with PCP PBTY seen in Figure 4.2C. The other images were obtained without staining; consequently only the core is visible. The hollow structure inside the spheres can be observed in the case of the fluorescent particles (Figure 4.2B). The image suggests that the grafted polypeptide can protect the surface against the action of the etchant agent in agreement with the results published by Zhang et al. on silica particles coated with polyvinylpyrrolidone, PVP.[47,48] The nonfluorescent composites, PCP PTYR, adopted a completely different architecture (Figure 4.2D). In comparison with the sample before etching, Figure 4.2C, the formation of the pores from the surface can be noted. The particles underwent a

slight shrinkage. A closer inspection of the fluorescent mesoporous structures gave another interesting detail: the dark "belt" present inside the empty particle and the full rattle core correspond to the size of the silica colloid after covalent doping with FITC–APS adduct. Therefore it can be hypothesized that the layer of the silica-dye adduct can act as a sacrifice which lowers the etching of the silica seed. As a proof-of-concept, a control experiment was developed as follows: bare fluorescent silica without carying a polypeptide shell, Figure 4.2E, were chosen and subjected to the same etching conditions as the former. As seen in the Figure 4.2F the morphology of the silica is identical with the one of the fluorescent composite particles. Figure 4.3 shows the control silica at different times of etching. Before exposure to NaOH, control silica particles had a good uniformity, as seen in Figure 4.3A (D = 176.5 ± 9 nm from TEM). The tendency to pack in 2D hexagonal arrays can be easily noted. After one day of the base incubation, Figure 4.3B, particles began to slightly excavate. The size stated essentially constant to 164 ± 7.5 nm. The formation of the pores from the surface can be seen in the second day, Figure 4.3C. The edge of the particles does not have the clarity and the sharpness of the initial spheres visualized in Figure 4.3A. Still, particles size remained constant and was evaluated as 171 ± 15 nm. The edges had a low contrast in the electron beam, a signature of a lower electron population due to internal etching. After 3 days, small voids inside the particle began to form and their morphology is presented in Figure 4.3D. Very interesting are the tunnels between the voids, seen at a higher magnification. These passages were also observed for PCP PLYS hybrids (Figure 4.4A and B).

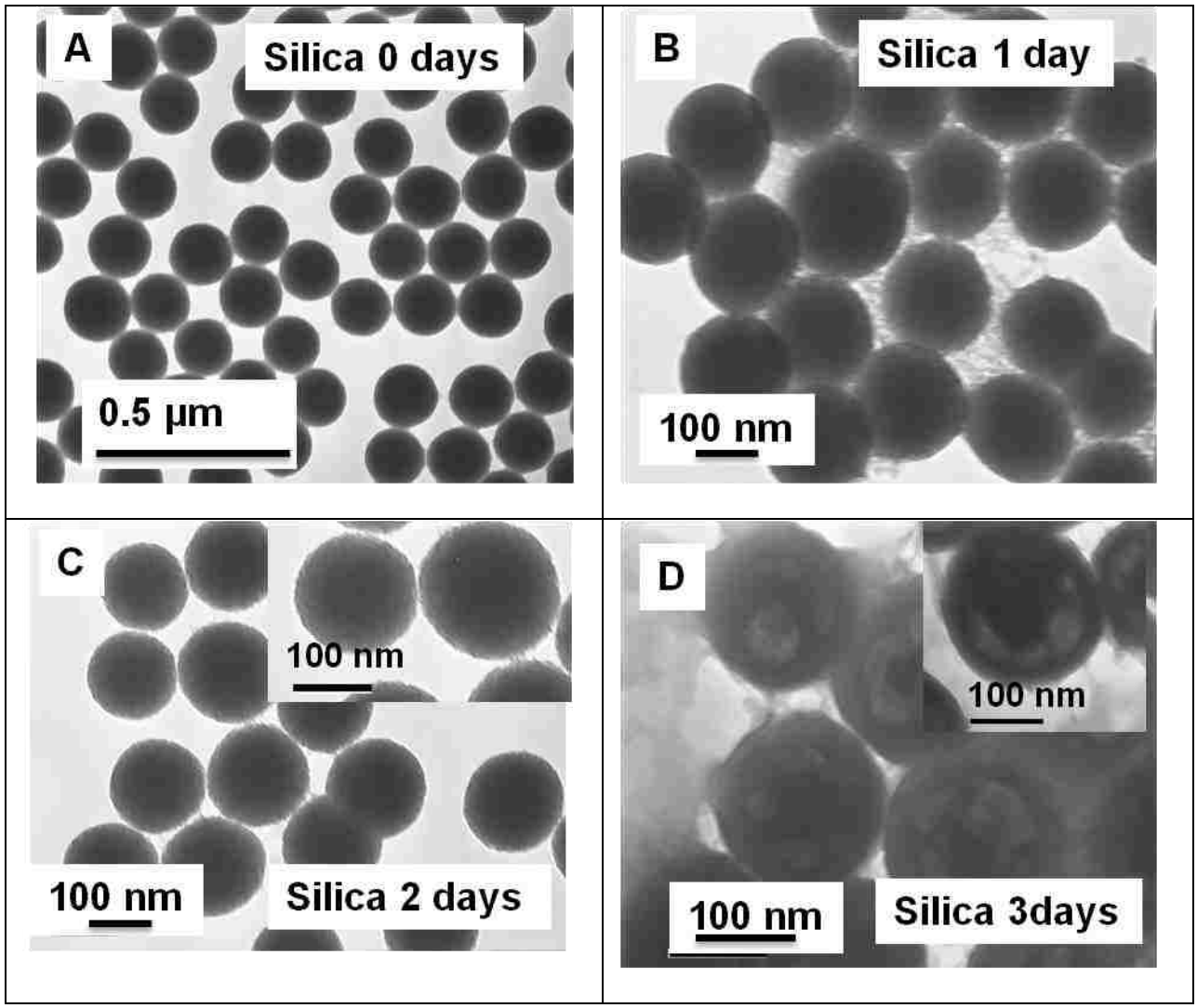

Figure 4.3 TEM micrographs recorded at different stages of etching the silica cores (CR760A top) with 3 mM NaOH (pH= 12.6): (A) 0 days, (B) after 1 day, (C) after 2 days (zoom inset) (D) after 3days (zoom inset), (E) after 4 days (zoom inset), (F) after 5 days (zoom), (G) after 6 days (zoom inset) and (H) after 7 days (zoom inset).

Figure 4.3 continued

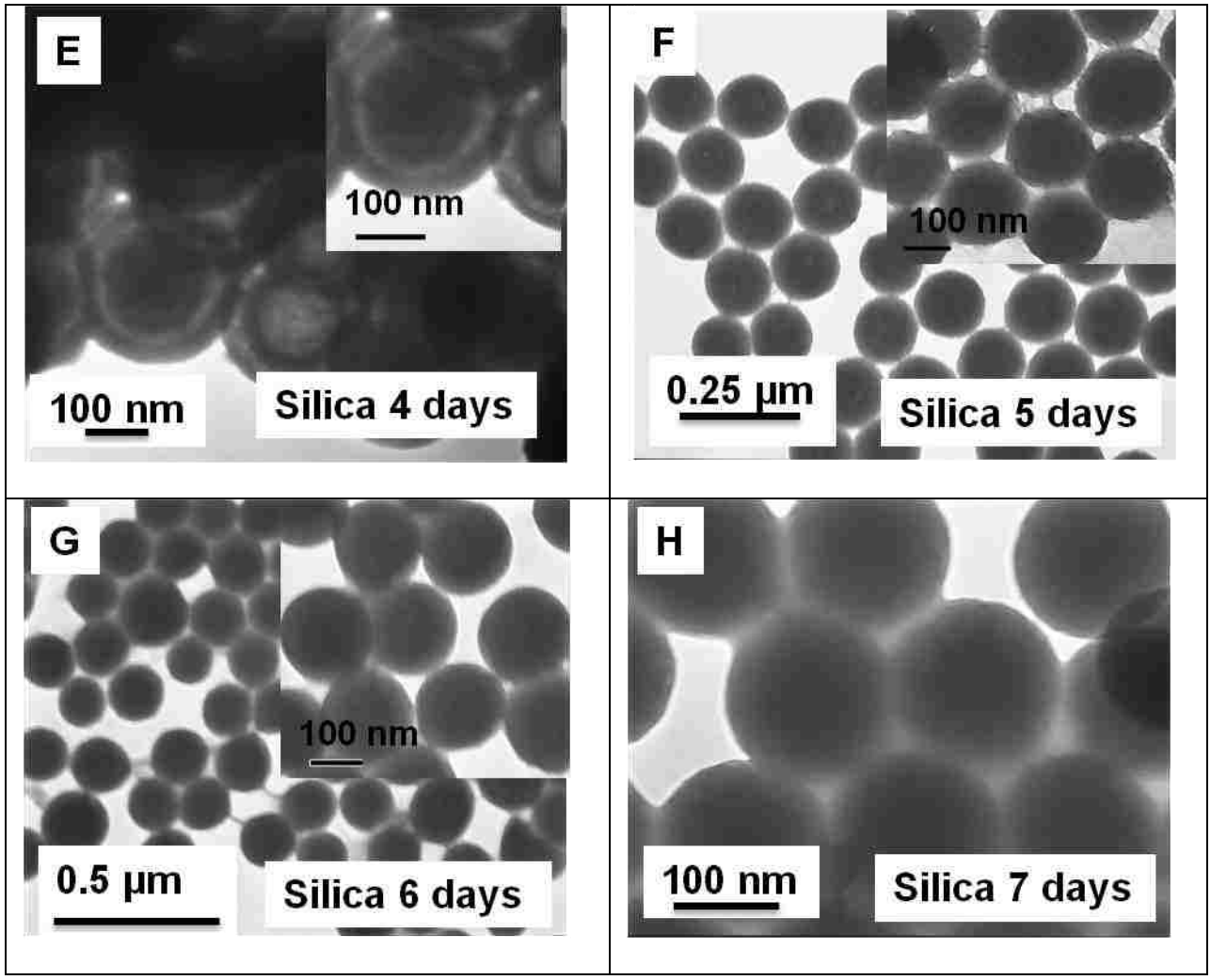

The control experiment on bare fluorescent silica revealed the possibility to also obtain morphologies such as void-belt-void-belt, as illustrated in Figure 4.3E. After 4 days of etching in 3mM NaOH solution, particles had an outer and an inner membrane, with voids in between. Most probably the small voids observed in day 3 merged into bigger structures separated by those tendon-like silica. Intriguing are the particles with an empty core formed along with the ones that have a full core. The density of the etched particles decreased in time due to the hydrolysis of the silane network. The Si—O—Si bonds of the 3-aminopropyltriethoxy silane

hydrolyze faster into Si—OH bonds due to less crosslinking when compared to the TEOS siloxane.

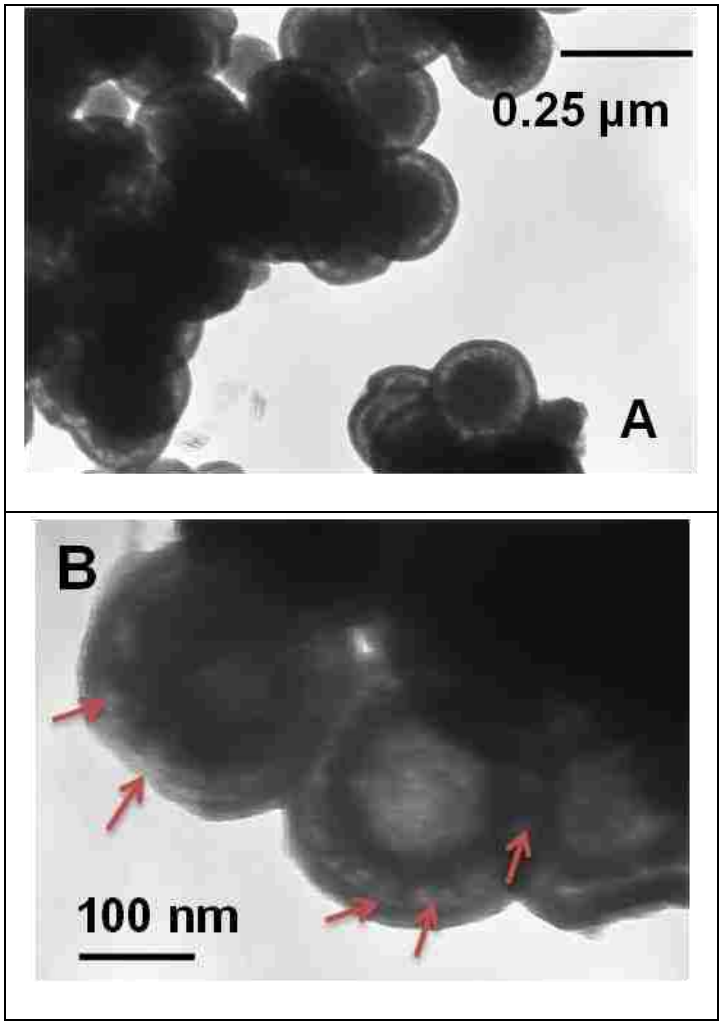

Figure 4.4 TEM images of (A) mesoporous PCP PLYS showing their morphology and (B) tunnels between the inner and outer membrane (marked with red arrows).

TEM size evaluation suggested the treatment with a basic etchant caused control particles to swell up to 268 ± 11 nm in the 4th day while those coated with a polypeptide corona slightly decreased in size. The decrease might be explained by the attractive forces associated with the mass of the corona which might induce the collapse of the outer membrane to the interior. Most of the particles did not change the spherical shape due to a symmetric and uniform coverage with

polypeptide. Yet, the sharp increase in size for silica was not seen in DLS measurements, Figure 4.5A..

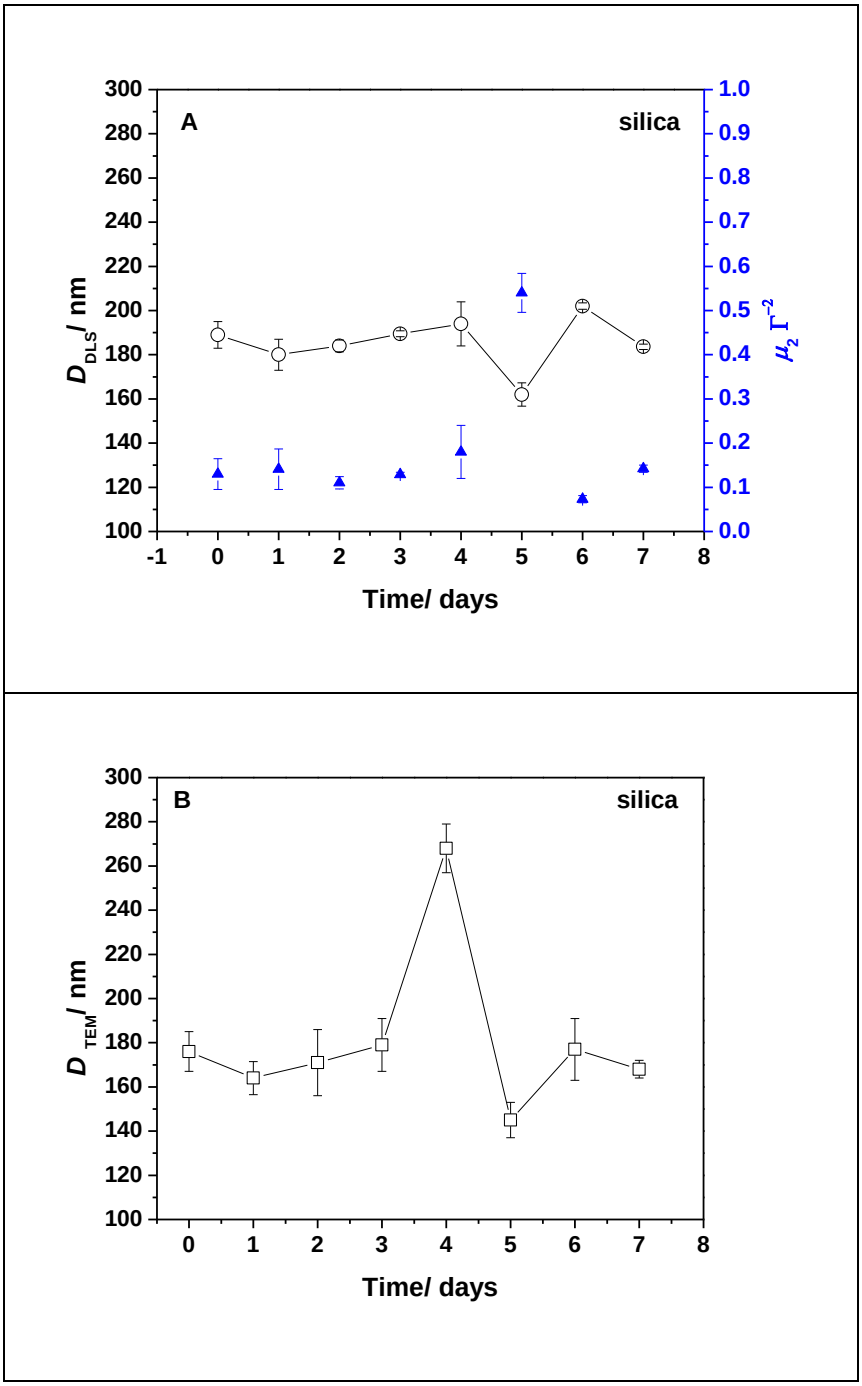

Figure 4.5 Diameter as a function of time (days) for fluorescent silica from: (A) dynamic light scattering along with associated polydispersity index, $\mu_2 \cdot \Gamma^{-2}$,and (B) TEM.

The peaking value of diameter seen in the 4th day from TEM, Figure 4.5B, is most probably a dry-down artifact.

After 5 days of base exposure particles lost their belt-void-belt appearance, Figure 4.3F. A decrease in size was observed while the polydispersity index from DLS deviated significantly. The diameter of the particles scaled at 145 ± 8 nm. Particles underwent excavation, a sign that the sacrificial TEOS-APS layer was probably hydrolyzed and the base reached the silica seed. In the day 6 the size increased to 177.5 ± 14 nm, Figure 4.3G. In the last day of the experiment, Figure 4.3H, silica began to drop in size again. The edges of the spheres clearly show the porous appearance along with the fuzzy shell consisting of hydrolyzed silica. Still the etched beads maintained their spherical shape after seven days of the NaOH treatment. DLS data showed that the size of the etched colloid was not altered significantly from the initial value, with the exception of the 5th day. The constancy of the size is a very important feature from the perspective of potential applications which will be later described.

The production of the mesoporous silica particles has engendered contradictory findings about the possible pathways of the etching mechanism. For example, Park et al. found that the etching took place predominantly in the particle interior[55] while El-Toni et al. showed mesoporous structures formed by shell-to-core etching.[56] Liu et al. reported shrinkage of the particles in the alkaline solution[57] but Chen et al.[58] and Zhao et al.[59] showed particles which slightly swelled after the alkaline treatment. This report showed that the size of the fluorescent silica cores remained essentially constant while the size of polypeptide-coated particles slightly decreased, according with TEM. The size of mesoporous particles before and during etching is summarized in Table 4.2.

Table 4.2 Mesoporous Particles and Their Core Diameter from TEM Obtained Before and During Etching

Mesoporous particle	Diameter/nm
PCP PCBL	275 ± 18
PCP PLYS	234 ± 16
PCP PLYS inner core	137 ± 20
PCP PBTY-	200 ± 5
PCP PTYR	136 ± 18
Silica (CR760Atop) 0 days	176 ± 9
Silica-1 day	164 ± 7.5
Silica-2 days	171 ± 15
Silica-3 days-total	179 ± 12
Silica-3 days-inner core	132 ± 9
Silica-4 days-total	268 ± 11
Silica-4 days-filled inner core	174 ± 8
Silica-4 days-empty inner core	132.5 ± 9
Silica-5 days	145 ± 8
Silica-6 days	177.5 ± 14
Silica-7 days	168 ± 4

The etching of the fluorescent particles, both furnished with polypeptide corona and without, was predominantly seen in the interior. What seems to happen in the formation of the void fluorescent particles is illustrated in Scheme 4.2. These particles have an inner layer of the

FITC-APS adduct blended with TEOS. The network formed by APS during the hydrolysis-condensation process is less crosslinked and dense than the TEOS network. The excavation that takes place in the first two days removes only a superficial layer of TEOS from the outer surface of the silica. The main effect is most probably the creation of larger pores. This way the etchant molecules have an easy path to the interior of the particle. Consequently, exposed to water and catalyzed by the hydroxyl ions, OH^-, provided by the etchant, the Si-O-Si bonds from the APS network hydrolyze faster to Si-OH bonds than the denser TEOS. The weakness of the Si-O-Si bridges promotes the formation of the sparse small voids. As a consequence of the prolonged exposure to the basic environment, the voids begin to merge while being separated by thin tunnels.

The afore described mechanism was also proposed by Roca et al. for their gold-void-silica particles.[60] Double silica membranes or belts seen in the case of PCP PLYS particles and bare silica mesoporous particles match pretty closely with the intermediate particles used in the core production (See Chapter 8 for experimental details and Figure 4.6 for the radii values). Figure 4.6 shows the silica seeds which were fluorescently tagged with the FITC-APS adduct and TEOS and finally with a protective layer of TEOS. These particles were the precursors of PCP PLYS colloids. For example, the size of the silica seeds closely matches with the size of the inner core seen after etching of the PCP PLYS.

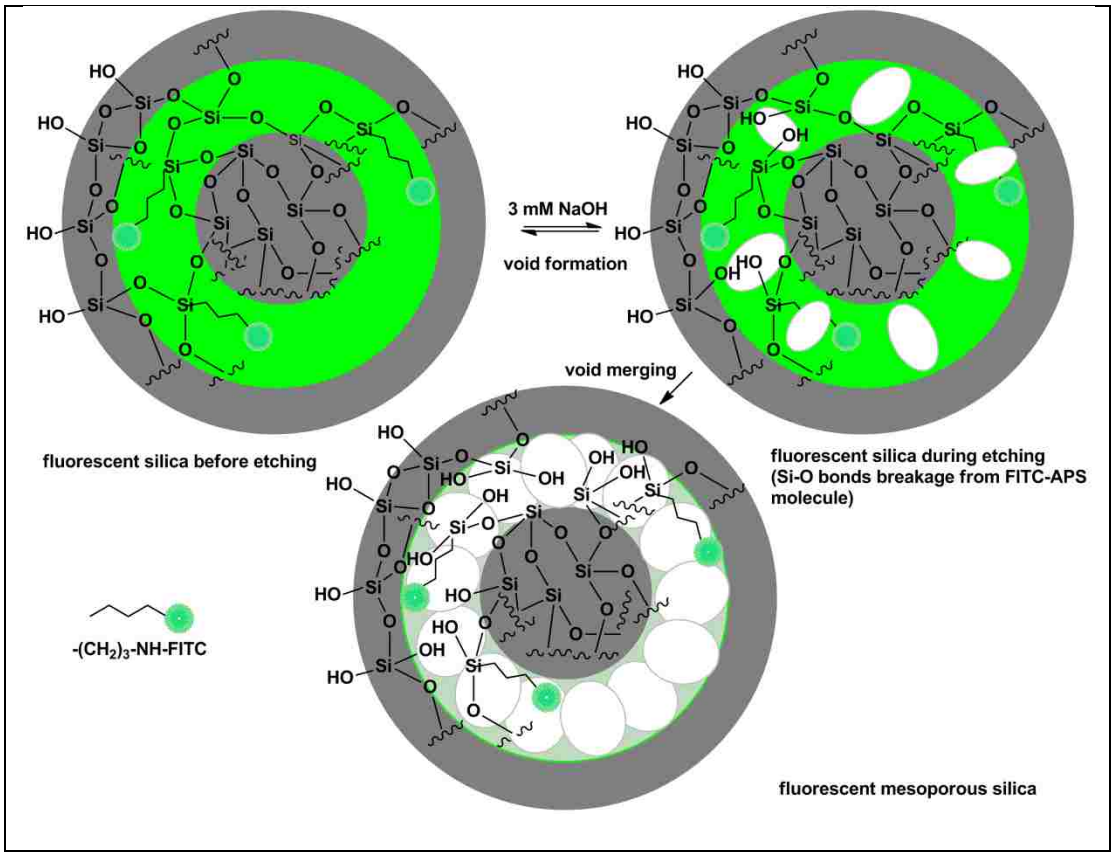

Scheme 4.2 Schematic illustration of the mesoporous fluorescent silica formation.

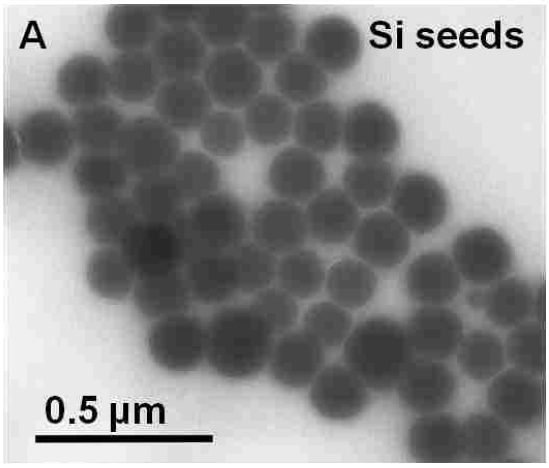

Figure 4.6 TEM images of the particles involved in the PCBL and PLYS-silica core preparation: (A) silica seeds (D = 154 ± 13 nm), (B) fluorescent core, Si-FITC-Si (D = 235 ± 12 nm) and (C) silica-protected core, Si-FITC-Si-Si, (D = 275 ± 18 nm).

Figure 4.6 continued

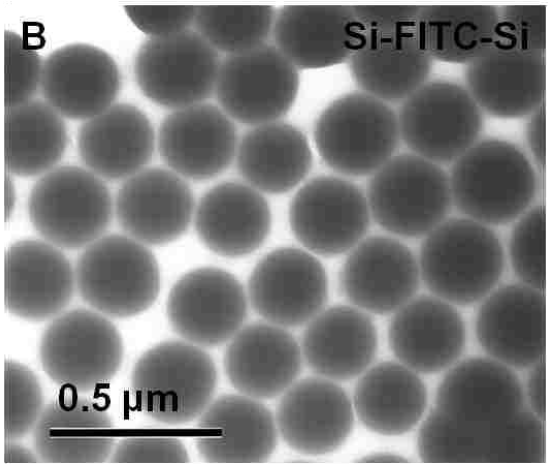

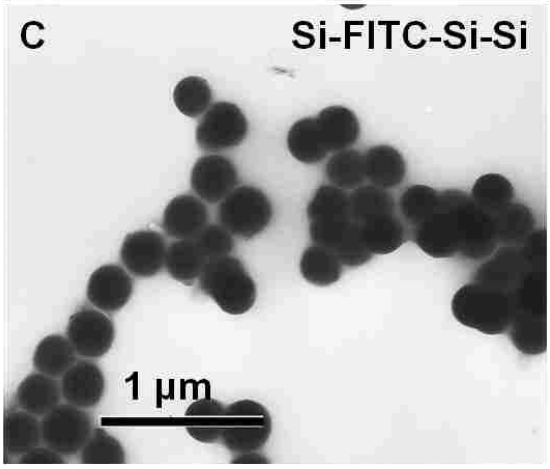

4.3.2 Applications of Mesoporous Polypeptide Composite Particles

After etching, the particles were still fluorescent. Figure 4.7 shows PCBL-silica and PLYS-silica particles. This is a very important feature of the technique involved in the particles fabrication which offers a multitude of advantages. Procedures for making fluorescent mesoporous particles require supplemental steps: after the formation of the voids, the colloid is labeled with FITC or other fluorescent dye. Further coatings with silica are not possible because the voids can be covered and the material loses its viability as a potential encapsulation candidate. Consequently, the dye might leak and can be easily bleached.

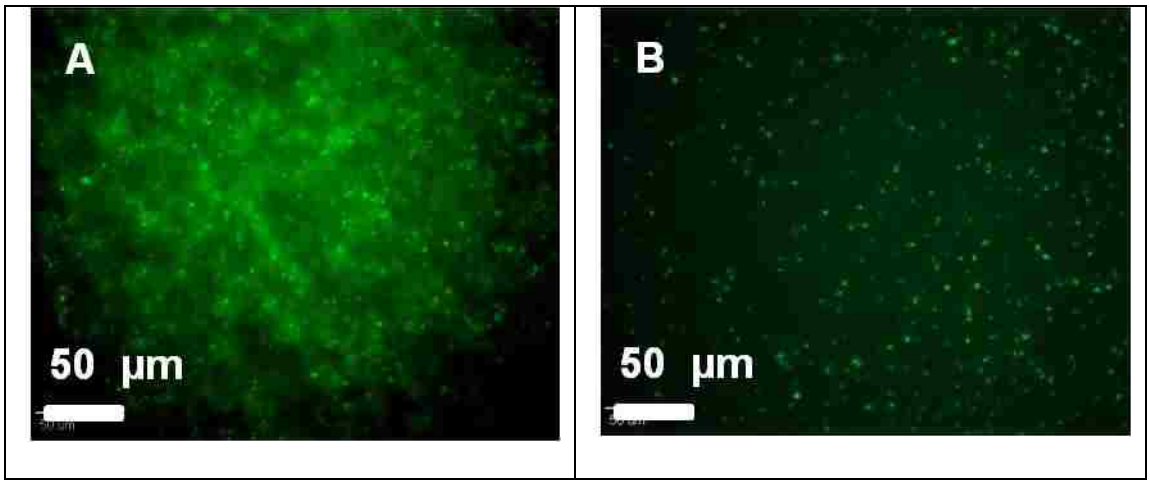

Figure 4.7 Fluorescence images of polypeptide composite particles: (A) PCP PCBL(CR7160) before etching and (B) PCP PCBL (CR7160) after etching. Scale bar 50 μm.

Applications such as *in vivo* imaging might be affected because the free dye is bleached and flushed quickly from the cell making it fluorescently invisible.[61,62] In comparison, the present colloid is already protected against leaking and bleaching thus ensuring a longer time for use in applications such as imaging. Figure 4.8 reflects the control silica particles visualized in fluorescence light inside an *Arabidopsis thaliana* leaf.

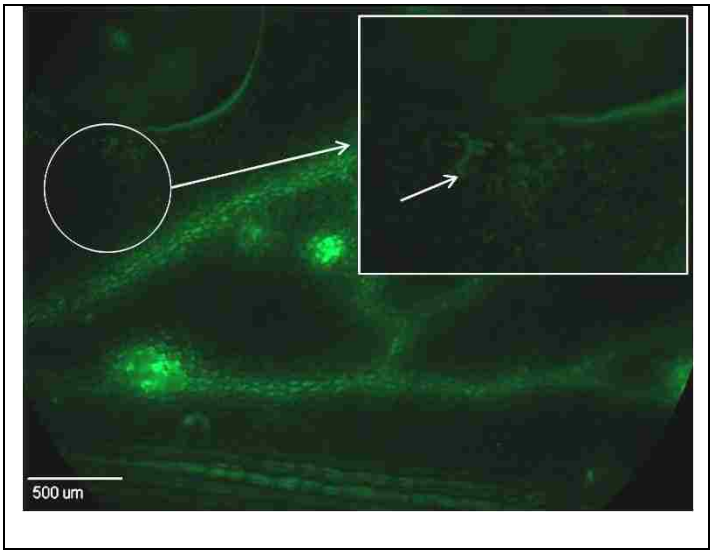

Figure 4.8 Fluorescent image of the fluorescent silica particles uptake in the vascular system of an *Arabidopsis thaliana* leaf and (inset) a zoom in the white circled area showing particles in the plant cells.

Despite their size (176 nm in diameter), particles were able to flow into the mainstream of the leaf's capillary system.

The stability and the good dispersion of the silica into the vessel's fluid seemed to hinder their aggregation, thus clogging the artery. Only two clusters can be seen in the image. Furthermore, some of the particles were able to penetrate through the cells walls and are visible in the inset. The protection against dye leakage and bleaching combined with the ability to penetrate into living cells makes the fluorescent silica particles, described in this chapter, potential candidates for *in vivo* imaging and, not the last, as probes.

4.3.3 Shell Haircut: Grafting Density and Secondary Structure

Inspired by the formation of the mesoporous hybrid particles in 3mM aqueous NaOH solution, another key approach of this work was developed: the use of NaOH etching to haircut the composite particle and asses the molecular weight of the polypeptide. Studies conducted up to present used HF as etchant[18] These experiments, especially the controls using vendor-purchased untethered polymer, are in their infancy. This section will be developed in Chapter 7, Section 7.5. Data on the cleaved PCBL along with the future experiments necessary to fulfill the goal of the project will be presented.

4.4 Conclusion

A facile and mild method, based on NaOH etching to manipulate hard silica cores into mesoporous morphologies was presented. This method, besides the good yields, can also be viewed as a convenient way to fluorescent mesoporous particles. The unique feature of the particles is that the fluorescent dye is protected from bleaching with a supplemental silica layer. The formation of the voids from the inside out was seen in both categories of colloids, simple fluorescent silica cores and fluorescent PCPs. In addition, the difference in morphologies

between a fluorescent particle and one lacking the fluorescent tag, pointed to selective etching of the dye-containing networks acting as a sacrificial layer and the heavy crosslinked TEOS strata. The less APS crosslinked network was hydrolyzed faster than the denser TEOS network. Voids occurred and upon prolonged exposure to the basic solution, they merged into silica-void-silica structures separated by the silica tendons or belts. The control particles retained enough fluorescence for bioimaging purposes. The fluorescence study showed they were transported through the vascular tract of *Arabidopsis thaliana* leaf and delivered to the plant cells. Observations made on the moderate etching of the silica with the formation of the mesoporous particles led to the idea of using NaOH of higher concentration and for a shorter time to haircut the polypeptide particle and measure the molecular weight of the grafted polypeptide, such a sensitive task in the *growing from* method. The combination of the thermogravimetric and chromatographic assays allowed the calculation of the grafting density and the chain population of the polypeptide-based hybrid particle. The cleavage experiments are presented in Chapter 7, Section 7.5. Several concluding remarks withdrawn from experiments carried out on cleaved PCBL are presented here. GPC experiments have shown that the cut off PCBL had a helical conformation and behaved like a rigid rod in the limits of Kratky – Porod model. The small random coil residues identified by FTIR did not impact the rodlike behavior. This behavior compared with the other polymers of different molecular weight underline the fact that not only the secondary structure of the PCBL was conserved but also the *grafting from* method can be considered a good way to produce well-behaved rigid rod polypeptides.

4. 5 References and Notes

(1) Li, Z.; Barnes, J. C.; Bosoy, A.; Stoddart, J. F.; Zink, J. I. Mesoporous silica nanoparticles in biomedical applications. *Chemical Society Reviews* **2012**, *41*, 2590-2605.

(2) O'Farrell, N.; Houlton, A.; Horrocks, B. R. Silicon nanoparticles: applications in cell biology and medicine. *International Journal of Nanomedicine* **2006**, *1*, 451-472.

(3) Chiappini, A.; Chiasera, A.; Berneschi, S.; Armellini, C.; Carpentiero, A.; Mazzola, M.; Moser, E.; Varas, S.; Righini, G. C.; Ferrari, M. Sol-gel-derived photonic structures: fabrication, assessment, and application. *J. Sol-Gel Sci. Technol.* **2011**, *60*, 408-425.

(4) Rother, D.; Sen, T.; East, D.; Bruce, I. J. Silicon, silica and its surface patterning/activation with alkoxy- and amino-silanes for nanomedical applications. *Nanomedicine* **2012**, *6*, 281-300.

(5) Vivero-Escoto, J. L.; Huxford-Phillips, R. C.; Lin, W. Silica-based nanoprobes for biomedical imaging and theranostic applications. *Chemical Society Reviews* **2012**, *41*, 2673-2685.

(6) Wang, S. B. Ordered mesoporous materials for drug delivery. *Microporous and Mesoporous Materials* **2009**, *117*, 1-9.

(7) Stober, W.; Fink, A.; Bohn, E. Controlled Growth of Monodisperse Silica Spheres in the Micron Size Range. *Journal of Colloid and Interface Science* **1968**, *26*, 62-69.

(8) Bogush, G. H.; Tracy, M. A.; Zukoski, C. F. Preparation of monodisperse silica particles - control of size and mass fraction. *Journal of Non-Crystalline Solids* **1988**, *104*, 95-106.

(9) Zhang, J. H.; Zhan, P.; Wang, Z. L.; Zhang, W. Y.; Ming, N. B. Preparation of monodisperse silica particles with controllable size and shape. *J. Mater. Res.* **2003**, *18*, 649-653.

(10) Midmore, B. R. Preparation of a novel silica-stabilized oil/water emulsion. *Colloids and Surfaces A: Physicochemical and Engineering Aspects* **1998**, *132*, 257-265.

(11) Morrison, S. A.; Cahill, C. L.; Carpenter, E. E.; Harris, V. G. Production scaleup of reverse micelle synthesis. *Industrial & Engineering Chemistry Research* **2006**, *45*, 1217-1220.

(12) Viger, M. L.; Live, L. S.; Therrien, O. D.; Boudreau, D. Reduction of self-quenching in fluorescent silica-coated silver nanoparticles. *Plasmonics* **2008**, *3*, 33-40.

(13) Santra, S.; Yang, H.; Dutta, D.; Stanley, J. T.; Holloway, P. H.; Tan, W. H.; Moudgil, B. M.; Mericle, R. A. TAT conjugated, FITC doped silica nanoparticles for bioimaging applications. *Chem. Commun.* **2004**, 2810-2811.

(14) Lu, Z. Y.; Xu, J. Q.; Han, Y. D.; Song, Z. Q.; Li, J.; Yang, W. S. Robust fluorescein-doped silica nanoparticles via dense-liquid treatment. *Colloids and Surfaces a-Physicochemical and Engineering Aspects* **2007**, *303*, 207-210.

(15) Wieringa, R. H.; Siesling, E. A.; Geurts, P. F. M.; Werkman, P. J.; Vorenkamp, E. J.; Erb, V.; Stamm, M.; Schouten, A. J. Surface grafting of poly (L-glutamates). 1. Synthesis and characterization. *Langmuir* **2001**, *17*, 6477-6484.

(16) Zheng, W. W.; Frank, C. W. Surface-Initiated Vapor Deposition Polymerization of Poly (γ-benzyl-L-glutamate): Optimization and Mechanistic Studies. *Langmuir* **2010**, *26*, 3929-3941.

(17) Balamurugan, S. S.; Soto-Cantu, E.; Cueto, R.; Russo, P. S. Preparation of Organosoluble Silica-Polypeptide Particles by "Click" Chemistry. *Macromolecules* **2010**, *43*, 62-70.

(18) Borase, T.; Iacono, M.; Ali, S. I.; Thornton, P. D.; Heise, A. Polypeptide core-shell silica nanoparticles with high grafting density by N-carboxyanhydride (NCA) ring opening polymerization as responsive materials and for bioconjugation. *Polymer Chemistry* **2012**, *3*, 1267-1275.

(19) Fong, B.; Russo, P. S. Organophilic colloidal particles with a synthetic polypeptide coating. *Langmuir* **1999**, *15*, 4421-4426.

(20) Fong, B.; Turksen, S.; Russo, P. S.; Stryjewski, W. Colloidal crystals of silica-homopolypeptide composite particles. *Langmuir* **2004**, *20*, 266-269.

(21) Kar, M.; Pauline, M.; Sharma, K.; Kumaraswamy, G.; Sen Gupta, S. Synthesis of Poly-L-glutamic Acid Grafted Silica Nanoparticles and Their Assembly into Macroporous Structures. *Langmuir* **2011**, *27*, 12124-12133.

(22) Kar, M.; Vijayakumar, P. S.; Prasad, B. L. V.; Sen Gupta, S. Synthesis and Characterization of Poly-L-lysine-Grafted Silica Nanoparticles Synthesized via NCA Polymerization and Click Chemistry. *Langmuir* **2010**, *26*, 5772-5781.

(23) Soto-Cantu, E.; Turksen-Selcuk, S.; Qiu, J. H.; Zhou, Z.; Russo, P. S.; Henk, M. C. Silica-Polypeptide Composite Particles: Controlling Shell Growth. *Langmuir* **2011**, *26*, 15604-15613.

(24) Oosterling, M. L. C. M.; Willems, E.; Schouten, A. J. End-grafting of (co)polyglutamates and (co)polyaspartates onto Si-OH containing surfaces. *Polymer* **1995**, *36*, 4463-4470.

(25) Tsubokawa, N.; Kobayashi, K.; Sone, Y. Grafting of Polypeptide from Carbon Black by the Ring-Opening Polymerization of γ-Methyl l-Glutamate N-Carboxyanhydride Initiated by Amino Groups on Carbon Black Surface. *Polymer Journal* **1987**, *19*, 1147-1155.

(26) Soto-Cantu, E.; Cueto, R.; Koch, J.; Russo, P. S. Synthesis and Rapid Characterization of Amine-Functionalized Silica. *Langmuir* **2012**, *28*, 5562-5569.

(27) Lim, Y. T.; Kim, J. K.; Noh, Y.-W.; Cho, M. Y.; Chung, B. H. Multifunctional Silica Nanocapsule with a Single Surface Hole. *Small* **2009**, *5*, 324-328.

(28) Yoon, T.-J.; Kim, J. S.; Kim, B. G.; Yu, K. N.; Cho, M.-H.; Lee, J.-K. Multifunctional Nanoparticles Possessing A "Magnetic Motor Effect" for Drug or Gene Delivery. *Angewandte Chemie International Edition* **2005**, *44*, 1068-1071.

(29) Jiao, J. X.; Xu, Q.; Li, L. M. Porous TiO2/SiO2 composite prepared using PEG as template direction reagent with assistance of supercritical CO2. *Journal of Colloid and Interface Science* **2007**, *316*, 596-603.

(30) Urata, C.; Tamura, Y.; Yamauchi, Y.; Kuroda, K. Preparation of mesostructured silica-micelle hybrids and their conversion to mesoporous silica modified controllably with immobilized hydrophobic blocks by using triethoxysilyl-terminated PEO-PPO-PEO triblock copolymer. *J. Mater. Chem.* **2011**, *21*, 3711-3717.

(31) Liu, Y.; Ju, M. H.; Wang, C. Q.; Zhang, L. X.; Liu, X. Q. Preparation of monodisperse mesoporous carbon microspheres from poly(furfuryl alcohol)-silica composite microspheres produced in a microfluidic device. *J. Mater. Chem.* **2011**, *21*, 15049-15056.

(32) Zhai, Z.; Wang, Y. J.; Lu, Y. C.; Luo, G. S. Preparation of Monodispersed Uniform Silica Spheres with Large Pore Size for Fast Adsorption of Proteins. *Industrial & Engineering Chemistry Research* **2010**, *49*, 4162-4168.

(33) Melnyk, I. V.; Zub, Y. L.; Veron, E.; Massiot, D.; Cacciaguerra, T.; Alonso, B. Spray-dried mesoporous silica microspheres with adjustable textures and pore surfaces homogenously covered by accessible thiol functions. *J. Mater. Chem.* **2008**, *18*, 1368-1382.

(34) Negishi, H.; Miyamoto, A.; Sakaki, K.; Endo, A. Electrophoretic deposition of mesoporous silica powder synthesized by spray-drying method. *Journal of the Ceramic Society of Japan* **2011**, *119*, 168-172.

(35) Okuyama, K.; Abdullah, M.; Lenggoro, I. W.; Iskandar, F. Preparation of functional nanostructured particles by spray drying. *Advanced Powder Technology* **2006**, *17*, 587-611.

(36) Kelly, T. L.; Yano, K.; Wolf, M. O. Nanoscale Control over Phase Separation in Conjugated Polymer Blends Using Mesoporous Silica Spheres. *Langmuir* **2011**, *26*, 421-431.

(37) Li, G. L.; Tai, C. A.; Neoh, K. G.; Kang, E. T.; Yang, X. L. Hybrid nanorattles of metal core and stimuli-responsive polymer shell for confined catalytic reactions. *Polymer Chemistry* **2011**, *2*, 1368-1374.

(38) Mekaru, H.; Fujimaki, M.; Awazu, K.; Takahashi, M. Resist-less patterning on SiO2 by combination of X-ray exposure and vapor HF etching. *Microsystem Technologies-Micro-and Nanosystems-Information Storage and Processing Systems* **2011**, *16*, 1339-1346.

(39) Qi, D. M.; Yuan, Y.; Zhang, R.; Xu, J.; Yang, L. Preparation and characterization of silica/PMMA composites with highly dispersed silica-grafting and crosslinking. *Acta Polymerica Sinica* **2011**, 1258-1265.

(40) Shen, R. P.; Mu, B.; Du, P. C.; Liu, P. Preparation of Photo-Sensitive Degradable Polymeric Nanocapsules from Dendrimer Grafted Nano-Silica Templates. *Soft Materials* **2011**, *9*, 382-392.

(41) Caruso, F.; Caruso, R. A.; Mohwald, H. Nanoengineering of inorganic and hybrid hollow spheres by colloidal templating. *Science* **1998**, *282*, 1111-1114.

(42) Chandrawati, R.; van Koeverden, M. P.; Lomas, H.; Caruso, F. Multicompartment Particle Assemblies for Bioinspired Encapsulated Reactions. *J. Phys. Chem. Lett.* **2011**, *2*, 2639-2649.

(43) Cui, J. W.; Wang, Y. J.; Hao, J. C.; Caruso, F. Mesoporous Silica-Templated Assembly of Luminescent Polyester Particles. *Chem. Mat.* **2009**, *21*, 4310-4315.

(44) Shon, J. K.; Kim, H.; Kong, S. S.; Hwang, S. H.; Han, T. H.; Kim, J. M.; Pak, C.; Doo, S.; Chang, H. Nano-propping effect of residual silicas on reversible lithium storage over highly ordered mesoporous SnO2 materials. *J. Mater. Chem.* **2009**, *19*, 6727-6732.

(45) Grzelczak, M.; Correa-Duarte, M. A.; Liz-Marzan, L. M. Carbon nanotubes encapsulated in wormlike hollow silica shells. *Small* **2006**, *2*, 1174-1177.

(46) Okada, A.; Nagao, D.; Ishii, H.; Konno, M. Direct observation of micron-sized silica rattles to demonstrate movability of inner spheres in the silica compartment suspended in aqueous media. *Soft Matter* **2012**, *8*, 3442-3445.

(47) Zhang, Q.; Ge, J. P.; Goebl, J.; Hu, Y. X.; Lu, Z. D.; Yin, Y. D. Rattle-Type Silica Colloidal Particles Prepared by a Surface-Protected Etching Process. *Nano Research* **2009**, *2*, 583-591.

(48) Zhang, Q.; Zhang, T. R.; Ge, J. P.; Yin, Y. D. Permeable silica shell through surface-protected etching. *Nano Letters* **2008**, *8*, 2867-2871.

(49) Guhathakurta, S.; Subramanian, A. Effect of hydrofluoric acid in oxidizing acid mixtures on the hydroxylation of silicon surface. *Journal of the Electrochemical Society* **2007**, *154*, P136-P146.

(50) Sugimoto, H.; Tajima, M. Photoluminescence imaging of multicrystalline Si wafers during HF etching. *Japanese Journal of Applied Physics Part 2-Letters & Express Letters* **2007**, *46*, L339-L341.

(51) Deng, T.-S.; Zhang, Q.-F.; Zhang, J.-Y.; Shen, X.; Zhu, K.-T.; Wu, J.-L. One-step synthesis of highly monodisperse hybrid silica spheres in aqueous solution. *Journal of Colloid and Interface Science* **2009**, *329*, 292-299.

(52) Nozawa, K.; Gailhanou, H.; Raison, L.; Panizza, P.; Ushiki, H.; Sellier, E.; Delville, J. P.; Delville, M. H. Smart control of monodisperse Stber silica particles: Effect of reactant addition rate on growth process. *Langmuir* **2005**, *21*, 1516-1523.

(53) Rao, K. S.; El-Hami, K.; Kodaki, T.; Matsushige, K.; Makino, K. A novel method for synthesis of silica nanoparticles. *Journal of Colloid and Interface Science* **2005**, *289*, 125-131.

(54) Liu, D.; Li, Y.; Deng, J.; Yang, W. Synthesis and characterization of magnetic Fe3O4-silica-poly(Î³-benzyl-L-glutamate) composite microspheres. *Reactive and Functional Polymers* **2011**, *71*, 1040-1044.

(55) Park, S.-J.; Kim, Y.-J.; Park, S.-J. Size-Dependent Shape Evolution of Silica Nanoparticles into Hollow Structures. *Langmuir* **2008**, *24*, 12134-12137.

(56) El-Toni, A. M.; Khan, A.; Ibrahim, M. A.; Labis, J. P.; Badr, G.; Al-Hoshan, M.; Yin, S.; Sato, T. Synthesis of double mesoporous core-shell silica spheres with tunable core porosity and their drug release and cancer cell apoptosis properties. *Journal of Colloid and Interface Science* **2012**, *378*, 83-92.

(57) Liu, S.; Wong, Y.; Wang, Y.; Wang, D.; Han, M. Y. Controlled Release and Absorption Resonance of Fluorescent Silica-Coated Platinum Nanoparticles. *Advanced Functional Materials* **2007**, *17*, 3147-3152.

(58) Chen, H. M.; Hu, T.; Zhang, X. M.; Huo, K. F.; Chu, P. K.; He, J. H. One-Step Synthesis of Monodisperse and Hierarchically Mesostructured Silica Particles with a Thin Shell. *Langmuir* **2010**, *26*, 13556-13563.

(59) Zhao, L.; Zhao, Y. F.; Han, Y. Pore Fabrication in Various Silica-Based Nanoparticles by Controlled Etching. *Langmuir* **2010**, *26*, 11784-11789.

(60) Roca, M.; Haes, A. J. Silica-Void-Gold Nanoparticles: Temporally Stable Surf ace-Enhanced Raman Scattering Substrates. *J. Am. Chem. Soc.* **2008**, *130*, 14273-14279.

(61) Schroeder, N. E.; MacGudwin, A. E. Incorporation of a fluorescent compound by live Heterodera glycines. *Journal of Nematology* **2007**, *39*, 43-49.

(62) Hedgecock, E. M.; Culotti, J. G.; Thomson, J. N.; Perkins, L. A. Axonal guidance mutants of caenorhabditis-elegans identified by filling sensory neurons with fluorescein dyes. *Developmental Biology* **1985**, *111*, 158-170.

CHAPTER 5
PHYSICAL PROPERTIES OF SILICA POLY(CARBOBENZYLOXY-L-LYSINE) COMPOSITE PARTICLES: METHODS TO INVESTIGATE THE REVERSE RANDOM COIL-TO-HELIX CONFORMATIONAL CHANGE IN M-CRESOL AS A TEMPERATURE RESPONSE

5.1 Introduction

Stimuli-responsive peptide-conjugated silica nanoparticles have captured attention in the last decade. These hybrid materials provide an opportunity to design novel materials that combine the biological functionality and the enormous chemical versatility of the polypeptide with the features of colloidal particles (stability, facile surface modification, low cost and most of all easy manipulation in gravitational and magnetic fields). Composite particles featuring a homopolypeptide shell can be considered useful models that can help understanding the tethering mechanism behind virus infection.

Polypeptides undergo structural changes induced by various factors such as pH, temperature and solvent. Studies focused on this field have reported controversial results but all highlighted the importance of understanding such phenomenology. The most widely investigated polypeptide from this point of view is PBLG. Zimm and Bragg[1] and then Applequist[2,3] have demonstrated that a cooperative thermally induced helix-coil occurs in many polypeptides. Zimm's theoretical approach agreed with the experimental observations accounted by Doty, Blout et al.[4-7] on poly(γ-benzyl-L-glutamate), PBLG. This homopolypeptide underwent a helix-coil transition dependent upon temperature and solvent composition. The interval of the transition was strictly related to the molecular weight of the PBLG. Zimm also evaluated the parameters of the helix formation based on previous theoretical predictions and coupled them with the optical rotation results.[1] One conclusion stated that optical rotation depends linearly on the fraction of helical residues. Karasz et al. measured the effects of deuteration and solvent

composition on helix-coil transition by optical rotation and calorimetry.[8] The transition thermodynamics was approached through the prism of Zimm-Bragg theory. A well-defined transition temperature for PBLG in dichloroacetic acid, DCA, (37% vol.)-chloroform (63% vol.) mixture was identified. The heat capacity associated with the transition was determined by calorimetry.[9] Watanabe et al. measured the dielectric constant and electric birefringence of PBLG in DCA–EDC, 1,2-dichloroethane, mixture. Addition of DCA in a small amount (~0.1%) caused a sharp change of these properties which was assigned to a helix-coil transition.[10] Ackermann et al. investigated the thermodynamics of the PBLG transition in the same solvent mixture by polarimetric measurements.[11] The critical transition temperature increased with the PBLG concentration, at constant solvent composition. This trend was also noted when the PBLG solution had equal concentration but the amount of DCA increased. Both studies seem to agree that parameters such as transition enthalpy or cooperativity are greatly dependent on concentration, temperature and solvent composition.

A less studied polypeptide with a structure similar to that of PBLG is poly(N^{ε}-carbobenzyloxy-L-lysine), PCBL. In the early 1970's the Fujita group reported a reverse random coil-to-helix transition of PCBL in m-cresol.[12,13] The data gathered by optical rotation dispersion, ORD, were fitted to the Moffit-Yang equation[14] to obtain the Moffit parameter[15] which further was used to calculate the fraction of helix during the transition from coil-to-helix. The solvent changes its viscosity with temperature.[16] The intriguing aspect in the occurrence of the transition is the unusually strong cooperativity. Omura et al. measured the optical rotation and investigated the dielectrical behavior of the dilute solutions.[17] The conformational change was assumed to evolve in all-or-none fashion, in good agreement with Karasz et al. reports.[18] The transition temperature was found to depend significantly on the molecular weight of the polypeptide: as the

molecular weight value increased the temperature moved to lower values around 27°C. The transition temperature interval increased with the decrease in the molecular weight. These observations were in good agreement with the early reports on PBLG. Fasman et al. noticed that the helix stability for PCBL is lower than for PBLG.[19] A mixture of 36% dichloroacetic acid, DCA in chloroform was sufficient to induce the transition while PBLG needed a 68%. In support of these observations came the work by Applequist and Doty.[20] They investigated PCBL of different molecular weights by light scattering, viscosity and flow birefringerence. The structure of the molecules was found to be stiffer than for a random coil especially for those polymers with a lower persistence length. Even having the same backbone structure, PCBL helices seemed to be more flexible than PBLG helices. Such behavior could be supported by Kratky-Porod "worm-like" model[21] but with the condition of having imperfect helices. The helix defects could be explained by the manner in which the amino acid side chains pack. PCBL has a bulkier side chain than PBLG therefore their freedom of motion in the helix is restricted to some extent. This feature can be considered a source of the instability among the intramolecular H-bonding, causing frequent breaks in the helix. Further confirmation on such occasional bends in the shape of the molecule was found from light scattering of the high molecular weight polymer. Such low-stability helical polypeptides were also reported at that time.[22,23] The net variation of the helix stability in the same solvent pointed out to have a great dependence of the helical structure on the nature of the side chains. It was shown that particular side chain can arrest the helix formation.[24]

The change in conformational structure motivated in-depth studies on thermodynamic and kinetic aspects, especially of helix-to-coil transition. The widely accepted model was proposed by Zimm and Bragg.[25] This model used as main parameters the free-energy preference and the cooperativity to form a helix. The dependence of the partition function on the H-bonding

was calculated. Since its formulation, the Zimm-Bragg model was used in many studies describing the kinetics and the thermodynamics of the helix-coil transition in both equilibrium and non-equilibrium. Recent investigations concentrated on the kinetics of the helix nucleation.[26-34] Various models were proposed such as temperature jump kinetics,[35,36] Ising models,[37,38] or conformational diffusion.[29] All seem to agree to some extent with Zimm-Bragg theory: the formation of the first turn of the helix is dominated by a consistent reduction in entropy. This feature makes difficult the construction of the nascent helix but once formed the turn acts as a nucleus for other helices by adding H-bonds. In addition to entropic effects, a boundary tension was explained to occur as a consequence of missing H-bonds at the adjacent segments.[25] The competition between available degrees of freedom in the coil and the helix fragments respectively, was shown to impact greatly the cooperativity in the helix-coil transition.[39]

Tethering the polypeptide on a surface may affect the dynamics when compared with the free polymer because of restrictions on the freedom degree. The first study on the PCBL silica-tethered magnetic colloid performed in Russo laboratory showed a consistent variation in size of the composite particle suspended in m-cresol as a function of the temperature as shown in Figure 5.1. Data corresponding to cycle 4 on cooling didn't seem to agree with the cycle 3 on heating. The possible causes and their effects on the measurements will be addressed in the Results and Discussion section.

This chapter concerns the study of the reversible, inverse-type helix-to-coil transition in m-cresol of PCBL tethered on silica as a response to temperature variation. The polypeptide hybrid particle was prepared by ring-opening polymerization of corresponding N-carboxyanhydride[40,41] using amino-functionalized silica cores as an initiator. The cores are

simple Stöber silica with slight modifications.[42-46] In order to expand the field of applications silica cores were covalently-labeled with fluorescein isothiocyanate, FITC.

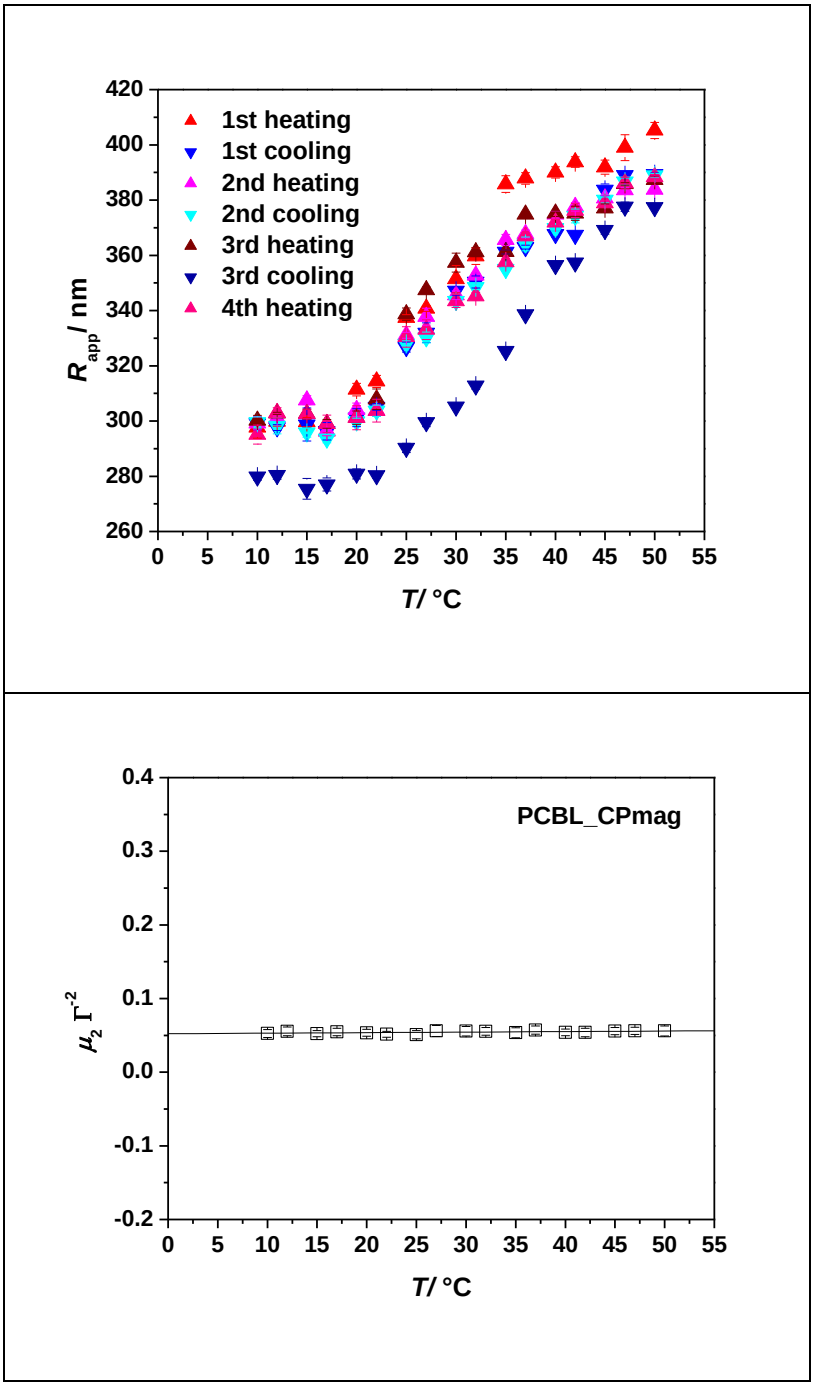

Figure 5.1 Dynamic light scattering data: (A) apparent radius, R_{app}, as a function of the scattering vector magnitude, q, and (B) polydispersity index, $\mu_2\ \Gamma^{-2}$ of PCBL-CPmag.

The combination of light and small angle X-ray scattering techniques was mainly used to test the following hypothesis: as a consequence of conformational changes the colloid size may vary in size with the temperature both on heating and cooling mode. The novelty of this work arises from the fact that the polypeptide chain free motion was partially arrested by attachment to a well-defined core in terms of the size and the curvature. In addition to this, different grafting densities were used to investigate the crowding effect on the transition. Observations on the PCBL-CP nurtured on a silica bead having a magnetic nugget were previously made in this group.[47] ^{1}H NMR experiments were also conducted to determine the longitudinal or spin-lattice relaxation time, T1. NMR measurements were not possible for the particles whose transition appears in Figure 5.1A and Figure 5.7A because they were magnetic. Modulated differential scanning calorimetry was used as a complementary method to investigate thermal behavior of the tethered and untethered polypeptide during the coil-to-helix transition. The data gathered with this blend of techniques point to a complicated landscape for the coil-to-helix transition in PCBL-m-cresol.

5.2 Materials.

Nε-carbobenzyloxy-L-lysine, CBL, (99%) was purchased from Acros Organics. Triphosgene (99%) was obtained from TCI America. Anhydrous solvents such as ethyl acetate, EtOAc, tetrahydrofuran, THF, hexanes were procured from Sigma Aldrich. Tetraethylorthosilicate, TEOS, 3-aminopropyltriethoxy silane, APTS, sodium bicarbonate, fluorescein isothiocyanate (99%) were also purchased from Sigma Aldrich. Absolute ethyl alcohol 200 proof ACS/USP grade was obtained from Pharmco-AAPER. Ammonium hydroxide 28-30% ACS grade was purchased from BDH Aristar. All reagents were used without further purification. Deionized water (18 mΩ) was drawn from a Barnstead Nanopure instrument.

5.3 Syntheses.

The preparatory steps involved in the production of PCBL-coated silica particles are presented elsewhere (Chapter 8, Section 8.4, 8.7, 8.8.2, 8.8.7 and 8.8.8).

5.4 Results and Discussion

5.4.1 Confirmation of the Polypeptide on the Core Surface.

Polypeptide composite particles carying a shell comprised of poly(N^{ε}-carbobenzyloxy-L-lysine), PCBL-CPs, were prepared by the *growing from* method. Details on the preparation are available in Chapter 8. The visualization of the PCBL-CPs was achieved by TEM, as shown in Figure 5.2. The staining procedure involving exposure to OsO_4 vapors, revealed the presence of the polypeptide corona (the dark shadow) surrounding the silica hard cores.

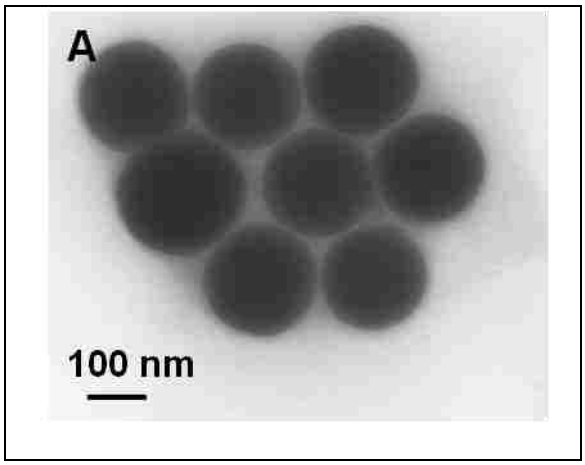

Figure 5.2 TEM micrographs of PCBL-CPs stained with OsO_4: PCBL-CP100 (A) (CR810B), PCBL-CP55 (B) CR810A) and PCBL-CP175L (C) (CR7188). The shadow around the particle is the polypeptide shell.

Figure 5.2 continued

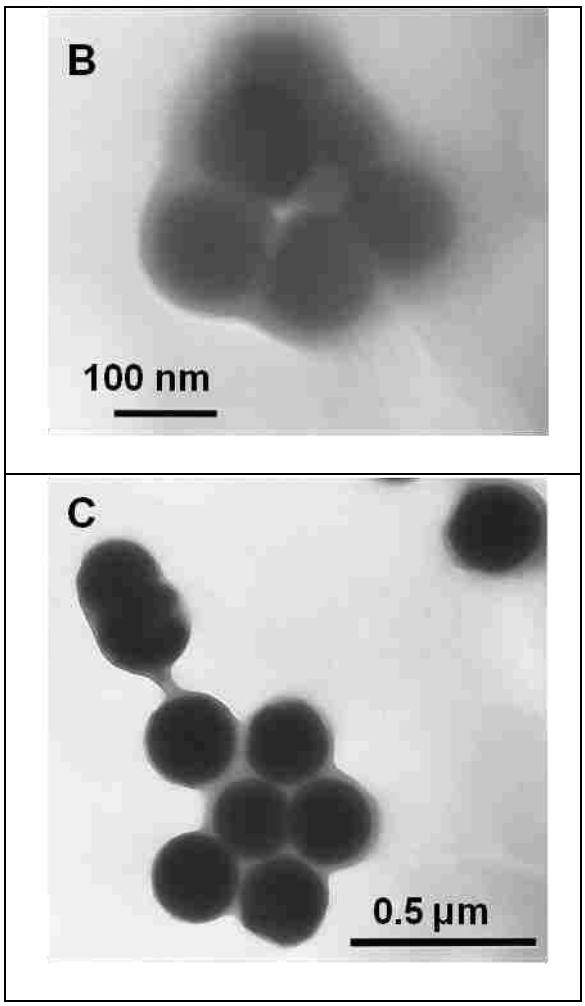

In the abbreviated particle name, the numbers denote the radius of the silica core and H/L is the grafting density, high/low, with amino groups prior polymerization, (e.g., PCBL175H). The presence of the PCBL on the particle surface was also investigated by thermogravimetric analysis, TGA. Figure 5.3 displays TGA traces of the silica cores, amino-functionalized particles and polypeptide-coated particles. The weight loss associated with the peptide loading onto the silica surface is listed in Table 5.1 for all samples employed in this investigation.

Table 5.1 Sample Code, Percentage Loss and Grafting Density with amino Groups for PCBL-CP samples

Sample Code	Shell Mass Loss (%)	$S_{spec.}$ /m^2 g^{-1}	σ /mmol m^{-2}	σ /mmol g^{-1}	NH_2 groups /nm^2	silane layers*
PCBL175L (CR7188)	55.8	8.66	$0.026 \pm 1.3\times10^{-3}$	0.23 ± 0.011	16 ± 0.8	4
PCBL175H (CR7160)	34.6	8.66	$0.034 \pm 1.7\times10^{-3}$	0.29 ± 0.014	20 ± 1.0	5
PCBL100H (CR810B)	13.5	15.15	$0.006 \pm 0.3\times10^{-3}$	0.17 ± 0.008	4 ± 0.2	1
PCBL55H (CR810A)	55.5	27.5	$0.003 \pm 1.5\times10^{-4}$	0.09 ± 0.004	2 ± 0.1	1

*the maximum number of aminosilanes *per* nm^2 is 4.[48]

The weight loss up to 200°C is due to adsorbed water. The decomposition from 200 to ~600°C can be assigned to the polypeptide coating the particle surface. PCBL-CPs were designed to have different surface coverage: from a crowded to a sparse population. The first step in achieving such grafting was the control over the number of the initiator molecules (e.g. amino groups) attached on the surface. The TGA profiles allowed the computation of the initiator grafting density using the following formula:[49,50]

$$\sigma_{APTS} = \frac{w_{\text{Si-APTS}} - w_{Si} \times [1 - w_{\text{Si-APTS}}]}{M \times S_{\text{spec}} \times [1 - w_{\text{Si-APTS}}]} \qquad Eq.\,5.1$$

where $w_{\text{Si-APTS}}$ and w_{Si} are the measured fractional weight losses associated with decomposition of the amino groups and silica cores respectively, M is the molecular weight of the grafted amino silane (APTS) and S_{spec} represents the specific surface area of the silica nanoparticles.

PCPs having a larger core, Figure 5.3A, had $0.026 \pm 1.3\times10^{-3}$ mmol m^{-2} grafting density with initiators. Considering a surface specific area of 8.66 m^2 g^{-1} and the silica density of silica 1.96 g cm^{-3} the number of initiators estimated per nm^2 was 16 ± 0.8. This value revealed that the amino silane condensed into four subsequent layers because, for monolayer coverage, only 3-5 silanol groups[51] are available for condensation of the organosilane molecules, leading to four amino

functionalities per nm^2.[52] The projection of an organosilane on the surface was taken as 0.25 nm^2, the most agreed value. PCBL-CP175H, Figure 5.3B had a higher amino grafting density estimated to $0.034 \pm 1.7\times10^{-3}$ $mmol\bullet m^{-2}$, with 20 ± 1.0 initiators arranged into five layers. Lower loadings with amino moieties were achieved for PCBL-CP100H, Figure 5.3C and PCBL-CP55H, Figure 5.3D. The first had $0.006 \pm 0.3\times10^{-3}$ $mmol\bullet m^{-2}$ functions equivalent to 4 ± 0.2 initiators per nm^2. For the second the grafting density was designed even lower, $0.003 \pm 1.5\times10^{-4}$ $mmol\bullet m^{-2}$ meaning 2 ± 0.1 functional moieties per nm^2. Both last-discussed PCBL-CPs had monolayer distribution of the amino silane on their surface. In order to compute the initiator efficiency the polypeptide was cut off from the surface by dissolution of the silica core in ~10% NaOH. Chapter 8 presents the detailed strategy and calculations.

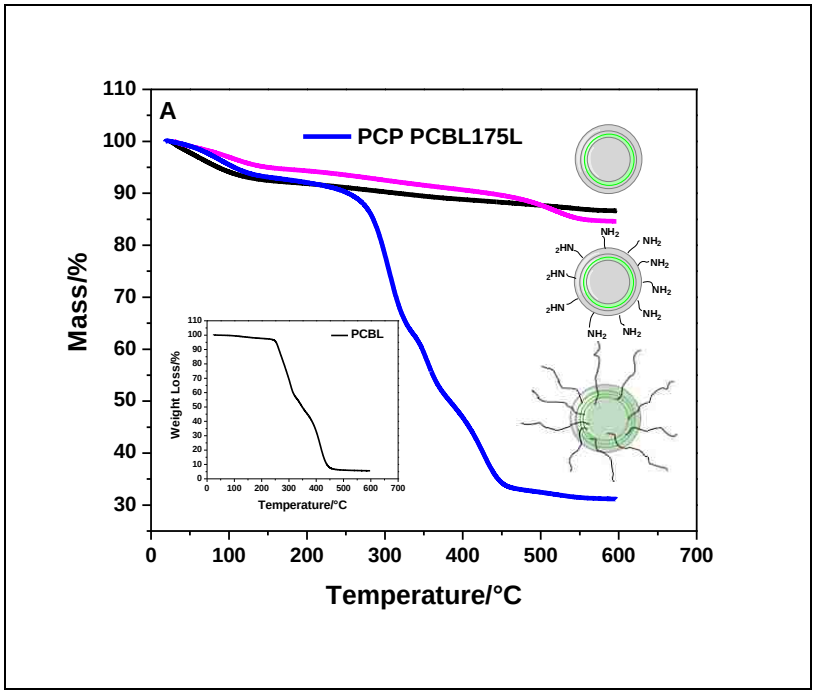

Figure 5.3 TGA profile of silica cores (−), amine-functionalized particles (−) and PCBL-CPs (−): (A) PCBL-CP175L (inset untethered PCBL), (B) PCBL-CP175H, (C) PCBL-CP100H and (D) PCBL-CP55H.

Figure 5.3 continued

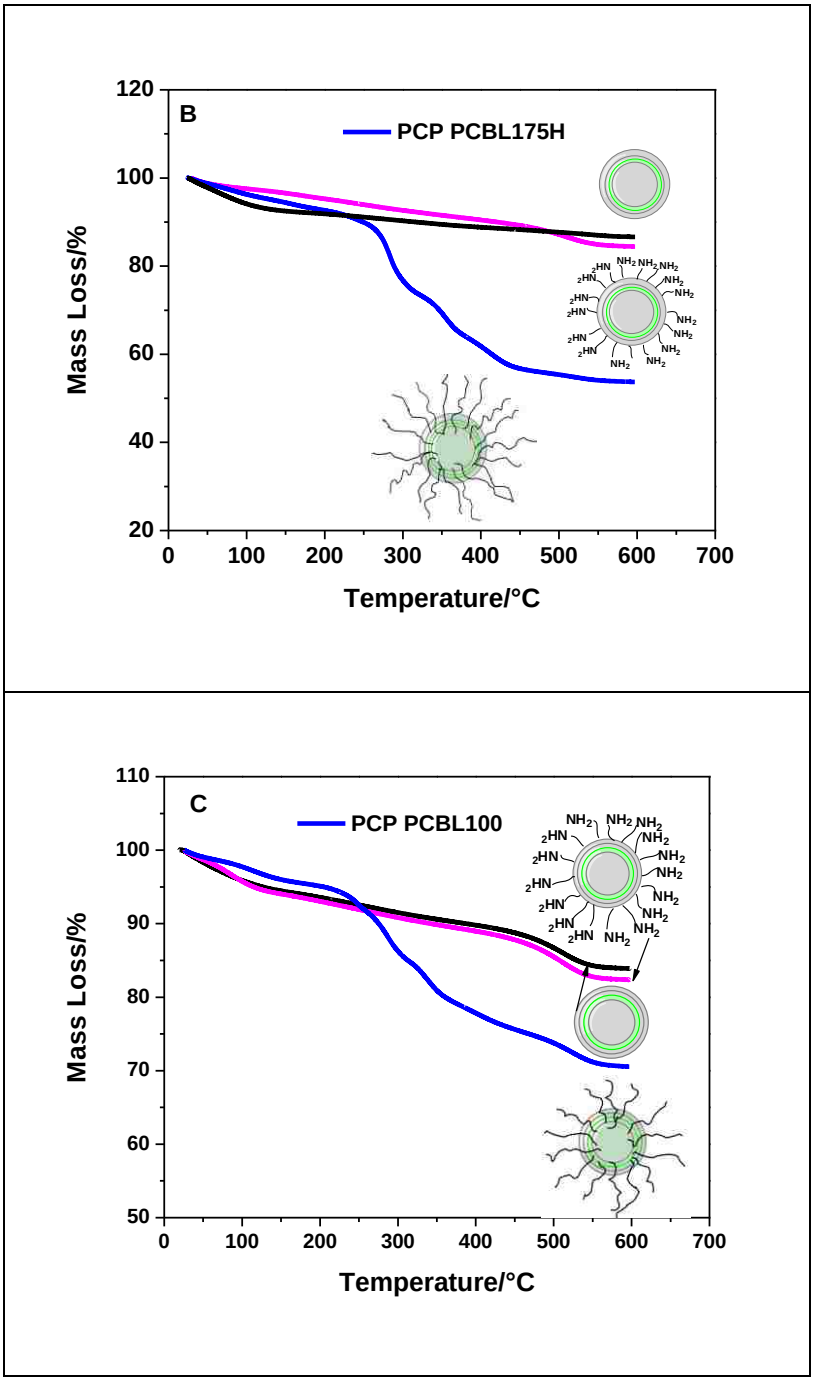

Figure 5.3 continued

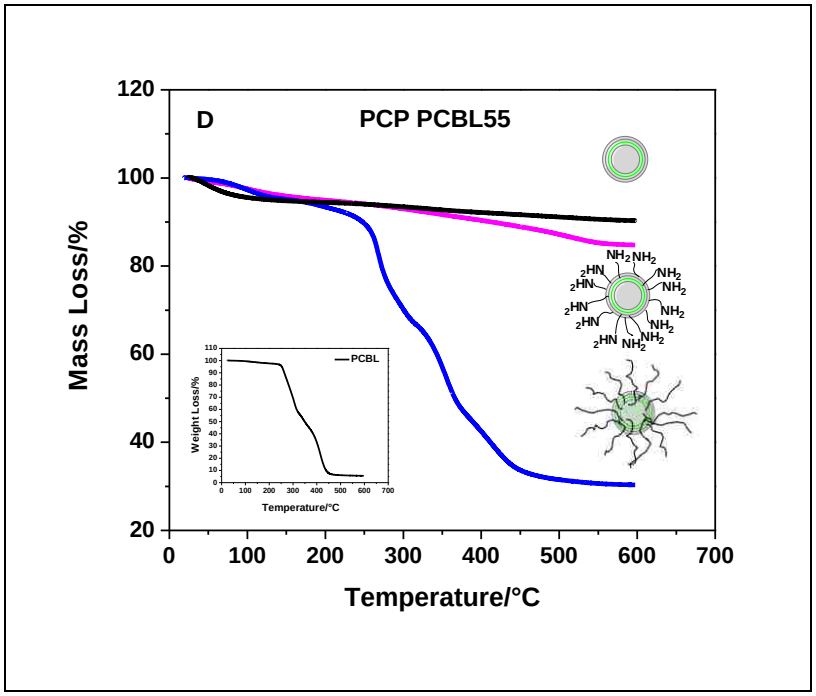

It was found that PCBL-CP175L had a grafting density of 0.9 ± 0.045 μmol•m^{-2} polypeptide, meaning 209,000 ± 10,000 chain per particle. Taking in account the initiator grafting density, 26 ± 1.3 μmol·m^{-2}, this leads to 3.5% grafting efficiency. Indeed this number suggests that many amino groups were not able to initiate the ROP of NCA into homopolypeptide chains. Small traces of moisture could also result in the initiation of the polymer chains which might grow as free polymer in the solution. In multilayer disposition the organosilanes carrying the functional groups can polymerize in a vertical fashion. That means some of the amino groups can be "buried" inside of a sublayer, thus they are hindered from initiating the polymerization. Only the functional moieties from the top layer can actively participate in the ROP of NCA. Consequently, in a multilayer arrangement, the aminosilane can act both as an activator and a passivator in the same time. The amino group content from the silica surface was also evaluated by zeta potential at low pH (1.46) because amino moieties are

charged.[48,52-54] Figure 5.4 presents the dependency of the surface charge on the grafting density and the number of the functionalities calculated from TGA.

PCBL-CPs with a higher calculated number of functional groups in a multilayer disposition had similar potential with the PCPs having monolayer of amino groups. This result confirmed the assumptions made upon calculations from TGA and clearly proves that for multilayer an important part of the functional groups are not available for initiating the polymerization due to steric hindrance.

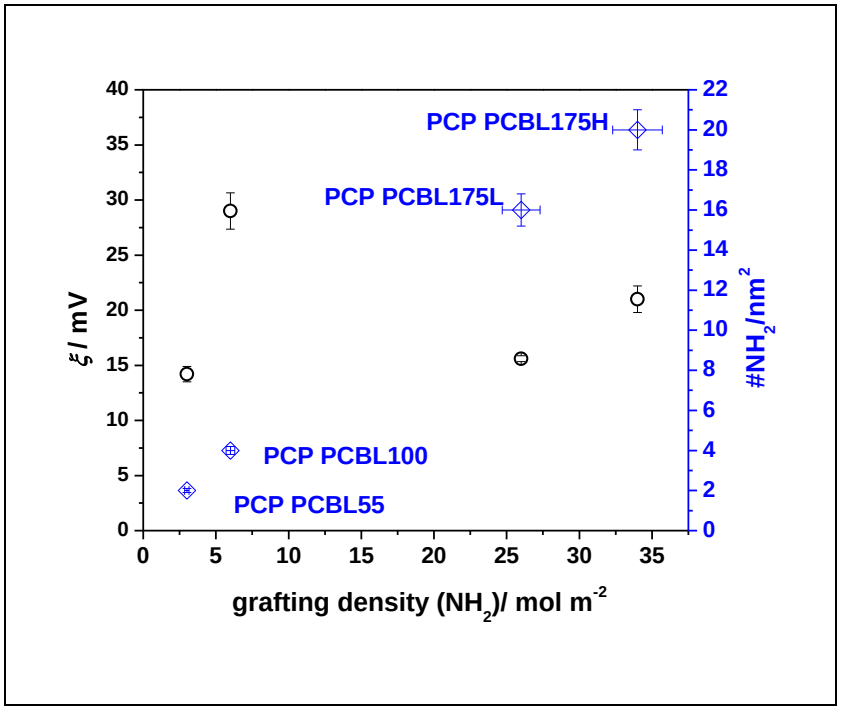

Figure 5.4 Zeta potential as a function of amino grafting density and the number of amino groups per squared nanometer.

5.4.2 Light Scattering

The size of the PCBL-CPs was investigated, first, by light scattering assays. Dynamic light scattering was a convenient tool to measure the deviation in the particle size during the inverse helix-to-coil transition as a function of the temperature.

In the Introduction section was presented the first study on this transition when the PCBL was tethered to a magnetic silica bead. The profile of the data gave rise to concerns regarding the presence of the free polymer in the solution. Free polypeptide can affect the viscosity of the solution. Because the Stökes-Einstein relation uses the solvent viscosity in the radius calculations, a divergence between the real medium viscosity and the one used in calculations can affect the results. In order to test such issues, the original sample of magnetic PCBL-CP (now almost 10 years old) was separated from the old solvent and suspended in a fresh one by centrifugation. The size of the PCBL-CPs was tested first at 20°C and 45°C by multi-angle DLS in both the old and fresh solvent for comparison purposes, as shown in Figure 5.5.

Once the old solvent was replaced with a fresh one the fitting of the size improved. The polydispersity index slope fitting, the insets of the Figure 5.5A1 and 5.5B1 has a higher value than the slope from fitting the polydispersity data of the sample in fresh solvent, insets of the Figure 5.5C1 and Figure 5.5D1.

The profile of the apparent diffusion coefficients and apparent radius presented in Figure 5.5A and 5.5A1 can be explained in two ways: the particles could coalesce in aggregate structures or the viscosity of the medium was not the same when fitting the data as was mentioned in the Introduction section. Yet, the difference in size computed at low and high angles is low for an aggregated colloid. In order to have more information about the factor that could affect the trend of the size displayed in Figure 5.1A, the viscosities of the old and fresh solvent was measured and plotted against temperature as seen in Figure 5.6.

The profile of the apparent diffusion coefficients and apparent radius presented in Figure 5.5A and 5.5A1 can be explained in two ways: the particles could coalesce in aggregate

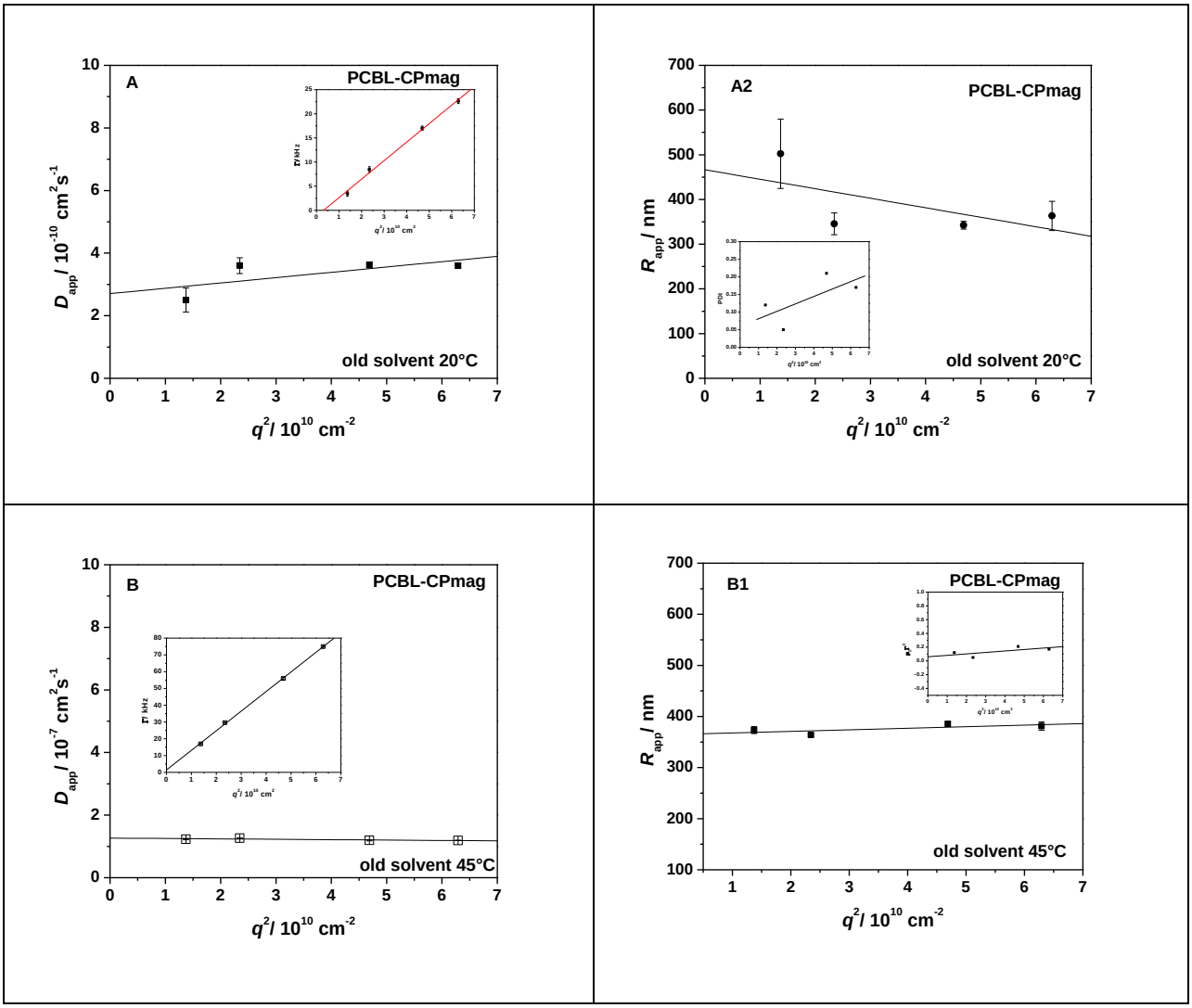

Figure 5.5 Dynamic light scattering representation of PCBL-CPmag: (A) apparent diffusion coefficients as a function of scattering vector magnitude, *q*, (inset) first cumulant versus q^2 (old solvent, 20°C), (A1) apparent radius as a function of scattering vector magnitude, *q*, (inset) polydispersity index, μ_2 Γ^{-1} (old solvent 20°C), (B) apparent diffusion coefficients as a function of scattering vector magnitude, *q*, (inset) first cumulant versus q^2 (old solvent, 45°C), (B1) apparent radius as a function of scattering vector magnitude, *q*, (inset) polydispersity index, μ_2 Γ^{-1} (old solvent 45°C), (C) apparent diffusion coefficients as a function of scattering vector magnitude, *q*, (inset) first cumulant versus q^2 (fresh solvent, 20°C), (C1) apparent radius as a function of scattering vector magnitude, *q*, (inset) polydispersity index, μ_2 Γ^{-1} (fresh solvent 20°C) and (D) apparent diffusion coefficients as a function of scattering vector magnitude, *q*, (inset) first cumulant versus q^2 (fresh solvent, 45°C), (D1) apparent radius as a function of scattering vector magnitude, *q*, (inset) polydispersity index, μ_2 Γ^{-1} (fresh solvent 45°C).

Figure 5.5 continued

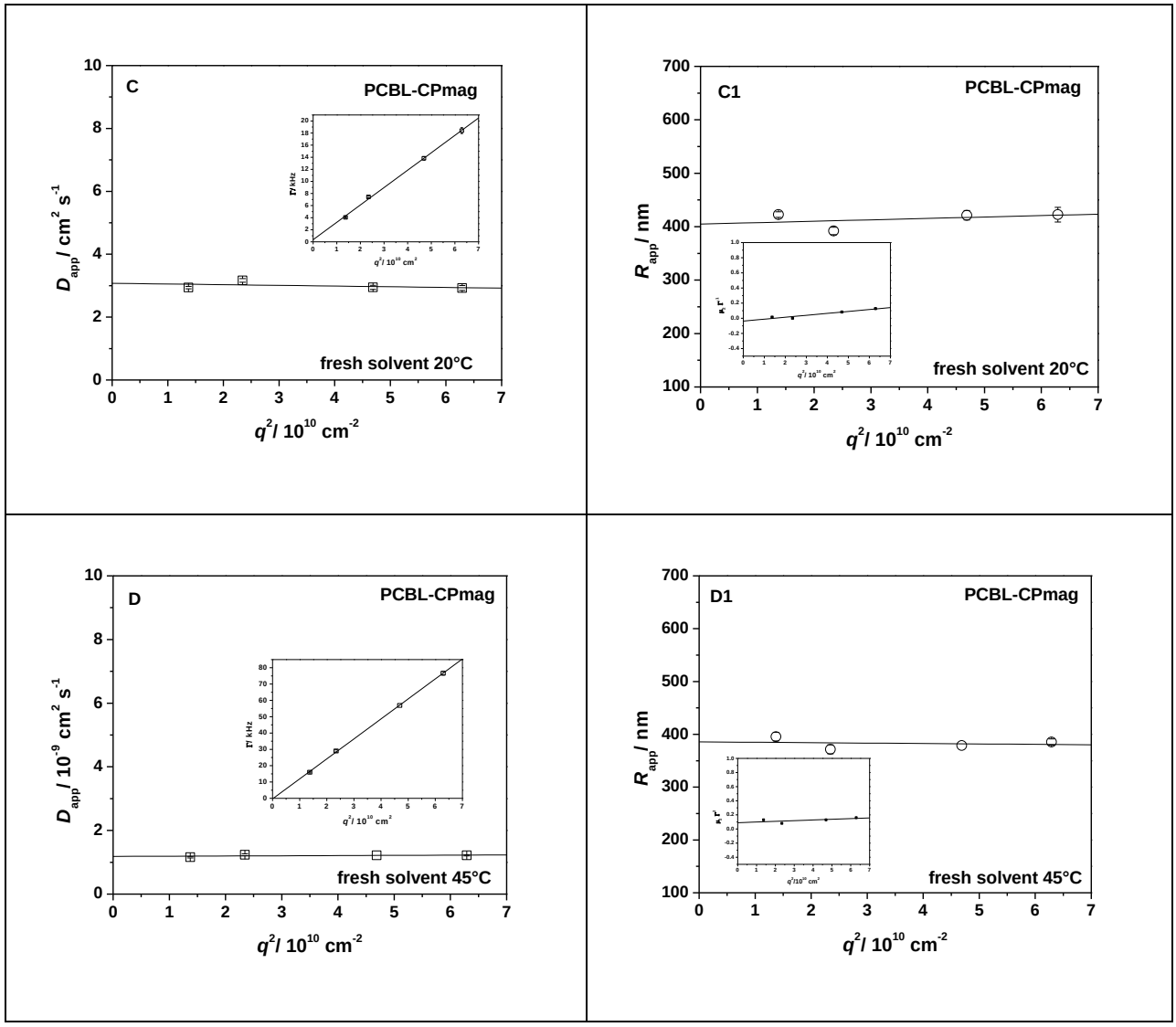

structures or the viscosity of the medium was not the same when fitting the data as was mentioned in the Introduction section.

The profile of the apparent diffusion coefficients and apparent radius presented in Figure 5.5A and 5.5A1 can be explained in two ways: the particles could coalesce in aggregate structures or the viscosity of the medium was not the same when fitting the data as was mentioned in the Introduction section. Yet, the difference in size computed at low and high

angles is low for an aggregated colloid. In order to have more information about the factor that could affect the trend of the size displayed in Figure 5.1A, the viscosities of the old and fresh solvent was measured and plotted against temperature as seen in Figure 5.6.

The Figure 5.6 shows evidence of altered solvent. The values of the measured viscosity didn't overlap with those reported in the literature and the fresh solvent. Over time, m-cresol can absorb water and can undergo oxidation. Fresh m-cresol is colorless or slight amber-like color; instead the old one had a strong yellow to red coloration. These data suggest that the lower viscosity of the old solvent due to both free polypeptide in solution and its degradation might affect the size measurements as seen in Figure 5.1A. PCBL-CPmag composite suspended in fresh solvent was subjected to multiple cycles on both heating and cooling using one-angle dynamic light scattering instrument from Malvern. The flatness of R_{app} versus q^2 plots (Figure 5.5) suggests one-angle measurements should be valid.

Figure 5.7 shows a significant difference in the size trend with the temperature as displayed in Figure 5.1A. At low temperatures the polypeptide is in a random coil conformation. The Figure 5.7A shows a descending trend of the radius up to 30°C followed by a sharp increase and then falls again to smaller values. The abbreviation of this trend will be presented later in this document. The polydispersity index, Figure 5.7A1 seems to remain relatively constant up to 30°C but began to rise in values and level out again but in this plot the error bars make it difficult to be certain of the behavior. The intensity plot against the temperature interval 15-50°C, Figure 5.7A2, suggested a sharp decrease followed by an increase and after a flat zone can be identified. Since the data were collected at the same angle and were viscosity corrected, a linear profile of the intensity was expected.

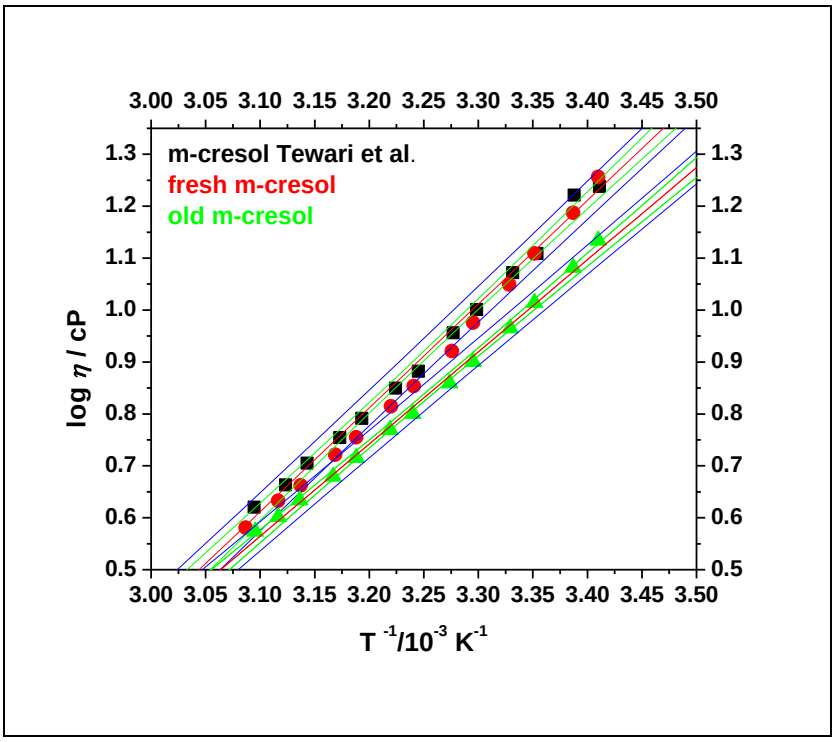

Figure 5.6 The ten base logarithmic representations of the old and fresh m-cresol as well as the literature reported values as a function of inverse Kelvin temperature. The red lines are the linear fits. The green and blue lines represent the upper and the lower confidence and prediction limits.

Hence, the plots presented in Figure 5.7 suggest that the transition of PCBL-tethered on silica might be more complex than a simple coil-to-helix conformational change. Besides the still "alive" fluctuation in size with temperature of the ten years old PCBL-CPmag, these experiments also reflects the stability of the CPs with time.

The newly produced (by the present author) nonmagnetic PCBL-CPs were analyzed in the same fashion as Turksen's magnetic counterparts. Preliminary experiments were performed, first, to evaluate whether the PCBL-CPs behaved as a uniform colloid. Measurements were performed at the extremities of the transition temperature interval, 15°C and 50°C respectively. Figure 5.8 shows the data recorded at 15°C.

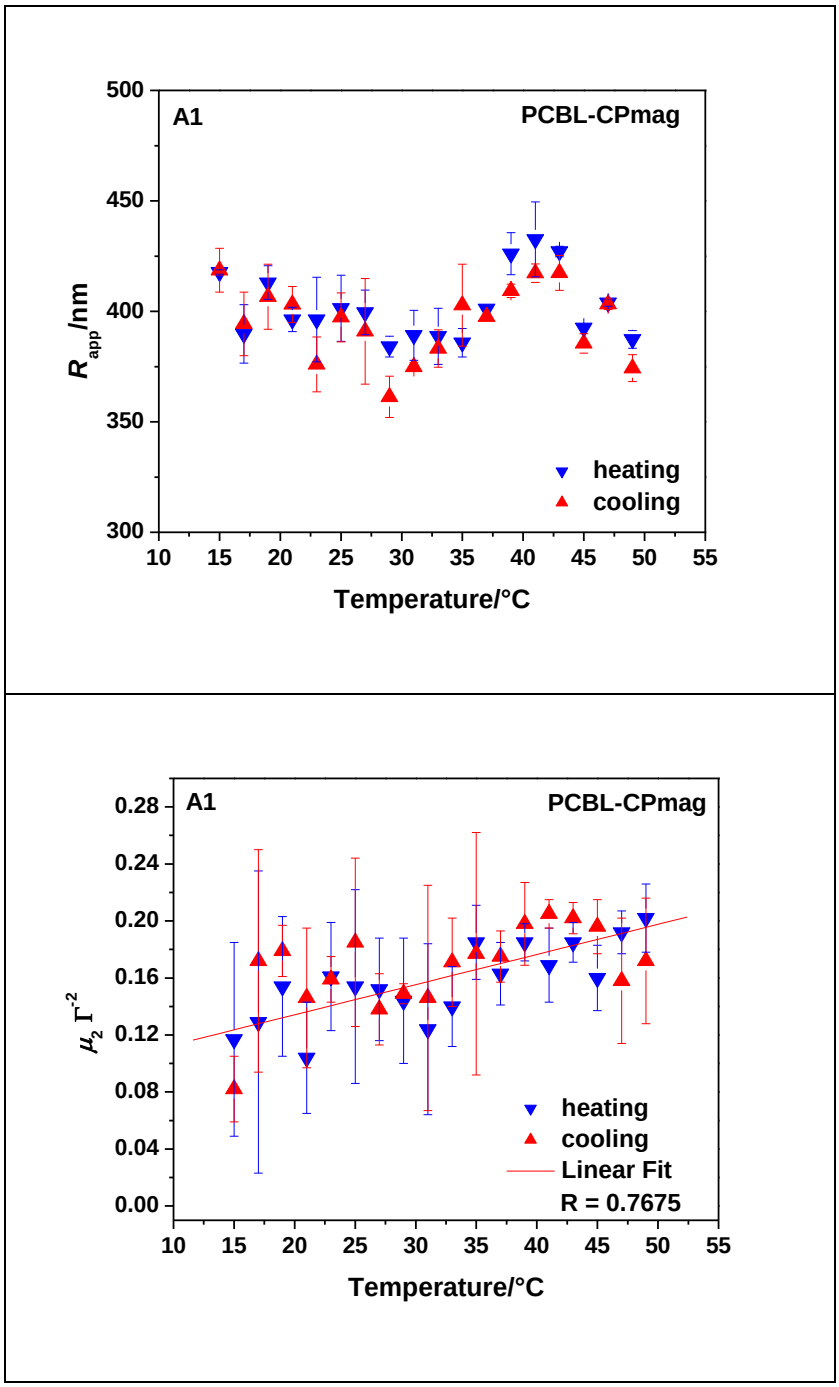

Figure 5.7 Dynamic light scattering data: (A) apparent radius, R_{app}, as a function of the temperature, (A1) polydispersity index, $\mu_2 \cdot \Gamma^{-2}$ as a function of the temperature and (A2) the intensity profile as a function of the temperature. The red and blue lines represent the linear regression applied to the data.

Figure 5.7 continued

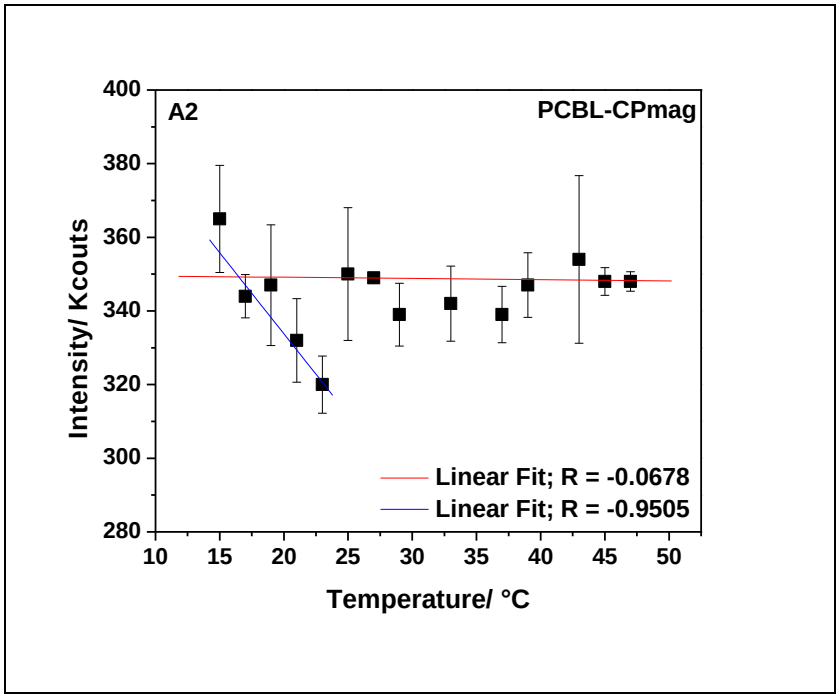

Because the contribution from the smaller particles becomes more evident at higher angles, a broad distribution could interfere greatly with the data interpretation regarding the shell transition. As shown in Figure 5.8, particles did not show significant angle dependence, and in agreement with TEM images these PCBL-CPs can be considered monodisperse. After the independent trend of the radius with the angle was confirmed by multi-angle measurements, the one-angle Malvern instrument was used to examine the reversibility of the transition. At least four cycles on heating-cooling modes were recorded for each sample. The values of the radius are reported as an average over three sets of measurements, each of 600s duration. Samples were equilibrated 30 min. at each temperature before the measurement. Figure 5.9A shows the trend recorded for PCBL-CP175L.

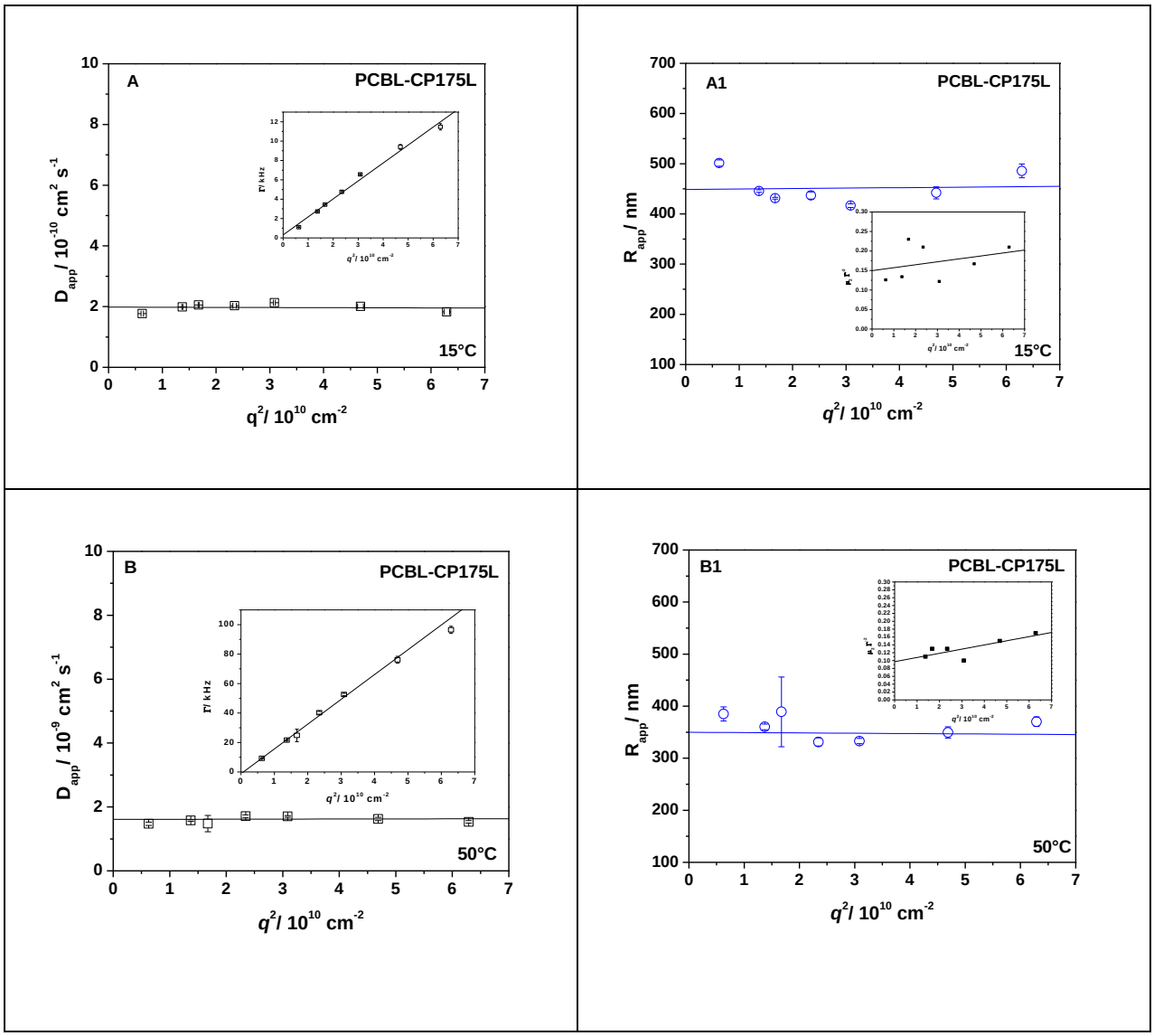

Figure 5.8 Light scattering results for PCPs dispersed in m-cresol as a function of squared scattering vector magnitude: apparent diffusion coefficients, D_{app} (A) PCBL-CP175L (15°C, CR7188), (B) PCBL-CP175L (50°C, CR7188), (C) PCBL-CP175H (15°C, CR7160), (D) PCBL-CP175H (50°C, CR7160), (E) PCBL-CP50H (15°C, CR810A), (F) PCBL-CP50H (50°C, CR810A), (G) PCBL-CP100H (15°C, CR810B), (H) PCBL-CP50H (50°C, CR810B) insets represent the decay rates as a function of squared scattering vector magnitude, and apparent radius, R_{app} (A1) PCBL-CP175L (15°C, CR7188), (B1) PCBL-CP175L (50°C, CR7188), (C1) PCBL-CP175H (15°C, CR7160), (D1) PCBL-CP175H (50°C, CR7160), (E1) PCBL-CP50H (15°C, CR810A), (F1) PCBL-CP50H (50°C, CR810A), (G1) PCBL-CP100H (15°C, CR810B), (H1) PCBL-CP50H (50°C, CR810B), insets represent the polydispersity index, $\mu_2 \cdot \Gamma^{-2}$, as a function of squared scattering vector magnitude. The red line is fitting excluded the angles at which the fitting was not linear.

Figure 5.8 continued

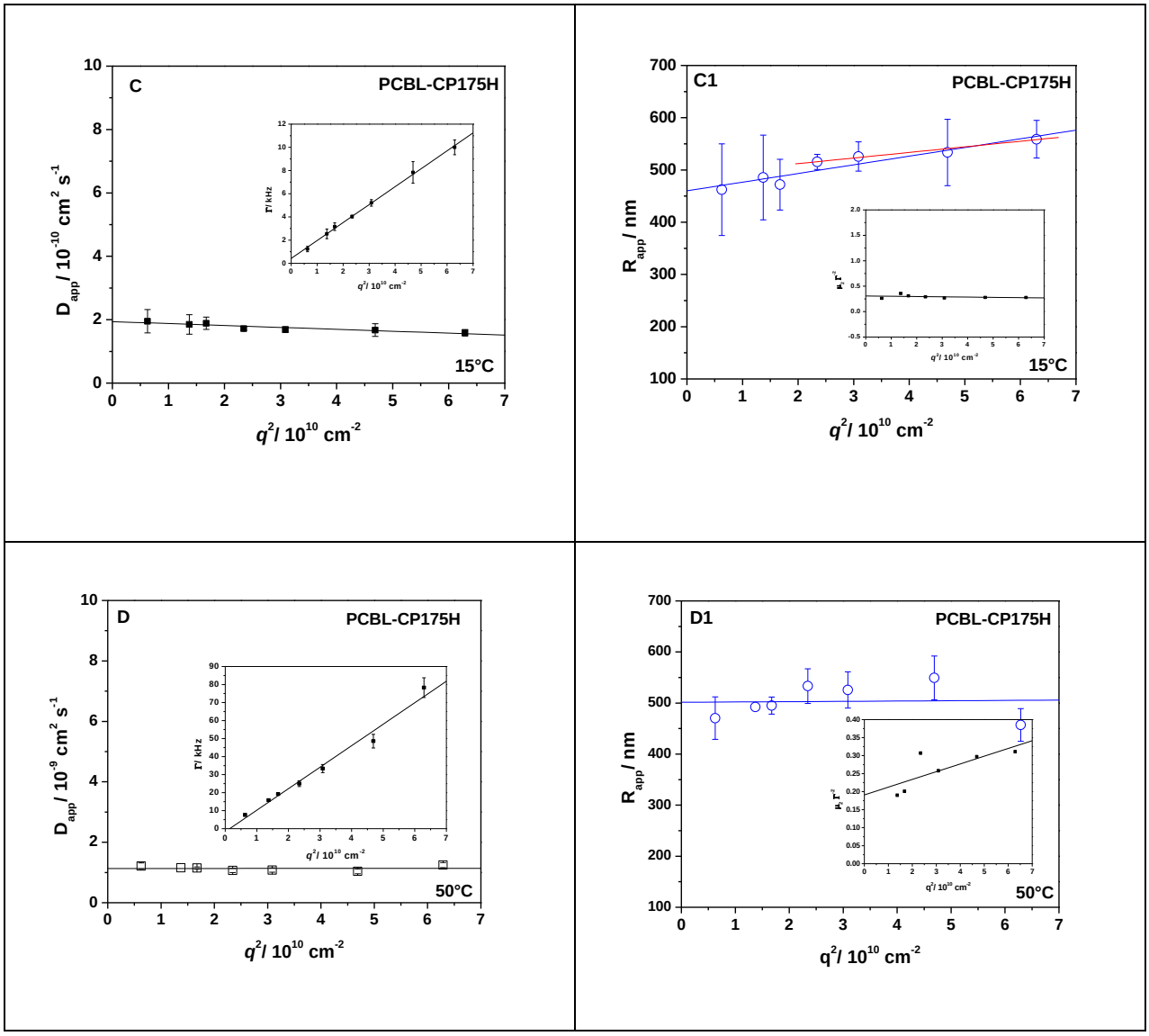

Figure 5.8 continued

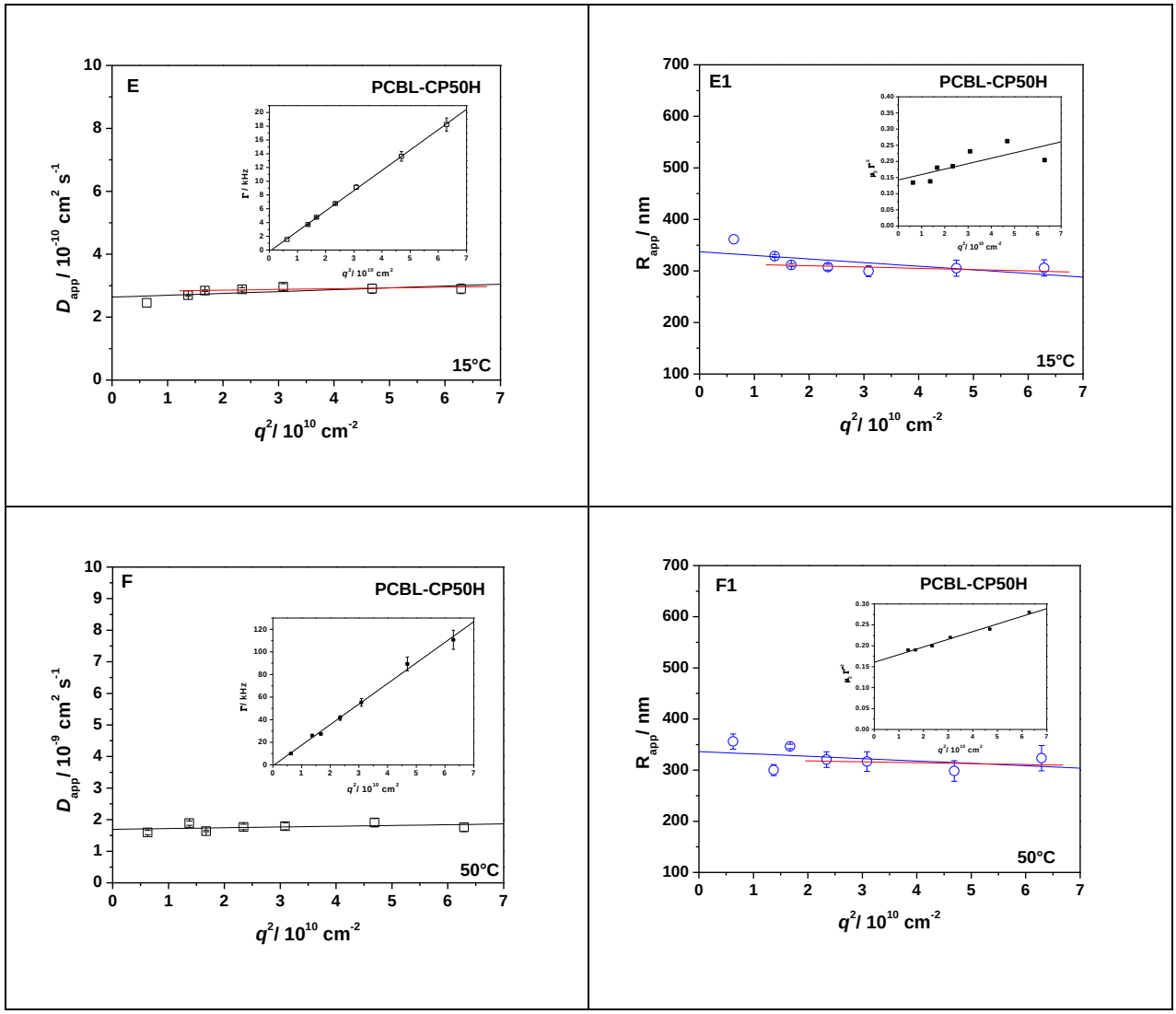

Figure 5.8 continued

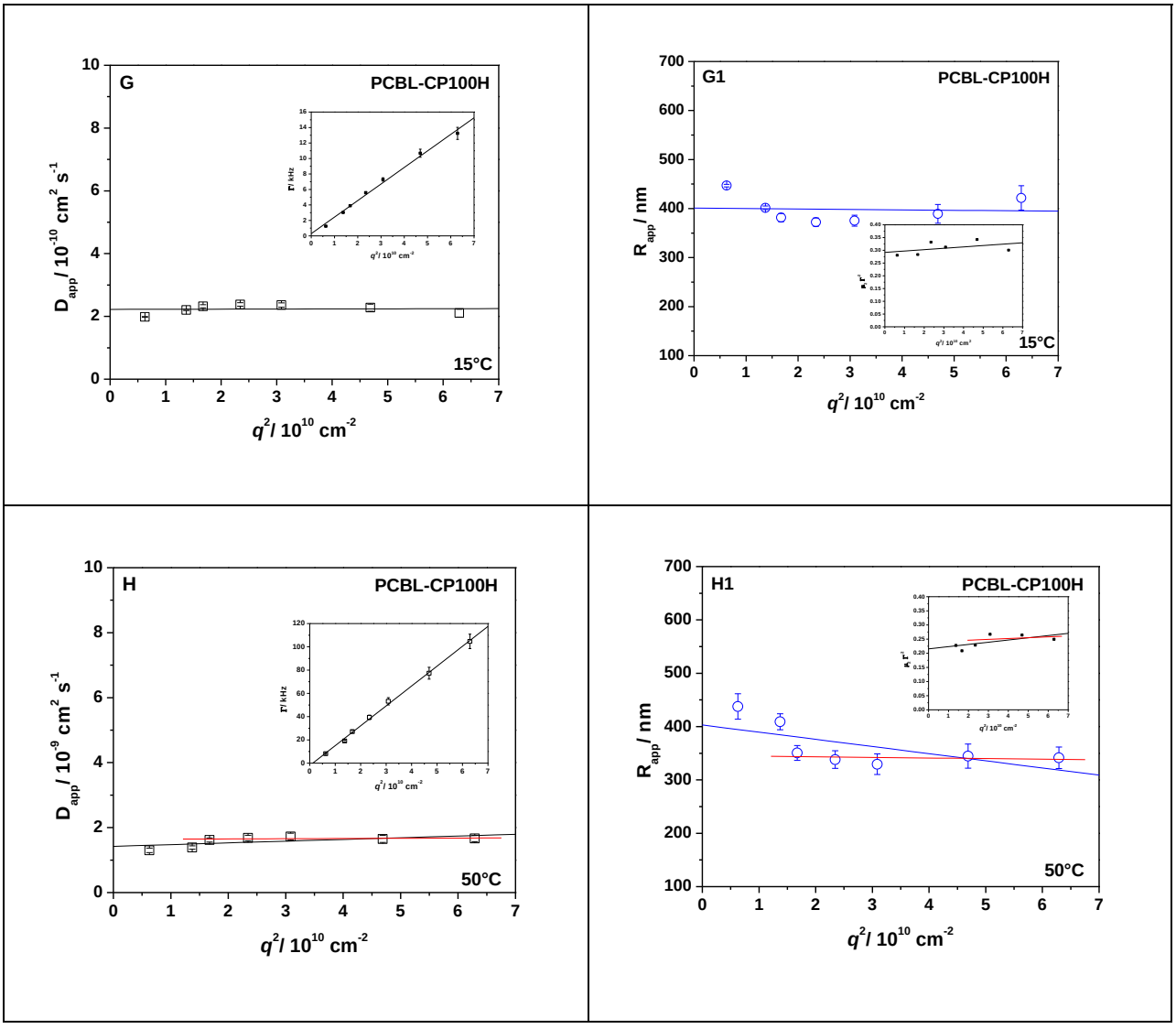

After the independent trend of the radius with the angle was confirmed by multi-angle measurements, the one-angle Malvern instrument was used to examine the reversibility of the transition. At least four cycles on heating-cooling modes were recorded for each sample. The values of the radius are reported as an average over three sets of measurements, each of 600s duration. Samples were equilibrated 30 min. at each temperature before the measurement. Figure 5.9A shows the trend recorded for PCBL-CP175L.

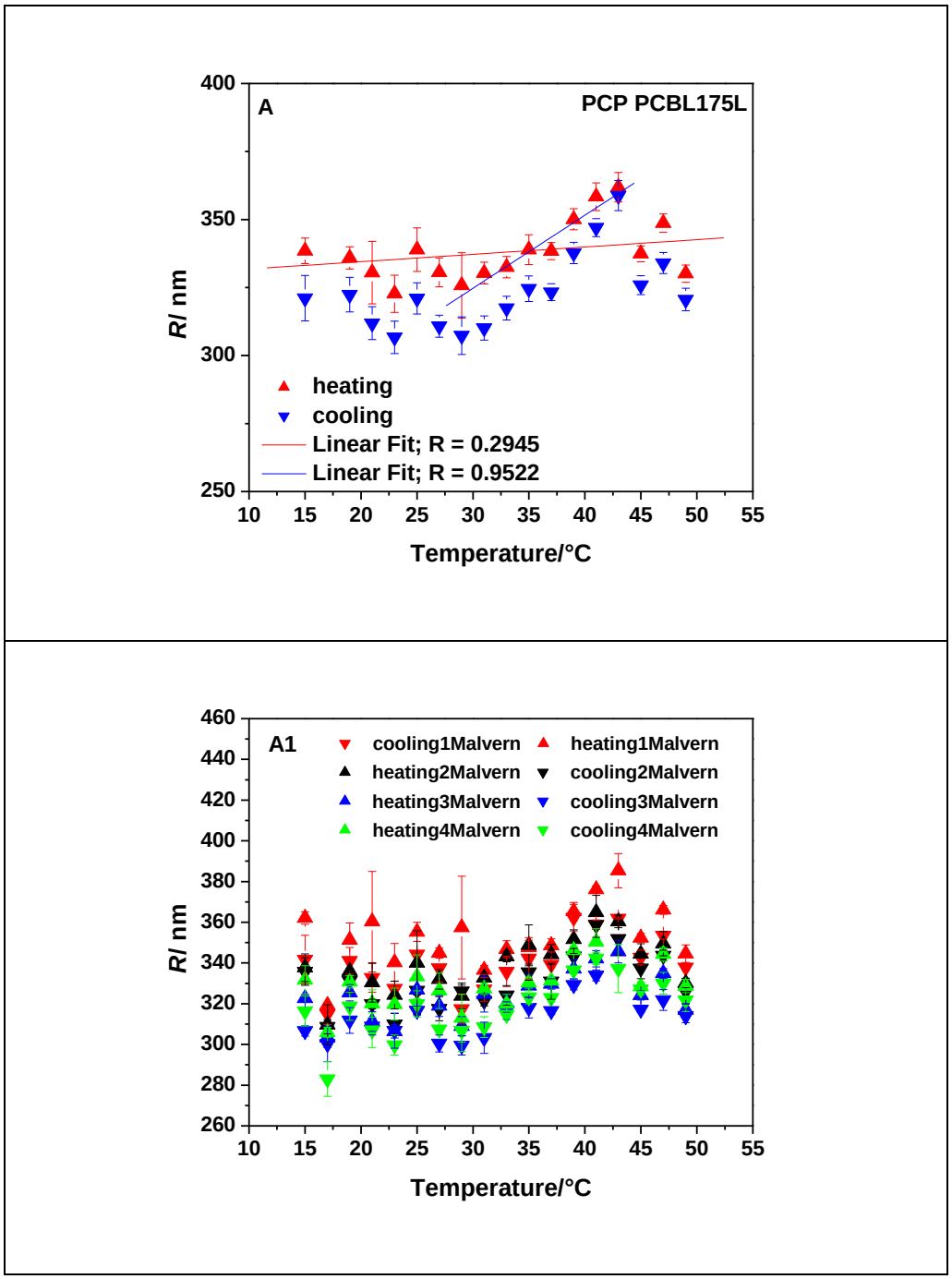

Figure 5.9 One angle dynamic light scattering results: (A) average apparent radius on cooling-heating as a function of temperature, for PCBL-CP175L, (A1) radius versus temperature trend over four cycles on heating-cooling for PCBL-CP175L (CR7188), (A2) polydispersity index, μ_2/Γ^2, as a function of temperature for all four heating-cooling cycles, and (B) control experiment showing independent trend of the radius with the temperature for polystyrene latex in water. The measurement for PCP PCBL175L was performed in m-cresol.

Figure 5.9 continued

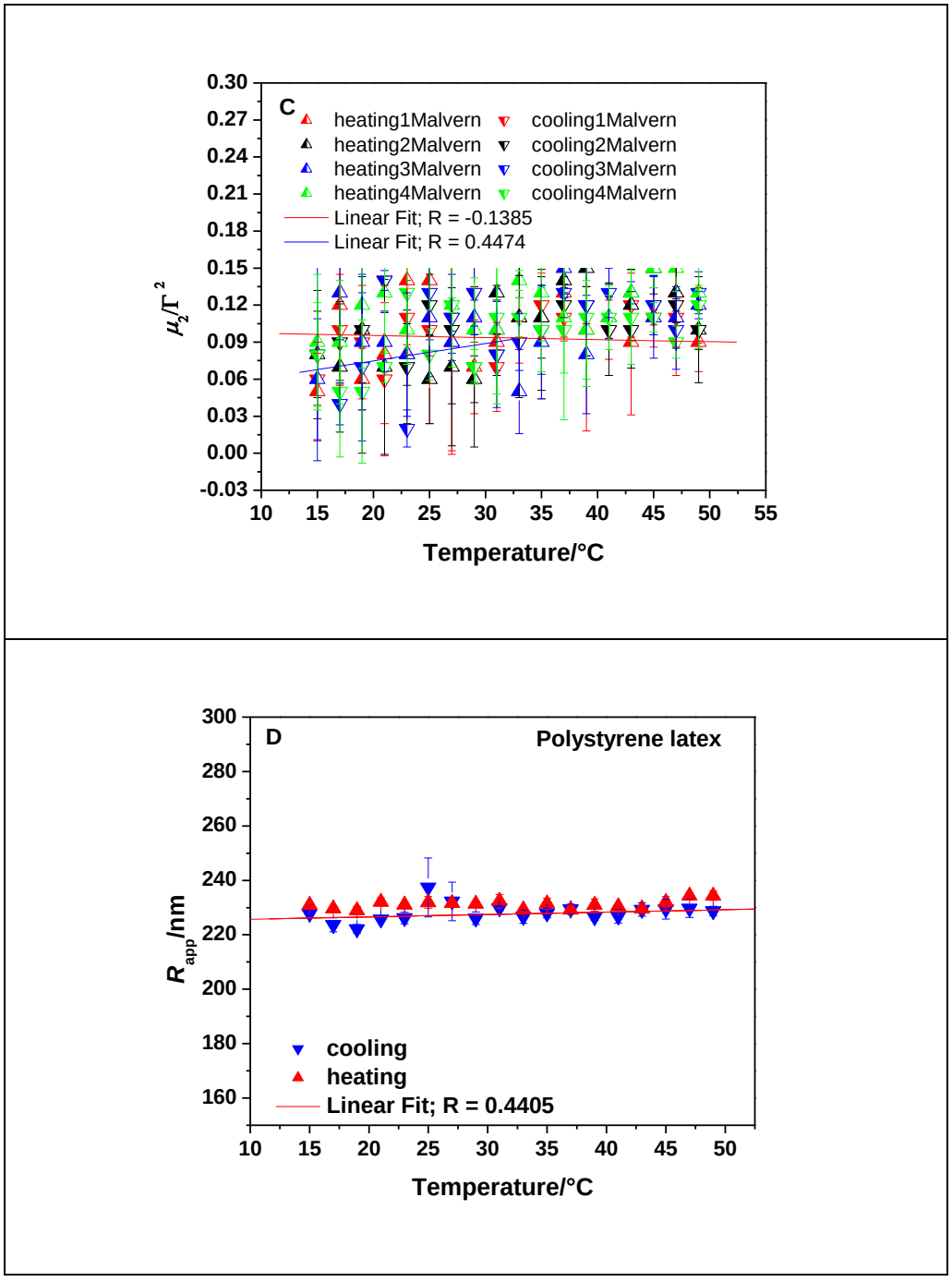

One-angle measurements required less time than multi-angle thus giving faster an image of the PCBL-CPs behavior. On heating, the particle size decreased from 338 nm at 15°C to about 325 nm at 29-31°C followed by a visible increase to about 350 nm at 43-45°C and then

decreased again to 330 nm at 50°C. This trend was abbreviated DID. A similar behavior can also be seen on cooling mode: a drop from 320 nm to 310 at 29-30°C, an increase to about 358 nm at 43-45°C and also a decrease to 320 nm at 50°C. Figure 5.9A1 reflects the total number of cooling-heating cycles averaged in Figure 5.9A. The reversibility of the helix-to-coil transition is clearly proven. Moreover particles did show a good "memory" of the temperature point or cycle. The hysteresis seen within a cycle may be considered an artifact of the different rates on cooling and heating even the sample was equilibrated at each temperature point. The polydispersity index, $\mu_2\ \Gamma^{-2}$, shown in Figure 5.9A2 can be correlated with the radius trend. While the radius decreased, first, up to 29-31°C, the index, $\mu_2\ \Gamma^{-2}$ increased until about 25°C and decreased around 29-31°C pointing to both an alteration and a recovery of the particle uniformity. In the next temperature interval, 31- 45, 47°C, marked by an increase in radius, the uniformity was again altered. In the hottest region of the transition 45- 50°C, the polydispersity index decreased, and so the radius. This trend was abbreviated as IDID. In order to test against artifacts stemming from the instrument, a control experiment was devised. Polystyrene latex beads were measured at the same temperatures and the size obtained is reflected in Figure 5.9B. The radius values can be easily fitted on a flat line proving their angle independence. Comparing Figure 5.9A and Figure 5.9B it is safe to assume that the t radius fluctuation seen for PCBL-CP175L is real and due to the particle's shell behavior.

Before discussion on the other samples involved in the study, several words should be spent on describing the curvature of the core and its influence on the polypeptide arrangement onto the particle surface. Figure 5.10 shows the relationship between the radius of the core and the thickness of the shell. In the case of the PCBL-CP175H and PCBL-CP175L the radius of the core, *R*, is higher than the thickness of the shell, t. The polypeptide disposition onto the surface

of these particles should be more similar with that of the grafted polymers on flat surfaces. For a radius approximately equal with the thickness, PCBL-CP100H, the polypeptide might "feel" the curvature of the surface. A sensible smaller core radius than thickness favors the star-like configuration of the particle.

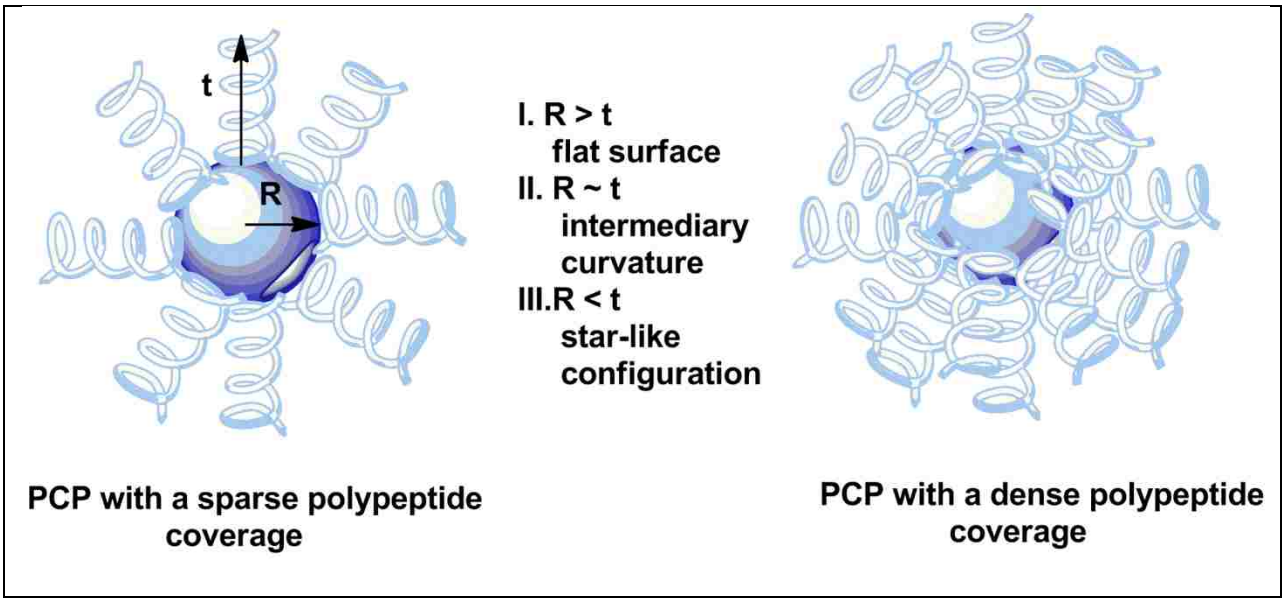

Figure 5.10 Idealized models of sparse and dense covered particles and the relationship between core radius, *R* and the shell thickness, *t*.

Bearing this in mind, let's examine the other three samples. PCBL175H presented in Figure 5.11A followed the same trend as seen for PCBL-CP175L but at a lower radius deviation and also the polydispersity index, Figure 5.11A1.

In the case of the PCBL-CP100H, Figure 5.11B, the DID behavior is clearly seen in the 15-27°C, 30 – 43°C and 45 – 50°C temperature interval. The uniformity of the particles, Figure 5.11B1 altered, translated in the increase of the polydispersity index up to 45°C and after showed stabilization to smaller constant values. In comparison, the DID fluctuation of the PCBL-CP55H radius, the "star PCBL-CP", Figure 5.11C is visible especially in the 27, 30 – 43°C and 45- 50°C interval. The $\mu_2\ \Gamma^{-2}$ index, Figure 5.11C1, did not vary consistently, rather settling around 0.2.

Table 5.2 summarizes the values for the radius of the composite particles studied in this work at the extremities of the temperature interval and as well as the variation of the size between the middle point of the temperature interval and its limits.

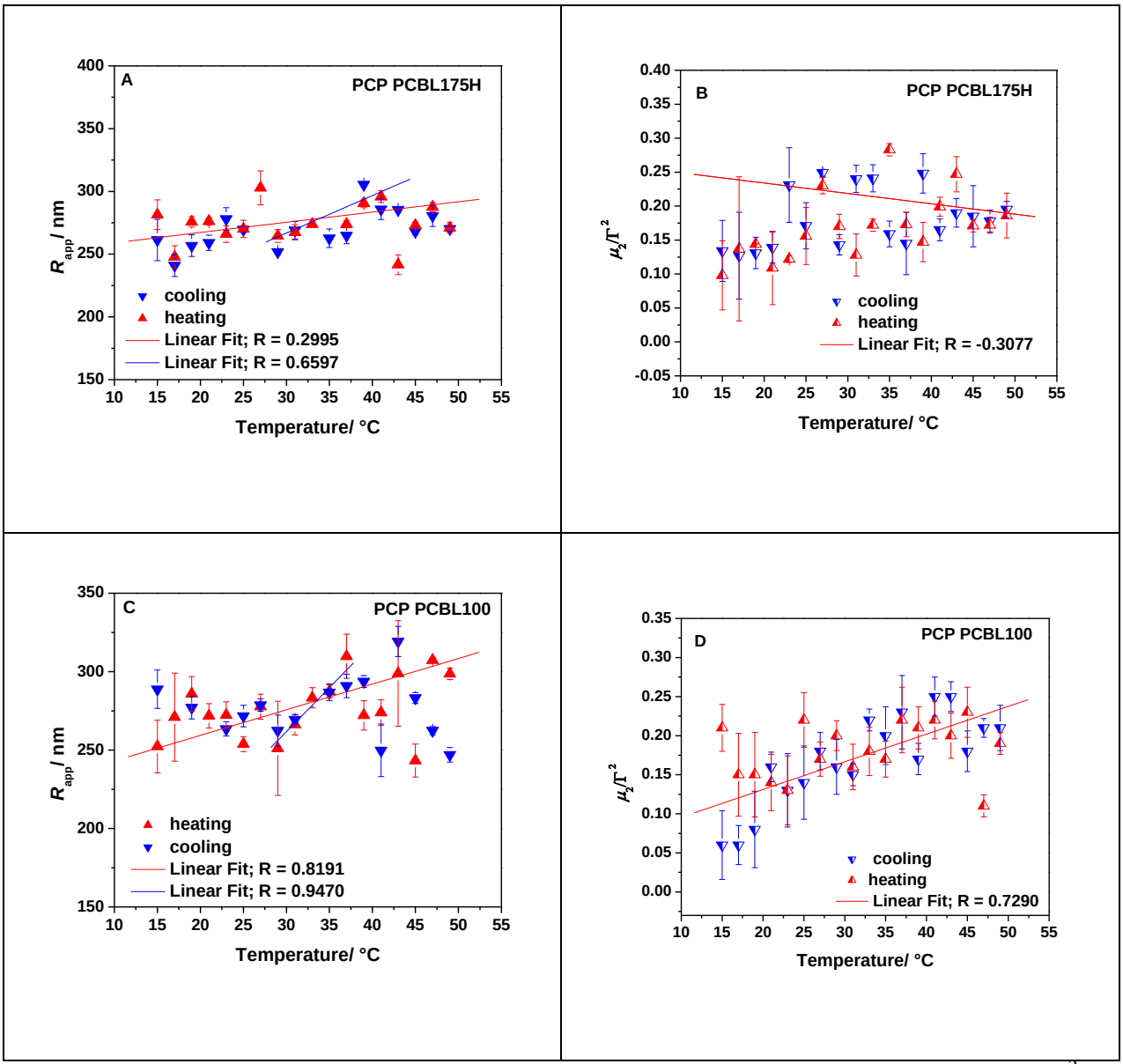

Figure 5.11 Variation of the apparent radius, R_{app} and the polydispersity index, $\mu_2\ \Gamma^{-2}$ as a function of the temperature recorded in m-cresol for (A, A1) PCBL-CP 175H (CR7160), (B, B1) PCBL-CP100H (CR810B) and (C, C1) PCBL-CP55H (CR710A) gathered at one angle. Red lines represent the linear regression applied to the data.

Figure 5.11 continued

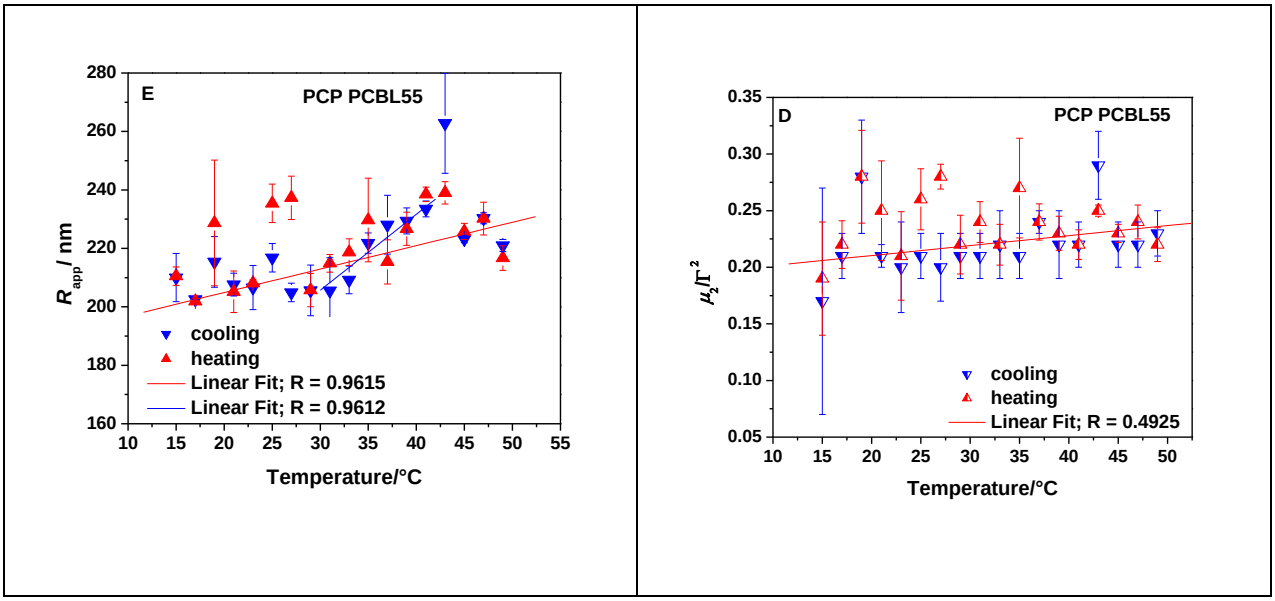

Table 5.2 Code, Radius of the Core, Radius Difference Between Low and High Limits of Transition Temperature Interval, Transition Midpoint Radius, Transition Midpoint and Transition Width for PCBL Silica Composites Recorded at One-Angle.

Code	R_{core}/nm	$\Delta(R_{cold}-R_{mid})$nm	R_{mid}/nm	$\Delta(R_{hot}-R_{mid})$/nm	Transition Midpoint/°C	Transition Width/°C
PCBL175L* (CR7188)	175	57	327.5	41.5	29	25 - 35
PCBL175H* (CR7160)	175	34	318	48	35	27 - 43
PCBL100H (CR810B)	100	30	257	52	29	23 - 47
PCBL55H (CR810A)	55	17	222	22	35	30 - 43

The DID behavior of the PCBL-CPs noted for PCBL-CP175L and confirmed by the other three PCBL-CP samples was also investigated by multiangle measurements, as reflected in Figure 5.12. Indeed the multiangle values agreed with the ones recorded at one angle, so the size trend.

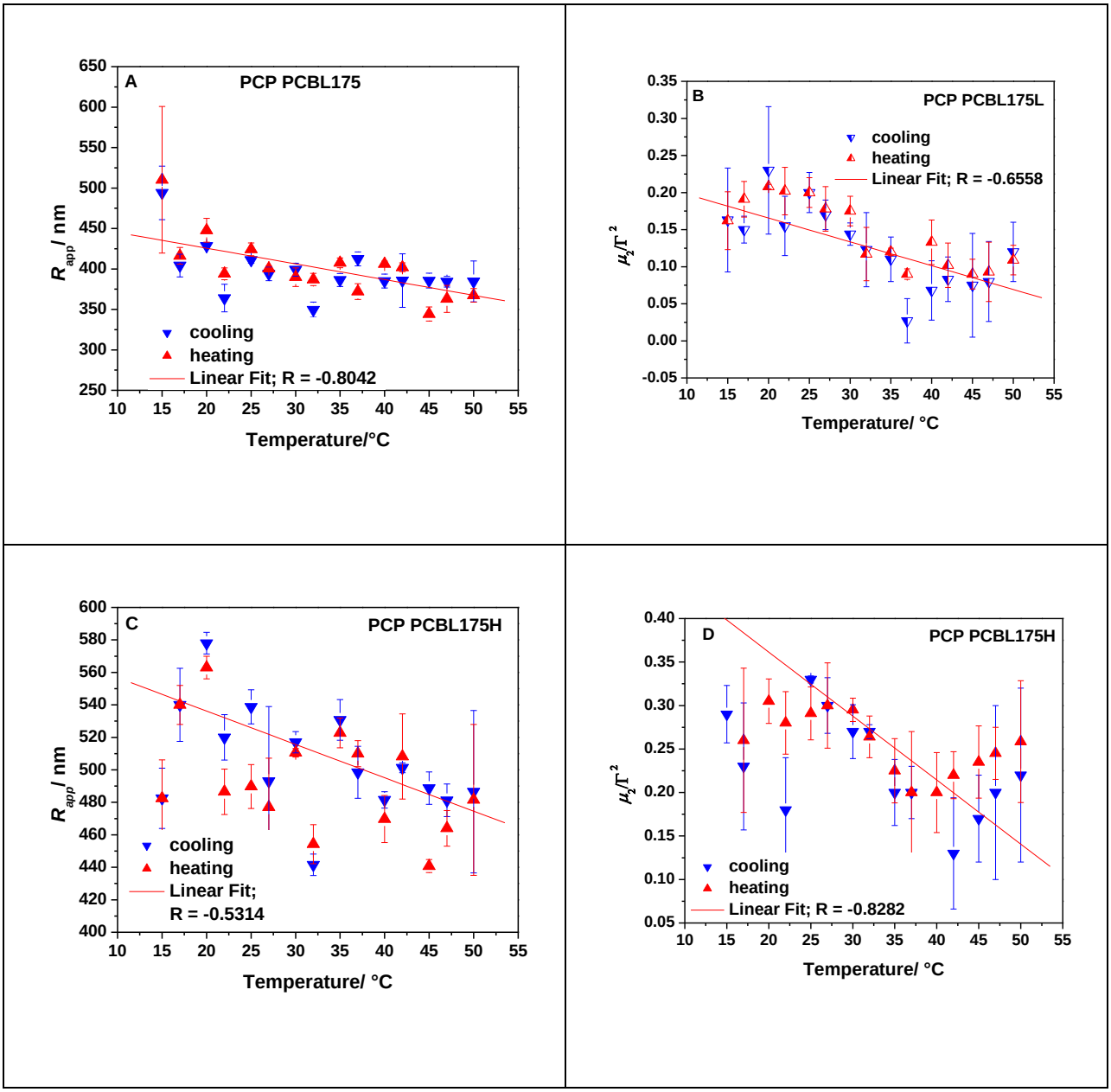

Figure 5.12 Apparent radius, R_{app}, as a function of temperature, for (A) PCBL-CP175L (CR7188), (B) PCBL-CP175H (CR7160), (C) PCBL-CP100H (CR810B), (D) PCBL-CP55H (CR810A) and polydispersity index, $\mu_2\ \Gamma^{-2}$, for (A1) PCBL-CP175L, (B1) PCBL-CP175H, (C1) PCBL-CP100H, (D1) PCBL-CP55H. The data were collected in m-cresol at 45°, 50° and 60° angles for each temperature and then averaged. The red and the blue lines represent linear regressions applied to the data.

Figure 5.12 continued

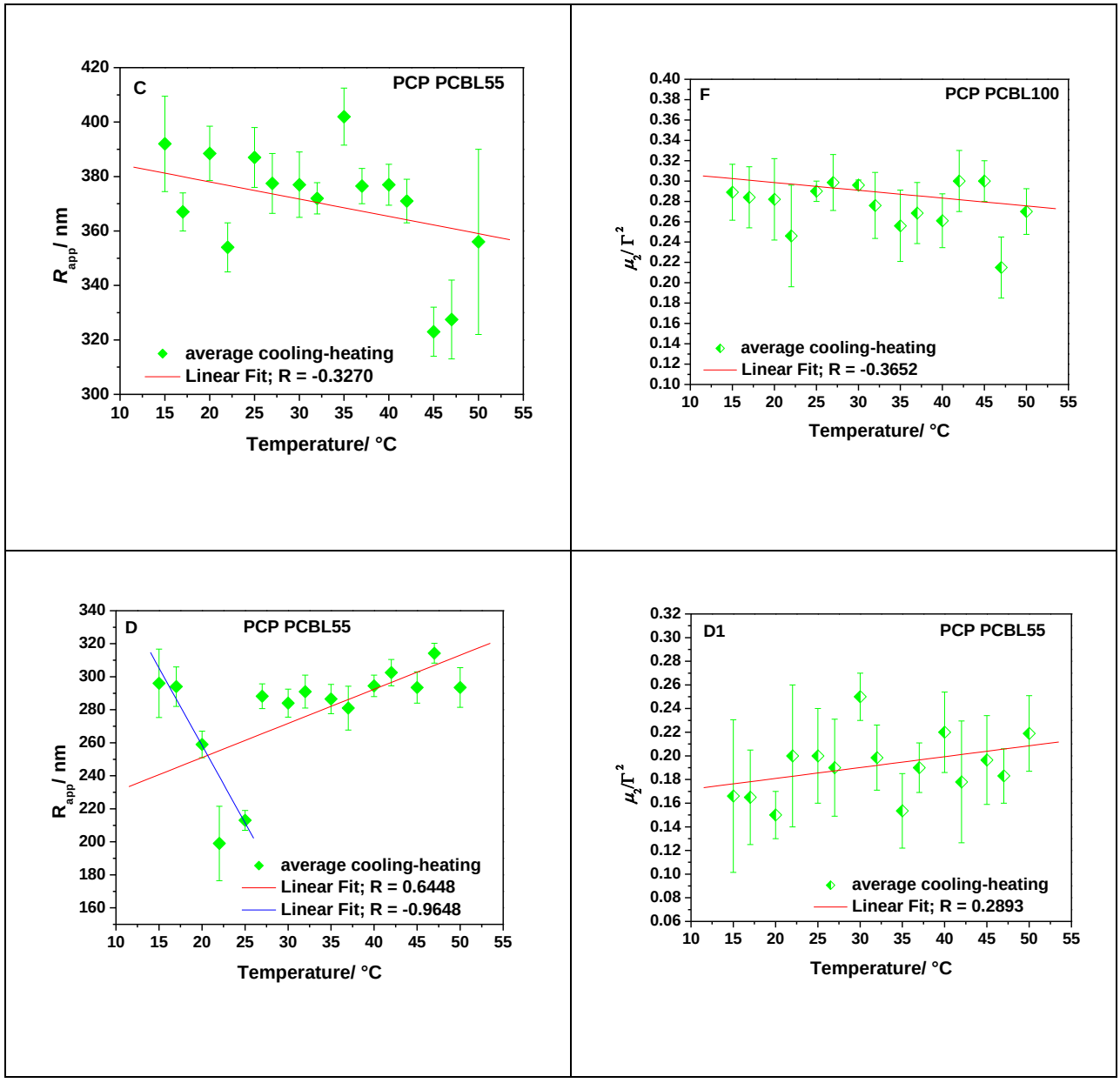

The multiangle measurement added additional information on DID trend of the particle size and polydispersity index, $\mu_2\ \Gamma^{-2}$. For example, in Figure 5.12A and Figure 5.12D, the drop in the radius within the 15 – 30, 32°C temperature interval is more prominent than in one angle measurements. Figure 5.12C confirmed that the decrease in size recorded in 40 – 50°C interval is sharp, as also seen in Figure 5.9A. The trend IDID for the $\mu_2\ \Gamma^{-2}$ index was also confirmed,

Figures 5.12A1, 5.12B1, 5.12C1 and 5.12D1. The intensities corresponding to the solution scattering were plotted against the temperature. As stated before, a linear trend was expected if no structural changes (e.g. aggregation, conformational changes) happen in the system. The intensity profiles of the two PCBL-CP samples shown in Figure 5.13A and Figure 5.13B is different than that of polystyrene latex. The PCBL-CP175L scattering decreases up to 25-27°C, then levels until the temperature reaches 40°C and finally decreases. The PCBL-CP50H intensity decreases over entire temperature interval.

The design of the experiments described above conducted both at one-angle and multi-angle allowed samples to equilibrate at each temperature for 30 minutes. Thus, it was interesting to investigate the behavior of the polypeptide shell when temperature equilibrium was not reached. Figure 5.14 displays several approaches to these non-equilibrated measurements.

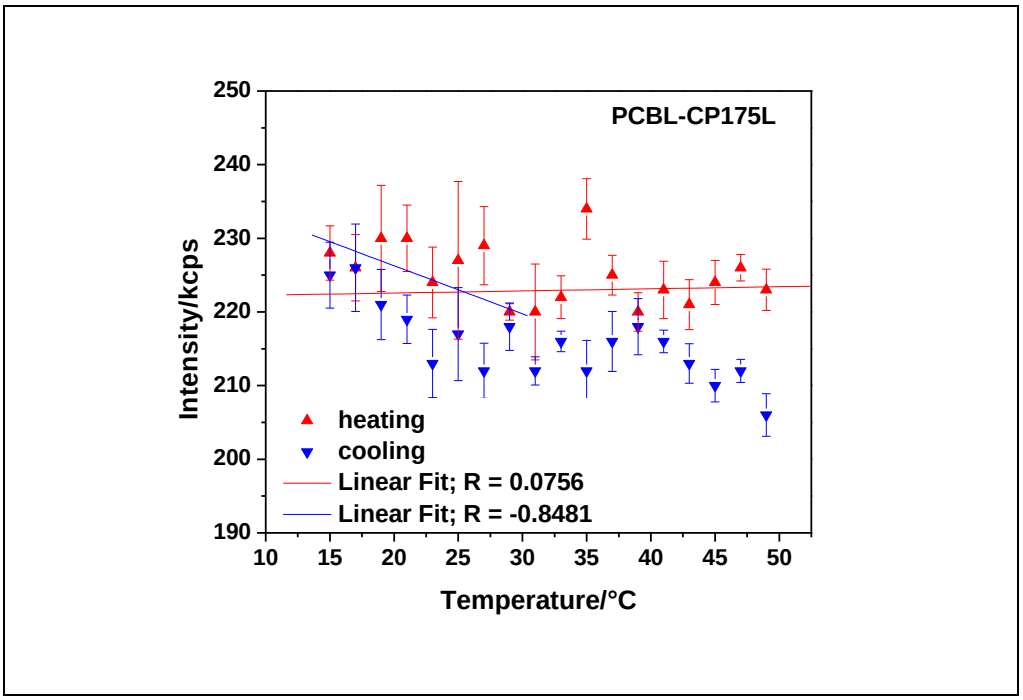

Figure 5.13 Scattering intensities as a function of the temperature for (A) PCBL-CP175L (CR7188), (B) PCBL-CP50H (CR810A) and (C) PS latex as control collected at one-angle. The red and the blue lines represent linear regressions applied to the data.

Figure 5.13 continued

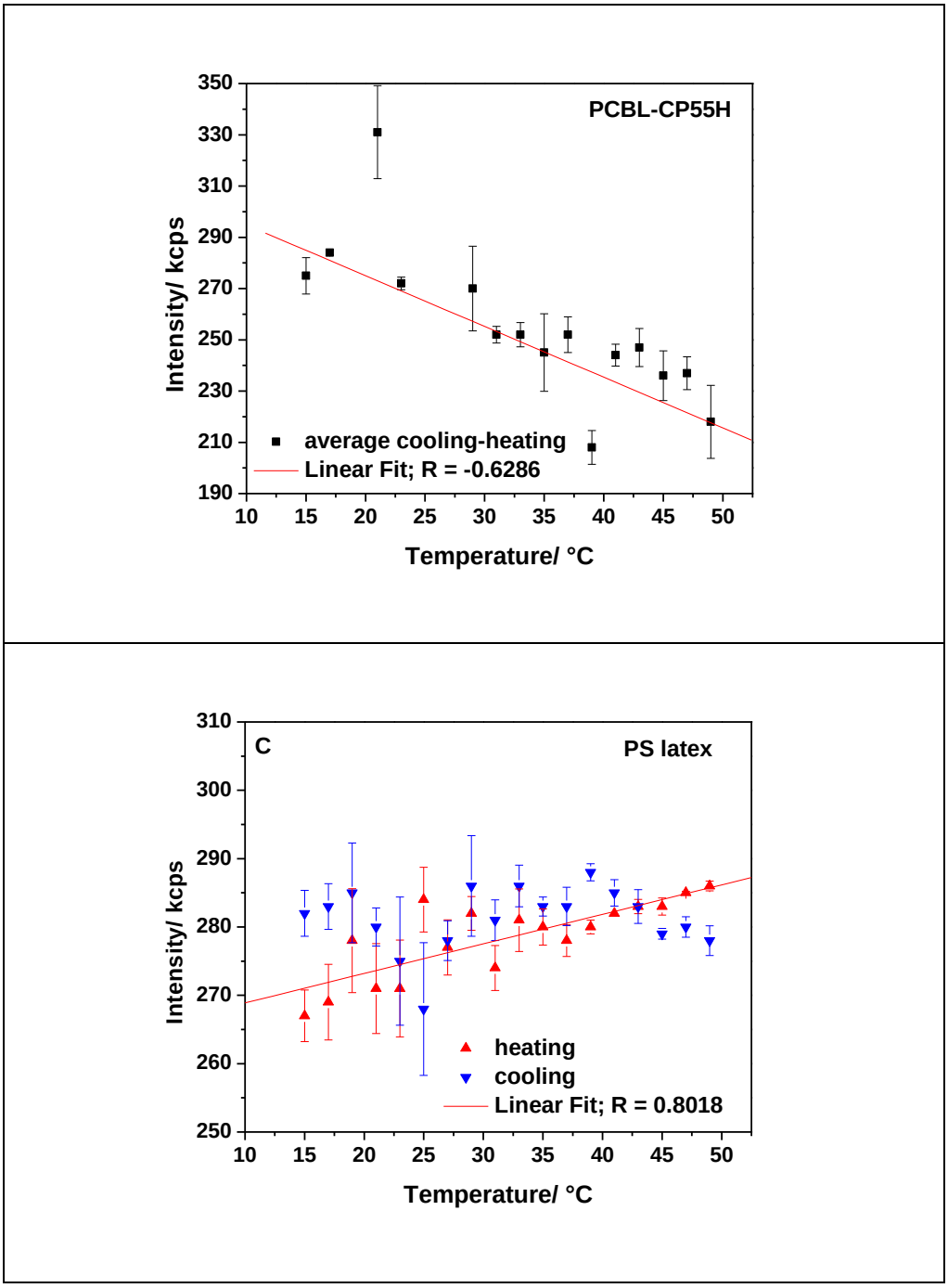

The intensity profiles of the two PCBL-CP samples shown in Figure 5.13A and Figure 5.13B is different than that of polystyrene latex. The PCBL-CP175L scattering decreases up to

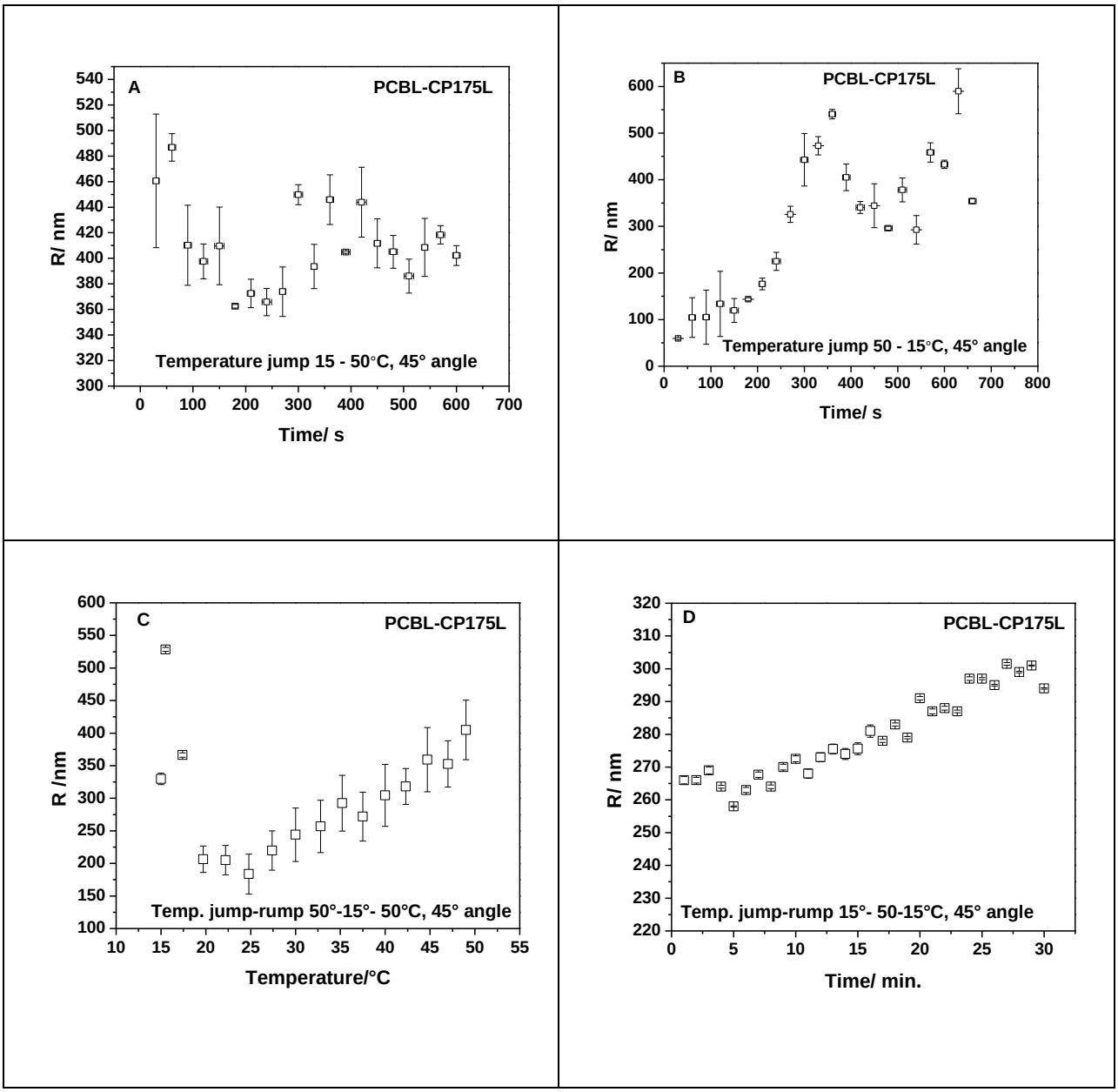

Figure 5.14 Dynamic light scattering data for PCBL-CP175L gathered at one-angle, 45°: (A) apparent radius as a function of time when the temperature jumped from 15° to 50°C, (B) apparent radius as a function of time when the temperature was jumped from 50°C to15°C, (C) apparent radius as a function of temperature when the temperature was jumped from 50°C to 15°C followed by rump to 50°C and (D) apparent radius as a function of time when the temperature was jumped from 50°C to 15°C followed by rump to 50°C.

25-27°C, then levels until the temperature reaches 40°C and finally decreases. The PCBL-CP50H intensity decreases over entire temperature interval.

The design of the experiments described above conducted both at one-angle and multi-angle allowed samples to equilibrate at each temperature for 30 minutes. Thus, it was interesting to investigate the behavior of the polypeptide shell when temperature equilibrium was not reached. Figure 5.14 displays several approaches to these non-equilibrated measurements.

The set-up of the experiments involved two DLS instruments available in the laboratory, DLS1 and DLS2. Noteworthy, before any experiment started it was necessary to determine the best optical settings for intensity. Since the DLS2 apparatus was used to collect the correlation functions associated with the sample scattering, the sample was inserted in the DLS2 set at 45° to adjust the pinhole-aperture and the filter for a scattering intensity between 200- 300 kHz. Further, in the temperature jump experiment, the sample was inserted in the holder cell of DLS1 instrument. The cell holder was isolated with a custom made Delrin cover and it was cooled for 1 hour using an attached cooling bath. In the same time the cell holder of the DLS2 instrument was heated at 50°C. The cell insertion of this instrument has a toluene bath. After one hour the sample was quickly switched from 15° to 50°C and the correlation functions was recorded over short runs of 60s each over 30-35 minutes. In the temperature jump-rump measurement the cooling bath of the DLS2 instrument was set to rump again. For example, if the sample was jumped from 15°C (DLS1) to 50°C (DLS2) the cooling system of DLS2 was set to rump back to 15°C. In this case the temperatures were also recorded until reached the interval limit (e.g. 15°C) and stabilized around its value. Figure 5.14A and 5.14B show the profile of the apparent radius recorded on 15° to 50°C and 50° to 15°C. The trend of the radius seemed to have common features with the equilibrated experiments in terms of size fluctuation. Yet, several details must be discussed regarding the data analysis. The radius values displayed on the plots were taken as average between 3rd cumulant and one-exponential fitting algorithms. The Stökes-Einstein

equation employed in size calculations used the solvent viscosity corrected for the temperature of the DLS2 cell holder toluene bath. It is true that the real temperature of the sample was not 50°C in the 15° to 50°C jump experiment. The sample "warmed" gradually until reached 50°C. The "perfect" experiment needs to allow the recording of the real sample temperature. This is attainable by inserting of a probe thermometer in the vial. These measurements can be considered only as "crude" observations on the shell behavior when exposed to extreme temperature variation. The jump-rump experiments, Figure 5.14C and Figure 5.14D did allow the recording of the ramp temperature but still differences in solvent viscosity as described are present.

In order to further demonstrate the occurrence of the reverse helix-to-coil transition in tethered PCBL system and as well to have a clearer image of how the grafting density might affect it a "mid-age" PCBL-CP nonfluorescent sample, five years old, was subjected to the same investigation by light scattering as the above described samples. The fluctuation of the size with the temperature is displayed in Figure 5.15. The PCBL-CP65 have a light coverage with polypeptide (a mixture of APS and passivators methyltrimethoxy silane, MTMS, was used to functionalize the silica surface) and also a lower polypeptide load (~30%).

Figure 5.15A shows a noisy fluctuation in the radius size up to 30°C. A smooth increase can be noted both in cooling and heating mode which "breaks" in a noisy slightly descending trend. The same evolution was observed for the polydispersity index, Figure 5.15A1. The profile of the size as a function of the temperature was similar with that of the magnetic and nonmagnetic fluorescent PCBL-CPs. The mid-point transition was around 37°C. The intensity, Figure 5.15A2, was found to decrease from low to high temperature interval limits. Combining the information about a low grafting density with initiator which would result in a sparse surface

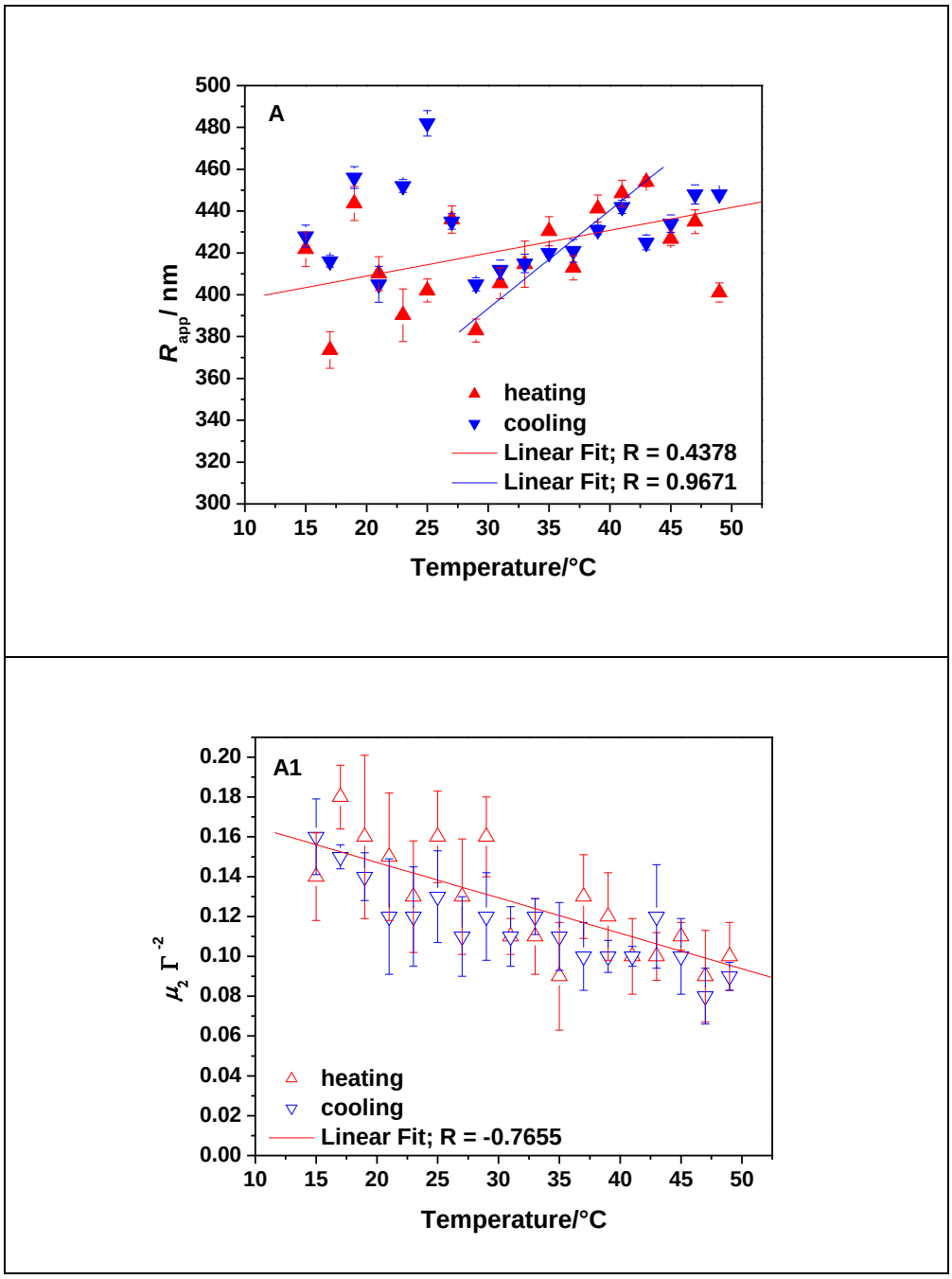

Figure 5.15 Dynamic light scattering data for PCBL CP65 (ES453A): (A) apparent radius, R_{app}, as a function of temperature, (A1) polydispersity index, $\mu_2 \cdot \Gamma^{-2}$, as a function of temperature and (A2) intensity as a function of temperature. The red and the blue lines represent linear regressions applied to the data.

Figure 5.15 continued

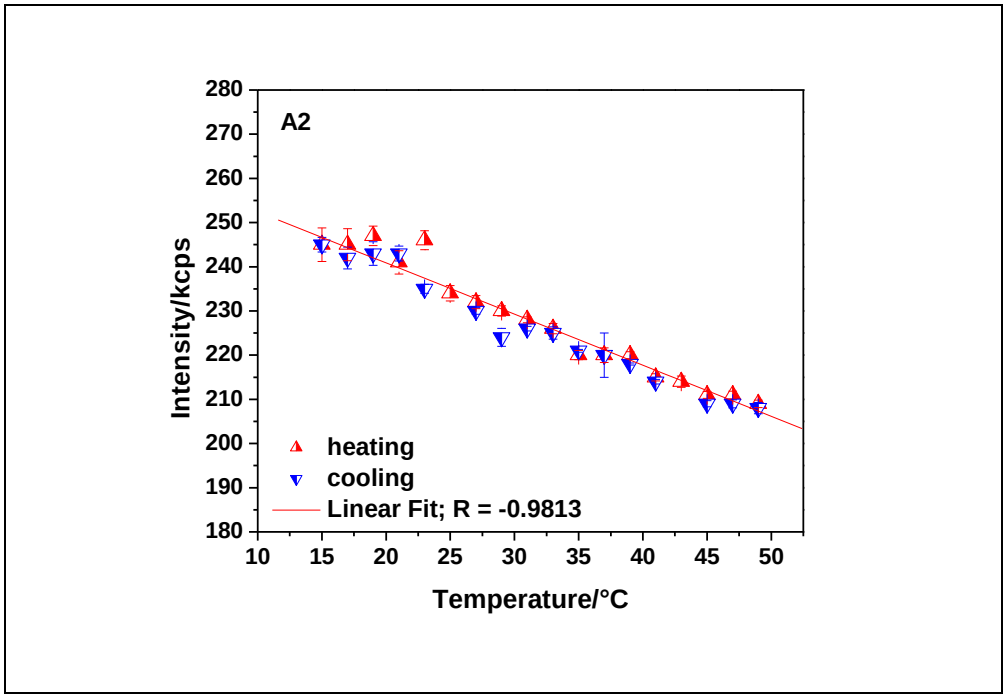

with polymer chains, the percentage of polypeptide load and the transition mid-point it can be concluded that the polypeptide had short chains (lower molecular weight) which underwent transition at a higher temperature as reported by the Fujita's group for free untethered polypeptide.

5.4.3 Nuclear Magnetic Resonance

M-cresol and tethered PCBL were analyzed first by simple ^{1}H NMR. Figure 5.16A shows the spectra of the bulk solvent collected at different temperatures. The signal from methyl protons was very stable and was centered at ~1 ppm. The OH proton instead shifted downfield with increased temperature. In order to test the possibility of a reversible OH shifting the sample was cooled down from 45°C to 25°C and compared with the initial spectrum collected at 25°C. It can clearly be seen that the two 25°C spectra match perfectly in the OH region. Another detail was present in the 45°C spectrum. One of the aromatic proton signal slightly shifted downfield

when compared with 25°C. In Figure 5.16B the characteristic peaks for tethered PCBL can be seen. The amide protons from the backbone and side chain can be seen at 7ppm and 6ppm at 25°C. Upon increasing the temperature the peak corresponding to backbone amide proton shifted downfield to about 5.5ppm and became less intense, while the side chain NH proton didn't change. This shift and decrease in intensity can be correlated with the formation of the α-helix. In a random coil disposition the backbone moves more freely than a rigid rodlike helical structure. At elevated temperatures the motion is more restricted, the fast contribution probably comes from the coil tail flanking the rigid rods. The side chains also lose some degree of freedom since they are folding around the helix axis. A supplemental evidence for coil-to-helix transition is reflected by the α(H) proton, Figure 5.16C. At 25°C when the polypeptide is essentially a random coil the α(H) signal is very sharp and well-resoluted. Once the temperature increased at 45°C at which the polymer is helical the α(H) peak almost disappeared. Once the rigid helix become to form, the α-CH fragment is hindered by being packed inside the helix, consequently the signal should decrease or disappear. Instead the neighbor signal from β(H) proton became sharper, a fingerprint of more freedom to move when compared with α(H). Similar with m-cresol, the aromatic contribution of protons was different at ambient and high temperatures. The Ar(H) shift downfield was also seen. It can be speculated that the peak position changes in the region of the amide and α(H) protons can be a consequence of H-bonding with the formation of α-helix. The aromatic shift can be a signature of relaxation from a $\pi - \pi$ stacking disposition between side chains and solvent-side chains, most probable in a random coil configuration at low temperature.

The shift in the OH signal with the temperature might suggest not only a change in viscosity but also a change in solvent conformation. The aromatic molecules carying pendant

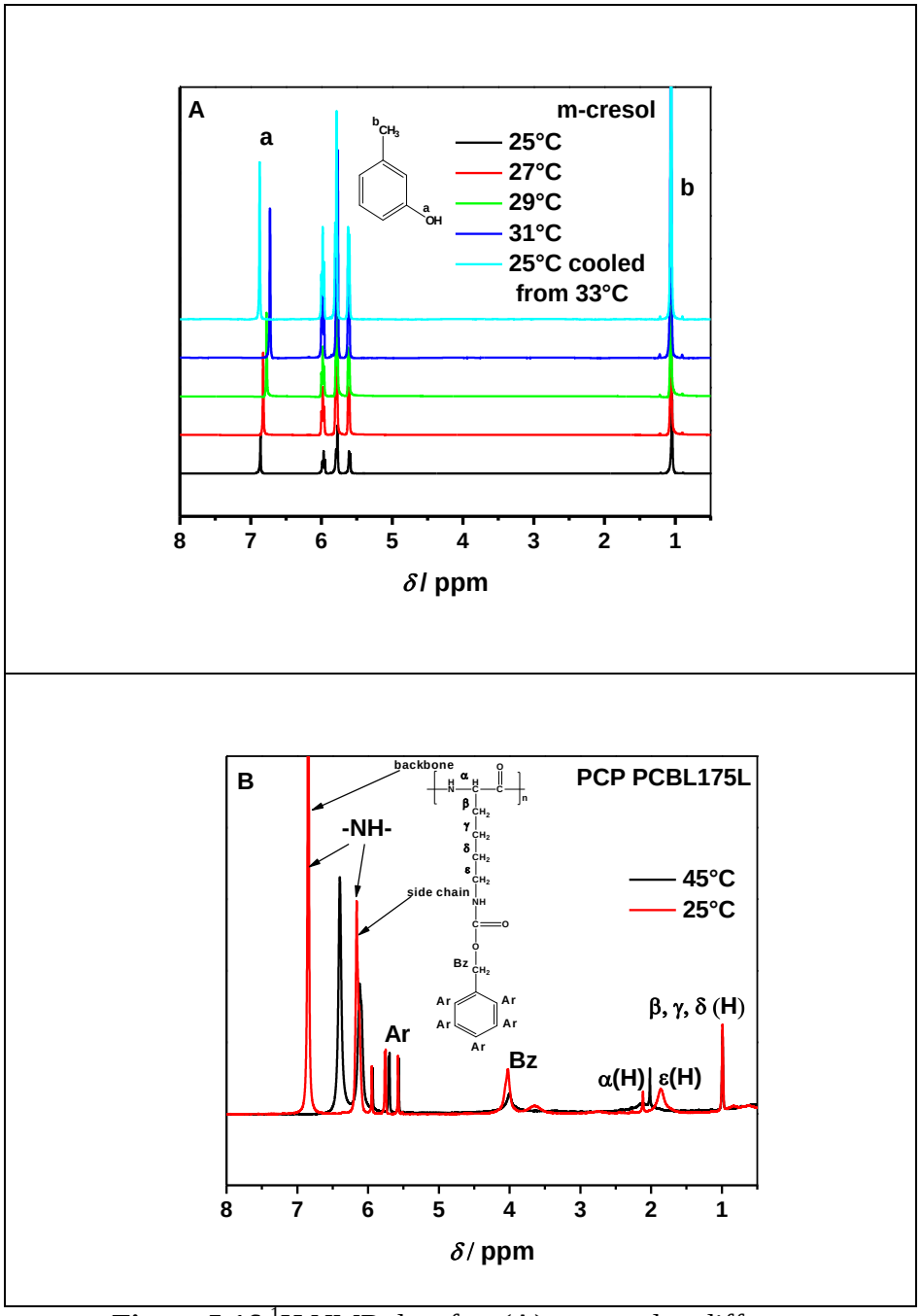

Figure 5.16 ^{1}H NMR data for: (A) m-cresol at different temperatures, (B) tethered PCBL at 25°C and 45°C and (C) zoom of ─NH─/ Ar and α(H) proton regions. Measurements B and C were performed in deuterated m-cresol.

Figure 5.16 continued

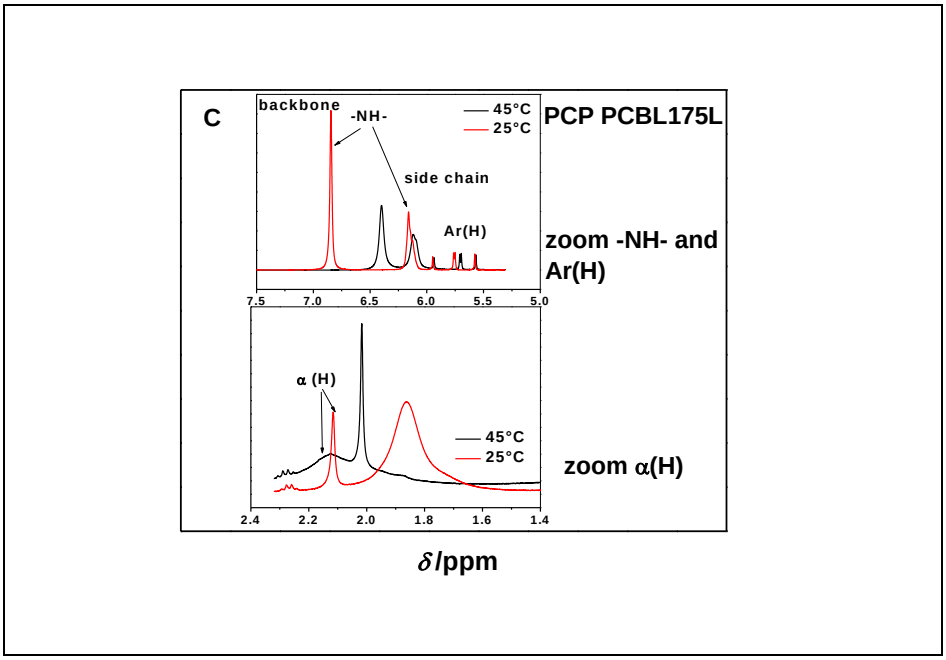

free OH and CH_3 groups in *meta* positions have the possibility to associate through H-bonds and $\pi - \pi$ interactions. Figure 5.17 displays the comparative areas of the signal shifts for m-cresol and untethered polypeptide. It seems, the solvent shows deviations in the same temperature interval as the PCBL.

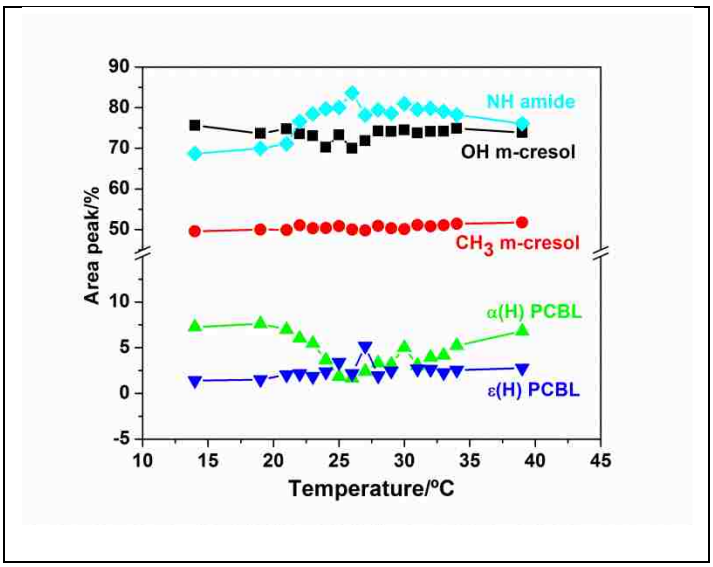

Figure 5.17 Percentage of proton area peak as a function of the temperature for m-cresol and PCBL.

In order to get more information about the transition, the spin-lattice relaxation times were measured. NMR relaxation measurements are more sensitive to both local motions of the side chain residues and the global motion of the polymer chain. For illustration Figure 5.18A displays the T1 times and the corresponding signal shifts downfield for amide proton as a function of the temperature for tethered polypeptide. The amide proton T1s increase with the temperature for both samples but at different amplitudes. Figure 5.18B shows the solvent viscosity-corrected T1 times. The spectrum for untethered polypeptide shows the occurrence of two relaxation T1 modes starting at 35°C. The tethered polypeptide does not reflect such tendency, but slight deviations can be also observed at 35°C. The similarity between the profiles of the lower and highly populated surface is evident. The best representation that reflects the transition for coil-to-helix of PCBL in m-cresol is displayed in Figure 5.19.

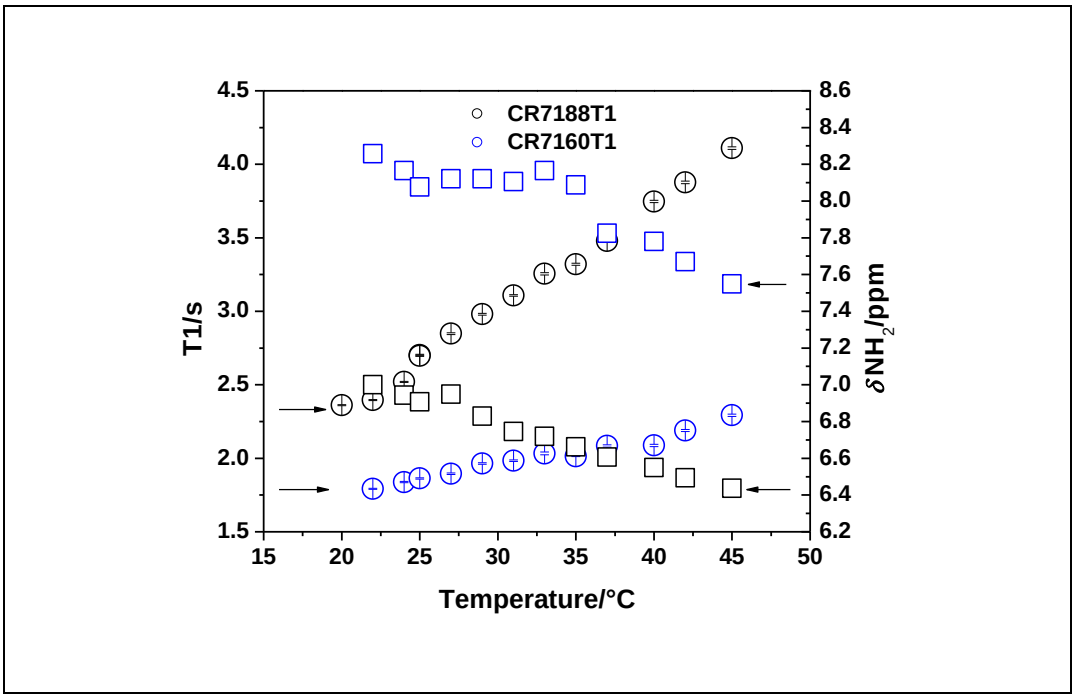

Figure 5.18 (A) Representation of T1 relaxation times and signal shifts as a function of the temperature and (B) T1 relaxation times corrected or solvent viscosity versus temperature for composite particles and untethered polypeptide. The line is the eye guide.

Figure 5.18 continued

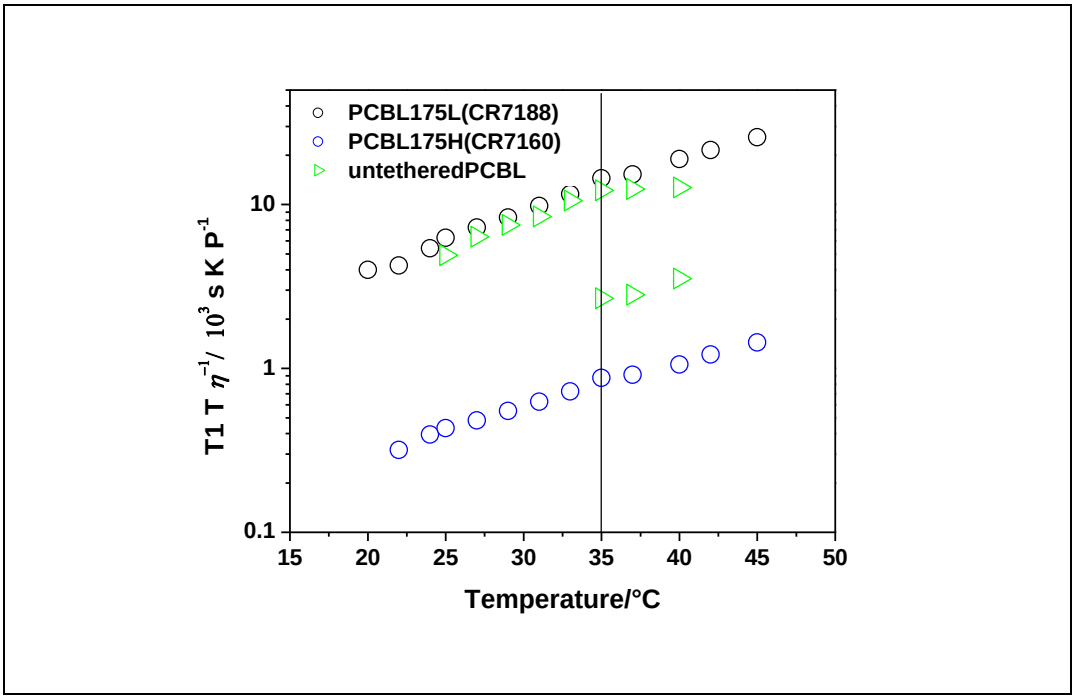

Tethered polypeptides presented in Figure 5.19A show three domains of relaxations. At lower temperatures up to 25°C, region **i**, the relaxation is rather constant. Then a gradual increase of the proton relaxation occurred within domain **ii**. The high temperature interval was marked by a sharp increase of T1s (region **iii**). In Figure 5.19B the untethered PCBL behaved in the same manner. The net difference can be noted at higher temperatures. One of the two split modes showed an increase with temperature of the T1 while the other decreased. The coexistence of the three domains is in agreement with the DID trend reflected in DLS data. Together these data suggest that the transition of the PCBL in m-cresol induced by temperature is not a pure coil-to-helix. Moreover the transition might undergo through intermediary conformations. The elevation of the relaxation times is in agreement with the other reports by McCormick et al.,[55] Ponomarenko et al.,[56] and Raby et al.,[57] to mention only few of them. The decrease in the relaxation times, thus faster correlation times, is associated with the increased mobility. At low

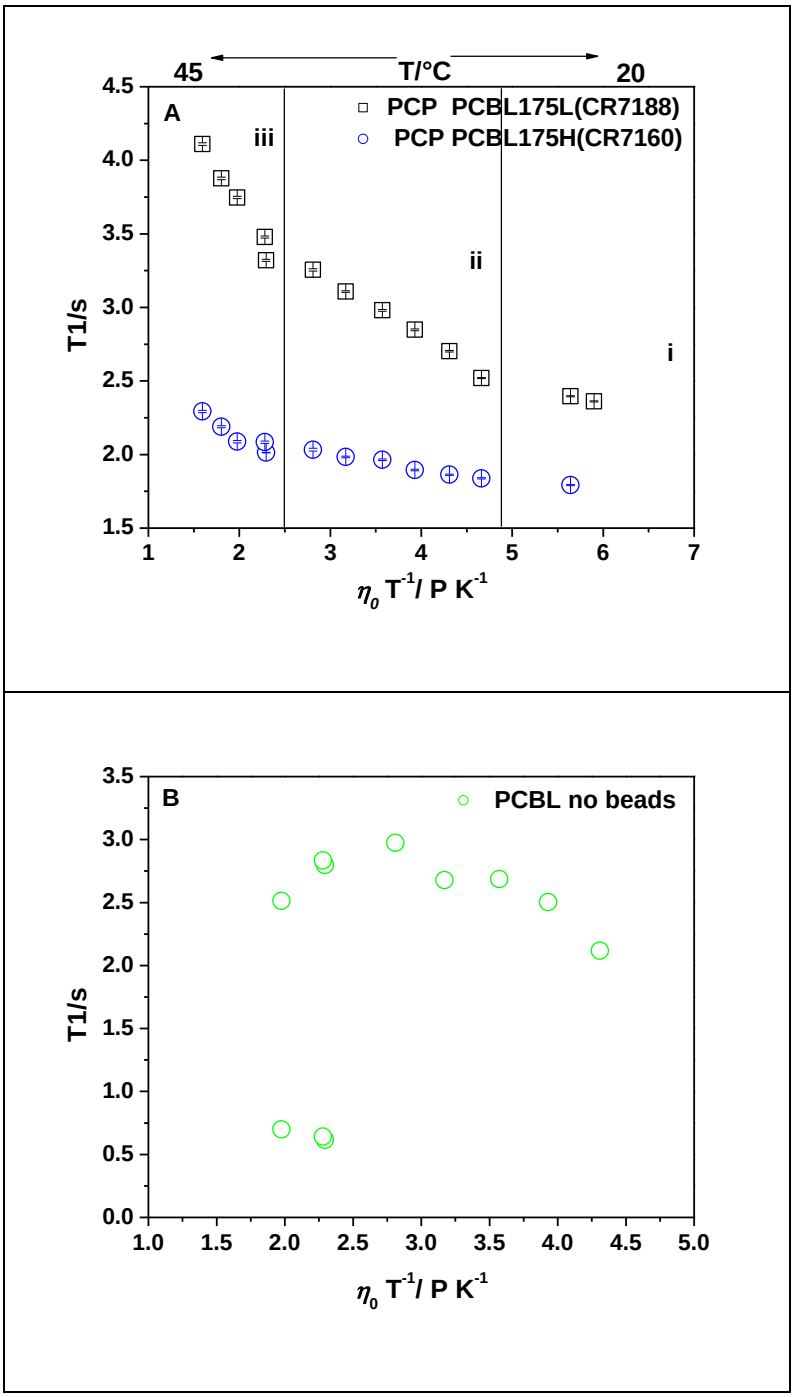

Figure 5.19 Solvent viscosity- and temperature-corrected NMR relaxation spin-lattice T1 times for (A) tethered PCBL (PCBL-CP175L(CR7188) and PCBL-CP175H(CR7160)) and (B) untethered PCBL.

temperatures the polypeptide backbone and its side segments moves freely with no restrictions. The high mobility enables polypeptide protons to relax faster. The solvent change in viscosity

with temperature elevation arrests the free motion once the backbone starts to fold into α-helical turns and increases T1s. Since the bulky carbobenzyloxy side group is packed inside the helix, the contribution to relaxation from PCBL side chains is lower to negligible. This is true for a rigid rod-like conformation and is clearly reflected by the PCBL tethered on the silica beads. PCBL is known to behave more like a wormlike polymer.[20] The helical segments are interrupted by random coil fragments which makes the PCBL rod flexible. The number of backbone flexures increase with the molecular weight.[57] These flexures were also suspected in poly(γ-benzyl-L-glutamate) during helix coil transition.[58] The descending high-amplitude T1s seen in Figure 5.19B around 35°C can be attributed to the motion of polymer from the coil flexures and from the random coil fragments flanking the ends of the rods. The ascendant T1s can be associated with the slower movement of the polypeptide packed in helical rod-like segments. The motion of these fragments is slower thus the relaxation times, T1s, increase.

5.4.4 Differential Scanning Calorimetry

The inverse helix-to-coil transition of tethered PCBL in m-cresol as a function of the temperature was also investigated by differential scanning calorimetry, DSC. Thermal behavior of the untethered PCBL was investigated early by Fujita group.[13] Figure 5.13A displays the thermograms obtained for m-cresol, tethered and untethered PCBL along with several control samples at a flow rate of 5°C min^{-1}. The endothermic events seen for PCBL-CP175L, PCBL-CP175H and untethered PCBL in the 29 - 40°C temperature interval, gave a rough image on their thermal behavior. Other reports pointed out the major difficulties in understanding the thermodynamics of helix-coil transition.[59,60] The broad range of the transition interval was associated with a low enthalpy and, in some situations the fully helical structure was never attained. The traditional DSC method is widely used to study the thermal transitions in materials.

Difficulties arise when the material's thermal behavior involves multiple processes. The sensitivity and the resolution of the simple DSC might not suffice such complex transitions. As shown in Figure 5.20A the DSC thermograms do confirm some thermal events in the above mentioned temperature interval but at low resolution. In order to overcome such inconvenience, samples were subjected to modulated differential scanning calorimetry, MDSC, an extension of the DSC. In a typical MDSC experiment, the total heat flow is separated into the kinetic and the heat capacity components, thus increasing the amount of structural information gained at a higher resolution and sensitivity. Figure 20B shows the reversible heat flow. PCBL-CP175H had two endothermic events in the 27 - 40°C temperature interval. Such events can be translated through the PCBL-CP tendency to evolve from a less to a more organized state. Noteworthy, the first endotherm is broader followed immediately by a narrower and a sharper endothermic transition.

MDSC was also a convenient tool to obtain an image about the cooperativity between the solvent and the polymer resulting in coil-to-helix transition. The bulk solvent seen in Figure 5.20C had three dominant endothermic relaxation peaks. The heat flow was 2°C min^{-1} and the modulation was performed every 60s period with 0.318s. The structural changes in m-cresol are the result of the intra and intermolecular interactions. H-bonding and $\pi - \pi$ stacking are the most probable interactions occurring in the bulk m-cresol. At sub-ambient temperatures the solvent viscosity is high pointing to a maximum of "packing" due to these connections. Upon increasing the temperature the viscosity thinning is translated through the increased freedom of the molecules to move due to weak and loose interactions. The endotherms at elevated temperatures reflect the intra and intermolecular H-bonding. The solution of PCBL in m-cresol, Figure 5.20D, showed multiple endothermic events. At the low temperatures similar relaxation signals were

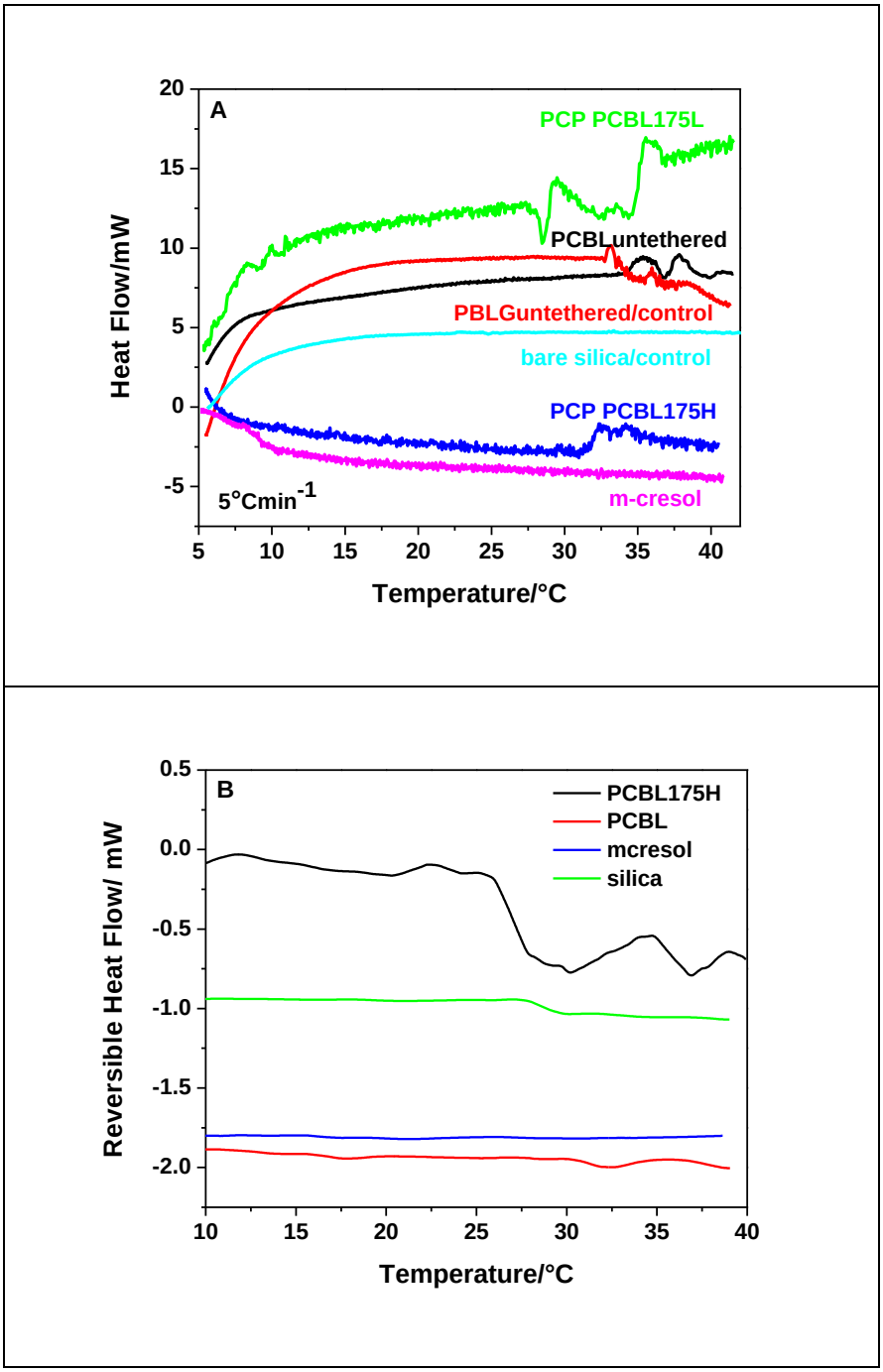

Figure 5.20 (A) DSC thermograms collected at a heat flow of 5°C min^{-1}, (B) modulated DSC thermograms recorded in m-cresol for tethered PCBL, untethered PCBL, silica cores and solvent, (C) zoomed MDSC for m-cresol and (D) zoomed MDSC for untethered PCBL.

Figure 5.20 continued

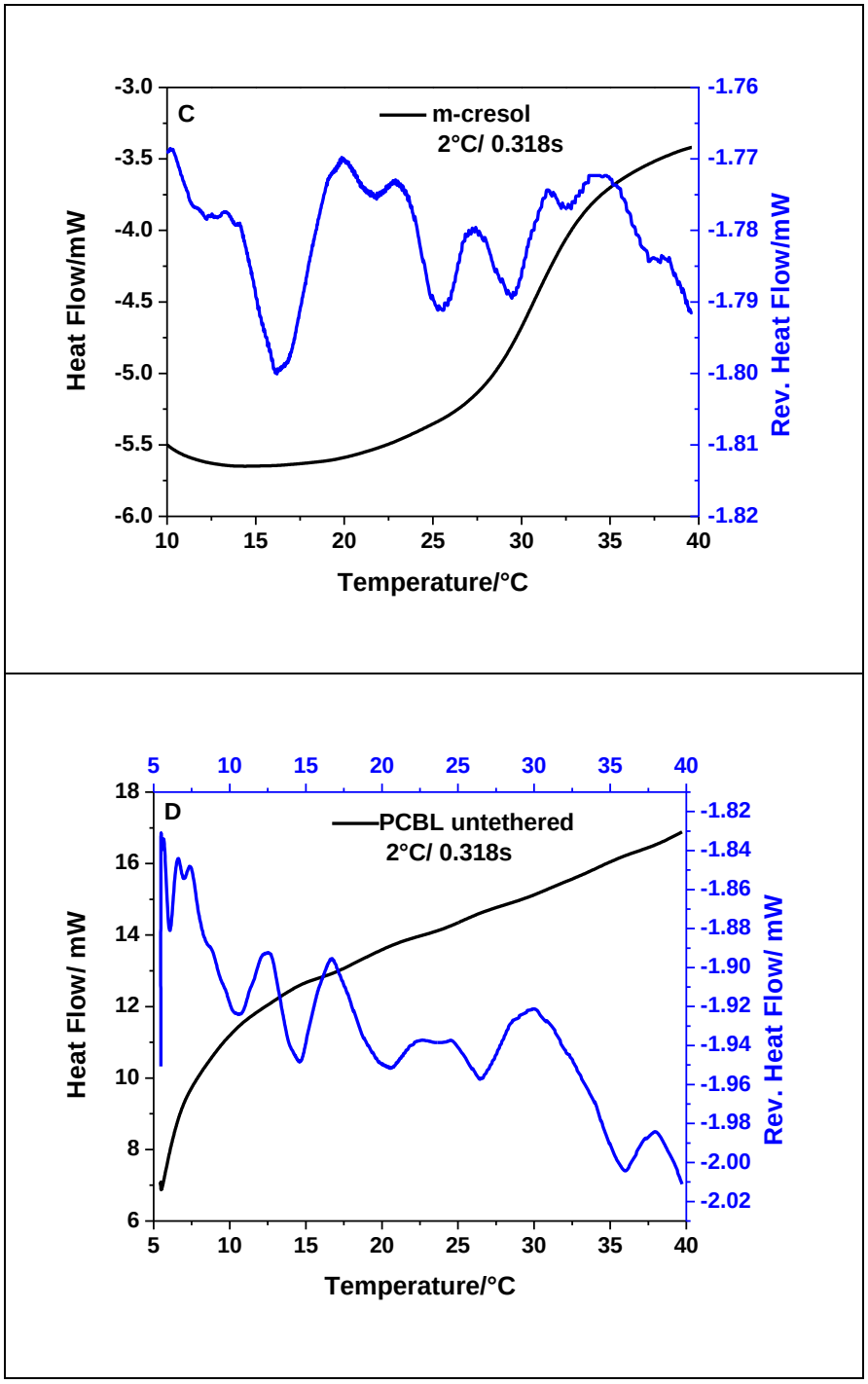

visible for both solvent and PCBL solution. One supplemental peak was present in the same region of temperature in PCBL solution. These events suggest that besides interactions between

the solvent in bulk present in a larger amount than polymer new interactions solvent- polymer took place. The pendant side chain of the PCBL had a high probability to stack with the aromatic ring of the solvent. The H-bonding between OH groups of the m-cresol and backbone and side chain NH were also very probably. Upon temperature increase the entropic-enthalpic exchange between solvent and PCBL promotes the formation of the helix, the more organized state seen as a sharp peak for both untethered and tethered polypeptide. The middle thermal endotherms at 20-27°C seen in Figure 5.20D could be a reflection of the breakage of solvent- polymer H-bonds with the formation of the polymer – polymer H-bonding.

5.4.5 Small Angle X-Ray Scattering

The growing interest in composite particles comprising especially responsive shells made SAXS a viable characterization tool. Many studies showed that the particulate changes in shell conformation can be resolved by SAXS. Figure 5.21 presents the SAXS data collected for PCBL-CP175H. Qualitative information about the PCBL-CP can be withdrawn. Since the PCBL-CPs have a hard silica core, the fluctuations in the scattering profile at different temperatures should emerge only from the shell. Such visible variations are also ensured by the electron contrast between the silica core and polypeptide shell.

The intensity profiles gathered at 25°, 29° and 50°C do not show significant difference from each other. At higher temperature particles seem to scatter less. This may be true if they decreased slightly in size. Such size variation would come from the conformational change suffered by shell because the core size is constant at all time. Other cause of the difficulty in data interpretation can be assigned to baseline errors. Further experiments will shed more light into these issues. Unfortunately, quantitative information could not be gathered in the q range that particles were analyzed. A Guinier regime could not be delimited to calculate the particle size.

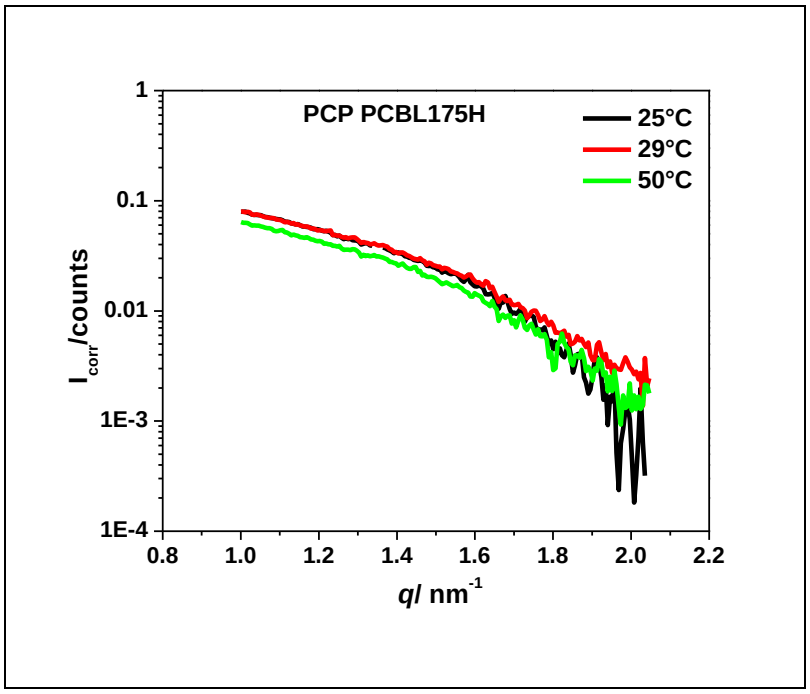

Figure 5.21 2D SAXS scattering profiles for PCBL-CP175H gathered at 25°C, 29°C and 50°C.

The radius of gyration or Guinier radius can be calculated from the Gaussian decay of the initial scattering intensity:[61]

$$I(q) = I(0)\exp\left(-\frac{1}{3}R_g^2 q^2\right) \qquad Eq.5.2$$

where R_g is Guinier radius and q is the scattering vector magnitude.

The cross section scattering of a core-shell particle is directly correlated to the corresponding form factor:[62-67]

$$P(q) = [V_{core}^2(\rho_{core} - \rho_{shell})^2 f_{core}(q,R)^2 + 2V_{core}V_{shell}(\rho_{core} - \rho_{shell})(\rho_{shell} - \rho_{solv})f_{shell}(q,R)f_{core}(q,R) + V_{shell}^2(\rho_{shell} - \rho_{solv})^2 f_{shell}(q,R)^2] \qquad Eq.5.3$$

where $f_x(q,R)$ is the normalized scattering amplitude of a homogenous sphere, and can be defined as:[68]

$$f(q,R) = \frac{3[\sin(qR) - qRcos(qR)]}{(qR)^3} \qquad Eq.5.4$$

V_x is the volume define as $4\pi R^3/3$, ($R_{shell} = R_{total} - R_{core}$) and ρ is the density.

A detailed analysis using equation 5.3 and a more critical consideration of baseline errors should be performed before reading too much into the SAXS data. All together the DLS, NMR, MDSC and SAXS data point to a not simple pure coil-to-helix transition of the PCBL in m-cresol. Moreover transition states can be expected.

5.4.6 Understanding the Reversible Coil-to-Helix Transition.

The helical conformation is the most common secondary structure occurring in proteins. Most of the traditional studies investigated the helix-coil transition in free polymers. Attachment to the surface may influence the transition in terms of the free energy.[69,70] Chains tethered to a surface with one-end would behave differently than free ones mainly due to the restriction on the degree of freedom for the chain motion.[71,72] In this study, PCBL was grafted onto silica beads of different sizes. As shown in Figure 5.10, the polypeptide can be considered grafted on a flat-like surface or lying in a star-like disposition. It is also known that the reverse coil-to-helix transition of PCBL in m-cresol as a function of temperature occurs on the basis of a strong cooperativity.[12,17,19,73] In the attempt to explain the evolution from a less ordered to a highly ordered state, one must take into consideration the key factor, H-bonding.[74-76] M-cresol in bulk can form H-bonds due to the polar OH groups. Additionally, the aromatic ring is a good source for π-π stacking. At low temperatures, the bulk solvent is probably well-packed due to these interactions and NMR data also suggested such interactions. Once the temperature increases, the molecules gain entropy and their degree of freedom increases. On the other side, polypeptide chains experience interactions due to side chains and due to the backbone. In the binary system solvent-polypeptide, three types of interactions compete with each other: solvent-solvent,

polymer-polymer and solvent-polymer. Several studies evaluated the enthalpy associated with the peptide unfolding and have indicated that the contribution from the side chain to side chain interaction is much smaller than the contribution from the solvation of the peptide backbone.[59] Consequently the solvent acts like a spy molecule and inserts with its OH groups into these weak H-bonds of the polypeptide. The effect of m-cresol aromatic ring folding over the one of the polypeptide side chain protective groups has to be also taken in consideration.[77] During helix formation, the side moieties of PCBL align themselves along the helical axis.[75] At low temperatures, the polymer is well-solvated and essentially in an extended random coil conformation. Once the temperature elevates, the solvent-polypeptide H-bonds become loose and the polar sites of the backbone are "seeing" each other due to the departure of the solvent in the bulk state. A close proximity of such polar sites would result in the formation of H-bonds between C==O and NH backbone groups which also promotes the formation of a helix turn and polypeptide folding. The creation of the helix is entropically driven but once the first turn forms it can act as a nucleus for the rest of the remnant chain. In addition, the fact that the polypeptide chain is fixed with one end to the surface induces more stress whose compensation can be made on energy penalty.

The hypothesis formulated in the preceding paragraph on the transition complexity is sustained and confirmed first by DLS data. Figure 5.22 shows the four transient states proposed for PCBL transition. From one- and multi-angle DLS size fluctuation profiles, several states can be distinguished. At 15°C the chains are fully extended by the solvent in a random coil state. The H-bonding is dominated mainly by solvent-polymer interaction. The increase in the temperature causes a drop in PCBL-CP size suggesting a collapsed state. This corresponds with the solvent going in the bulk and the occurrence of a "naked" backbone.[76] This configuration can be

imagined by the fallen chains on the silica surface as illustrated in Figure 5.22B. The helix-forming temperature interval is characterized by a transition midpoint at which at least 50% helical fraction is present. During the interval marked by a sharper increase in size, the alternation of the random coil and the helical segments is probably the most favored constitution for the nascent rod-like polymer during collapsed chain-helix transition.[70] The formation of the loose helices is also promoted by the density of chains grafted on the surface.[72,78,79] The sample presented in Figure 5.9A had a grafting density of 0.9 μmol m^{-2} which translates to about 200,000 chains per particle. A dense population of chains would impact the transition by broadening its temperature interval as shown in for PCBL-CP175H and the inter-chain interactions can have as result the interrupted helical structure.[78] The loose conformation, Figure 5.22C, is reflected by an increase in the radius around 43-45°C. The drop in the colloid size at even higher temperatures suggests the transition from a loose helix into a more compact one, Figure 5.22D.

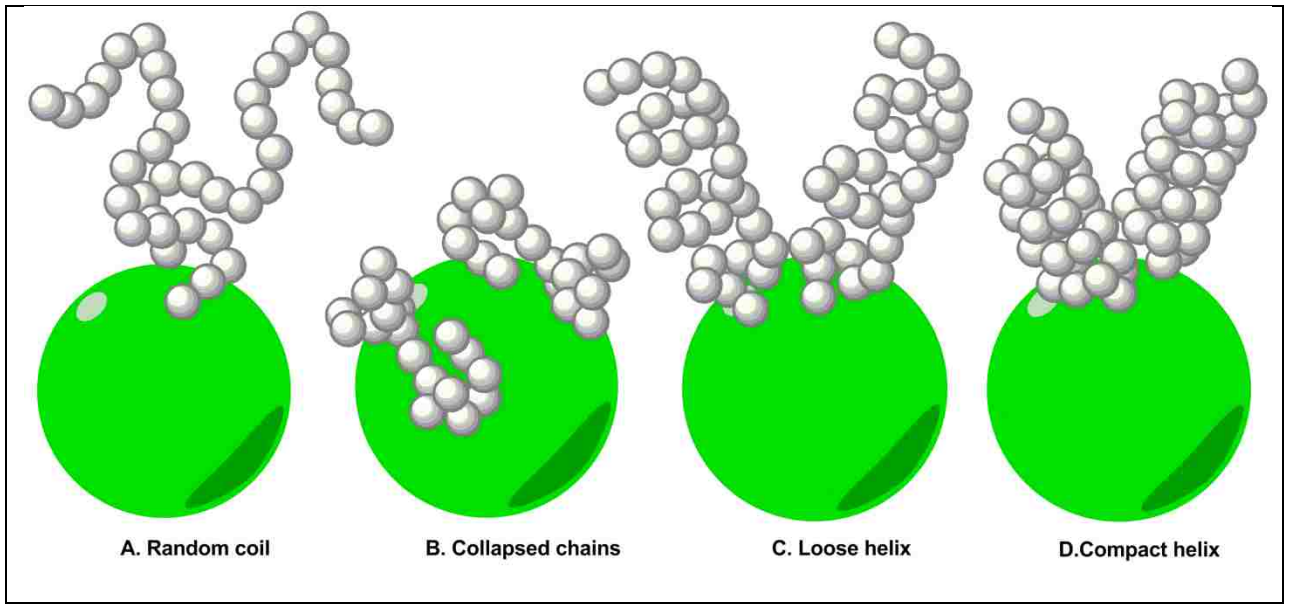

Figure 5.22 Schematic illustration of transient states associated with reverse coil-to-helix transition of PCBL in m-cresol as a function of temperature. The green circle symbolizes the silica bead and the grey circles the monomeric repeat unit of the polypeptide. Not drawn to scale.

The contribution from random coil segment flanking the end of the rod is insignificant and the chains can be treated as rigid rods. The schematic of the four states random coil, collapsed chains, loose helix and compact helix are illustrated in the Figure 5.22.

The confirmation of the rigid rod-like conformation was obtained by GPC means (details on Chapter 7). The representation of the radius as a function of the molecular weight in a semilogaritmic fashion revealed that the radius for the haircut polypeptide scaled well with the Flory exponent *v* equal to 1, characteristic for helix conformation.

The confirmation of these transient states especially transition from a loose helix to a compact helix was also supported by MDSC measurements. Moreover, as shown in Figure 5.20A, three endothermic humps were present in the MDSC profile of the tethered polypeptide at 17-23°C, broad 27-35°C and sharp 37°C and can be assigned to coil-to-collapsed chain, collapsed chain-to-helix and helix-to-helix transitions, respectively. The transition states, especially the collapsed chain, found in this work are in good agreement with the work published by Kemp et al[80] but on a reversed trend. Samulski et al. also observed these transient states at higher temperature but different system.[81]

The most intriguing feature of this transition is its reversibility. DLS multiple cycles on heating-cooling mode showed the good “memory” of the polypeptide undergoing from coil-to helix and back to coil state. Supplemental confirmation that supported the reversible character of the transition was gained by spin-lattice relaxation time, T1, measurements. PCBL-CP175L was cooled from 45°C directly to 25°C. The relaxation time measurement gained at 25°C was scaling with the first one, at the same temperature, within experimental error.

The DLS data revealed other useful information about the temperature responsive PCPs. Figure 5.23A shows the plot of the polypeptide radius in a random coil versus helix

configuration. The intersection between the coil, coil-to-collapsed chain sizes and collapsed chain-to-loose helix and loose helix-to-compact helix can be regarded as the most probable temperature at which the polypeptide has both random coil and helix segments. The position of such point depends greatly on the relationship between the curvature of the surface that holds the polymer and the grafting densities. PCBL-CP175H had a broader collapsed chain-to-loose helix and loose helix-to-compact helix temperature interval transition than PCBL-CP175L. The higher grafting density with amino function confirmed by zeta potential measurements could result in a higher loading with polymer. As discussed before, the polypeptide shell disposition of the two PCBL-CPs with a core of 175 nm, was considered similar with a polymer grafted on a flat surface. At high grafting, chains interpenetrate and most extend to relieve crowding.

Stretching of the chains in a collapsed state most probably balance with helix formation. Once the shell feels the surface curvature an energy penalty must be paid to stabilize the nascent helix due to the increased angle between the rods. This is seen for PCBL-CP100H and PCBL-CP55H even though the last had a low grafting density with functional groups, therefore less polymer chains on the surface. It is true that the relationship between the shell thickness and the core radius dictated the tethering disposition but no dependent trend can be attributed to them *per se* as shown in Figure 5.23B.

This study can be considered a good model to study the tethering of biological molecules such as viruses on the surfaces of different curvatures. One example is *Influenza* virus whose infecting mechanism is not fully understood. Thus, PCBL-CPs can mimic the infected cells. The expansion-contraction of the PCPs during transition can be also exploited in application regarding self-annealing of colloidal crystals. Due to the reversible trend of the transition, PCPs can be used as good platforms to study memory shaped materials.

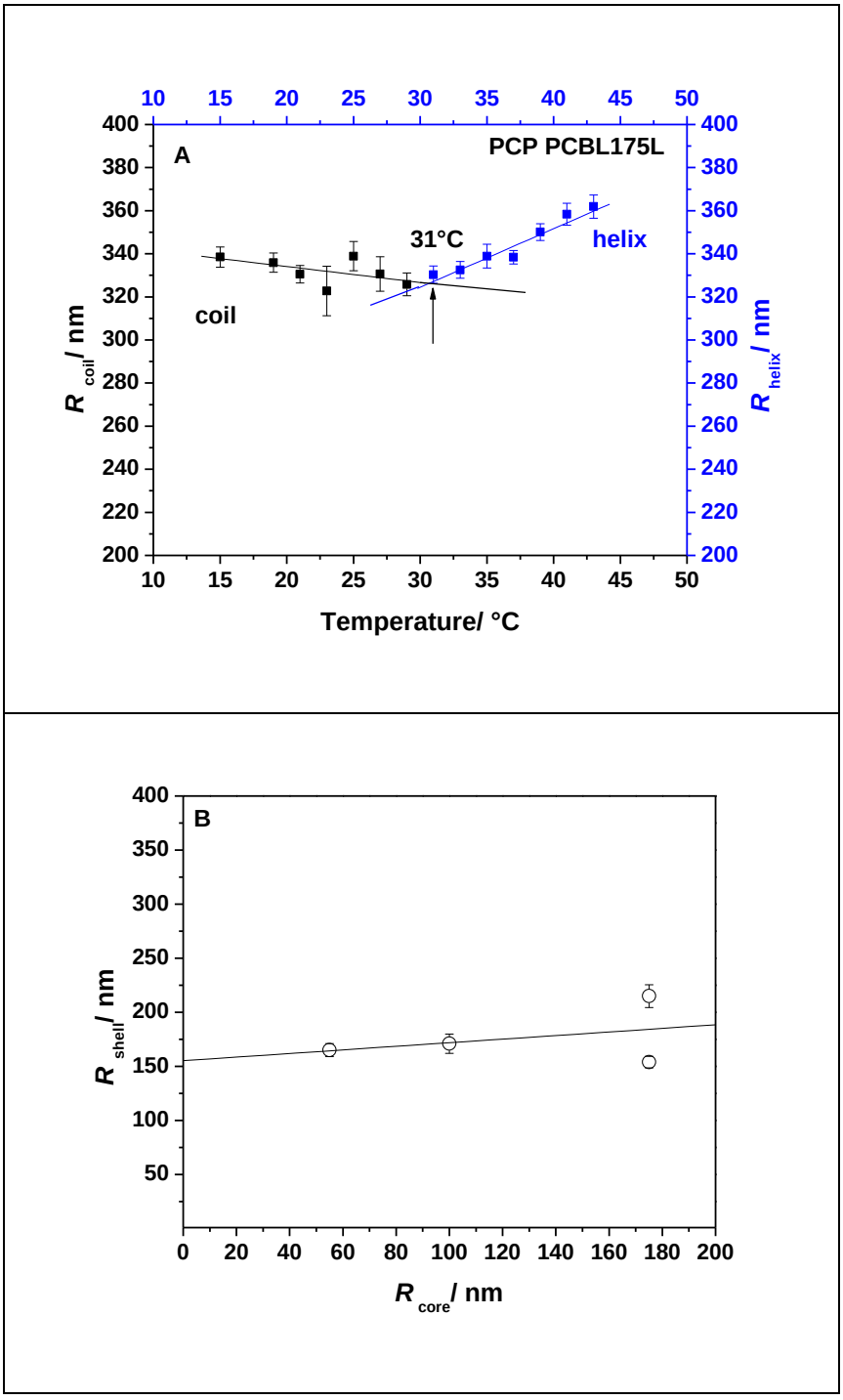

Figure 5.23 (A) tethered polypeptide radius in the coil and helix state as a function of the temperature and (B) shell radius as a function of the core radius. The shell radius was taken as an average over the values recorded on 15°-50°C temperature interval.

5.5 Conclusion

Polypeptide composite particles, PCPs, having a shell consisting of poly(Nε-carbobenzyloxy-L-lysine), PCBL were prepared by ring opening polymerization of corresponding N-carboxyanhydride, initiated by the amino group furnishing the surface of silica core. The confirmation of the polypeptide shell was possible by TEM, TGA and DLS assays. The combination of the TGA and zeta potential measurements offered the possibility to evaluate the amount of the amino functional group grafted onto the surface of the different sized silica cores. High and low graft densities were achieved. The zeta potential values measured agreed with the TGA measurements and supported the idea that in a multilayer disposition the functional groups act both as an initiator and a passivator as well. The variation of the shell size during inverse helix-to-coil transition as a function of the temperature in m-cresol was followed by DLS. After the independent behavior with the angle of the PCPs was confirmed the samples were measured at one angle, in order to obtain a faster image of the size behavior. All PCP samples aligned to a decrease-increase-decrease, DID, behavior. The reflection of the size changes was also seen in the DLS polydidpersity index, $\mu_2\ \Gamma^{-2}$ (IDID). The DID trend was also confirmed by multiangle measurements. The relaxation times corrected for the solvent viscosity increased with elevated temperature pointed to a sequestration of the free motion. Three regions were distinguished. MSDC measurements revealed that the transition evolves through two consecutive organized states. Together with the NMR data DSC measurements also showed the crucial role of the solvent in the transition occurrence. Due to similar structure with the polypeptide side chain m-cresol can interact through $\pi - \pi$ stacking. H-bonding between the solvent and polymer is another feature that can explain the unusual high cooperativity. Based on the DLS, NMR, MSDC and SAXS data four transient states could be proposed: random coil,

collapsed chain, loose helix and compact helix. The transition interval and its middle point were greatly dependent on the grafting density and the polypeptide loading. The intersection between the polypeptide size in random coil and helix was regarded as the point at which the polymer existed equally in both conformations. The thickness of the shell was found to be independent on the radius core.

5.6 References and Notes

(1) Zimm, B. H.; Doty, P.; Iso, K. Determination of the parameters for helix formation in poly-γ-benzyl-L-glutamate. *Proceedings of the National Academy of Sciences of the United States of America* **1959**, *45*, 1601-1604.

(2) Applequist, J. On helix-coil equilibrium in polypeptides. *J. Chem. Phys.* **1963**, *38*, 934-&.

(3) Rifkind, J.; Applequist, J. Helix interruption constant for poly-L-glutamic acid from pressure dependence of optical rotation. *J. Am. Chem. Soc.* **1964**, *86*, 4207-&.

(4) Doty, P.; Bradbury, J. H.; Holtzer, A. M. Polypeptides .4. The molecular weight, configuration and association of poly-γ-benzyl-L-glutamate in various solvents. *J. Am. Chem. Soc.* **1956**, *78*, 947-954.

(5) Doty, P.; Holtzer, A. M.; Bradbury, J. H.; Blout, E. R. Polypeptides .2. The configuration of polymers of γ-benzyl-L-glutamate in solution. *J. Am. Chem. Soc.* **1954**, *76*, 4493-4494.

(6) Doty, P.; Lundberg, R. D. The contribution of the alpha-helical configuration to the optical rotation of polypeptides and proteins. *Proceedings of the National Academy of Sciences of the United States of America* **1957**, *43*, 213-222.

(7) Doty, P.; Yang, J. T. Polypeptides .7. Poly-γ-benzyl-L-glutamate - the helix-coil transition in solution. *J. Am. Chem. Soc.* **1956**, *78*, 498-500.

(8) Karasz, F. E.; Oreilly, J. M. Deuteration and solvent composition effects in helix-coil transition of poly-γ-benzyl-L-glutamate. *Biopolymers* **1966**, *4*, 1015-&.

(9) Karasz, F. E.; Oreilly, J. M.; Bair, H. E. Thermal helix-coil transition in poly-γ-benzyl-L-glutamate. *Nature* **1964**, *202*, 693-&.

(10) Watanabe, H.; Yoshioka, K.; Wada, A. Electrooptical and dielectric investigations on the conformation and the electrical properties of poly-γ-benzyl-L-glutamate in mixed solvents. *Biopolymers* **1964**, *2*, 91-101.

(11) Ackerman.T; Neumann, E. Experimental thermodynamics of helix-random coil transition .1. Influence of polymer concentration and solvent composition in PBG-DCA-EDC system. *Biopolymers* **1967**, *5*, 649-&.

(12) Matsuoka, M.; Norisuye, T.; Teramoto, A.; Fujita, H. Solution properties of synthetic polypeptides .15. Helix-coil transition in poly(ε-carbobenzyloxy L-lysine). *Biopolymers* **1973**, *12*, 1515-1532.

(13) Nakamoto, K.; Suga, H.; Seki, S.; Teramoto, A.; Norisuye, T.; Fujita, H. Solution properties of synthetic polypeptides .19. Heat-capacity measurements on system of poly(ε-carbobenzyloxy-L-lysine) and meta-cresol in helix-coil transition region. *Macromolecules* **1974**, *7*, 784-789.

(14) Moffitt, W.; Yang, J. T. The optical rotatory dispersion of simple polypeptides .1. *Proceedings of the National Academy of Sciences of the United States of America* **1956**, *42*, 596-603.

(15) Moffitt, W. The optical rotatory dispersion of simple polypeptides .2. *Proceedings of the National Academy of Sciences of the United States of America* **1956**, *42*, 736-746.

(16) Tewari, U. S.; Vasudevan, P.; Ramakrishna, V. Viscosity behavior of ortho-cresol, meta-cresol and para-cresol melts. *Indian Journal of Chemistry* **1975**, *13*, 720-721.

(17) Omura, I.; Teramoto, A.; Fujita, H. Dielectric-dispersion of polypeptide solutions .2. Helix-coil transition of "poly(ε-carbobenzoxy-L-lysine) in m-cresol. *Macromolecules* **1975**, *8*, 284-290.

(18) Karasz, F. E.; Oreilly, J. M.; Bair, H. E. Helix-coil transition in poly-ε-carbobenzoxy-L-lysine. *Biopolymers* **1965**, *3*, 241.

(19) Fasman, G. D.; Idelson, M.; Blout, E. R. Synthesis and conformation of high molecular weight poly-ε-carbobenzyloxy-L-lysine and poly-L-lysine.HCL. *J. Am. Chem. Soc.* **1961**, *83*, 709.

(20) Applequist, J.; Doty, P. In *Polyamino Acids, Polypeptides, and Proteins*; Stahmann, M. A., Ed.; The University of Wisconsin Press, p. 161-175: Madison, 1962.

(21) Kratky, O.; Porod, G. Rontgenuntersuchung geloster fadenmolekule. *Recueil Des Travaux Chimiques Des Pays-Bas-Journal of the Royal Netherlands Chemical Society* **1949**, *68*, 1106-1122.

(22) Bradbury, E. M.; Brown, L.; Downie, A. R.; Elliott, A.; Hanby, W. E.; McDonald, T. R. R. Alpha-helices and a new polypeptide fold in poly-β-benzyl-L-aspartate. *Nature* **1959**, *183*, 1736-1737.

(23) Karlson, R. H.; Norland, K. S.; Fasman, G. D.; Blout, E. R. The helical sense of poly-β-benzyl-L-aspartate-synthesis and rotatory dispersion of copolymers of beta-benzyl-L and d-aspartate with γ-benzyl-L-glutamate. *J. Am. Chem. Soc.* **1960**, *82*, 2268-2275.

(24) Blout, E. R.; Deloze, C.; Bloom, S. M.; Fasman, G. D. The dependence of the conformations of synthetic polypeptides on amino acid composition. *J. Am. Chem. Soc.* **1960**, *82*, 3787-3789.

(25) Zimm, B. H.; Bragg, J. K. Theory of the phase transition between helix and random coil in polypeptide chains. *J. Chem. Phys.* **1959**, *31*, 526-535.

(26) Causgrove, T. P.; Dyer, R. B. Nonequilibrium protein folding dynamics: laser-induced pH-jump studies of the-helix-coil transition. *Chemical Physics* **2006**, *323*, 2-10.

(27) Gruenewald, B.; Nicola, C. U.; Lustig, A.; Schwarz, G.; Klump, H. Kinetics of the helix-coil transition of a polypeptide with nonionic side groups, derived from ultrasonic relaxation measurements. *Biophysical Chemistry* **1979**, *9*, 137-147.

(28) Huang, C. Y.; Getahun, Z.; Wang, T.; DeGrado, W. F.; Gai, F. Time-resolved infrared study of the helix-coil transition using C-13-labeled helical peptides. *J. Am. Chem. Soc.* **2001**, *123*, 12111-12112.

(29) Huang, C. Y.; Getahun, Z.; Zhu, Y. J.; Klemke, J. W.; DeGrado, W. F.; Gai, F. Helix formation via conformation diffusion search. *Proceedings of the National Academy of Sciences of the United States of America* **2002**, *99*, 2788-2793.

(30) Sano, T.; Yasunaga, T. Kinetics of helix-coil transition of polypeptides in solution by the relaxation methods. *Biophysical Chemistry* **1980**, *11*, 377-386.

(31) Skolnick, J. Theory of the kinetics of the helix coil transition in 2-chain, coiled coils1. Infinite-chain limit. *Macromolecules* **1984**, *17*, 2158-2173.

(32) Skolnick, J. Theory of the kinetics of the helix coil transition in 2-chain, coiled coils. 2. The finite chain. *Macromolecules* **1985**, *18*, 232-243.

(33) Valles, J. L.; Sagues, F. Monte-carlo simulation of the kinetics of the helix coil transition in a synthetic DNA. *Chemical Physics Letters* **1985**, *122*, 459-464.

(34) van Giessen, A. E.; Straub, J. E. Coarse-grained model of coil-to-helix kinetics demonstrates the importance of multiple nucleation sites in helix folding. *Journal of Chemical Theory and Computation* **2006**, *2*, 674-684.

(35) De Sancho, D.; Best, R. B. What Is the Time Scale for alpha-Helix Nucleation? *J. Am. Chem. Soc.* **2011**, *133*, 6809-6816.

(36) Serrano, A. L.; Tucker, M. J.; Gai, F. Direct Assessment of the α-Helix Nucleation Time. *Journal of Physical Chemistry B* **2011**, *115*, 7472-7478.

(37) Badasyan, A. V.; Giacometti, A.; Mamasakhlisov, Y. S.; Morozov, V. F.; Benight, A. S. Microscopic formulation of the Zimm-Bragg model for the helix-coil transition. *Physical Review E* **2010**, *81*.

(38) Buchete, N. V.; Straub, J. E. Mean first-passage time calculations for the coil-to-helix transition: The active helix Ising model. *Journal of Physical Chemistry B* **2001**, *105*, 6684-6697.

(39) Vorov, O. K.; Livesay, D. R.; Jacobs, D. J. Helix/Coil Nucleation: A Local Response to Global Demands. *Biophysical Journal* **2009**, *97*, 3000-3009.

(40) Daly, W. H.; PochÃ©, D. The preparation of N-carboxyanhydrides of Î±-amino acids using bis(trichloromethyl)carbonate. *Tetrahedron Letters* **1988**, *29*, 5859-5862.

(41) Poche, D. S.; Moore, M. J.; Bowles, J. L. An unconventional method for purifying the N-carboxyanhydride derivatives of γ-alkyl-L-glutamates. *Synthetic Communications* **1999**, *29*, 843-854.

(42) Bogush, G. H.; Tracy, M. A.; Zukoski, C. F. Preparation of monodisperse silica particles - control of size and mass fraction. *Journal of Non-Crystalline Solids* **1988**, *104*, 95-106.

(43) Deng, T.-S.; Zhang, Q.-F.; Zhang, J.-Y.; Shen, X.; Zhu, K.-T.; Wu, J.-L. One-step synthesis of highly monodisperse hybrid silica spheres in aqueous solution. *Journal of Colloid and Interface Science* **2009**, *329*, 292-299.

(44) Rao, K. S.; El-Hami, K.; Kodaki, T.; Matsushige, K.; Makino, K. A novel method for synthesis of silica nanoparticles. *Journal of Colloid and Interface Science* **2005**, *289*, 125-131.

(45) Stober, W.; Fink, A.; Bohn, E. Controlled Growth of Monodisperse Silica Spheres in the Micron Size Range. *Journal of Colloid and Interface Science* **1968**, *26*, 62-69.

(46) Zhang, J. H.; Zhan, P.; Wang, Z. L.; Zhang, W. Y.; Ming, N. B. Preparation of monodisperse silica particles with controllable size and shape. *J. Mater. Res.* **2003**, *18*, 649-653.

(47) Turksen, S. Ph. D. Dissertation, Synthesis and Characterization of Superparamagnetic Silica-homopolypeptide Composite Particles. Louisiana State University, 2006.

(48) Campelj, S.; Makovec, D.; Drofenik, M. Functionalization of magnetic nanoparticles with 3-aminopropyl silane. *Journal of Magnetism and Magnetic Materials* **2009**, *321*, 1346-1350.

(49) Balamurugan, S. S.; Soto-Cantu, E.; Cueto, R.; Russo, P. S. Preparation of Organosoluble Silica-Polypeptide Particles by "Click" Chemistry. *Macromolecules* **2010**, *43*, 62-70.

(50) Bartholome, C.; Beyou, E.; Bourgeat-Lami, E.; Chaumont, P.; Zydowicz, N. Nitroxide-mediated polymerizations from silica nanoparticle surfaces: "Graft from" polymerization of styrene using a triethoxysilyl-terminated alkoxyamine initiator. *Macromolecules* **2003**, *36*, 7946-7952.

(51) Cousinie, S.; Gressier, M.; Alphonse, P.; Menu, M. J. Silica-based nanohybrids containing dipyridine, urethan, or urea derivatives. *Chem. Mat.* **2007**, *19*, 6492-6503.

(52) Soto-Cantu, E.; Cueto, R.; Koch, J.; Russo, P. S. Synthesis and Rapid Characterization of Amine-Functionalized Silica. *Langmuir* **2012**, *28*, 5562-5569.

(53) van de Waterbeemd, M.; Sen, T.; Biagini, S.; Bruce, I. J. Surface functionalisation of magnetic nanoparticles: quantification of surface to bulk amine density. *Micro & Nano Letters* **2010**, *5*, 282-285.

(54) Kralj, S.; Drofenik, M.; Makovec, D. Controlled surface functionalization of silica-coated magnetic nanoparticles with terminal amino and carboxyl groups. *Journal of Nanoparticle Research* **2011**, *13*, 2829-2841.

(55) McCormick, M.; Reimer, J. R. A. NMR studies of structural phase transitions in random copolymers. *Macromolecules* **2003**, *36*, 477-485.

(56) Ponomarenko, E. A.; Tirrell, D. A.; MacKnight, W. J. Stoichiometric complexes of synthetic polypeptides and oppositely charged surfactants in organic solvents and in the solid state. *Macromolecules* **1996**, *29*, 8751-8758.

(57) Raby, P.; Budd, P. M.; Heatley, F.; Price, C. Nuclear magnetic-relaxation of alpha-C-13-nuclei of helical poly(γ-hexyl-L-glutamate) and poly(γ-benzyl-L-glutamate). *Journal of Polymer Science Part B-Polymer Physics* **1991**, *29*, 451-456.

(58) Allerhan.A; Oldfield, E. Determination of rotational mobilities of backbone and side-chain carbons of poly(γ-benzyl L-glutamate) in helical and random-coil states from measurements of C-13 relaxation-times and nuclear overhauser enhancements. *Biochemistry* **1973**, *12*, 3428-3433.

(59) Richardson, J. M.; Makhatadze, G. I. Temperature dependence of the thermodynamics of helix-coil transition. *Journal of Molecular Biology* **2004**, *335*, 1029-1037.

(60) Scholtz, J. M.; Marqusee, S.; Baldwin, R. L.; York, E. J.; Stewart, J. M.; Santoro, M.; Bolen, D. W. Calorimetric determination of the enthalpy change for the alpha-helix to coil

transition of an alanine peptide in water. *Proceedings of the National Academy of Sciences of the United States of America* **1991**, *88*, 2854-2858.

(61) Stribeck, N. *X-Ray Scattering of Soft Matter*; Springer Berlin Heidleberg: New York, 2007.

(62) Balmer, J. A.; Mykhaylyk, O. O.; Schmid, A.; Armes, S. P.; Fairclough, J. P. A.; Ryan, A. J. Characterization of Polymer-Silica Nanocomposite Particles with Core-Shell Morphologies using Monte Carlo Simulations and Small Angle X-ray Scattering. *Langmuir* **2011**, *27*, 8075-8089.

(63) Ballauff, M. Nanoscopic polymer particles with a well-defined surface: Synthesis, characterization, and properties. *Macromol. Chem. Phys.* **2003**, *204*, 220-234.

(64) Dingenouts, N.; Norhausen, C.; Ballauff, M. Observation of the volume transition in thermosensitive core-shell latex particles by small-angle X-ray scattering. *Macromolecules* **1998**, *31*, 8912-8917.

(65) Ooi, W.-Y.; Fujita, M.; Pan, P.; Tang, H.-Y.; Sudesh, K.; Ito, K.; Kanayama, N.; Takarada, T.; Maeda, M. Structural characterization of nanoparticles from thermoresponsive poly(N-isopropylacrylamide)-DNA conjugate. *Journal of Colloid and Interface Science* **2012**, *374*, 315-320.

(66) Pavlopoulou, E.; Portale, G.; Christodoulakis, K. E.; Vamvakaki, M.; Bras, W.; Anastasiadis, S. H. Following the Synthesis of Metal Nanoparticles within pH-Responsive Microgel Particles by SAXS. *Macromolecules* **2010**, *43*, 9828-9836.

(67) Berndt, I.; Pedersen, J. S.; Lindner, P.; Richtering, W. Influence of shell thickness and cross-link density on the structure of temperature-sensitive - Poly-N-isopropylacrylamide-poly-N-isopropylmethacrylamide core-shell microgels investigated by small-angle neutron scattering. *Langmuir* **2006**, *22*, 459-468.

(68) Kratochvil, P. In *Light Scattering from Polymer Solutions*; Huglin, M. B., Ed.; Academic Press: New York, 1972, p 333-379.

(69) Buhot, A.; Halperin, A. On the helix-coil transition in grafted chains. *Europhysics Letters* **2000**, *50*, 756-761.

(70) Buhot, A.; Halperin, A. Extension Behavior of helicogenic polypeptides. *Macromolecules* **2002**, *35*, 3238-3252.

(71) Wang, Y. L.; Chang, Y. C. Synthesis and conformational transition of surface-tethered polypeptide: Poly(L-lysine). *Macromolecules* **2003**, *36*, 6511-6518.

(72) Wang, Y. L.; Chang, Y. C. Synthesis and conformational transition of surface-tethered polypeptide: Poly(L-glutamic acid). *Macromolecules* **2003**, *36*, 6503-6510.

(73) Hayashi, T.; Emi, S.; Nakajima, A. Helix-coil transition of poly(ε-carbobenzyloxy-L-lysine) in m-cresol. *Polymer* **1975**, *16*, 396-400.

(74) Badasyan, A. V.; Tonoyan, S. A.; Mamasakhlisov, Y. S.; Giacometti, A.; Benight, A. S.; Morozov, V. F. Competition for hydrogen-bond formation in the helix-coil transition and protein folding. *Physical Review E* **2011**, *83*.

(75) Wei, Y. J.; Nadler, W.; Hansmann, U. H. E. Side-chain and backbone ordering in homopolymers. *Journal of Physical Chemistry B* **2007**, *111*, 4244-4250.

(76) Scheraga, H. A.; Vila, J. A.; Ripoll, D. R. Helixâ€“coil transitions re-visited. *Biophysical Chemistry* **2002**, *101â€“102*, 255-265.

(77) Kaposta-Stanca, E. C.; Su, Z.; Simon, J. P.; Hurtado, P.; Gamblin, D.; Davis, B. *Hydrogen bonding vs. dispersive interactions: carbohydrate-p-cresol complexes*, University of Oxford, 2007/2008.

(78) Wang, J.; Lu, H.; Ren, Y.; Zhang, Y. F.; Morton, M.; Cheng, J. J.; Lin, Y. Interrupted Helical Structure of Grafted Polypeptides in Brush-Like Macromolecules. *Macromolecules* **2011**, *44*, 8699-8708.

(79) Kastantin, M.; Tirrell, M. Helix Formation in the Polymer Brush. *Macromolecules* **2011**, *44*, 4977-4987.

(80) Kemp, J. P.; Chen, J. Z. Y. Helical structures in proteins. *Biomacromolecules* **2001**, *2*, 389-401.

(81) Samulski, E. T.; Chien, M.; Wade, C. G. Polypeptide sidechain secondary structure and helix-coil transition - NMR relaxation study. *Journal of Polymer Science Part C-Polymer Symposium* **1974**, 335-340.

CHAPTER 6
POLYCOLLOIDS: PREPARATION AND CHARACTERIZATION OF CROSS-LINKED POLYTYROSINE-SILICA HYBRID COLLOIDS

6.1 Introduction

Tyrosine, TYR is a unique amino acid with versatile chemical properties. Bearing a phenol group in the side chain, TYR can form different types of hydrogen bonds.[1] Upon deprotonation, the tyrosinyl anion can be further oxidized to a neutral radical by direct proton release.[2] Hydrogen bonding also plays a key role in the conformation of polytyrosine PTYR obtained from TYR polymerization. Several studies were devoted to elucidate the PTYR structure. While in most organic solvents this homopolypeptide assumes an α-helical conformation,[3-7] in aqueous solution PTYR has an antiparallel *β*-conformation as the degree of ionization of hydroxyl groups from phenol ring decreases.[8-15] Hamada et al. investigated the conformation of PTYR in dimethylformamide DMF by small-angle X-ray scattering (SAXS) and found a right-handed α-helix.[16] Other extensively used techniques in analyzing homopolymers of amino acids are circular dichroism CD and optical rotation ORD. Polypeptides having aromatic rings in their side chain do not show the typical CD spectrum of the secondary structure.[17-22] The cause arises from overlapping of the optical rotation of aromatic chromophores and optical activity of the backbone's amide chromophore. Circular dichroism was used by various research groups in their effort to elucidate the secondary structure of polytyrosine and contrasting conclusions were withdrawn. Beychok et al. dissolved PTYR in water at pH 11.2 and reported a helical conformation. Dissolution above pH 12 followed by back titration to pH 11.2 revealed a random coil structure.[23] On the contrary, Friedman et al. investigations found different spectrum patterns while PTYR was retaining its helical conformation. They suggested that the difference

in the degree of ionization of the phenol rings might be responsible for such behavior.[24] Watanabe et al. were able to separate the CD component of the backbone of the tyrosyl fragments using fluorescence detected circular dichroism FDCD. The presence of the two negative peaks centered at 213 nm and 222 nm, were attributed to the α-helix conformation when dissolved in methanol. Transition from helical to β-sheet structure was induced by addition of aqueous NaOH.[25] In addition to CD and ORD, Wen et al. used viscosity and infrared spectroscopy (IR) and found a random coil conformation in dimethyl sulfoxide DMSO. Upon addition of dichloroacetic acid DCA, PTYR underwent to a coil-to-helix transition, its completion being attained at 20% DCA.[26] Beside the above mentioned methods, nuclear magnetic resonance (NMR)[6] and vibrational circular dichroism VCD[27] were used to elucidate PTYR conformation. Theoretical methods pointed to a right-handed α-helix conformation.[28]

The unique nature of tyrosine, a hydrophobic side chain comprised of a phenol ring moiety, indicates TYR a potential candidate for many biological applications. The rigid side chain, conductive even at low entropic energy loss, can interact with antigens. Thus, tyrosine is ideal for recognition of antibodies.[29-37] Phosphorylation of sidechain hydroxyl groups by tyrosine kinases plays an important role in signal transduction processes.[38]

Tyrosine residues can be easily coupled to di- and trityrosine adducts. Such processes take place naturally; a good example is post-translational modification of proteins. Resilin, found in insects and anthropods, increases dramatically its elasticity due to intermolecular crosslinking.[39,40] Other tyrosine coupling products were found in keratin,[41] collagen,[42,43] cuticlin,[44] elastin,[45,46] extensin[47] and fibroin.[41] Tyrosine also takes advantage over N-terminus amino acids (lysine), terminal carboxyl groups (aspartic acid, glutamic acid) or cysteine's thiol

group in protein modification. Hydrophobic tyrosine has a higher site-specificity than hydrophilic amino acids because fewer TYR residues are exposed to the protein surface.

Chemical cross-linking is an appealing tool for engineering the architecture of proteins. Many oxidative reactions were developed by researchers over the years.[48-51] Enzymatic reactions were also employed, especially tyrosine coupling catalyzed by peroxidases.[52-57] *Horseradish peroxidase*-assisted coupling is one of the most utilized enzymatic approaches in cross-linking tyrosine residues. During its enzymatic cycle,[58-60] HRP assists the formation of a free radical in the phenol moiety. Recently Minamihata et al. genetically introduced at the C-terminus of *Escheria coli* alkaline phosphatase, a peptide tag containing tyrosine moieties which were further cross-linked by incubation in HRP and H_2O_2.[36] Grupen's group and collaborators coupled hydroxy-arylated oligosaccharides with tripeptides having tyrosine.[61] Heijnis et al. isolated the dimer of α-lactalbumin and studied its cross-linking path. Structural modeling indicated that intermolecular cross-linking of tyrosine is favored.[62]

In the late 1990s Kodadek's group develop a fast and versatile method for coupling peptides bearing tyrosine residues: photo-induced cross-linking of unmodified proteins, PICUP. They photogenerated an oxidant specie involving tris-bipyridylruthenium (II) for coupling of associated proteins containing tyrosine.[63,64] Cross-linked products in very high yields were obtained with irradiation times less than 1s.

The formation of amyloids *β*-protein (Aβ) deposits (fibrils and neurotoxic oligomers) is a progressive neurodegenerative process. These deposits were believed to be the key factor causing diseases such as Alzheimer's. Bitan et al. used PICUP to understand earliest the stages of Aβ oligomerization.[65-71] Covalent linkage through PICUP system made possible the stabilization of prion proteins (PrP) aggregates in their native structure, proving that degradation

of structural features involved in prion propagation were not affected by the cross-linking procedure.[72] Clérico et al. explored the cross-linking pattern when signal peptides were linked to *E. coli* signal recognition particle.[73]

In the present work polytyrosine was grown on silica particles. The hybrid colloids are of particular interest because they can serve as models for improved understanding of the behavior of protein-caged materials like viruses. Many methods to immobilize polymers or biomacromolecules onto particles exist, but *growing from* was chosen because it yields a higher grafting density and a thicker shell is obtained with fewer steps. In this approach the surface is functionalized with initiating groups that promote the polymerization upon addition of monomer.[74]A drawback of this method is the characterization of grafted polymer. Yet etching silica core with either solution of hydrofluoric acid, HF, complexes containing fluorine[75-78] or alkaline aqueous solution (NaOH, KOH)[79,80] can circumvent the challenge. Concerns regarded the degradation of the polypeptide chain as well as a consequence of etching. This group has reported poly(γ-benzyl-L-glutamate), PBLG and poly(Nε-carbobenzyloxy-L-lysine), PCBL polypeptide-coated silica colloids.[74,81,82] Even though the properties of the polytyrosine-based hybrid are appealing from the point of view of biological application, no work has been attempted to explore the direct growth of PTYR homopolypeptide on colloid surfaces. Indirectly, in an effort to understand cell adhesion, Auenheimer et al. studied the amount of cyclic arginine-glycine-aspartate (RGD) protein radio labeled with ^{125}I of tyrosine containing RGD bound to different surfaces.[83] Fan et al. used fluorescence immunostaining with tyrosine hydroxylase to evaluate the effect of surface roughness on central neural cells (*Substantia nigra*) adherence to silicon wafers.[84]

This work concerns the use of cross-linking methods to prepare polycolloids. The versatility of the photopolymerization, PICUP, method is compared with polymerization assisted by enzymatic *Horseradish peroxidase*. The use of PICUP procedure to cross-link proteins is extended to the colloidal size domain to attempt the production of poly(colloids). Because the colloidal particles do not naturally aggregate, unlike amyloids peptide fragments so successfully stitched together using PICUP, they were made with magnetic inclusions to draw them close in chains.

6.2 Materials

O-benzyl-L-tyrosine (99%) was purchased from Indofine Chemical Company, Inc., and Sigma-Aldrich, triphosgene (99%) was obtained from Acros Organics. Hydrobromic acid solution (HBr) (30 %) in acetic acid, NaOH, tetraethylorthosilicate (TEOS) (99%), 3-amino-propyl-tetraorthosilicate (APS, 99%), cobalt chloride hexahydrate ($CoCl_2$ x $6H_2O$), sodium borohydride ($NaNH_4$) (%), citric acid (%), phosphate monobasic, NaH_2PO4, phosphate dibasic, Na_2HPO4, anhydrous magnesium sulfate ($MgSO_4$), sodium bicarbonate, Na_2CO_3, Peroxidase, from horseradish, type VI, essentially salt-free, lyophilized poeder, 274 units/ mg solid, tris(2,2´ bipyridyl)dichloro-ruthenium(II) hexahydrate, anhydrous (≥99.9%) dimethylsulfoxide were obtained from Sigma-Aldrich. Anhydrous solvents such as tetrahydrofuran (THF), hexanes, ethyl acetate (EtOAc) were purchased from Aldrich and used as received. Absolute anhydrous ethyl alcohol 200 proof ACS/USP grade was obtained from Pharmco-AAPER. Ammonium hydroxide 28-30% ACS grade was purchased from BDH Aristar. All reagents were used without further purification. Deionized water (18 mΩ) was drawn from a Barnstead Nanopure instrument.

6.3 Results and Discussion

6.3.1 Core and Polypeptide Precursor Preparation.

Silica non-magnetic cores were prepared following the well-known Stöber method with modifications.[85,86] The synthetic route for the fabrication of the Co-nugget silica particles followed Kobayashi procedure[87] and is shown in the Scheme 6.1.

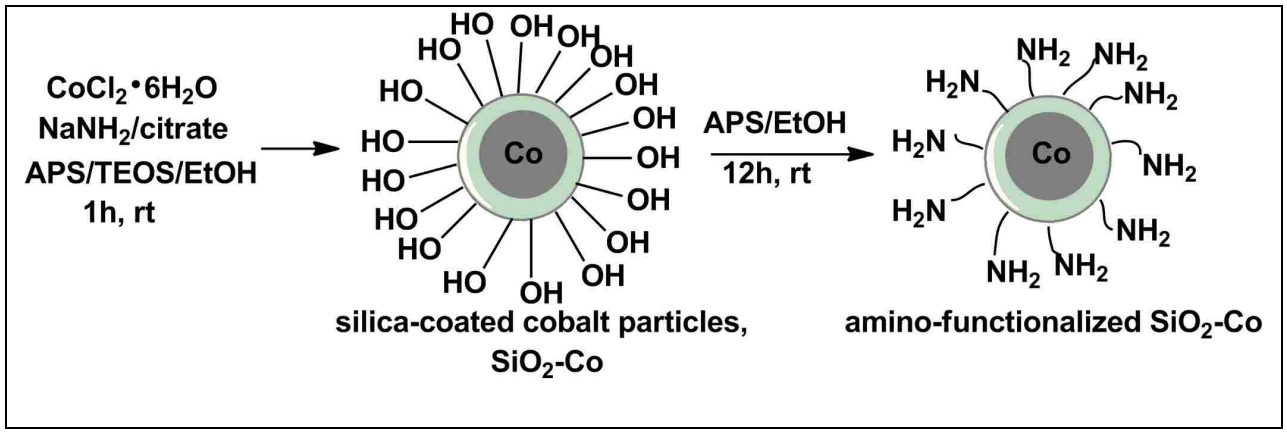

Scheme 6.1 Schematic representation of preparation of amino-functionalized silica-coated cobalt particles

The reduction of cobalt salt, $CoCl_2 \cdot 6H_2O$, in the presence of sodium borohydride, $NaNH_4$, yielded cobalt particles with a diameter of 15 nm measured by TEM. Due to their sensitivity to oxygen exposure, cobalt nougats were covered immediately after their preparation with a protective silica layer in a one-pot reaction. The addition of 3-aminopropyl-triethoxysilane, APS primed the surface for the TEOS on the cobalt surface. Cobalt particles do not have hydroxyl, OH, groups on the surface like silica necessary in TEOS polymerization. Instead cobalt has a high affinity to form coordination complexes with amino carriers. The morphology of the synthesized cores is presented in Figure 6.1.

The size distribution of the non- and magnetic cores was investigated by multi-angle dynamic light scattering, as shown in Figure 6.2.

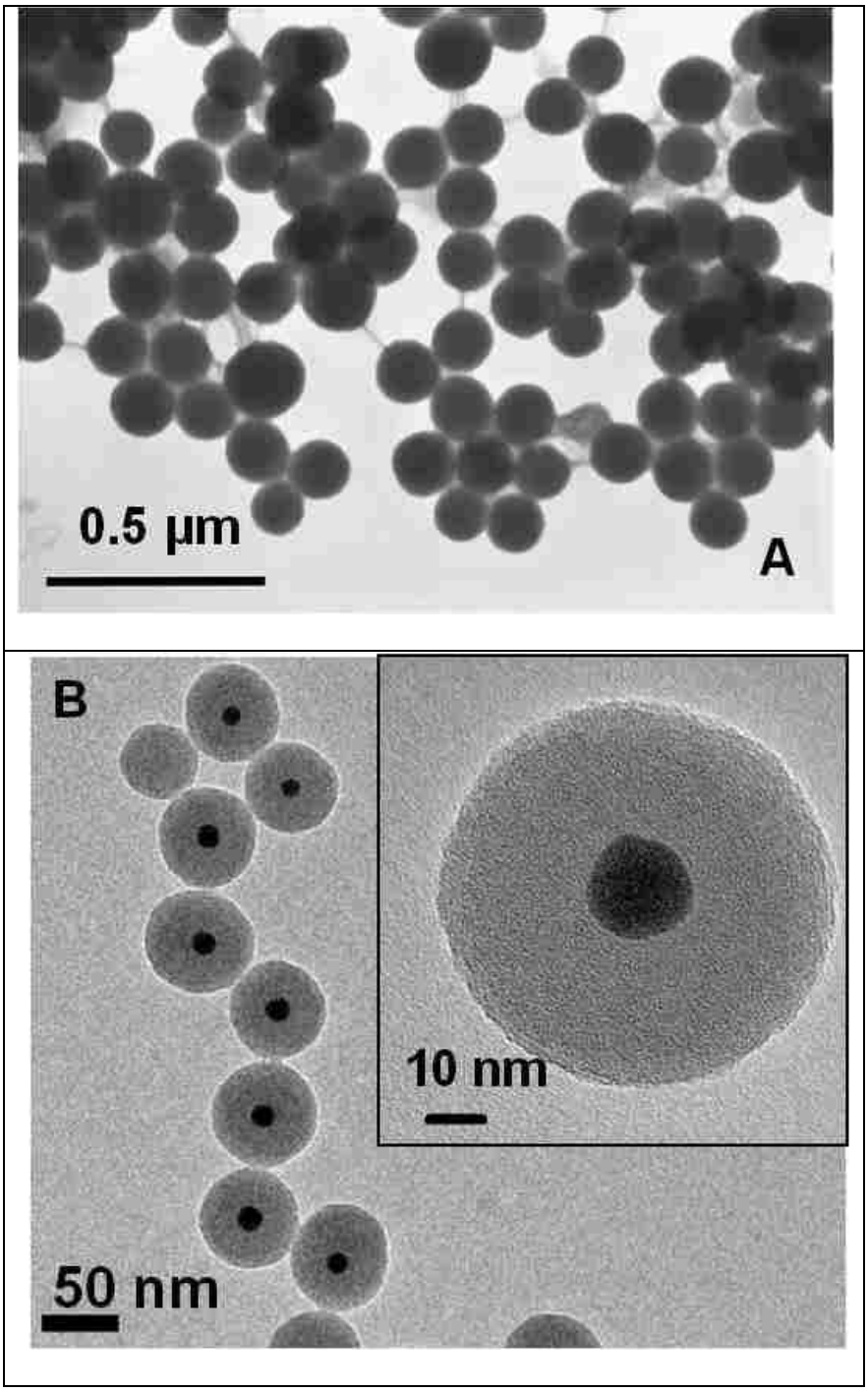

Figure 6.1 TEM images of silica cores (A) and HRTEM of silica-coated cobalt particles (B).

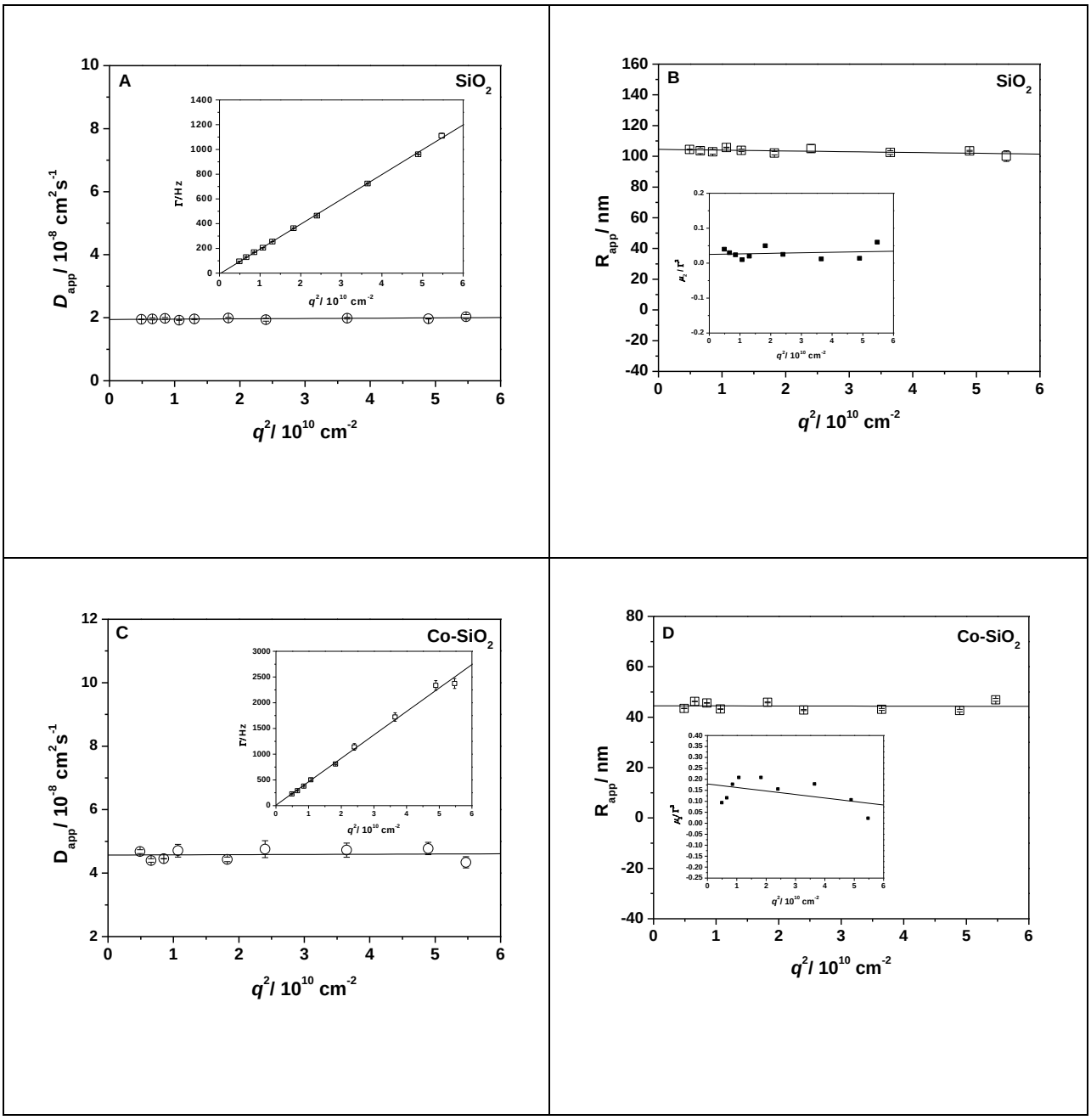

Figure 6.2 Apparent diffusion coefficients, D_{app}, and the decay rates (inset) as a function of the squared scattering vector magnitude, q, for silica (A) and silica-coated cobalt particles (C); apparent radius, R_{app} and polydispersity index, $\mu_2\ \Gamma^{-2}$, (inset) versus q^2 for silica (CR7124) (B) and silica-coated cobalt colloids (CR842mag) (D). Measurements were performed in water (silica) and ethanol (cobalt-coated silica) at 25°C over 9 angles from 30° to 120°.

DLS results show that these particles were uniform because no angle dependency was noted, Figures 6.2B and6.2D. This argument applies better to large particles than to small ones. Table 6.1 summarizes the core sizes evaluated by DLS.

Table 6.1 Sample, Solvent, Temperature, Radius and Polydispersity Index of Silica and Silica-coated Cobalt Particles from Multi-angle Measurements

Sample	Solvent	Temperature/ °C	Radius/ nm	PDI, $\mu_2 \Gamma^{-2}$
Silica 230 (CR7124)	Ethanol	25	124 ± 4.7	0.05 ± 0.04
Co-silica (CR842mag)	Ethanol	25	44.4 ± 0.23	0.16 ± 0.04
Silica 620 (CR10165)	Water	25	620 ± 16	0.35 ± 0.03

Even though the size of the magnetic particles was much smaller than the size of the bare silica they were slower diffusers, Figure 6.2C. The movement of the particles in the solution is dominated by friction which is size dependent.

Due to the size of the cobalt inclusion (less than 20 nm), the silica-coated cobalt particles were expected to show superparamagnetic behavior. Such particles align when exposed to a permanent magnetic field but lose the orientation instantly, once the magnetic field is removed. The magnetic behavior was visualized with an optical microscope as displayed in Figure 6.3.

Indeed before exposure to a magnetic field provided by a neodymium magnet, particles were diffusing randomly. Once the magnet was placed close to the capillary containing the particles, they began to align. After fifteen minutes clear strings of particles could be seen as shown in the Figure 6.3, middle. The removal of the magnet caused the chained particles to instantly move randomly as individual particles again.

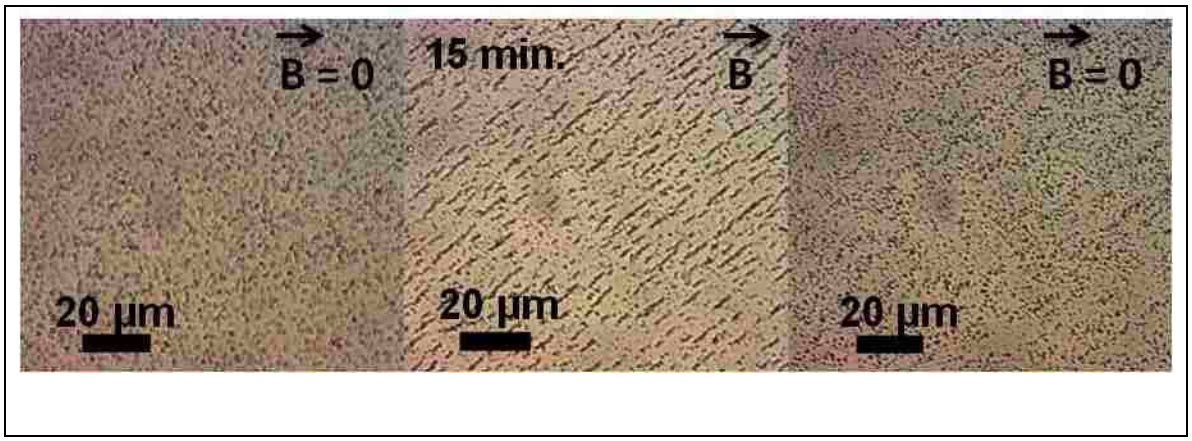

Figure 6.3 Optical micrographs of silica-coated cobalt particles (CR842mag) before exposure to a magnetic field (left), fifteen minutes under exposure (middle) and immediately after the magnetic field was removed. The magnet was placed at ~45° to the capillary containing the particles.

The polypeptide monomer precursor, o-benzyl-L-tyrosine N-carboxyanhydride, BTY-NCA, was prepared by adapting the Poché et al. procedure[88,89] as illustrated in Scheme 6.2.

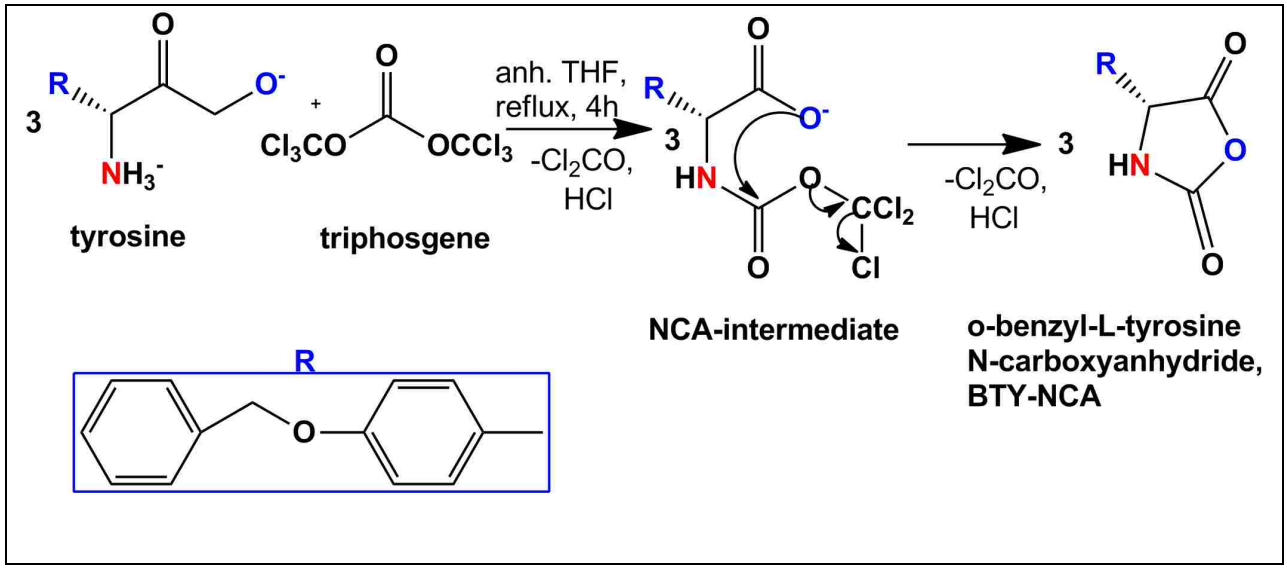

Scheme 6.2 Representation of BTY-NCA formation using triphosgene as the ring closure agent.

The closure of the BTY-NCA ring was performed with triphosgene. The protected aminoacid was selected for NCA preparation because, without the protective benzyl groups, the NCA

formation can evolve simultaneously with *in-situ* polymerization initiated by the free hydroxyl groups. The reaction product was analyzed by FTIR. The spectrum presented in Figure 6.4 shows the characteristic peaks of BTY-NCA. The characteristic bands of carbonyl groups C=O can be seen at 1840 and 1774 cm^{-1}. The stretching of the —NH— occurred at ~3300 cm^{-1}. The peaks seen at 3000 and 2800- 2900 cm^{-1} correspond to benzyl and —CH_2— symmetric and asymmetric stretching.

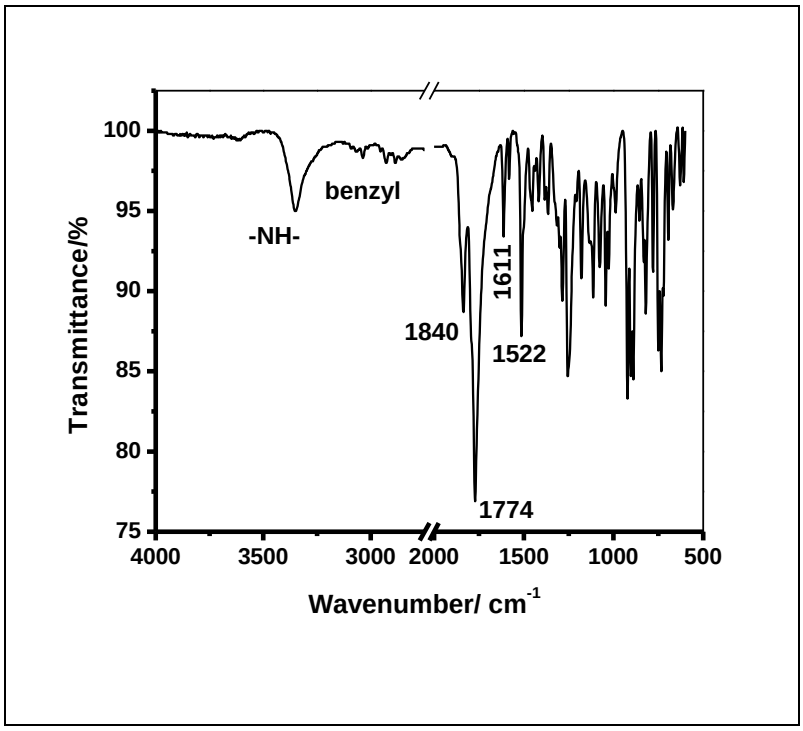

Figure 6.4 FTIR spectrum of o-benzyl-L-tyrosine N-carboxyanhydride, BTY-NCA.

6.3.2 Preparation of Polytyrosine Composite Particles.

The preparation of PCPs having a shell consisting of benzyl-protected poly(L-tyrosine), PCP PBTY, was achieved by employing *growing from* method.[74,90-92] Three batches, two non-magnetic (PTYR PCP230 and PTYR PCP620, the number indicates the diameter of the core) and one Co-nougat composite particles were prepared in the same fashion. Scheme 6.3 illustrates the

synthesis of magnetic composites. Amino-functionalized particles were reacted with polypeptide precursor, o-benzyl-L-tyrosine N-carboxyanhydride. After the reaction completed, the PCP PBTY particles were collected by centrifugation and washed several times (3-4) with THF by centrifugation-redispersions to remove any unreacted polypeptide. In order to convert poly(o-benzyl-L-tyrosine) to unprotected poly(L-tyrosine) the former was treated with HBr/CH_3COOH, 33%. The purification of the PCP PTYR colloid was performed with toluene and acetone by centrifugation-redispersion to remove benzyl bromide. Then the particles were neutralized with 3mM NaOH solution and finally were washed with deionized water using centrifugation-redispersion method. The cleavage of the benzyl protective side group yielded a water-dispersible product, PCP PTYR, carrying free hydroxyl groups.

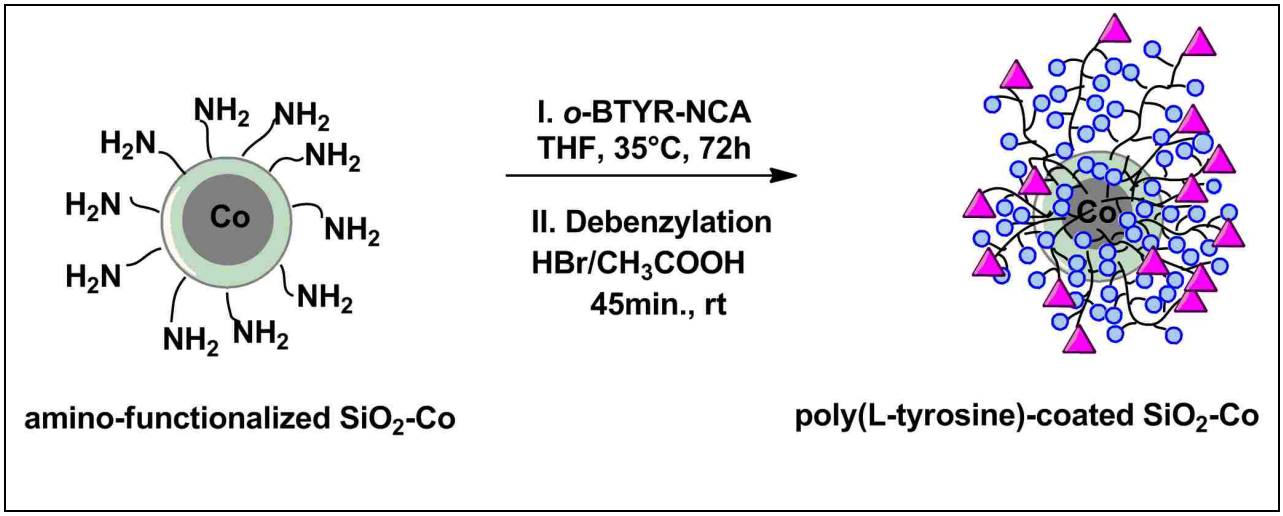

Scheme 6.3 Schematic representation of magnetic poly(L-tyrosine) composite particles prepared by the *growing from* method.

A picture of the PCP PTYR particles is shown in Figure 6.5. Figure 6.5A shows the presence of the polypeptide shell seen as the dark corona surrounding the silica core which is not visible in Figure 6.1A of plain silica or Figure 6.5B showing the magnetic PTYR PCPs. The visualization

of the shell was achieved by exposing the particles deposited on the TEM grid to OsO_4 vapors to increase the electron contrast.

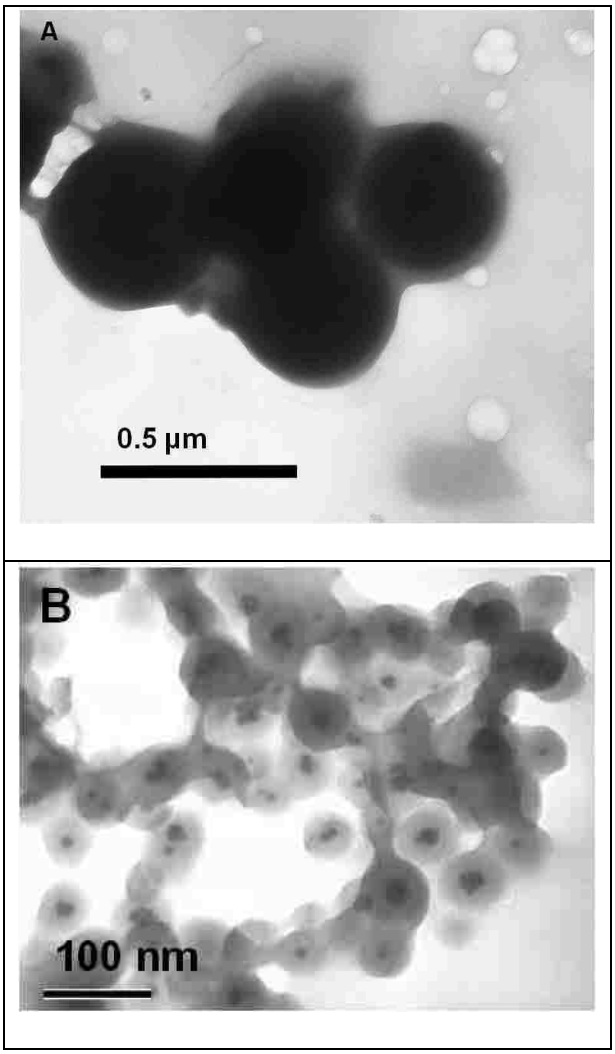

Figure 6.5 TEM image of PCP PTYR: (A) non-magnetic, PTYR PCP230 (CR856) stained with OsO4 and (B) magnetic PTYR PCPs (CR9151) without staining.

The size of the PCPs was evaluated by dynamic light scattering. Table 6.2 summarizes the data gathered using this technique.

Table 6.2 Sample, Measurement, Solvent, Temperature, Radius and Polydispersity Index of Poly(L-tyrosine) Polypeptide Composite Particles Measured by DLS

Sample	Measurement	Solvent	Temperature/ °C	Diameter/nm	$\mu_2\ \Gamma^{-2}$
PBTY PCP230 (CR836)	Malvern	m-cresol	17-41	631 ± 33	0.33 ± 0.08
PTYR PCP230 (CR856)	Multi-angle	water	25	823 ± 30	0.33 ± 0.08
PTYR PCP230 (CR856)	Malvern	DMSO	25	568 ± 4	0.37 ± 0.03
PBTY PCPmag (CR9151)	Multi-angle	m-cresol	25	610 ± 33	0.38 ± 0.01
PTYR PCP620 (CR10.190A)	Malvern	DMSO	25	728 ± 54	0.79 ± 0.29

The analysis by multi-angle or one-angle (Malvern) DLS encountered complications stemming from the insolubility of the PBTY in conventional solvents. Sharing a phenyl ring in their structure, PBTY was dispersed in m-cresol. The particles seemed to give a good dispersion. PBTY PCP230 was measured by Malvern as an average over 10 runs performed at 17°C, 23°C, 31°C, 35°C, 37°C and 41°C. At each temperature the data were corrected for solvent viscosity (see Chapter 5, Figure 5.6). After deprotection, PTYR PCPs were expected to disperse well in water. Multi-angle measurements at 25°C showed that the particles tend to coalesce. This trend is evidenced by the angle-dependent profile of the apparent radius, Figure 6.6A and the ascending polydispersity index, Figure 6.6B.

The non-magnetic particle aggregation can be caused by the H-bonding between hydroxyl groups of the phenolic side chain. It is also possible that the some of the chains are still protected with benzyl groups. Another suitable solvent for PTYR is dimethylsulfoxide, DMSO. The size of the PTYR PCP230 and PTYR PCP620 was evaluated by Malvern in DMSO. All other samples were measured at one-angle. The magnetic interaction due to slight magnetic remanence can be responsible for magnetic particle aggregation.

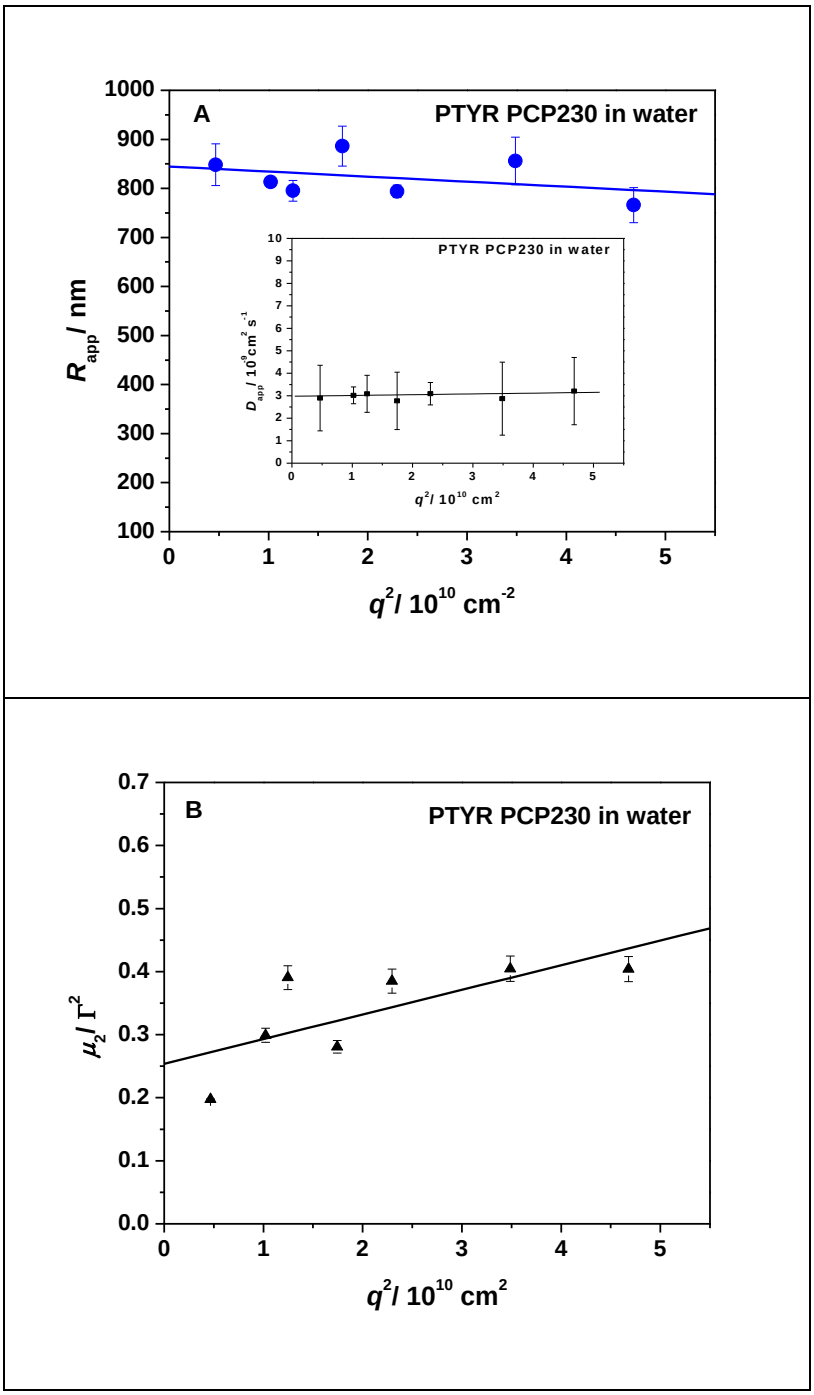

Figure 6.6 Typical DLS data for non-magnetic PTYR PCP230 (CR856): (A) apparent radius, R_{app}, as a function of squared scattering vector magnitude, q^2, (inset) apparent diffusion coefficients, D_{app}, as a function of q^2 (inset) and (B) polydispersity index, $\mu_2 \cdot \Gamma^{-2}$, as a function of q^2. Data recorded in water, at 25°C. Run time 100s.

Additional confirmation of the polypeptide shell came from TGA measurements. Figure 6.7 displays TGA traces of silica cores before functionalization, PBTY PCP, PTYR PCP and untethered poly(L-tyrosine) for both non-magnetic and magnetic PCPs.

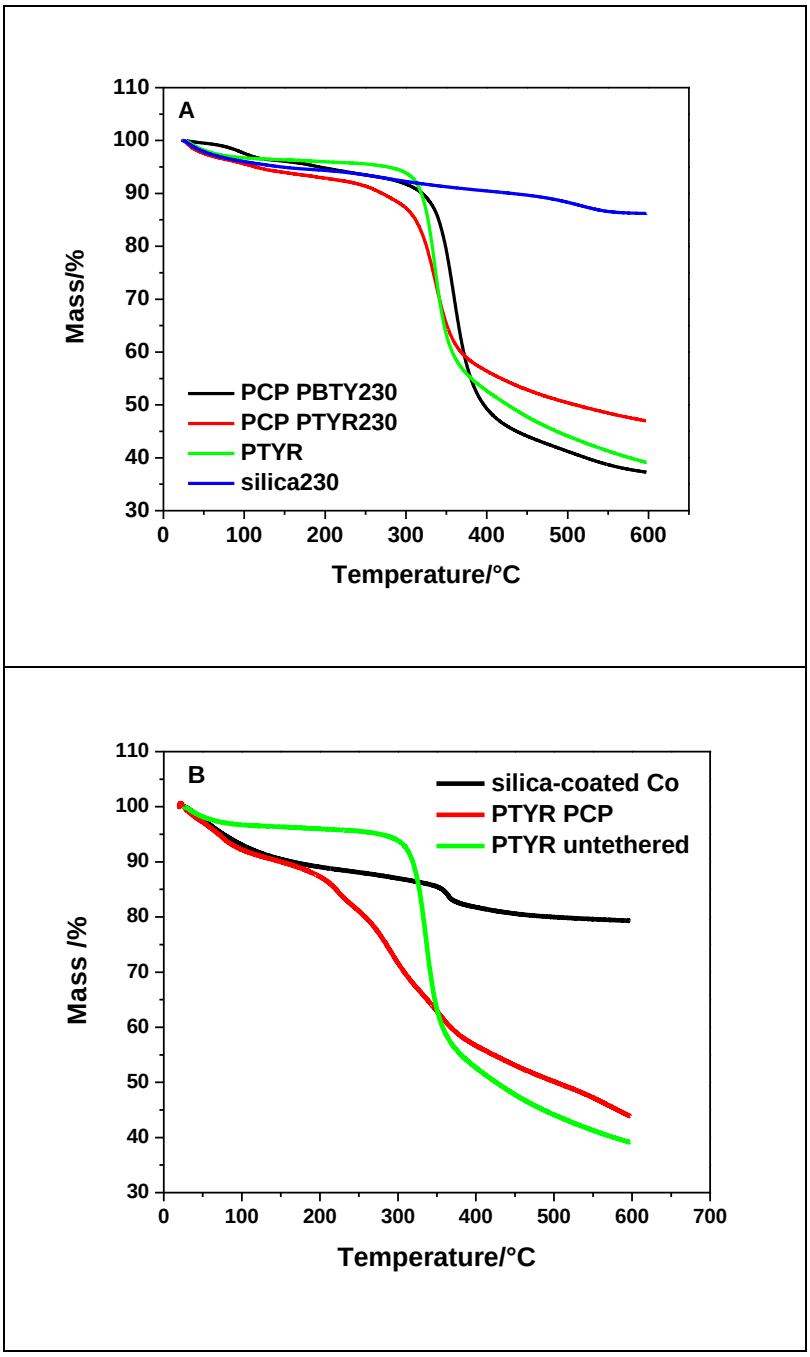

Figure 6.7 TGA traces for the steps involved in preparation of (A) non-magnetic PTYR PCP230 and (B) magnetic PTYR PCPs. The TGA response of the untethered poly(L-tyrosine) is also shown. Scan rate 10°C·min^{-1}.

The weight loss up to 200°C is due to the water. In the case of the PCP PBTY and PCP PTYR the decomposition occurring in the 200 and 600°C temperature interval corresponds to the grafted PTYR. The large core non-magnetic PCPs were designed to have a very sparse coverage with polypeptide. The TGA traces of this sample are seen in Figure 6.8A suggest a small polypeptide load.

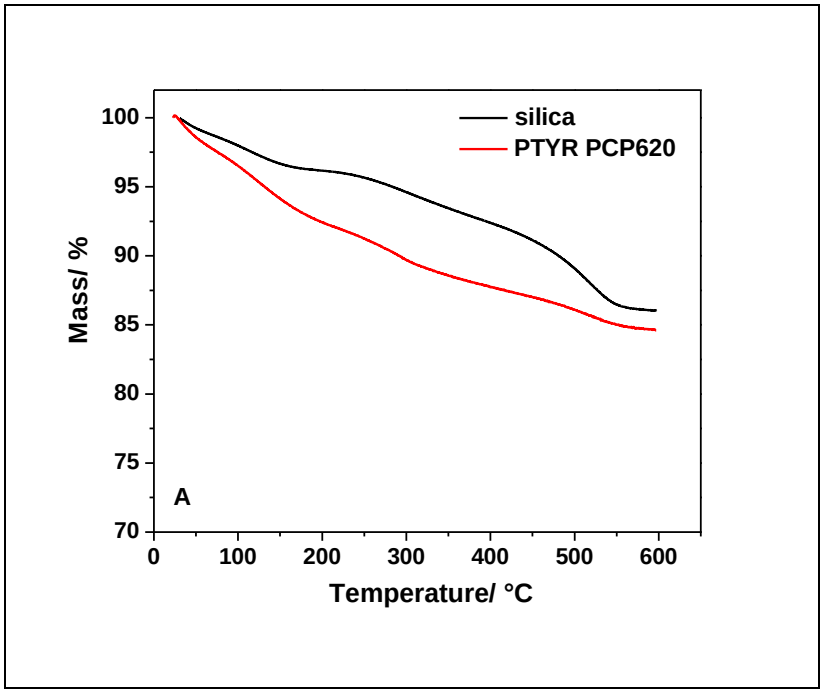

Figure 6.8 Typical thermogravimetric analysis data: (A) percentage of mass loss and (B) derivative mass loss as a function of the temperature for untethered PTYR, silica-tethered PTYR (CR10.190A) and plain silica. Scan rate was 10°C·min^{-1}.

Figure 6.8 continued

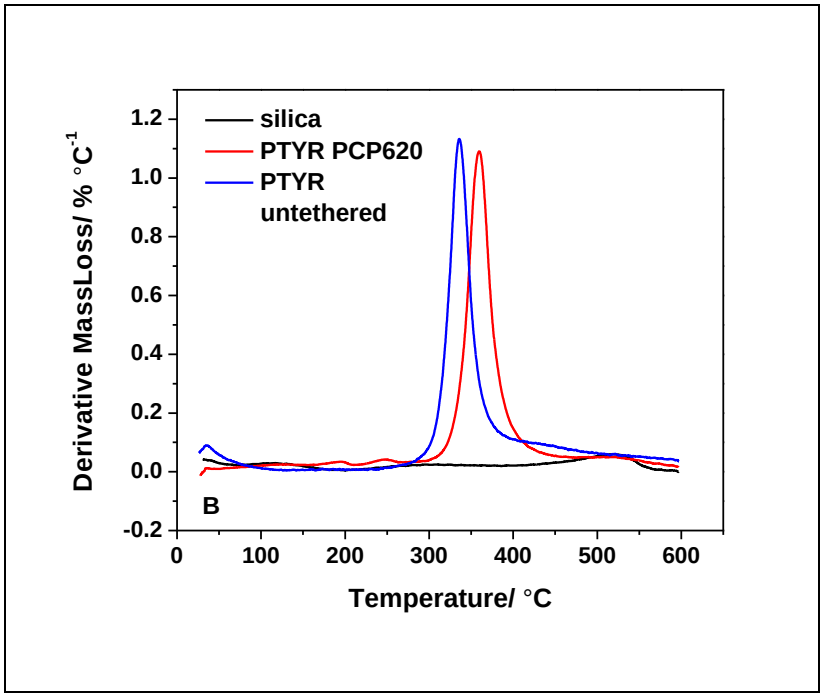

Yet, such a low difference in mass loss between the plain silica cores and the PTYR composite particles can be questionable as being due to the presence of the polymer. In order to clarify this doubt, the derivative of mass loss was plotted against temperature. Figure 6.8B shows the peak associated with the decomposition of the untethered and silica-tethered PTYR with the maxima situated between 300-400°C. This peak is not present in the trace of the plain silica. The overlapping of the two events of free untethered PTYR and PTYR PCP proves that the small difference in mass lost during decomposition is due to the polypeptide and not to the other artifacts (e.g. solvent, impurities). In Table 6.3 is listed the percent polypeptide loading for each sample of PCPs.

The FTIR spectra of PCPs benzyl protected and unprotected, Figure 6.8 shows the characteristic adsorption bands of siloxane bond, Si—O—Si, at 1048 cm^{-1}.

Table 6.3 Code and Weight Loss from TGA for PCPs Samples

Code	Weight Loss from TGA/ %
PBTY PCP230	50
PTYR PCP230	40
PTYR PCP620	2
PTYR PCPmag	35

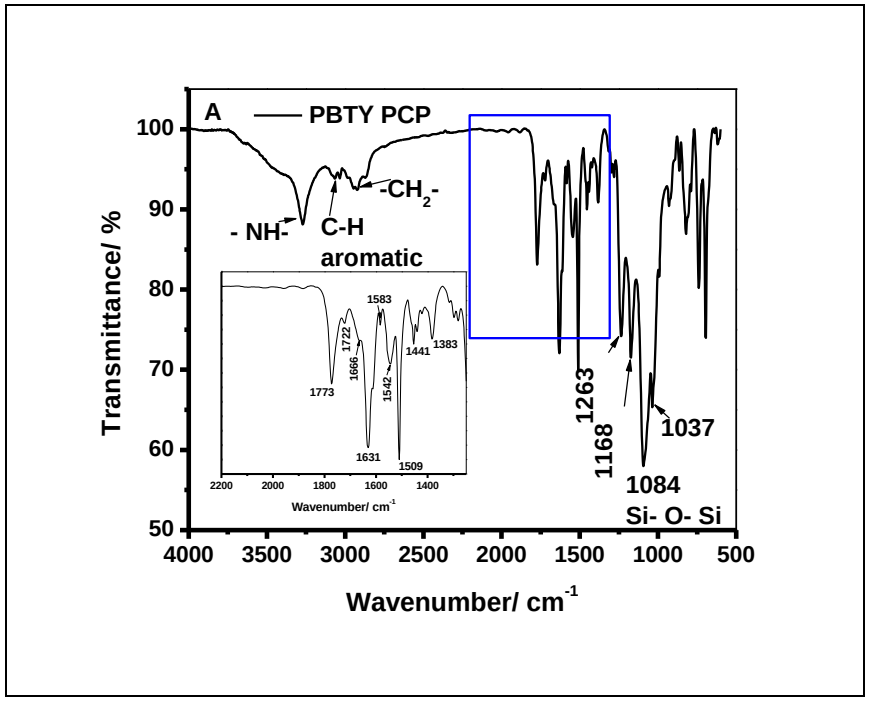

Figure 6.9 FTIR spectra of (A) PCP PBTY and (B) PCP PTYR. The insets show the expanded region from 2200 to 1250 cm^{-1}.

Figure 6.9 continued

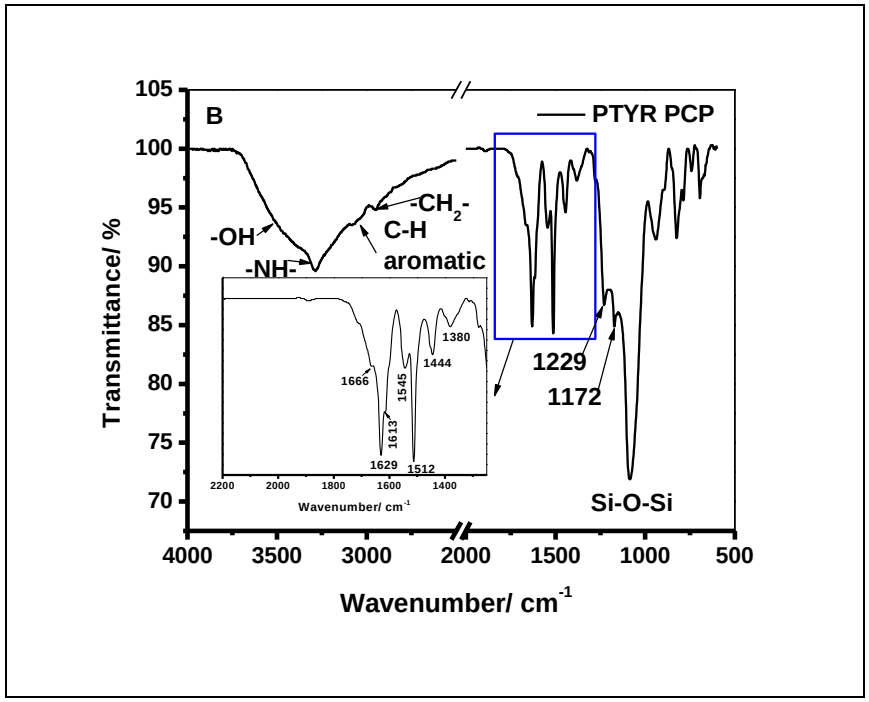

The specific bands shown in the inset for PCP PBTY, Figure 6.9A, correspond to a mixture of helical and random coil polypeptide. The dominant secondary structure of the composite material is random coil, reflected through the presence of the amide I peak at 1635 cm^{-1} and the amide II at 1510 cm^{-1}. The α-helix amide I band assigned to C=O stretch is located at 1668 cm^{-1} (small shoulder) and the amide II corresponding to in-plane NH bending and C─N stretching vibration is found at 1545 cm^{-1}. Beside the peaks corresponding to helical and random coil assignments, other distinct bands were evident in the spectrum at 1635 cm^{-1} possible overlap, 1610 cm^{-1} and 1510 cm^{-1}. These adsorption bands can be assigned to skeletal vibration of the tyrosine ring and to its protective benzyl side chain as well. The absorption of the ether linkage C(Ar)—O—CH_2—C(Ar) is visible at 1263 cm^{-1} and 1168 cm^{-1}. The cleavage of the benzyl protective groups of the side chains is reflected by the occurrence of the broad peak around 3300- 3500 cm^{-1}

specific to—OH adsorption. In addition, a significant decrease in the intensity of the aromatic C—H stretch at ~3000 cm^{-1} can be also seen. The polypeptide chains have a dominant random coil structure (amide I, 1629 cm^{-1}, amide II, 1512 cm^{-1}) with small traces of α-helix (amide I, 1666 cm^{-1}, amide II, 1545 cm^{-1}). The presence of the silica particles is marked in both FTIR spectra by the intense peak at 1048 cm^{-1}.

6.3.3 Photo-induced Cross-linking of Unmodified Polypeptides, PICUP.

The photo-cross-linking reaction, PICUP, involving ruthenium bipyridyl complex was performed at room temperature in a phosphate buffer solution following the Kodadek et al. procedure.[63,64] First, the reaction was carried out without any attempt to obtain regular shapes. In order to design a shaped material, an appealing technique is illustrated in Scheme 6.4: the alignment of the magnetic composite particles followed by shining visible light of 470 nm wavelength through a Ronchi ruling. Particles shadowed by the dark stripes of the ruling cannot cross-link because the light is obstructed to illuminate them. Therefore, the cross-linking will be possible only in illuminated areas. This procedure can facilitate the preparation of a polycolloid of a precise length. For example, a Ronchi ruling having 50 μm wide grid lines can yield of 50 μm long polycolloid chains. The mechanism of the PICUP reaction, especially the catalysis of the ruthenium complex, is not completely understood. Yet, the tentatively accepted route suggests that excitation with visible light of 452 nm wavelength induces the oxidation of Ru(II) to Ru(III). In the same time, ammonium persulfate loses the peroxide bond, —O—O—, and produces a sulfate anion and a sulfate radical. Further the Ru(III) ion attacks the aromatic ring of tyrosine unit extracting a proton from the immediate proximity of the Ar—OH group leaving behind a free electron and finally reduces back to Ru(II). A nearby tyrosine unit can provide the former an electron to suffice the deficit for a double bond while linking in the *ortho* position.

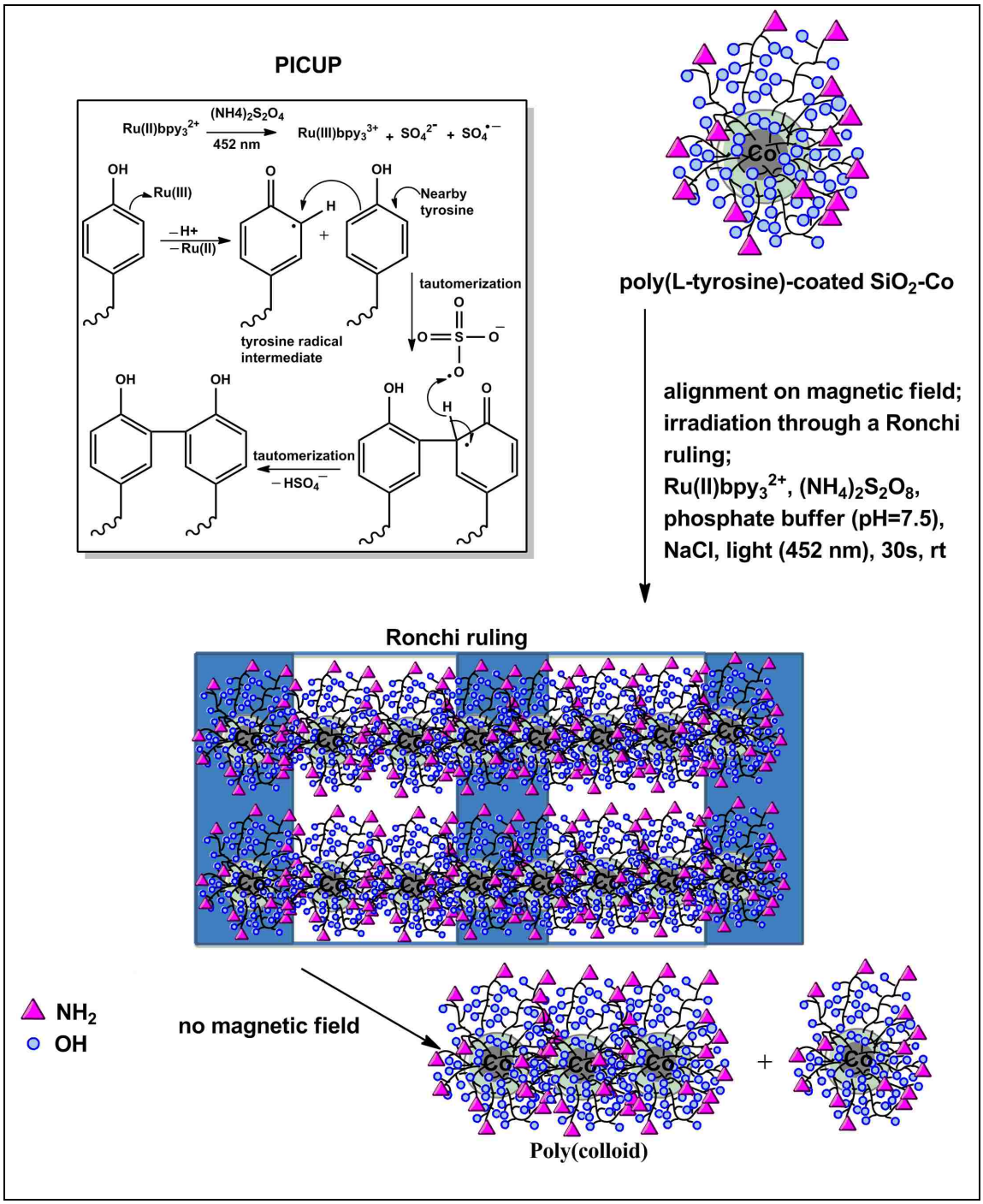

Scheme 6.4 Idealized illustration of magnetic polycolloid preparation through PICUP reaction using magnetic PCP PTYR and, inset, the accepted mechanism for ruthenium complex catalysis.

At this step the sulfate radical donates the electron necessary to reform the double bond of the later tyrosine unit and receives the proton in change.

The versatility of the PICUP method was compared with that of the cross-linking reaction using the enzyme *Horseradish peroxidase*, HRP, as a cross-linking catalyst. Both methods used the same medium (phosphate buffer) at slightly different pH, 6.5 and 7, respectively. Yet, the net distinction between these two methods is made by the reaction time. The reaction time in the case of PICUP is equal with the duration of illumination and varies roughly from 2 to 15 minutes while the HRP approach requires, in general, 3 hours. HRP cross-linking necessitates the addition drop by drop of 5% H_2O_2 over 2 hours and another hour for complete reaction. HRP is a much more expensive catalyst when compared with Ru bipyridyl complex. In Figure 6.10A are shown the non-magnetic PCPs before the HRP-mediated cross-linking. Figure 6.10B and Figure 6.10C show the cross-linked adduct at low and high magnification.

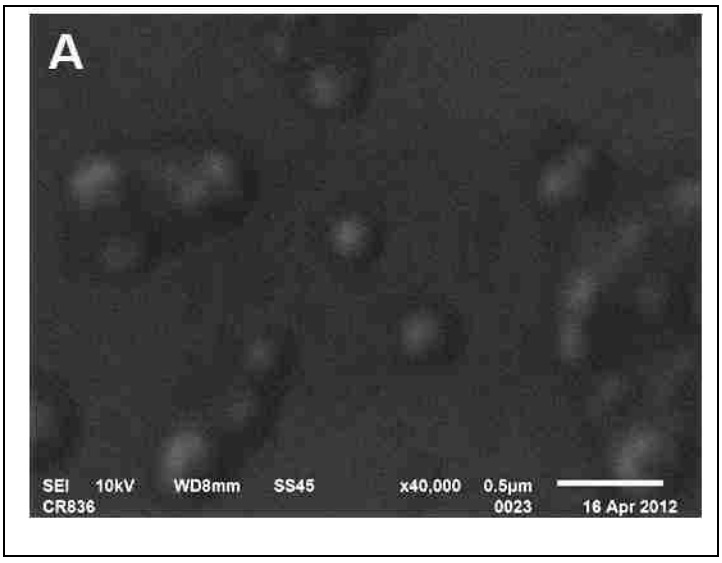

Figure 6.10 SEM pictures of (A) PBTY CP and (B) polycolloid obtained by *Horseradish peroxidase*-catalyzed cross-linking without magnetic alignment (lower magnification) and (C) the same polycolloid at higher magnification.

Figure 6.10 continued

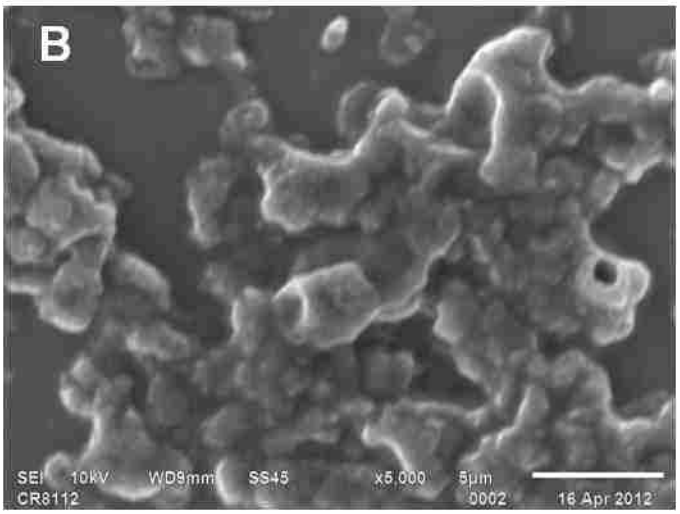

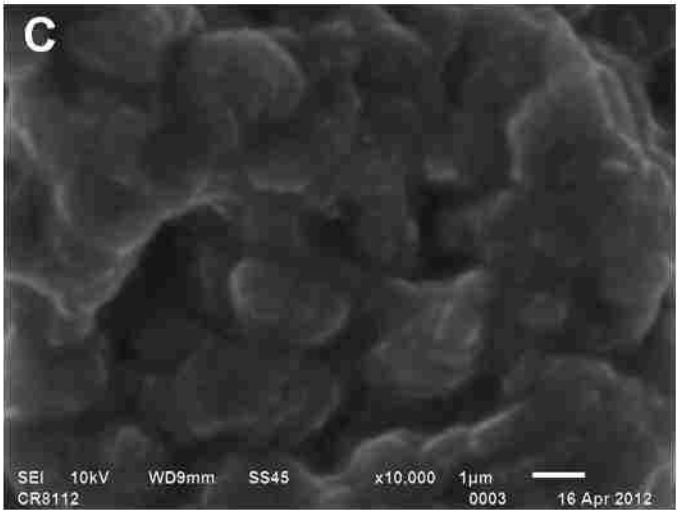

Silica beads are embedded in the polymer network due to the intra- and inter-cross-linking. The heavy cross-linking is a result of high grafting density with polypeptide.

PTYR PCPs chemically photo-cross-linked *via* PICUP were also characterized by FTIR. Figure 6.11 shows the disappearance of several specific signals when compared with the PBTY

and PTYR PCPs. The disappearance of the peaks seen at 1229 and 1172 cm^{-1} for PTYR PCPs and also the band at 1380 cm^{-1} suggest the formation of linkages between tyrosine units.

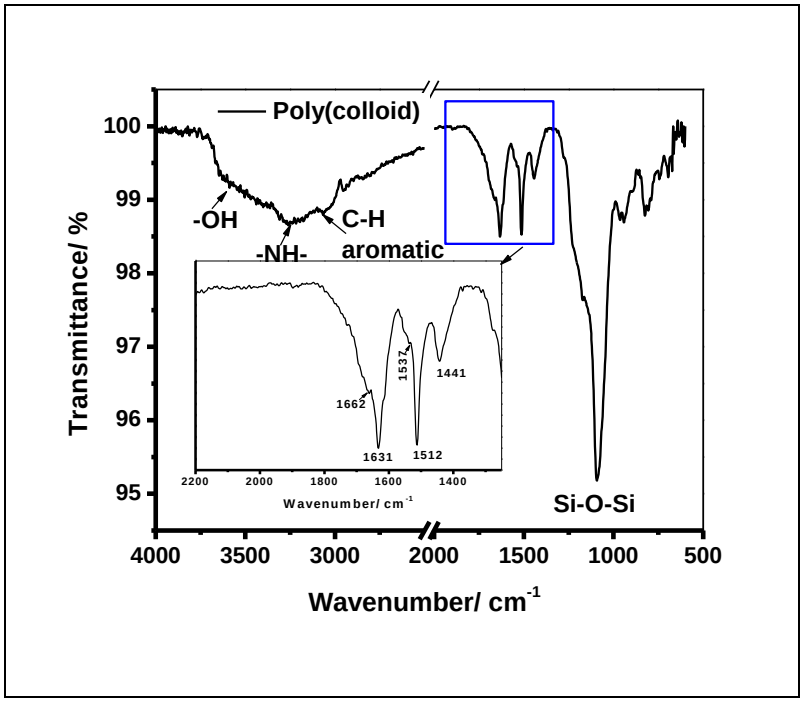

Figure 6.11 FTIR spectrum of cross-linked PTYR PCPs using the PICUP method

Non-magnetic PCPs particles presented in Figure 6.5A were photo-cross-linked using patterned surfaces as shown in Figure 6.12. One wall of the clear disposable square cuvettes was detached by using a syringe needle (25G, 5/8") heated with a torch yielding three-wall cuvette for the purpose of the easy reagent addition. The same flamed needle was used to draw lines on the bottom of the cuvette. Then it was covered with aluminum foil which had scratched lines overlaying with the ones drawn as described before. Another setting was obtained by drawing circles on the bottom of a cuvette and the rest of the wall was colored in black using a permanent marker. The light- emitting diode, LED, of 470 nm wavelength was set to illuminate the cuvettes from the bottom.

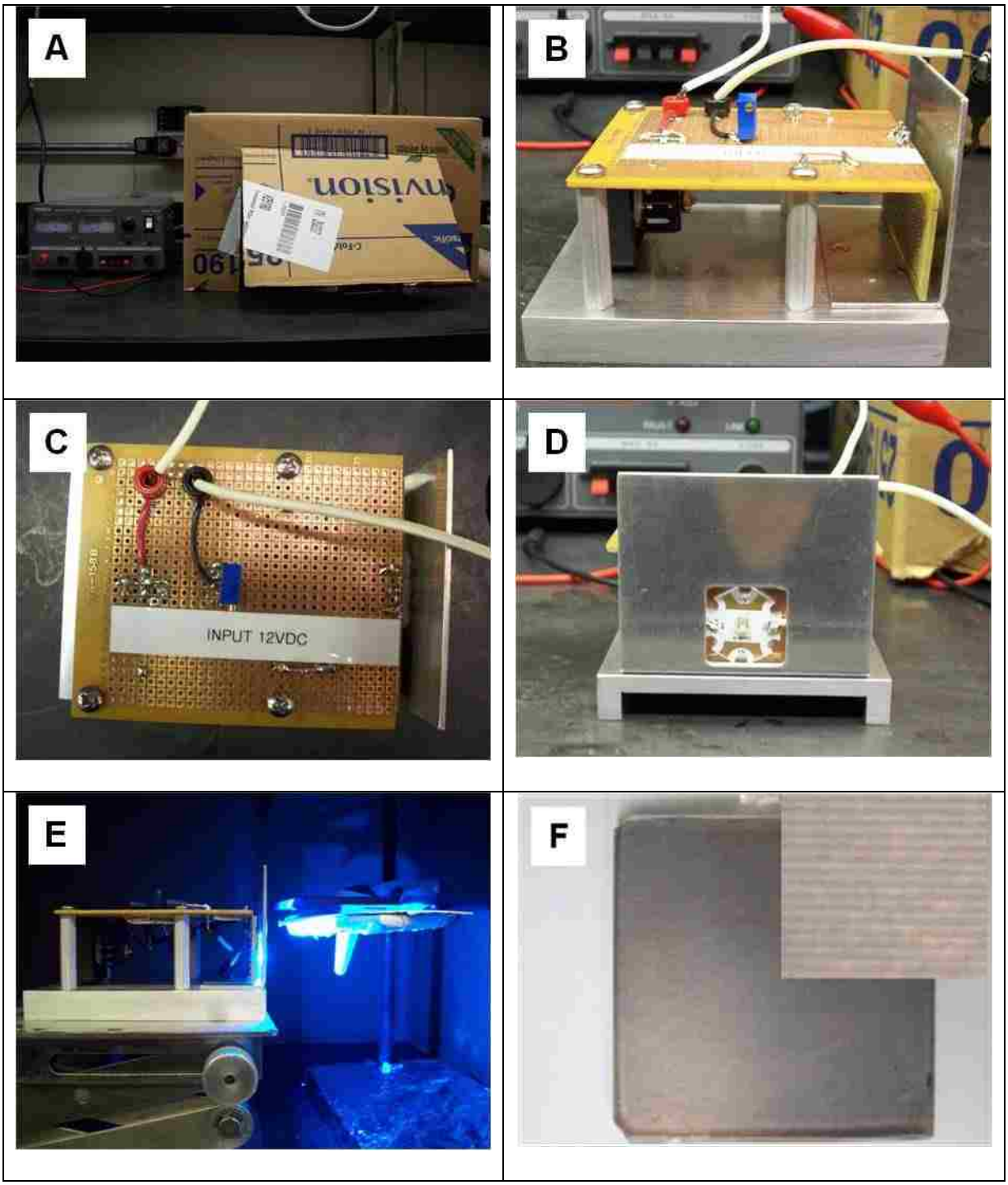

Figure 6.12 Components used in the PICUP reaction: (A) TENMA Regulated DC power supply and the photopolymerization box, (B) LED source 470 nm wavelength, lateral view, (C) LED source 470 nm wavelength, top view, (D) LED source 470 nm wavelength, front view, (E) illumination set-up from the lateral position, and (F) Ronchi ruling (50 μm), spacings (inset).

Figure 6.13 displays several polycolloids obtained using the PICUP method. The sample shown in Figure 6.13A and Figure 6.13A1 was obtained with no patterning. Non-magnetic PCP particles were deposited in a thin layer on a three-wall cuvette by sedimentation overnight inside a Petri dish with water set aside in a vial cap to prevent the evaporation of buffer solution from the sample. The Petri dish was kept in the box further used for the photo-crosslinking. Then the Ru complex was added inside the box in the dark followed by the ammonium persulfate. The cuvette was illuminated from the bottom for 15 min. SEM showed that the cross-linked particles seemed to self-assemble into maple leaf-like structures. The high magnification image visualized the edge of these shapes and shows deeply imbedded particles into the polymerization adduct.

The polycolloid shown in Figure 6.13B and 6.13B1 was obtained using the patterned cuvette. The morphology of this product resembled a crystal-like branched structure. The simple drawing of stripes with the torched syringe needle couldn't result in smooth and straight edges. The imperfections of the stripes were filled by the PTYR PCPs and after cross-linking they displayed the shape of those defects. Similar to the photo-polymerization product exhibited in Figure 6.13A, the particles are difficult to distinct due to the heavy cross-linked shell. The particle used in these reactions (Figure 6.5A) had a relatively small silica core and a thick shell. In order to visualize the colloid after cross-linking PTYR PCPs with a big core and a very sparse PTYR-populated shell was used. The polycolloid displayed in Figure 6.13C and 6.13C1 was obtained by mixing the two kinds of PTYR PCPs aforementioned in a ratio 50:50. The SEM image shows that macrocycle polycolloids similar to macrocycle untethered polymer can be obtained easily by simply drawing circles on the cuvette bottom as shown in Figure 6.12G. In the high- magnification image, the big core particles (PCP PTYR620) can be clearly seen along with the small-cored ones (PCP PTYR230).

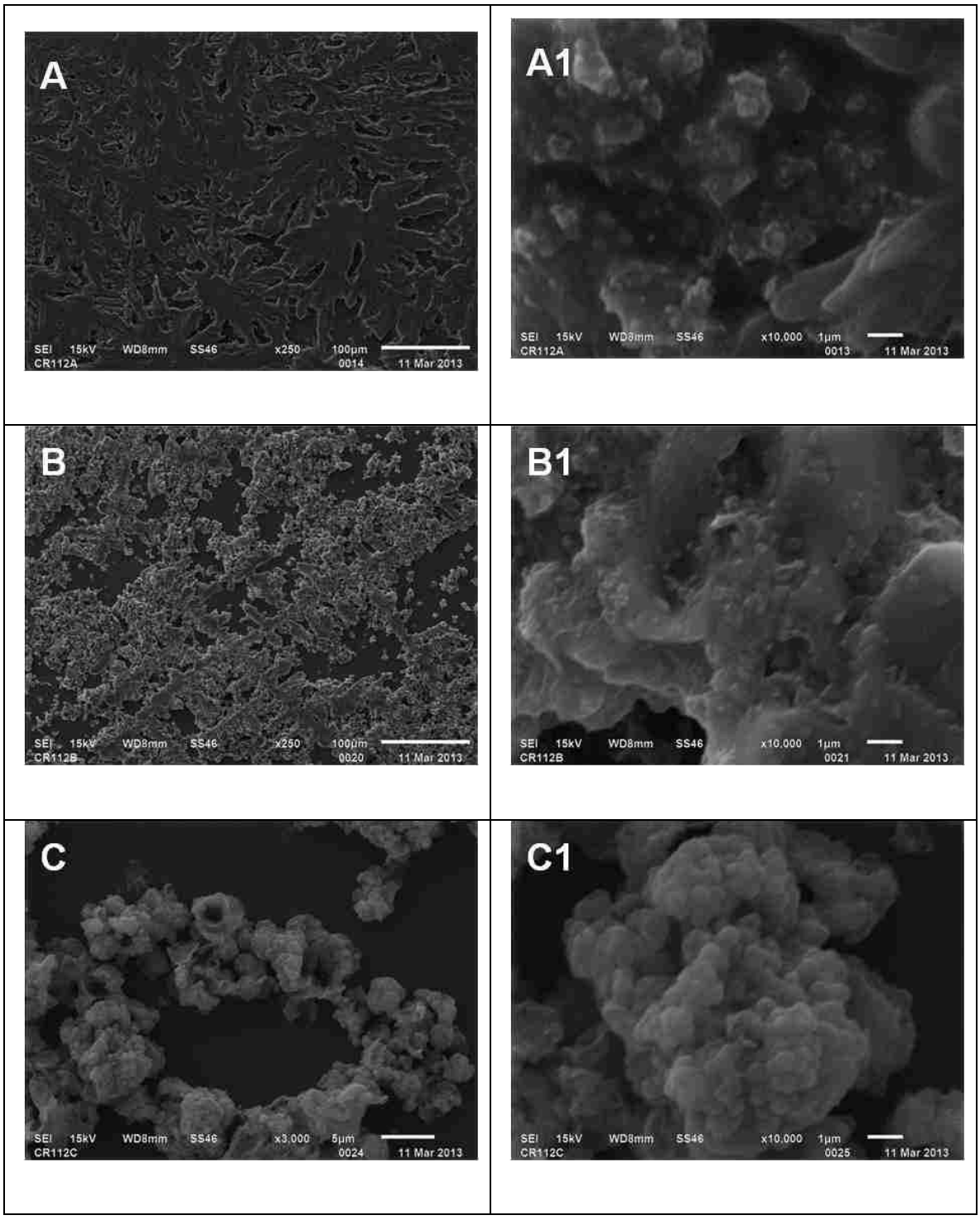

Figure 6.13 SEM images of (A) cross-linked PTYR PCP230 (CR11.2A) showing maple leaf-like structure, (A1) zoom into circled (A) area, (B) cross-linked PTYR PCP230 into crystal-like shape, (B1) zoom into circled (B) area, (C) crosslinked 50:50 mixture of PTYR PCP230 and PTYR PCP620 into macrocycle-like structure and (C1) zoom into the circled (C) area.

The polycolloid shown in Figure 6.13B and 6.13B1 was obtained using the patterned cuvette. The morphology of this product resembled a crystal-like branched structure. The simple drawing of stripes with the torched syringe needle couldn't result in smooth and straight edges. The imperfections of the stripes were filled by the PTYR PCPs and after cross-linking they displayed the shape of those defects. Similar to the photo-polymerization product exhibited in Figure 6.13A, the particles are difficult to distinct due to the heavy cross-linked shell. The particle used in these reactions (Figure 6.5A) had a relatively small silica core and a thick shell. In order to visualize the colloid after cross-linking PTYR PCPs with a big core and a very sparse PTYR-populated shell was used. The polycolloid displayed in Figure 6.13C and 6.13C1 was obtained by mixing the two kinds of PTYR PCPs aforementioned in a ratio 50:50. The SEM image shows that macrocycle polycolloids similar to macrocycle untethered polymer can be obtained easily by simply drawing circles on the cuvette bottom as shown in Figure 6.12G. In the high-magnification image, the big core particles (PCP PTYR620) can be clearly seen along with the small-cored ones (PCP PTYR230).

Not only non-magnetic but Co-nugget particles were cross-linked using PICUP method. The exposure of the magnetic PTYR PCPs to an external magnetic field induces the alignment of the particles in chains in the same fashion as the cores seen in Figure 6.3. The shells of the particles are forced to interpenetrate. The photo-cross-linking enables the formation of the permanent chains due to the formation of the dityrosine linkages. The magnetic polycolloid obtained using Ronchi ruling is shown in Figures 6.14A and 6.14A1. The TEM images show a specimen with a very high electron contrast. This is due to the Ru traces present in the sample. Yet, particles seem to be "locked" in the chain-like fashion. The TEM images were obtained

without staining with OsO_4 and that explains the smaller appearance of PCPs compared to Figure 6.5B.

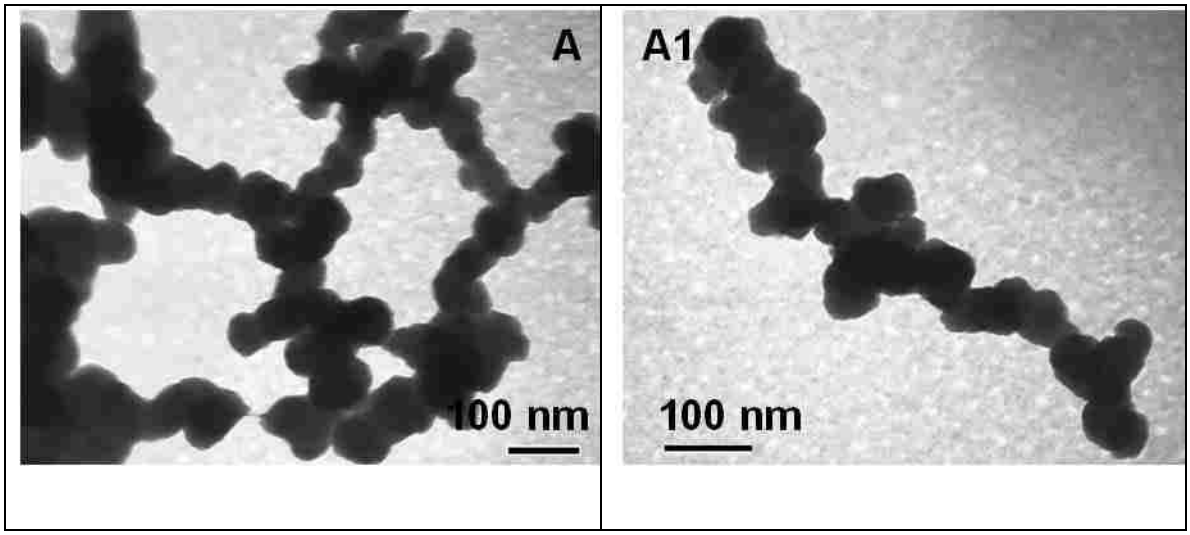

Figure 6.14 TEM images of cross-linked Co-nugget PTYR PCP at (A) lower and (A1) higher magnification.

Polycolloid obtained either through the HRP or the PICUP approach can be considered a good candidate for specific applications. Due to their high PTYR load, these PCPs may be useful in post-translational modification of proteins through tyrosine side chain coupling.[36] The nature of the tyrosine unit is hydrophobic (despite the presence of –OH groups) while the most protein amino acid units are hydrophilic. The modification of the protein through the hydrophilic residues is not effective because these residues are exposed on the surface. While the population of the hydrophilic residues exposed on the surface is high, tyrosine units are less. Therefore the coupling through the hydrophobic tyrosine residues is more effective because is more site-selective. Furthermore, tyrosine is a neutral amino acid over a broad range of pH. Consequently, the modification of the proteins through tyrosine coupling can be a more effective way for protein modification. The advantage of using the PTYR PCPs in such processes is that they provide a higher number of tyrosine units per surface area, thus increasing the effectiveness of

the site-specific coupling. Grafted on a smaller core, PTYR PCPs can be up-taken into the living bodies and used, for example, in antibody recognition as a result of tyrosine capability to interact with specific antigens.[33] Magnetic PCPs may be also useful in such an application because they have the ability to be guided with external magnetic fields to less accessible sites. Labeled with a fluorescent core they can be easily visualized during and after cross-linking. Another opportunity to use the PCPs and the PICUP method is to stabilize protein aggregates.[68] A number of fatal diseases are associated with the folding of the soluble amyloid-like fibrils into insoluble aggregates. Coupling the small aggregates formed at the incipient stages of the disease may slow down or even stop further growth of the aggregates.

Besides several possible applications described above the polycolloid can be used as a platform for drug encapsulation and drug delivery. After photo-polymerization, the silica cores can be easily dissolved with either NaOH or HF yielding a cross-linked vesicle-like morphology which can be loaded with drugs.

Future efforts will be focused on perfecting the patterned poly(colloid). The smoothness and narrowness of the striped cuvettes will be attained by using better tools (e.g. Dremel tool). Other means such as microfluidic devices are also considered for this work.

6.4 Conclusion

This work was devoted to expanding the architectural repertoire of polypeptide composite particles and their potential applications. PTYR PCPs, non-magnetic or having a cobalt intrusion, were synthesized *via* the *growing from* method. The non-magnetic PCPs were prepared in two batches with a dense and a very sparse polypeptide shell. The difference in their size core was about three times. The presence of the polypeptide on the silica beads was evidenced by TEM, TGA, DLS and FTIR. Poly(L-tyrosine) had mostly a random coil structure

with remnant α-helix. The effectiveness of the PICUP method was compared with the HRP-mediated cross-linking. While both procedures yielded heavily cross-linked adducts, only PICUP allowed architectural maple-like, crystal-like and chain-like structure. This procedure requires no stirring and a very short reaction time when compared with the HRP-catalyzed approach. The desired architectures of the polycolloid were obtained by using patterned squared cuvettes by simple drawing with a flamed syringe needle or a permanent marker. The design concept used to prepare the polycolloid opens the door to an entire palette of the unusual morphologies. This method presented here may be employed further in engineering precisely defined cross-linked polypeptide composite materials.

6.5 References and Notes

(1) Takahashi, R.; Noguchi, T. Criteria for determining the hydrogen-bond structures of a tyrosine side chain by Fourier transform infrared spectroscopy: Density functional theory analyses of model hydrogen-bonded complexes of p-cresol. *Journal of Physical Chemistry B* **2007**, *111*, 13833-13844.

(2) Berthomieu, C.; Hienerwadel, R. Vibrational spectroscopy to study the properties of redox-active tyrosines in photosystem II and other proteins. *Biochimica Et Biophysica Acta-Bioenergetics* **2005**, *1707*, 51-66.

(3) Applequi. J; Mahr, T. G. Conformation of poly-L-tyrosine in quinoline from dielectric dispersion studies. *J. Am. Chem. Soc.* **1966**, *88*, 5419-&.

(4) Troxell, T. C.; Scheraga, H. A. Use of electric dichroism to study polymer conformation. *Biochemical and Biophysical Research Communications* **1969**, *35*, 913-&.

(5) Damle, V. N. On helix-coil equilibrium in 2-stranded and 3-stranded complexes involving complementary polynucleotides and oligonucleotides. *Biopolymers* **1970**, *9*, 353-&.

(6) Bradbury, E. M.; Stephens, R. M.; Giancott.V; Cranerob.C conformational studies of poly(L-tyrosine) in solvent mixtures of dimethylsulfoxide with water and trimethylphosphate. *Polymer* **1972**, *13*, 33-&.

(7) Quadrifo. F; Ius, A.; Crescenz.V conformation of poly-L-tyrosine in solution. *Makromolekulare Chemie* **1970**, *136*, 241-&.

(8) Conio, G.; Patrone, E.; Salaris, F. Conformational transitions of poly(L-tyrosine) in mixed water-ethanol solvents. *Macromolecules* **1971**, *4*, 283-&.

(9) Conio, G.; Trefilet.V; Patrone, E. Stability of beta-helical and alpha-helical conformations of poly-L-tyrosine. *Makromolekulare Chemie* **1972**, *154*, 311-&.

(10) Cosani, A.; Palumbo, M.; Terbojevich, M.; Peggion, E. Potentiometric and CD study on beta-random coil transition of poly-L-tyrosine in aqueous-solution. *International Journal of Peptide and Protein Research* **1974**, *6*, 457-463.

(11) Patrone, E.; Conio, G.; Brighett.S Conformation of poly-L-tyrosine in aqueous solution. *Biopolymers* **1970**, *9*, 897-&.

(12) Peggion, E.; Cosani, A.; Terbojev.M Solution properties of synthetic polypeptides - assignment of conformation of poly(L-tyrosine) in water and in ethanol-water solutions. *Macromolecules* **1974**, *7*, 453-459.

(13) Auer, H. E.; Patton, E. Kinetics of disordered chain-to-beta transformation of poly(L-tyrosine) in aqueous-solution. *Biophysical Chemistry* **1976**, *4*, 15-21.

(14) Cosani, A.; Palumbo, M.; Terbojevich, M.; Peggion, E. A Potentiometric and CD study on the β-random coil transition of poly-L-tyrosine in Aqueous solution. *International Journal of Peptide and Protein Research* **1974**, *6*, 457-463.

(15) Patton, E.; Auer, H. E. Conformational states of poly(L-tyrosine) in aqueous-solution. *Biopolymers* **1975**, *14*, 849-869.

(16) Hamada, F.; Ishimuro, Y.; Hayashi, T.; Nakajima, A. Conformation study on poly(L-tyrosine) in dimethyl formamide by small-angle X-ray-scattering. *Biopolymers* **1977**, *16*, 2351-2361.

(17) Baba, M.; Hamaguch.K; Ikenaka, T. States of tyrosyl residues and circular dichroism of Kunitz trypsin inhibitor. *Journal of Biochemistry* **1969**, *65*, 113-&.

(18) Cathou, R. E.; Kulczyck.A; Haber, E. Structural features of gamma-immunoglobulin antibody and their fragments . Circular dichroism studies. *Biochemistry* **1968**, *7*, 3958-&.

(19) Coleman, J. E. Carbonic anhydrase-azosulfonamide complexes - spectral properties. *Journal of Biological Chemistry* **1968**, *243*, 4574-&.

(20) Green, N. M.; Melamed, M. D. Optical rotatory dispersion circular dichroism and far-ultraviolet spectra of avidin and streptavidin. *Biochemical Journal* **1966**, *100*, 614-&.

(21) Welsh, E. J.; Frangou, S. A.; Morris, E. R.; Rees, D. A. Tyrosine optical-activity as a probe of the conformation and interactions of fibronectin. *Biopolymers* **1983**, *22*, 821-831.

(22) Yang, C. C.; Chang, C. C.; Hayashi, K.; Suzuki, T.; Ikeda, K.; Hamaguch.K optical rotatory dispersion and circular dichroism of cobrotoxin. *Biochimica Et Biophysica Acta* **1968**, *168*, 373-&.

(23) Beychok, S.; Fasman, G. D. Circular dichroism of poly-L-tyrosine. *Biochemistry* **1964**, *3*, 1675-&.

(24) Friedman, S.; Tso, P. O. P. Circular dichroic spectrum of poly-L-tyrosine in aqueous solution. *Biochemical and Biophysical Research Communications* **1971**, *42*, 510-&.

(25) Watanabe, K.; Muto, K.; Ishii, T. Conformational analysis of poly(L-tyrosine) and tyrosyl oligomers based on backbone circular dichroism spectra obtained by fluorescence-detected circular dichroism. *Biospectroscopy* **1997**, *3*, 103-111.

(26) Wen, K. J.; Woody, R. W. Conformational studies of poly(L-tyrosine) - helix-coil transition in dimethyl sulfoxide dichloroacetic acid mixtures. *Biopolymers* **1975**, *14*, 1827-1840.

(27) Yasui, S. C.; Keiderling, T. A. Vibrational circular-dichroism of polypeptides .6. Polytyrosine alpha-helical and random-coil results. *Biopolymers* **1986**, *25*, 5-15.

(28) Pao, Y. H.; Longwort.R; Kornegay, R. L. Optical rotatory dispersion of poly-L-tyrosine in solution. *Biopolymers* **1965**, *3*, 519-&.

(29) Mian, I. S.; Bradwell, A. R.; Olson, A. J. Structure, function and properties of antibody-binding sites. *Journal of Molecular Biology* **1991**, *217*, 133-151.

(30) Fellouse, F. A.; Li, B.; Compaan, D. M.; Peden, A. A.; Hymowitz, S. G.; Sidhu, S. S. Molecular recognition by a binary code. *Journal of Molecular Biology* **2005**, *348*, 1153-1162.

(31) Friedman, A. A.; Tucker, G.; Singh, R.; Yan, D.; Vinayagam, A.; Hu, Y. H.; Binari, R.; Hong, P. Y.; Sun, X. Y.; Porto, M.; Pacifico, S.; Murali, T.; Finley, R. L.; Asara, J. M.; Berger, B.; Perrimon, N. Proteomic and Functional Genomic Landscape of Receptor Tyrosine Kinase and Ras to Extracellular Signal-Regulated Kinase Signaling. *Science Signaling* **2011**, *4*.

(32) Koide, A.; Gilbreth, R. N.; Esaki, K.; Tereshko, V.; Koide, S. High-affinity single-domain binding proteins with a binary-code interface. *Proceedings of the National Academy of Sciences of the United States of America* **2007**, *104*, 6632-6637.

(33) Koide, S.; Sidhu, S. S. The Importance of Being Tyrosine: Lessons in Molecular Recognition from Minimalist Synthetic Binding Proteins. *Acs Chemical Biology* **2009**, *4*, 325-334.

(34) Mahajan, K.; Coppola, D.; Chen, Y. A.; Zhu, W. W.; Lawrence, H. R.; Lawrence, N. J.; Mahajan, N. P. Ack1 Tyrosine Kinase Activation Correlates with Pancreatic Cancer Progression. *American Journal of Pathology* **2012**, *180*, 1386-1393.

(35) Zemlin, M.; Klinger, M.; Link, J.; Zemlin, C.; Bauers, K.; Engler, J. A.; Schroeder, H. W.; Kirkham, P. M. Expressed murine and human CDR-H3 intervals of equal length exhibit distinct repertoires that differ in their amino acid composition and predicted range of structures. *Journal of Molecular Biology* **2003**, *334*, 733-749.

(36) Minamihata, K.; Goto, M.; Kamiya, N. Site-Specific Protein Cross-Linking by Peroxidase-Catalyzed Activation of a Tyrosine-Containing Peptide Tag. *Bioconjugate Chem.* **2011**, *22*, 74-81.

(37) Wu, J. H.; Zhang, L. S.; Fanaroff, A. C.; Cai, X. J.; Sharma, K. C.; Brian, L.; Exum, S. T.; Shenoy, S. K.; Peppel, K.; Freedman, N. J. G Protein-Coupled Receptor Kinase-5 Attenuates Atherosclerosis by Regulating Receptor Tyrosine Kinases and 7-Transmembrane Receptors. *Arteriosclerosis Thrombosis and Vascular Biology* **2012**, *32*, 308-U325.

(38) Ullrich, A.; Schlessinger, J. Signal transduction by receptors with tyrosine kinase-activity. *Cell* **1990**, *61*, 203-212.

(39) Andersen, S. O. Cross-links in resilin identified as dityrosine + trityrosine. *Biochimica Et Biophysica Acta* **1964**, *93*, 213-&.

(40) Elvin, C. M.; Carr, A. G.; Huson, M. G.; Maxwell, J. M.; Pearson, R. D.; Vuocolo, T.; Liyou, N. E.; Wong, D. C. C.; Merritt, D. J.; Dixon, N. E. Synthesis and properties of crosslinked recombinant pro-resilin. *Nature* **2005**, *437*, 999-1002.

(41) Raven, D. J.; Earland, C.; Little, M. Occurrence of dityrosine in tussah silk fibroin and keratin. *Biochimica Et Biophysica Acta* **1971**, *251*, 96-&.

(42) Labella, F.; Waykole, P.; Queen, G. Formation of insoluble gels and dityrosing by action of peroxidase on soluble collagens. *Biochemical and Biophysical Research Communications* **1968**, *30*, 333-&.

(43) Waykole, P.; Heidemann, E. Dityrosine in collagen. *Connective Tissue Research* **1976**, *4*, 219-222.

(44) Fujimoto, D. Occurrence of dityrosine in cuticlin, a structural protein from ascaris cuticle. *Comparative Biochemistry and Physiology B-Biochemistry & Molecular Biology* **1975**, *51*, 205-207.

(45) Labella, F.; Keeley, F.; Vivian, S.; Thornhil.D Evidence for dityrosine in elastin. *Biochemical and Biophysical Research Communications* **1967**, *26*, 748-&.

(46) Held, M. A.; Tan, L.; Kamyab, A.; Hare, M.; Shpak, E.; Kieliszewski, M. J. Di-isodityrosine is the intermolecular cross-link of isodityrosine-rich extensin analogs cross-linked in vitro. *Journal of Biological Chemistry* **2004**, *279*, 55474-55482.

(47) Brady, J. D.; Sadler, I. H.; Fry, S. C. Di-isodityrosine, a novel tetrameric derivative of tyrosine in plant cell wall proteins: A new potential cross-link. *Biochemical Journal* **1996**, *315*, 323-327.

(48) Brown, K. C.; Yu, Z. H.; Burlingame, A. L.; Craik, C. S. Determining protein-protein interactions by oxidative cross-linking of a glycine-glycine-histidine fusion protein. *Biochemistry* **1998**, *37*, 4397-4406.

(49) Stayner, R. S.; Min, D. J.; Kiser, P. F.; Stewart, R. J. Site-specific cross-linking of proteins through tyrosine hexahistidine tags. *Bioconjugate Chem.* **2005**, *16*, 1617-1623.

(50) Seim, K. L.; Obermeyer, A. C.; Francis, M. B. Oxidative Modification of Native Protein Residues Using Cerium(IV) Ammonium Nitrate. *J. Am. Chem. Soc.* **2011**, *133*, 16970-16976.

(51) Joshi, N. S.; Whitaker, L. R.; Francis, M. B. A three-component Mannich-type reaction for selective tyrosine bioconjugation. *J. Am. Chem. Soc.* **2004**, *126*, 15942-15943.

(52) Williams, R. A.; Blanch, H. W. Covalent immobilization of protein monolayers for biosensor applications. *Biosensors & Bioelectronics* **1994**, *9*, 159-167.

(53) Ren, L. G.; Chen, X. W.; Luechapanichkul, R.; Selner, N. G.; Meyer, T. M.; Wavreille, A. S.; Chan, R.; Iorio, C.; Zhou, X. A.; Neel, B. G.; Pei, D. H. Substrate Specificity of Protein Tyrosine Phosphatases 1B, RPTP alpha, SHP-1, and SHP-2. *Biochemistry* **2011**, *50*, 2339-2356.

(54) Kwon, O. H.; Ito, Y.; Ueda, M.; Tanaka, A.; Imanishi, Y. Hydrophobilization of esterase by genetic combination with polyproline or polytyrosine at the carboxyl terminal. *Biochimica Et Biophysica Acta-Protein Structure and Molecular Enzymology* **1998**, *1388*, 239-246.

(55) Figueroa-Espinoza, M. C.; Morel, M. H.; Surget, A.; Rouau, X. Oxidative cross-linking of wheat arabinoxylans by manganese peroxidase. Comparison with laccase and horseradish peroxidase. Effect of cysteine and tyrosine on gelation. *Journal of the Science of Food and Agriculture* **1999**, *79*, 460-463.

(56) Lewandowski, A. T.; Small, D. A.; Chen, T. H.; Payne, G. F.; Bentley, W. E. Tyrosine-based "activatable pro-tag": Enzyme-catalyzed protein capture and release. *Biotechnology and Bioengineering* **2006**, *93*, 1207-1215.

(57) Lewandowski, A. T.; Yi, H. M.; Luo, X. L.; Payne, G. F.; Ghodssi, R.; Rubloff, G. W.; Bentley, W. E. Protein assembly onto patterned microfabricated devices through enzymatic activation of fusion pro-tag. *Biotechnology and Bioengineering* **2008**, *99*, 499-507.

(58) Boeriu, C. G.; Oudgenoeg, G.; Spekking, W. T. J.; Berendsen, L.; Vancon, L.; Boumans, H.; Gruppen, H.; Van Berkel, W. J. H.; Laane, C.; Voragen, A. G. J. Horseradish peroxidase-catalyzed cross-linking of feruloylated arabinoxylans with β-casein. *Journal of Agricultural and Food Chemistry* **2004**, *52*, 6633-6639.

(59) Oudgenoeg, G.; Hilhorst, R.; Piersma, S. R.; Boeriu, C. G.; Gruppen, H.; Hessing, M.; Voragen, A. G. J.; Laane, C. Peroxidase-mediated cross-linking of a tyrosine-containing peptide with ferulic acid. *Journal of Agricultural and Food Chemistry* **2001**, *49*, 2503-2510.

(60) Michon, T.; Chenu, M.; Kellershon, N.; Desmadril, M.; Gueguen, J. *Horseradish peroxidase* oxidation of tyrosine-containing peptides and their subsequent polymerization: A kinetic study. *Biochemistry* **1997**, *36*, 8504-8513.

(61) ter Haar, R.; Wildschut, J.; Sugih, A. K.; Moller, W. B.; de Waard, P.; Boeriu, C. G.; Heeres, H. J.; Schols, H. A.; Gruppen, H. Proof of principle for the synthesis of hydroxy-aryl esters of glycosidic polyols and non-reducing oligosaccharides with subsequent enzymatic coupling to a tyrosine-containing tripeptide. *Carbohydrate Research* **2011**, *346*, 1005-1012.

(62) Heijnis, W. H.; Dekker, H. L.; de Koning, L. J.; Wierenga, P. A.; Westphal, A. H.; de Koster, C. G.; Gruppen, H.; van Berkel, W. J. H. Identification of the Peroxidase-Generated Intermolecular Dityrosine Cross-Link in Bovine α-Lactalbumin. *Journal of Agricultural and Food Chemistry* **2011**, *59*, 444-449.

(63) Fancy, D. A.; Kodadek, T. Chemistry for the analysis of protein-protein interactions: Rapid and efficient cross-linking triggered by long wavelength light. *Proceedings of the National Academy of Sciences of the United States of America* **1999**, *96*, 6020-6024.

(64) Kodadek, T. J. D., TX), Fancy, David A. (Dallas, TX), Johnston, Stephen A. (Dallas, TX); Board of Regents, The University of Texas System (Austin, TX): United States, 2003.

(65) Bitan, G.; Kirkitadze, M. D.; Lomakin, A.; Vollers, S. S.; Benedek, G. B.; Teplow, D. B. Amyloid β-protein (Aβ) assembly: Aβ40 and Aβ42 oligomerize through distinct pathways. *Proceedings of the National Academy of Sciences of the United States of America* **2003**, *100*, 330-335.

(66) Bitan, G.; Lomakin, A.; Teplow, D. B. Amyloid beta-protein oligomerization - Prenucleation interactions revealed by photo-induced cross-linking of unmodified proteins. *Journal of Biological Chemistry* **2001**, *276*, 35176-35184.

(67) Bitan, G.; Tarus, B.; Vollers, S. S.; Lashuel, H. A.; Condron, M. M.; Straub, J. E.; Teplow, D. B. A molecular switch in amyloid assembly: Met(35) and amyloid beta-protein oligomerization. *J. Am. Chem. Soc.* **2003**, *125*, 15359-15365.

(68) Bitan, G.; Teplow, D. B. Rapid photochemical cross-linking - A new tool for studies of metastable, amyloidogenic protein assemblies. *Accounts Chem. Res.* **2004**, *37*, 357-364.

(69) Bitan, G.; Vollers, S. S.; Teplow, D. B. Elucidation of primary structure elements controlling early amyloid beta-protein oligomerization. *Journal of Biological Chemistry* **2003**, *278*, 34882-34889.

(70) Li, H. Y.; Monien, B. H.; Lomakin, A.; Zemel, R.; Fradinger, E. A.; Tan, M. A.; Spring, S. M.; Urbanc, B.; Xie, C. W.; Benedek, G. B.; Bitan, G. Mechanistic Investigation of the Inhibition of Aβ42 Assembly and Neurotoxicity by Aβ42 C-Terminal Fragments. *Biochemistry* **2010**, *49*, 6358-6364.

(71) Urbanc, B.; Betnel, M.; Cruz, L.; Bitan, G.; Teplow, D. B. Elucidation of Amyloid β-Protein Oligomerization Mechanisms: Discrete Molecular Dynamics Study. *J. Am. Chem. Soc.* **2010**, *132*, 4266-4280.

(72) Piening, N.; Weber, P.; Hogen, T.; Beekes, M.; Kretzschmar, H.; Giese, A. Photo-induced crosslinking of prion protein oligomers and prions. *Amyloid-Journal of Protein Folding Disorders* **2006**, *13*, 67-77.

(73) Clérico, E. M.; Szymańska, A.; Gierasch, L. M. Exploring the interactions between signal sequences and E. coli SRP by two distinct and complementary crosslinking methods. *Peptide Science* **2009**, *92*, 201-211.

(74) Soto-Cantu, E.; Turksen-Selcuk, S.; Qiu, J. H.; Zhou, Z.; Russo, P. S.; Henk, M. C. Silica-Polypeptide Composite Particles: Controlling Shell Growth. *Langmuir* **2011**, *26*, 15604-15613.

(75) Chen, Z. M.; Gang, T.; Zhang, K.; Zhang, J. H.; Chen, X.; Sun, Z. Q.; Yang, B. Ag nanoparticles-coated silica-PMMA core-shell microspheres and hollow PMMA microspheres with Ag nanoparticles in the interior surfaces. *Colloids and Surfaces a-Physicochemical and Engineering Aspects* **2006**, *272*, 151-156.

(76) Li, G. L.; Liu, G.; Kang, E. T.; Neoh, K. G.; Yang, X. L. pH-responsive hollow polymeric microspheres and concentric hollow silica microspheres from silica-polymer core-shell microspheres. *Langmuir* **2008**, *24*, 9050-9055.

(77) Park, J. H.; Kim, Y. G.; Oh, C.; Shin, S. I.; Kim, Y. C.; Oh, S. G.; Kong, S. H. Fabrication of hollow silver spheres by MPTMS-functionalized hollow silica spheres as templates. *Materials Research Bulletin* **2005**, *40*, 271-280.

(78) Wong, L.; Suratwala, T.; Feit, M. D.; Miller, P. E.; Steele, R. The effect of HF/NH_4F etching on the morphology of surface fractures on fused silica. *Journal of Non-Crystalline Solids* **2009**, *355*, 797-810.

(79) Zhang, L.; Gu, F. X.; Tong, L. M.; Yin, X. F. Simple and cost-effective fabrication of two-dimensional plastic nanochannels from silica nanowire templates. *Microfluidics and Nanofluidics* **2008**, *5*, 727-732.

(80) Zhang, Q.; Ge, J. P.; Goebl, J.; Hu, Y. X.; Lu, Z. D.; Yin, Y. D. Rattle-Type Silica Colloidal Particles Prepared by a Surface-Protected Etching Process. *Nano Research* **2009**, *2*, 583-591.

(81) Fong, B.; Russo, P. S. Organophilic colloidal particles with a synthetic polypeptide coating. *Langmuir* **1999**, *15*, 4421-4426.

(82) Fong, B.; Turksen, S.; Russo, P. S.; Stryjewski, W. Colloidal crystals of silica-homopolypeptide composite particles. *Langmuir* **2004**, *20*, 266-269.

(83) Auernheimer, J.; Haubner, R.; Schottelius, M.; Wester, H.-J.; Kessler, H. Radio-Analytical Determination of the Coating Efficiency of Cyclic RGD Peptides. *Helvetica Chimica Acta* **2006**, *89*, 833-840.

(84) Fan, Y. W.; Cui, F. Z.; Hou, S. P.; Xu, Q. Y.; Chen, L. N.; Lee, I. S. Culture of neural cells on silicon wafers with nano-scale surface topograph. *Journal of Neuroscience Methods* **2002**, *120*, 17-23.

(85) Stober, W.; Fink, A.; Bohn, E. Controlled Growth of Monodisperse Silica Spheres in the Micron Size Range. *Journal of Colloid and Interface Science* **1968**, *26*, 62-69.

(86) Bogush, G. H.; Tracy, M. A.; Zukoski, C. F. Preparation of monodisperse silica particles - control of size and mass fraction. *Journal of Non-Crystalline Solids* **1988**, *104*, 95-106.

(87) Kobayashi, Y.; Horie, M.; Konno, M.; Rodriguez-Gonzalez, B.; Liz-Marzan, L. M. Preparation and properties of silica-coated cobalt nanoparticles. *Journal of Physical Chemistry B* **2003**, *107*, 7420-7425.

(88) Daly, W. H.; Poché, D. The preparation of N-carboxyanhydrides of α-amino acids using bis(trichloromethyl)carbonate. *Tetrahedron Letters* **1988**, *29*, 5859-5862.

(89) Poche, D. S.; Moore, M. J.; Bowles, J. L. An unconventional method for purifying the N-carboxyanhydride derivatives of gamma-alkyl-L-glutamates. *Synthetic Communications* **1999**, *29*, 843-854.

(90) Borase, T.; Iacono, M.; Ali, S. I.; Thornton, P. D.; Heise, A. Polypeptide core-shell silica nanoparticles with high grafting density by N-carboxyanhydride (NCA) ring opening polymerization as responsive materials and for bioconjugation. *Polymer Chemistry* **2012**, *3*, 1267-1275.

(91) Turksen, S. Ph. D. Dissertation, Synthesis and Characterization of Superparamagnetic Silica-homopolypeptide Composite Particles. Louisiana State University, 2006.

(92) Liu, D.; Li, Y.; Deng, J. P.; Yang, W. T. Synthesis and characterization of magnetic Fe_3O_4-silica-poly(gamma-benzyl-L-glutamate) composite microspheres. *Reactive & Functional Polymers* **2011**, *71*, 1040-1044.

CHAPTER 7
FUTURE WORK

7.1 Self- and Mutual Diffusion of a Rodlike Polymer

The aim of this project is to study self- and mutual diffusion of rodlike polymers using dynamic light scattering, DLS, and pulse field gradient (pulse gradient spin echo) nuclear magnetic resonance, PGSE. The distinction between the two types of diffusion is that mutual or cooperative diffusion represents the motion of the rod in response to a weak local concentration gradient while self diffusion is friction driven. Self diffusion is proportional with the squared distance traveled by the diffuser in time and is friction dependent.[1]

$$D_{self} = \frac{\langle x^2 \rangle}{t} \qquad Eq.\ 7.1$$

$$D_{self} = \frac{k_B T}{f} \qquad Eq.\ 7.2$$

where D_{self} is the self diffusion coefficient, x is the distance, t is the time, k_B is the Boltzmann constant, T is the absolute temperature and f the friction coefficient.

A rod-shaped molecule moves parallel and transverse to its own axis. The average motion is given by:[2]

$$D_s = D^0 = \frac{1}{3}\left(D_{\parallel}^0 + 2D_{\perp}^0\right) \quad Eq.\ 7.3$$

where D_s is the self-diffusion coefficient, D^0 is the diffusion coefficient at concentration extrapolated to zero, $D_{\parallel}^0$ is the parallel motion and $D_{\perp}^0$ is the transverse motion to the axis. In the dilute regime the friction coefficients are the same, $f_m = f_s$ and thermodynamic driving terms that affect mutual diffusion are absent. Consequently D_s and D_m are also equal. In semidilute conditions, the contribution from transverse diffusion becomes negligible. The diffusion can be expressed then:

$$D = \frac{1}{2} D^0 \qquad Eq. 7.4$$

Usually, self diffusion coefficients are measured by PGSE or fluorescence photobleaching recovery, FPR, or other advanced methods developed largely in response to the rapid development of transport theories in the late 1970s and early 1980s. The mutual diffusion coefficients are usually measured by DLS. Studies were conducted before on different molecules with different conformations such as polyelectrolytes,[1] globular proteins,[3] stiff and random coil polymers,[4,5] etc. Most of these results found a disagreement between the values of diffusion coefficients collected by both DLS and PGSE. In a typical sample, D_s rises while D_m falls with the concentration. They agree at zero concentration, practically the dilute limit. A disagreement between DLS and PGSE was noted by the amyloids community.[6] For the short amyloids the two techniques agree but once the fibrils become longer they start to diverge. On the assumption that $f_{self} = f_{mutual}$, the discrimination between D_m and D_s can be eliminated if the corrections for thermodynamic force and solvent back flow are made:[7]

$$\frac{D_m}{D_s} = \frac{M}{RT} \times \frac{\partial \Pi}{\partial c} \times (1 - \bar{\nu}\, c) \qquad Eq. 7.5$$

where M is the molecular weight, RT is the gas constant multiplied by the absolute temperature, Π is the osmotic pressure, c is the concentration and $\bar{\nu}$ is the partial specific volume.

The rodlike configuration of polypeptides qualifies them as appealing candidates for investigating the dynamical behavior. The most studied polypeptide from this perspective is poly(γ-benzyl-L-glutamate), PBLG. Self and mutual diffusion of the PBLG was explored using FPR and DLS by this group,[2,8,9] and by others. It is difficult sometimes to find the best model to study rodlike polymers.

Early studies showed that PBLG is not quite a rigid rod as might be expected.[10-12] The best model found is poly(γ-stearyl-L-glutamate), PSLG.[13-15] Having the long stearyl chains pointing out from the backbone, PSLG has a stable α-helix conformation, without random coil interruptions as PBLG does. This polypeptide was studied before in the Russo group[16,17] and also by other researchers.[18,19] PSLG is easy to prepare and easy to obtain in a very narrow molecular weight distribution by fractionation. Polypeptides mimic natural molecules, some of them involved in fatal diseases. Using PSLG as model, one can introspect then, the behavior of the amyloid fibers, responsible for Alzheimer's disease. A real monodisperse sample of amyloids is difficult to obtain. The study of a rigid rod-like conformation usually uses light scattering. For example, in the case of a short rod-like PSLG prepared in this laboratory, both DLS and PGSE excellently agreed as shown in Figure 7.1A.

PGSE returned two modes of decay from the correlation functions: fast and slow. In such situation one might suspect two things: the contribution from the rotation of the rod and the solvent contribution. The easiest way to test the later is to plot the intensity associated to the echo pulse against the concentration. As shown in Figure 7.1B the signal declines at elevated concentration. At increased concentration, the higher population of rods hinders the free motion of the solvent molecules. The rotational contribution can be tested with a rodlike polypeptide which has the capability to undergo helix-coil transition in a single solvent. Poly(ε-carbobenzyloxy-L-lysine), PCBL is the polypeptide of choice due to its well-documented inverse helix-to-coil transition in m-cresol.[20-23]

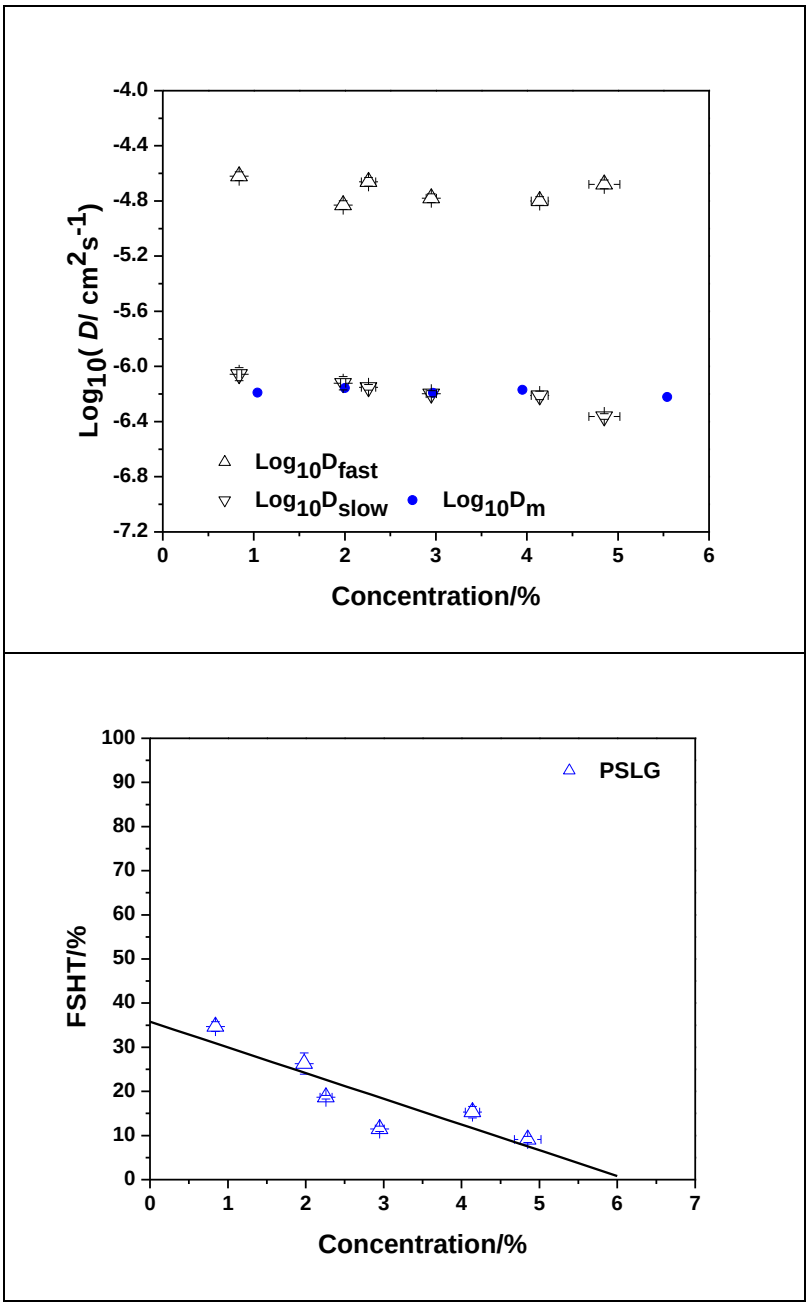

Figure 7.1 Logarithmic representation of the self and mutual diffusion coefficients collected by PGSE and DLS as a function of the concentration (A) and the intensity of the echo signal as a function of the concentration (B).

Finally, this project is devoted to research the limit at which DLS and PGSE techniques will disagree measuring the rigid rodlike PSLG. It will be completed in collaboration with Prof. Ernst Von Meerwall from Akron University, Akron, OH.

7.2 Physical Properties of Silica Poly(N^{ε}-carbobenzyloxy-L-lysine)-based Colloids: Methods to Investigate the Reverse Random Coil-to-Helix Conformational Change

7.2.1 Optical Rotatory Dispersion, ORD

Optical rotatory dispersion, ORD was largely used on early studies focused on polypeptides conformation. ORD was the main tool to investigate the inverse helix-to-coil transition of PCBL in m-cresol as a function of the temperature. This part of the project described in Chapter 5 will be completed using a future locally available ORD or in collaboration with another laboratory.

7.2.2 Nuclear Magnetic Resonance: Spin-Spin Relaxation Times, T2 Measurements

New investigations regarding spin-spin relaxation times, T2 are under way in completion to T1 measurements. These studies are meant to help in having clearer image of the mechanistic pathway the PCBL transition undergoes.

7.2.3 Spectroscopic Assay: UV-VIS

PCP PCBL particles can be excellent platforms to obtain gold-decorated PCPs by physical adsorption of colloidal gold to the terminal amine groups of the PCBL chains, as shown in Figure 7.2. This material can find potential use in sensing. Regardless of the size of the colloidal gold, these advanced PCPs can be useful tools for monitoring the helix-coil transition. It is hypothesized that the gold emission signal will shift according with the transition states of the polypeptide.

7.3 Saturn Belts

The project entitled “Saturn belts” will borrow ingredients from the projects described in several chapters of this document. The idea is illustrated in Figure 7.3. The architecture is similar with that of ABA block copolymers. There is one simple question this project is willing to answer: “Can we make ABA colloids or colloidal amphiphiles?” Briefly, particles with magnetic inclusions, either iron or cobalt, superparamagnetic or paramagnetic are coated with silica.

Optional, the complex of FITC-APS can be embedded into them, with supplemental silica protective coating.

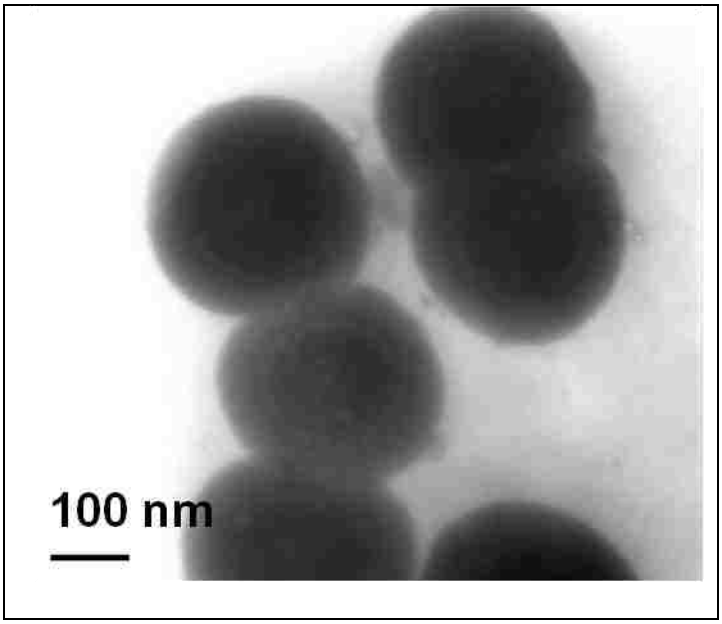

Figure 7.2 TEM micrograph of PCP PCBL(175)L decorated with colloidal gold (D = 5 nm).

Further particles are prepared for surface chemistry. If click chemistry will be employed to graft the polypeptide, the surface will be primed with azide functional groups. The *growing from* method uses a surface functionalized with amino groups. Once the surface of the particles has the desired functionality, they are aligned in a magnetic field. The polypeptide corona will grow only in the free area while the contact surface between particles is not accessible for growth. After magnetic field removal, another polypeptide can be grown. Aligned, they can also be crosslinked to resemble chain-like structure. This architectural colloid can be used as suspension for high power cars and bridges and to mimic an artificial muscle.

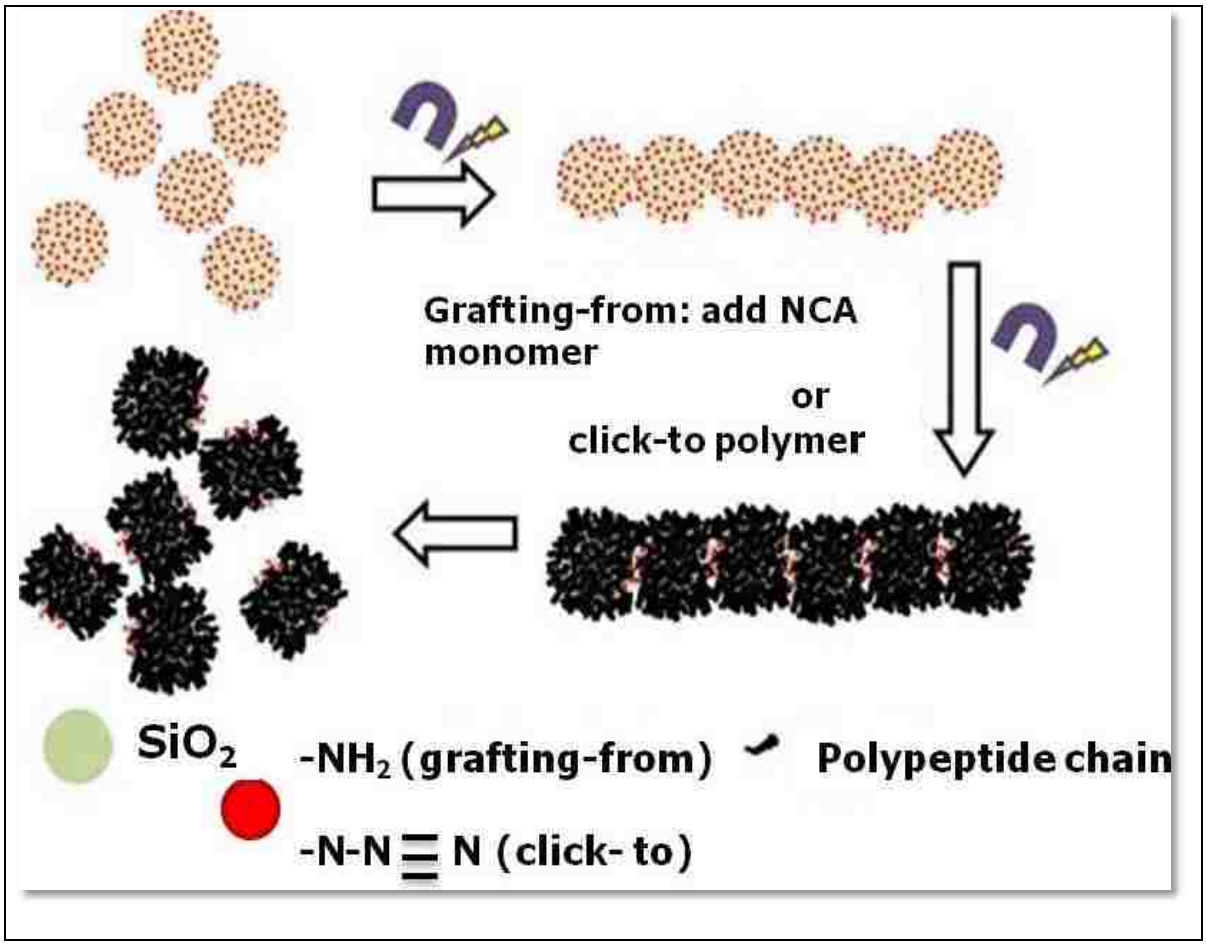

Figure 7.3 Schematic representation of the Saturn Belt production

7.4 Light-emitting Colloidal Hybrids, LECH.

Magnetic dye-doped silica colloids have attracted more and more attention lately because of their bifunctionality.[24] Iron oxide particles were intensely studied for *in vivo* and *in vitro* biomedical applications, such as magnetic resonance imaging and drug delivery.[25,26] Dye-coated silica colloids qualified as good candidates for biolabeling and bioimaging.[27] He et al. obtained stable Cy5 dye doped silica fluorescent nanoparticles (SFNP) with the shell consisting of biomolecules (e.g. polylysine, insulin) of different isoelectric points.[28] These hybrids gave good results in recognition of breast cancer cells. Wu et al. obtained photoswitchable and thermotunable multicolor fluorescent silica nanoparticles grafted with poly(N-isopropylacrylamide (PNIPAM)) brushes labeled with fluorescence resonance energy transfer

(FRET) donors as potential materials for human stem cell labeling, photodynamic therapy and so on.[29]

The purpose of this project will be two-fold: a) synthesis of magnetic, azo-dye loaded silica polypeptide-based hybrids; and, b) characterization of hybrids by IR, XPS, TGA, DLS, TEM, SEM and UV-Vis. A third tunable property, helix-coil transition of the polypeptide, PCBL, will be investigated along with magnetic properties and dye's photochromism. This colloid is envisioned as a multi-purpose, responsive material.

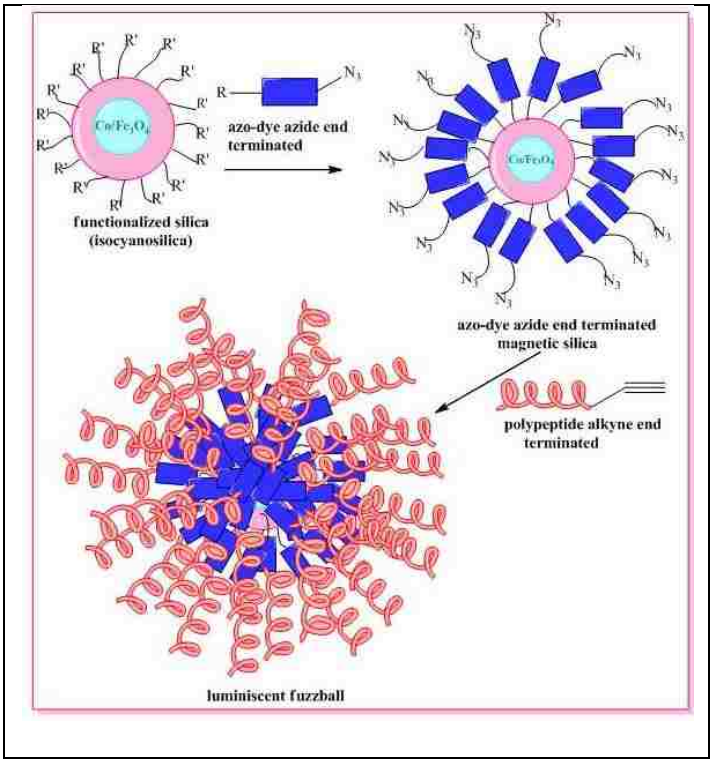

Figure 7.4 Schematic illustration of LECH preparation

It is predicted that the polypeptide shell will wiggle as a response to the trans-cis transition (photochromism, Figure 7.4) induced by the photolysis of the azochromophore.

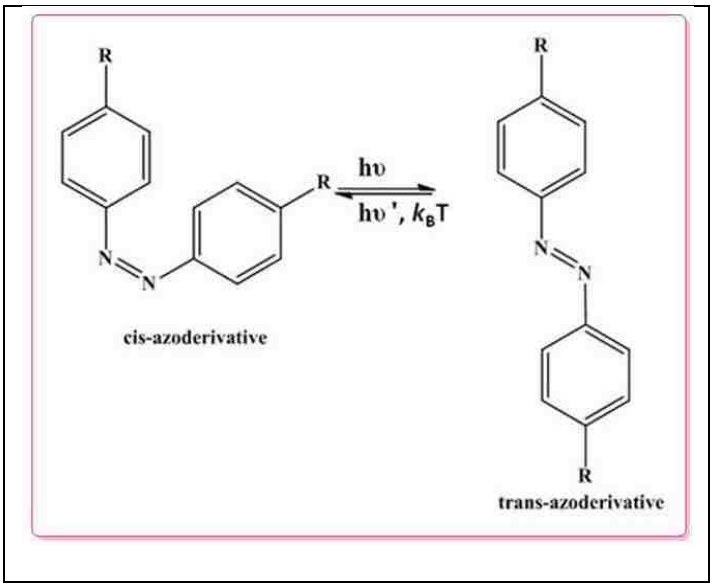

Figure 7.5 Trans-cis transition of azo-derivatives (photochromism)

The photochromic behavior is taking advantage of the azo-dye shape change to produce switchable receptors. Both kinds of transition (helix to coil for polypeptide and trans-cis for azo-dye) can be initiated by raising the temperature and light irradiation. The question is how they will interact? Can one block the other? Upon irradiation, an increase in viscosity might occur (photoviscosity effect) due to azo-dye conformation changes.

7.5 Shell Haircut: Grafting Density and Secondary Structure

In this section the work performed to measure the molecular weight of the polypeptide cleaved from the particles made by the *growing from* method will be described. Future experiments necessary to complete the project will also be presented.

Inspired by the formation of the mesoporous hybrid particles in 3mM aqueous NaOH solution, another key aspect of this work was developed: the use of NaOH etching to haircut the composite particle and assess the molecular weight of the polypeptide. Studies conducted up to present used HF as etchant[30] A dilute 3mM NaOH solution required a long time to form voids inside the silica beads. It was hypothesized that a more concentrated basic solution and a shorter

time of exposure to such conditions will “dissolve” silica cores leaving the polypeptide intact. This hypothesis was made on the basis of the thermogravimetric analysis which clearly showed that the particles still have polypeptide on the surface after deprotection and etching. Preliminary tests (Figure 7.6) have shown that ~10% NaOH and 40 minutes were sufficient to cause bare control fluorescent silica dissolution.

Figure 7.6 Control fluorescent silica cores with no polypeptide loading before (left) and after (right) etching for 40 min. in ~10% NaOH solution.

The original yellow turbid solution became transparent yellow and a thin layer of silicates (white transparent) have deposited on the bottom. Because the polypeptide can play a protective role against etching, a longer time was expected for complete disappearance of the silica core in the case of polypeptide-based colloid. Upon suspension in ~10% NaOH, starting from THF as a solvent, PCP PCBL hybrid lost its core and the cleaved shell polymer was collected by centrifugation. Dissolution in DMF followed by precipitation with water (2 times) and drying *in vacuo* overnight gave a white solid sample which was further analyzed by gel permeation chromatography, GPC/MALS. Figure 7.7A shows GPC/MALS chromatograms for PCBL cut from the particle, obtained by using Zimm model.

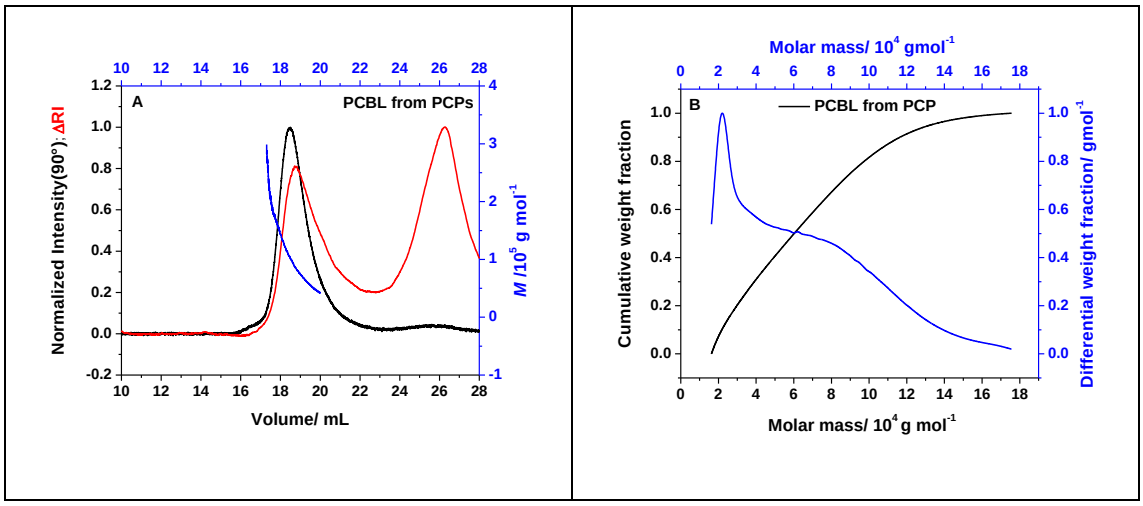

Figure 7.7 GPC/MALS traces and the mass plots of (A) PCBL from shell (CR7188) and cumulative and differential weight fraction of (B) PCBL from shell (CR7188). The chromatograms were recorded in DMF + 0.1M LiBr at 25°C and the refractive index was taken, *dn/dc* = 0.123 ± 0.002mL g^{-1} in accordance with Applequist and Doty.[31]

Table 7.1 summarizes data obtained by GPC/MALS.

Table 7.1 Sample Code, Number-Average Molecular Weight, M_n, Weight-Average Molecular Weight, M_w, Polydispersity Index, M_w/M_n and Gyration Radius for Cleaved PCBL

Sample code	M_n	M_w	(M_w/M_n)	Gyration Radius/Å
PCBL-1	60,000±1.2%	77,000±0.7%	1.27(1.4%)	200±17.7%

FTIR spectrum presented in Figure 7.8 shows the characteristic N−H stretching of the amine at 3290 cm^{-1} along with other specific peaks of PCBL-1: amide I band at 1651 cm^{-1} and 1626 cm^{-1} amide II at 1537cm^{-1} and C=O stretch of ester at 1689 cm^{-1}. The assignment of the characteristic bands was in accordance with data published by Fasman et al.[20] The split signal detected for amide I can be associated with α-helix conformation (1651 cm^{-1}) and traces of random coil (1626 cm^{-1}). The evidence of a random coil residue in addition with GPC data suggests that in the *growing from* approach polymer does not grow uniform and small "caps" can be present on the surface along with longer chains. It is also possible that, during etching, some long chains could

be broken. Indeed the chromatogram displayed in the Figure 7.7A shows a small shoulder at higher elution volume.

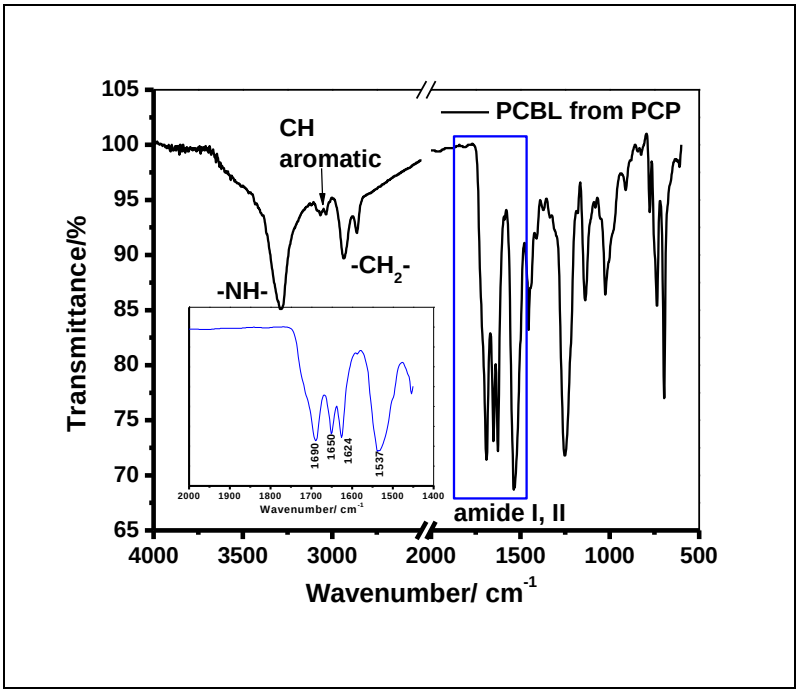

Figure 7.8 FTIR spectrum of PCBL-1 (CR7188) cleaved from the particle with ~10% NaOH.

The corresponding weight-average molecular weight, M_w, was 3,300 Da which gives a degree of polymerization, DP, of about 12.

The presence of the secondary structure other than α-helix can be explained on the basis of the monomer units number necessary whether to form, or not, a helix. A degree of polymerization of 12 is probably not enough to form a stable helix. Consequently the most of oligomers peaking at higher values of the elution volume are probably in a stable random coil secondary structure, as also seen in the FTIR spectrum.

The assessment of the shell's polymer size in terms of the molecular weight is important but also the evaluation of the grafting density is the most sensitive issue in the *grafting from* methodology. The combination of the GPC/MALS and TGA measurements made possible the computation of the chain population using the formula:

$$\sigma = \frac{f^{-1}w_{200-600} - w_{\mathrm{Si}} \times [1 - f^{-1}w_{200-600}]}{M \times S_{\mathrm{spec.}} \times [1 - f^{-1}w_{200-600}]} \times 10^6 \ (\mu\mathrm{mol} \cdot \mathrm{m}^{-2}) \qquad \text{Eq. 7.6}$$

where f^{-1} is the fraction of the polypeptide ashes, $w_{200\text{-}600}$ is the weight loss associated with polypeptide degradation between 200°C and 600°C, w_{Si} is the weight loss of the silica core in the same temperature interval, 200-600°C, M is the molecular weight of the polypeptide, and S_{spec} is the surface specific area. The calculation of the molar grafting density, σ, have used weight loss profiles from TGA shown in Figure 7.9, and the GPC/MALS results reflecting the value of the molecular weight for the grafted polypeptide. This approach followed Bartholome et al.[32] which was corrected by Balamurugan et al.[33] The factor f^{-1} ($0 < f < 1$) represents the fraction of the polypeptide ashes and it is taken as 0.94 from the inset TGA trace profile for the free polypeptide, assuming a hypothetical 1 gram of composite particle. The term $w_{200\text{-}600}$ is associated with the decomposition of the polypeptide shell between 200°C and 600°C. The w_{silica} is the fraction lost by silica cores in the same temperature interval as the polypeptide and it is measured before grafting the polypeptide. It is assumed that the weight loss is mostly due to water and hydroxyl groups from the silica surface and it will be the same in the case of the composite particle. In the denominator, the weight average molecular weight of the polypeptide, M_{w}, was taken as 77,000, measured by GPC/MALS. The surface specific area, S_{spec}, was calculated considering a core of radius 175 nm and the density of the silica 1.98 g mol^{-1}. The result was 8.66 m^2 g^{-1}. According with Figure 4.11, $w_{200\text{-}600}$ was 0.92-0.31= 0.61 and w_{silica} was 0.92-0.87= 0.04. Introducing the data into the surface density expression, led to σ = 0.9 μmol m^{-2}. To calculate the population of the chains from the silica core surface, first the aria of the core needed to be computed. Multiplying this amount, $4\pi R^2_{\mathrm{core}}$, with the grafting density, σ, and Avogadro's number, N_{A}, returned a population of about 200,000 chains per particle.

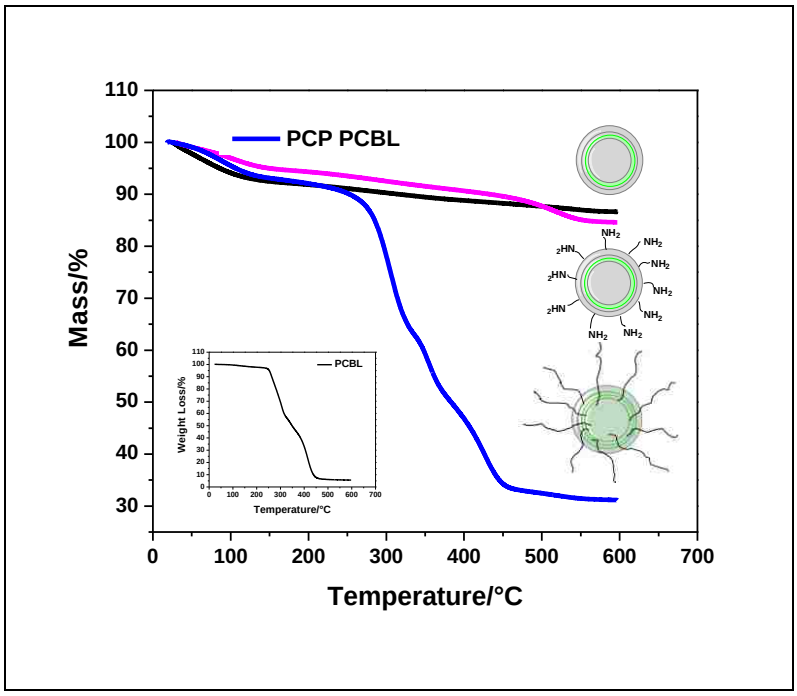

Figure 7.9 TGA traces for fluorescent silica core, amino-functionalized fluorescent silica and PCP PCBL (CR7188) particle used in the cleavage experiment.

The grafting density, expressed in number of chains per particle alone, it is not useful information if the profile of the cut off polypeptide is not described in terms of its secondary structure. Polypeptides, as well as proteins, carry information imbedded in their conformation. Understanding the polypeptide structures helps to also understand more complex processes such as protein folding. Consequently, the first concern after the cleavage of the PCBL from the composite's core was to investigate its conformation. The most common secondary structure for polypeptides is α-helix and was confirmed by FTIR. The stabilization of secondary configuration is ensured by intramolecular H-bonding which gives a rodlike structure. A rodlike behavior enables extraordinary properties and PCBL should be expected to behave in the same manner. Because the stability of the helical structure is the most important feature in a large palette of applications concerning responsive materials, it was of crucial importance to determine whenever the haircut polypeptide behavior was a reflection of a rodlike shape. A plot of radius,

R, versus molecular weight, *M*, appears in Figure 7.10 and shows the stiff rod conformation of the cut off PCBL. The deviation of data corresponding to the two polymers PCBL from PCP and lab prepared can be assigned to the difference in refractive index increment used in data analysis. The graphical representation was constructed by also plotting a lab-synthesized by the primary amino initiation and not tethered PCBL of medium molecular weight, PCBL lab prerpared (Table 7.2).

Table 7.2 Sample Code, Weight–Average Molecular Weight and Polydispersity Index of Cleaved and Lab-prepared PCBL Samples Used in This Study.

Sample Code	M_w/g mol^{-1}	M_w/M_n
PCBL from PCP	77,000	1.27
PCBL lab prepared	202,000	1.10

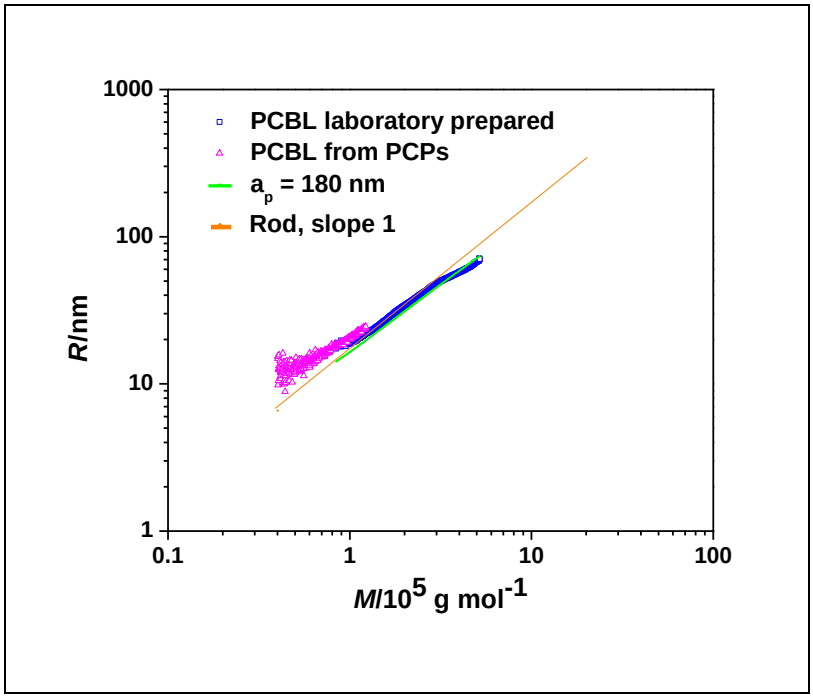

Figure 7.10 Conformation plot for different molecular weight of the PCBL; PCBL from PCPs (CR7188) and PCBL Russo's laboratory-prepared.

Deviations from the rigid rod behavior become evident with the increase in the molecular weight. In a log – log representation, PCBL lab prepared with a calculated persistence length, a_p,

of 1600Å, gave a Flory scaling parameter, ν_f,[34,35] ($Rg \sim M^{\nu}_f$) of ~0.80 for higher values of M (Figure 7.11).

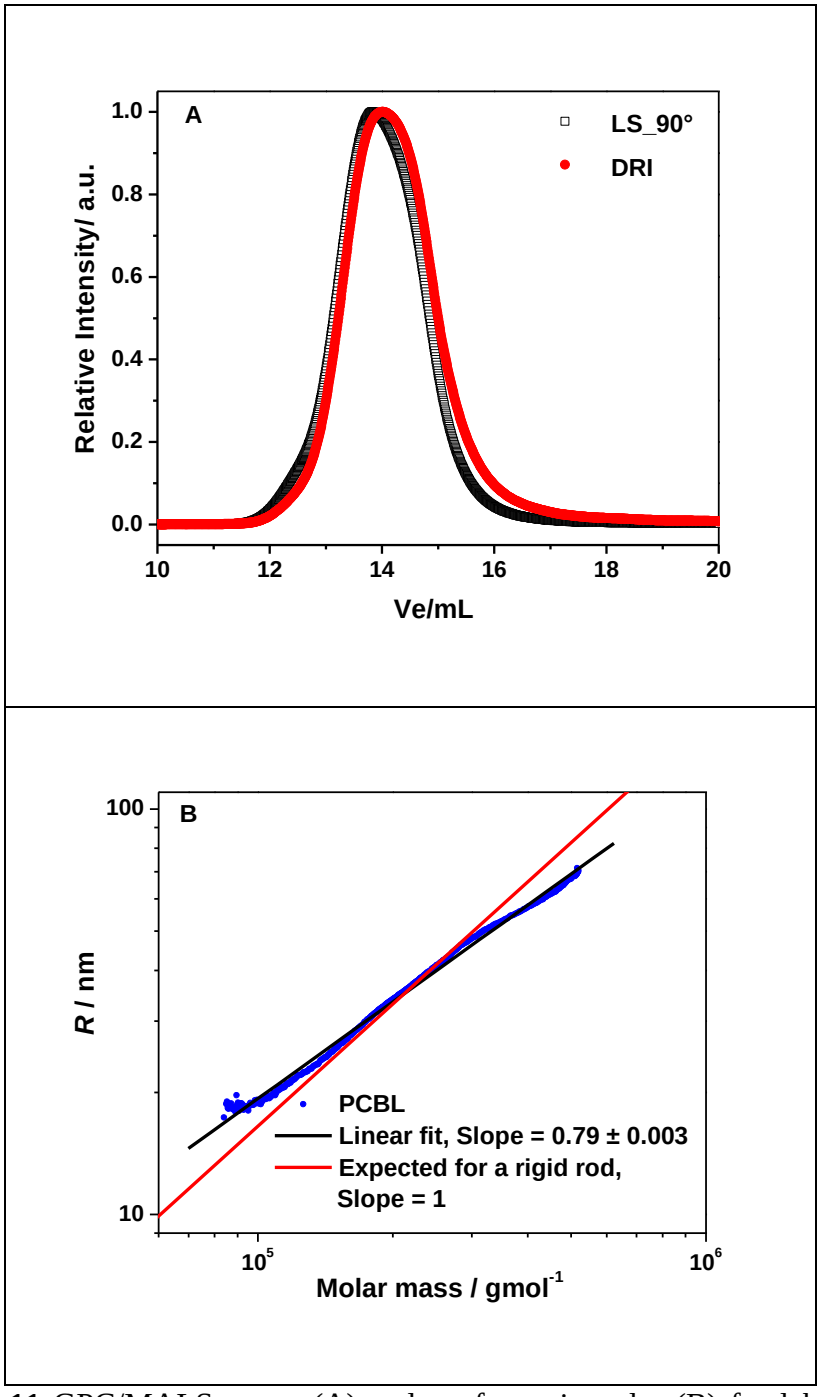

Figure 7.11 GPC/MALS traces (A) and conformation plot (B) for lab-prepared PCBL (Mw = 202,000 kDa). Adapted with permission.[36]

Variations from rigid rodlike conformation in helicogenic solvents, as seen in Figure 4.13B,were reported before especially for PBLG.[5,16,17,37-41] This finding might be an indication that Kratky – Porod model does not extend to the whole range of the molecular weight. It is also true that PCBL, as well as PBLG, seem to have higher values of the persistence length for a rigid rod conformation and increases with molecular weight.[41] Applequist and Doty compared a PCBL chain of 262 Å persistence length with the values obtained for other rigid molecules such as deoxyribonucleic acid (a_p = 500 Å) and cellulose trinitrate (a_p = 117 Å) and found that the shape of the molecule is that of a free-draining coil.[31] The wormlike model can be reconciled with the dynamical behavior of the PCBL on the base of the enhanced flexibility for PCBL helix. Studies performed on helix-coil transition of PCBL in helicogenical solvents or mixtures have pointed out to a "broken" conformation.[20-23,42] The helices could be interrupted, consequently the chains might have missing intramolecular H-bonds which ultimately create multiple bends. Thus, the behavior of the PCBL-2 sample analyzed in this work can be explained through the prism of broken helices. Yet, several other speculations can be added to the picture of the PCBL conformational behavior. The polydispersity of the sample can be an artifact of the aggregation. It is also true that PCBL's structure might favor branching, if the protective side chain benzyl groups are missing. Either debenzylation occurring in time or a not fully protected monomer precursor used in the polymerization, can constitute sources of branching. Hence questions can be posed on the GPC detection limit for very polydisperse high molecular polymers and a good option to answer can be asymmetric flow field flow fractionation, AF4.[43,44]

The future work requires control experiments on untethered, vendor-purchased PCBL. GPC\MALS will be used to evaluate molecular weights and polydispersity index. The polymer will be subjected to the same conditions of etching: 3h in aqueous 10% NaOH and also a longer

time (e.g. 48h). The non-etched polymer will be another sample to analyze. Before GPC\MALS experiments, the refractive index of the samples will be determined using a refractometer. These measurements will be the first indicators whether the polymer will undergo degradation.

7.6 References and Notes

(1) Pecora, R. Dynamics of biological polyelectrolytes. *Macromolecular Symposia* **2005**, *229*, 18-23.

(2) Bu, Z. M.; Russo, P. S.; Tipton, D. L.; Negulescu, II Self-diffusion of rodlike polymers in isotropic solutions. *Macromolecules* **1994**, *27*, 6871-6882.

(3) Le Bon, C.; Nicolai, T.; Kuil, M. E.; Hollander, J. G. Self-diffusion and cooperative diffusion of globular proteins in solution. *Journal of Physical Chemistry B* **1999**, *103*, 10294-10299.

(4) Callaghan, P. T.; Pinder, D. N. Self-diffusion of random-coil polystyrene determined by pulsed field gradient nuclear magnetic-resonance - dependence on concentration and molar mass. *Macromolecules* **1981**, *14*, 1334-1340.

(5) Jamil, T.; Russo, P. S.; Negulescu, I.; Daly, W. H.; Schaefer, D. W.; Beaucage, G. Light-scattering from random coils dispersed in solutions of rodlike polymers. *Macromolecules* **1994**, *27*, 171-178.

(6) Baldwin, A. J.; Anthony-Cahill, S. J.; Knowles, T. P. J.; Lippens, G.; Christodoulou, J.; Barker, P. D.; Dobson, C. M. Measurement of amyloid fibril length distributions by inclusion of rotational motion in solution NMR diffusion measurements. *Angew. Chem.-Int. Edit.* **2008**, *47*, 3385-3387.

(7) Kanematsu, T.; Sato, T.; Imai, Y.; Ute, K.; Kitayama, T. Mutual- and self-diffusion coefficients of a semiflexible polymer in solution. *Polymer Journal* **2005**, *37*, 65-73.

(8) Russo, P. S.; Baylis, M.; Bu, Z. M.; Stryjewski, W.; Doucet, G.; Temyanko, E.; Tipton, D. Self-diffusion of a semiflexible polymer measured across the lyotropic liquid-crystalline-phase boundary. *J. Chem. Phys.* **1999**, *111*, 1746-1752.

(9) Delong, L. M.; Russo, P. S. Thermodynamic and dynamic behavior of semiflexible polymers in the isotropic-phase. *Macromolecules* **1991**, *24*, 6139-6155.

(10) Doty, P.; Bradbury, J. H.; Holtzer, A. M. Polypeptides .4. The molecular weight, configuration and association of poly-gamma-benzyl-L-glutamate in various solvents. *J. Am. Chem. Soc.* **1956**, *78*, 947-954.

(11) Doty, P.; Holtzer, A. M.; Bradbury, J. H.; Blout, E. R. Polypeptides .2. The configuration of polymers of gamma-benzyl-L-glutamate in solution. *J. Am. Chem. Soc.* **1954**, *76*, 4493-4494.

(12) Doty, P.; Yang, J. T. Polypeptides .7. Poly-gamma-benzyl-L-glutamate - the helix-coil transition in solution. *J. Am. Chem. Soc.* **1956**, *78*, 498-500.

(13) Poche, D.; Daly, W. H.; Russo, P. S. Synthesis and thermal-behavior of linear and star branched poly(gamma-stearyl-alpha,L-glutamate). *Abstracts of Papers of the American Chemical Society* **1990**, *200*, 132-POLY.

(14) Poche, D. S.; Daly, W. H.; Russo, P. S. Synthesis and some solution properties of poly(gamma-stearyl alpha,L-glutamate). *Macromolecules* **1995**, *28*, 6745-6753.

(15) Poche, D. S.; Russo, P. S.; Daly, W. H. Solution characterization of linear and star-branched semiflexible polymers of gamma-stearyl-alpha,L-glutamate. *Abstracts of Papers of the American Chemical Society* **1990**, *200*, 211-POLY.

(16) Jamil, T.; Russo, P. S. Dynamic light-scattering from a semiflexible polymer at very low concentrations. *J. Chem. Phys.* **1992**, *97*, 2777-2782.

(17) Jamil, T.; Russo, P. S.; Daly, W. H.; Negulescu, I. Static and dynamic light-scattering of a random coil polymer in rodlike polymer-solution. *Macromolecular Symposia* **1994**, *79*, 81-85.

(18) Ando, I.; Yin, Y. G.; Zhao, C. H.; Kanesaka, S.; Kuroki, S. Diffusion of rod-like polypeptides in the liquid crystalline and isotropic phases as studied by high field-gradient NMR spectroscopy. *Macromolecular Symposia* **2005**, *220*, 61-73.

(19) Yin, Y. G.; Zhao, C. H.; Sasaki, A.; Kimura, H.; Kuroki, S.; Ando, I. Diffusional behavior of polypeptides in the isotropic, biphasic, and liquid crystalline phases as studied by the pulse field-gradient spin-echo H-1 NMR method. *Macromolecules* **2002**, *35*, 5910-5915.

(20) Fasman, G. D.; Idelson, M.; Blout, E. R. Synthesis and conformation of high molecular weight poly-epsilon-carbobenzyloxy-L-lysine and poly-L-lysine.HCl. *J. Am. Chem. Soc.* **1961**, *83*, 709-&.

(21) Hayashi, T.; Emi, S.; Nakajima, A. Helix-coil transition of poly(epsilon-carbobenzyloxy-L-lysine) in m-cresol. *Polymer* **1975**, *16*, 396-400.

(22) Matsuoka, M.; Norisuye, T.; Teramoto, A.; Fujita, H. Solution properties of synthetic polypeptides .15. Helix-coil transition in poly(epsilon-carbobenzyloxy L-lysine). *Biopolymers* **1973**, *12*, 1515-1532.

(23) Nakamoto, K.; Suga, H.; Seki, S.; Teramoto, A.; Norisuye, T.; Fujita, H. Solution properties of synthetic polypeptides .19. Heat-capacity measurements on system of poly(epsilon-

carbobenzyloxy-L-lysine) and meta-cresol in helix-coil transition region. *Macromolecules* **1974**, *7*, 784-789.

(24) Ren, C. L.; Li, J. H.; Chen, X. G.; Hu, Z. D.; Xue, D. S. Preparation and properties of a new multifunctional material composed of superparamagnetic core and rhodamine B doped silica shell. *Nanotechnology* **2007**, *18*, 6.

(25) Santra, S.; Tapec, R.; Theodoropoulou, N.; Dobson, J.; Hebard, A.; Tan, W. H. Synthesis and characterization of silica-coated iron oxide nanoparticles in microemulsion: The effect of nonionic surfactants. *Langmuir* **2001**, *17*, 2900-2906.

(26) Bruce, I. J.; Sen, T. Surface modification of magnetic nanoparticles with alkoxysilanes and their application in magnetic bioseparations. *Langmuir* **2005**, *21*, 7029-7035.

(27) Yao, G.; Wang, L.; Wu, Y. R.; Smith, J.; Xu, J. S.; Zhao, W. J.; Lee, E. J.; Tan, W. H. FloDots: luminescent nanoparticles. *Analytical and Bioanalytical Chemistry* **2006**, *385*, 518-524.

(28) He, X.; Chen, J.; Wang, K.; Qin, D.; Tan, W. Preparation of luminescent Cy5 doped core-shell SFNPs and its application as a near-infrared fluorescent marker. *Talanta* **2007**, *72*, 1519-1526.

(29) Wu, T.; Zou, G.; Hu, J. M.; Liu, S. Y. Fabrication of Photoswitchable and Thermotunable Multicolor Fluorescent Hybrid Silica Nanoparticles Coated with Dye-Labeled Poly(N-isopropylacrylamide) Brushes. *Chem. Mat.* **2009**, *21*, 3788-3798.

(30) Borase, T.; Iacono, M.; Ali, S. I.; Thornton, P. D.; Heise, A. Polypeptide core-shell silica nanoparticles with high grafting density by N-carboxyanhydride (NCA) ring opening polymerization as responsive materials and for bioconjugation. *Polymer Chemistry* **2012**, *3*, 1267-1275.

(31) Applequist, J.; Doty, P. In *Polyamino Acids, Polypeptides, and Proteins*; Stahmann, M. A., Ed.; The University of Wisconsin Press, p. 161-175: Madison, 1962.

(32) Bartholome, C.; Beyou, E.; Bourgeat-Lami, E.; Chaumont, P.; Zydowicz, N. Nitroxide-mediated polymerizations from silica nanoparticle surfaces: "Graft from" polymerization of styrene using a triethoxysilyl-terminated alkoxyamine initiator. *Macromolecules* **2003**, *36*, 7946-7952.

(33) Balamurugan, S. S.; Soto-Cantu, E.; Cueto, R.; Russo, P. S. Preparation of Organosoluble Silica-Polypeptide Particles by "Click" Chemistry. *Macromolecules* **2010**, *43*, 62-70.

(34) Flory, P. *Principles of Polymer Chemistry*; Cornell, Ithaca: New York, 1957.

(35) Flory, P. J.; Matheson, R. R. Statistical thermodynamics of semirigid macromolecules - chains with interconvertible rodlike and random-coil sequences in equilibrium. *J. Phys. Chem.* **1984**, *88*, 6606-6612.

(36) Soto-Cantu, E. PhD Dissertation, Synthesis and Surface Characterization of Silica-Polypeptide Composite Particles. Louisiana State University, 2008.

(37) Mitchell, J. C.; Woodward, A. E.; Doty, P. Polypeptides .16. The polydispersity and configuration of low molecular weight poly-gamma-benzyl-L-glutamates. *J. Am. Chem. Soc.* **1957**, *79*, 3955-3960.

(38) Dawkins, J. V.; Hemming, M. Gel-permeation chromatography - universal calibration for rigid rod and random coil polymers. *Polymer* **1975**, *16*, 554-560.

(39) Grubisic, Z.; Reibel, L.; Spach, G. Application de la technique de fractionnement sur gel aux polypeptides de synthese. *Comptes Rendus Hebdomadaires Des Seances De L Academie Des Sciences Serie C* **1967**, *264*, 1690-&.

(40) Grubisic, Z.; Rempp, P.; Benoit, H. A universal calibration for gel permeation chromatography. *Journal of Polymer Science Part B-Polymer Letters* **1967**, *5*, 753-&.

(41) Temyanko, E.; Russo, P. S.; Ricks, H. Study of rodlike homopolypeptides by gel permeation chromatography with light scattering detection: Validity of universal calibration and stiffness assessment. *Macromolecules* **2001**, *34*, 582-586.

(42) Omura, I.; Teramoto, A.; Fujita, H. Dielectric-dispersion of polypeptide solutions .2. Helix-coil transition of "poly(epsilon-carbobenzoxy-L-lysine) in m-cresol. *Macromolecules* **1975**, *8*, 284-290.

(43) Podzimek, S. In *Light Scattering, Size Exclusion Chromatography and Asymmetric Flow Field Flow Fractionation*; John Wiley & Sons, Inc., p 1-36.

(44) Podzimek, S. In *Light Scattering, Size Exclusion Chromatography and Asymmetric Flow Field Flow Fractionation*; John Wiley & Sons, Inc., p 259-305.

CHAPTER 8
SYNTHETIC PROCEDURES AND CHARACTERIZATION TECHNIQUES

Synthetic procedures

NOTE: 1. Chemicals used in the preparation of the materials described in the following sections are listed in the chapters 3,4,5,6 and 7 after Introduction section.

2. All particles prepared were stored as suspensions.

3. Yield was calculated by taking an aliquot of a given silica-based suspension (usually 1mL) in a vial and was dried either at 100°C for 2-3h (plain silica cores) or in vacuo overnight (polypeptide composite particles). The weight observed was used to calculate the total yield and the solids concentration of the suspensions.

4. Abbreviations

8.1 Preparation of Silica Particles by Sol-Gel Method[1,2](Chapter 3)

Silica particles were prepared by a modified Stöber procedure in medium and large batches as described below.

8.1.1 Medium-Size Batch

In a two-neck 1000 mL round-bottomed flask connected to an overhead mechanical stirrer, 500 mL of EtOH was mixed with 40 mL of ammonium hydroxide (28%) to ensure a basic pH (9- 10, pH paper). Moderate stirring of the mixture (150-200 rpm) was performed over 15- 20 min. Then a solution of TEOS (13.3 mL) in 53 mL of EtOH was added quickly, ~10 – 15s, (using a glass funnel with a long and wide leg) under vigorous stirring (~400 rpm) at 22-25°C and reacted for 2h. The obtained colloid was transferred in a tall bottle and a small aliquot was kept for further characterization.

Typical yield: 5.2 g ($c = 8.6\ mg \cdot mL^{-1}$).

8.1.2 Large-Size Batch

A larger batch of Stöber silica can be prepared using a 2000 mL two-neck flask in the same fashion as described above. Ethanol (1250 mL) and ammonium hydroxide (28%, 100mL) were mixed together and the same moderate stirring rate and time was kept as for medium batch. After homogenization, TEOS (33.25mL) in EtOH (132.5mL) was added fast and the reaction continued as described in section 8.1.1.

NOTE: If a lower pH than 9 was noted after homogenization of the solution S1 for 15- 20 min., supplemental ammonium hydroxide was added to adjust to the optimal value (9- 10).

Typical yield: 11.2 g ($c = 7.4\ mg \cdot mL^{-1}$).

8.2 Preparation of Silica Particles by Reverse Microemulsion[3]

Cyclohexane, water, aqueous ammonia and surfactant were mixed together to form the reverse microemulsion. In a typical experiment, 17.5 mL of surfactant Igepal CO-520 and 225 mL cyclohexane were fed in a 500 mL three-neck flask connected to an overhead mechanical stirrer. Then, 5 mL of ammonium hydroxide (28%) was added and the mixture was stirred for 10 min. at 300 rpm. While the rate of the stirring was kept constant, 5 mL of TEOS was added fast (10 – 15 s) and the reaction continued overnight at room temperature. Methanol (50-60mL) was used to break the reverse microemulsion and extract the particles. The extracted particles were washed 3 times with methanol, 3 times with a mixture of methanol/water by centrifugation-redispersion. Finally they were stored in methanol.

Yield: 200 mg, ($c = 10 mg \cdot mL^{-1}$).

8.3 Preparation of Fluorescent Molecules FITC/APS[4-6] and RhB/APS[7-10] (Chapters 4,5 and 6)

8.3.1 Rhodamine B-APS Molecule

Rhodamine B (0.485 g, 0.001 mol) was dissolved in 20 mL chloroform in a round bottom flask wrapped in aluminum foil, immersed in an oil bath and connected to an azeotropic distillation adapter (Dean Stark). This adapter had a condenser attached to it. The mixture of the dye was stirred and heated to the boiling point of the chloroform (61.2^{o}C). Then 3-aminopropyltriethoxy silane (0.223 mL, 0.001 mol) was injected dropwise into the hot solution while being stirred. The water formed during the condensation was collected via azeotropic adapter over r 30 min. and collected in the Dean Stark attachment. After water removal, the chloroform was distilled off from the reaction mixture and red crystals were obtained which were stored in brown bottles or transparent vials wrapped in aluminum foil.

Yield: 0.684g (100%)

FTIR: C=O (1772 cm^{-1}), Si-O-C (1114 cm^{-1}, 1070 cm^{-}1, 1101 cm^{-1}).

8.3.2 FITC-APS Molecule

Fluorescein isothiocyanate (50 mg, 0.12 mmol) and 10 mL of absolute ethanol were suspended in a 50 mL round-bottomed flask capped with a septum. The mixture was magnetically stirred for 30 min. and 3-aminopropyltriethoxy silane (0.5 mL, 1.2 mmol) was injected into the solution through the septum. The reaction proceeded for 18 h in the dark to prevent the dye from bleaching.

Yield: 0.081g (100%).

8.4 Synthesis of Fluorescent Covalently Tagged Silica Particles[4-6,11] (Chapter 5 and 6)

After the formation of the silica seeds (see Section 8.1.1), a separatory funnel containing 75 mL TEOS five times diluted with EtOH (375 mL) was attached to the two neck flask. The

flow of the dropping solution was adjusted for 1 drop per minute (~ 50 μL). Using a syringe, a volume of 8 mL of FITC–APS adduct was injected into the silica seed suspension. The round bottom flask was wrapped in aluminum foil to prevent dye bleaching. The reaction proceeded for 36 h under continuous stirring (200 rpm) at room temperature. Fluorescent particles were washed copiously with ethanol by repeated centrifugations-dispersions to a loose precipitate settled on the bottom of the PTFE tubes until the washing alcohol was not giving fluorescence signal when illuminated with a 488 nm wavelength laser.

Typical yield: 19 g (c = 18 mg·mL^{-1}).

8.5 Protective Coating of Fluorescent Silica Particles.[11] (Chapter 5 and 6)

Silica coating was performed on particles as described in the previous step (8.4) in order to prevent dye leaking and bleaching. Control over the size of the final particle was intermediated by the use of the calculations by Zhang et al.:

$$d = d_0(V/V_0)^{1/3} \qquad \text{Eq. 8.1}$$

where d is the final diameter of 375 nm, d_0 is the initial size of the silica seeds, V_0 is the initial volume of the TEOS used in silica seeds preparation and V is the TEOS needed for a target particle size. Several sizes were prepared ranging from 250 nm to 1.3 μm. The detailed procedure for a target size of 375 nm is described below.

From the original fluorescent suspension (8.4), 100 mL (4.74 g) were taken and diluted to 200 mL total volume in a beaker. This mixture was first sonicated with an ultrasonicator operating at 40 amps for 5 min. to ensure a good dispersion of particles within the solution. Then the suspension was quickly transferred into a 500 mL two-neck round bottom flask connected to an overhead mechanical stirrer and wrapped in aluminum foil. Ammonia, 43 mL was added to create a basic environment validated by pH paper. This mixture was stirred for 15 – 20 min. for

homogenization. Separately 6 mL TEOS was diluted four times with absolute EtOH (24 mL) and the solution was swirled for homogenization. This mixture was transferred into a small separatory funnel (125 mL) attached to the two-neck flask containing the fluorescent particles. The flow rate was 50 μL per minute under continuous vigorous stirring (~400 rpm) at room temperature. The reaction continued over 24 h. Particles were washed 3-4 times with ethanol by centrifugation-dispersion and stored in brown bottles as alcoholic suspension.

Typical yield: 5.92 g (c = 215 mg·mL^{-1}).

8.6 Preparation of FITC Covalently Labeled Silica by Reverse Emulsion[3]

Cyclohexane, water, aqueous ammonia (28%) and surfactant were mixed together to form the reverse microemulsion. In a typical experiment, 17.5 mL of surfactant Igepal CO-520 and 225 mL cyclohexane were fed in a 500 mL three-neck flask connected to an overhead mechanical stirrer. Then, 5 mL of aqueous ammonia and 2 mL of FITC/APS complex were added and the mixture was vigorously stirred for 10 min. at 300 rpm to form the emulsion droplets. The flask was covered with aluminum foil to prevent dye bleaching. While the rate of the stirring was kept constant, 5 mL of TEOS was added fast, 5 – 10s, and the reaction continued overnight at room temperature. Methanol (50-60mL) was used to break the reverse microemulsion and extract the particles. The extracted particles were washed by centrifugations-dispersions to lose precipitates 3 times with methanol, 3 times with a mixture of methanol/water and finally with methanol until the supernatant didn't fluoresce when irradiated with a blue laser. The particles were dispersed in methanol as the storage solvent.

Yield: 245 mg (c = 1 mg·mL^{-1}).

8.7 Functionalization of Silica Surface with Amino Groups[12-14] (Chapters 4, 5 and 6)

The functionalization with amino groups used 3-aminopropy triethoxysilane, APS as an amination agent. The volume of the amino precursor, APS, was computed as a function of the desired surface coverage. In a typical preparation, an aliquot of silica-protected fluorescent particles (~10 mL) was diluted with absolute ethanol (see Table 8.3). The suspension was sonicated for five minutes prior to use and quickly transferred into a 250 mL two-neck round-bottom flask attached to an overhead mechanical stirrer and protected with aluminum foil. Afterwards APS was injected into the mixture with a syringe. The reaction proceeded for 18 h under stirring (200 rpm) at room temperature. The particles were washed by centrifugation-dispersion to lose precipitates with ethanol until the ninhydrin test was negative indicating the absence of free amino groups in the suspension. For testing small aliquots (1 mL) of supernatant from the centrifuge tubes were loaded in vials placed in a water bath set at 45°C. Two drops (~100 μL) of a 10% alcoholic solution of ninhydrin was added. The presence of free amino group was indicated by a purple to blue coloration. Afterwards, the particles were washed by centrifugation-dispersion twice with anhydrous THF and stored in a dark vial suspended in the same solvent, anhydrous THF. The amounts of the particles, the desired coverage with amino groups and the volume of the amino silane are listed in Table 8.3

Table 8.1 Amino-Silica Prepared for This Work Following the Section 8.7 Recipe

Silica		Amino-silica			Volume	#NH_2/groups	Chapter/
Abbreviation	Mass /mg	Abbreviation	Solvent /mL	Yield / mg	of APS/μL	nm^{-2}	Section
SF1(175) (CR797A)	770	SFA1 (CR7157)	90	600	15	4NH2 (100%APS)	Ch6, Ch5
SF1(175) (CR797A)	900	SFA2 (CR7184A)	90	820	20	2NH2 (100%APS)	Ch6, Ch5
SF2(100) (CR7151)	350	SFA3 (CR83A)	40	280	12	4NH2 (100%APS)	Ch6

Table 8.1 continued

Silica Abbreviation	Mass /mg	Amino-silica Abbreviation	Solvent /mL	Yield /mg	Volume of APS/μL	#NH2/groups nm^{-2}	Chapter / Section
SF3(55) (CR7153B)	300	SFA4 (CR84A)	40	240	19	4NH2 (100%APS)	Ch6
S1(105) (CR7124)	620	SA5 (CR7153A)	90	525	70	4NH2 (100%APS)	Ch5
S1(105) (CR7124)	360	SA6 (CR822)	50	300	30	4NH2 (100%APS)	Ch7

8.8 Magnetic Particles with a Magnetite, Fe_3O_4, Core (Chapter 3)

8.8.1 Preparation of Ferrofluid[15-17]

A 500 mL three-neck flask connected to an in-line N_2 source, using a long needle, a mechanical overhead stirrer and a condenser attached to a cooling bath was loaded with 150 mL of deionized, degassed water (overnight, by bubbling dry N_2) and two aqueous solutions of iron chlorides prepared separately as follows: (I) 3.97 g of $FeCl_2 \bullet 4H_2O$ and (II) 6.33 g $FeCl_3$ and 4 mL of deionized, degassed water were added to each vial and injected sequentially into the three-neck flask. The light brown mixture was heated under vigorous stirring (300 rpm) at 80°C. Then 60 mL of 10 M NaOH were injected slowly through a septum over a period of 40 min while the temperature was kept at 80°C. The solution changed color from light brown to dark brown and finally became the color of the black mud. After the addition of the base, temperature was maintained at 80°C another 30 min. Then 100 mL solution of 0.6 M sodium citrate was added and the temperature was increased to 95°C. Heating and stirring continued for 90 min. The black slurry was cooled down to the room temperature while stirring continued. The black mud was poured into a large beaker (1000mL) containing 400 mL of acetone. The particles precipitated almost instantaneously. The precipitation step was repeated twice. Particles were collected with a strong Nd magnet each time by binding them to the flask's wall surface. The exposure time to the magnetic field varied as a function of the dispersion concentration and volume. In order to

collect all particles the dispersion was separated into 200 mL beakers each containing ~100mL of magnetic solution. A volume of 100 mL and a concentration of~20 $mg \cdot mL^{-1}$ of ferrofluid required 3-5 minutes of magnet exposure for complete separation. Finally they were dispersed in water and had the consistency of a well-dispersed ferrofluid. In order to remove the excess base and citrate coating, iron particles were dialyzed over deionized, degassed water by using a 6-8 KDa cutoff membrane made from regenerated cellulose which had been previously boiled in deionized water for 15 min. The dialysis took place in a glove bag over a period of 3 days in an inert N_2 atmosphere to prevent particle oxidation. The dialysis water (deionized and degassed) was changed every 6 hours initially, and then over a longer period of time until the pH changed from 13 to 7. Finally the ferrofluid was washed twice with fresh deionized degassed water and stored as an aqueous solution (~150 mL) in an Erlenmeyer flask capped with a glass stopper insulated with parafilm.

Yield: 4.13 g ($c = 275\ mg \cdot mL^{-1}$).

8.8.2 Silica Coating of Magnetite Particles by Sol-Gel Method[1,2,11,16,18-20] (Chapter 3)

The protective silica coating of the magnetite particles was accomplished by using the well-known Stöber procedure with some modifications.[1,2,11,16,18-20] A 250 mL two-neck flask was charged with a mixture of 85 mL absolute ethanol and 22.7 mL deionized and degassed water. To this mixture 20mL of (1.14 g of solids) magnetite dispersion was added and the dispersion was sonicated for 30 min. Then the flask was connected to an overhead stirrer and 3 mL of ammonium hydroxide (28%) were added. The mixture was stirred vigorously for 15-20 min. and the pH was measured. The optimum pH value for silica coating is 9. In a separate vial 1 mL of TEOS was diluted with 5 mL of absolute ethanol. The alcoholic solution containing the silanization precursor was injected into the ferrofluid mixture drop by drop, over 30 min. while

the mixture was vigorously stirred. The reaction continued for 12 h. The particles were then washed 3× with absolute ethanol and then 3× with deionized water using a magnet for separation. Finally they were suspended in water.

Yield: 2.1 g (c = 15.7mg·mL^{-1}).

8.8.3 Silica Coating of Magnetite Particles by Reverse Emulsion[3]

This procedure used the magnetite particles described in the section 8.8.1.

Typically, 300 mL of cyclohexane, 24 mL Igepal CO-520 were mixed in a three-neck 500 mL flask connected to an overhead mechanical stirrer. Aqueous ammonia (28%), 7 mL, was added and the mixture was stirred vigorously (300 rpm) for 20 min. to allow the formation of the reverse emulsion droplets. An aliquot (~3mL) of original magnetic dispersion (suspended in water) was suspended in 10mL of cyclohexane by centrifugation-redispersion at least 5-6 times. After the concentration of the suspension was determined as described in the introductory notes, 2.4mL of dispersion containing 17 mg magnetic particles previously ultrasonicated were introduced into the emulsion batch, while stirring. The stirring, at the same rate, was kept for another 15 min. TEOS, 6 mL was finally added to the above mixture and the reaction continued overnight, under stirring and at room temperature. Methanol (50-60mL) was used to break the emulsion. The particles were washed by centrifugation-dispersion several times with methanol, a mixture of methanol/water and again methanol. They were finally stored as a suspension (~40 mL) in methanol.

Yield: 250mg (c = 6.25 mg·mL^{-1}).

8.8.4. Fluorescent Labeling of Silica-coated Magnetite Particles via Sol-Gel (Chapter 3)

Silica coated magnetite was suspended in a basic ethanol solution (S1) in a 200 mL two-neck round bottom flask connected to an overhead mechanical stirrer. The mixture was sonicated

with a probe sonicator for 5 min. to ensure a good dispersion of the particles. In a separate vial, an alcoholic solution of TEOS (S2) was prepared. This solution and the amount of the fluorescent complex were injected simultaneously in the flask. The reaction was carried out at room temperature, with stirring (200-300 rpm) for 12 h. The particles were washed 3× with absolute ethanol, 3× with deionized water and finally suspended in absolute ethanol. A magnet was used to separate particles by immobilization to the side wall of the flask. The amounts of the dye complex and alcoholic solutions are listed in the Table 8.4.

Table 8.2 Sample Code, Amounts of the Ferrofluid, Solutions S1 and S2, Amounts of the Dye Molecule and Yields for Preparation of the Fluorescent Magnetite Particles.

Sample Code	Ferrofluid/g	Solution 1 (S1) EtOH/water/mL	Solution 2 (S2) TEOS/EtOH/mL	Dye complex	Yield/g
Si-RhB-Si-Fe_3O_4	0.42	34/8.5	0.21/5	68.2 mg	0.50
Si-FITC-Si-Fe_3O_4	1.15	92/23	0.575/7	5 mL	1.75

8.8.5 Fluorescent Labeling of Silica-coated Magnetite Particles via Reverse Emulsion[3]

In order to obtain FITC covalently labeled silica coated magnetite particles, the batch described in the step 8.8.3 was used. Typically, after overnight stirring of the magnetic sol, 1.5 mL of the FITC/APS was added and the reaction was carried out for another 18 h under stirring at room temperature. Methanol was used to break the emulsion. The particles were washed several times with methanol, a mixture of methanol/water and again methanol using a magnet. They were finally stored as a suspension (~40 mL) in methanol.

Yield: 210 mg ($c = 5.25 mg \cdot mL^{-1}$).

8.8.6 Preparation of Silica-protected Fluorescent Ferrofluid via Sol-Gel (Chapter 3)

The silica coating performed at this step had the role to prevent dye bleaching and leaking. The procedure followed the same well-known Stöber procedure as described in the previous steps. The magnetic sol used was described in the section 8.8.4.

Fluorescein isothiocyanate tagged ferrofluid (1.34 g) was dispersed in 107 mL absolute ethanol and 27 mL deionized water inside a two-neck flask. The mixture was probe sonicated for 5 min. The flask was connected to an overhead mechanical stirrer and 3.5 mL aqueous ammonia (28%) were added to ensure the basic pH (9) for condensation. The suspension was stirred (150 rpm) for 15-20 min. In a separate vial, a solution consisting of 12 ml absolute ethanol and 567.5 μL TEOS was prepared. This solution was added drop by drop to the magnetite mixture using a buret. The reaction continued for 12 h. Then the particles were washed 3× with absolute ethanol, 3× with deionized water using a magnet and finally suspended in absolute ethanol.

Yield: 1.56 g (c = 11mg·mL^{-1}).

8.8.7 Functionalization of Fluorescent Silica-coated Magnetite Particle Surface with Bromine Groups.[3,21-24] (Chapter 3)

Silica-protected fluorescent magnetite particles (0.33 g) were suspended twice in dry toluene (~30mL) using a magnet. Then they were loaded as a dispersion (50mL toluene was used) in a three-neck flask immersed in an oil bath and connected to an in-line N_2 and an overhead stirrer. To test for water traces, 5 mL of toluene was collected by distillation using a Dean Stark adaptor and a condenser attached to a cooling bath. The stirring rate was 150 rpm. In a separate vial 151 μL of (3-bromopropyl)trichlorosilane was mixed with 1 mL toluene. This mixture was injected in the ferrofluid suspension dropwise under stirring and N_2 bubbling. The reaction continued for 18 h at 80°C and afterwards was cooled down to room temperature. Finally the particles were subjected 6× to centrifugation and redispersion in absolute ethanol and stored in the same solvent .

Yield: 0.39 g (c = 7.8 mg·mL^{-1}).

8.8.8 Functionalization of Fluorescent Silica-coated Magnetite Particle Surface with Azide Groups.[3,21-24] (Chapter 3)

An amount of 0.226 g of brominated ferrofluid was ultrasonicated in 100 mL dry DMF for 5 min. and quickly transferred to a three-neck flask connected to an in-line N_2 bubbler and an overhead mechanical stirrer. In a separate vial, tetrabutylammonium iodide (0.038 g, 0.001 mol) was added to 2 mL of dry DMF. This mixture and sodium azide (1.51 g, 0.023 mol) was subsequently introduced into the ferrofluid suspension under vigorous stirring (300 rpm). The mixture was heated at 80°C for 24 h and then cooled down to room temperature. The particles were washed three times with toluene and three times with DMF; each time, a magnet was used to separate the particles from the rinse.

Yield: 0.30 g ($c = 2.8\ mg \cdot mL^{-1}$).

8.9. Preparation of Magnetic Particles with a Cobalt Nugget[25]

8.9.1 Preparation of Silica-coated Cobalt Particles (Chapter 6)

In a four-neck flask capped with septa and fitted to a Branson probe ultrasonicator operating at 40% amplitude (sonicating horn 1/2″), 200 mL of freshly prepared 4×10^{-4}M $NaBH_4$ aqueous solution containing 4×10^{-4}M citric acid was added. Cobalt precursor, $CoCl_2$, 200 μL 0.4M in deionized degassed water was injected through the septum using a syringe with a long needle (gauge 18, 10 in. long). The nitrogen flow rate and the ultrasonication power were adjusted to prevent solution from frothing. The formation of the cobalt particles was manifested immediately after $CoCl_2$ addition by an intense grey coloration. Separately, a solution consisting of absolute ethanol, 800 mL, APS, 14.4 μL and TEOS, 169 μL (1/9 ratio APS/TEOS), was prepared (refer to this as solution C). After 1 min. of mixing $CoCl_2$ and $NaNH_4$ solutions, solution C was added rapidly to ensure silica protective coating of cobalt particles. The reaction continued 1 h under N_2 bubbling and ultrasonication. After 1 h the cobalt containing sol was left

to rest undisturbed overnight. Then particles were collected both *via* a magnet and by centrifugation. They were washed several times with absolute ethanol and finally suspended (~15mL) in the same solvent.

Yield: 65 mg (c = 4.3 $mg \cdot mL^{-1}$).

NOTE All aqueous solutions were degassed by bubbling dry N_2: the water used to prepare $CoCl_2$ (overnight) and citric acid solutions and these solutions after their preparation (30-45 min.).

8.9.2 Functionalization of Silica-coated Cobalt Particles with Amino Groups[26] (Chapter 6)

In a 500 mL two-neck flask connected to an overhead mechanical stirrer, the cobalt particles obtained in the previous step were suspended in 200 mL of absolute ethanol. A solution 25:75 of amino silane, AEAPTMS and passivator MTMS, 200 μL, was injected and the reaction continued 18 h under moderate stirring (150 rpm). The particles were collected by centrifugation and washed with absolute ethanol until no free amino groups were detected. This procedure is described in section 8.7. They were also washed twice with anhydrous THF and finally suspended in the same solvent.

NOTE At all steps involving ferrofluid suspension μ-metal was used to shield against the magnetic field from the hot/stirrer plate. The metal foils were inserted between the flask and the hot plate. Two of these foils were enough to completely screen the magnetic field.

8.10 Preparation of Polypeptides and Their Monomer Precursors (Chapters 3, 4, 5and 6)

8.10.1 Preparation of *γ*-Stearyl-L-glutamate, SLG

L-glutamic acid (16 g, 0.11M), *t*-butanol (170 mL) and γ-stearyl alcohol (117.6 g, 0.434 M) were fed into a three-neck flask immersed in an oil bath and connected to a condenser. An in-line N_2 bubbler was also attached to the flask. The temperature was raised to 40°C, under

magnetic stirring, and then 12 mL of sulfuric acid was added dropwise, using a dropping funnel. The mixture was further heated at 65°C for 45 min., by which time a clear solution formed. The oil bath was removed and 12 mL (0.084 M) of trimethylamine was added dropwise while stirring continued. A white precipitate formed. Afterwards the stirring was stopped. Ethanol (300 mL), deionized water (20 mL) and triethylamine (34 mL, 0.242 M) were added to give a thick white solid cake upon standing 30 min. The cake was allowed to rest overnight to complete precipitation. The solid was suction filtered and hot methanol (400 mL) and hot ethyl acetate (400 mL) were used to rinse the white solid sitting on the filter paper inside the funnel. Then the partially dried solid was transferred into a large beaker charged with 1000 mL mixture of 1:1 *n*-butanol and deionized water. The mixture was heated to 95°C, under magnetic stirring until it became clear (about 60 min.). After dissolution, the mixture was allowed to cool down to room temperature. White crystals began to form and a complete crystallization was obtained overnight. The crystalline white solid was recovered by filtration and was vacuum dried at ambient temperature for 12 h.

Yield: 27.15 g (63.14%).

8.10.2 Preparation of *γ*-Stearyl-L-glutamate N-carboxyanhydride, SLG-NCA.[27]

Dry *γ*-stearyl-L-glutamate (5.1 g, 0.0125 molar) and anhydrous THF were added to a three- neck round bottom flask equipped with a condenser attached to a cooling bath, a stirring bar, and connected to a nitrogen bubbler in-line to ensure the inert atmosphere and release the pressure formed during reaction. The flask was heated to 50°C using an oil bath, and triphosgene (1.26 g, 0.0042 molar) was added under stirring. After a clear solution formed over 1 h, the reaction continued for another hour. The mixture was concentrated to 1/3 of its volume and poured into twice its volume of cold, dry *n*-hexane. A white precipitate began to form and the

complete crystallization was obtained overnight upon refrigeration. In a glovebag filled with dry N_2, the crystals were filtered by suction filtration and washed with cold hexane. The white solid was redissolved in dichloromethane and shaken with sodium carbonate (a small amount) and filtered through a pad of Celite deposited on cotton. The filtrate was concentrated and cold hexane was poured slowly into it. The recrystallization was performed thrice. Finally the white solid was dried *in vacuo* and freshly used in the next step.

Yield: 3.97–4.24 g, 75-80%

8.10.3 Synthesis of N^{ε}-carbobenzyloxy-L-lysine N-carboxyanhydride, CBL – NCA and o-benzyl-L-tyrosine N-carboxyanhydride, oBTYR-NCA.[27,28]

The amounts of the chemicals involved in the preparation are listed in the Table 8.4.

Table 8.3 NCA Name and Ingredients Used in the Polypeptide Precursor Synthesis.

NCA Name	Solvent	NCA precursor, CBL/oBTYR			Triphosgene		
	Anh. EtOAc/ mL	Mass/ g	Molarity/ mmol	Mw/ $g \cdot mol^{-1}$	Mass/ g	Molarity/ mmol	Mw/ $g \cdot mol^{-1}$
CBL-NCA	150	5.021	18.0	280.32	1.8	6.0	296.75
o-BTYR-NCA	150	4.66	18.4	271.31	1.82	6.1	296.75

In a N_2-filled glove bag, anhydrous (Sigma) ethyl acetate, EtOAc, 150 mL was mixed with the amount of the NCA precursor in a flame-dried three-neck round-bottom flask. The flask was immersed in an oil bath and connected to dry N_2 (passed through Drierite with indicator). A condenser attached to a cooling bath was also connected to the flask and capped with a glass stopper. Under N_2 bubbling and magnetic stirring the slurry was brought to reflux. In a separate vial the desired amount of the triphosgene was weighed inside the hood in a glove bag filled with dry N_2. The content of the vial was quickly added to the refluxing mixture and the reaction continued until the solution became clear (4-5 h). In situation when after 90–120 min. the solution was still turbid, supplemental amounts (0.2 g) of solid triphosgene were fed into the

mixture. After the solution turned clear, the reflux was kept for another hour. The clear solution was allowed to cool down to room temperature while stirring and bubbling nitrogen continued. Overnight, the solution was kept in the freezer at -5°C. Removal of unreacted amino acid and HCl was performed by washing oily NCA in a separatory funnel with icy water (75 mL) and icy solution (0.5%) of $NaHCO_3$ (75 mL). Two layers formed each time and the upper was the organic phase of interest. Afterwards, the NCA was dried over anhydrous $MgSO_4$ until the drying powder didn't show clumping. The clear solution of NCA was then suction filtered through Whatman 90 mm filter paper. The drying steps and the filtration were performed in a glove bag. The volume of the mixture was reduced to 1/3 by evaporation inside the glove bag placed in the hood. Finally dry cold dry (Aldrich) hexane (100 mL) was poured slowly in the NCA solution. White crystals of NCA started to form. The crystallization took place overnight in the freezer at -5°C. The recrystallization was repeated twice in a glove bag filled with dry nitrogen as follows: NCA was dissolved in a minimum amount (15-20 mL) of dry THF and then cold dry hexane was poured slowly and the flask gently swirled until white crystals began to form. The flask was capped with septum and placed inside the freezer overnight for a complete crystallization.

Yield: CBL-NCA- 4.43g, 86%; oBTYR-NCA-4.18g, 82%.

NOTE 1. The dissolution of the NCA in THF during recrystallization steps might require warming the mixture. The flask containing NCA solution should be attached to a bubbler to release the pressure caused by the THF vapors. Preheated water (T~ 30-35°C) can be used to warm the mixture with continuous swirling.

2. Triphosgene is a toxic chemical. Therefore, the reaction is conducted in a well-ventilated hood and the HCl/phosgene gas formed during reaction should be passed through an

ammonia hydroxide solution for neutralization purposes. This is realized by connecting the bubbler to a flask containing aqueous ammonia. The triphosgene should be weighed inside the hood.

8.10.4 Preparation of Alkyne-terminated Poly(*γ*-stearyl-L-glutamate), PSLG, and Alkyne-terminated Poly(N^{ε}-carbobenzyloxy-L-lysine), PCBL for Click Chemistry (Chapter 3)

The alkyne-terminated polypeptides were prepared by ring-opening polymerization of the N-carboxyanhydrides of γ-stearyl-L-glutamate and N^{ε}-carbobenzyloxy-L-lysine respectively. The reagents used are listed in Table 8.5.

Table 8.4 Reaction Conditions Used in the Synthesis of Polypeptides.

Polypeptide	Solvent DCM/mL	Monomer Concentration/%	[M]/[I]	SLG-NCA		Propargyl amine	
				Mass/g	Mol	Mass/g	Mol
PSLG-Alkyne	50	2	100	1.0	0.002	0.001	0.0004
PCBL-Alkyne	50	2.4	100	1.2	0.004	0.002	0.002

The amount of the NCA was weighed inside a glove bag into a 50 mL round-bottom flask. To this, the solvent, anhydrous (Aldrich) dichloromethane, DCM, was added and the flask was capped with a rubber septum. The mixture was swirled until the NCA completely dissolved. Then the initiator, propargyl amine was dissolved in 1 mL of the solvent inside the glove bag and was injected into the NCA solution using a syringe. The flask was immersed in a water bath set at 30°C and connected to an in-line nitrogen bubbler to release pressure formed during reaction. The polymerization of NCA was allowed to continue for 72 h until no gas bubbling was noticed. Purification of the alkyne-polypeptides was performed as follows: the alkyne-PSLG mixture was concentrated to a thick solution by bubbling dry nitrogen and precipitated in acetone (~75 mL).

The so-obtained polypeptide was suction filtered through Whatman filter paper 55 mm circles, washed with acetone (~50 mL) on the filter paper and dried *in vacuo* overnight.

Yield: 0.82 g

The alkyne-PCBL mixture was concentrated in the same manner as afore described alkyne-PSLG, precipitated in water (75 mL) and then suction filtered through the same filter paper type. Then the solid was redissolved in 20 mL of DMF and precipitated again in water (75 mL). The purified polypeptide was suction filtered dried *in vacuo* overnight.

The presence of the alkyne end-group was confirmed using FTIR and MALDI-TOF mass spectrometry (Chapter 3).

Yield: 1 g

8.11 Preparation of Polypeptide Composite Particles Without a Magnetic Core

8.11.1 Preparation of Poly(Nε-carbobenzyloxy-L-lysine) Composite Fluorescent Silica Particles (Chapter 4and 5)

In a flame-dried round-bottom flask the designated volume of anhydrous (Aldrich) THF was loaded. To this amount of solvent CBL-NCA was added (see Table 8.7). The flask was capped with a rubber septum and stirred until the CBL-NCA completely dissolved to a clear solution. To this mixture amino functionalized particles were added under the inert atmosphere ensured by the glove bag. The flask, immersed in a water bath set to 35°C, was rapidly connected to a bubbler to release the CO_2 formed during the reaction. After three days the production of the gas stopped an indication for reaction completion. The particles were subjected to centrifugation and dispersion five-six times with THF and finally suspended also in THF. They were stored in dark vials. The batches of the PCP PCBL particles prepared after this recipe are listed in Table 8.7.

Table 8.5 PCBL PCP Particles by the *Growing From* Method and the Chapter Number of the Dissertation Where They Have Been Used

Amino-silica			PCP		Chapter/ Section
5Abbreviation	Mass/mg	Solvent/mL	Abbreviation	Yield/mg	
SFA1(CR7157)	400	50	PCP PCBL(175)H*(CR7160)	600	Ch5, Ch4
SFA2(CR7184A)	600	50	PCP PCBL(175)L(CR7188)	800	Ch5, Ch4
SFA4(CR84A)	180	50	PCP PCBL(55)L(CR810A)	250	Ch5
SFA3(CR83A)	255	50	PCP PCBL(100)H(CR810B)	320	Ch5

*The number represents the core radius and H, L high and low loading with amino groups.

8.11.2 Synthesis of Poly(o-benzyl-L-tyrosine) Composite Silica Particles, PBTY (Chapter 6)

Anhydrous (Aldrich) tetrahydrofuran, THF, was loaded into a flamed dried 150 mL round-bottom flask. Polypeptide precursor, *o*-benzyl-L-tyrosine N-carboxyanhydride, *o*BTYR-NCA, was added and the flask capped with a septum. The mixture was swirled until it became clear. Then, amine-functionalized silica particles were added along with a stir bar. These reactions were performed in a glove bag under inert atmosphere of nitrogen. The flask was connected to a bubbler to release the CO_2 formed during reaction. The reaction continued for 72 h at 35°C. After the gas release stopped the particles were washed 6× with THF by centrifugation/dispersion and finally stored in anhydrous THF. The amounts of the reagents used in all PBTY PCPs syntheses are listed in Table 8.8.

Table 8.6 Hybrid Particle, Solvent, Amine-core Amount, NCA, Yield and the Chapter PCP Particles Have Been Used.

Hybrid	Solvent/mL	Amine-core Amount/g	NCA/g	Yield/g	Chapter
PBTY PCP230*L (CR7161)	50	0.175	2.5	0.2	4,6
PBTY PCP230 (CR836)	50	0.196	2	0.3	6

Table 8.6 continued

Hybrid	Solvent/mL	Amine-core Amount/g	NCA/g	Yield/g	Chapter
PBTY PCP620 (CR10.180)	50	0.47	1.6	0.5	6

*The numbers represent the core diameter

8.12 Preparation of Polypeptide Composite Particles with a Magnetic Nugget

8.12.1 Surface Grafting of Alkyne End-terminated PSLG and Alkyne End-terminated PCBL on Azido-fluorescent Silica-coated Magnetite Particles through Huisgen's 1,3-Dipolar Addition (Chapter 3)

The reagent amounts used in synthesis are listed in Table 8.9.

Table 8.7 Synthesized Hybrid Name, Amounts of Azido-functionalized Ferrofluid, Polypeptide, CuBr, PMDETA and Solvent and the Yield of Particles Obtained from Click Reaction.

Hybrid	Azide-ferrofluid/g	Polypeptide/g	CuBr/g	PMDETA/mL	Solvent/mL	Yield/g
PSLG-click	0.230	0.6	0.091	0.26	30	0.25
PCBL-click	0.155	0.3	0.091	0.26	30	0.172

Azido-magnetic silica was dispersed in 10 mL of dry solvent (anhydrous (Aldrich) toluene for PSLG-click) and (anhydrous (Aldrich) tetrahydrofuran, THF for PCBL-click) inside a three-neck flask which was connected to a nitrogen line, a water condenser and an overhead mechanical stirrer. This suspension was degassed for 10- 15 min. In a separate vial the alkyne-polypeptide was dissolved in 10 mL of the reaction solvent (toluene/THF) and was degassed for 10 min. In another vial CuBr was weighed and dissolved in 10 mL of the solvent (toluene/THF). The vial was capped with a rubber septum and the mixture was stirred and degassed for 10 min. To the CuBr mixture, PMDETA was added using a syringe. These degassed solutions of alkyne polypeptide and CuBr were injected sequentially into the three-neck flask containing the azido-functionalized ferrofluid. The flask was immersed in an oil bath and heated to 60°C for 1 h and

then to 40°C for 24 h. The reaction mixture was cooled down to the ambient temperature and the particles were separated by a magnet. Washings with the solvent used during click reaction were performed 3× to remove unreacted polypeptide. Afterwards the hybrid particles were dispersed in chloroform and extracted with water, a sodium salt solution of EDTA , and again with water to remove the copper. After copper removal the click colloid was washed 3× with chloroform (PSLG-click) or THF (PCBL-click). The coupling reaction for PCBL-click was also repeated using anhydrous (J.T. Baker) dimethylformamide, DMF.

8.12.2 Preparation of Poly(o-benzyl-L-tyrosine) Composite Silica Particles with Cobalt Inclusions (Chapter 6)

In a glovebag under nitrogen atmosphere BTYR-NCA (1 g) was added to anhydrous THF (30 mL) in a 50 mL flame-dried flask equipped with a stirring bar and capped with rubber septum. To this mixture, an aliquot of amino-functionalized particles (13.5mL, c=0.5 mg/mL) dispersed in anhydrous THF was injected into NCA solution. The flask was connected through tubing to a graduated cylinder placed upside-down in a beaker and filled with oil. This setting was used to monitor the release the CO_2 during reaction. The reaction was performed over 3 days (no gas release noticed). The particles were collected by centrifugation. Several washings (4x) using centrifugation-dispersion method with THF were necessary to remove unreacted monomer. The obtained particles were stored as a dispersion (~8mL) in dry THF.

Yield: 7 mg (c = 0.8 mg·mL^{-1}).

8.13 Deprotection of the Side Chains[29,30]

The amounts of the chemicals used in synthesis are listed in the Table 8.10. An amount of polypeptide-coated silica particles was placed in a Teflon tube and the storage solvent (anhydrous THF) reduced until the mixture became a slurry. Then a volume of HBr/CH_3COOH (33%) (Aldrich) was added inside the hood. The tube was quickly capped and the mixture stirred

magnetically for 45 min. The light brown mixture was washed with toluene, acetone, neutralized with 3.5 mM NaOH, washed with water twice. Finally particles were dispersed in water. The amounts of the chemicals used in synthesis are listed in the Table 8.10.

Table 8.8 Reaction Conditions for Deprotection of Benzyl-protected Poly(L-tyrosine)-coated Composite Particles

Sample	Amount of the Particles/g	Volume of HBr/CH_3COOH/mL	Yield of deprotected particles/g**	Chapter
PLYS175*H (CR7160)	0.2	2	0.14	5,6
PTYR230L (CR7161)	0.21	5	0.15	5
PTYR230 (CR856)	0.19	6	0.18	7
PTYRmag (CR10.190B)	0.025	0.5	0.017	7
PTYR620 (CR10.190A)	0.2	3	0.185	7

*the number 175 is the core radius and 230 and 620 represent the diameter of the core. The abbreviation "mag" means magnetic PCPs with cobalt intrusions.
**Based upon aliquot analysis

8.14 Aging with 3 mM NaOH Solution (Chapter 4)

Particles subjected to aging (~50 mg) were concentrated to a slurry by removal of almost all storage solvent, using centrifugation. The 3 mM NaOH solution (3 mL) was poured over the thick suspension of particles. The aging took place in a glass vial under gentle stirring for 36 h. Particles were washed several times (six) with deionized water by centrifugation-dispersion and stored in water.

Yield: 40 – 45 mg

8.15 Particle Haircut with 10% NaOH (Chapter 7)

An amount of the PCBL-coated silica particles (40 mg; Section 8.11.1) was mixed with 2 mL of 10% NaOH aqueous solution. The mixture was stirred for 2 h. After aging, a white layer formed containing the polymer from the shell, which was separated by centrifugation (7,000

rpm). The white solid was washed 3× with water and collected each time by centrifugation. Finally the white solid was dried *in vacuo* at 40°C overnight.

Yield: 12 mg

8.16 Immobilization of Lipase from *Candida Rugosa* by Adsorption onto the PSLG-click Composite Particles[31,32] (Chapter 3)

PSLG click-particles (44 mg) were dispersed in absolute ethanol several times using a magnet. Particles were kept in 5 mL of the same solvent for 1 h. They were further washed with deionized water and a phosphate buffer solution (0.05M, pH=7.0). Separately a solution of lipase (2 mg•mL^{-1}) was prepared in phosphate buffer. The particles were suspended in 5 mL of lipase solution and kept overnight at 30°C and under gentle stirring. Finally the particles were washed copiously with the buffer solution to remove the free lipase and were stored in the buffer (~5mL) for further investigations.

Yield: 35 mg (c = 7.5 mg·mL^{-1}).

8.17 Enzymatic *Horseradish peroxidase*-catalyzed Cross-linking of PTYR PCPs (Chapter 6)

In a scintillation vial 2.5 ml of PTYR PCPs (c = 10 mg•mL^{-1}, Section 8.13, (CR856)) were suspended in phosphate buffer (pH=7). The enzyme catalyst, *Horseradish peroxidase* was first dissolved in the phosphate buffer (0.5 mL) and then added to the vial containing PCPs. The mixture components were mixed by vortex for 1 min. Hydrogen peroxide (5.0% aqueous solution, 2 mL) was added dropwise to the mixture at room temperature under air and gentle magnetic stirring. The reaction was complete after a total of 3h. Then the cross-linked material was washed by dispersion-sedimentation-decantation 3× with the phosphate buffer.

Yield: 20 mg, (c = 4 mg·mL^{-1}).

8.18 Photo-cross-linking of PTRY PCPs Using Photo-induced Cross-linking of Unmodified Peptides, PICUP (Chapter 6)

PICUP cross-linking reactions were carried out in a buffer comprised of 15 mM sodium phosphate (pH=7.5) and150mM NaCl. The ruthenium catalyst, $Ru(bpy)_3Cl_2$ was dissolved in the above described buffer in as a 3.125mM (2mL) solution and stored in a vial wrapped with aluminum foil until use. A stock solution (5mL, 62.5mM) of ammonium persulfate, was prepared in the same buffer. The PCPs solution was placed in either 1 mL Eppendorf tubes or disposable squared cuvettes modified as shown in Chapter 6. Some of these cuvettes were patterned on their bottom to allow the production of an architectural polycolloid. Some had drawn lines with a flamed syringe needle, other had circles and the rest covered with a black permanent marker. In the case of the magnetic PCPs a Ronchi ruling was positioned underneath the cuvette. The irradiation of the reaction mixtures used a light emitting diode of 470 nm wavelength, situated at a distance between 2 and4 cm from the sample. The exposure time varied between 5 and 10 minutes. The nonmagnetic PCPs were allowed first to sediment in a thin layer on the cuvette bottom. The magnetic PCPs were aligned using an external magnetic field provide by a permanent magnet. After the particles were settled on the bottom or aligned the catalyst was added in the dark using a simple cardboard box with a front-cut window. After 1 min. the ammonium persulfate was added and the visible light source was turned on. After reaction completion particles were gently suspended in the fresh buffer and kept for further analysis. All the settings are available in Chapter 6 as pictures. Table 8.11summarizes the amounts of the reagents and parameters used for PICUP reactions. The yield is assumed 100%.

Table 8.9 Reaction Conditions for Polycolloid Preparation by PICUP Method

Sample	Amount PCPs/mg	Solvent/mL	Catalyst/μL	APS/μL	Shape	Setting	Exposure Time/min.
Picup-1	40	0.5	30	60	random	Eppendorf	5
Picup-2	60	0.75	20	40	maple leaf	three-wall cuvette	7
Picup-3	60	0.75	20	40	crystal-like	three-wall cuvette	10
Picup-4	80	1.2	30	60	macrocycle	three-wall cuvette	15
Picup-5	10	0.5	20	40	chains	three-wall cuvette	25

*Picup-1 (CR11.1A), Picup-2 (CR11.2A), Picup-3 (CR11.2B), Picup-4 (CR11.2C) and Picup-5(CR11.2D)

Table 8.10 Supplemental Batches of Amino-Silica Prepared as Described in Section 8.7 and Not Used in This Work (Available Upon Request)

Silica		Amino-silica		
Abbreviation	Mass used/mg	Abbreviation	Initiator used	Yield/mg
S1 (CR7124)	1200	SA1(CR7130A)	APS ($4NH_2/100Å^2$)	900
S1(CR7124)	1200	SA2(CR7130B)	APS:MTMS (25:75)	800
S2(CR10169)	3200	SA3(CR10178)	APS ($2NH_2/100Å^2$)	2500
SF1(CR797A)	770	SFA1(CR7158)	APS:MTMS (25:75)	500
SF1(CR797A)	900	SFA2(CR7184B)	APS:MTMS (25:75)	600
SF2(CR7101B)	1000	SFA3(CR7163A)	AUDTES	720
SF2(CR7101B)	1000	SFA4(CR7162)	APS	740
SF2(CR7101B)	1000	SFA5(CR7163B)	AEAPTMS	720
SF2(CR7101B)	1000	SFA6(CR7167)	APS:MTMS (25:75)	700
SF2(CR7101B)	1000	SFA7(CR7168A)	AUDTES:MTMS (25:75)	720
SF2(CR7101B)	1000	SFA8(CR7168B)	AEAPTMS:MTMS (25:75)	700

Table 8.10 continued

Silica		Amino-silica		
Abbreviation	Mass used/mg	Abbreviation	Initiator used	Yield/mg
SF4(CR7153B)	300	SFA10(CR814)	APS:MTMS (25:75)	260
MSCo1(CR760B)	50	MSACo1(CR7185A)	AEAPTMS	40
MSCo2(CR713B)	60	MSACo2(CR7185B)	AEAPTMS:MTMS (25:75)	45
MSCo3(CR7120)	50	MSACo3(CR815)	AEAPTMS:MTMS (25:75)	45

Table 8.11 Supplemental batches of PCPs by Growing From synthesized but Not Used in This Work

Amino-silica		PCP		
Abbreviation	Mass used/mg	Abbreviation	Yield	Mass Loss TGA/%
SFA1(CR7158)	92	PCP PCBL(CR7164)	60	5
SFA2(CR7162)	600	PCP PCBL(CR7166A)	400	4
SFA10(CR814)	195	PCP PCBL(CR821)	220	4
MASCo1(CR7185A)	30	PCP PBTY(CR7187)	40	35
MASCo2(CR815)	30	PCP PBTY(CR7187)	45	43

Abbreviations: Sx- nonfluorescent silica; SFx:-fluorescent silica; SAy-nonfluorescent amino-silica; SFAy-fluorescent amino-silica; MSCo-magnetic silica-coated cobalt; MSACo-magnetic amino-silica-coated cobalt

Characterization Techniques

8.19 Dynamic Light Scattering, DLS

A custom-built, multi-angle apparatus using an ALV-5000/E digital autocorrelator and a 632.8 nm laser source was used to measure the size of the composite particles at each step during their preparation. Silica magnetic/nonmagnetic cores were dispersed in anhydrous ethanol

filtered through a 0.02μm Whatman filter with a guard 0.1 μm PTFE filter. Benzyl-protected polytyrosine silica hybrids were dispersed in dry THF. After deprotection the colloid was dispersed in pure water. Solvents such as ethanol and THF were filtered through 0.1 μm Whatman PTFE filter and water through 0.1 μm Millipore filter. Measurements were achieved at multiple scattering angles from θ= 30º to 90º. The size evaluation was made as follow: first the apparent diffusion coefficient was computed from $D_{app}= \Gamma/q^2$, where Γ represents the decay rate of the electric field autocorrelation function $g^{(1)}(\tau)$ and q is the scattering vector magnitude, expressed as $q= 4\pi n\sin(\theta/2)/\lambda_o$, n being the solvent refractive index, θ the scattering angle and λ_o the wavelength in vacuo. Stokes- Einstein equation, $D = kT/(6\pi\eta_o R_h)$, was used then to calculate the hydrodynamic radius, R_h. In this equation D represents the extrapolation of D_{app} to $q = 0$, k is the Boltzmann's constant, T is the absolute temperature at which the experiments were carried out and η_o is the solvent viscosity. The hydrodynamic radius is the actual radius when particles diffuse independently. In order to evaluate the particle uniformity, the dimensionless ratio of the second cumulant to the square of the first (polydispersity index), μ_2/Γ^2 is analyzed. Another qualitative indicator of dispersity is the q-independence of D_{app}: at higher angles the scattering contribution from larger particles diminishes rendering smaller particles relatively more visible.

8.20 Transmission Electron Microscopy, TEM

Transmission electron microscopy images of magnetic particles at different stages were obtained using a high resolution STEM (JEOL-2010 CX operating at 200KVand a JEOL 100-CX with an accelerating voltage of 80KV electron microscopes were used for nonmagnetic particles. A dilute sample solution was prepared by dispersion of 20μL of particles in 1mL of appropriate solvent (water, ethanol, THF of dimethylformamide, DMF). The sol was sonicated 1-2 min. to ensure a good dispersion of particles in the solution. From this solution a drop was

placed on top of a 400 mesh carbon-coated grid (Electron Microscopy Sciences) and dried either in the air, overnight or 2-3 hours in the vacuum. Particles having a polypeptide corona were placed on the bottom of a Petri dish and further exposed to only OsO_4 vapors for 15- 20 min. The small silica particles obtained by reverse emulsion polymerization were stained with uranyl acetate to obtain a better contrast. Particle size visualized in the transmission electron microscope was analyzed using NIH Image J processor.

8.21 Scanning Electron Microscopy, SEM

Scanning electron microscopy, SEM, has been used to visualize the polycolloid material and some of the PCPs and their cores. The images were recorded with a JSM-6610 apparatus. The instrument has a rotating stage which can take 7 samples. The resolution depth is 3 nm. Samples were prepared as follow: the stubs were first cleaned with ethanol to remove potential impurities. The stubs used had 12.7 mm diameter. Each stub is mounted on a pin which had 8 mm height and a diameter of 3.2 mm (1/8"). Carbon conductive double adhesive coated sheet was placed on top of the stub by thumb pressing. Small pieces of mica sheets from Tedpella, Inc. were glued on the sticky conductive sheet. The specimen was grounded to the stub on the mica as drops with a digital pipette and allow to air dry 2-3 days or overnight in the vacuum at ambient temperature. Before visualization the non-conductive samples were sputter coated with a layer of Pt for 4 min. (1 min= 15 nm Pt deposition).

8.22 Fourier-Transform Infrared Spectroscopy, FTIR

Fourier transform infrared spectroscopy, FTIR, was used to confirm the characteristic adsorption bands. Spectra were obtained with a Bruker Tensor 27 FT-IR instrument having a Pike Miracle single-bounce attenuated total reflectance (ATR) cell and a ZnSe single crystal. The powder samples were directly deposited on the crystal. Composite particles were analyzed in

solution using the special cell attachment for liquid samples. The solvent was scanned first for background subtraction.

8.23 Confocal Light Microscopy, CLM

A Leica TCS SP2 confocal microscope, CLM, operating in reflection mode investigated the surface details of the morphologies. A YOKOGAWA, CSU22(2) confocal unit equipped with home built microscopic optics coupled to the rheometer instrument further described in the section was used to visualize the behavior of the fluorescent particles at Institute of Liquid Crystals, Kent State University, Kent, OH.

8.24 Optical/Polarized Light Microscopy, OM/POM

Optical images of particles suspended in liquid crystal solutions were recorded with an Olympus polarized light optical microscope, model BH2, equipped with an Amscope color CCD camera.

8.25 Nuclear Magnetic Resonance Spectroscopy, NMR

Proton spin-lattice relaxation times (T_1) were measured at a field of 9.39T on a Bruker DPX-400 NMR spectrometer over the temperature range 20° to 38° C, at intervals of 2° C. The temperature interval was reduced to 1° C over the range 38° C to 45° C. The sample was allowed to equilibrate at least 5 minutes, at each temperature, in order to minimize temperature gradients over the volume of the NMR sample. Using a spectral window of 12 ppm, 32,000 data points were collected. Data was zero-filled once prior to Fourier transformation. Data processing and T_1 calculation were conducted using Bruker's Topspin software, version 1.3.

8.26 Matrix Assisted Laser Desorption/Ionization Time of Flight Mass Spectroscopy, MALDI-TOF

A Bruker PROFLEX III MALDI-TOF mass spectrometer was used to obtain the matrix-assisted laser desorption/ionization time of flight spectra of alkyne-PSLG and PCBL. The matrix used was dithranol and the solvents were chloroform and acetone, respectively.

8.27 Electrospray Ionization, ESI

ESI spectra were obtained with an Agilent Technologies, 6210 Time-of-flight LC/MS device under nitrogen flow. The electric field used for fragmentation was set at 215V. The samples were dissolved in chloroform and subjected to 12 scans each ranging between 0.195-0.375 minutes.

8.28 Differential Scanning Calorimetry/Modulated Differential Scanning Calorimetry, DSC/MDSC

DSC and MDSC were carried out using a 2920 MDSC V2 6A instrument from TA Instruments at a scan rate of 2 and 5 °C·min^{-1} under nitrogen, for both heating and cooling. Samples, 40 μL solution in m-cresol, were placed in the DSC liquid cells. The sample weight was in the range of mg. The reference consisted of a pan filled with m-cresol identical to that used to hold the samples.

8.29 Thermogravimetric Analysis, TGA

Thermogravimetric analysis, TGA, of samples was obtained with a TGA Q50 apparatus from TA Instruments under nitrogen flow and a heating rate of 10°C min^{-1}. Several experiments were conducted under air atmosphere at the same heating rate for the magnetite containing colloids.

8.30 Gel Permeation Chromatography/Multiangle Light Scattering, GPC/MALS

The molecular weight of the alkyne-PSLG was measured by gel permeation chromatography with multiangle light scattering, GPC-MALS. An instrument equipped with an Agilent 1100 solvent degasser, Agilent 1100 pump and Agilent 1100 autosampler was used for separation. The instrument had a 10 μm, 50 x 7.8 mm guard column and two Phenogel 300 x 7.8 mm columns from Phenomenex, Torrance, CA: (1) 10 μm, 10^5 Å (10K-1000K) and (2) 10 μm, MXM, (100-10000K). The detection was assured by a Wyatt Dawn DSP-F multiangle light scattering detector, with a He-Ne laser and a Hitachi L-7490 differential index detector (32 x 10^5 RIUFS). An injection volume of 100 μL was used for separation. The mobile carrier was THF (1 mL min^{-1}) stabilized with 250 ppm BHT for PSLG and DMF + 0.1 N LiBr for PCBL. The refractive index of PSLG was taken as 0.080 ± 0.002 mL·g^{-1}.[33] The refractive index of PCBL was taken as 0.123 mL·g^{-1}.[34]

8.31 Asymmetric Flow Field Flow Fractionation, AF4

Size measurements as well fractionation of stratified silica colloid were performed with an AF4 instrument, Eclipse 2 Separation System from Wyatt Technology Corporation, Santa Barbara, CA. The apparatus was equipped with a pump connected to an in-line vacuum degasser and an autosampler (1100 series, Agilent Technologies, Palo Alto, CA). This setting was used to deliver the mobile phase, deionized water with 200 ppm sodium azide, upon injection onto AF4 channel. A Mylar spacer of 490 μm thickness and a trapezoidal shape with a tip-to-tip length of 24 cm, an inlet width of 2.15 cm and an outlet width of 0.6 cm respectively, formed the assembly of the flow channel. The accumulation wall consisted of regenerated cellulose membrane (Wyatt) with a cutoff of 10 KDa. The instrument had connected an Optilab rEX differential

refractive index (DRI) detector and a Heleos multi angle light scattering, MALS, detector. The scattering measurements used a GaAs 50mW laser source with a wavelength λ_0 = 658 nm.

8.32 X-ray Photoelectron Spectroscopy, XPS

The surface composition of the particles at all stages was investigated with a Kratos Analytical Axis 165 X-ray photoelectron spectrometer (XPS) with Al Kα-radiation with an energy of 1.48 KeV and a takeoff angle of 90°. For each sample, a high resolution spectrum and a survey spectrum of individual elements were recorded with pass energies of 40 and 80 eV, respectively. The peak locations were calibrated based on a C1s signal at 284 eV. Samples were dried in vacuo to a powder state. They were deposited on the copper conductive tape attached to the instrument sample holder.

8.32 X-ray Powder Diffraction, XRD

X-ray powder diffraction (XRD) analysis was performed at Center for Advanced Materials and Devices, CAMD, in a custom built instrument, using CoKα radiation (λ = 1.7902 Å). The apparatus is equipped with a double crystal monochromator with silica (111) and germanium (220) crystals, a huber four-cycle goniometer capable of step size as low as 0.0001°, and a Canberra high purity germanium solid state detector. The sample holders consisted of quartz cut 6° from 0001 with 50 μm sample depth. The data were analyzed with MDI's Jade software. The samples were dried in vacuo overnight and grinded to fine powders.

8.33 Small Angle X-ray Scattering, SAXS

SAXS measurements were performed at Stanford Linear Accelerator Center, SLAC, Stanford, California in the Stanford Synchrotron Radiation, Laboratory, SSRL, at the station bL1-4. Data collected were normalized by counts:

$$Counts = I_0 \times T \times t \qquad Eq.8.11$$

where I_0 is the incident intensity, T is the transmission and t the rum time. The beam at SSRL is stable within a few percent, therefore the term $\boldsymbol{I_0}$ from equation 1 may be skipped and the counts expression simplified to:

$$Counts = I_{pre} \times T \times t \qquad Eq.8.2$$

The correction for transmission is expressed by:

$$T = \frac{I_{pst} \times I_{pre(0)}}{I_{pre} \times I_{post(0)}} \qquad Eq.8.3$$

where I_{pre} is the pre-sample ion chamber reading, I_{pst} is the post-sample ion chamber reading, $I_{\text{pre(0)}}$ is the pre-sample ion chamber reading in air, no sample and $I_{\text{pst(0)}}$ is the post-sample ion chamber reading in air, no sample.

The final expression used to normalize by counts is:

$$Counts = \frac{I_{pst} \times I_{pre(0)}}{I_{pst(0)}} \times t \qquad Eq.8.4$$

The parameters involved in transmission correction were collected first with the ion chamber in place. Run time for pre- and post air with no sample readings was 300s. Then the heating stage from Mettler was positioned inside the sample chamber and the reading in air was repeated. Then the sample (a solution in a glass capillary from Charles Supper Company, D = 1.0 mm, wall thickness = 0.01 mm and length = ~80 mm) was fixed onto the hot stage and the readings pre- and post- with sample in place were recorded. After beam horizontal and vertical alignment of the capillary in the beam the ion chamber was removed and controlled temperature dependant runs were performed by using the Mettler hot stage. It has to be mentioned that the centering of the sample was facilitated by a camera which records the position of the capillary in the beam. The run time was 700s with an equilibration between runs of 5 minutes. The same procedure was followed for the solvent, m-cresol, itself with a run time of 1000s. The data were corrected as

described above. The solvent scattering was subtracted from the sample and the scattering difference was plotted against scattering vector magnitude, *q*, in a semilogaritmic representation. Conversion of the corrected intensity to natural logarithm and plotting agains *q* gave the Guinier representation of the acquired data.

8.34 Rheology

The rheological behavior was studied using a HAAKE MARS instrument with parallel plates belonging Prof. Chanjoong Kim from Institute of Liquid Crystals, Kent University, Kent, OH.

8.35 Superconducting Quantum Interference Device, SQUID

Magnetic measurements were performed on a SQUID magnetometer (Quantum Design MPM S XL-7) belonging to Prof. Carlos Rinaldi from University of Puerto Rico Mayaguez.

8.36 References and Notes

(1) Bogush, G. H.; Tracy, M. A.; Zukoski, C. F. Preparation of Monodisperse Silica Particles - Control of Size and Mass Fraction. *Journal of Non-Crystalline Solids* **1988**, *104*, 95-106.

(2) Stober, W.; Fink, A.; Bohn, E. Controlled Growth of Monodisperse Silica Spheres in the Micron Size Range. *Journal of Colloid and Interface Science* **1968**, *26*, 62-69.

(3) Zhao, L.; Zhao, Y. F.; Han, Y. Pore Fabrication in Various Silica-Based Nanoparticles by Controlled Etching. *Langmuir* **2010**, *26*, 11784-11789.

(4) Lee, M. H.; Beyer, F. L.; Furst, E. M. Synthesis of monodisperse fluorescent core-shell silica particles using a modified Stober method for imaging individual particles in dense colloidal suspensions. *Journal of Colloid and Interface Science* **2005**, *288*, 114-123.

(5) Lu, Z. Y.; Xu, J. Q.; Han, Y. D.; Song, Z. Q.; Li, J.; Yang, W. S. Robust fluorescein-doped silica nanoparticles via dense-liquid treatment. *Colloids and Surfaces a-Physicochemical and Engineering Aspects* **2007**, *303*, 207-210.

(6) Nakamura, M.; Shono, M.; Ishimura, K. Synthesis, characterization, and biological applications of multifluorescent silica nanoparticles. *Anal. Chem.* **2007**, *79*, 6507-6514.

(7) Gao, X.; He, J.; Deng, L.; Cao, H. Synthesis and characterization of functionalized rhodamine B-doped silica nanoparticles. *Optical Materials* **2009**, *31*, 1715-1719.

(8) Ma, D.; Guan, J.; DÃ©nommÃ©e, S. P.; Enright, G.; Veres, T.; Simard, B. Multifunctional Nano-Architecture for Biomedical Applications. *Chem. Mat.* **2006**, *18*, 1920-1927.

(9) Nedelcev, T.; Racko, D.; Krupa, I. Preparation and characterization of a new derivative of rhodamine B with an alkoxysilane moiety. *Dyes and Pigments* **2008**, *76*, 550-556.

(10) Ren, C. L.; Li, J. H.; Chen, X. G.; Hu, Z. D.; Xue, D. S. Preparation and properties of a new multifunctional material composed of superparamagnetic core and rhodamine B doped silica shell. *Nanotechnology* **2007**, *18*, 6.

(11) Zhang, J. H.; Zhan, P.; Wang, Z. L.; Zhang, W. Y.; Ming, N. B. Preparation of monodisperse silica particles with controllable size and shape. *J. Mater. Res.* **2003**, *18*, 649-653.

(12) Fong, B.; Russo, P. S. Organophilic colloidal particles with a synthetic polypeptide coating. *Langmuir* **1999**, *15*, 4421-4426.

(13) Soto-Cantu, E.; Cueto, R.; Koch, J.; Russo, P. S. Synthesis and Rapid Characterization of Amine-Functionalized Silica. *Langmuir* **2012**, *28*, 5562-5569.

(14) Soto-Cantu, E.; Turksen-Selcuk, S.; Qiu, J. H.; Zhou, Z.; Russo, P. S.; Henk, M. C. Silica-Polypeptide Composite Particles: Controlling Shell Growth. *Langmuir* **2011**, *26*, 15604-15613.

(15) Massart, R. Preparation of Aqueous Magnetic Liquids in Alkaline and Acidic Media. *Ieee Transactions on Magnetics* **1981**, *17*, 1247-1248.

(16) Philipse, A. P.; Vanbruggen, M. P. B.; Pathmamanoharan, C. Magnetic Silica Dispersions - Preparation and Stability of Surface-Modified Silica Particles With A Magnetic Core. *Langmuir* **1994**, *10*, 92-99.

(17) Yang, D.; Hu, J. H.; Fu, S. K. Controlled Synthesis of Magnetite-Silica Nanocomposites via a Seeded Sol-Gel Approach. *J. Phys. Chem. C* **2009**, *113*, 7646-7651.

(18) Deng, Y. H.; Wang, C. C.; Hu, J. H.; Yang, W. L.; Fu, S. K. Investigation of formation of silica-coated magnetite nanoparticles via sol-gel approach. *Colloids and Surfaces a-Physicochemical and Engineering Aspects* **2005**, *262*, 87-93.

(19) Ma, Z.; Guan, Y.; Liu, H. Superparamagnetic silica nanoparticles with immobilized metal affinity ligands for protein adsorption. *Journal of Magnetism and Magnetic Materials* **2006**, *301*, 469-477.

(20) Salgueiriño-Maceira, V.; Correa-Duarte, M. A.; Spasova, M.; Liz-Marzán, L. M.; Farle, M. Composite Silica Spheres with Magnetic and Luminescent Functionalities. *Advanced Functional Materials* **2006**, *16*, 1266-1266.

(21) Balamurugan, S. S.; Soto-Cantu, E.; Cueto, R.; Russo, P. S. Preparation of Organosoluble Silica-Polypeptide Particles by "Click" Chemistry. *Macromolecules* **2010**, *43*, 62-70.

(22) Ranjan, R.; Brittain, W. J. Tandem RAFT polymerization and click chemistry: An efficient approach to surface modification. *Macromol. Rapid Commun.* **2007**, *28*, 2084-2089.

(23) Ranjan, R.; Brittain, W. J. Combination of living radical polymerization and click chemistry for surface modification. *Macromolecules* **2007**, *40*, 6217-6223.

(24) Ranjan, R.; Brittain, W. J. Synthesis of high density polymer brushes on nanoparticles by combined RAFT polymerization and click chemistry. *Macromol. Rapid Commun.* **2008**, *29*, 1104-1110.

(25) Kobayashi, Y.; Horie, M.; Konno, M.; Rodriguez-Gonzalez, B.; Liz-Marzan, L. M. Preparation and properties of silica-coated cobalt nanoparticles. *Journal of Physical Chemistry B* **2003**, *107*, 7420-7425.

(26) Turksen, S. PhD, Louisiana State University, 2006.

(27) Daly, W. H.; Poché, D. The preparation of N-carboxyanhydrides of α-amino acids using bis(trichloromethyl)carbonate. *Tetrahedron Letters* **1988**, *29*, 5859-5862.

(28) Poche, D. S.; Moore, M. J.; Bowles, J. L. An unconventional method for purifying the N-carboxyanhydride derivatives of γ-alkyl-L-glutamates. *Synthetic Communications* **1999**, *29*, 843-854.

(29) Wang, Y. L.; Chang, Y. C. Synthesis and conformational transition of surface-tethered polypeptide: Poly(L-glutamic acid). *Macromolecules* **2003**, *36*, 6503-6510.

(30) Chaikittisilp, W.; Lunn, J. D.; Shantz, D. F.; Jones, C. W. Poly(L-lysine) Brush-Mesoporous Silica Hybrid Material as a Biomolecule-Based Adsorbent for CO_2 Capture from Simulated Flue Gas and Air. *Chem.-Eur. J.* **2011**, *17*, 10556-10561.

(31) Deng, H. T.; Xu, Z. K.; Liu, Z. M.; Wu, J.; Ye, P. Adsorption immobilization of Candida rugosa lipases on polypropylene hollow fiber microfiltration membranes modified by hydrophobic polypeptides. *Enzyme and Microbial Technology* **2004**, *35*, 437-443.

(32) Deng, H. T.; Xu, Z. K.; Wu, J.; Ye, P.; Liu, Z. M.; Seta, P. A comparative study on lipase immobilized polypropylene microfiltration membranes modified by sugar-containing polymer and polypeptide. *Journal of Molecular Catalysis B-Enzymatic* **2004**, *28*, 95-100.

(33) Poche, D. S.; Daly, W. H.; Russo, P. S. Synthesis and Some Solution Properties of Poly(Gamma-Stearyl Alpha,L-Glutamate). *Macromolecules* **1995**, *28*, 6745-6753.

(34) Applequist, J.; Doty, P. In *Polyamino Acids, Polypeptides, and Proteins*; Stahmann, M. A., Ed.; The University of Wisconsin Press, p. 161-175: Madison, 1962.

APPENDIX A: PERMISSION

Cornelia Rosu <crosu1@tigers.lsu.edu> Apr 11 (5 days ago)

to Sibel

Dear Dr. Selcuk,

I would like to request permission to use Figure 4.33 from the 2004 Louisiana State University dissertation entitled "Synthesis and Characterization of Superparamagnetic Silica-Homopolypeptide Composite Particles" of which you are the author. It will be used as dissertation material for illustrative purposes.

Kind regards,

Cornelia Rosu

Selcuk, Sibel Apr 12 (4 days ago)

to me

Dear Cornelia,

Here by with this email I grant you the permission to use Figure 4.33 from the LSU Dissertation entitled "Synthesis and Characterization of Superparamagnetic Silica-Homopolypeptide Composite Particles".

I wish you the best of luck in your defense and your future endeavors.

Best,
Sibel Selcuk

Sibel Selcuk , Ph.D.

Chief Scientist

Hentoga Research Group

(w) 317-390-3136

(fax) 317-486-2985

email: sibel.selcuk@hrglab.com

permission request

Inbox x

Cornelia Rosu <crosu1@tigers.lsu.edu> Apr 11 (5 days ago)

to Erick

Dear Dr. Soto-Cantu,

I would like to request permission to use Figure 4.36 and Figure 4.37 from the Louisiana State University dissertation entitled "Synthesis and Surface Characterization of Silica-Polypeptide Composite Particles" of which you are the author. It will be used as dissertation material for illustrative purposes.

Kind regards,

Cornelia Rosu

Erick Soto-Cantu Apr 11 (5 days ago)

to me

Dear Cornelia Rosu:

According to LSU's Thesis and Dissertation Guidelines (http://gradlsu.gs.lsu.edu/files/item10745.pdf):
"*The copyright of any thesis or dissertation resides with the individual student author, by virtue of Part VII of the University Bylaws and Regulations, p. 47.*"

Therefore, I as the author of Louisiana State University dissertation entitled "Synthesis and Surface Characterization of Silica-Polypeptide Composite Particles" have the right to grant permission to use the figures you requested.

Permission Granted

Regards,

Erick Soto-Cantu

VITA

Cornelia Rosu was born in Vatra Dornei, Suceava County, Romania. She attended the Industrial High School in Suceava county and graduated in 1989. Cornelia studied Chemistry and Physics at the "Al. I. Cuza", Iasi, Romania and graduated in 1996. She taught chemistry and physics from the mid to high school level for a number of years. In 2007, Cornelia was admitted in the chemistry doctoral program at Louisiana State University, Chemistry Department where she joined Prof. Paul Russo's group. In 2011 Cornelia won the Dow award for excellence in macromolecular studied and in 2013 she was awarded with the ASC Excellence in Polymer Research. Cornelia is a doctoral candidate and she is expected to receive the degree of Doctor of Philosophy in the August 2013 commencement.